ADDRESSING CHALLENGES IN CATALYSIS AND ENERGY: SELECTIVE GRAFTING FUNCTIONALITY ONTO MESOPOROUS SILICAS AND ORGANIC HYDRIDES FOR THE REGENERATION OF AMMONIA BORANE, A HYDROGEN STORAGE MATERIAL

by

Jonathan Douglas Webb

A thesis submitted to the Department of Chemistry

In conformity with the requirements for

the degree of Doctor of Philosophy

Queen's University

Kingston, Ontario, Canada

(September, 2011)

Abstract

Ordered mesoporous silicas have been shown to have a variety of useful applications ranging from adsorbents for containments to supports for catalysts. While these materials have received a good deal of attention in the literature there is still much opportunity for new technologies. We present research describing a novel approach to incorporate functionality onto the pore surfaces of these materials as well as a highly active catalyst for the Suzuki-Miyaura reaction.

Our approach to selectively graft functionality on to the pore walls of the mesoporous silicas SBA-15 and MCM-41 involves treating the materials loaded with a structure directing agent (SDA), with hexamethyldisilazane that passivates the external surface through silylation. Once the SDA is removed the mesopores can be functionalized selectively using standard methods. A test designed to look at the passivation layer is also described.

The catalyst developed is designated Pd-SBA-15-SH(g) and it is active for the Suzuki-Miyaura reaction. The activity, recyclability and leaching of Pd-SBA-15-SH(g) was found to be superior to related materials. A mechanistic analysis suggests the catalyst is a reservoir for soluble Pd metal.

A key challenge that is holding back wide scale application of ammonia borane (NH_3BH_3) as a hydrogen storage material for mobile applications is the dearth of regeneration strategies. Presented are our forays into the development of an organic hydride based regeneration strategy. The first phase of the project focused on the reaction between Hantzsch esters and $B(C_6F_5)_3$. N-substituted Hantzsch esters were found to transfer hydride to boron in >90 % yield. Mechanistic

analysis of the reaction suggests either a SET mechanism or a highly asynchronous transition state. A novel hydride transfer equilibrium promoted by $B(C_6F_5)_3$ was observed and it operated at temperatures below -10 ºC.

N,*N*-ditertbutyl-dihydroimidazole is also an effective hydride donor to $B(C_6F_5)_3$ as well as other Lewis acids that are more relevant mimics to those invoked in regeneration schemes. When the redistribution of $B(SPh)_3$ is carried out with *N*,*N*-ditertbutyl-dihydroimidazole in the presence of NEt_3 and CH_2Cl_2 at 50 ºC, $BH_2(NEt)_3(SPh)$ is formed. CH_2Cl_2 functions as a thiol scavenger under the reaction conditions. 1-Octene trapping experiments provided indirect evidence for the formation of diborane, a critical component in the regeneration of NH_3BH_3.

Preface

This thesis is divided into two parts which discuss research advances that we have made in developing applications of ordered mesoporous silicas and a regeneration strategy for the potential hydrogen storage material, ammonia borane (NH_3BH_3). Part A of this thesis concentrates on my research efforts into applications of mesoporous silicas and Chapter 1 serves as a general introduction into these materials, their applications and methods of functionalization. Building on the literature precedents introduced in Chapter 1, Chapter 2 describes advances that we have made towards the goal of selectively localizing functional groups in the pores of SBA-15 and MCM-41. A common application of mesoporous silicas is as supports for metal catalysts and Chapter 3 describes a study of Pd-SBA-15-SH(g), a material which serves as a catalyst for the Suzuki-Miyaura reaction. The research approach adopted in Chapter 2 and Chapter 3 was to use physical methods and mechanistic tests to elucidate how the properties of these materials dictated their function with the ultimate goal of improving their design.

The same methodological approach was adopted in Part B of this thesis which describes the development of hydride transfer reactions from organic molecules to boron Lewis acids. This work was initiated in 2007 and the aim of the project was to develop an organic hydride based regeneration scheme for the hydrogen storage material NH_3BH_3. At the time, there were very few reports that described hydride transfer from organic molecules to boron and they were not well understood. Chapter 4 serves as an introduction to NH_3BH_3 as a hydrogen storage material, in addition to the critical issue of proposed routes for its regeneration. Chapter 5 describes the hydride transfer from Hantzsch esters to the Lewis acid $B(C_6F_5)_3$. The reaction was amenable to a mechanistic study, which ultimately lead to a picture of the structural features of these 1,4-

dihydropyridines that were important for efficient reaction. This work leads into Chapter 6 which describes the use of dihydroimidazoles as hydride donors to boron Lewis acids that are more relevant from a regeneration point of view. An NMR study of these reactions provides direct evidence for multiple hydride transfers to boron and indirect evidence of the formation of diborane, an important precursor to NH_3BH_3.

Acknowledgements

For the better part of the last six years I have been a member of the Crudden group. It has been a fantastic experience and I must first acknowledge my supervisor. To Cathy: Thank-you for providing the most creative of work environments and for being my advocate not only professionally but creatively throughout my time in your lab. It truly has been a pleasure working for you!

When I first started graduate school, even though I had some prior undergraduate research experience I was still very much green and I was taught the nuts and bolts of being a chemist by a number of predecessors in the lab, hopefully I have learned my lessons well and with humility. I must point out in particular Dave Edwards whose raw intelligence as well as enthusiasm for all things chemical, especially in the field of physical organic chemistry, has provided me with much inspiration. Thanks also for the spirited discussions and factoids which have served me well.

I have had the pleasure of working with some extremely talented people over the course of my time in the Crudden lab and in the Queen's Chemistry Department. There are some people would need special recognition:

- To my research collaborators Véronique Laberge and Chris Lata. Not only did we work together in the lab but we also became the best of friends.
- To the most fantastic of post-docs Thomas Wood, Daisuke Imao, Stephanie MacQuarrie, Xiaowei Wu and most recently Patrick Eisenberger for your passion for research, excellent discussions and creativity. There is a piece of all of you in this thesis. Tom do you want another Rusty-Nail?
- To the bay and my compatriots, Steve Dickson, Jenny Du, Ben Glasspoole and Jeremy Praetorius what a pleasure it was working alongside all of you. You kept me focused through those though days. Time does fly doesn`t it and I wish you all the luck in the future.
- To the newbies, you all have great assets, work hard and have fun please…

- To Derek Pratt for giving me the opportunity to lecture and to be the teaching assistant for your undergraduate third year organic chemistry course. I learned more from this experience than anyone can imagine.
- Pat Cashin thanks for My Bar and I hope you find success in Law School.
- Thanks to the Stan Brown, the David Zechel and the Philip Jessop groups for the use of instruments which aided the studies described herein. Thanks to Françoise Sauriol and Ruiyao Wang for Solid State NMR spectra and X-ray crystallographic analysis respectively.

I must also acknowledge others for there for their support and inspiration:

- To my former supervisors Steve Westcott, Tom Baker, Matt Sigman and David Thorn thanks for the opportunity to work in your research groups. Matt Sigman you provided the ideal environment for me to learn about mechanistic analysis, Katrina Jensen is fantastic and was the ideal collaborator. To Tom Baker and David Thorn for the opportunity to work at LANL and teaching me about the challenges of boron based hydrogen storage.
- Steve Westcott you get your own bullet because without you I would not be at this position today. You were an amazing mentor and you are a great friend, I am your boy Sludgy and a true blue Wild Toad.

I must acknowledge NSERC and Queen`s University for graduate scholarships and a travel grant respectively. These funds made it possible for me to focus on the task at hand.

Last but definitely not least to my family, without your love and encouragement I would not have been able to tough it out all these years. This thesis is for you!

Statement of Originality

I hereby certify that all of the work described within this thesis is the original work of the author. Any published (or unpublished) ideas and/or techniques from the work of others are fully acknowledged in accordance with the standard referencing practices.

(Jonathan Webb)

(September, 2011)

Table of Contents

List of Schemes

List of Figures

List of Tables

List of Abbreviations

Å	angstrom
AAC	azide-alkyne cycloaddition
A.C.S.	American Chemical Society
Ac	acetyl
AcOH	acetic acid
AES	atomic emission spectroscopy
AIBN	azobis(isobutyronitrile)
Anal. Calc.	analysis calculated
APTES	3-aminopropyl triethoxysilane
APTMEES	3-aminopropyltris(methoxyethoxyethoxy)silane
Ar	aryl
ASNC	arrays of silica nano-channels
atm	atmosphere
BET	Brunauer Emmett Teller
BINAP	2,2'-bis(diphenylphosphino)-1,1'-binaphthyl
BJH	Barrett Joyner Halenda
bmim	1,3-butylmethylimidazolium
BN	boron nitride
BNH_x	polyborazylene
Bn	benzyl
nBu	n-butyl
bpy	2,2'-bipyridine
br	broad
c	centi,
^oC	degree Celsius
cal	calorie
cat	catalyst, cat, catechol
cc	co-condensed
CDB	cyclodiaminoborane

ClPTES	3-chloropropyltriethoxysilane
ClPTMS	3-chloropropyltrimethoxysilane
cm^{-1}	wave number
CN	cyano
Co.	company
cod	1,5-cyclooctadiene
CP	cross-polarization
Cp	cyclopentyldienyl
Cp*	1,2,3,4,5-pentamethylcyclopentyldienyl
CSLM	confocal scanning laser microscopy
CTAB	cetyltrimethylammonium bromide
CTB	cyclotriborazane
Cy	cyclohexyl
D	diameter
d	day, dog, doublet
Δ	delta, chemical shift
Dabco	1,4-diazabicyclo[2.2.2]octane
DADB	diammoniate of diborane
DCE	1,2-dichloroethane
DEM	diethoxymethane
DHP	1,4-dihydropyridine
dmpe	1,2-dimethylphosphinoethane
DMB	1,4-dimethoxybenzene
DME	dimethoxyethane
DMF	N,N-dimethylformamide
DOE	United States Department of Energy
dppf	1,1'-bis(diphenylphosphino)ferrocene
e^-	electron
EA	elemental analysis
ee	enantioselectivity
EI	electron impact
E^o	standard electrode potential

EO	ethylene oxide
equiv.	equivalent
Et	ethyl
Et_2O	diethylether
EtOAc	ethylacetate
EtOH	ethanol
ESI	electron spray ionization
ESR	electron spin resonance spectroscopy
em	emission
emim	1,3-ethylmethylimidazolium
endo	endothermic
ex	excitation
exo	exothermic
EXSY	exchange spectroscopy
F127	$poly(ethyleneoxide)_{106}$–$poly(propyleneoxide)_{70}$–$poly(ethyleneoxide)_{106}$
$Fc^{0/+}$	ferrocene reference electrode
FDU-#	Fundan University material – number
FID	flame ionization detector
FITC	fluorescein isothiocyanate
FLP	frustrated Lewis pair
FSM-#	folded sheets mesoporous materials-number
FT-IR	Fourier Transform infra-red spectroscopy
g	gram
ΔG	free energy
GC	gas chromatography
gge	gasoline gallon equivalent
GNP	gold nanoparticle
GNR	guns and roses
h	hour, hexet
ΔH	enthalpy
ΔH_{aff}	hydride affinity
Hz	hertz

HBcat	catechol borane, 1,3,2-benzodioxaborole
HBpin	pinacol borane, 4,4,5,5-tetramethyl-1,3,2-dioxaborolane
HLADH	horse liver alcohol dehydrogenase
HMBC	heteronuclear multiple bond correlation
HMDS	hexamethyldisilazane
HRTEM	high resolution transmission electron microscopy
HSQC	heteronuclear single quantum correlation
ICP-MS	inductively coupled plasma mass spectroscopy
iPr	isopropyl
J	coupling, joule constant
k	rate constant, kilo
K	Kelvin
K_b	binding constant
K_{eq}	equilibrium constant
KIE	kinetic isotope effect
KIT-#	Korea Advanced Institute of Technology material - number
k_{obs}	observed rate constant
L	litre
LA	Lewis acid
λ	wavelength
λ_{ex}	excitation wavelength
LANL	Los Alamos National Laboratory
LB	Lewis base
M	molar, mega
m	multiplet, metre, milli, meta, monkey
MAS	magic angle spinning
MCM-#	Mobile composite material-number
Me	methyl
MeCN	acetonitrile
MeOH	methanol
min	minute
mol	mole percent

mol%	mole %
MPTMS	3-mercaptopropyltrimethoxysilane
MS	mass spectrometry
MW	molecular weight
n	nonet, nano
N_3PTES	3-azido-propyltriethoxysilane
NADH	nicotinamide adenine dinucleotide
NHC	N-heterocyclic carbene
NLSSQ	non-linear least square
NMR	nuclear magnetic resonance
nOc	n-octyl
NOESY	nuclear overhauser effect spectroscopy
^{o}	degree
OF#	orthoformamide-number
ORTEP	Oak Ridge Thermal Ellipsoid Plot Program
OTf	triflate
ov	overlapping
P	pressure
p	pentet, para
P123	poly(ethyleneoxide)$_{20}$–poly(propyleneoxide)$_{70}$–poly(ethyleneoxide)$_{20}$
PAB	polyaminoborane
Pd/C	palladium on carbon
PEM	polymer electrolyte membrane
PIB	polyiminoborane
PG	passivating group
Ph	phenyl
pin	pinacol
PMMA	polymethylmethacylate
PNNL	Pacific Northwest National Laboratory
PO	propylene oxide
ppb	parts per billion
ppm	parts per million

Pr	propyl
psi	pressure per square inch
PTFE	polytetrafluoroethylene, Teflon
PVP	polyvinylpyridine
py	pyridine
q	quartet
re-	reloaded
rpm	rotations per minute
rt	room temperature
rxn	reaction
S	surface area
s	singlet, second
ΔS	entropy
SBA-#	Santa Barbara material – number
SDA	structure directing agent
SET	single electron transfer
SEM	scanning electron microscopy
STDEV	standard deviation
STP	standard temperature and pressure
t	triplet
$t_{1/2}$	half life
tBu	tert-butyl
tBuOH	tert-butanol
TEM	transmission electron microscopy
TEOS	tetraethoxysilane
THF	tetrahydrofuran
TMB	1,3,5-trimethylbenzene
TMEDA	tetramethylethylenediamine
TMP	tetramethylpipieridine
TMS	trimethylsilyl
TMSCl	trimethylsilylchloride
TMSOEt	ethoxytrimethylsilane

TOF	turn over frequency, time of flight
Tol	toluene
TON	turn over number
UV	ultraviolet
V	volt, volume
Vol	volume
VT	variable temperature
VTS	vinyltrichlorosilane
W	Watt
W/O	water in oil
wt	weight, wild toad
XPS	X-ray photoelectron spectroscopy
XRD	X-ray diffraction
XAES	X-ray Auger induced spectroscopy

Chapter 1

General Introduction to Functionalization of Ordered Mesoporous Silicas

1.1 Introduction

Ordered porous materials have received much attention in the literature over the last 20-30 years.[1] This diverse class of solids includes zeolites, metal-organic frameworks, mesoporous/macroporous silicas, and mesoporous organosilicas as well as mesoporous metal-oxides.[1-4] There are three pore size ranges represented in these materials, 1 – 2 nm, 2 – 50 nm and >50 nm, and they are termed micropores, mesopores and macropores, respectively.[5] At a basic level, these solids are interesting because their high surface area, which is in some cases greater than 1000 m^2 g^{-1}, affords them the ability, in principle, to have excellent surface contact throughout the material with the surrounding medium, which can be gas or solvent.[1] Another beneficial property of porous solids is that they have a high void space to pore volume ratio. In other words, they are less dense than a chemically similar non-porous material. These materials are also often robust, and it is these intrinsic properties that can account for the applicability of ordered porous solids as catalysts or catalyst supports, as adsorbents for a range of molecules including organics, metals and gases, as templates for nanoparticle synthesis and as low dielectric constant materials for electronic applications.[1]

Key to the many successful applications of porous solids is suitable functionalization of the material. Mesoporous silicas, for example, have received much attention in the literature not only because they are easily synthesized and have good stability but also because their silanol containing surfaces are amenable to functionalization with a diverse array of organic,

organometallic and inorganic groups. The synthesis, structure, functionalization and applications of mesoporous silicas have been aptly reviewed by a number of research groups.[6-13] The focus of this chapter will be to introduce ordered mesoporous silicas as well as the various methods used to functionalize these solids. As will be seen there is significant interest in developing strategies to pattern functionality on the surfaces of silicas as well as to selectively graft functional groups on various domains such as the external, mesopore and micropore surfaces. This discussion will lead into the first research chapter of this thesis that deals with the development of a strategy to selectively functionalize the mesopores of these materials to the exclusion of other surfaces.

1.1.1 Ordered Mesoporous Silicas

Ordered mesoporous silicas were first reported in 1990 when the Kuroda group[14, 15] demonstrated that Kanemite, a layered (i.e. lamellar) silicate, could restructure into a 2D hexagonally ordered material with high surface area (~ 1000 m^2/g) on treatment with cationic ammonium salts.[16] It is believed thet the mesostructure arose from fragmentation and folding of the silica layers about the ammonium surfactant,[17] this material was later named FSM-16 (folded sheet mesoporous material-16).[18] Subsequent to the work of Kuroda in 1992 Mobile Corporation[19, 20] reported a related material MCM-41 (Mobile composite material-41) which had similar structural properties to FSM-16. Instead of a folding sheet mechanism, MCM-41 is believed to arise from a surfactant templation process.[7] The pore walls of FSM-16 and MCM-41 are amorphous and this is typical of mesoporous silicas. Prior to the development of these materials, only mesoporous silicas with irregularly shaped pores and broad pore size distributions were known.[21, 22] By contrast FSM-16 and MCM-41 have a regular pore structure and a narrow pore size distribution centered between 2 - 4 nm depending on the synthesis conditions.

Subsequent to the initial reports of FSM-16 and MCM-41 there have been a plethora of reports of new classes of mesoporous silica materials with a range of mesostructures (**Scheme 1-1**).[7] The names of common ordered mesoporous silicas and general details describing their structures and syntheses are described in **Table 1-1**. Of these solids, the most commonly employed mesoporous silicas are SBA-15 (Santa Barbara material-15)[23, 24] and MCM-41. The details of the structure of these materials will be discussed later on in this chapter.

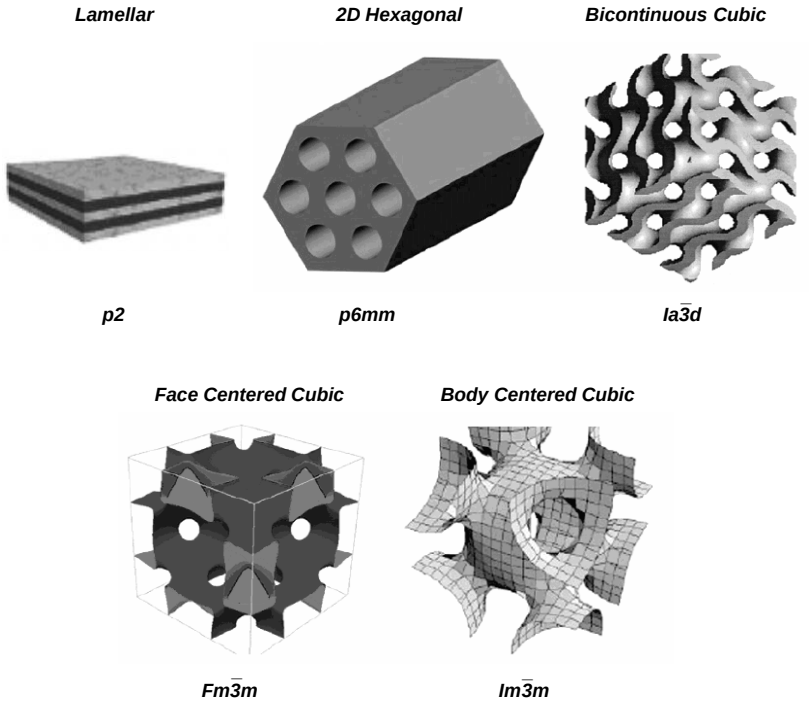

Scheme 1-1. Models of common pore structures for mesoporous silicas with associated pore symmetries, adapted from reference 7 with permission

Table 1-1. Some representative ordered mesoporous silicas and general notes regarding their structure and synthesis

Material	Mesostructure	Surfactant	Silica[a] Surfactant Interaction[b]	Templating pH
MCM-41	2D-Hexagonal	CTAB	S^+I^-	Basic
MCM-48	Cubic	Gemini[c]	S^+I^-	Basic
FDU-12	Face Centered Cubic	F127, TMB[d]	$S^+X^-I^+$	Acidic
FSM-16	2D-Hexagonal	CTAB	Folded Sheet	Basic
KIT-6	Bicontinuous Cubic	P123,[e] Butanol	$S^+X^-I^+$	Acidic
SBA-15	2D-Hexagonal	P123	$S^+X^-I^+$	Acidic
SBA-16	Body Centered Cubic	F127	$S^+X^-I^+$	Acidic

[a] Tetraethoxysilane is the common silica source although others may be used; [b] S = surfactant, I = inorganic network i.e. silica, X = halide; [c] Gemini = $[CH_3(CH_2)_nNMe_2(CH_2)_mNMe_2(CH_2)_pCH_3][Br]_2$ n = 8 – 22, m = 2 – 6, p = 1 – 22; [d] F127 = $EO_{106}PO_{70}EO_{106}$ EO = ethylene oxide, PO = propylene oxide and TMB = 1,3,5-trimethylbenzene [e] P123 = $EO_{20}PO_{70}EO_{20}$

1.1.2 Surfactant Templation Process for the Synthesis of Mesoporous Silicas

As was mentioned above, SBA-15 and MCM-41 are synthesized using a surfactant templation process. Materials are generated by dissolving a structure directing agent (SDA) into an acidic or basic aqueous solution. The SDA for the synthesis of SBA-15 is the triblock copolymer P123 and the SDA for the synthesis of MCM-41 is cetyltrimethylammonium bromide (CTAB) (**Scheme 1-2**). Under typical synthetic conditions, these SDAs exist in solution as micelles. Formation of the mesostructured silica-SDA network is initiated by adding an inorganic precursor such as tetraethoxysilane (TEOS) to the solution (**Scheme 1-3**).

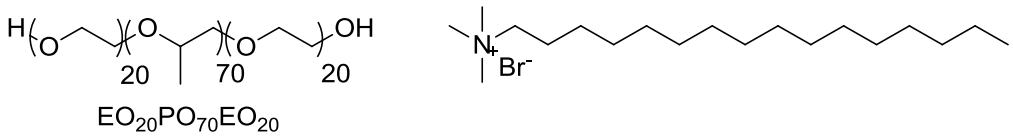

Scheme 1-2. Structural directing agents P123 (left) and CTAB (right)

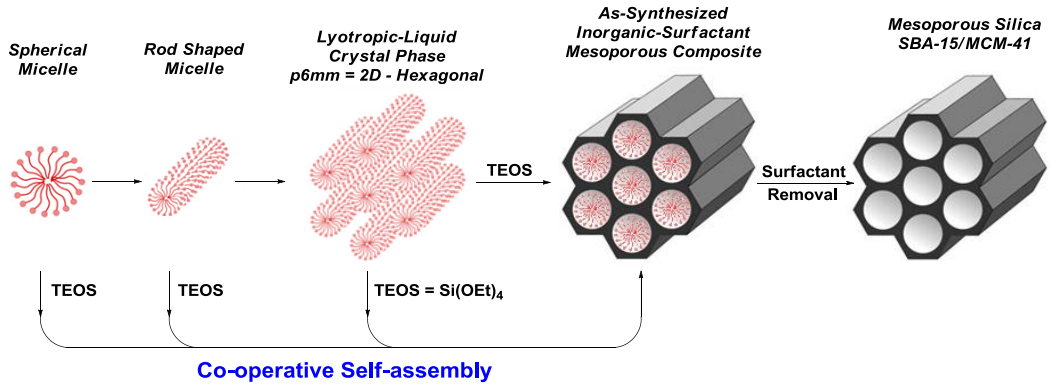

Scheme 1-3. Surfactant templation process for the synthesis of SBA-15 and MCM-41, adapted from reference 6 with permission

The mesophase about which the silica network of SBA-15 and MCM-41 condenses is formed by a co-operative self-assembly process that involves the SDA and the inorganic precursor, which is undergoing hydrolysis and is condensing under the material synthesis conditions (**Scheme 1-3**).[25-28] The interplay between the condensing inorganic precursor and the SDA(s) as well as the temperature, pH and concentration all control the structure of the developing mesophase. There are six different types of SDA to silica network interactions summarized in **Scheme 1-4** as delineated by Stucky and co-workers.[6, 7, 25] The interaction that dominates under acidic (pH < 2) conditions is $S^{+}X^{-}I^{+}$, which is the cooperative assembly interaction relevant for the synthesis of SBA-15. Under these low pH conditions the inorganic precursor carries a net positive charge.[23, 24] By contrast $S^{+}I^{-}$ electrostatic interactions operates

during the synthesis of MCM-41. MCM-41 is synthesized at high pH (>10) in the presence of cationic ammonium salts.[20, 25] Under these pH conditions the inorganic precursor (Si-OH pKa ~ 6) carries a net negative charge.[23] At the end of the templation process the inorganic-surfactant composites of SBA-15 and MCM-41 are subjected to a static hydrothermal treatment, the purpose of which is to increase the condensation of the silica framework.[23, 29] After hydrothermal treatment, the mesoporous silica is recovered and is considered to be in its as-synthesized state.

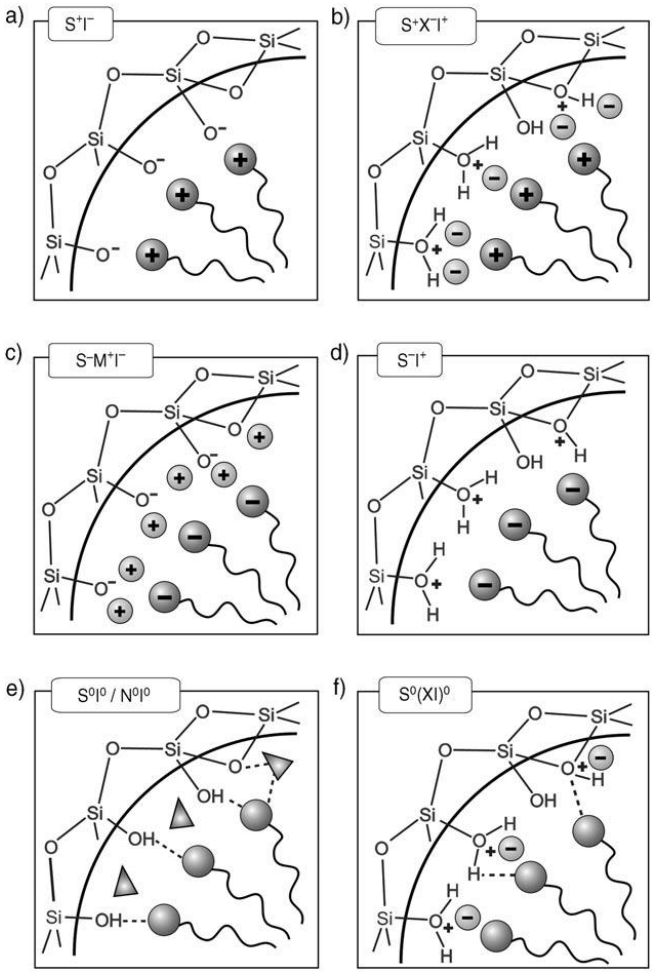

Scheme 1-4. Types of SDA-Silica interactions relevant to the synthesis of mesoporous silicas; a)-d) are electrostatic interactions and e)-f) are hydrogen bonding interactions where S or N = surfactant, X = halide, I = inorganic silica, reproduced from reference 6 with permission

The as-synthesized mesoporous silicas as-SBA-15 and as-MCM-41 contain residual SDA within the pores of the material which is removed by an extraction procedure.[30] The two common approaches for removing the SDA are calcination, usually at 550 °C, and solvent extraction. The calcination conditions are sufficiently aggressive to remove all organic content from the mesoporous silica and they will also promote increased condensation of the silica framework.[31] Surfactant solvent extraction is milder and typically less effective at removing the SDA. The most effective procedures remove >90 % of the residual SDA.[23, 32] Solvent extraction is carried out either by suspending the material in solvent or by placing the material in a Soxhlet extractor. There are a number of publications dedicated to the study of different solvent extraction conditions; approaches taken vary from washing with neutral or acidic (pH < 4) ethanol[23, 32] and supercritical CO_2[33] to the use of dilute solutions of oxidants such as $KMnO_4$[34] and H_2O_2.[35] Other novel ways of extracting the SDA involve the use of microwave irradiation[36] or UV light in conjunction with acid or oxidants.[37] That said, hot neutral or acidic ethanol (pH < 4) are the most commonly employed solvent extraction procedures for as-SBA-15 and as-MCM-41.

1.1.3 Structure of SBA-15 and MCM-41

The pore structure and surface characteristics of MCM-41 and SBA-15 are complex. As mentioned earlier these materials have 2D hexagonal mesostructures (**Figure 1-1**). The average pore size of MCM-41 and SBA-15 depends on the synthesis conditions but generally MCM-41 (2 – 4 nm)[19] has smaller pores than SBA-15 (6 – 8 nm).[23, 24] The pore wall thickness also differs between the two materials (SBA-15 ≈ 3 – 6 nm,[23, 24] MCM-41 ≈ 1 nm[7, 38]) and SBA-15 has a rougher pore surface than MCM-41.[39] The pores of SBA-15 have been described as being corrugated because the width of a pore appears to vary periodically by about 1.5 nm along their

length.[40] Embedded within the walls of the mesopores of SBA-15 are micropores.[30] Micropores result from the protrusion of the ethylene-oxide blocks of the SDA P123 into the walls of the material. The micropore content of SBA-15 depends heavily on the hydrothermal treatment, with the amount decreasing with higher temperatures and prolonged heating times.[41-45] Under more aggressive hydrothermal treatment conditions, micropores transform into larger secondary mesopores that connect the main mesochannels of SBA-15. Finally, the surfaces of the mesoporous silicas SBA-15 and MCM-41 are populated with silanols; the density ($N_{OH} \approx 3.7$ nm^{-2} for SBA-15 and $N_{OH} \approx 3$ nm^{-2} for MCM-41)[46] and types of which (**Scheme 1-5**)[47] again depend on the method of preparation and drying procedure.

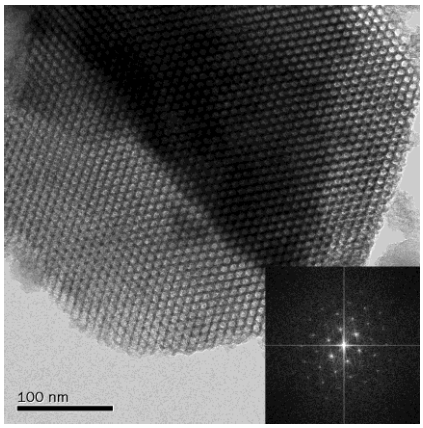

Figure 1-1. A TEM image depicting the 2D hexagonal periodic structure of an SBA-15 particle

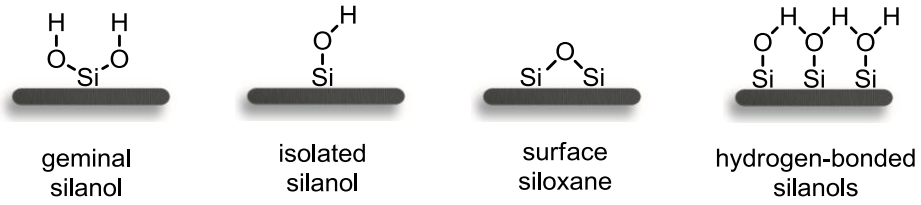

Scheme 1-5. Types of surface silanols on mesoporous silicas

1.1.4 Functionalization of SBA-15 and MCM-41

There are two methods used to functionalize mesoporous silicas; post-synthetic functionalization "post-grafting" and co-condensation (**Scheme 1-6**).[6, 8-10] These methods differ in terms of when the organo-silane is introduced. Post-grafting involves treating the silica with an organo-silane after the material is synthesized and the SDA has been extracted, whereas functionalization by co-condensation involves adding the organo-silane during the surfactant templation process.

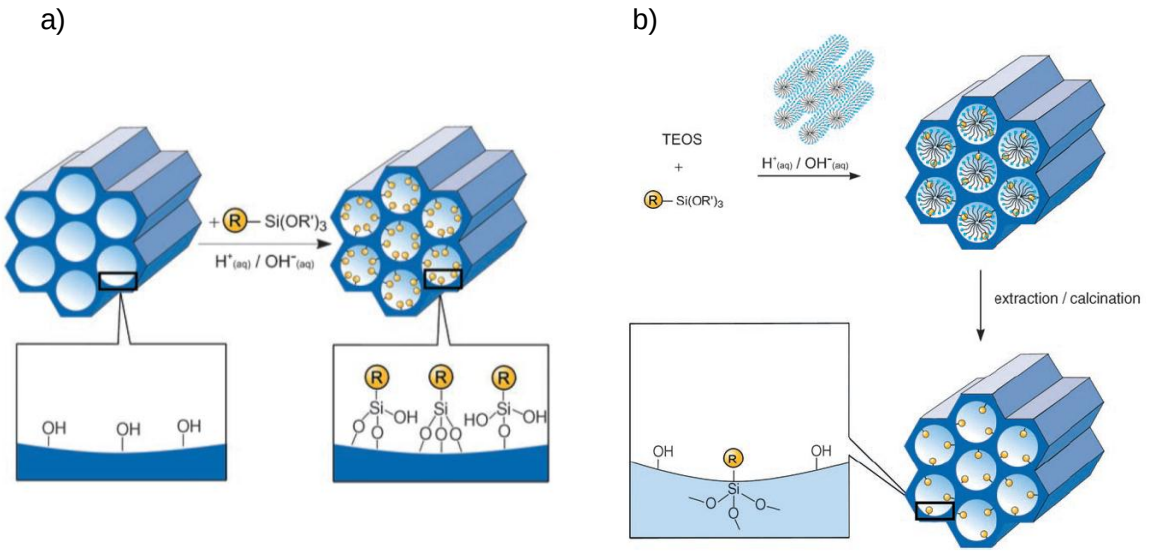

Scheme 1-6. Functionalization of mesoporous silicas by a) post-synthetic grafting and b) co-condensation, reproduced from reference 6 with permission

Post-synthetic functionalization "Post-grafting"

Functionalization of mesoporous silica by post-grafting involves reaction of the silanol containing surface with an organo-silane, the general types of which are listed in **Scheme 1-7**, including alkoxy/chloro silanes and silazanes.[48] Post-grafting is often carried out in organic

solvent with a gross excess of reagent.[49] Not all surface bound silanols are accessible to functionalization by this method, notably hydrogen bonded silanols are unreactive.[47] It is also noteworthy that strained surface-bound siloxanes are amenable to functionalization as was noted by Blümel and Brunel.[50, 51] For these reasons it is difficult to achieve complete surface coverage, for practical purposes surface coverage is limited to 85 %.[8] A key benefit of post-grafting is that it does not degrade the structural order of the material significantly.[8] Although it is noted that the surface area and pore size does decrease by this method of functionalization, the amount by which these values diminish depends on the size of the organo-silane employed. Taken to the extreme, the functional group can block the pores of the material if it is large enough.[45] An advantage of post-grafting in comparison to co-condensation is that one can employ organo-silanes which may not survive the acidic or basic conditions of the templation process. The main drawback of this approach, however, is it results in an in-homogeneous distribution of functional groups on the surface of the material.[52] It is expected that, for example, the pore edges of SBA-15 and MCM-41 are functionalized preferentially because those silanols are more accessible.

$$R'O-SiR_3 \; < \; R'_2N-SiR_3 \approx Cl-SiR_3$$

Scheme 1-7. Common organo-silanes used in the functionalization of mesoporous silicas listed in order of their approximate reactivity

The choice of solvent for post-grafting is also important when attempting to avoid formation of multilayers or dense clustering of functionality on the surface. The Asefa group[53] illustrated that solvent choice is crucial when functionalizing materials with polar organosilanes such as 3-aminopropyltriethoxysilane (APTES). They noted that when non-polar solvents such as toluene were employed, up to 3 – 4 mmol g^{-1} of ATPES could be grafted onto the material. The

silica possessed a densely functionalized surface and APTES aggregation was also observed. By contrast, polar-protic solvents such as ethanol and isopropanol provided lower loadings (1 – 2 mmol g^{-1}) and improved spatial distribution of functional groups. Asefa also reported,[54] that the control protic solvents imparted over APTES grafting was crucial in obtaining a highly active catalyst for the Henry reaction between nitromethane and benzaldehyde. Note that less polar organo-silanes which include 3-mercaptopropyl trimethoxysilane (MPTMS) are less prone to this type of substantial aggregation when post-grafting is carried out in apolar solvents.[53]

Vapor deposition can also be used to functionalize mesoporous silicas. This method requires that the organosilane is volatile.[6, 55, 56] The process is performed under vacuum, and often at high temperatures, 150 ºC or greater. A benefit of vapor phase post-grafting over solvent based approaches is that one can exert good control over the extent of functionalization and the dispersion of functional groups by finely tuning the reaction conditions.

Co-condensation

In contrast to post-grafting, the main benefit of co-condensation is the improved distribution of functional groups on the surface of the material, which is believed to be more random than in post-grafting which tends to produce islands of functionality. Stack[49] examined the effectiveness of co-condensation at widely distributing functionality by varying the loading of 3-azido-propyl triethoxysilane (N_3PTES) from 0 – 8 mol % relative to the initially added TEOS. Under these conditions it was found the functional group was incorporated linearly as the initial loading was increased and that site isolation of the organo-silane could be achieved at low loadings of N_3PTES (~ 0.2 mol%). At 8 mol%, their co-condensation method resulted in an SBA-15-N_3 material with ~ 1 mmol g^{-1} of organic functionality, an amount comparable to effective post-grafting. They visualized the distribution of the incorporated N_3PTES on SBA-15-N_3 as a

function of initial loading by reacting the material with 1-ethynylpyrene under Cu mediated azide-alkyne Huisgen click cyclization conditions. They characterized the resulting material designated SBA-15-pyrene by fluorescence and examined the spectra for bands associated with monomer and excimer emission (**Figure 1-2**). At 0.2 mol% loading, the monomer emission is prevalent while the excimer prevails at 8 mol%, demonstrating site-isolation and close positioning of azide functional groups respectively on SBA-15-N_3. The main drawback of the co-condensation method for functionalization is it often diminishes the structural order of the resulting mesoporous silica because it disrupts the condensation of the silica network during the templation process, and for this reason, is believed to be limited to 25 mol% as a maximum. However, for practical purposes the loadings of organo-silanes is often less than 25 mol%.[6] Another drawback of this method it that the organo-silane can be trapped in the walls of the silica possibly affecting its accessibly, an issue that must be taken into consideration if the material is going to serve as a catalyst. Also, care must be exercised to ensure that the functional group will survive the templation process and subsequent SDA removal. This can impact the extraction procedure chosen for example, calcination is typically not employed and caution must be taken if acid is required.[6, 8]

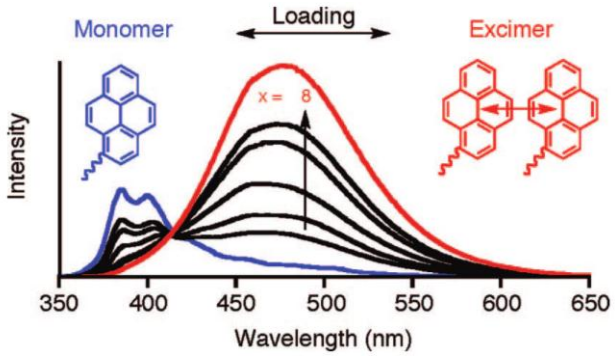

Figure 1-2. Fluorescence overlay for SBA-15-pyrene where the x mol % of the initially added N_3PTES was varied from x = 0.2, 0.5, 1, 2, 3, 4, 8, reproduced from reference 49 with permission

Beyond the Stack report discussed above,[49] a benefit of co-condensation is that one can exercise some control over where the functional groups become localized on the resulting material. Bein[57, 58] has been able to illustrate that functionality can either be localized on the external surface, within the core and/or distributed throughout the pores of his spherical mesoporous silicas. As will be seen later on in this discussion, the Bein[57, 58] protocol is an example of selective grafting. For instance his group demonstrated that aminopropyl groups become preferentially more localized on the external surface of silica particles when the addition is delayed relative to TEOS from 0 min to 30 min. The localization of the amines was inferred based on Zeta-potential measurements of acidified nanospheres (**Figure 1-3**). Note that increasing charge due to the presence of ammonium groups on the exterior of the nanospheres results in a higher Zeta-potential.

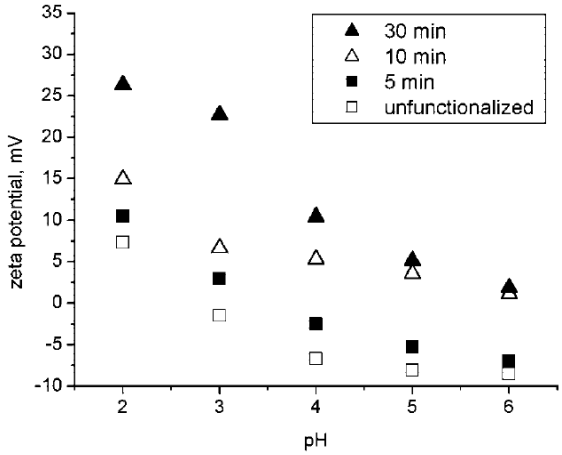

Figure 1-3. Zeta-potential of mesoporous silica spheres where APTES addition to the templation process was delayed from 5 – 30 min, reproduced from reference 58 with permission

1.1.5 Controlled Functionalization of Mesoporous Silicas

There is great interest in developing methods to pattern functionality onto the surface of mesoporous silicas. In broad strokes, there are two levels of patterning, molecular scale control over the distribution of functional group(s) and selective grafting which involves exerting control over which surfaces of the material are functionalized.[8-10, 59-62] Applications of mesoporous silicas are the driving force behind the development of these approaches to functionalization. For instance, ensuring that functional groups are close in space can increase the catalytic activity of a material.[10, 59, 63] Beyond mere patterning of functional groups, selective mesopore functionalization may be able to increase the regio or enantio-selectivity of a reaction if the pores serve as a restricting environment.[59-62] An emerging application for mesoporous silicas is as drug delivery materials. Key to this type of type of usage is selective functionalization of the external surface the particle,[9, 64] the purpose of which is to graft a group that has the capacity to recognize a particular type of tissue without clogging the pores. The pores must be left untouched because

they will serve as a reservoir for the drug substance. Also mesoporous silicas have been employed as templates for nanoparticle synthesis and it has been indicated that selective functionalization of the pores is desirable because functionality localized on the external surface of the silica can lead to less controlled nucleation and particle growth. [65, 66]

1.1.6 Patterning Functional Groups on Mesoporous Silicas

Patterning functional groups on a silica surface is accomplished by chemically linking the two groups, which are expected to reside next to one another, followed by post-grafting the resulting organo-silane. The functionality is then liberated by cleaving the linkage between the two groups. This approach has been utilized by Davis[63] and Katz.[67] Davis grafted a disulfide onto SBA-15 and subsequently reduced and oxidized the functional group (**Scheme 1-8a**). The results, respectively, were materials with mercaptopropyl and sulfonic acid groups in close proximity on the surface. He showed that a patterned sulfonic acid material was a more active and selective catalyst for the formation of bisphenol-A from the reaction of phenol with acetone. Katz utilized a xanthate protection/deprotection strategy to pattern silica with two mercaptopropyl and one aminopropyl group within ~3 Å of each other (**Scheme 1-8b**). They also observed that some level of patterning could be achieved by sequentially post-grafting xanthate and carbamate protected organo-silanes, the effect was ascribed to self-association of similar functionalities on the surface.

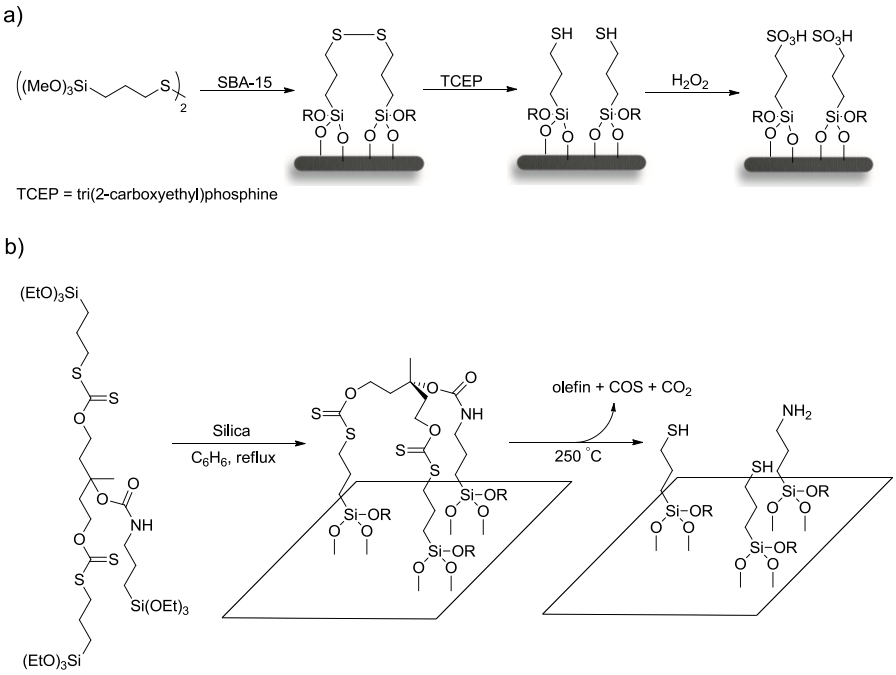

Scheme 1-8. Patterning functionality onto silica based on a post-grafting strategy; a) grafting disulfide; b) grafting a tethered trialkoxysilane

1.1.7 Selective Grafting

Selective grafting is an umbrella term that refers to a mode of functionalization that preferentially localizes groups onto specific surface domains of porous silica.[8-10, 59-62] It encompasses preferential functionalization of the external or internal surfaces. The next chapter of this thesis will discuss our foray into localizing functionality within the mesopores of SBA-15 and MCM-41 (**Scheme 1-9**). There are two approaches to selective grafting functionality onto mesoporous silicas: diffusion controlled and pore protection. Diffusion controlled selective grafting assumes that the silanols on the external surface are more accessible to post-grafting than those within the pores. Pore protection assumes that the SDA contained within the mesopores of as-synthesized materials can protect that domain from being functionalized. External surface

functionalization is then accomplished by treating silica with a substoichiometric quantity of an organo-silane which, based on the methods just described, should react with those silanols on the outer surface before those contained within the mesostructure. Preferential pore functionalization is achieved by utilizing either the diffusion controlled or pore protection method to passivate/cap silanols on the external surface with a silylating agent **Scheme 1-9**. It is assumed that after successful external passivation only those silanols within the mesopores remain accessible to functionalization using a traditional post-grafting procedure. As will be seen, the challenge with selective grafting procedures is characterizing the resulting materials and demonstrating that the techniques were successfully employed.

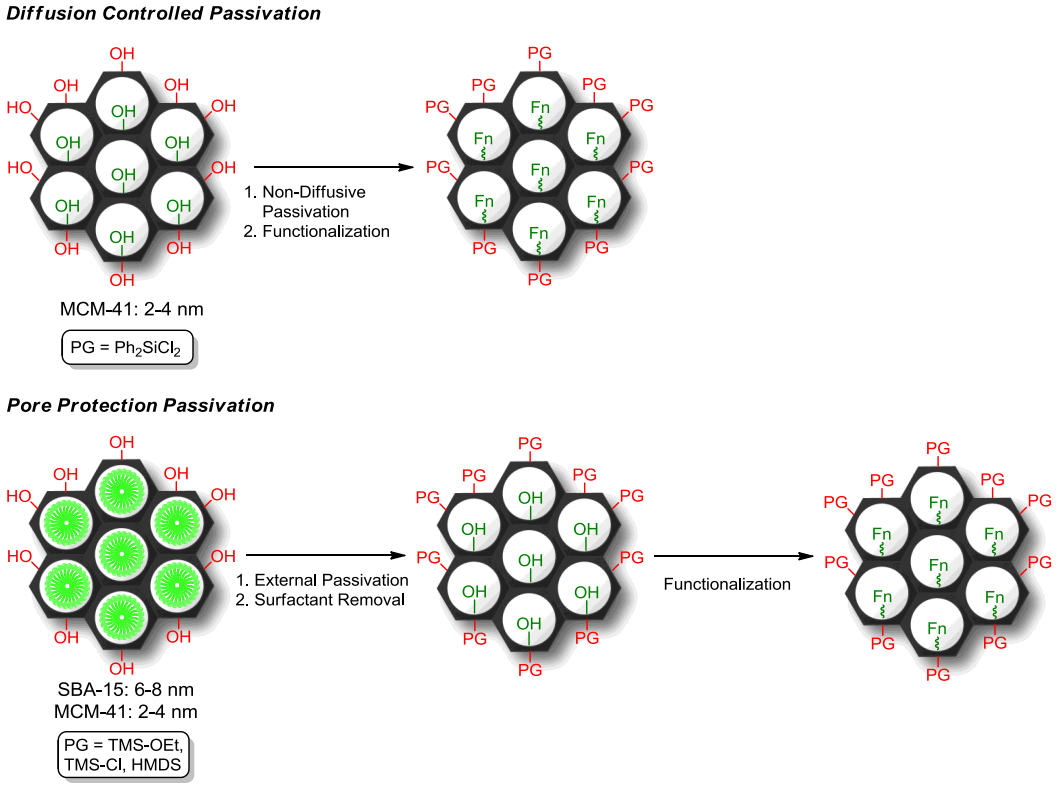

Scheme 1-9. General methods to selectively localize functionality within the mesopores of SBA-15 and MCM-41; PG = passivating group

Selective Grafting Functionality onto the external surface of mesoporous silica

Brühwiler[64] recently evaluated the underlying assumptions of diffusion controlled and pore protection methods of selective grafting as they pertain to localizing aminopropyl functionality on the external surface of mesoporous silicas. The group utilized morphology controlled materials denoted as spherical SBA-15 particles and ASNC's (arrays of silica nano-channels), which are analogous to MCM-41. Brühwiler`s plan is to eventually employ externally functionalized materials in a drug delivery technology; the purpose of the functionality will be to modulate how the silicas interact with biological tissues. To visualize the localization of the amino groups, the materials were reacted with FITC (fluorescein isothiocyanate), a fluorescent dye, and they were imaged by CSLM (confocal scanning laser microscopy). While the authors reach a number of interesting conclusions, their detection method does not necessarily inform on how effective their selective grafting strategy was across the bulk material. This is a common limitation of detection methods for selective grafting and we intend to address this problem with our research. That said, Brühwiler does report results from three different particles, in an effort to mitigate this particular concern.

Both as-synthesized and calcined versions of SBA-15 and ASNC particles were treated with small quantities of amino-propyl trialkoxysilanes in hexane for 10 min. After the trialkoxysilane adsorbed onto silica, the material was recovered and cured at 80 °C to promote grafting. The materials were then treated with FITC and imaged (**Figure 1-4**). The trialkoxysilanes screened in this study were believed to have varying mobilities through the pores of mesoporous silicas, decreasing from APTES>BTESPA>APTMEES. Notwithstanding the results discussed in the next paragraph, the Brühwiler[64] study demonstrated that the mobility of

these trialkoxysilanes is solvent dependent. These organosilanes had higher mobilities in more polar solvents such as acetone and THF.

The amino group distribution on the as-synthesized materials illustrates the effectiveness of the pore protection selective grafting strategy (**Figure 1-4b**), whereas distribution on the calcined materials informs on the diffusion controlled strategy (**Figure 1-4a**). It was found that diffusion controlled selective grafting with SBA-15 failed regardless of the organo-silane employed, presumably due to the relatively large pore size 6 – 8 nm of the material. Diffusion controlled selective grafting was only effective with the smaller pored (2 – 4 nm) ASNC particles when the organo-silane was APTMEES, evidenced by the fact that fluorescence was only observed on the boundary of the particles.

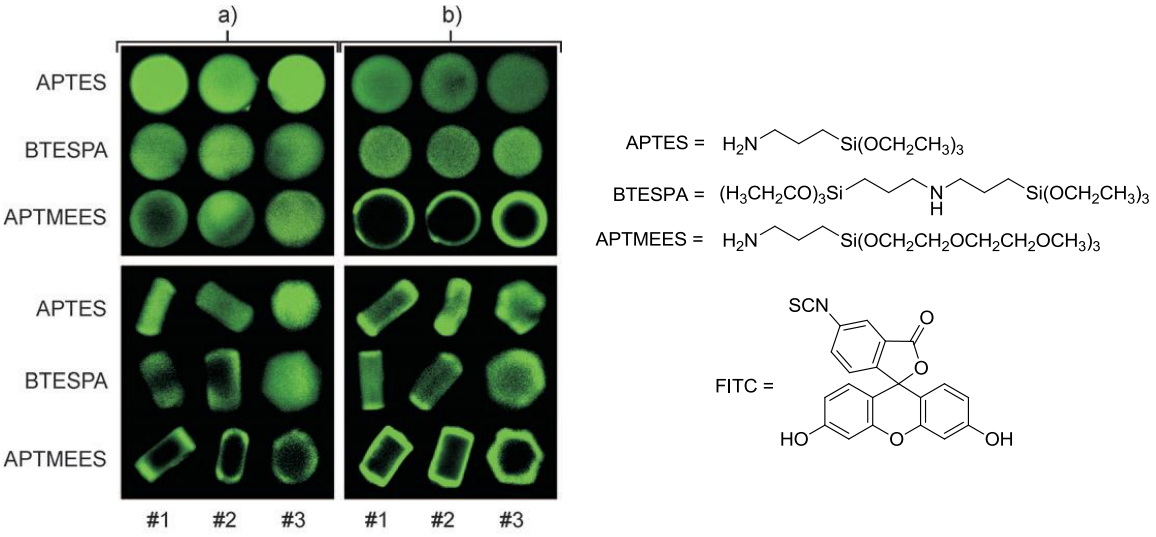

Figure 1-4. CSLM results from the Brühwiler study of external functionalization depicting the localization of amine functionality on SBA-15 (top) and ASNC (bottom) particles after treatment with an FITC dye; a) calcined materials; b) as-synthesized material, reproduced from reference 64 with permission

The pore protection selective grafting results showed again that APTMEES was the optimum organo-silane. The strategy was effective for both the SBA-15 and ASNC materials. Interestingly APTES failed on both materials, Brühwiler makes a special note that this result is particularly interesting because APTES is routinely employed by groups interested in externally functionalizing mesoporous silicas.[68, 69] Therefore, it is likely that these materials contain amino propyl groups throughout the pore structure and are not actually selectively grafted.

To illustrate the problem that Brühwiler pointed out with literature methods to externally functionalize mesoporous silica, we can consider the recent reports by Shantz[68] and Lin (**Scheme 1-10**).[69] Shantz was interested in attaching a polymer on the external surface of SBA-15 while Lin was interested in site isolation of amino and acid groups for novel catalytic applications. Note in **Scheme 1-10** that both researchers are suggesting that the amino groups are localized exclusively on the external surfaces while sulfur is contained within the pores. Using an analogous protocol to that discussed below, the opposite orientation of functionality is also purported to have been achieved. Both Shantz[68] and Lin[69] attempted to achieve external functionalization utilizing a pore protection procedure that is more aggressive than that which failed for Brühwiler.[64] These grafting procedures employed microwave irradiation[68] or heat[69] and an excess of reagent. Their methods are essentially a standard post-grafting protocol with one difference; there is SDA in the mesopores of the materials. Recall that by contrast, to achieve external functionalization, Brühwiler[64] adsorbed a small amount of bulky organo-silane onto the surface at room temperature and then cured the isolated material. Considering that Brühwiler demonstrated that APTES incorporates throughout his materials under mild conditions, it is likely that Shantz and Lin also failed to achieve selective external functionalization, even though they suggest that they have. The difficulty with research in this field is the lack of a reliable and consistent method to analyze

and verify selective grafting. In the absence of such a method, researchers typically just do not address the possibility that the SDA was not effective at protecting the mesostructure under their selective grafting conditions, they rely instead on supposed literature precedent.

a)

b)

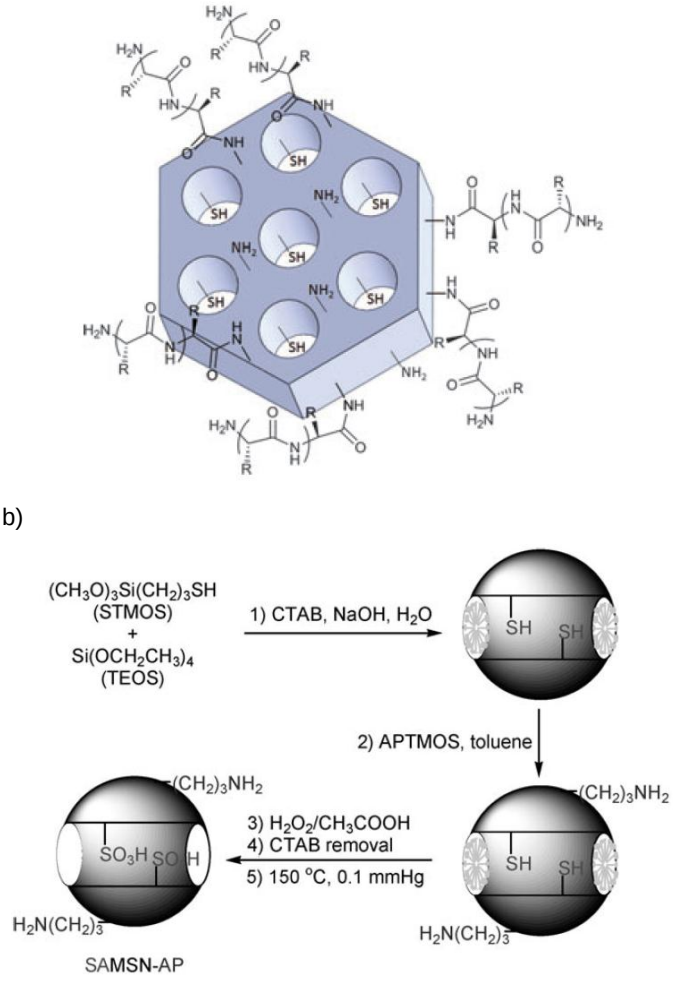

Scheme 1-10. Graphics published by a) Shantz and b) Lin to describe their selective grafted materials, reproduced from references 68 and 69 with permission

Schüth[70] took an entirely different approach to pore protection selective grafting to achieve external functionalization with magnetic cobalt particles. Instead of using the SDA P123 to protect silanols within the mesopores of SBA-15, the material was calcined and a methyl-methacrylate (MMA) polymerization was carried out. The polymerization closed the mesostructure allowing for Co nanoparticles to be adsorbed on the external surface. The nanoparticles were protected by coating them with furyl alcohol which carbonized when the pores were reopened by calcination at 850 ºC. Successful external functionalization was inferred because of the lack of pore blocking effects, which were observed when P123 was used to block the pores. The Schüth[70] report hints at the possibilty that the amount of P123 retained in as-synthesized SBA-15 is insufficient to block the pore domain from functionalization in certain cases. This point is something we explore in our own research and will be discussed in greater detail in Chapter 2. While interesting, calcination limits the applicability of Schüth method of external functionalization because organo-silanes will decompose with such a heat treatment. That said, they utilized their method to generate a magnetically separable Pd hydrogenation catalyst.[71]

Diffusion Controlled Passivation: Selective Functionalization of Mesopores

As mentioned earlier, diffusion controlled and pore protection selective grafting strategies can be used with slight modifications to localize functional groups within the pore structure mesoporous silicas. Such selective grafting approaches will be termed from now on: diffusion controlled passivation and pore protection passivation (**Scheme 1-9**). Recall, to accomplish preferential mesopore functionalization both strategies employ a step designed to deactivate silanols localized on the external surface through reaction with a passivating agent.

Passivating agents are typically silylating agents such as diphenylsilyl dichloride (Ph_2SiCl_2), trimethylsilyl chloride (TMS-Cl) or hexamethyldisilazane (HMDS). The objective, ideally, is to cap reactive external silanols with TMS or Ph_2Si groups and to leave those silanols localized on the interior of the mesostructure unmodified and available for functionalization.

Diffusion controlled passivation can only be applied to materials with small pores (2 – 4 nm) as was effectively illustrated by Brühwiler.[64] The seminal work in this field was reported by Thomas.[72] Calcined MCM-41 was treated with a small amount of Ph_2SiCl_2 in THF, care was taken that the silylating agent would be a limiting reagent with respect to the estimated silanol content of the material. The concept was that the external silanols would be more accessible and thus more reactive toward the passivating agent than the silanols localized within the meso-structure of the material. The result would be Ph_2Si capping of externally localized silanols and a meso-structure that was largely unmodified. The material recovered, sPh_2Si-MCM-41, was subsequently functionalized using APTES and acidified to yield sPh_2Si-MCM-41-NH_3.

To evaluate the effectiveness of their strategy, sPh_2Si-MCM-41-NH_3 was treated a Ru-cluster that selectively binds to amines and serves as a contrast agent in HRTEM images (**Scheme 1-11**). This material was compared with MCM-41-NH_3, generated using established post-grafting procedures. The authors noted that sPh_2Si-MCM-41-NH_2 had lower contrast on the external surface as compared to MCM-41-NH_2, although this might be hard for the reader to see. Unfortunately, as with other selective grafting reports there was little discussion about how well the images chosen for publication represent the properties of the bulk material. Nonetheless, Thomas utilized this procedure in subsequent publications to assess whether the concave mesopore walls of MCM-41 could enhance the selectivity of supported hydrogenation[59, 61, 62, 73-75] and allylic amination[60, 62, 76] catalysts. For example, they grafted Rh diamine hydrogenation

catalysts onto MCM-41 and demonstrated that enhanced enantioselectivity and activity was achieved relative to homogeneous control reactions (**Scheme 1-12**). They ascribed these effects to benefits from carrying the reaction out exclusively within the mesopores of MCM-41, but remarkably did not provide a control where conventional grafting strategies were employed to generate a catalyst. Such a control is conspicuously absent from all their studies but would seem necessary to ascertain if there was any benefit to deactivating the external surface. Any conclusion that selective grafting can benefit catalysis is only as good as the controls that are performed; it is only through analysis with standard grafted materials that one can gauge whether the effects of externally immobilized functionality are null, positive or negative on the properties of a catalyst.

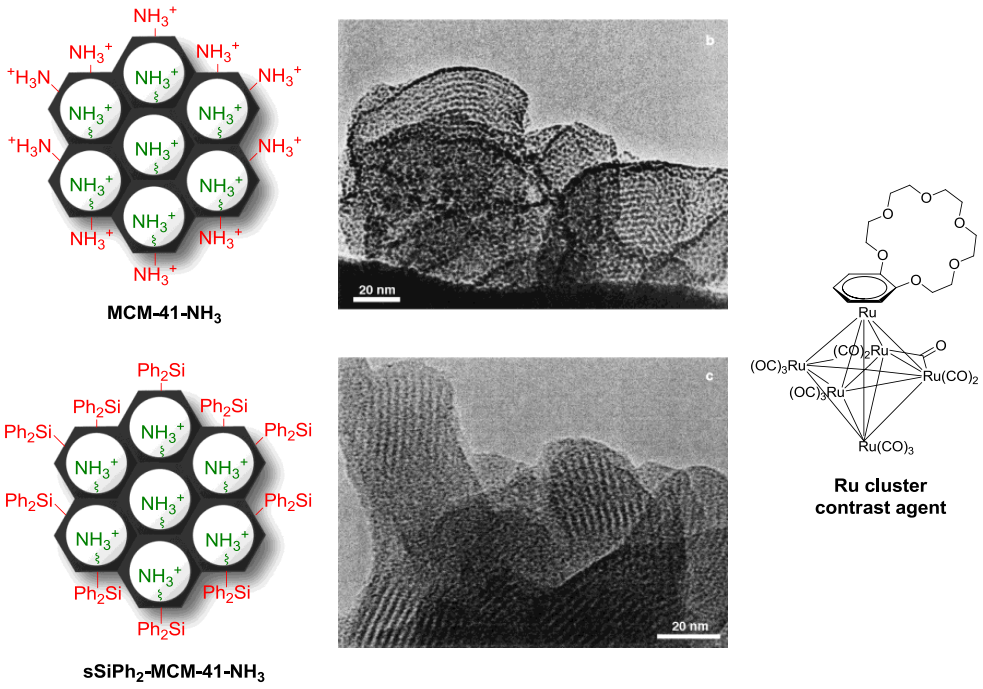

Scheme 1-11. The localization of functionality on MCM-41-NH_3 and sPh_2Si-MCM-41-NH_3 as postulated by Thomas based on results of an HRTEM analysis of materials stained with a Ru cluster contrast agent, HRTEM images were reproduced from reference 72 with permission

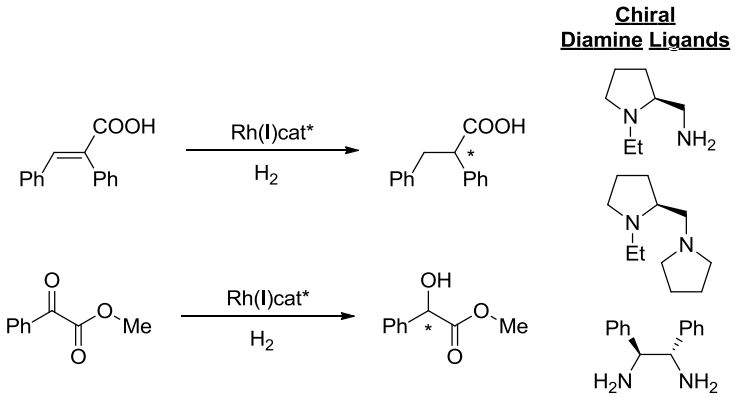

Scheme 1-12. Sample symmetric hydrogenations performed using Thomas-type selective grafted Rh-diamine catalyst functionalized MCM-41, from references 73-75. The heterogeneous catalysts were more active and selective than homogeneous counterparts

Pore Protection Passivation: Selective Functionalization of Mesopores

The limitation of diffusion controlled passivation as described earlier is that it can be only be effective on mesoporous silicas with small pore sizes (2 - 4 nm). Further, it is only as good as the mobility of the passivating agent employed.[64] If under the reaction conditions, the passivating agent readily passes through the mesopores, there will be limited preferential capping of the external surface. Pore protection passivation selective grafting addresses these issues by blocking the mesostructure with the SDA employed in the templation process used to synthesize the material (**Scheme 1-9**). The role of the surfactant is to limit the accessibility of the mesostructure of the material to the passivating agent. The passivating agent is typically added in large excess to the estimated total reactive silanol content of the material to ensure effective protection of the exterior of the material.

The first application of pore protection passivation selective grafting strategy, which unfortunately was not particularly successful, was reported by the Ruiz-Hitzky group.[77] As-

synthesized (as-MCM-41) was treated with TMSCl to passivate the external surface and the SDA was subsequently extracted to give sTMS-MCM-41. The isolated material was then post-grafted with phenylpropyldimethyl-chlorosilane ($PhPrMe_2SiCl$). The passivation step was evaluated by N_2 physisorption and elemental (EA) analysis, techniques which informed on textural properties of the material such as surface area (S_{BET}), pore volume and organic content. The group concluded that preferential passivation of the external surface was achieved by comparing the textural properties of sTMS-MCM-41 to standard MCM-41. Unfortunately, their analysis is questionable as they failed to consider that their passivation approach incorporated 1.2 mmol g^{-1} TMS into the material. This amount represents a high loading of TMS considering that the loading limit of mesoporous silica is ~ 3 mmol g^{-1}. Therefore, it is reasonable to conclude that significant reaction occurred within the mesopores considering they were only able to post-graft 0.15 mmol g^{-1} $PhPrMe_2SiCl$ onto their sTMS-MCM-41. If, as Ruiz-Hitzky *et al.* claim, the mesopores were unmodified by the passivation procedure it would be expected that at least 6 times that quantity of $PhPrMe_2SiCl$ would be post-grafted onto the material since the interior of the material represents ~ 90% of the surface area.[61] Therefore, the Ruiz-Hitzky conclusions are suspect, and again, the proper comparisons of sTMS-MCM-41 to fully TMSCl silylated MCM-41 were not made. Additionally, also observe that their conclusions are inconsistent with the observations of Jaroneic[78] who utilized a similar protocol to this passivation procedure to achieve high loadings of functionality on MCM-41 materials. In this report TMSCl was not only used to functionalize the material but also to simultaneously extract the SDA. The approach is likely ineffective because the HCl formed when TMSCl reacts with silanols facilitates removal of the SDA. As was noted earlier acid is often used in the solvent extraction of mesoporous silicas especially those synthesized using cationic ammonium surfactants.[32] We will discuss in Chapter 2

a more effective external passivation procedure for as-MCM-41 which employs the silylating agent hexamethylsilazane (HMDS) instead of TMSCl.

Pore protection passivation has also been employed to generate SBA-15 materials that are useful for the synthesis of Ag and Au nanoparticles/ nanowires. The passivating agents used were TMSCl[79-82] and HMDS.[65, 66] It was mentioned by the Asefa group[65, 66] that external passivation of SBA-15 was necessary to achieve good quality nanoparticle formation and that non-passivated materials resulted in large agglomerates which were localized on the external surface (**Figure 1-5**). Absent from these reports, however, is a detailed analysis of how the textural properties of the pore protected passivated sTMS-SBA-15 materials compared with materials generated using the established functionalization procedures. Such information is critical to assess the extent to which, if any, mesopore passivation occurred. This point is particularly important because significant mesopore passivation might be beneficial for this application. It could reduce the number of nucleation sites available for nanoparticle growth creating better dispersion and less agglomeration. If mesopore passivation does in fact occur, it might be more apt to think of these procedures as generating entirely passivated SBA-15, not just externally passivated SBA-15.

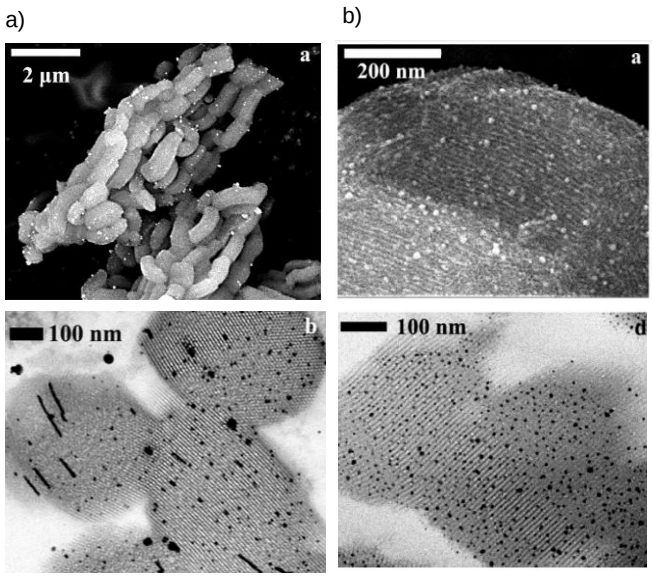

Figure 1-5. (top) SEM and (bottom) TEM images of Ag nanoparticles formed on; a) non-external passivated SBA-15 materials; b) TMSCl passivated SBA-15. Notice the comparatively larger and more irregularly shaped particles are present on the non-passivated materials, reproduced from reference 65 with permission

1.1.8 Selective Grafting Micropores and Mesopores of SBA-15

As was mentioned earlier, embedded in the mesopore walls of SBA-15 are micropores which contribute to surface roughness. The Yang group[83] developed an approach to differently functionalize the mesopores and micropores of SBA-15 based on this fact. Previous work by the same group[84] demonstrated that the SDA P123 can be extracted from the mesopores of SBA-15 without liberating the polymer occluded in the micropores by treating the as-synthesized material with concentrated H_2SO_4. The micropores were then liberated in a separate step by heating the material to 250 ºC. The Yang group[83] took full advantage of their extraction procedure by differently functionalizing these domains (**Scheme 1-13**). After the acid treatment, the silanols localized on the mesopores were treated with TMSCl, capping them. The micropores were then

exposed by a heat treatment as was evidenced by N_2 physisorption analysis and functionalized with a vinyl trichlorosilane (VTS). Textural characterization of these materials showed a decrease in microporosity after this step as these pores were filled with VTS. The VTS grafted material was then treated with Pd which preferentially localized in the micropore domain evidenced by physisorption and Solid State NMR analysis. The metal was reduced under a stream of H_2 at 300 ºC and the resulting nanoparticles were 2.0 ± 0.5 nm in size as measured by HRTEM. Their small size was used as evidence of being occluded in micropores.

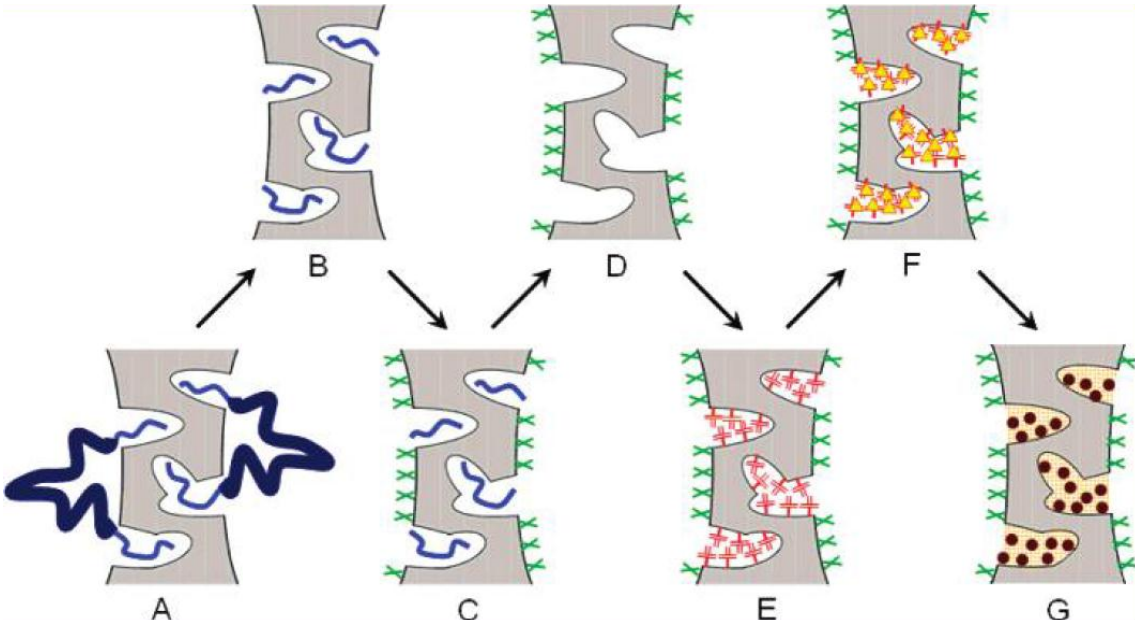

Scheme 1-13. Yang approach to selective mesopore and micropore functionalization; A) as-SBA-15; B) after H_2SO_4 treatment; C) after TMSCl post-grafting; D) after thermolysis at 250 ºC; E) after VTS post-grafting; F) after Pd complexation; G) after reduction and nanoparticle formation, reproduced from reference 83 with permission

1.1.9 Selective Grafting and Mesoporous Silicon

Recently, there have been two reports by the Gooding group[85, 86] on the generation of selectively functionalized mesoporous silicon materials. The goal was to generate materials designed to study bio-sensing/ drug delivery applications. Recall that there is great interest in these fields to have differently functionalized external and porous surfaces. On the exterior, the functionality will be designed to recognize a cell type and promote adhesion and the pores will be modified with a functionality designed to modulate drug uptake and release. The bio-hybrid material can be used to monitor drug-uptake and cell behavior. Their initial report[85] in this area utilized a solvatophobic strategy to selectively functionalize their material (**Scheme 1-14**); the approach is not entirely different from the previously discussed diffusion controlled method of selective grafting.

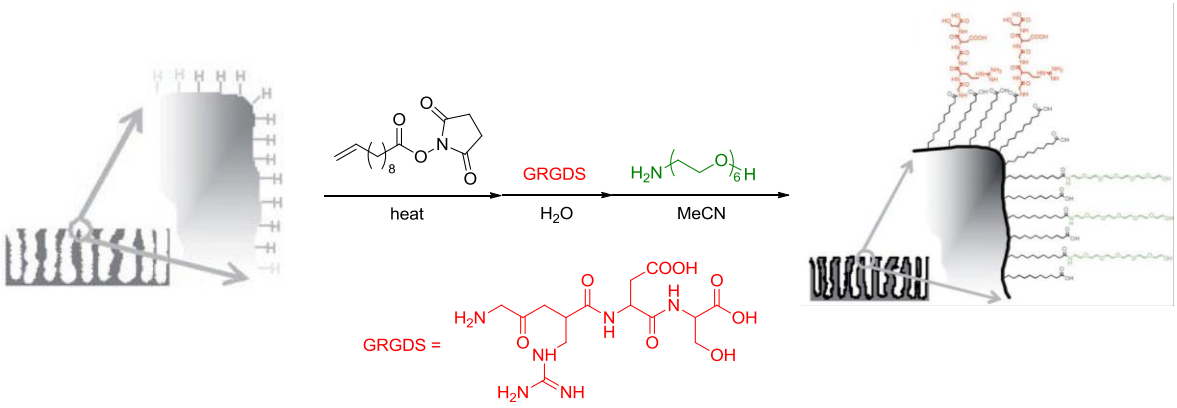

Scheme 1-14. Solvatophobic approach to selective grafted mesoporous silicon rugate filter, adapted from reference 85 with permission

Mesoporous silicon rugate filters (pore diameter 12 nm) were functionalized on the external and internal surfaces via hydrosilylation with 10-succinimidylundecenoate. The resulting material now had mesopores which were sufficiently hydrophobic that they would not wet on

exposure to water. This allowed for functionalization of the external surface selectively with the water soluble peptide (GRGDS). The mesopores were then functionalized by switching the solvent to acetonitrile and adding an amine to solution. Gooding characterized the mesopores spectroscopically and demonstrated that the peptide was bound to the external surface by quantifying cell adhesion relative to controls. Subsequently, the group noted[86] that even slight oxidation on the Si-H mesopore surface will lead to wetting on exposure to water allowing that domain to be functionalized with the peptide chain. For this reason, they pursued a more general selective grafting approach.

Gooding's new approach is to use Cu mediated azide-alkyne Huisgen click cyclization reactions to modify the external and internal surfaces of the rugate filters with different functional groups. The freshly prepared material is functionalized by a hydrosilylation reaction with a dialkyne. They found that ligand-less Cu mediated a click cyclization of an azide functionalized peptide selectively on the external surface. The resulting material was examined by FT-IR and X-ray photoelectron spectroscopy (XPS). Adding tetramethylethylenediamine (TMEDA) to click solutions then allowed for functionalization of the mesostructure. Gooding postulated that the ligand-less Cu does not modify the mesopores of these materials because it is either too prone to deactivation by disproportionation and/or because it is adsorbed on formed triazoles too readily. As with the previous solvatophobic selective grafting method, the click-based approach was also capable of adsorbing cells onto the external surface.

1.2 Summary

Ever since the first reports in the 1990`s mesoporous silicas have been shown to be useful for a number of applications. Key to the interest in these materials is the ease of their functionalization and there is greated attention being placed on developing and demonstrating approaches to localizing functional groups on the external and pore surfaces. The next chapter will discuss our forays into this field and will describe a selective grafting approach that localizes functionality within the mesopores of SBA-15 and MCM-41.

1.3 References

(1) Davis, M. E. *Nature* **2002**, *417*, 813-821.

(2) Soler-Illia, G.; Sanchez, C.; Lebeau, B.; Patarin, J. *Chem. Rev.* **2002**, *102*, 4093-4138.

(3) Cundy, C. S.; Cox, P. A. *Chem. Rev.* **2003**, *103*, 663-702.

(4) Farha, O. K.; Hupp, J. T. *Acc. Chem. Res.* **2010**, *43*, 1166-1175.

(5) Sing, K. S. W.; Everett, D. H.; Haul, R. A. W.; Moscou, L.; Pierotti, R. A.; Rouquerol, J.; Siemieniewska, T. *Pure Appl. Chem.* **1985**, *57*, 603-19.

(6) Hoffmann, F.; Cornelius, M.; Morell, J.; Fröba, M. *Angew. Chem. Int. Ed.* **2006**, *45*, 3216-3251.

(7) Wan, Y.; Zhao, D. *Chem. Rev.* **2007**, *107*, 2821-2860.

(8) Stein, A.; Melde, B. J.; Schroden, R. C. *Adv. Mater.* **2000**, *12*, 1403-1419.

(9) Brühwiler, D. *Nanoscale* **2010**, *2*, 887-892.

(10) Slowing, I. I.; Vivero-Escoto, J. L.; Trewyn, B. G.; Lin, V. S. Y. *J. Mater. Chem.* **2010**, *20*, 7924-7937.

(11) Corma, A. *Chem. Rev.* **1997**, *97*, 2373-2420.

(12) De Vos, D. E.; Dams, M.; Sels, B. F.; Jacobs, P. A. *Chem. Rev.* **2002**, *102*, 3615-3640.

(13) Kumar, P.; Guliants, V. V. *Microporous Mesoporous Mater.* **2010**, *132*, 1-14.

(14) Yanagisawa, T.; Shimizu, T.; Kuroda, K.; Kato, C. *Bull. Chem. Soc. Jpn.* **1990**, *63*, 988-92.

(15) Yanagisawa, T.; Shimizu, T.; Kuroda, K.; Kato, C. *Bull. Chem. Soc. Jpn.* **1990**, *63*, 1535-7.

(16) Inagaki, S.; Fukushima, Y.; Kuroda, K. *J. Chem. Soc. Chem. Commun.* **1993**, 680-2.

(17) Kimura, T.; Kuroda, K. *Adv. Funct. Mater.* **2009**, *19*, 511-527.

(18) Inagaki, S.; Fukushima, Y.; Kuroda, K. *Stud. Surf. Sci. Catal.* **1994**, *84*, 125-32.

(19) Kresge, C. T.; Leonowicz, M. E.; Roth, W. J.; Vartuli, J. C.; Beck, J. S. *Nature* **1992**, *359*, 710-712.

(20) Beck, J. S.; Vartuli, J. C.; Roth, W. J.; Leonowicz, M. E.; Kresge, C. T.; Schmitt, K. D.; Chu, C. T. W.; Olson, D. H.; Sheppard, E. W. *J. Am. Chem. Soc.* **1992**, *114*, 10834-10843.

(21) Di Renzo, F.; Cambon, H.; Dutartre, R. *Microporous Mater.* **1997**, *10*, 283-286.

(22) Chiola, V.; Ritsko, J. E.; Vanderpool, C. D. US Patent 3556725, 1971.

(23) Zhao, D.; Huo, Q.; Feng, J.; Chmelka, B. F.; Stucky, G. D. *J. Am. Chem. Soc.* **1998**, *120*, 6024-6036.

(24) Zhao, D.; Feng, J.; Huo, Q.; Melosh, N.; Fredrickson, G. H.; Chmelka, B. F.; Stucky, G. D. *Science* **1998**, *279*, 548-552.

(25) Huo, Q.; Margolese, D. I.; Ciesla, U.; Feng, P.; Gier, T. E.; Sieger, P.; Leon, R.; Petroff, P. M.; Schuth, F.; Stucky, G. D. *Nature* **1994**, *368*, 317-321.

(26) Lindén, M.; Schunk, S. A.; Schüth, F. *Angew. Chem. Int. Ed.* **1998**, *37*, 821-823.

(27) Flodström, K.; Teixeira, C. V.; Amenitsch, H.; Alfredsson, V.; Lindén, M. *Langmuir* **2004**, *20*, 4885-4891.

(28) Monnier, A.; Schüth, F.; Huo, Q.; Kumar, D.; Margolese, D.; Maxwell, R. S.; Stucky, G. D.; Krishnamurty, M.; Petroff, P.; Firouzi, A.; Janicke, M.; Chmelka, B. F. *Science* **1993**, *261*, 1299-1303.

(29) Huo, Q.; Margolese, D. I.; Stucky, G. D. *Chem. Mater.* **1996**, *8*, 1147-1160.

(30) Kruk, M.; Jaroniec, M.; Ko, C. H.; Ryoo, R. *Chem. Mater.* **2000**, *12*, 1961-1968.

(31) Zhang, F.; Yang, H.; Yan, M. Y.; Yu, C.; Tu, B.; Zhao, D. *J. Phys. Chem. B* **2005**, *109*, 8723-8732.

(32) Lang, N.; Tuel, A. *Chem. Mater.* **2004**, *16*, 1961-1966.

(33) Van, G., Rafael; Calleja, G.; Stucky, G. D.; Melero, J. A.; Garcia, R. A.; Iglesias, J. *Langmuir* **2003**, *19*, 3966-3973.

(34) Lu, A.; Li, W.; Schmidt, W.; Schueth, F. *J. Mater. Chem.* **2006**, *16*, 3396-3401.

(35) Yang, L. M.; Wang, Y. J.; Luo, G. S.; Dai, Y. Y. *Microporous Mesoporous Mater.* **2005**, *81*, 107-114.

(36) Tian, B.; Liu, X.; Yu, C.; Gao, F.; Luo, Q.; Xie, S.; Tu, B.; Zhao, D. *Chem. Commun.* **2002**, 1186-1187.

(37) Xiao, L.; Li, J.; Jin, H.; Xu, R. *Microporous Mesoporous Mater.* **2006**, *96*, 413-418.

(38) Feuston, B. P.; Higgins, J. B. *J. Phys. Chem.* **1994**, *98*, 4459-4462.

(39) Prouzet, E.; Boissière, C.; Kim, S. S.; Pinnavaia, T. J. *Microporous Mesoporous Mater.* **2009**, *119*, 9-17.

(40) Gommes, C. J.; Friedrich, H.; Wolters, M.; de Jongh, P. E.; de Jong, K. P. *Chem. Mater.* **2009**, *21*, 1311-1317.

(41) Joo, S. H.; Ryoo, R.; Kruk, M.; Jaroniec, M. *J. Phys. Chem. B* **2002**, *106*, 4640-4646.

(42) Ryoo, R.; Joo, S. H.; Jun, S. *J. Phys. Chem. B* **1999**, *103*, 7743-7746.

(43) Impéror-Clerc, M.; Davidson, P.; Davidson, A. *J. Am. Chem. Soc.* **2000**, *122*, 11925-11933.

(44) Hoang, V.; Huang, Q.; Eić, M.; Do, T.; Kaliaguine, S. *Langmuir* **2005**, *21*, 2051-2057.

(45) Ryoo, R.; Ko, C. H.; Kruk, M.; Antochshuk, V.; Jaroniec, M. *J. Phys. Chem. B* **2000**, *104*, 11465-11471.

(46) Shenderovich, I. G.; Buntkowsky, G.; Schreiber, A.; Gedat, E.; Sharif, S.; Albrecht, J.; Golubev, N. S.; Findenegg, G. H.; Limbach, H. *J. Phys. Chem. C* **2003**, *107*, 11924-11939.

(47) Zhao, X. S.; Lu, G. Q.; Whittaker, A. K.; Millar, G. J.; Zhu, H. Y. *J. Phys. Chem. B* **1997**, *101*, 6525-6531.

(48) Deschner, T.; Liang, Y.; Anwander, R. *J. Phys. Chem. C* **2010**, *114*, 22603-22609.

(49) Nakazawa, J.; Stack, T.,Daniel P. *J. Am. Chem. Soc.* **2008**, *130*, 14360-14361.

(50) Blümel, J. *J. Am. Chem. Soc.* **1995**, *117*, 2112-2113.

(51) Brunel, D.; Cauvel, A.; Di Renzo, F.; Fajula, F.; Fubini, B.; Onida, B.; Garrone, E. *New J. Chem.* **2000**, *24*, 807-813.

(52) Lim, M. H.; Stein, A. *Chem. Mater.* **1999**, *11*, 3285-3295.

(53) Sharma, K. K.; Anan, A.; Buckley, R. P.; Ouellette, W.; Asefa, T. *J. Am. Chem. Soc.* **2008**, *130*, 218-228.

(54) Sharma, K.; Asefa, T. *Angew. Chem. Int. Ed.* **2007**, *46*, 2879-2882.

(55) Zhang, F.; Sautter, K.; Larsen, A. M.; Findley, D. A.; Davis, R. C.; Samha, H.; Linford, M. R. *Langmuir* **2010**, *26*, 14648-14654.

(56) Ek, S.; Iiskola, E. I.; Niinistö, L. *Langmuir* **2003**, *19*, 3461-3471.

(57) Cauda, V.; Schlossbauer, A.; Kecht, J.; ZuÌˆrner, A.; Bein, T. *J. Am. Chem. Soc.* **2009**, *131*, 11361-11370.

(58) Kecht, J.; Schlossbauer, A.; Bein, T. *Chem. Mater.* **2008**, *20*, 7207-7214.

(59) Thomas, J. M.; Johnson, B. F. G.; Raja, R.; Sankar, G.; Midgley, P. A. *Acc. Chem. Res.* **2003**, *36*, 20-30.

(60) Thomas, J. M. *Angew. Chem. Int. Ed.* **1999**, *38*, 3588-3628.

(61) Thomas, J. M.; Maschmeyer, T.; Johnson, B. F. G.; Shephard, D. S. *J. Mol. Catal. A.* **1999**, *141*, 139-144.

(62) Thomas, J. M.; Raja, R. *Acc. Chem. Res.* **2008**, *41*, 708-720.

(63) Dufaud, V.; Davis, M. E. *J. Am. Chem. Soc.* **2003**, *125*, 9403-9413.

(64) Gartmann, N.; Brühwiler, D. *Angew. Chem. Int. Ed.* **2009**, *48*, 6354-6356.

(65) Asefa, T.; Lennox, R. B. *Chem. Mater.* **2005**, *17*, 2481-2483.

(66) Xie, Y.; Quinlivan, S.; Asefa, T. *J. Phys. Chem. C* **2008**, *112*, 9996-10003.

(67) Bass, J. D.; Katz, A. *Chem. Mater.* **2006**, *18*, 1611-1620.

(68) Lunn, J. D.; Shantz, D. F. *Chem. Commun.* **2010**, *46*, 2926-2928.

(69) Huang, Y.; Xu, S.; Lin, V. S. Y. *Angew. Chem. Int. Ed.* **2011**, *50*, 661-664.

(70) Lu, A.; Li, W.; Kiefer, A.; Schmidt, W.; Bill, E.; Fink, G.; Schüth, F. *J. Am. Chem. Soc.* **2004**, *126*, 8616-8617.

(71) Lu, A.; Schmidt, W.; Matoussevitch, N.; Bönnemann, H.; Spliethoff, B.; Tesche, B.; Bill, E.; Kiefer, W.; Schüth, F. *Angew. Chem. Int. Ed.* **2004**, *43*, 4303-4306.

(72) Shephard, D. S.; Zhou, W.; Maschmeyer, T.; Matters, J. M.; Roper, C. L.; Parsons, S.; Johnson, B. F. G.; Duer, M. J. *Angew. Chem. Int. Ed.* **1998**, *37*, 2719-2723.

(73) Raja, R.; Thomas, J. M.; Jones, M. D.; Johnson, B. F. G.; Vaughan, D. E. W. *J. Am. Chem. Soc.* **2003**, *125*, 14982-14983.

(74) Jones, M. D.; Raja, R.; Thomas, J. M.; Johnson, B. F. G.; Lewis, D. W.; Rouzaud, J.; Harris, K. D. M. *Angew. Chem. Int. Ed.* **2003**, *42*, 4326-4331.

(75) Raynor, S. A.; Thomas, J. M.; Raja, R.; Johnson, B. F. G.; Bell, R. G.; Mantle, M. D. *Chem. Commun.* **2000**, 1925-1926.

(76) Johnson, B. F. G.; Raynor, S. A.; Shephard, D. S.; Mashmeyer, T.; Meurig, T. J.; Sankar, G.; Bromley, S.; Oldroyd, R.; Gladden, L.; Mantle, M. D. *Chem. Commun.* **1999**, 1167-1168.

(77) de Juan, F.; Ruiz-Hitzky, E. *Adv. Mater.* **2000**, *12*, 430-432.

(78) Antochshuk, V.; Jaroniec, M. *Chem. Commun.* **1999**, 2373-2374.

(79) Zhang, Z.; Dai, S.; Blom, D. A.; Shen, J. *Chem. Mater.* **2002**, *14*, 965-968.

(80) Sun, J.; Ma, D.; Zhang, H.; Liu, X.; Han, X.; Bao, X.; Weinberg, G.; Pfänder, N.; Su, D. *J. Am. Chem. Soc.* **2006**, *128*, 15756-15764.

(81) Lin, D.; Jiang, Y.; Wang, Y.; Sun, S. *J. Nanomater.* **2008**, 473791.

(82) Huang, X.; Yang, M.; Wang, G.; Zhang, X. *Microporous Mesoporous Mater.* **2011**, *144*, 171-175.

(83) Yang, C.; Lin, H.; Zibrowius, B.; Spliethoff, B.; Schüth, F.; Liou, S.; Chu, M.; Chen, C. *Chem. Mater* **2007**, *19*, 3205-3211.

(84) Yang, C.; Zibrowius, B.; Schmidt, W.; Schüth, F. *Chem. Mater*. **2004**, *16*, 2918-2925.

(85) Kilian, K.; Böcking, T.; Gaus, K.; Gooding, J. J. *Angew. Chem. Int. Ed.* **2008**, *47*, 2697-2699.

(86) Guan, B.; Ciampi, S.; Le Saux, G.; Gaus, K.; Reece, P. J.; Gooding, J. J. *Langmuir* **2011**, *27*, 328-334.

Chapter 2

Selective Grafting and Mesoporous Templated Silicas

2.1 Research Objectives

As was discussed in Chapter 1, mesoporous silicas are often functionalized by post-synthetic grafting (post-grafting) of organic groups.[1, 2] Materials processed in this way have functionality on exterior and pore surfaces. This distribution of functional groups has been cited as undesirable for a number of applications including catalysis, templates for nanoparticle synthesis and as drug delivery agents.[3-7] We were interested in developing a selective grafting protocol to localize functionality preferentially within the pores of mesoporous silicas, specifically SBA-15 and MCM-41. Two approaches to this type of selective grafting have been described in the literature; these strategies are termed diffusion controlled passivation[6] and pore protection passivation.[3-5, 8-11] Both methods focus on deactivating silanols on the external surface by reacting them with passivating agents, typically silylating agents such as trimethylsilyl chloride (TMSCl) or hexamethyldisilazane (HMDS).

This study will focus on developing the pore protection passivation method of selective grafting, which was described in detail in Chapter 1. Recall that pore protection passivation utilizes the structure directing agent (SDA), which is P123 for SBA-15 and CTAB for MCM-41, contained within the pores of the as-synthesized materials as a barrier to protect the silanols localized on that domain from being silylated. [3-5, 7-11] The ideal end result after extraction of the SDA is a passivated external surface and an internal mesopore surface populated with silanols that are available for functionalization. Conspicuously absent in the literature that addresses pore protection passivation is a discussion comparing the textural properties of selective grafted

materials to materials synthesized using conventional methods. There is also a lack of rigorous tests designed to probe the overall effectiveness of the various strategies described in the literature.[6, 7] The goal of this work is to address both concerns.

The first phase of this research project evaluated pore protection passivation protocols reported in the literature[3-5, 7-11] and compared these materials to those synthesized conventionally.[1,2] From this data we developed a method to better protect the internal mesostructure of SBA-15 from unwanted silylation. This approach was also extended to MCM-41. The last section of this chapter describes our forays into the development of new selective grafting tests and we report a new method to evaluate the passivation layer formed on the external surface of SBA-15 and MCM-41.

2.2 Results & Discussion

2.2.1 Literature Methods for the Pore Protection Passivation with as-SBA-15

Our initial work focused on an assessment of literature methods for the pore protection passivation of SBA-15 as described in Chapter 1.[3-5, 7-11] There were two procedures of interest and both involve treatment of as-synthesized SBA-15 (as-SBA-15 where the prefix as- stands for as-synthesized) with a large excess of a strong silylating agent such as hexamethyldisilazane (HMDS)[3, 4] or trimethylsilyl chloride (TMSCl).[5, 9-11] These reports assumed that their procedures selectively passivated the external surface of SBA-15 and this assumption was based on the idea that P123 completely protects the interior surface of the as-SBA-15 materials (**Scheme 2-1**). We will show that this is not the case. When HMDS was employed as the passivating agent, treatment was carried out in toluene at room temperature overnight,[3, 4] while the TMSCl treatment was carried out at 80 °C for 8 h.[5] To provide insight into the extent of silylation, the textural properties of the resulting "selective grafted" materials termed sHMDS-SBA-15 and sTMSCl-SBA-15

(where the prefix s denotes selective grafted) were compared to those of unfunctionalized SBA-15 and a fully silylated SBA-15 material, TMS-SBA-15 (**Figure 2-1** and **Table 2-1**). It should be noted that the original reports of these procedures omitted any discussion of such comparisons, which would have provided critical information regarding how successful their approaches were at preventing pore silylation. As can be seen in **Figure 2-1** and **Table 2-1** sHMDS-SBA-15 and sTMSCl-SBA-15 have surface areas, pore volumes and pore sizes that are intermediate between SBA-15 and TMS-SBA-15. The parameter C_{BET} (BET parameter) is a qualitative indicator of the hydrophobicity of a surface within a series of closely related materials.[12] Thus, a decrease in C_{BET} represents an increase in hydrophobicity, for example TMS-SBA-15 has a C_{BET} of 45 compared to 110 for SBA-15. The C_{BET} for sTMSCl-SBA-15 and sHMDS-SBA-15 were significantly lower than the C_{BET} of unfunctionalized SBA-15 suggesting that these materials are significantly hydrophobic and this observation is mirrored by increase in carbon content as measured by elemental analysis. Note that it is assumed based on nitrogen physisorption analysis that the external surface of these materials is a minor contributor to the overall surface area, 5 – 10 %;[13] therefore, it would be expected that selective external surface passivation would result in a minor change in the bulk carbon content and hydrophobicity of the material. On a whole the textural properties of sTMSCl-SBA-15 and sHMDS-SBA-15 suggest that these materials are significantly silylated, and that passivation occurred not only on the external surface, as desired, but also within the mesostructure.

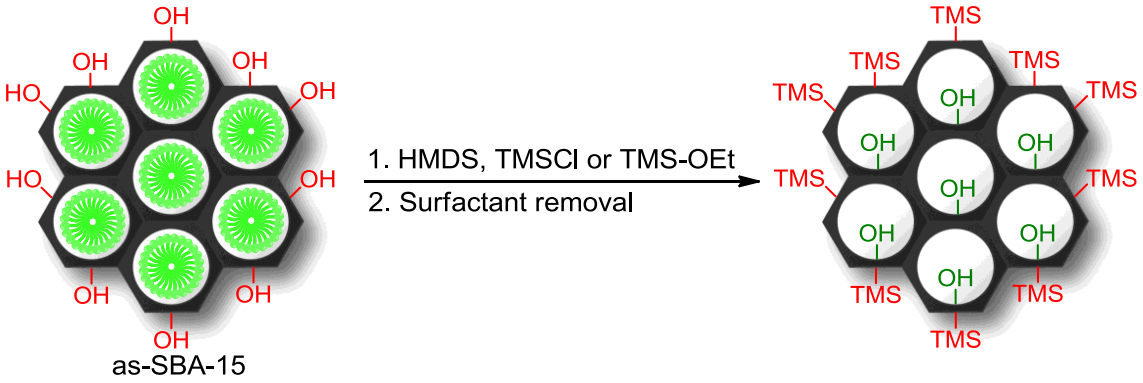

Scheme 2-1. Pore protection passivation of SBA-15 assuming as-SBA-15 behaves as a closed pore material[3-5, 7-11]

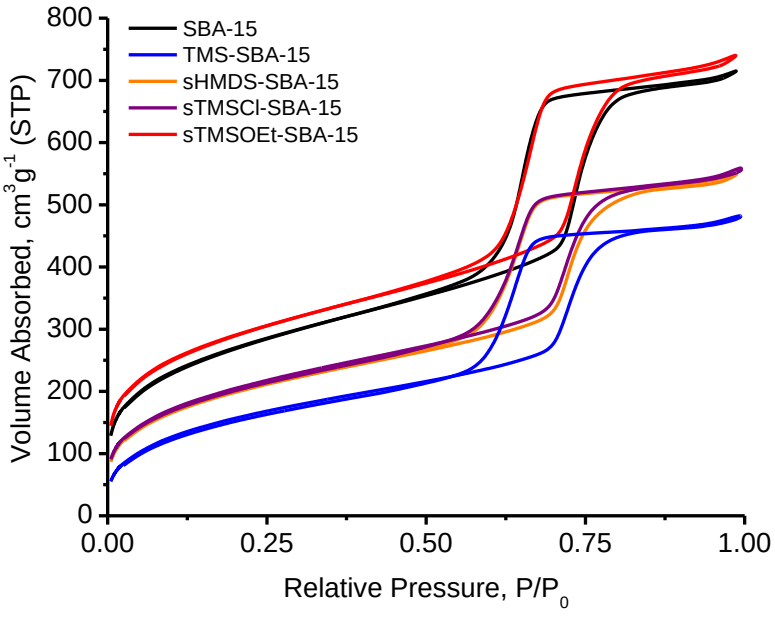

Figure 2-1. Nitrogen physisorption overlay for the selective grafting survey of SBA-15 using literature methods

Table 2-1. Summary of textural properties for the selective grafting survey of SBA-15 using literature methods[a]

Material	S_{BET},[b] m^2 g^{-1}	C_{BET}[c]	D_{BJH},[d] nm	V_p,[d] cm^3 g^{-1}	C, wt%
SBA-15	977	110	7.9	1.06	2.9
TMS-SBA-15	595	45	7.4	0.69	11.3
sHMDS-SBA-15	734	75	7.4	0.79	9.4
sTMSCl-SBA-15	754	73	7.4	0.80	8.9
sTMSOEt-SBA-15	1040	150	7.6	1.09	3.3

[a] Reaction conditions: See Experimental for details; [b] BET surface area; [c] BET parameter; [d] Pore diameter (D_{BJH}) and pore volume (V_p) calculated using BJH adsorption branch for pores 1.0 – 300 nm in diameter

What is clear from the data in **Figure 2-1** and **Table 2-1** is that previously reported procedures for pore protection passivation result in significant silylation of SBA-15. It can be inferred that the quantity of P123 retained within the pores of the as-SBA-15 material is not particularly effective at protecting silanols within the mesoporous structure from these passivating agents. This effect has been previously observed by Schüth in 2004,[14] who reported selectively grafting cobalt nanoparticles onto the external surface of SBA-15. In that publication, it was found that as- SBA-15 allowed for the intrusion of Co particles into the mesoporous structure, and to prevent this unwanted effect they protected the pores with poly-methylmethacrylate instead of the structural directing agent P123. Another concern was that toluene might have had the capacity to extract P123. To address this possibility, a pore protection passivation control was carried out in neat HMDS. The recovered material had similar textural properties to sHMDS-SBA-15. From this point forward, to obviate the concerns about toluene as a solvent, all attempts at pore protection passivation with SBA-15 were carried out using neat

silylating agent. Additionally, as discussed in the Chapter 1, TMSCl generates HCl as it reacts with silanols, and since acid is known to facilitate P123 extraction TMSCl was abandoned as a passivating agent.

TMSOEt was also examined as a passivation agent (**Figure 2-1** and **Table 2-1**). It was found, in contrast to HMDS and TMSCl, that the resulting material had textural properties and carbon content similar to unmodified SBA-15. ^{13}C CP-MAS NMR spectroscopy was used to confirm the incorporation of TMS groups on the surface of the material (**Figure A-1 in Appendix A**). These resulte were encouraging because thet suggested that the mesostructure was unmodified but TMSOEt is a weak silylating agent and as will be shown later in the discussion the extent of passivation on the external surface is lower than that achieved with HMDS.

2.2.2 Reloading SBA-15 with P123

In our view, employing weaker silylating agents such as TMSOEt was not a satisfactory solution to the problems with the pore protection passivation approach to selective grafting, since incomplete silylation of the external surface will inevitably lead to functionality incorporating onto that domain during post-grafting. The challenge instead was to enhance P123's ability to protect silanols contained within the mesostructure. Physisorption analysis of various batches of as-SBA-15 (**Figure 2-2** and **Table 2-2**) revealed that the material consistently had a small but significant surface area (S_{BET} = 140 m^2 g^{-1}) and pore volume (V_P = 0.25 cm^3 g^{-1}). The inherent porosity of as-SBA-15 was thought to be one of reasons why the literature pore protection passivation procedures performed poorly. We contend that as-SBA-15 should not be thought of as a closed pore material, as others have assumed (Scheme 2-1).[3-5, 9] Instead as-SBA-15 should be considered a porous material (**Scheme 2-2**) and it was thought that incorporating additional P123

within the mesopores of as-SBA-15 might help enhance its ability to protect silanols from unwanted silylation.

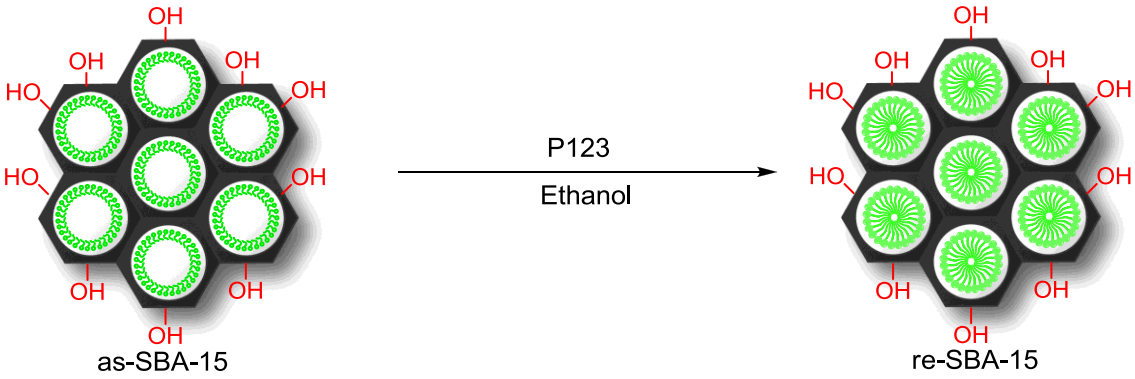

Scheme 2-2. Reloading P123 into as-SBA-15

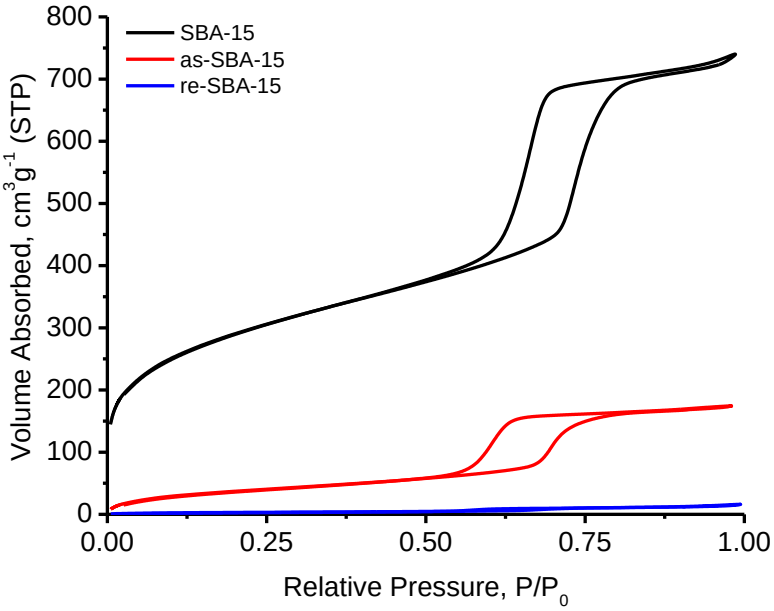

Figure 2-2. Nitrogen physisorption overlay for as-SBA-15 and re-SBA-15

Table 2-2. Summary of textural properties for as-SBA-15 and re-SBA-15[a]

Material	S_{BET},[b] m^2 g^{-1}	C_{BET}[c]	D_{BJH},[d] nm	V_p,[d] cm^3 g^{-1}	C, wt%
as-SBA-15	156	30	7.1	0.32	25.0
re-SBA-15	30	29	6.6	0.07	31.5

[a] Reaction conditions: See Experimental for details; [b] BET surface area; [c] BET parameter; [d] Pore diameter (D_{BJH}) and pore volume (V_p) calculated using BJH adsorption branch for pores 1.0 – 300 nm in diameter

The method we have developed results in the incorporation of additional P123 within the mesostructure and we term it *reloading* (**Scheme 2-2**). While the motivation behind reloading is similar to that of Schüth[14] who used polymethylmethacrylate to block the mesopores of SBA-15; our method will allow for the pores to be liberated by Soxhlet extraction rather than calcination, which would destroy the external passivation layer. The reloaded material, re-SBA-15 (where the prefix re- stands for reloaded), was prepared from as-synthesized SBA-15 (as-SBA-15) by suspending the material in a concentrated solution of P123 in ethanol (30 wt% P123 in EtOH). The suspension was stirred for one day and then filtered rapidly without washing either the material or the flask. The recovered material increased in mass by about 10 % and the carbon content increased by 6.5 % (**Table 2-2**).

While it is likely that there is some P123 adsorbed on to the exterior of the silica, controls and characterization of the material indicate that re-SBA-15 is not simply as-SBA-15 suspended in bulk P123. Note that no P123 is retained on the frit after filtering a concentrated solution of P123 in ethanol, demonstrating that P123 is soluble under the reloading conditions (30 wt% P123 in EtOH) rather than just suspended in solution. Furthermore, while the carbon content of re-SBA-15 (C = 31.5 wt%) is slightly higher than that of as-SBA-15 (C = 25 wt%), it is still substantially lower than what is expected for bulk P123 (C = 60 wt%). Based on rough

calculations, these elemental results suggest that re-SBA-15 is composed of ~ 50 wt% silica and ~ 50 wt% P123, which is compared to as-SBA-15 which is composed of ~ 60 wt% silica and ~ 40 wt% P123. Perhaps most significantly, physisorption analysis of re-SBA-15 (**Figure 2-2** and **Table 2-2**) showed that the surface area and pore volume of these materials were lower than those of as-SBA-15. Reloading of as-SBA-15 has been performed in this fashion multiple times (> 10) and the surface area drop depicted above is consistently observed with an error no-greater than 10 %. It can be inferred then that P123 was indeed incorporated within the pores of SBA-15 or is effectively blocking them because the magnitude of the surface area and pore volume decrease was much larger than the increase in mass of the material (a 10% increase in mass is observed along with an 80% drop in surface area **Table 2-2**).

2.2.3 Pore Protection Passivation with re-SBA-15

The next objective was to develop a procedure to selectively passivate the external surface (**Scheme 2-3**). The optimum conditions for the formation of a passivation layer were found to be 3 h in neat HMDS followed by a 2 day Soxhlet extraction with ethanol and heat treatment to 250 °C for 6 hrs. Increased passivation times (8 – 24 h) lead to materials that displayed textural properties consistent with significant pore silylation and use of alternate extraction conditions, such as an acetone Soxhlet, resulted in materials with larger amounts of residual surfactant.

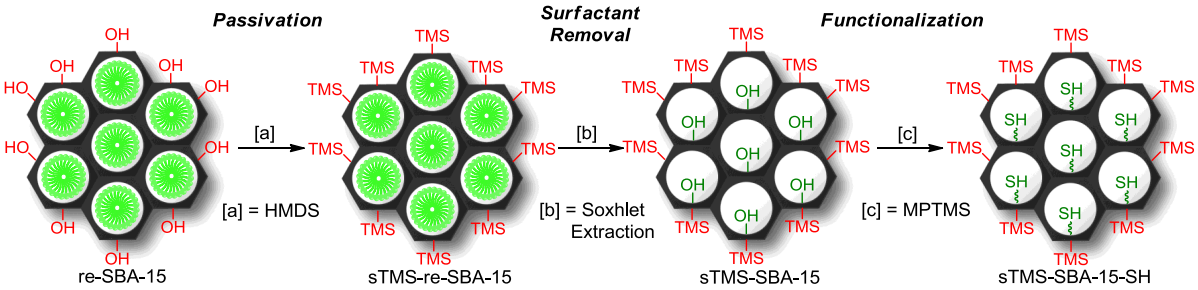

Scheme 2-3. General pore protection passivation selective grafting protocol using re-SBA-15

The textural properties of sTMS-re-SBA-15, which is pore protected and externally passivated SBA-15, prepared from re-SBA-15 were encouraging (**Figure 2-3** and **Table 2-3**). The material recovered immediately after treatment with HMDS before extraction of the SDA, sTMS-re-SBA-15, had a slightly increased surface area and pore volume compared with re-SBA-15, which was ascribed to extraction of a small amount of P123 and/or washing of physisorbed SDA from the external surface of the silica. The material recovered after extraction, sTMS-SBA-15, had a surface area of (963 m^2/g) which was 10 % lower than untreated SBA-15 (1064 m^2/g) and elemental analysis indicated that carbon content differed by 1.6 wt%. Both metrics indicate a significant improvement over previously reported methods (**Table 2-1**).[3-5, 8-11] Recall that the earlier procedures, which employed as-SBA-15 instead of re-SBA-15, resulted in large decreases in surface area, pore volume and a substantial increases in carbon content. It is reasonable to conclude then that the P123 retained in re-SBA-15 is better able to protect silanols from silylation.

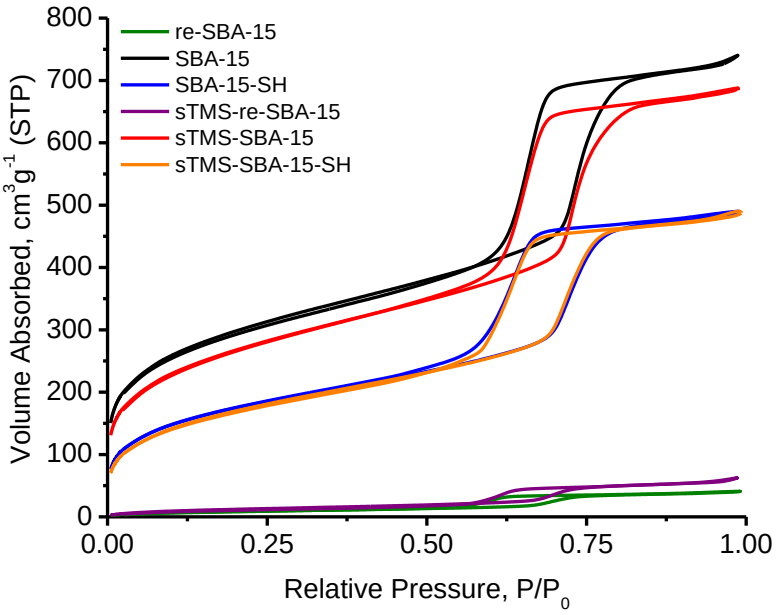

Figure 2-3. Nitrogen physisorption overlay for selective grafting with re-SBA-15

Table 2-3. Summary of textural properties for selective grafting with re-SBA-15[a]

Material	S_{BET},[b] m^2 g^{-1}	C_{BET}[c]	D_{BJH},[d] nm	V_p,[d] cm^3 g^{-1}	wt%	
					C	S
re-SBA-15	33	34	6.1	0.06	34.5[e]	-
sTMS-re-SBA-15	48	27	5.6	0.10	25.4	-
SBA-15	1064	185	7.5	1.08	3.0	-
sTMS-SBA-15	963	128	7.5	1.01	4.6	-
SBA-15-SH	636	90	7.1	0.77	8.8	3.9
sTMS-SBA-15-SH	627	68	7.1	0.77	9.9	3.9

[a] Reaction conditions: See Experimental for details; [b] BET surface area; [c] BET parameter; [d] Pore diameter (D_{BJH}) and pore volume (V_p) calculated using BJH adsorption branch for pores 1.0 – 300 nm in diameter; [e] as-SBA-15 for this batch of material has C = 28.7 wt%

As mentioned in the introduction, an important milestone in any selective grafting procedure is comparing the extent of functionalization of the passivated material with materials

generated using conventional post-grafting methods. sTMS-SBA-15 was functionalized with 3-mercaptopropyl(trimethoxysilane) (MPTMS) using a standard post-grafting protocol. The resulting material, sTMS-SBA-15-SH had remarkably similar textural properties (SBA-15-SH = 636 m^2 g^{-1} vs sTMS-SBA-15-SH = 627 m^2 g^{-1}) and sulfur content (SBA-15-SH and sTMS-SBA-15-SH = 1.2 mmol S/g) to SBA-15-SH which was made from SBA-15. The choice of MPTMS was made because the sulfur tag is easily quantified by elemental analysis, but in principle any trialkoxysilane could be grafted onto the surface of sTMS-SBA-15.

The pore protection passivation procedure was followed at each step by solid state NMR. The ^{13}C CP-MAS NMR spectra of re-SBA-15 (**Figure 2-4**) showed peaks attributable to the surfactant P123 and is largely identical to as-SBA-15. After treatment with HMDS a peak at 0 ppm and -13 ppm appeared in the ^{13}C (**Figure 2-4**) and ^{29}Si CP-MAS NMR spectra (**Figure A-2** in **Appendix A**), respectively. These peaks indicate that TMS was grafted onto the material. These spectra also demonstrate that the TMS functionality was retained after extraction. It is noteworthy that some ethanol, from the extraction protocol, was incorporated into/onto the silica surface. At a bare minimum, the ethanol detected in these spectra is not weakly adsorbed because after Soxhlet extraction the material was heated to 250 °C and dried under vacuum at 80 °C and the ethanol signals remained.

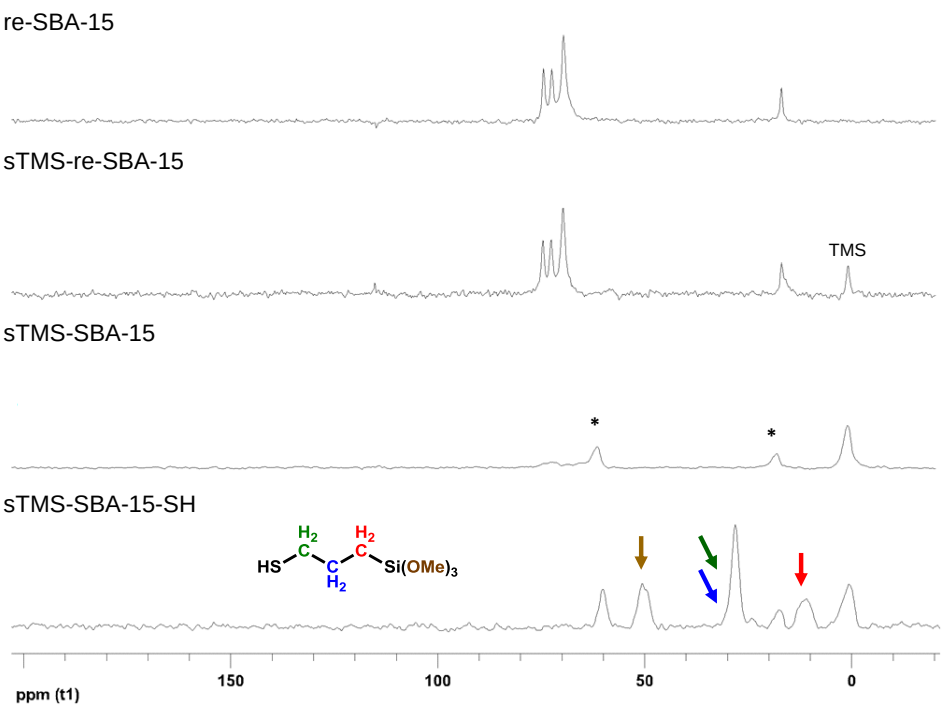

Figure 2-4. ^{13}C CP-MAS NMR overlay for selective grafted SBA-15 post-grafted with MPTMS, the asterisks denote ethanol incorporated during Soxhlet extraction

It has been proposed that ethanol becomes incorporated into these materials by nucleophilic attack at strained surface siloxane groups. This process was studied by Blümel[15] and is conceptually similar to epoxide ring opening, even though the mechanistic details are somewhat different. Ethanol incorporation generates new silanols (**Scheme 2-4**) and may serve to degrade the passivation layer on the external surface by providing new attachment points for grafting to take place. Note that strained surface siloxanes such as those depicted in **Scheme 2-4** are present, albeit likely at a low concentration, on silica surfaces dried at 25 ºC.[15] Another way the passivation layer can be degraded is by removal of TMS through nucleophilic attack by ethanol; based on the results of the solid-state NMR study this process, if operative, is relatively

slow under the Soxhlet conditions. The new peaks in the ^{13}C CP-MAS spectrum of sTMS-SBA-15-SH are consistent with silica bound mercaptopropyl chain.

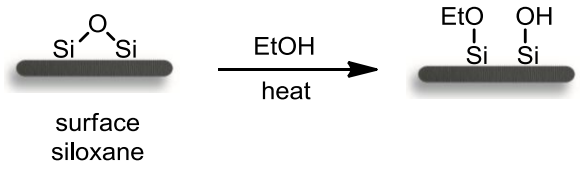

Scheme 2-4. Opening of strain siloxanes by ethanol attack

Unfortunately, the preceding material characterization of pore protected passivated SBA-15 has not provided definitive evidence that these silicas are indeed selectively grafted. Instead these techniques have established that the pore protection strategy is capable of generating a bi-functional material with surface bound TMS and thiol functional groups. What remains to be done is to establish whether our protocol results in the formation of an effective passivation layer on the external surface of SBA-15 that inhibits functionalization of any externally localized silanols. Our efforts along these lines will be presented after a brief discussion of pore protection passivation as applied to MCM-41.

2.2.4 Pore Protection Passivation with as-MCM-41

Recall that the early attempt at pore protection passivation of MCM-41 by Ruiz-Hitzky[8] was not successful because the HCl formed as a consequence of their attempted passivation procedure with TMSCl facilitated SDA extraction. Extraction of the cetyltrimethylammonium bromide (CTAB) SDA allowed for significant silylation of the meso-structure of their materials. While the Ruiz-Hitzky[8] results were unfortunate, it was our contention that pore protection passivation might be effective with MCM-41 if HMDS were employed as the passivating agent

instead of TMSCl (**Scheme 2-5**). HMDS was thought to be more appropriate because the by-products formed during the passivation step do not have the same capacity to promote surfactant extraction as does HCl.

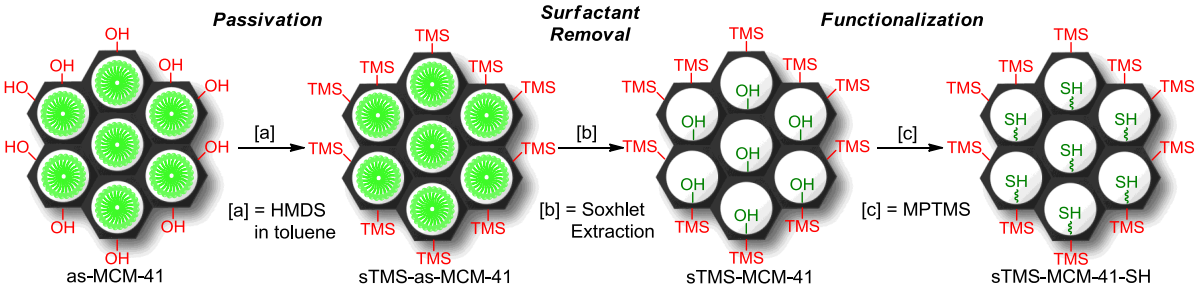

Scheme 2-5. General pore protection selective grafting protocol with as-MCM-41

Buoyed by the observation that as-MCM-41 had a closed pore structure based on physisorption analysis (**Figure 2-5** and **Table 2-4**) pore protection passivation was carried out using HMDS. As predicted, the recovered material still had a closed pore structure as measured by physisorption analysis. Extraction of CTAB was carried out using a procedure optimized by Tuel[16] that involved washing the material with ethanolic solutions of NH_4NO_3 (0.2 wt% NH_4NO_3). The recovered sTMS-MCM-41 had a surface area comparable to MCM-41 and it was significantly larger than that observed for TMS-MCM-41. A similar trend was also observed in the carbon content as measured by elemental analysis. These data suggest that only a small quantity of TMS was incorporated during the pore protection passivation treatment and is in line with the observations made with SBA-15 (**Figure 2-3** and **Table 2-3**). After post-grafting with MPTMS, sTMS-MCM-41-SH had similar textural properties to MCM-41-SH even though the sulfur content (sTMS-MCM-41-SH = 1.7 mmol S g^{-1} and MCM-41-SH = 2.2 mmol S g^{-1}) was slightly lower.

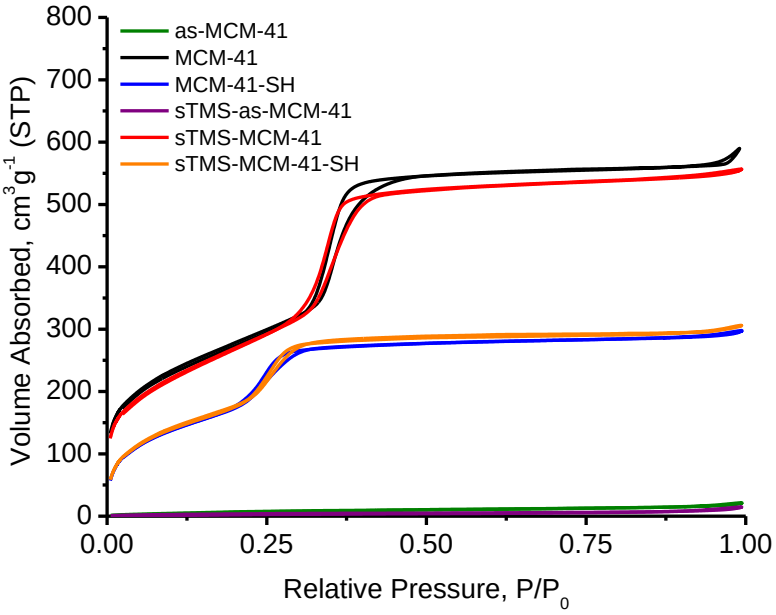

Figure 2-5. Nitrogen physisorption overlay for selective grafting with as-MCM-41

Table 2-4. Summary of textural properties for selective grafting with as-MCM-41[a]

Material	S_{BET},[b] m^2 g^{-1}	C_{BET}[c]	D_{BJH},[d] nm	V_p,[d] cm^3 g^{-1}	wt%	
					C	S
as-MCM-41	32	11	1.5	0.03	31.0	-
sTMS-as-MCM-41	15	21	1.6	0.02	31.3	-
MCM-41	1018	79	2.6	0.88	3.4	-
sTMS-MCM-41	1000	60	2.5	0.83	4.0	-
MCM-41-SH	653	42	2.0	0.40	11.0	6.8
sTMS-MCM-41-SH	670	43	2.0	0.41	10.6	5.3
TMS-MCM-41	706	26	2.2	0.54	10.8	-

[a] Reaction conditions: See Experimental for details; [b] BET surface area; [c] BET parameter; [d] Pore diameter (D_{BJH}) and pore volume (V_p) calculated using BJH adsorption branch for pores 1.0 – 300 nm in diameter

2.2.5 *En route* to a Method to Detect Selective Grafting

As discussed in the introduction, assays[6, 7] which have been developed to analyze the effectiveness of selective grafting strategies typically rely solely on microscopy to assess the materials. While microscopy is a valuable method, it can be challenging to determine how well the image(s) captured represent the properties of the bulk material.

Our approach to examining the effectiveness of selective grafting was different from the outset. It was our intent not to rely exclusively on microscopy for our evidence of selective grafting. Development of a method along these lines was initiated by former graduate student Dr. Daryl P. Allen. He synthesized the APTES functionalized silicas SBA-15-NH_2 and sTMS-SBA-15-NH_2 using procedures similar to those discussed above for SBA-15-SH and sTMS-SBA-15-SH. He then treated these materials with resin-bound bromocresol blue (**Scheme 2-6**). This resin turns blue upon exposure to amino groups and because of the size of the resin bead, is too large to enter the 6 – 8 nm pores of SBA-15. For this reason it was hypothesized that the resin should only be able to detect amino groups localized on the external surface of SBA-15. Optimally, the resin would turn blue on exposure to SBA-15-NH_2 and would not change color on exposure to sTMS-SBA-15-NH_2, because the amino groups are contained within the mesostructure. The test yielded encouraging results (**Figure 2-6**); the combination of resin-bound bromocresol blue and SBA-15-NH_2 formed a slightly blue-green suspension (Solution **3**). No color change was observed under similar conditions with sTMS-SBA-15-NH_2 (Solution **4**). Nonetheless, this data was not optimal because the resin response with SBA-15-NH_2 was not particularly intense. The limited sensitivity of the test was thought to be rooted in the inherent challenge of getting irregularly shaped surfaces to interact with one another.[17, 18] A second problem with the test relates to the functionalization of SBA-15 with APTES. APTES post-grafting is challenging due to the

propensity for this trialkoxysilane to form multilayers on surfaces and co-condense with itself to form aggregates.[19, 20] For these reasons we began to explore alternative approaches to detect selective grafting.

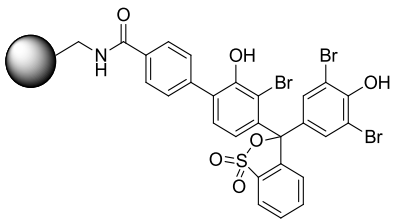

Scheme 2-6. Polystyrene bound bromocresol blue (bromocresol-blue resin)

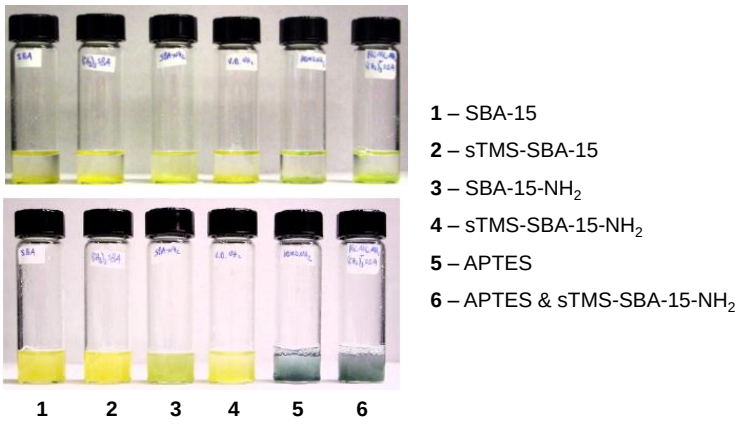

Figure 2-6. Results of Daryl Allen`s bromocresol-blue resin selective grafting test; top, initial solutions; bottom, after 5 h at room temperature

Inspired by Daryl Allen's resin test results, we also briefly examined the possibility of cross-linking SBA-15-NH_2 or SBA-15-SH particles. The crosslinking agent was an isocyanate polymer. It was thought that on exposure to the cross-linking agent the average particle size of SBA-15-NH_2 and SBA-15-SH would increase, while sTMS-SBA-15-NH_2 and sTMS-SBA-15-SH

would remain unchanged. Changes in particle size could be measured by SEM and laser diffraction. This test for selective grafting was abandoned early on because the average particle size of SBA-15-NH_2 did not change on treatment with the iso-cyanate polymer (**Figure A-3** and **Figure A-4** in **Appendix A**).

2.2.6 FloDots as a Possible Means to Detect Selective Grafting

The resin and cross-linking tests that were intended to evaluate selective grafting relied on the principle of size exclusion. When a particle is too large to enter the mesostructure, but designed nonetheless to react with a grafted functional group, it can only do so by interacting with the external surface(s). Continuing with this theme, we became interested in exploring the potential for a suitably functionalized nanoparticle to react with groups on the external surface of mesoporous silicas. Ideal particle properties for this application would be: well-defined morphology, narrow size distribution that is larger than the pore size of SBA-15 and MCM-41, i.e. > 10 nm in diameter, easily functionalized and fluorescent. Fluorescence would allow us to assess the effectiveness of selective grafting across a bulk amount of material. A literature search revealed that the nanoparticles called FloDots satisfied these criteria.

FloDots were developed and named by the Tan group[21-24] and are a type of non-porous fluorescent silica nanosphere. The particle size distribution is narrow and is dictated by method of preparation (10 - 100 nm in diameter).[21] The diameter of these particles ensures that they are too large to interact with the pores of SBA-15 and MCM-41. A wide variety of fluorescent dopants can be immobilized within the walls of FloDots;[21, 23] this study employs tris(2,2′-bipyridyl)dichlororuthenium(II) ($Ru(bpy)_3$). The silica walls entrap the fluorescent dye and serve to prevent leaching and photobleaching. A stability study by Tan[21] demonstrated that $Ru(bpy)_3$ doped FloDots are stable to constant excitation over the course of 1 h. Under similar conditions a

solution of $Ru(bpy)_3$ will bleach. Moreover the surface of FloDots has been functionalized with a variety of amine, thiol and carboxyl groups.

FloDots are synthesized by a reverse microemulsion method (**Scheme 2-7**), also termed water in oil (W/O) microemulsion.[22] The oil of the emulsion is cyclohexane and it is stabilized by a surfactant and co-surfactant system composed of Triton-X-100 (**Scheme 2-8**) and hexanol. The surfactant system also serves to keep the growing spheres separated. Tetraethoxysilane (TEOS) serves as the silica source for the FloDots and the fluorescent dopant, $Ru(bpy)_3$ is dissolved in the water. After addition of the reagents, the condensation of the silica spheres is initiated by addition of NH_3. $Ru(bpy)_3$ is entrapped within the silica walls as the particles grow. An optimization study by Tan[23] concluded that particle size is controlled by the pH and the ratios of water: surfactant: co-surfactant.

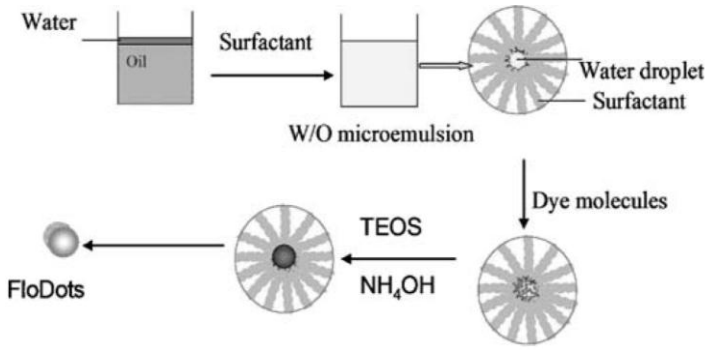

Scheme 2-7. Synthesis of $Ru(bpy)_3$ doped FloDots using reverse microemulsion method, reproduced from reference 21 with permission

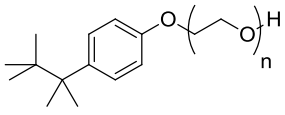

Scheme 2-8. Structure of Triton-X-100, n = 9 - 10[25]

The initial quantity of TEOS added to the microemulsion forms a core particle, but functionalization is best achieved by addition of a second portion of TEOS followed 30 min later by the trialkoxysilane(s) of choice.[22] The delayed addition is believed to favour localization of the functional group(s) on the external surface of FloDot.[22] Functionalization with phosphonate **1 (Scheme 2-9)** is critical as it mitigates agglomeration of the FloDots and reduces non-specific adsorption to hydrophobic surfaces, a property that will turn out to be important for detection of selective grafting. FloDots are isolated by centrifugation and washed repeatedly to remove excess $Ru(bpy)_3$. The FloDots were stored as dispersions in 1:1 ^{t}BuOH:H_2O which were stable for up to 1 month without evidence of sedimentation. The spherical morphology of FloDots synthesized for selective grafting detection was confirmed by TEM (**Figure 2-7**); the particle size distribution was found to be 82 ± 4 nm, which was comparable to that reported in the literature.[23]

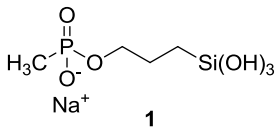

1

Scheme 2-9. Structure of phosphonate additive **1** for stabilization of FloDot suspensions

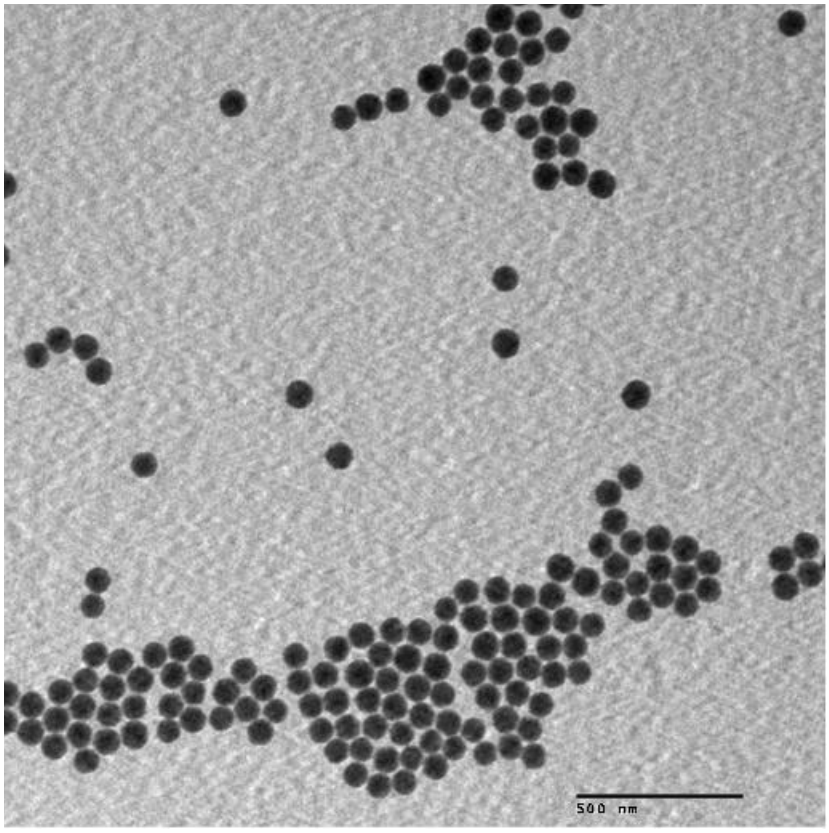

Figure 2-7. TEM of FloDots synthesized by the reverse microemulsion method

2.2.7 Reactivity of FloDots with MTS materials

As previously mentioned, FloDots are too large to enter the pores of SBA-15 and MCM-41; consequently, these particles can only interact with functionality localized on the exterior surface of these silicas. We were interested in exploring the possibility of reacting FloDots with functionalized mesoporous silicas and monitoring the outcome by fluorescence. We hypothesized that reaction of functionalized FloDots with mesoporous silicas grafted using conventional methods would result in a fluorescent material, while successful selective grafting would result a material that would not develop fluorescence. Ultimately, this approach was abandoned for

several reasons that will be discussed in the next few pages but observations made over the course of the reactivity study lead us to a selective grafting detection strategy that evaluates the passivation layer on the external surface. For this reason our efforts towards the development of a thiol-disulfide interchange and a Cu(I) mediated azide-alkyne Huisgen cycloaddition reaction between FloDots and mesoporous silica will be discussed below.

Thiol-disulfide exchange with FloDots and SBA-15

The thiol-disulfide interchange reaction shown in **Scheme 2-10** is an equilibrium process and was previously employed by the Tan group[26] to covalently link FloDots to oligonucleotides. In their system, the FloDots were functionalized with MPTMS and the oligonucleotides were tagged with a disulfide. We chose to adapt this strategy to detect selective grafting with mesoporous silicas. Thus, FloDots prepared in our lab were functionalized with MPTMS. Simultaneously, we prepared SBA-15-SS and sTMS-SBA-15-SS, which are mesoporous silicas functionalized with the hetero-disulfide **3** (**Scheme 2-11**). The Davis group[27] previously established that **3** readily undergoes thiol-disulfide interchange with excess MPTMS to form disulfide **4** as part of his strategy to pattern sulfur groups on the surface of SBA-15. Our goal was to observe a thiol-disulfide interchange upon treatment of SBA-15-SS with FloDots, leading to fluorescent mesoporous silica and no inter-change on treatment of sTMS-SBA-15-SS (**Scheme 2-12**).

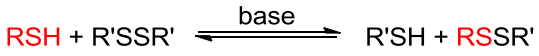

Scheme 2-10. Generalized thiol-disulfide interchange reaction

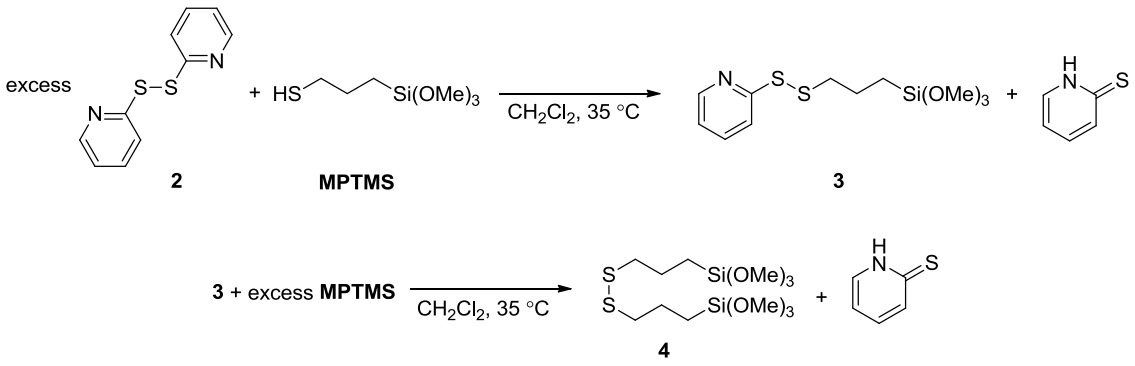

Scheme 2-11. Synthesis of heterodisulfide **3** and disulfide interchange with MPTMS to yield **4**

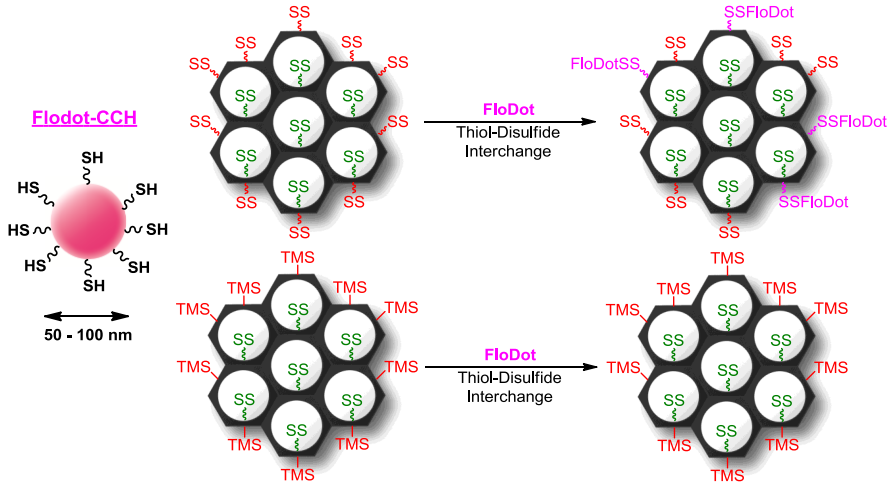

Scheme 2-12. Proposed selective grafting scheme based on the thiol-disulfide interchange reaction where silica was functionalized with disulfide **3** and FloDots were functionalized with MPTMS

Unfortunately, preferential adsorption of FloDots onto SBA-15-SS or SiO_2-SS, an amorphous silica analogue, was not observed under the interchange conditions, and instead non-specific adsorption appeared to be the dominant interaction, i.e. all the silicas became fluorescent. Although unsuccessful, this brief foray into disulfide chemistry did illustrate the importance of functionalizing FloDots with a phosphonate group which is critical to inhibiting non-selective

adsorption of these particles onto powdered silicas (**Figure 2-8**). FloDots that were not functionalized with phosphonate underwent complete non-specific adsorption onto all silica samples tested. These effects are illustrated in **Figure 2-9** by comparing the color of the supernatant for silicas treated with different FloDot batches. Notice that the supernatant is yellow for phosphonate **1** co-functionalized FloDots (vials 2 and 4), and clear for samples treated with phosphonate free FloDots (vials 1 and 5), indicating complete adsorption. This experiment suggests that the presence of phosphonate functionality reduces the amount of non-specific adsorption but does not eliminate the phenomena entirely, later we will show that washing steps are necessary to remove weakly adsorbed FloDots. Optical pictures are presented here because at this stage in the research project we anticipated that extensive reaction between FloDots and silica would be clearly visible by the naked eye, we learned that this was a false assumption and all subsequent detection screens are evaluated based on fluorescence measurements.

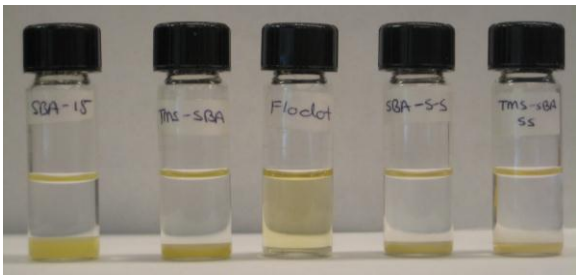

1 – SBA-15
2 – TMS-SBA-15
3 – FloDot
4 – SBA-15-SS
5 – sTMS-SBA-15-SS

Figure 2-8. Adsorption of MPTMS FloDots onto silicas, FloDots were not co-functionalized with phosphonate **1**

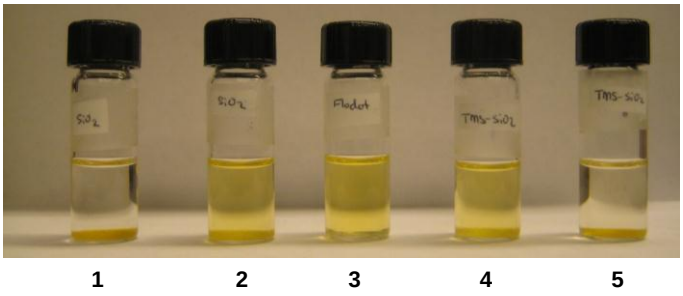

Figure 2-9. Adsorption of MPTMS FloDots onto amorphous SiO_2; vials 1 and 5 contain FloDots without phosphonate **1;** to vials 2 – 4 contain FloDots co-functionalized with **1**

Azide-Alkyne Cycloaddition with FloDots and MTS materials

The azide-alkyne Huisgen cycloaddition (AAC) reaction[28, 29] (**Scheme 2-13**) is one of a number of "Click reactions", a term and philosophy developed by Barry Sharpless and co-workers.[30] To be classified as a Click reaction a process must meet several criteria including being high yielding, modular with wide substrate scope, generate inoffensive by-products and purification must be simple i.e. non-chromatographic.[30] For these reasons, Click reactions such as AAC are often the ideal choice when attempting to assemble complex architectures from simple subunits.[31]

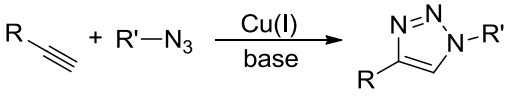

Scheme 2-13. Copper catalyzed azide-alkyne Huisgen cycloaddition (AAC)

Several groups have reported applications of AAC reaction with mesoporous silicas.[32-35] A good example was a report by the Stack group[33] which was outlined in Chapter 1. They used the AAC reaction to illustrate how the density of functionality changed with loading on co-

condensed SBA-15. An application of the AAC reaction by the Bein group[35] described the successful immobilization of the protein trypsin (4 nm in diameter)[36] within the pores of SBA-15. Their goal was to use the mesopores of SBA-15 to protect the enzyme from environmental factors that could lead to deactivation. The Bein report demonstrated that the AAC reaction could be effective at attaching a relatively large particle to the surface of mesoporous silica. Based on their results, we intended to explore the potential of the AAC reaction to graft FloDots onto mesoporous silica (**Scheme 2-14**).

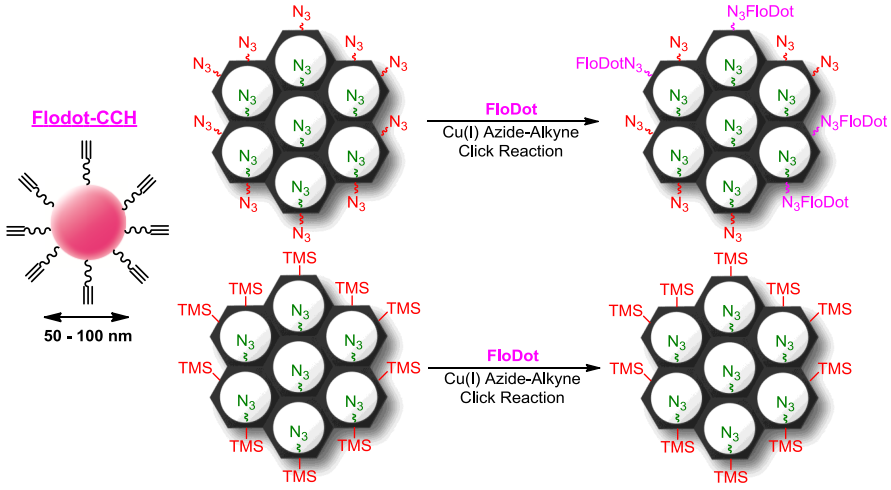

Scheme 2-14. Proposed selective grafting scheme based on the Cu catalyzed azide-alkyne cycloaddition reaction where silica was functionalized with an azide and FloDots were functionalized with alkyne **6**

To assess the capacity to carry out an AAC coupling between FloDots and silica, we synthesized FloDots functionalized with alkyne **6** (**Scheme 2-15**) and phosphonate **1** as well as silicas functionalized with propyl azide groups. The azide groups were initially incorporated on silicas, SBA-15-N_3, s-TMS-SBA-15-N_3, MCM-41-N_3, s-MCM-41-N_3 and SiO_2-N_3 using the

strategy outlined by Bein.[35] Their approach involves post grafting with 3-chloropropyltrimethoxysilane (ClPTMS) and subsequent substitution with NaN_3. In our hands, only partial conversion of chloropropyl groups on the surface were converted to azido-propyl groups was achieved, as determined by ^{13}C CP MAS NMR (**Figure 2-10**). Regardless, we thought sufficient reaction took place to permit us to carry out an AAC reaction between SiO_2-N_3 and the homogeneous alkyne **7** (**Scheme 2-16**) as a test of the AAC reaction conditions that would be employed with FloDots. After reaction the azide stretch at 2108 cm^{-1} in the FT-IR spectrum was undetectable, indicating that a significant number of the azides are reactive with **7** (**Figure 2-11**).

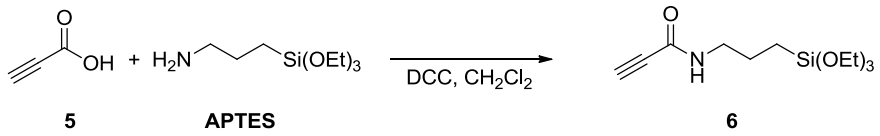

Scheme 2-15. Synthesis of alkyne **6**

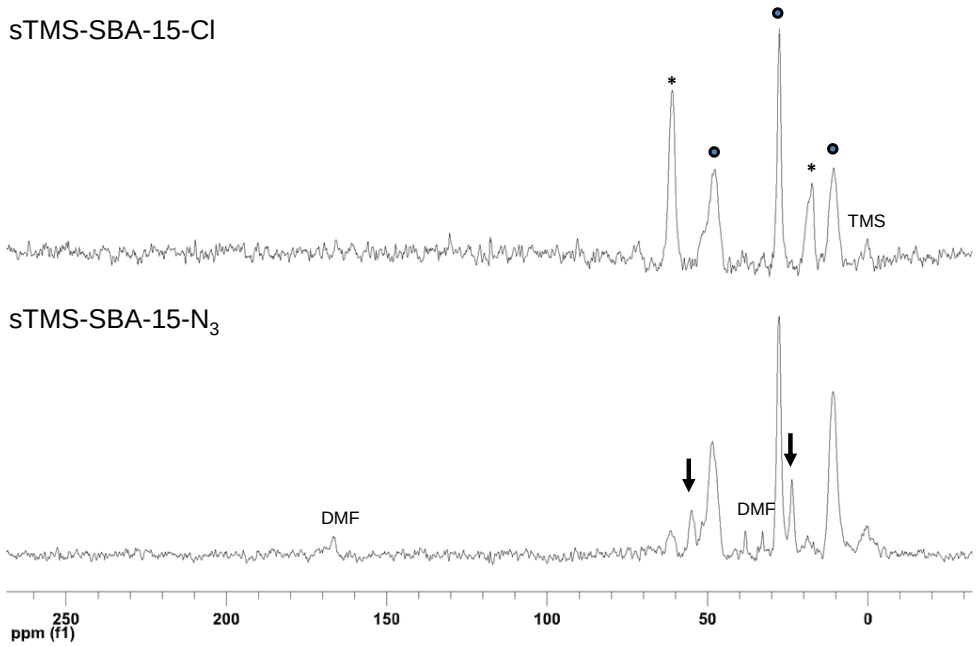

Figure 2-10. ^{13}C CP-MAS NMR overlay for the partial conversion of sTMS-SBA-15-Cl to sTMS-SBA-15-N_3 via an SN_2 reaction with NaN_3 in DMF, peaks consistent with ClPTMS (circle), N_3PTES (arrow) and ethanol (asterisk) are labeled

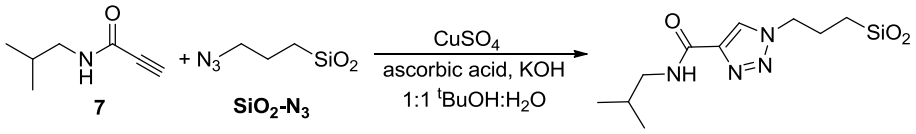

Scheme 2-16. Cu mediated AAC reaction between alkyne **7** and SiO_2-N_3

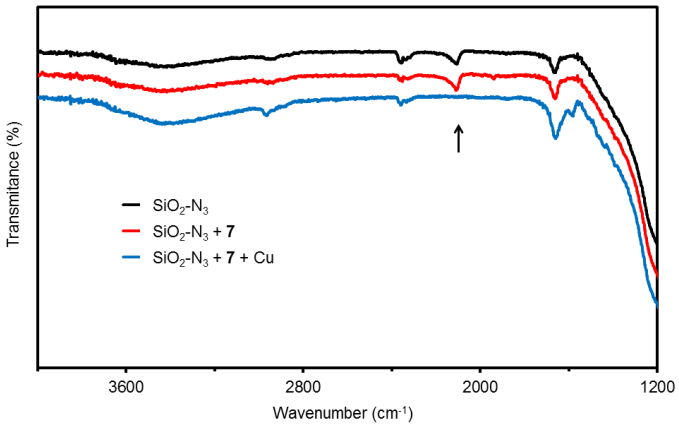

Figure 2-11. FT-IR spectra depicting the loss of the azide stretch at 2108 cm^{-1} upon AAC reaction of alkyne **7** with SiO_2-N_3

Initial attempts at AAC coupling of FloDots to SiO_2-N_3 proceeded with large amounts of non-specific adsorption, evidenced by significant increases in fluorescence in Cu-free controls. Non-specific adsorption was mitigated by treating SiO_2-N_3 with HMDS (TMS-SiO_2-N_3), the purpose of which was to silylate exposed silanols, and by washing the silica recovered from reaction with the ammonium surfactant CTAB dissolved in 4:1 H_2O:EtOH (5 wt% CTAB). When these protocols were instituted, FloDot and TMS-SiO_2-N_3 reactions carried out in the presence of Cu had marked increases in fluorescence as compared to the controls (**Figure 2-12**). These results infer, albeit indirectly, that AAC reaction between alkyne-functionalized FloDots and TMS-SiO_2-N_3 has occurred. All fluorescence spectra reported in this chapter were collected as DMF

suspension. The silica was dispersed by stirring the solutions in the spectrometer. The spectra are also normalized to the weight of silica added to the cuvette.

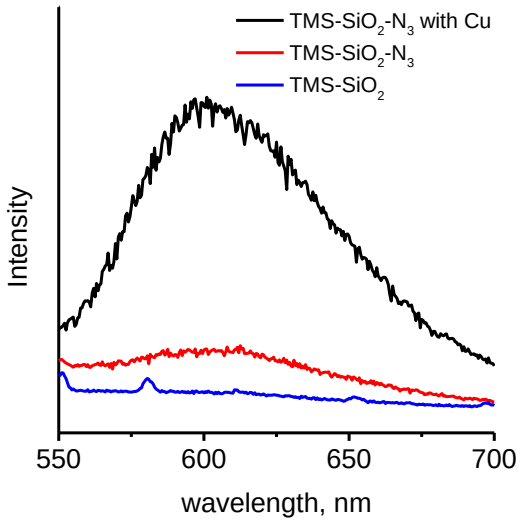

Figure 2-12. Fluorescence overlay (λ_{ex} = 450 nm) for the AAC reaction of FloDots with TMS-SiO_2-N_3. Spectra are normalized to the weight of silica added to the cuvette and dispersed in DMF (3.5 mL)

Subsequent to the TMS-SiO_2-N_3 results reported above, SBA-15-N_3, s-TMS-SBA-15-N_3 MCM-41-N_3 and s-MCM-41-N_3 materials were tested for selective grafting under the FloDot AAC reaction conditions; as with SiO_2-N_3, it was necessary to silylate each silica with HMDS after the NaN_3 treatment and prior to exposure to the FloDot AAC reaction conditions. Unfortunately, in both cases (**Figure 2-13**) the recovered selective and non-selective materials were equally fluorescent. In these fluorescent overlays a control reaction without Cu is shown (red line) demonstrating that non-specific adsorption of FloDots was not an issue under these conditions. Note that while it appears that selective grafted SBA-15 materials were slightly less fluorescent than standard grafted SBA-15-N_3; the same trend was not observed for MCM-41, so

we believe that the SBA-15 spectra were a happy accident as both classes of materials were treated in a similar fashion. The conclusion then from these data is that the AAC detection protocol was not reproducible in its current form. Moreover a TEM analysis **(Figure 2-14**) of SBA-15-N_3 and TMS-SBA-15 after exposure to Cu and FloDots show that the nanoparticles are less abundant on TMS-SBA-15. Note the size of FloDots relative to the mesopores confirming they are indeed too large to enter the pores of these silicas.

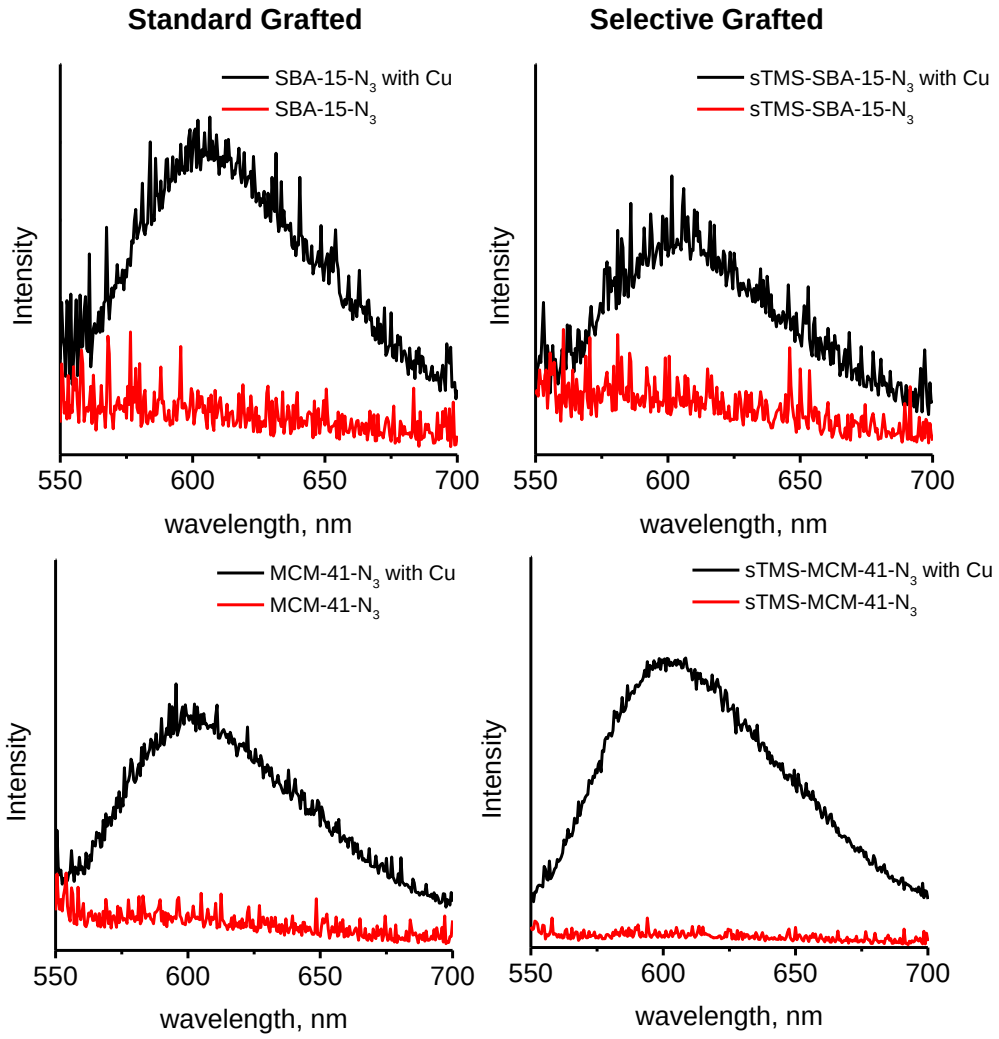

Figure 2-13. Fluorescence overlays (λ_{ex} = 450 nm) for the AAC reaction of FloDots with selective and non-selective grafted SBA-15 (top) and MCM-41 (bottom), with Cu (black lines) and without Cu (red lines); note all materials were silylated with HMDS prior to exposure to FloDots. Spectra are normalized to the weight of silica added to the cuvette and dispersed in 3.5 mL DMF

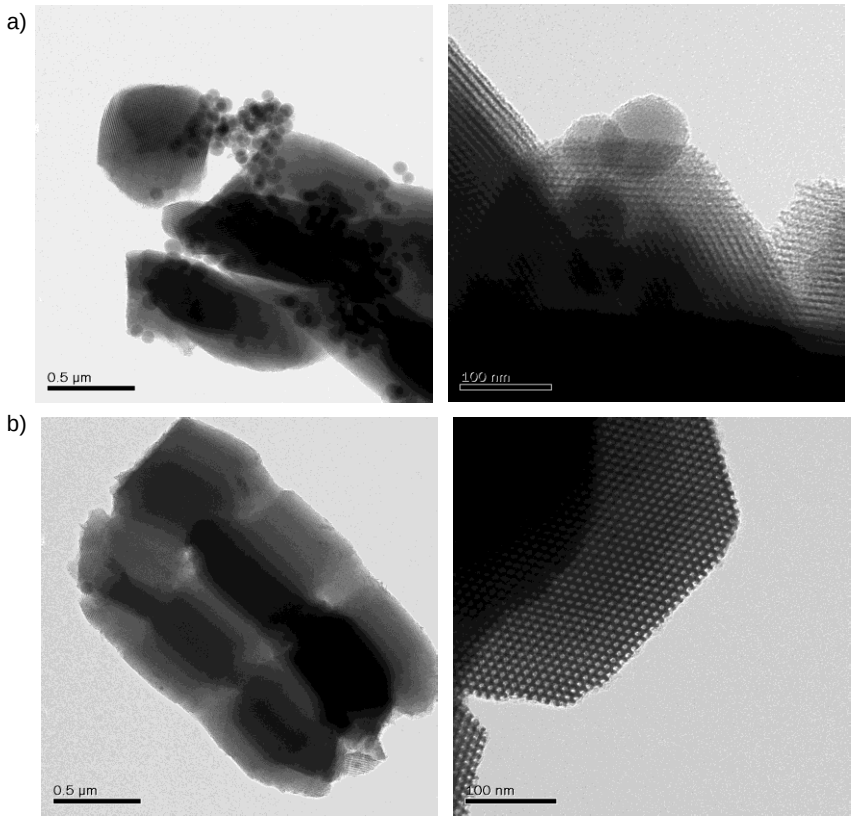

Figure 2-14. TEM images of SBA-15-N_3 and TMS-SBA-15 after exposure to FloDots and the AAC reaction conditions

While it is difficult to assess the exact reasons why selective grafting was not detected under these AAC conditions we thought a contributing factor to the failure of this approach was the method used to incorporate azide functionality on the surface of these silicas. Based on our work with Pd-SBA-15-SH(g), which will be discussed in Chapter 3,[37, 38] we were concerned that NaN_3 could degrade the surface of mesoporous materials by nucleophilic attack at silica[15] or it could be removing TMS groups under the substitution conditions.

To see if the AAC result was a consequence of how the silicas were functionalized with azide, MCM-41-N_3(g) was synthesized by post-grafting 3-azido-propyl triethoxysilane (N_3PTES

8) onto MCM-41 (**Scheme 2-17**). The silylated material after post-grafting was subjected to the AAC reaction conditions with FloDots. The fluorescence increase was less dramatic than with the materials functionalized by the substitution method described above due to the fact there was increased non-specific adsorption (**Figure 2-15**). These data prompted us to re-evaluate the AAC FloDot detection strategy. The AAC approach was ultimately abandoned because the fluorescent responses were relatively weak and the whole experimental protocol was inefficient requiring multiple functionalization steps and controls which were time consuming. We thought that it should be possible to develop a more efficient protocol.

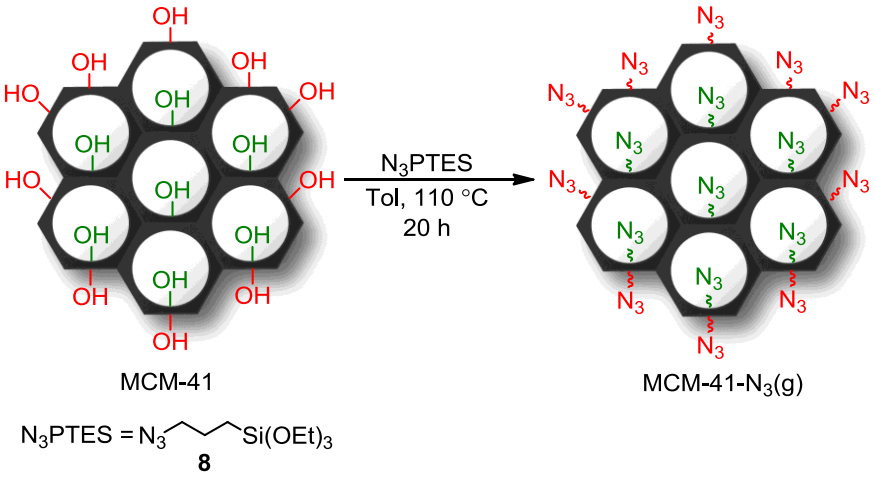

Scheme 2-17. Synthesis of MCM-41-N_3(g)

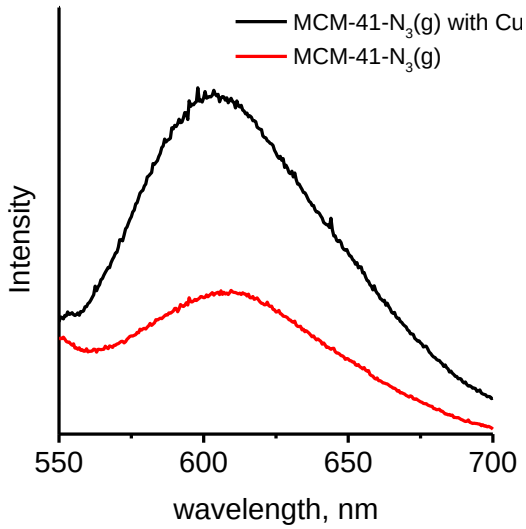

Figure 2-15. Fluorescence overlay (λ_{ex} = 450 nm) for the AAC reaction of FloDots with MCM-41-N_3(g), with Cu (black line) and without Cu (red line); note the material was silylated with HMDS prior to exposure to FloDots. Spectra are normalized to the weight of silica added to the cuvette and dispersed in 3.5 mL DMF

2.2.8 Adsorption of FloDots onto mesoporous silcas: A crude method to evaluate selective grafting passivation layer

While inefficient, the AAC strategy illustrated that FloDots irreversibly adsorb onto the surface of hydrophilic mesoporous silicas and that these particles do not assorb, to any large degree, onto hydrophobic silicas, i.e. silylated TMS-SBA-15 and TMS-MCM-41. It is then reasonable to assume, based on their size that FloDots should not adsorb onto externally passivated sTMS-SBA-15 and sTMS-MCM-41, removing the need for any post-grafting of azides or alkynes. We hypothesized that the differential affinity of FloDots for SBA-15 and sTMS-SBA-15 as well as MCM-41 and sTMS-MCM-41 could be used to detect the passivation layer (**Scheme 2-18**).

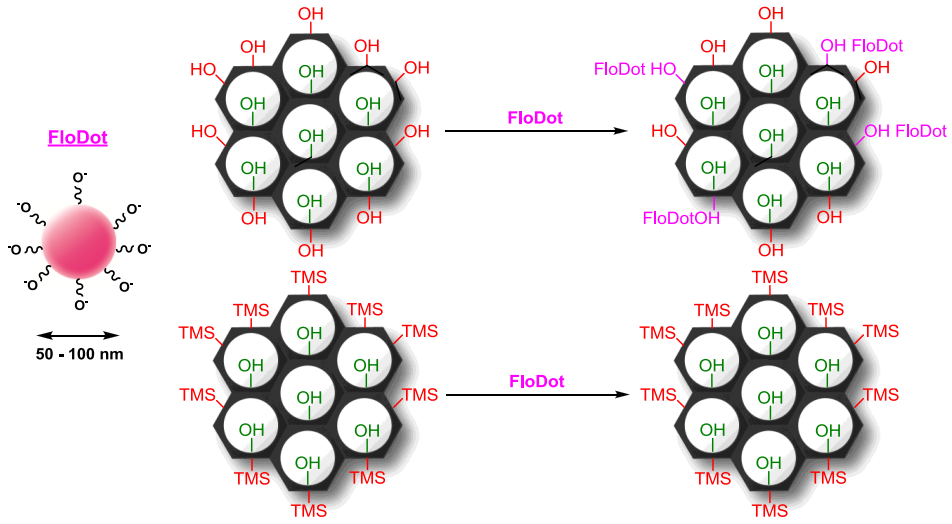

Scheme 2-18. Selective grafting detection scheme based on the differential adsorption of phosphonate **1** functionalized FloDots for hydrophilic and hydrophobic surfaces

This detection strategy allows for the evaluation of the passivation layer formed on the external surface of mesoporous materials immediately after surfactant removal. All other detection strategies discussed here (**Scheme 2-12** and **Scheme 2-14**) and elsewhere,[6, 7] evaluate materials only after functionalization. This approach (**Scheme 2-18**) allows for more rapid feedback regarding effectiveness of one's pore protection protocol. The obvious disadvantage of the adsorption approach is it does not evaluate whether the passivation layer will inhibit functionalization of the external surface during post-grafting. This disadvantage exists because there is no indication as to how sensitive FloDots are to the presence of silanols. Moreover, the detection scheme will not indicate whether or not those same silanols are accessible to functionalization with trialkoxysilanes. Regardless of these issues, it would nonetheless be useful to establish whether a passivation layer is formed on the external surface mesoporous silicas. In our view, the adsorption test for selective grafting served as a stop-gap to establish that

passivation indeed occurs, but it does not replace the need for a detection strategy to evaluate the second step of functionalization of selective grafted materials.

Evaluating Pore protection Passivation with SBA-15

To validate the FloDot adsorption test (**Scheme 2-18**) the literature pore protection passivation procedures were screened (**Figure 2-16**). This screening was performed alongside controls with SBA-15 and TMS-SBA-15 to establish benchmarks for FloDot adsorption on fully hydrophilic and hydrophobic surfaces. As shown in **Figure 2-16**, it was found that sHMDS-SBA-15 and sTMSCl-SBA-15 had reduced fluorescence as compared to SBA-15 and the adsorption was more similar to that observed with TMS-SBA-15. sTMSOEt-SBA-15 was the worst performing selective grafted material in this screen as expected because TMSOEt is a weak silylation agent. On the whole, these results confirmed that FloDots have the capacity to detect the effectiveness of passivation methods, even though these are less than ideal selective grafted materials (**Table 2-1**).

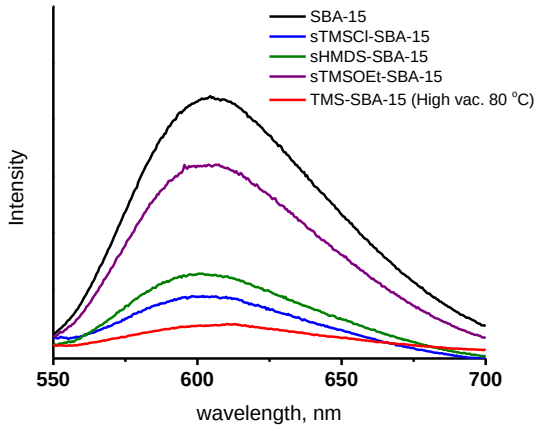

Figure 2-16. Fluorescence overlay (λ_{ex} = 450 nm) for the adsorption of FloDots on to selective grafted materials prepared using literature methods, as-SBA-15 was dried at 80 ºC under high vacuum prior to passivation. Spectra are normalized to the weight of silica added to the cuvette and dispersed in 3.5 mL DMF

Encouraged by the initial adsorption test results with the literature materials, we proceeded to test sTMS-SBA-15 prepared from re-SBA-15. When the surfactant was removed by ethanol extraction there was about a 50 % reduction in fluorescent intensity resulting from adsorbed FloDots as compared to the SBA-15 control (**Figure 2-17a**). The reduced fluorescence is put in context by considering that there is only a 10% difference in surface area and 1.6 % difference in carbon content between sTMS-SBA-15 and SBA-15 (**Table 2-3**). These results definitively indicate that passivation of silanols occurred preferentially on the external surface of re-SBA-15. As with the literature controls discussed above (**Figure 2-16**), the level of fluorescence was, however, still higher than the TMS-SBA-15 control. It was suspected that ethanol extraction step played a role in degrading the passivation layer.[39] To test this possibility sTMS-SBA-15 and sHMDS-SBA-15 were Soxhlet extracted with acetone (**Figure 2-17b**),

instead of ethanol. The level of FloDot adsorption on these materials was comparable to TMS-SBA-15, confirming that ethanol does in fact degrade the passivation layer to some degree. The background non-specific adsorption present in the acetone passivated materials is likely due to residual silanols on the external surface of these materials. It has been noted, and introduced in Chapter 1, that silylation of silica under the best conditions can only cap 85 % of the surface silanols, the rest are unreactive.[2] Thus, it is likely that FloDots are detecting residual silanols on the external surface.

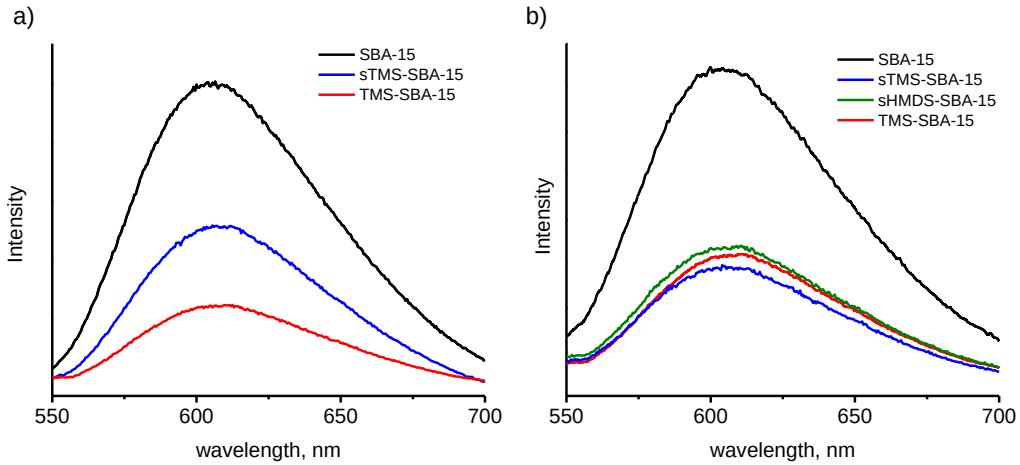

Figure 2-17. Fluorescence overlay **(**λ_{ex} = 450 nm) the adsorption of FloDots on to sTMS-SBA-15, re-SBA-15 was dried at 80 ºC under low vacuum prior to passivation; a) EtOH Soxhlet extraction; b) acetone Soxhlet extraction. Spectra are normalized to the weight of silica added to the cuvette and dispersed in 3.5 mL DMF

An additional factor that was determined to be critical to mitigate non-specific adsorption of FloDots was the drying temperature of the SBA-15 prior to silylation (**Figure 2-18**). The more aggressively we dried the silica prior to silylation, the lower the fluorescence resulting from FloDot adsorption. The drying conditions chosen are likely removing residual water from the

surface of the silicas, while some silanol condensation may be occurring to give strained surface siloxanes. This process should be slow at 1 atm and 250 ºC.[15, 40] It is known that wetter silica surfaces possess larger numbers of silanols that are deactivated towards silylation because they exist in stabilized hydrogen bonding networks.[40] The drying procedure is then important in dictating the extent of silylation and hence passivation that can be achieved of the external surface during the pore protection step. Based on this assessment, the adsorption of FloDots on fully silylated TMS-SBA-15 is a good estimation of the maximum extent of external surface passivation that can occur under a given drying procedure. It is for this reason the drying procedure used to prepare the SBA-15 samples for the different pore protection passivation treatments are reported alongside all the fluorescence overlays.

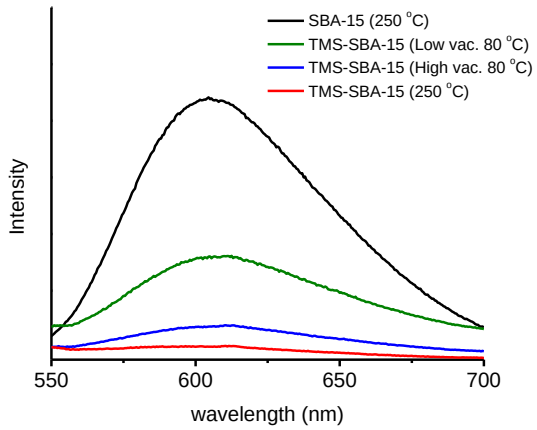

Figure 2-18. Fluorescence overlay **(**λ_{ex} = 450 nm) the adsorption of FloDots on to TMS-SBA-15, where SBA-15 was dried under different conditions prior to silylation. Spectra are normalized to the weight of silica added to the cuvette and dispersed in 3.5 mL DMF

The drying temperature for as-SBA-15 and re-SBA-15 prior to external passivation is limited to approximately 80 ºC because above this temperature the P123 SDA begins to degrade. Our new optimized drying procedure is an 80 ºC treatment under high vacuum and we are currently in the process of reproducing the passivation procedure (3 h in HMDS) and the fluorescence overlay depicted in **Figure 2-17** but have been unable to complete it due to time constraints. In lieu of this data included as **Figure A-8** in **Appendix A**, is a fluorescence overlay for 24 h HMDS pore protection treatment of re-SBA-15, the results are qualitatively similar to those reported in **Figure 2-17a**.

Evaluating Pore protection Passivation with MCM-41

sTMS-MCM-41 was also evaluated with the FloDot adsorption test (**Figure 2-19**). As with SBA-15, the fluorescence was reduced by about 50 % as compared to MCM-41. Recall that MCM-41 and sMCM-41 have similar surface areas and carbon contents. Again, this data strongly suggests the formation of a passivation layer on the external surface. We also attempted to use the adsorption test to examine selective grafted MCM-41 materials prepared by the diffusion controlled method outlined by Thomas.[6] Recall as introduced in Chapter 1 that diffusion controlled passivation involves treating calcined MCM-41 with a small amount Ph_2SiCl_2, sPh_2Si-MCM-41. Unfortunately, FloDots adsorbed similarly onto MCM-41 and the fully silylated Ph_2Si-MCM-41 control materials making the test inconclusive in this case, it appears that the passivation layer formed by Ph_2SiCl_2 is not hydrophobic enough to prevent FloDot adsorption. Note that the surfaces of calcined MCM-41 are activated by drying under high vacuum at 250 ºC immediately prior to passivation, so surface wetting is likely not a significant contributing factor.

Another detection strategy is then needed to reassess the Thomas approach to diffusion controlled selective grafting. [6]

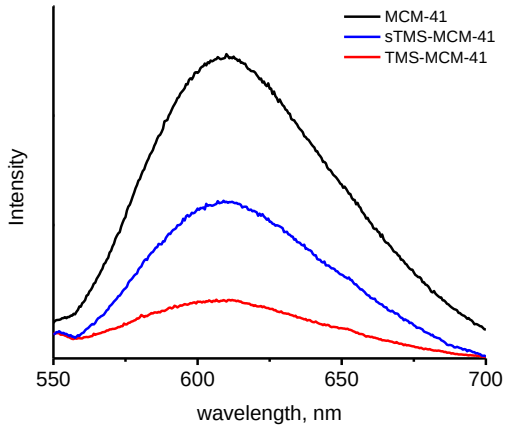

Figure 2-19. Fluorescence overlay (λ_{ex} = 450 nm) the adsorption of FloDots on to sTMS-MCM-41, as-MCM-41 was dried at 80 ºC under high vacuum prior to passivation. Spectra are normalized to the weight of silica added to the cuvette and dispersed in 3.5 mL DMF

2.2.9 Beyond FloDots, a new test for Selective Grafting

The FloDot adsorption test is a method that probes the passivation layer of selective grafted materials but does not provide any information about how effective the passivation layer will be at preventing functionalization of the external surface. While FloDots adsorb onto silanol containing domains, we have little to no information regarding how quantitatively they detect the presence of silanols. A perhaps more serious issue is that not all silanols are equally amenable to functionalization, even though they may adsorb FloDots.[40] Thus FloDots may be detecting the existence of silanols, but not necessary the presence of silanols that are available to react with trialkoxysilanes under post-grafting conditions. For this reason, a test that examines how

effectively functional groups are localized within the mesostructure of selective grafted materials is still highly desirable.

Inspired by the work and Lejeune,[41] we embarked on the development of such a test. The Lejeune group developed a method to synthesize sulfur functionalized mesoporous array's which were impregnated, indiscriminately on the external and internal surface, with the fluorescent dye Rhodamine B. In these materials Rhodamine B is contained within the pores and on the external surface of the silica. The pore diameter of the silicas was ~6 nm and they examined the extent of quenching of Rhodamine B fluorescence using differently sized (3.5 and 17 nm) gold nanoparticles (GNP).[42] They found that the GNPs which were 3.5 nm in diameter quenched fluorescence to a greater degree than those which were 17 nm in diameter. They ascribed the difference in fluorescence quenching to the different size of the particles because it was assumed that 17 nm GNPs were too large to interact with the pore structure of their materials and therefore are not able to get into close proximity to the dye molecules localized on that domain.

With this in mind, we began to examine changes in fluorescence of dye-doped selective grafted materials upon exposure to large quenchers. Instead of physically adsorbing a dye, we thought it better to chemically bind the fluorophore to the mesoporous material since mobility of the dye might complicate our analysis. Along these lines, we have successfully treated SBA-15-SH with pyrene maleimide (**Scheme 2-19**) and obtained a material that is fluorescent and the emission spectrum (**Figure 2-20**) collected is consistent with site-isolated pyrene.[33] The material is designated SBA-15-SH-pyrene and the absence of the excimer in the emission spectrum indicates that the bound pyrene molecules on the surface are well separated; therefore, there should be plenty of thiols still available to bind fluorescence quenchers.

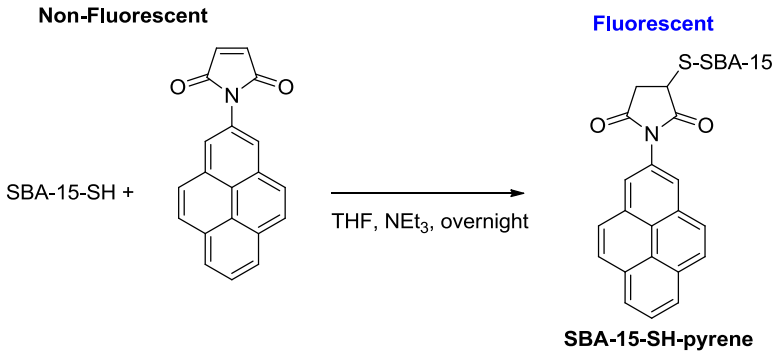

Scheme 2-19. Synthesis of SBA-15-SH-pyr, the molar ratio of thiol : pyrene was 50:1

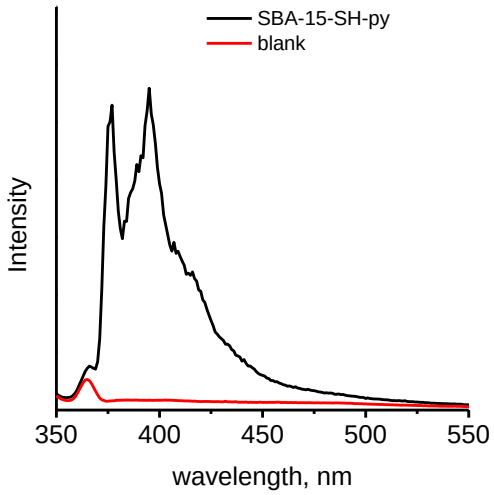

Figure 2-20. Fluorescence emission (λ_{ex} = 330 nm) spectrum of SBA-15-SH-pyrene

We intend to use fluorescence quenching to evaluate selective grafting. In this way, selective grafting can be inferred if the fluorescence of SBA-15-SH-pyrene and MCM-41-SH-pyrene is quenched to a greater degree upon exposure to 17 nm GNPs than sTMS-SBA-15-SH-pyrene and sMCM-41-SH-pyrene (**Scheme 2-20**). We anticipate that quenching in the control materials with 17 nm GNPs will be measurable, not only based on the Leujeune results but by the

fact that literature precedence suggests that the bulk of the pyrene loaded onto SBA-15-SH-pyrene and MCM-41-SH-pyrene might be localized near, or on the external surface. For example, Landry[43] showed that deprotection of amines occurs on the external surface of porous silicas prior to the mesostructure. Evaluation of the florescence quenching detection method is currently underway in our laboratory. It is our expectation that successful demonstration of this selective grafting test will complete the research goals outlined when we set-out to develop methodologies to localize functionality within the pores of mesoporous silicas.

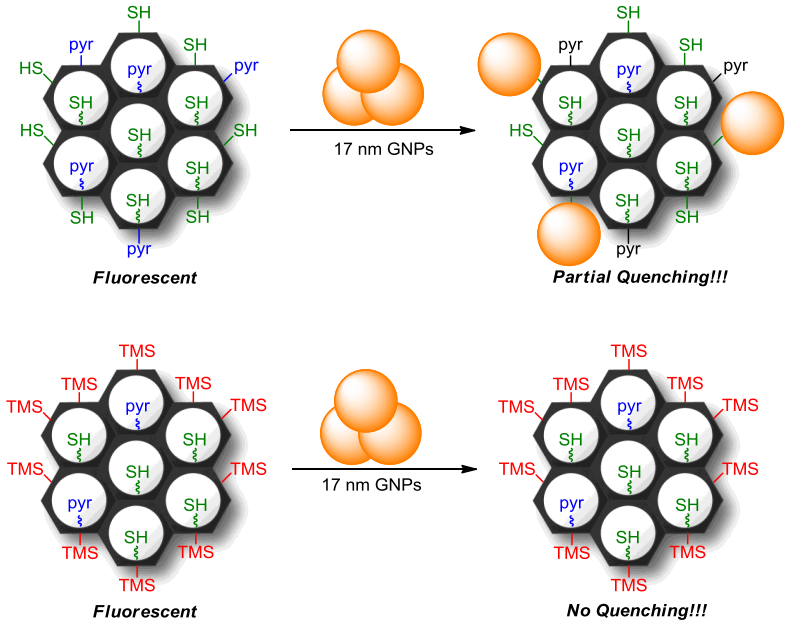

Scheme 2-20. Proposed selective grafting detection scheme based on differential fluorescence quenching by GNPs too large to enter the mesopores of SBA-15 and MCM-41

2.3 Conclusions

The goal of this study was to evaluate the pore protection passivation selective grafting strategy. Specifically, we set out to interrogate this functionalization approach and establish

whether or not it was capable of localizing functionality preferentially within the mesopores of SBA-15 and MCM-41. Other research groups[3-5, 8-11] have applied this approach to both classes of silica with varying success. The first step of this selective grafting protocol involves treating an as-synthesized mesoporous material with a strong silylating agent such as HMDS or TMSCl. We evaluated the textural properties of SBA-15 materials that were passivated using the existing literature procedures and concluded that significant silylation of the mesostructure occurred. Based on the available data, we postulated that the unwanted silylation was a result of the inherent porosity of as-synthesized SBA-15, as-SBA-15, resulting from the inability of the remaining P123 to completely block the pores. To mitigate the problem with as-SBA-15, a straight forward method to incorporate additional P123 SDA into the pores after the material was prepared was developed. The resulting re-SBA-15 was subjected to the passivation conditions with superior results. The material termed sTMS-SBA-15 had similar textural properties to SBA-15. Each material could also be functionalized with a similar quantity of MPTMS. Both observations suggest that minimal silylation of the mesostructure occurred during the passivation step on re-SBA-15. In this regard, the use of re-SBA-15 for pore protection passivation is an improvement over as-SBA-15. It was also found that pore protection passivation selective grafting can also be employed with as-MCM-41 when HMDS is the passivating agent.

The second phase of the project was to develop a method(s) that could assess the effectiveness of selective grafting across a bulk amount of material. Previous groups have relied solely on microscopy to characterize their approaches to selective grafting.[6, 7] The approaches that we evaluated employed FloDots which are silica nanospheres that are larger than the mesopores of SBA-15 and MCM-41, and as such they can only interact with the external surface of these materials. Attempts to develop a selective grafting protocol based on a thiol-disulfide interchange

or a Huisgen cyclization reaction between FloDots with mesoporous silicas were not entirely successful. However, these forays illustrated that FloDots tend to adsorb onto hydrophilic surfaces. This characteristic was exploited in the development of a method to evaluate the external passivation layer formed on sTMS-SBA-15 and sTMS-MCM-41. The test revealed that passivation layers are indeed formed but did not give information regarding whether or not these layers were sufficient to mitigate functionalization of the external surface. To address this challenge a new detection strategy has been proposed based on the expectation that large gold nanoparticles will differently quench the fluorescence of pyrene functionalized selective and non-selective mesoporous silicas, work on the quenching strategy is on-going.

2.4 Experimental

2.4.1 General

Reagents and solvents were obtained from Aldrich and used as obtained unless otherwise noted. 2,2'-Dithiodipyridine was purchased from TCI organic chemicals. Silica gel-100 (amorphous SiO_2) was purchased from Fluka. Transmission electron microscopy (TEM) images were collected on a JEOL 2011 STEM at the University of New Brunswick. Elemental analysis was performed on a Thermo Scientific Flash 2000 Organic Elemental Analyzer equipped with a CHNS-TCD detector, V_2O_5 was added to sulfur containing samples. Nitrogen adsorption/desorption isotherms were collected at 77 K on Micrometrics ASAP 2010 instrument. All SBA-15 and MCM-41 samples were degassed at 353 K prior to analysis. Surface area (S_{BET}) was calculated by the Brunauer-Emmett-Teller (BET)[44] method the region $P/P_0 = 0.07 – 0.20$. Pore size was measured from the maxima of the pore size distribution curve calculated by the Barrett-Joyner-Halenda (BJH)[45] method using the adsorption branch of the isotherm assuming a cylindrical pore structure. The pore volume was measured from the amount of gas adsorbed at a

relative pressure (P/P_0) of 0.99. ^{1}H and ^{13}C NMR spectra were collected on a Bruker Advance 300, 400 or 500 MHz NMR spectrometer as indicated, chemical shifts are reported in ppm and referenced to residual solvent. ^{13}C and ^{29}Si CP-MAS NMR spectra were collected on a 600 MHz NMR spectrometer with spin rates of 10 000 Hz. Fluorescence spectra were acquired on a PTI Fluorimeter equipped with an 814 Photomultiplier Detection System and LPS-220B Xenon Arc Lamp Power Supply.

2.4.2 Synthesis of SBA-15

The sol gel procedure was adapted from Stucky *et al*.[46] P123 (4.0 g) was weighed into a 500 mL glass jar fitted with a stir bar, distilled H_2O (30 mL) was added and the mixture stirred for 4 h at 35 °C until homogeneous. 2 M $HCl_{(aq)}$ was prepared by diluting 36.5 – 38.0 wt% HCl (20 mL) in distilled H_2O (100 mL) and was added to the above solution. The resulting mixture was stirred for 24 h at 35 °C. TEOS (9.0 mL) was added via syringe over a period of 1 min to the mixture which was stirred at 35 °C for another 24 h after which the stir bar was removed, the jar was sealed tightly for the hydrothermal treatment at 80 °C for 48 h. The as-synthesized material was recovered by filtration without washing and dried overnight in air and under vacuum with P_2O_5 as the desiccant. The surfactant was removed by Soxhlet extraction using 0.5 g or 1.0 g batches of as-synthesized SBA-15 (as-SBA-15). The material was doubly wrapped in filter paper (125 mm diameter) placed in a 100 mL thimble and was extracted with 95 % ethanol or acetone for 48 h, the temperature ranges and times between siphons were 70 – 75 °C, 12 min and 58 – 62 °C, 14 min for ethanol and acetone respectively. The recovered material was dried under vacuum and was heated in temperature controlled oven, programmed the following parameters: 1 °C/min ramp-up to 250 °C, hold for 480 min and a 1.5 °C/min ramp down to room temperature.

2.4.3 Synthesis of MCM-41

The sol-gel procedure was adapted from Beck *et al.*[47] CTAB (2.4 g) was weighed into a 1.5 L glass jar, distilled H_2O (120 mL) was added and the suspension was stirred at room temperature for 10 min followed by addition of 30 wt% $NH_4OH_{(aq)}$ (10.5 mL). After 15 min of vigorous stirring, TEOS (10.5 mL) was added by syringe to the suspension over a period of 1 min followed by an additional 1 h of mixing. The precipitate was recovered by filtration without washing and placed, while still wet, in a 1.5 L Teflon capped glass jar which was sealed tightly for a hydrothermal treatment in an oven at 80 °C for 24 h. The as-synthesized material was recovered and dried in air overnight and under vacuum with P_2O_5 as the desiccant. The surfactant was removed from the as-synthesized material by ethanol extraction in 750 mg batches.[16] To extract the surfactant the material (750 mg) was loaded into a 250 mL round bottom flask fitted with a stir bar. NH_4NO_3 (950 mg) was weighed and dissolved in distilled H_2O (25 mL) with stirring followed by the addition of anhydrous EtOH (450 mL) to create a 0.025 M solution. After mixing, a portion (75 mL) of the NH_4NO_3 stock solution was added to the round bottom flask containing the material. The suspension was stirred for 20 min at 60 °C and the material was recovered by hot filtration. This procedure was repeated 3 times and the material was dried under vacuum, one night at room temperature and one night at 80 °C, see **Table 2-4** for textural properties.

2.4.4 Synthesis of sHMDS-SBA-15 based on Asefa *et al.*

The synthesis was adapted from Asefa *et al*.[4] To a 50 mL round bottom flask fitted with a stir bar and septum was added as-SBA-15 (250 mg) and toluene (18 mL). Hexamethyldisilazane (1.8 mL) was added to the suspension via syringe and the flask was purged with Ar for 10 min, sealed and stirred vigorously at room temperature for 18 h. The solution was filtered and the recovered

powder washed with hexanes. The surfactant was removed using the ethanol Soxhlet extraction and heating procedure outlined above for SBA-15. The procedure furnished 110 mg of material, see **Table 2-2** for textural properties.

2.4.5 Synthesis of sTMSCl-SBA-15 based on Bao *et al.*

The synthesis was adapted from Bao *et al*.[5] To a 50 mL round bottom flask fitted with a stir bar and septum was added as-SBA-15 (250 mg) and toluene (18 mL). Chlorotrimethylsilane (1.8 mL) was added to the suspension and the flask was purged with Ar for 10 min, sealed and stirred vigorously at 80 °C for 8 h. The solution was filtered and recovered powder washed with hexanes. The surfactant was removed using the ethanol Soxhlet extraction and heating procedure outlined above for SBA-15. The procedure furnished 110 mg of material, see **Table 2-2** for textural properties.

2.4.6 Synthesis of sTMSOEt-SBA-15

To a 15 mL round bottom flask fitted with a stir bar was added as-SBA-15 (250 mg) and ethoxy trimethylsilane (2.5 mL). The suspension was stirred vigorously for 24 h, filtered and washed with hexanes. The surfactant was removed using the ethanol Soxhlet extraction and heating procedure outlined above for SBA-15. The procedure furnished 110 mg of material, see **Table 2-2** for textural properties and **Figure A-1** in **Appendix A** for ^{13}C CP-MAS NMR spectrum depicting a TMS peak at 0 ppm.

2.4.7 Synthesis of re-SBA-15 by reloading as-SBA-15 with P123

P123 (16.0 g) was dissolved in EtOH (56 mL) by gently heating the flask (~50 ºC for 5-10 min) after which the solution was allowed cooled to room temperature. as-SBA-15 (4.0 g) was then added and the suspension was stirred vigorously for 24 h. The solid material was recovered by

rapid filtration through a 12.5 cm diameter Büchner funnel, dried under vacuum, one night using P_2O_5 as the desiccant and one night at 80 °C. The surfactant was removed using the Soxhlet extraction and heating procedures outlined for SBA-15. The procedure furnished 4.2 g of material, see **Table 2-2** and **Table 2-3** for textural properties.

2.4.8 Synthesis of sTMS-SBA-15

To a 25 mL round bottom flask fitted with a stir bar and septum was added as-SBA-15 (1.00 g) and HMDS (10 mL). The suspension was stirred vigorously at room temperature for the 3 h, filtered and washed with hexanes. The surfactant was removed using the ethanol Soxhlet extraction and heating procedure outlined for SBA-15. The procedure furnished 350 mg of material, see **Table 2-3** for textural properties.

2.4.9 Synthesis of sTMS-MCM-41

To a 100 mL round bottom flask fitted with a stir bar and septum was added as-MCM-41 (900 mg) and freshly ketyl distilled toluene (65 mL). HMDS (6.5 mL) was added to the suspension and the flask was purged with Ar for 10 min, sealed and stirred vigorously at room temperature for 20 h. The solution was filtered and recovered powder washed with hexanes. The surfactant was removed using ethanol extraction and heating procedure outlined for MCM-41. The procedure furnished 400 mg of material, see **Table 2-4** for textural properties.

2.4.10 General procedure for grafting MPTMS, disulfide 3, ClPTMS or N_3PTES onto mesoporous and amorphous silicas

Prior to grafting, SBA-15, MCM-41 or SiO_2 were dried by heating to 80 ºC under high vacuum (< 1 mm Hg) overnight. In a typical procedure, to a 50 mL round bottom flask fitted with a stir bar and septum was added SBA-15, MCM-41 or SiO_2 (250 mg) and toluene (15 mL). One of MPTMS, **1**, ClPTMS, or N_3PTES (0.5 mL) was added via syringe and the suspension was stirred

at 110 ºC for 18 h followed by filtration and washing with hexanes (15 mL). The recovered powder was suspended in 95 % EtOH (15 mL) and stirred for 1 h at room temperature, filtered again and washed with 95 % EtOH (15 mL). The material was dried at 80 ºC under vacuum. The procedure furnished 230 mg of material. Representative textural properties of MPTMS functionalized SBA-15 and MCM-41 materials are reported in **Table 2-3** and **Table 2-4**. See **Figure 2-4** as well as **Figure A-5**, **Figure A-6** and **Figure A-7** in **Appendix A** for ^{13}C CP-MAS spectra of silicas functionalized with MPTMS, disulfide **1**, ClPTMS and N_3PTMS respectively.

2.4.11 General procedure for the synthesis of TMS-SBA-15, TMS-MCM-41, TMS-SiO_2 and other fully silylated silicas

Prior to silylation, SBA-15, MCM-41 or SiO_2 were dried by heating to 80 ºC under high vacuum (< 1 mm Hg) overnight. In a typical procedure, to a 15 mL round bottom flask fitted with a stir bar and septum was added SBA-15, MCM-41 or SiO_2 (300 mg). Hexamethyldisilazane (6 mL) was added to the powder via syringe and the suspension was stirred for 6 h at room temperature. The suspension was filtered, and washed with hexanes. The recovered powder was suspended in 95 % EtOH (15 mL) and stirred for 1 h at room temperature, filtered again and washed with 95 % EtOH (15 mL). The material was dried at 80 ºC under vacuum. The procedure furnished 250 mg of material, see **Table 2-1** and **Table 2-4** for textural properties of TMS-SBA-15 and TMS-MCM-41.

2.4.12 Synthesis of 2-((3-(trimethoxysilyl)propyl)disulfanyl)pyridine: 3

The synthesis was adapted from Davis *et al*.[27] To an oven dried 50 mL round bottom flask was added 2,2'-dithiodipyridine (3.36 g, 15.4 mmol) and dissolved in CH_2Cl_2 (40 mL) and the solution was heated to 40 °C. MPTMS (1.00 g, 5.10 mmol) was diluted in CH_2Cl_2 (10 mL) and added to the above solution dropwise using a syringe pump over 10 hrs. The reaction mixture was cooled

to room temperature and stirred at room temperature overnight. The solvent was removed under vacuum and the residue was purified by column chromatography (1.5:1 Hexanes:THF). Yield: 1.20 g (77 %). The spectra collected were in good agreement with literature reports.[27] ^{1}H NMR (500 MHz, CD_2Cl_2) δ: 0.75 (t, 2H, $^{3}J_{H\text{-}H}$ = 8 Hz, $SSCH_2CH_2CH_2Si$), 1.82 (p, 2H, $^{3}J_{H\text{-}H}$ = 8 Hz, $SSCH_2CH_2CH_2Si$), 2.84 (t, 2H, $^{3}J_{H\text{-}H}$ = 8 Hz, $SSCH_2CH_2CH_2Si$), 3.53 (s, 9H, $Si(OCH_3)_3$), 7.11 (m, 1H, *py*-SS), 7.68 (m, 1H, *py*-SS), 7.77 (m, 1H, *py*-SS), 8.44 (m, 1H, *py*-SS). ^{13}C NMR (100 MHz, CD_2Cl_2) δ: 8.7, 22.8, 42.0, 50.7, 119.7, 120.9, 137.3, 149.9, 161.0.

2.4.13 Synthesis of N-(3-(triethoxysilyl)propyl)propriolamide: 6

The synthesis was adapted from Santoyo-Gonzalez *et al*.[48] N,N-Dicyclohexylcarbodiimide (DCC) was distilled under vacuum prior to use. 3-Aminopropyltriethoxysilane (2.55 mL, 10.8 mmol) and propiolic acid (0.75 mL, 12.4 mmol) were added to CH_2Cl_2 (40 mL) in a 100 mL round bottom flask and cooled in an ice bath. DCC was weighed (2.45 g, 11.8 mmol) into a 4 dram vial, dissolved into CH_2Cl_2 (10 mL) and added dropwise to the above solution. The reaction mixture was stirred for 2 h, filtered cold and the filtrate was concentrated under vacuum. The crude product was further purified by chromatography (3:1, 2:1, 1:1 Hexanes:EtOAc). Yield: 2.10 g (70 %). The spectra collected were in good agreement with literature reports.[48] ^{1}H NMR (400 MHz, $CDCl_3$) δ: 0.66 (t, 2H, $^{3}J_{H\text{-}H}$ = 8 Hz, $NHCH_2CH_2CH_2Si$), 1.25 (t, 9H, $^{3}J_{H\text{-}H}$ = 8 Hz, $SiOCH_2CH_3$), 1.68 (p, 2H, $^{3}J_{H\text{-}H}$ = 8 Hz, $NHCH_2CH_2CH_2Si$), 2.76 (s, 1H, CC*H*), 3.32 (q, 2H, $^{3}J_{H\text{-}H}$ = 8 Hz, $NHCH_2CH_2CH_2Si$), 3.84 (q, 6H, $^{3}J_{H\text{-}H}$ = 8 Hz, $SiOCH_2CH_3$), 6.38 (br s, 1H NH); ^{13}C NMR (100 MHz, $CDCl_3$) δ: 7.77, 18.2, 22.4, 42.1, 58.5, 72.8, 77.6, 152.2. HRMS (ESI^+) exact mass calculated for $[M+H]^+$ required m/z 274.1469 ($C_{12}H_{24}NO_4Si$), found m/z 274.1468.

2.4.14 Synthesis of N-isobutylpropiolamide: 7

DCC was distilled under vacuum prior to use. Iso-butylamine (1.10 mL, 10.8 mmol) and propiolic acid (0.75 mL, 12.4 mmol) were added to CH_2Cl_2 (15 mL) in a 50 mL round bottom flask fitted with a stir bar and cooled in an ice bath. DCC (2.45 g, 11.8 mmol) was weighed into a 4 dram vial, dissolved into CH_2Cl_2 (10 mL) and added dropwise to the above solution. The reaction mixture was stirred for 1 h, filtered cold and the filtrate was concentrated under vacuum. The crude product was further purified by chromatography (3:1 Hexanes:EtOAc). Yield: 800 mg (60 %). The ^{1}H NMR ratio of amide rotational isomers was >10:1. Major isomer ^{1}H NMR (300 MHz, $CDCl_3$) δ: 0.98 (d, 6H, $^3J_{H\text{-}H}$ = 7 Hz, $NHCH_2CH(CH_3)_2$), 1.84 (m, 1H, $NHCH_2CH(CH_3)_2$), 2.79 (s, 1H, CC*H*), 3.13 (t, 2H, $^3J_{H\text{-}H}$ = 7 Hz, $NHCH_2CH(CH_3)_2$), 6.19 (br s, 1H, $NHCH_2CH(CH_3)_2$); ^{13}C NMR (100 MHz, $CDCl_3$) δ: 20.0, 29.4, 47.2, 73.0, 77.4, 152.3. HRMS (TOF EI^+) exact mass calculated for [M^+] required *m/z* 125.0841 ($C_7H_{11}NO$), found *m/z* 125.0846.

2.4.15 Synthesis of 3-azopropyltriethoxysilane: N_3PTES: 8

The synthesis was adapted from Gupta *et al*.[49] To a 100 mL round bottom flask fitted with a stir bar and septum was added NaN_3 (1.10 g, 16.6 mmol), tetrabutylammonium bromide (640 mg, 2.0 mmol) and acetonitrile (50 mL). 3-Chloropropyltriethoxysilane (2.00 mL, 8.30 mmol) was added to the suspension via syringe. The reaction mixture was heated at 80 ºC for 18 h. The solvent was removed under reduced pressure and pentane (100 mL) was added to the residue which was filtered through Celite which was washed also washed with pentane (200 mL). The filtrate was concentrated under vacuum giving a clear oil. Yield: 1.45 g (70 %). The spectra were consistent with literature reports.[49] ^{1}H NMR (400 MHz, C_6D_6) δ: 0.67 (t, 2H, $^3J_{H\text{-}H}$ = 8 Hz, $N_3CH_2CH_2CH_2Si$), 1.25 (t, 9H, $^3J_{H\text{-}H}$ = 8 Hz, $Si(OCH_2CH_3)_3$), 1.68 (p, 2H, $^3J_{H\text{-}H}$ = 8 Hz, $N_3CH_2CH_2CH_2Si$), 3.85 (t, 6H, $^3J_{H\text{-}H}$ = 8 Hz, $Si(OCH_2CH_3)_3$).

2.4.16 Attempted cross linking of SBA-15-NH_2 and sTMS-SBA-NH_2

To two 4 dram vials equipped with stir bars was added either SBA-15-NH_2 (250 mg) or sTMS-SBA-15 (250 mg) which was dispersed in THF (5 ml). To the suspensions was added poly[(phenyl-isocyanate) co-formaldehyde] (85 mg) and the mixtures were stirred overnight. The silicas were recovered by filtration and washed with copious amounts of THF, Et_2O and hexanes and dried under vacuum at room temperature. The particle size distributions of the resulting powders were measured by laser diffraction on a Mastersizer 2000 particle size analyzer provided by Malverin instruments (**Figure A-3** and **Figure A-4** in **Appendix A**).

2.4.17 Synthesis of MPTMS Functionalized FloDots

The synthesis was adapted from Tam *et al*.[22] Cyclohexane (7.5 mL), hexanol (1.8 mL), triton 100-X (1.66 g), Millipore H_2O (340 µL) and tris (2,2′-bipyridyl)dichlororuthenium (II) (0.115M, 120 µL) were added to a 4 dram vial fitted with a stir bar. The suspension was stirred for 10 min followed by the addition of TEOS (100 µL) and after an additional 10 min 30 wt% NH_4OH (60 µL) was added. The emulsion was stirred vigorously overnight at room temperature after which an additional portion of TEOS (50 µL) was added. After 30 min 42 wt % aqueous sodium 3-(trihydroxysilyl)propylmethylphosphonate (35 mg) and MPTMS (4.5 µL) was added to the emulsion which was stirred vigorously overnight at room temperature. The emulsion was broken by addition of 95 % ethanol (25 mL) and transferred to a centrifuge tube. The solution was centrifuged on a KR25i Ultra Centrifuge at 20 000 g for 10 min, the supernatant was discarded and the pellet was washed with 95 % EtOH (2 × 25 mL) and H_2O (1 × 25 mL). The resulting pellet was dispersed in 95 % EtOH (15 mL) with sonication for 10 min and residual particulates

were removed by centrifugation IEC HN-SII Centrifuge for 10 min at 2600 rpm (800 g). The pellet was discarded and the supernatant was a FloDot stock solution.

2.4.18 Synthesis of N-(3-(triethoxysilyl)propyl)propriolamide functionalized FloDots

The synthesis was adapted Tam *et al*.[22] Cyclohexane (7.5 mL), hexanol (1.8 mL), triton 100-X (1.66 g), Millipore H_2O (340 μL) and tris(2,2′-bipyridyl)dichlororuthenium(II) (0.115M, 120 μL) were added to a 4 dram vial fitted with a stir bar. The suspension was stirred for 10 min followed by the addition of TEOS (100 μL) and after an additional 10 min 30 wt% NH_4OH (60 μL) was added. The emulsion was stirred vigorously overnight at room temperature after which an additional portion of TEOS (50 μL) was added. After 30 min 42 wt % aqueous sodium 3-(trihydroxysilyl)propylmethylphosphonate (35 mg) and *N*-((3-triethoxysilyl)propyl)propiolamide **6** (5 μL) was added to the emulsion which was stirred vigorously overnight at room temperature. The emulsion was broken by addition of 95 % ethanol (25 mL) and transferred to a centrifuge tube. The solution was centrifuged on a KR25i Ultra Centrifuge at 20 000 g for 10 min, the supernatant was discarded and the pellet was washed with 95 % EtOH (2 × 25 mL) and H_2O (1 × 25 mL). The resulting pellet was dispersed in 1:1 ^{t}BuOH:H_2O (15 mL) with sonication for 10 min and residual particulates were removed by centrifugation on a IEC HN-SII Centrifuge for 10 min at 2600 rpm (800 g). The pellet was discarded and the supernatant was a FloDot stock solution.

2.4.19 Synthesis of sodium 3-(trihydroxysilyl)propylmethylphosphonate functionalized FloDots

The synthesis was adapted from Tam *et al*.[22] Cyclohexane (7.5 mL), hexanol (1.8 mL), triton 100-X (1.66 g), Millipore H_2O (340 μL) and tris(2,2′-bipyridyl)dichlororuthenium(II) (0.115M, 120 μL) were added to a 4 dram vial fitted with a stir bar. The suspension was stirred for 10 min followed by the addition of TEOS (100 μL) and after an additional 10 min 30 wt% NH_4OH (60

μL) was added. The emulsion was stirred vigorously overnight at room temperature after which an additional portion of TEOS (50 μL) was added. After 30 min 42 wt % aqueous sodium 3-(trihydroxysilyl)propyl methylphosphonate (35 mg) was added to the emulsion which was stirred vigorously overnight at room temperature. The emulsion was broken by addition of 95 % ethanol (25 mL) and transferred to a centrifuge tube. The solution was centrifuged on a KR25i Ultra Centrifuge at 20 000 g for 10 min, the supernatant was discarded and the pellet was washed with 95 % EtOH (2 × 25 mL) and H_2O (1 × 25 mL). The resulting pellet was dispersed in 1:1 ^tBuOH:H_2O (15 mL) with sonication for 10 min and residual particulates were removed by centrifugation IEC HN-SII Centrifuge for 10 min at 2600 rpm (800 g). The pellet was discarded and the supernatant was a FloDot stock solution.

2.4.20 Attempted detection of selective grafting: General method for thiol-disulfide interchange between FloDots and (sTMS)-SBA-15-ss, or SiO_2-SS

To a 1 dram vial was added SBA-15-ss, sTMS-SBA-15-ss or SiO_2-SS (35 mg) and the material was dispersed in 5:1 EtOH:NEt_3 (2 mL). To the suspension was added MPTMS functionalized FloDots (0.2 mL) from the EtOH stock solution. The suspension was sonicated for 10 min and the silicas were allowed to settle overnight. After washing with EtOH and H_2O both SBA-15-ss and sTMS-SBA-15 appeared similarly fluorescent under a UV lamp and the approach abandoned.

2.4.21 General method for the conversion of (sTMS)-SBA-15-Cl, (sTMS)-MCM-41-Cl, or SiO_2-Cl to (sTMS)-SBA-15-N_3, sTMS-MCM-41-N_3, or SiO_2-N_3

In a typical procedure, to a 25 mL round bottom flask fitted with a stir bar and septum was added SBA-15-Cl, sTMS-SBA-15-Cl, MCM-41-Cl, sTMS-MCM-41-Cl, or SiO_2-Cl (220 mg) and DMF (12 mL). To the suspension was added NaN_3 (44 mg) and the reaction mixture was stirred at 90 ^oC for 2 h. The suspension was filtered and washed with 95 % ethanol (10 mL) and H_2O (10 mL).

The recovered material was dispersed in H_2O (10 mL), stirred for 1 h and filtered again. The powder was washed with hexanes (10 mL) and dried under vacuum at 80 ºC. The procedure furnished 170 mg of material; see **Figure 2-11** for a representative IR spectrum (N_3 = 2108 cm^{-1}) of the recovered material and **Figure 2-10** for a spectral overlay that suggests that only a portion of the chloropropyl groups on the parent material are converted to azide.

2.4.22 Evaluating the AAC reaction conditions: reaction of N-isobutylpropiolamide with SiO_2-N_3

$Cu(SO_4)$ stock solution

$CuSO_4$•5 H_2O (5 mg, 0.02 mmol) was weighed and dissolved in distilled H_2O (1 mL). Ascorbic acid (14 mg, 0.08 mmol) and KOH (4 mg, 0.08 mmol) was weighed and dissolved in distilled H_2O (1.5 mL). To the ascorbate solution was added ^{t}BuOH (2.5 mL). The ascorbate solution was added to the Cu solution. On addition, the color of the Cu solution changed from clear blue to a turbid yellow.

AAC reaction and Control

Into two 4 dram vials (A and B) were weighed SiO_2-N_3 (35 mg) and *N*-isobutylpropiolamide **7** (125 mg, 1.00 mmol). To vial A was added 1:1 ^{t}BuOH:H_2O (2.5 mL) and the $CuSO_4$ stock solution (2.5 mL). To vial B was added 1:1 ^{t}BuOH:H_2O (5.0 mL). Both vials were shaken to disperse silica and the materials were allowed to settle overnight. The powders were recovered by filtration and were washed with H_2O (10 mL), EtOH (10 mL) and Et_2O (10 mL). The procedure furnished 25 mg of material, see **Figure 2-11** for representative FT-IR spectra that showed the azide stretch disappeared when the reaction was carried out in the presence of Cu.

2.4.23 Attempted detection of selective grafting: General method for AAC reaction between FloDots and (sTMS)-SBA-15-N_3, (sTMS)-MCM-41-N_3 or SiO_2-N_3

Note: All materials were silylated with HMDS as described for SBA-15, MCM-41 and SiO_2 immediately prior to use in this screening procedure. Failure to do so, will lead to large amounts of non-specific adsorption. Also, the screens were performed in a N_2 glove bag that was purged for 30 min.

Cu(SO_4) stock solution

$CuSO_4$•5 H_2O (10 mg, 0.02 mmol) was weighed and dissolved in distilled H_2O (2.5 mL). Ascorbic acid (38 mg, 0.20 mmol) and KOH (10 mg, 0.20 mmol) was weighed and dissolved in distilled H_2O (2.5 mL). To the ascorbate solution was added ^{t}BuOH (5 mL). The ascorbate solution was added to the Cu solution. On addition the color of the Cu solution changed from clear blue to a turbid yellow.

AAC reactions and Controls using SBA-15 or MCM-41 as an example

Into six 4 dram vials (A-F) was weighed different SBA-15 or MCM-41 materials (35 mg) as noted in **Table 2-5**. To vial A-C was added 1:1 ^{t}BuOH:H_2O (2.0 mL), the FloDot stock solution (0.5 mL) and the $CuSO_4$ stock solution (2.5 mL). To vials D-F was added 1:1 ^{t}BuOH:H_2O (4.5 mL) and the FloDot stock (0.5 mL). All vials were shaken to disperse silica and the materials were allowed to settle overnight. The solutions were centrifuged with an IEC HN-SII Centrifuge for 5 min at 2600 rpm (800 g) and the supernatant was discarded. To desorb weakly bound FloDots the pellets were treated with CTAB (150 mg) and 4:1 H_2O:EtOH (3 mL) and the suspension was heated to dissolve the surfactant after which the vial was filled with H_2O. The suspension was centrifuged again and the pellet was washed using the same procedure two twice after which the pellet was washed in a similar manner with a 10 wt% EDTA solution. The silica was recovered by filtration and washed with copious quantities of H_2O, 95 % EtOH and Hexanes.

This procedure furnished 25 mg of material. The fluorescence spectra of the materials were collected by stirring the sample and by setting the excitation wavelength at λ_{ex} = 450 nm and the emission range at λ_{em} = 500 – 700 nm with a step size and residence time of 0.5 nm and 1 sec respectively. For each analysis, 5 mg of silica was weighed and transferred to a quartz cuvette (10 mm) fitted with a stir bar, and the silica was dispersed in DMF (3.5 mL). For representative results see **Figure 2-12** and **Figure 2-13**.

Table 2-5. SBA-15 and MCM-41 materials employed in an AAC selective grafting screen

Vial	Material	
	SBA-15	MCM-41
A	SBA-15-N_3	MCM-41-N_3
B	sTMS-SBA-15-N_3	sTMS-MCM-41-N_3
C	TMS-SBA-15	TMS-MCM-41
D	SBA-15-N_3	MCM-41-N_3
E	sTMS-SBA-15-N_3	sTMS-MCM-41-N_3
F	TMS-SBA-15	TMS-MCM-41

2.4.24 Attempted detection of selective grafting: General method for the differential adsorption of FloDots onto (sTMS)-SBA-15 or (sTMS)-MCM-41

Into three 4 dram vials (A-C) was weighed different SBA-15 or MCM-41 materials (35 mg) as noted in **Table 2-6**. To the vials A-C was added 1:1 ^{t}BuOH:H_2O (4.5 mL) and the FloDot stock solution (0.5 mL). All vials were shaken to disperse silica and the materials were allowed to settle overnight. The solutions were centrifuged IEC HN-SII Centrifuge for 5 min at 2600 rpm (800 g) and the supernatant was discarded. To desorb weakly bound FloDots the pellets were treated with CTAB (150 mg) and 4:1 H_2O:EtOH (2 mL) and the resulting suspension heated to dissolve the surfactant after which the vial was filled with H_2O. The silica was recovered by filtration and

washed with copious quantities of H_2O, 95 % EtOH and Hexanes. This procedure furnished 25 mg of material. The fluorescence spectra of the materials were collected by stirring the sample and by setting the excitation wavelength at λ_{ex} = 450 nm and the emission range at λ_{em} = 500 – 700 nm with a step size and residence time of 0.5 nm and 1 sec respectively. For each analysis 5 mg of silica was weighed and transferred to a quartz cuvette (10 mm) fitted with a stir bar, and the silica was dispersed in DMF (3.5 mL). For representative results see **Figure 2-17**, **Figure 2-18** and **Figure 2-19**.

Table 2-6. SBA-15 and MCM-41 materials employed in an FloDot adsorption selective grafting screen

Vial	Material	
	SBA-15	MCM-41
A	SBA-15	MCM-41
B	sTMS-SBA-15	sTMS-MCM-41
C	TMS-SBA-15	TMS-MCM-41

2.4.25 Reaction of pyrene-maleimide with SBA-15-SH: SBA-15-SH-pyrene

To a 10.00 mL volumetric flask was added pyrene-maleimide (3 mg, 0.01 mmol) which was diluted up to 10.00 mL using ketyl distilled THF to give a 1 mM solution. To a 1 dram vial was added SBA-15-SH (50 mg, 0.06 mmol S at 1.2 mmol S/g) which was suspended in THF (1 mL). To the suspension was added 1 mL of the pyrene-maleimide (0.001 mmol pyrene) stock solution. After which NEt_3 (50 μL) was added to the silica suspension. The reaction mixture was allowed to stand overnight at room temperature and the solution was decanted. The material was recovered by filtration and washed with copious amounts of THF and hexanes. The material was dried under vacuum at room temperature. The fluorescence spectra of the materials were

collected by stirring the sample and by setting the excitation wavelength at λ_{ex} = 330 nm and the emission range at λ_{em} = 350 – 600 nm with a step size and residence time of 0.5 nm and 1 sec respectively. For the analysis 3 mg of silica was weighed in a 4 dram vial and was suspended in DMF (10.0 mL). A portion (0.5 mL) of the silica solution was transferred to a quartz cuvette (10 mm) fitted with a stir bar, and the suspension was diluted to 3.5 mL with DMF. See **Figure 2-20** for a representative collected a spectrum that consistent with monomeric pyrene emission.

2.5 References

(1) Hoffmann, F.; Cornelius, M.; Morell, J.; Fröba, M. *Angew. Chem. Int. Ed.* **2006**, *45*, 3216-3251.

(2) Stein, A.; Melde, B. J.; Schroden, R. C. *Adv. Mater.* **2000**, *12*, 1403-1419.

(3) Asefa, T.; Lennox, R. B. *Chem. Mater.* **2005**, *17*, 2481-2483.

(4) Xie, Y.; Quinlivan, S.; Asefa, T. *J. Phys. Chem. C* **2008**, *112*, 9996-10003.

(5) Sun, J.; Ma, D.; Zhang, H.; Liu, X.; Han, X.; Bao, X.; Weinberg, G.; Pfänder, N.; Su, D. *J. Am. Chem. Soc.* **2006**, *128*, 15756-15764.

(6) Shephard, D. S.; Zhou, W.; Maschmeyer, T.; Matters, J. M.; Roper, C. L.; Parsons, S.; Johnson, B. F. G.; Duer, M. J. *Angew. Chem. Int. Ed.* **1998**, *37*, 2719-2723.

(7) Gartmann, N.; Brühwiler, D. *Angew. Chem. Int. Ed.* **2009**, *48*, 6354-6356.

(8) de Juan, F.; Ruiz-Hitzky, E. *Adv. Mater.* **2000**, *12*, 430-432.

(9) Zhang, Z.; Dai, S.; Blom, D. A.; Shen, J. *Chem. Mater.* **2002**, *14*, 965-968.

(10) Lin, D.; Jiang, Y.; Wang, Y.; Sun, S. *J. Nanomater.* **2008**, 473791.

(11) Huang, X.; Yang, M.; Wang, G.; Zhang, X. *Microporous Mesoporous Mater.* **2011**, *144*, 171-175.

(12) Sing, K. S. W.; Everett, D. H.; Haul, R. A. W.; Moscou, L.; Pierotti, R. A.; Rouquerol, J.; Siemieniewska, T. *Pure Appl. Chem.* **1985**, *57*, 603-19.

(13) Thomas, J. M.; Maschmeyer, T.; Johnson, B. F. G.; Shephard, D. S. *J. Mol. Catal. A.* **1999**, *141*, 139-144.

(14) Lu, A.; Li, W.; Kiefer, A.; Schmidt, W.; Bill, E.; Fink, G.; Schüth, F. *J. Am. Chem. Soc.* **2004**, *126*, 8616-8617.

(15) Blümel, J. *J. Am. Chem. Soc.* **1995**, *117*, 2112-2113.

(16) Lang, N.; Tuel, A. *Chem. Mater.* **2004**, *16*, 1961-1966.

(17) Rebek, J.; Gavina, F. *J. Am. Chem. Soc.* **1974**, *96*, 7112-14.

(18) Rebek, J.; Brown, D.; Zimmerman, S. *J. Am. Chem. Soc.* **1975**, *97*, 454-5.

(19) Sharma, K. K.; Anan, A.; Buckley, R. P.; Ouellette, W.; Asefa, T. *J. Am. Chem. Soc.* **2008**, *130*, 218-228.

(20) Brühwiler, D. *Nanoscale* **2010**, *2*, 887-892.

(21) Yao, G.; Wang, L.; Wu, Y.; Smith, J.; Xu, J.; Zhao, W.; Lee, E.; Tan, W. *Anal. Biochem. Chem.* **2006**, *385*, 518-524.

(22) Bagwe, R. P.; Hilliard, L. R.; Tan, W. *Langmuir* **2006**, *22*, 4357-4362.

(23) Bagwe, R. P.; Yang, C.; Hilliard, L. R.; Tan, W. *Langmuir* **2004**, *20*, 8336-8342.

(24) Zhao, X.; Bagwe, R. P.; Tan, W. *Adv. Mater.* **2004**, *16*, 173-176.

(25) Sigma Aldrich, *Product Information Triton X-100* [http://www.sigmaaldrich.com/etc/medialib/docs/Sigma/Product_Information_Sheet/1/t8532pis.Par.0001.File.tmp/t8532pis.pdf] Retrieved: 06/27/2011.

(26) Hilliard, L. R.; Zhao, X.; Tan, W. *Anal. Chim. Acta* **2002**, *470*, 51-56.

(27) Dufaud, V.; Davis, M. E. *J. Am. Chem. Soc.* **2003**, *125*, 9403-9413.

(28) Tornøe, C. W.; Christensen, C.; Meldal, M. *J. Org. Chem.* **2002**, *67*, 3057-3064.

(29) Rostovtsev, V. V.; Green, L. G.; Fokin, V. V.; Sharpless, K. B. *Angew. Chem. Int. Ed.* **2002**, *41*, 2596-2599.

(30) Kolb, H. C.; Finn, M. G.; Sharpless, K. B. *Angew. Chem. Int. Ed.* **2001**, *40*, 2004-2021.

(31) Binder, W. H.; Kluger, C. *Curr. Org. Chem.* **2006**, *10*, 1791-1815.

(32) Guan, B.; Ciampi, S.; Le Saux, G.; Gaus, K.; Reece, P. J.; Gooding, J. J. *Langmuir* **2011**, *27*, 328-334.

(33) Nakazawa, J.; Stack, T.,Daniel P. *J. Am. Chem. Soc.* **2008**, *130*, 14360-14361.

(34) Ortega-Munoz, M.; Lopez-Jaramillo, J.; Hernandez-Mateo, F.; Santoyo-Gonzalez, F. *Adv. Synth. Catal.* **2006**, *348*, 2410-2420.

(35) Schlossbauer, A.; Schaffert, D.; Kecht, J.; Wagner, E.; Bein, T. *J. Am. Chem. Soc.* **2008**, *130*, 12558-12559.

(36) Hudson, S.; Cooney, J.; Magner, E. *Angew. Chem. Int. Ed.* **2008**, *47*, 8582-8594.

(37) Webb, J. D.; MacQuarrie, S.; McEleney, K.; Crudden, C. M. *J. Catal.* **2007**, *252*, 97-109.

(38) Glasspoole, B. W.; Webb, J. D.; Crudden, C. M. *J. Catal.* **2009**, *265*, 148-154.

(39) Beller, M.; Fischer, H.; Herrmann, W. A.; Oefele, K.; Brossmer, C. *Angew. Chem. Int. Ed. Engl.* **1995**, *34*, 1848-9.

(40) Zhao, X. S.; Lu, G. Q.; Whittaker, A. K.; Millar, G. J.; Zhu, H. Y. *J. Phys. Chem. B* **1997**, *101*, 6525-6531.

(41) Fousseret, B.; Mougenot, M.; Rossignol, F.; Baumard, J.; Soulestin, B.; Boissière, C.; Ribot, F.; Jalabert, D.; Carrion, C.; Sanchez, C.; Lejeune, M. *Chem. Mater.* **2010**, *22*, 3875-3883.

(42) Jana, N. R.; Gearheart, L.; Murphy, C. J. *Langmuir* **2001**, *17*, 6782-6786.

(43) Cheng, K.; Landry, C. C. *J. Am. Chem. Soc.* **2007**, *129*, 9674-9685.

(44) Brunauer, S.; Emmett, P. H.; Teller, E. *J. Am. Chem. Soc.* **1938**, *60*, 309-319.

(45) Barrett, E. P.; Joyner, L. G.; Halenda, P. P. *J. Am. Chem. Soc.* **1951**, *73*, 373-380.

(46) Zhao, D.; Huo, Q.; Feng, J.; Chmelka, B. F.; Stucky, G. D. *J. Am. Chem. Soc.* **1998**, *120*, 6024-6036.

(47) Beck, J. S.; Vartuli, J. C.; Roth, W. J.; Leonowicz, M. E.; Kresge, C. T.; Schmitt, K. D.; Chu, C. T. W.; Olson, D. H.; Sheppard, E. W. *J. Am. Chem. Soc.* **1992**, *114*, 10834-10843.

(48) Ortega-Munoz, M.; Lopez-Jaramillo, J.; Hernandez-Mateo, F.; Santoyo-Gonzalez, F. *Adv. Synth. Catal.* **2006**, *348*, 2410-2420.

(49) Malvi, B.; Sarkar, B. R.; Pati, D.; Mathew, R.; Ajithkumar, T. G.; Gupta, S. S. *J. Mater. Chem.* **2009**, *19*, 1409-1416.

Chapter 3

Palladium Immobilized on SBA-15 as a Suzuki-Miyaura Catalyst

3.1 Introduction

3.1.1 Suzuki-Miyaura Cross-Coupling and Supported Pd Complexes

Cross-coupling describes a subset of metal catalyzed reactions that involve the formation of a new bond between two different organic fragments. The literature in this field is extensive and this discussion will be focused primarily on the Suzuki-Miyaura reaction, which is the metal catalyzed coupling of a C-X fragment with a C-BY_2 fragment to yield a new C-C bond (**Scheme 3-1**).[1] Aryl or vinyl groups are the most commonly employed organic fragments coupled, although significant advances in the use of alkyl substrates have been reported recently.[2-6] The X groups are typically I, OTf, Br or Cl (listed their approximate order of reactivity). The BY_2 structural motif is also highly variable; among the more popular functional groups employed are boronic acids, esters or trifluoroborate salts.[1, 7] The seminal publications of the Suzuki-Miyaura reaction[8, 9] appeared in 1979 and development over the last 3 decades has made the reaction an indispensible tool in synthetic chemistry, which was reflected by the award of the 2010 Nobel Prize in Chemistry to Akira Suzuki.[10]

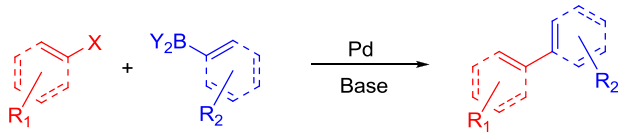

Scheme 3-1. General depiction of the Suzuki-Miyaura reaction

The Suzuki-Miyaura reaction has seen wide spread application in the pharmaceutical industry owed to the relatively low toxicity of organo-boron reagents, broad substrate scope,

selectivity and functional group tolerance.[11-13] An example of a drug substance whose synthesis involves the use of a Suzuki-Miyaura reaction is Losartan (**Scheme 3-2**),[14] which is an angiotensin II receptor antagonist prescribed to treat hypertension.

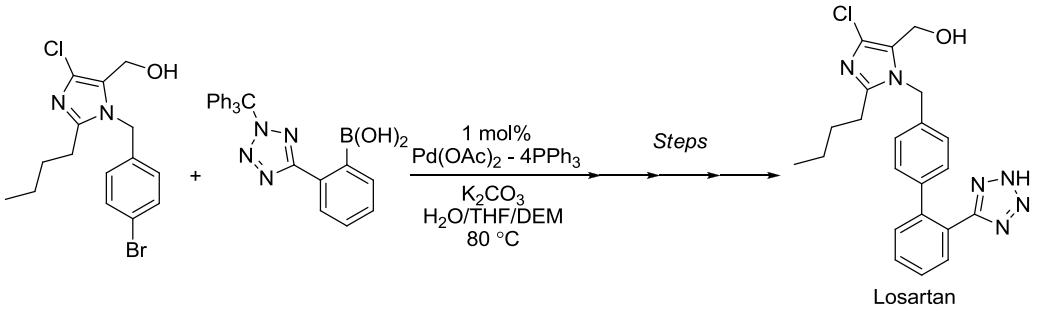

Scheme 3-2. Synthesis of Losartan

The Suzuki-Miyaura reaction also allows the biaryl motif present in agrochemicals and pharmaceutical agents[11, 13, 15] to be constructed in a single step. Compared to laborious and wasteful strategies which do not rely on catalysis, this approach is remarkably efficient. The synthesis of the pharmaceutical agent Valsartan can be used as an example of how the Suzuki-Miyaura reaction can reduce synthetic complexity. Using the Suzuki-Miyaura reaction, the biaryl core of Valsartan is constructed in one step, whereas an alternative approach without a cross-coupling reaction would require 5 steps (**Scheme 3-3**).[16-18]

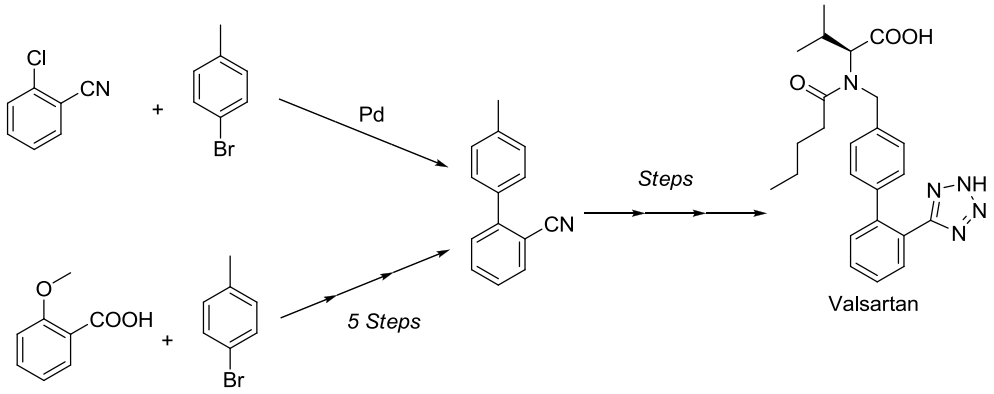

Scheme 3-3. General synthetic routes to Valsartan

On an industrial scale, the challenge with the Suzuki-Miyaura reaction and other palladium mediated processes is remediation of the spent metal catalyst from the product.[15, 19, 20] Effective remediation strategies are important, particularly in the pharmaceutical industry, because the concentration of Pd in crude reaction products can exceed 1000 ppm.[19] Compared to the loose guideline of 10 ppm for the total Pt group content in a pharmaceutical agent, this number is obviously untenable.[11, 19, 20] Currently there are no specific guidelines for the total Pd content permissible in a pharmaceutical agent since the daily dose of the pharmaceutical agent will affect the level of Pd that is permissible (i.e. higher dosage drugs will have lower overall heavy metal tolerance numbers than low dose drugs). However, it is worth noting that these guidelines are meant to err on the side of caution since the effects of biological exposure to the metal are not well understood and all available data points to low levels of toxicity if any.[11, 19, 20]

There are several approaches to metal remediation.[19] Distillation, for example, can be effective in some cases but is limited to compounds with low boiling points and those which do not possess structural motifs that can isomerize. Crystallization can be used as well; the challenge is to find conditions that keep Pd in solution while the product precipitates. Additives may be

added to solution to increase the solubility of Pd, such that it will not incorporate into the product as it crystallizes.[19] The use of additives in purification is exemplified in the synthesis of Losartan, the addition of 10 mol% tributylphosphine to the organic layer prior to crystallization reduces the Pd content in the product to less than <50 ppm.[14] Alternatively, the synthesis of a drug substance may be modified to move the coupling reaction to an earlier point in the synthesis with the hope that the subsequent purification steps will lower the Pd content to acceptable levels.[19]

Another approach to Pd remediation involves the addition of adsorbents also termed scavengers.[19, 21, 22] These materials, which adsorb Pd, are added to a solution containing the contaminated product. After adsorption of Pd, the scavenger is filtered away; thus useful scavengers must have desirable filtration properties. Several different types of scavengers have been employed for Pd remediation and include; trimercaptotriazine, activated carbons, functionalized polystyrene beads and silicas. An example of the successful application of the scavenger approach would be in the synthesis of the active pharmaceutical agent, E2040 (**Scheme 3-4**).[23] After the coupling step, the polystyrene bound amine DIAION^{TM} CR20 was added to the crude product and it was able to reduce the Pd content from 2000 – 3000 ppm to < 10 ppm. The purified intermediate was then carried onto E2040 which had acceptable levels of residual Pd.

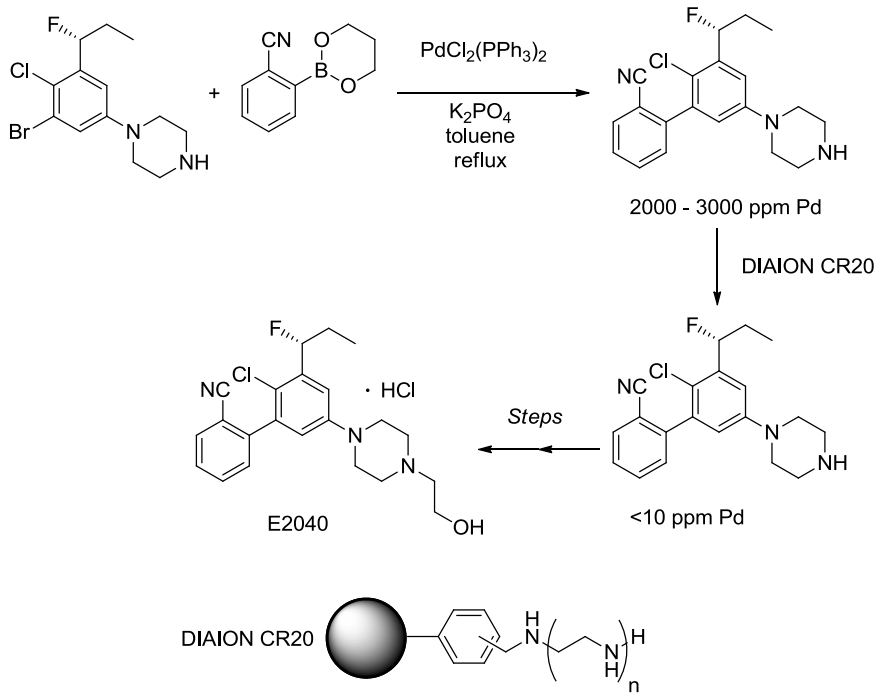

Scheme 3-4. Application of DIAION^{TM} CR20 in the synthesis of E2040

An alternative to remediation of spent homogeneous Pd catalysts from products is to immobilize them prior to reaction.[24-27] In this way, ideally large amounts of the metal would never become incorporated into the reaction products and therefore would not require remediation. With little to no measurable amounts of Pd in the product, the metal could then be removed easily by a filtration step, if the metal was immobilized on support, or by extraction, if the metal was immobilized in an immiscible solvent. Both approaches would obviate or reduce the need for additional metal scavenging. Another advantage of an immobilized catalyst is the recovered material may be reusable.

As with scavenging, immobilizing Pd catalysts is an active field of research and there are a number of strategies that have been reported in the literature. The field is vast and has been

aptly reviewed by a number of groups.[24-27] For expediency the following discussion will summarize the different approaches for immobilizing Pd onto a solid support and the examples highlighted will illustrate the general utility of each strategy. The field of solid phase immobilization will be subdivided into three broad classes of supported Pd catalysts: Class I, immobilized Pd particles, Class II, immobilized Pd complexes and Class III, immobilized Pd onto functional materials.

Class I catalysts represent the simplest way of immobilizing Pd and the approach involves adsorption of the metal or nanoparticles onto an unfunctionalized support such as an inorganic oxide, carbon or silica.[24] After the metal is adsorbed onto the support a second processing step is typically used to convert/reduce the adsorbed metal into particles. An illustrative example of this is Pd/C which is a readily available inexpensive source of Pd. An organic syntheses[28] procedure outlines the preparation of Pd/C which can be generated by adsorption of $PdCl_2$ onto activated carbon and followed by reduction with formaldehyde or under an atmosphere of hydrogen.

The first use of Pd/C as a catalyst for the Suzuki-Miyaura reaction was reported by Marck in 1994.[29] This publication and others[30] have demonstrated the general usefulness of this material for the Suzuki-Miyaura reaction. It is noteworthy that aryl-I, Br, Cl and OTf reagents can all act as substrates, although high yields with aryl-Cl's are typically only achieved after the addition of ligands. While the activity of Pd/C is impressive, some drawbacks are common to this class of immobilized catalyst. Namely, the weak nature of the binding of Pd to the unfunctionalized supports results in significant amounts of leaching into products.[30] Furthermore, these catalysts often display poor recyclability ascribed to agglomeration of Pd, i.e. formation of

Pd-black.[30] There is also an inverse relationship between Pd nanoparticle size and activity toward the Suzuki-Reaction.[31]

The properties of Class I catalysts can be improved by impregnating Pd within porous supports such as polymers, mesoporous silicas or zeolites for which there are many examples.[24] The role of the pore structure of a support is to limit particle size and reduce agglomeration. For example 5 – 10 nm Pd nanoparticles were immobilized within SBA-15 by adding $PdCl_2$ during the sol-gel synthesis step and reducing the recovered material under a stream of hydrogen gas.[32] The nanoparticles had similar dimensionality to the pores of the material. The impregnated Pd-SBA-15 was shown to be a recyclable catalyst with an average yield of 98 (95 – 99)% after 5 runs at a 0.2 mol% loading. Unfortunately, no data was provided as to leaching and the stability of the pore network on recycling, [32] an issue we deem important. Stability of the support to the Suzuki-Miyaura reaction conditions is a consideration which is often overlooked in catalytic studies but is important as will be seen in the Results and Discussion.

More recently Durap[33] reported an example of Pd impregnated zeolite-Y (Pd-Y) in which, the Pd was confined to the void spaces in the pore structure. The surprising characteristic of their material was that it had activity at room temperature for the coupling of boronic acids with aryl bromides. This result is interesting as most supported catalysts for the Suzuki reaction are not active except at elevated temperatures. Leaching was reported to be minimal based on ICP-AES studies of used catalysts. Pd-Y was recyclable, with average yield of 91 (98 – 81) % over 15 runs.

While the former example is clearly exceptional, Class II materials are the more commonly seen type of supported catalyst for the Suzuki-Miyaura reaction. Typical palladium ligand architectures are represented in Class II materials including phosphines,[34, 35] carbenes,[36]

pincers,[37] and palladacycles.[38, 39] There are two ways to generate immobilized Pd complexes: pre-synthesize the complex and graft it onto support or immobilize a designer ligand onto support and treat the material with Pd.[24, 25] Research in this field is diverse but can be exemplified by the work of García.[39] In their work, palladacycle **cat-1** was synthesized and immobilized onto a variety of supports including two polymers, polystyrene and polyacrylate, and two inorganic oxides, MCM-41 and amorphous SiO_2 (**Scheme 3-5**). The catalysts generated were all active towards the Suzuki-Miyaura reaction, and couplings with Ar-Br and Ar-Cl substrates were reported. They highlighted that under aqueous conditions **cat-1**-MCM-41 and **cat-1**-SiO_2 were significantly more active than their polymeric counterparts. **cat-1**-MCM-41 was recyclable with an average yields >99 % over 8 runs with minimal leaching. Even though the leaching was low, detailed studies of this and related systems have established that the catalyst functions by decomposition of the Pd complex to nanoparticles or "homogeneous Pd". The mechanism of action of supported Pd catalysts will be discussed later on.

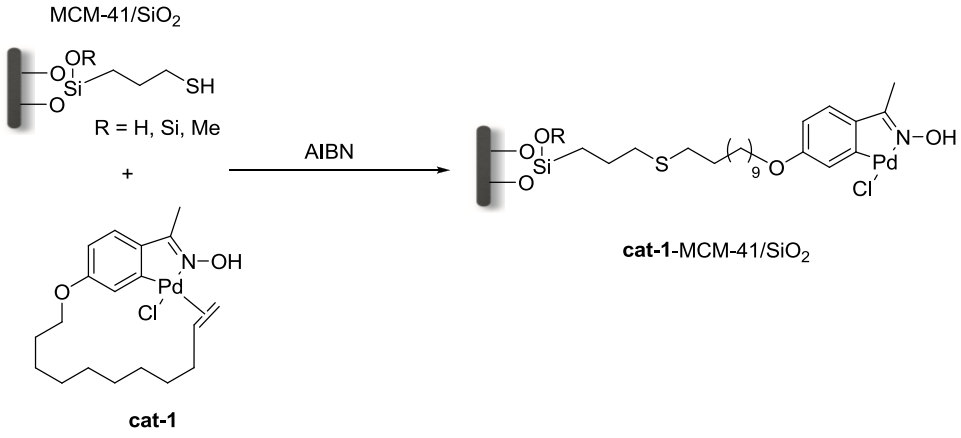

Scheme 3-5. An example of a Class II catalyst which were reported by García from reference 39

While many of these Class II materials are highly active, and recyclable with low leaching there are still drawbacks to this approach of immobilization.[24, 25] As indicated by the work of García[39] the ligand and/or the complex must be pre-synthesized. This adds cost to resulting supported catalyst. Moreover, as will be discussed in the next subsection, the vast majority of supported Pd catalysts for cross-coupling reactions operate as a reservoir for a homogeneous active metal species, including **cat-1**-MCM-41,[39] begging the question as to the usefulness of this approach. If the supported complex is going to decompose and is not the active catalyst in reaction, the wisdom of synthesizing designer ligands is questionable, especially if there are more cost effective alternatives.

Class III Pd loaded catalysts sit somewhere between those in Class I or Class II.[24] They are generated by adsorption of nanoparticles or a readily available Pd source onto a functional material. Class III catalysts differ from those in Class II, in that the functionality on support is readily available from commercial sources. Again all the standard support classes are represented. It should be noted that the supports for Class III materials can double as effective metal scavengers for Pd.[40, 41] The effectiveness of Class III materials at preventing leaching and agglomeration is somewhat related to the strength of interaction of Pd with the supported functionality.[42] As will be seen in the Results and Discussion, thiols can ensure leaching levels of < 0.1 % of the initially added Pd. A representative example of a Class III material is the commerically available catalyst PdEnCat. Developed by Ley,[43] PdEnCat composed of Pd loaded, sometimes along with phosphine ligands such as PPh_3 or BINAP, in a polyurea matrix. PdEnCat materials are active catalysts for the Suzuki-Miyaura reaction with leaching levels in the low ppm range.[44]

Another type of Class III material is Pd loaded mercaptopropyl modified mesoporous silicas described by our group,[40, 45-49] Shimizu,[50] and Jones.[51] These materials have been shown to be active catalysts for the Suzuki-Miyaura reaction among other cross-couplings reactions, which are recyclable and react with low levels of leaching. This class of material will be the focus of work presented in the Results and Discussion. Collectively, these materials illustrate an elegant approach to immobilizing Pd. The mercaptopropyl ligand is commerically available and inexpensive; the same cannot be said for many of ligands used in the Class II materials discussed above. While the Pd-EnCat,[43] has a similar advantages to the thiol loaded materials, the distinct advantage of our strategy over this commercial alternative is the extremely low level of leaching (<1 ppm).

3.1.2 Heterogeneity or Homogeneity of Supported Cross-coupling Catalysts

There has been much attention paid to the nature of the active species in cross-coupling reactions catalyzed by supported Pd catalysts.[25, 31, 42, 52] At issue is the question: are these heterogeneous catalysts truly heterogeneous? After much debate the consensus is these materials are reservoirs for an active soluble molecular palladium catalyst. There are still a few research groups claiming to have developed truly heterogeneous Pd cross-coupling catalysts.[53, 54] However, these researchers are in the minority in this field and their results are often ambiguous and/or inconclusive. As a general rule it does not matter whether the metal loaded on support is initially in Pd^{2+} or Pd^{0} oxidation states or in nanoparticle form, a homogeneous catalyst will universally result.[25, 31, 42, 52] As far as this discussion is concerned a homogeneous catalyst is defined as a soluble species with a single active site and a heterogeneous catalyst is an insoluble species, such as metal supported on a material. These definitions are consistent with and were

adapted from publications devoted to the discussion of distinguishing between homogeneous and heterogeneous catalysis.[55]

The proposed mechanism for the Suzuki-Miyaura reaction carried out with a supported catalyst has been characterized as being boomerang like (**Scheme 3-6**).[30, 56] The metal is leached from support into solution upon oxidative addition of the aryl-halide, hence the support being referred to as a reservoir.[57] The soluble metal complex then enters a typical cross-coupling catalytic cycle and undergoes transmetallation and reductive elimination forming product and a Pd^0 species. The metal then undergoes anyone of the following processes: re-enters the catalytic cycle, agglomeration and/or re-deposition onto the support, which completes the boomerang.

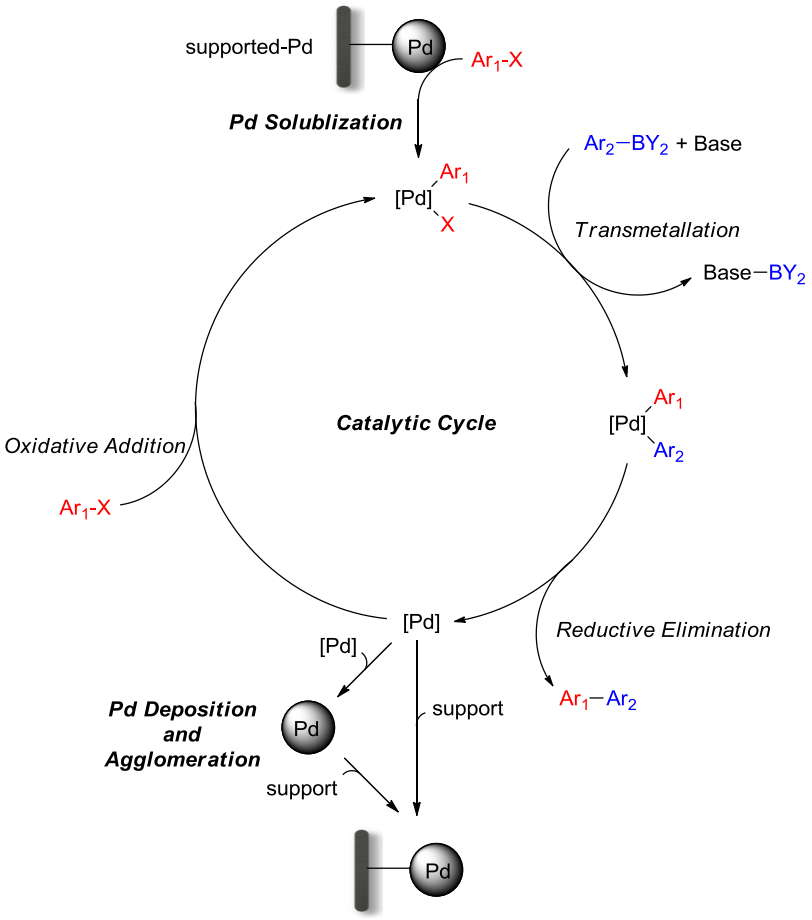

Scheme 3-6. Proposed mechanism for the Suzuki-Miyaura reaction with an immobilized catalyst

The evidence in support of the proposed mechanism has come from studies that examined the leaching of Pd, as well as others that have applied a variety of heterogeneity tests.[25, 31, 42, 52] With regard to leaching, it has been shown for example with Pd/C that the concentration of Pd increases in solution, as measured by ICP-MS, during reaction and the metal re-deposits on support once the aryl-halide has been consumed (**Figure 3-1**).[58] Our group[57] also demonstrated an aryl-halide effect on Pd foil under Suzuki-Miyaura conditions. We found that pitting of the foil

only occurred on the portion that was heated above 80 °C and furthermore that the leached Pd eventually re-deposited onto cooler areas of the surface not far from the reactive zone. The pitting and re-deposition was characterized by scanning electron microscopy (SEM) and X-ray photoelectron spectroscopy (XPS) and control reactions indicated that it only occurred in the presence of aryl-halide. Also, there have been studies focused on understanding leaching from immobilized Pd nanoparticles which have shown that it occurs from surface defect sites.[31] More evidence in support of the boomerang mechanism which was acquired from performing common heterogeneity tests will be discussed below alongside brief descriptions of these tests.

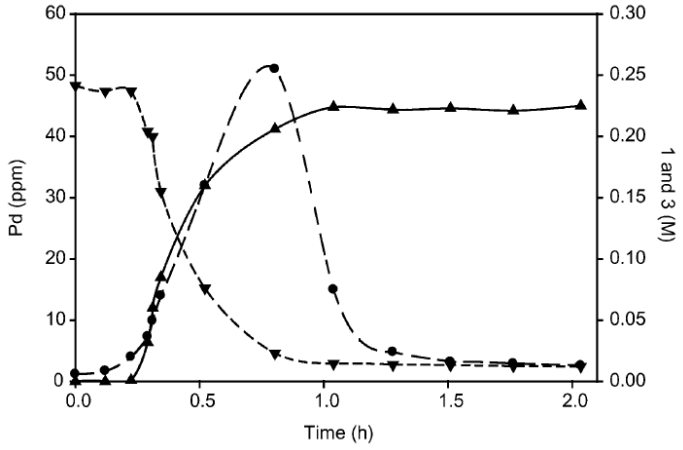

Figure 3-1. A Reaction Profile for a Pd/C Catalyzed Suzuki-Miyaura Reaction, aryl bromide (inverted triangle), biaryl product (triangle) and soluble Pd (circle), reproduced from reference 58 with permission

3.1.3 Heterogeneity Tests

TEM and pXRD Studies

Analyzing a recovered supported catalyst by transmission electron microscopy (TEM) and powder X-ray diffraction (pXRD) is a good way to begin the assessment of catalyst homogeneity or heterogeneity. It is common to observe Pd nanoparticles on supported catalysts after use in a coupling reaction.[24, 25, 52] Observation of particles/nanoparticles in these ways can provide good initial evidence that a heterogeneous species may be involved at some point on the reaction pathway.[55] It is important to note that observation of particles in this manner does not provide information regarding their catalytic competence. In addition the absence of nanoparticles is also insufficient to conclusively rule out the possibility of a heterogeneous reaction pathway, as the particles may be too small and/or too dilute to be detected easily. While TEM and pXRD studies are a good first step in a mechanistic study, they are also ambiguous in the absence of other data.[55]

Kinetic Analysis

Catalysis is a kinetic phenomenon and analysis of reaction profiles can provide critical information regarding the nature of the active catalyst.[55] The data obtained from reaction profiles are best corroborated with information gleaned from TEM and pXRD studies.[55] In regard to coupling reactions catalyzed by immobilized Pd, reaction profiles often exhibit induction periods (**Figure 3-1**).[58] Induction periods reflect the time required to generate the active catalyst, and are often related to breakdown of metal-ligand bonds necessary to the generation of soluble Pd.[42] The induction period of immobilized Pd^{2+} catalysts are on their own ambiguous because it may only reflect the time required to reduce the metal. Reaction profiles can in some cases be corroborated

with Pd leaching data (**Figure 3-1**). In these reactions the Pd concentration has been shown to increase as the coupling proceeds, demonstrating that solubilization of the catalyst can occur. [58]

Filtration Test

Evidence of catalyst homogeneity or heterogeneity can be obtained by employing filtration tests. The simplest form of the test is referred to as the hot filtration test and involves filtration of the hot reaction mixture at low conversion through a frit capable of removing small particles of immobilized catalyst (**Scheme 3-7**).[55] After filtration the solution is monitored for reaction. Note that any insoluble reagents, such as the base need to be added again to the filtrate.[42] If no further conversion is observed in the filtrate then the filtration test suggests the active catalyst is heterogeneous because it did not pass through the frit. On the other hand, conversion in the filtrate is conclusive evidence of a homogeneous process. Care must be taken when employing this test on coupling reactions because any cooling of the solution during filtration can lead to catalyst deactivation/deposition giving erroneous results.[42] For this reason, the observation of no reaction after filtration is not necessarily conclusive of a heterogeneous reaction because it might be difficult to assess how much the catalyst cooled during filtration.[57, 59]

A report by Rothenberg[60] highlighted an interesting application of the filtration test with the Suzuki-Miyaura reaction. They utilized a nanoporous membrane, which divided the reactor in two and while reagents were added to both sides, catalyst was only added to one. The researchers observed conversion on both sides of the membrane and their results were consistent with a catalyst that is likely molecular or a small particle (<< 5 nm).

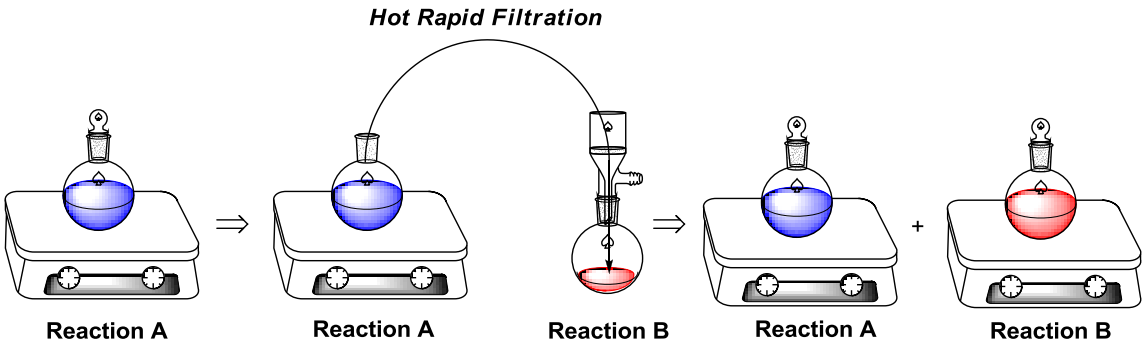

Scheme 3-7. Representation of the hot filtration test

Catalyst Poisoning

Addition of poisons to reactions can be used to distinguish between homogeneous and heterogeneous catalysts. In particular solid phase poisons have been applied to assess the heterogeneity of supported Pd catalysts for variety of coupling reactions.[52, 61, 62] The assumption behind this approach is solid poisons added to reaction mixtures that containing a supported catalyst are only able to scavenge homogeneous species from solution (**Scheme 3-8**). This assumption is reasonable because it is difficult to get efficient reaction between large irregularly shaped surfaces. Thus, product formation in the presence of a solid poison would suggest a heterogeneous catalyst bound to support and cessation of catalysis would suggest a soluble homogeneous catalyst.

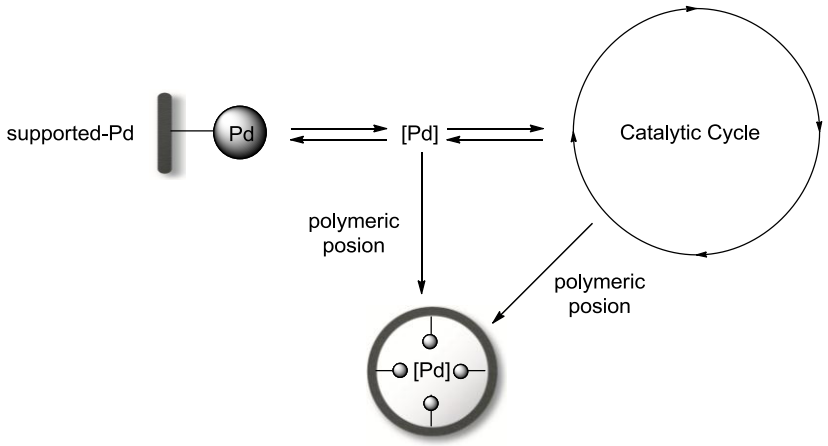

Scheme 3-8. Interception of a soluble Pd catalyst by a polymeric solid phase poison, from reference 61

Common solid phase poisons for Pd catalysis are listed in **Scheme 3-9**. These materials also double as scavengers.[40, 51, 61] The most commonly employed poisons are polyvinylpyridine (PVP) and Quadrapure™ TU, which is a thiourea functionalized macroporous polystyrene. SiO_2-SH and SiO_2-NH_2 are amorphous silicas which are functionalized with aminopropyl and mercaptopropyl groups.[51, 61] Solid phase poisons have provided much evidence in support of the homogeneous boomerang mechanism discussed above because product formation arrests in their presence.[51, 61, 62] The drawback of using poisons to assess homogeneity and heterogeneity is they probe the active catalyst indirectly.

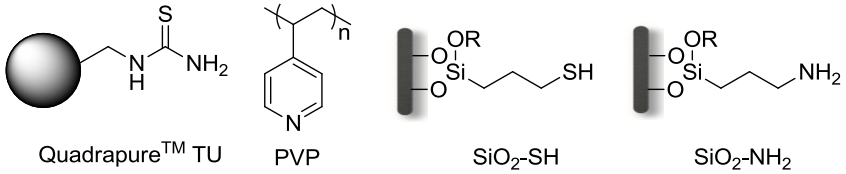

Scheme 3-9. Typical solid phase poisons

The Three-Phase Test

The three-phase test was inspired by Rebek's[63, 64] work in the 1970's directed towards detecting reactive intermediates. The central assumption is that it is difficult for compounds bound to two different solid supports to react with each other, thus any reaction between the supports must be the result of a homogeneous species. The experimental setup of the three-phase test (**Scheme 3-10**) is similar to a typical reaction except that a supported reagent is included. In the case of Suzuki-Miyaura reaction the supported reagent is typically an aryl-halide.[39, 65] After coupling the supported reagent is recovered and is analyzed for evidence of product formation. If cross-coupling occurred on support, the conclusion is that a homogeneous catalyst must be operating under the reaction conditions. If no conversion of the supported reagent is observed then the catalyst must be heterogeneous. The three-phase test is superior to the solid phase poisons discussed above because it assesses the active catalyst directly.

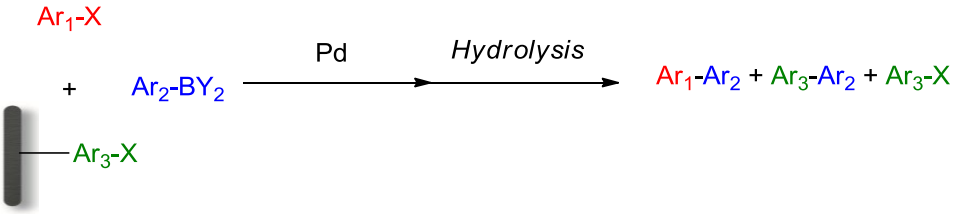

Scheme 3-10. A general description of the three-phase test

There are a couple of considerations to be taken into account when performing and interpreting results from the three-phase test. It is necessary to perform the test in the presence of all reagents as it is possible that one of these species participates in the formation of a soluble catalyst.[65] As discussed in the context of the Suzuki-Miyaura reaction, it is believed that the oxidative addition of aryl-halides to Pd promotes leaching from the support.[57] Furthermore, it is

necessary to observe product formation in solution, as this confirms that an active catalyst was formed under the reaction conditions. Also, a critical point that is often overlooked is that product formation is more rapid in solution than on support; therefore, it is possible that the in solution reaction can reach completion before the supported reagent has had an opportunity to react.[51, 52] The consequences of this scenario will be addressed in the Results and Discussion but a very good test that all of the above conditions are met is to calibrate the three-phase test against known *homogeneous catalysts*. In this way it is possible to get a measure of the extent of reaction that can occur on the supported reagent under the reaction conditions of interest.

To summarize the preceding discussions, there are a number of ways to access homogeneity or heterogeneity of an immobilized catalyst. When making an assessment of true catalyst heterogeneity or homogeneity based on these tests it is important to carefully interpret data from a variety of different sources because no single test is infallible or entirely conclusive on its own.

3.2 Research Objectives

As part of our program developing mesoporous metal scavengers, it was found that mercaptopropylated SBA-15 (abbreviated SBA-15-SH(g), where (g) indicates that the functionality was introduced by post-grafting) was an effective scavenger of Pd in solution. Upon treatment of a 0.01 M $Pd(OAc)_2$ THF solution with SBA-15-SH(g) the metal content was reduced 500 000 fold, outperforming both amorphous SiO_2-SH and commercial scavengers.[40] Interestingly, we found that the SBA-15-SH(g) recovered from this scavenging protocol was itself an active catalyst for Suzuki-Miyaura, Mizoroki-Heck and Sogonshira reactions, with low levels of leaching. Furthermore, results from hot-filtration and three-phase tests suggested that the material was a functionally heterogeneous catalyst, an unusual observation because at the time the

vast majority of supported Pd complexes were believed to act as reservoirs for a homogeneous species.

At the outset of this project there was some difficulty in generating a reproducibly active Pd-SBA-15-SH(g) catalyst, and this was obviously an issue that needed to be addressed. Fellow graduate student Kevin McEleney, post-doctoral fellow Stephanie MacQuarrie and I were tasked with solving the reproducibility problem and addressing the nature of the active species. The Suzuki-Miyaura coupling of bromoacetophenone (**1**) and the pinacol ester of phenylboronic acid (PhBpin, **2**) was chosen as the test reaction to evaluate catalyst activity, recycling, stability and heterogeneity (**Scheme 3-11**).[46] My responsibility was to study the post-grafted mercaptopropyl material Pd-SBA-15-SH(g), Kevin McEleney was responsible for the work on the co-condensed material, Pd-SBA-15-SH(cc) and Stephanie MacQuarrie worked with commerically available mercaptopropylated amorphous silica, Pd-SiO_2-SH.

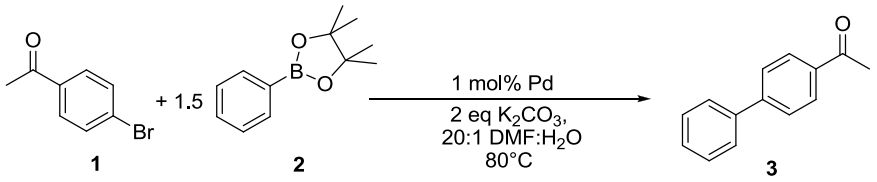

Scheme 3-11. Suzuki-Miyaura test reaction for the Pd-SBA-15-SH(g) catalyst

3.3 Results and Discussion

3.3.1 Synthesis of Pd-SBA-15-SH(g)

The first step was optimizing the synthesis of a reproducibly active Pd-SBA-15-SH(g) or Pd-SBA-15-SH(cc) catalyst because at the outset, the activity of these materials was irreproducible. Our initial foray into this problem was to address the molar ratio of S:Pd on the

material. In fact, it was found this was a critical variable that must be controlled to achieve an active catalyst. For all catalysts discussed subsequently, the sulfur content was measured by elemental analysis (EA). Screening for the optimum molar ratio was performed by Stephanie MacQuarrie using amorphous silica analogue, Pd-SiO_2-SH (**Table 3-1**), and it was found that S:Pd ratios greater than 4:1 resulted in a catalytically inactive material. A 2:1 S:Pd ratio was chosen as the best balance between catalyst activity (98 % yield) and Pd leaching (0.06 %), which was in the ppb range as measured by ICP-MS. Materials synthesized with a 2:1 S:Pd ratio were found to be reproducibly active catalysts.

Table 3-1. Effect of S:Pd ratio on catalytic activity and Pd leaching[a]

Entry	Material	S:Pd	Yield,[b] %	Pd Leached,%[c]
1	Pd-SiO_2-SH	1:1	86	0.3
2	Pd-SiO_2-SH	2:1	98	0.06
3	Pd-SiO_2-SH	3:1	72	0.02
4	Pd-SiO_2-SH	4:1	25	0.03
5	Pd-SiO_2-SH	8:1	0	-

[a] Reaction conditions: 0.75 mmol PhBpin, 0.50 mmol **1**, 1 mol% Pd-SiO_2-SH(g), 1.00 mmol K_2CO_3, 0.50 mmol *p*-dimethoxybenzene (DMB) as internal standard, 20:1 DMF:H_2O (0.l M in BrAcPh), 80 ºC for 18 h; [b] Determined by GC-FID; [c] Measured by ICP-MS and based on the amount of Pd added to the reaction mixture

SBA-15-SH(g), was obtained from Soxhlet extracted SBA-15 (**Scheme 3-12**). SBA-15 was heated with 3-mercaptopropyl(trimethoxysilane) (MPTMS) in toluene at 110 ºC overnight. The sulfur content of SBA-15-SH(g) (0.8 – 1.1 mmol g^{-1} S) varied with the batch of SBA-15. Pd-SBA-15-SH(g) was made by treating SBA-15-SH(g) with $Pd(OAc)_2$ trimer dissolved in THF.

After 1 h, the solution was filtered and the filtrate was colorless. ICP-MS analysis of the filtrate confirmed that >99.9 % of the initially added Pd was loaded onto SBA-15-SH(g) and representative textural properties are reported in **Table 3-2**.

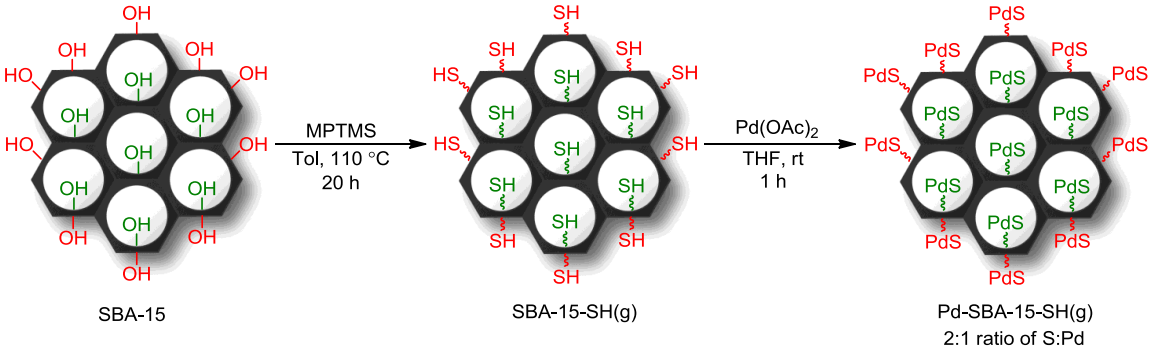

Scheme 3-12. Synthesis of Pd-SBA-15-SH(g)

Table 3-2. Summary of some representative textural properties for the synthesis of Pd-SBA-15-SH(g)[a]

Material	S_{BET},[b] m^2 g^{-1}	C	D_{BJH},[c] nm	V_p,[c] cm^3 g^{-1}
SBA-15	1076	145	8.5	1.13
SBA-15-SH(g)[d]	753	97	7.5	0.82
Pd-SBA-15-SH(g)	360	57	7.3	0.44

[a] Reaction conditions: See Experimental for details; [b] BET surface area; [c] Pore diameter (D_{BJH}) and pore volume (V_p) calculated using BJH adsorption branch for pores 1.0 – 300 nm in diameter; [d] SBA-15-SH(g) had 3.6 wt% S (1.1 mmol S g^{-1}) as measured by elemental analysis

3.3.2 Suzuki Reaction Conditions

Initially, the Suzuki-Miyaura test reaction was performed in air, but analysis of the reaction mixture suggested that these conditions resulted in significant quantities of biphenyl, a homocoupling product. It was found that upon completion of the Suzuki-Miyaura reaction, the

catalyst would continue to convert the excess PhBpin to biphenyl (**Table 3-3**). After 8 h in air there was a 25 % yield of biphenyl and 98-99 % yield of the biaryl product **3**. The amount of biphenyl then continued to increase to 33 % after 24 h under the reaction conditions. Complete conversion of excess PhBpin to biphenyl was achieved under an O_2 atmosphere. However, formation of the homocoupled product could be prevented by performing the reaction under an Ar atmosphere.[66] Thus, all reactions discussed from this point forward were performed under an Ar atmosphere unless otherwise stated. An Ar atmosphere also resulted in decreased Pd leaching as well as improved catalyst activity. Reactions preformed under Ar also required approximately half the time to reach completion (**Table 3-3**). The effectiveness of these immobilized catalysts at retaining Pd can be inferred by looking at the reaction mixture because the material settles to the bottom of the test tube leaving a supernatant that almost colorless (**Scheme 3-13**).

Table 3-3. Effect of atmosphere on the Suzuki Miyaura reaction[a]

Entry	Atm	Time, h	Yield,[b] %	Pd Leached	
				ppm[c]	%[d]
1	Air	8	98-99	0.40 ± 0.05	0.32 ± 0.05
2	Ar	4	98-99	0.16 ± 0.05	0.12 ± 0.05

[a] Reaction conditions: 0.75 mmol PhBpin, 0.50 mmol **1**, 1 mol% Pd-SBA-15-SH(g), 1.00 mmol K_2CO_3, 0.50 mmol *p*-dimethoxybenzene (DMB) as internal standard, 20:1 DMF:H_2O (0.l M in BrAcPh), 80 ºC; [b] Determined by GC-FID; [c] Measured by ICP-MS; [d] Based on the amount of Pd added to the reaction mixture.

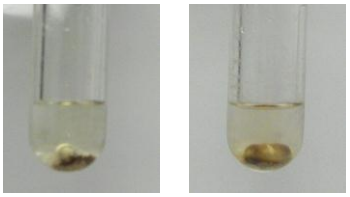

Scheme 3-13. Images of a Suzuki-Miyaura reaction catalyzed by Pd-SBA-15-SH(g)

The consumption of aryl-halide **1** and PhBpin was plotted with formation of biaryl **3** (**Figure 3-2**). It was found that consumption of PhBpin at short reaction times outpaced that of **1** and formation of **3**. However, upon completion of the reaction only 1.0 equivalent of PhBpin had been consumed. Recall that 1.5 equivalents of PhBpin were added initially, as using excess boronate ester is typical for Suzuki-Miyaura cross-couplings.[1] The enhanced PhBpin consumption at short reaction times is consistent with partial hydrolysis of the ester to $PhB(OH)_2$. Corroborating evidence for this assertion was the observation of free pinacol in GC chromatograms. A more detailed assessment of the behavior of PhBpin under the reaction conditions is not possible without further study because of the complex nature of the system. The data does indicate that PhBpin consumption is not a good measure of product formation.

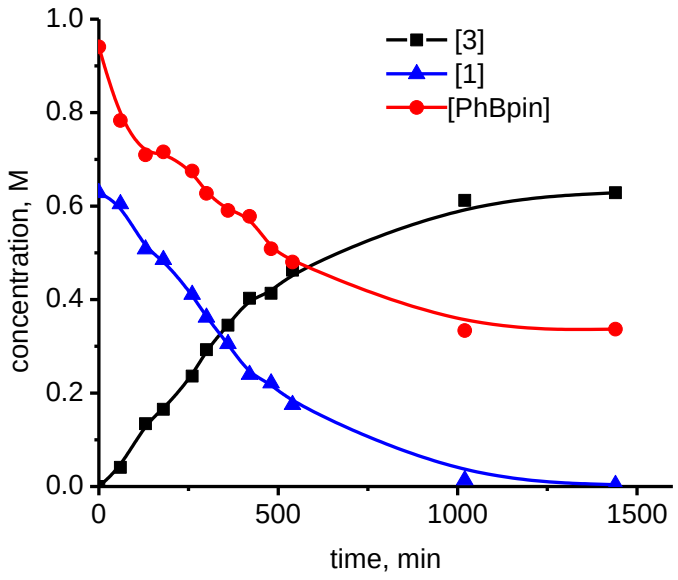

Figure 3-2. Reaction profile for the Suzuki-Miyaura reaction catalyzed by Pd-SBA-15-SH(g)

The longevity of the catalyst was assessed by measuring the turnover number (TON) (**Table 3-4**). Pd-SBA-15-SH(g) had the highest TON value, (Entry 2) at >10 000, of the three catalytic materials assessed. Our values are comparable to other supported cross-coupling catalysts, although catalysts giving TONs greater than 100 000 are known.[24] It is interesting to note that the TOF at low conversion under Ar (entry 2) and air (entry 4) are of similar magnitude, suggesting that at short reaction times both systems operate with a similar catalytic species. The TOF at short times under Ar for Pd-SBA-15-SH(g) was higher than that the value measured at prolonged reaction times, even though conversion of **1** was below 30 %. The shift between the TOF's was relatively rapid and may reflect a change in the active catalyst or catalyst speciation.

Table 3-4. Summary of TON and TOF values for the various supported silica catalysts[a]

Entry	Catalyst	mol% Pd	Atm	TOF (h^{-1})[b]	TON[b]
1	Pd-SBA-15-SH(g)	0.004	Ar	400	
2	Pd-SBA-15-SH(g)	0.009	Ar	2200,[c] 490	>10 000
3	Pd-SBA-15-SH(g)	0.013	Ar	720	
4	Pd-SBA-15-SH(g)	0.009	Air	2200[c]	4800
5	Pd-SBA-15-SH(cc)	0.009	Ar	900	3450
6	Pd-SBA-15-SH(cc)	0.009	Air	590	2750
7	Pd-SiO_2-SH	0.013	Ar	130	6800
8	Pd-SiO_2-SH	0.013	Air	190	5100

[a] Reaction conditions: 18.8 mmol PhBpin, 12.5 mmol **1**, 25.0 mmol K_2CO_3, 12.5 mmol *p*-dimethoxybenzene (DMB) as internal standard, 20:1 DMF:H_2O (0.36 M in BrAcPh) at 80 ºC; [b] Determined by GC-FID; [c] TOF after 1 h of reaction with 20% yield of **3**

3.3.3 Recyclability

The recyclability of Pd-SBA-15-SH(g) was assessed (**Table 3-5**), and was found to have good reusability. It was found that the catalyst activity and yields were maintained until the second recycle (entries 3 and 4) after which longer reaction times were required. The amount of Pd leached increased with catalyst reuse, but was still under 1 % (0.63 ppm) of the initially added Pd after 4 recycles. Pd-SBA-15-SH(g) outperformed the other two supported catalysts assessed, with better reusability and Pd-leaching data (**Figure 3-3**).

Table 3-5. Summary of recycling data for Pd-SBA-15-SH(g)[a]

Recycle	Time, h	Yield,[b] %	Pd Leached	
			ppm[c]	%[d]
0	4	99	0.01	0.01
1	4	99	0.01	0.01
2	4	99	0.04	0.03
3	8	91	0.25	0.25
4	8	97	0.63	0.60

[a] Reaction conditions: See Experimental for details; [b] Determined by GC-FID; [c] Measured by ICP-MS; [d] Based on the amount of Pd added to the reaction mixture

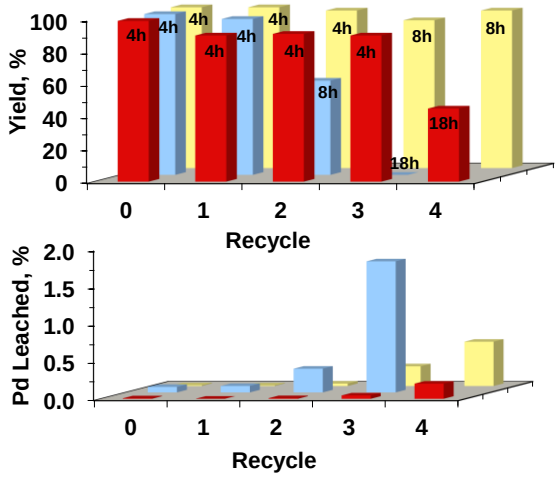

Figure 3-3. Recycling and leaching data for Pd-SiO_2-SH (red), Pd-SBA-15-SH(cc) (blue) and Pd-SBA-15-SH(g) (yellow)

We were interested in the textural properties of the used catalytic materials to gain insight into modes of catalyst deactivation during recycling. The ultimate goal would be to take the lessons learned and apply them to improve catalyst design. A TEM of Pd-SBA-15-SH(g) before use showed a material with a highly ordered meso-structure and there was no evidence of Pd

nanoparticles (**Figure B-1** in **Appendix B**). TEMs after use in air and under Ar indicated that the materials retained their mesostructure (**Figure 3-4**). Interestingly, no Pd nanoparticles were observed for Pd-SBA-15-SH(g) employed under an air atmosphere while nanoparticles were observed under Ar. Air may stabilize Pd in solution by limiting the accumulation of Pd(0).[66-68]

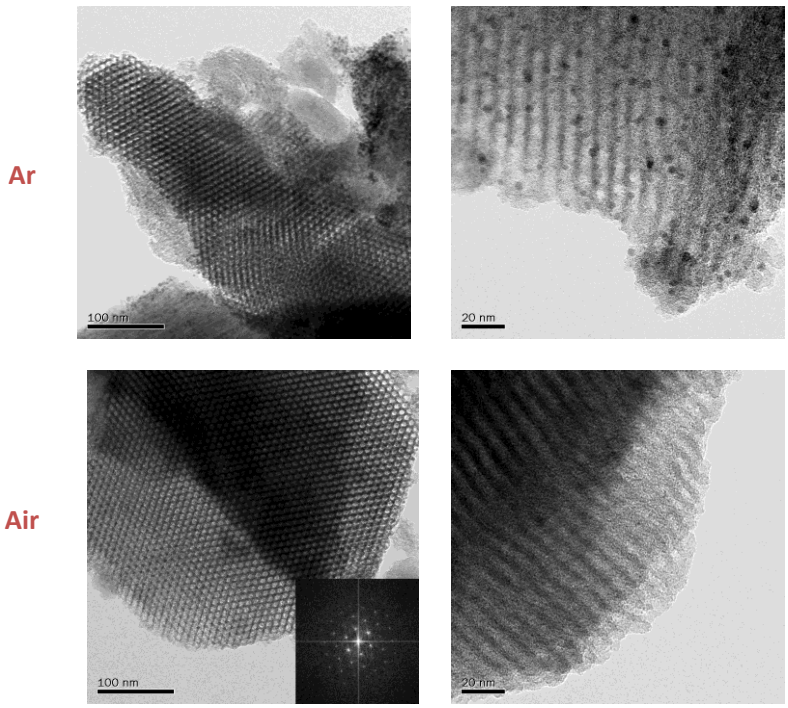

Figure 3-4. TEM images of used Pd-SBA-15-SH(g), the inlay represents a Fourier Transform of the image

The nanoparticles formed under Ar were found to have a size range limited by the dimensions of the mesopores of Pd-SBA-15-SH(g) (**Figure 3-5**). Recall that the pores of SBA-15 are 6 – 8 nm in diameter, and no nanoparticles were observed with a diameter larger than 6 nm, with the majority falling between 3-5 nm. Thus, it seems that a function of the mesopores of these materials may be to restrict nanoparticle growth.[69] It was subsequently observed by Stephanie MacQuarrie[49] that in more highly interconnected materials such as KIT-6, which has a bi-

continous structure, the mesopores do not restrict nanoparticle growth. Rather the pores facilitate redistribution of Pd to the external surface. Combined, these two observations indicate that the role of the mesopores depends on the structure of the silica support.

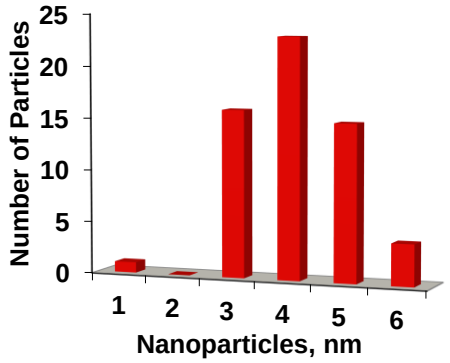

Figure 3-5. Size distribution of nanoparticles formed under an Ar atmosphere

The concentration of nanoparticles was too low to be visualized using wide angle pXRD (**Figure B-2** and **Figure B-3** in **Appendix B**). However, an XPS and XAES (X-ray induced Auger spectroscopy) study by fellow graduate student Kevin McEleney[70] concluded that the changes to the Pd environment on the surface of these materials after use was consistent with reduction of the metal during reaction.

It is well understood that smaller Pd nanoparticles have higher activity towards cross-coupling reactions.[31] The rational is that the smaller the nanoparticle the larger the proportion of the Pd atoms that are in proximity to the surface and thus assessable to the reagents. Restriction of particle growth by mesopores may be one reason for the increased recyclability of Pd-SBA-15-SH(g) as compared to Pd-SiO_2-SH, which does not possess an ordered pore system or narrow pore size distribution. Consistent with this assertion Pd supported on SiO_2-SH shows evidence of unrestricted Pd nanoparticle growth (**Figure 3-6**).

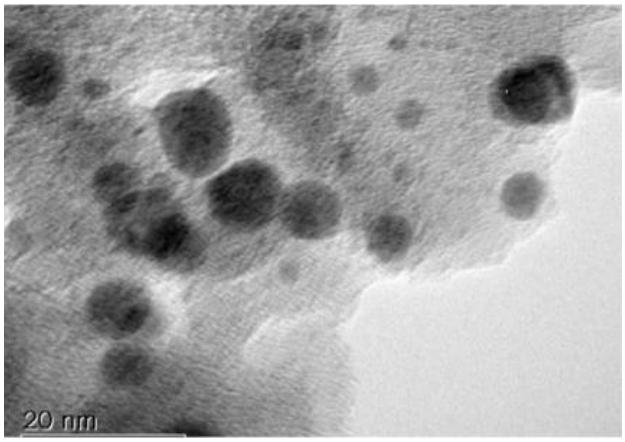

Figure 3-6. TEM image of used Pd-SiO_2-SH

Textural characterization of Pd-SBA-15-SH(g) by N_2 physisorption analysis revealed that the structure of the material did degrade with increased exposure to the reaction conditions (**Figure 3-7**). This can be inferred from the decrease in surface area (S_{BET}), pore diameter (D_{BJH}) and pore size (V_P) of the material (**Table 3-6**). The loss of order was also observed qualitatively by TEM as there was an increase in the number of disordered domains (**Figure 3-4**). pXRD of Pd-SBA-15-SH(g) before and after use showed a reduction in peak intensities and the cell parameter (**Figure B-4** and **Table B-1** in **Appendix B**). All of these observations are consistent restructuring of the pore system and reduced structural order of the material.

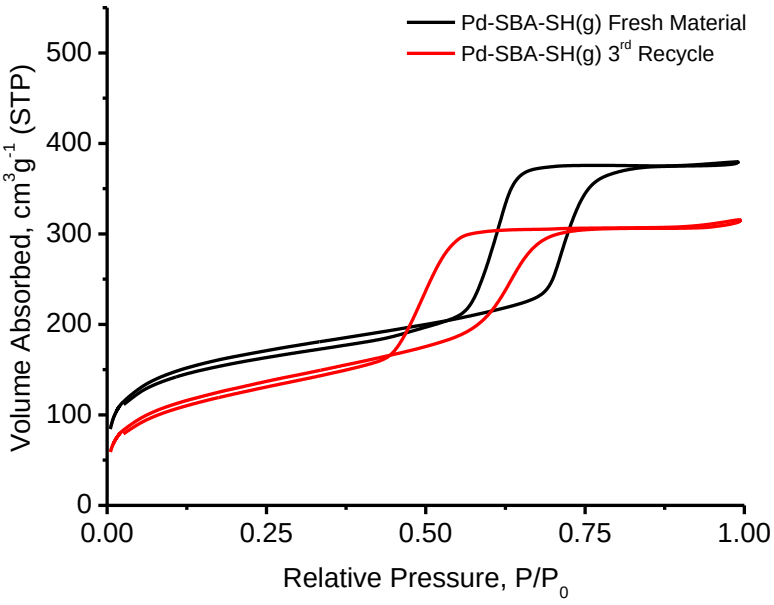

Figure 3-7. Nitrogen physisorption overlay for Pd-SBA-15-SH(g)

Table 3-6. Summary of textural properties for Pd-SBA-15-SH(g)[a] on recycle[b]

Recycle	S_{BET},[c] m^2 g^{-1}	D_{BJH},[d] nm	V_p,[d] cm^3 g^{-1}
0	580	6.8	0.53
1	427	5.8	0.43
2	467	5.3	0.43
3	466	4.6	0.38

[a] SBA-15-SH(g) has 2.9 wt% S (0.91 mmol g^{-1}) as measured by elemental analysis prior to Pd loading; [b] Reaction conditions: See Experimental for details; [c] BET surface area; [d] Pore diameter (D_{BJH}) and pore volume (V_p) calculated using BJH adsorption branch for pores 1.0 – 300 nm in diameter

It is likely that restructuring upon re-use played a role in reducing catalytic activity. Reduced pore volume and size will result in inferior contact between the reagents in solution and the Pd, which is predominately localized on the interior material surface. When taken to the extreme, a collapse of the pore system would be expected to result in loss of catalytic activity, as the bulk of the Pd would be inaccessible to reagents in solution. In fact, fellow graduate students Kevin McEleney[46] and Ben Glasspoole[47] observed that mesostructure collapse in Pd-SBA-15-SH(cc) and Pd-MCM-SH(g) is accompanied by a complete loss of catalytic activity.

A variety of control experiments illustrated that the basic reaction conditions were chiefly responsible for the restructuring of the Pd-SBA-15-SH(g).[47] The effect of base on SBA-15-SH(g) under conditions mimicking those used for Suzuki-Miyaura reaction was dramatic: within 4 h of exposure to hot (80 ºC) aqueous base under the reaction conditions, complete loss of the mesostructure was observed **Figure 3-8** and **Table 3-7**. The detrimental effect of base was not unexpected considering silica is soluble at high pH. The route to degradation is likely attack of base on the silica framework. Interestingly though, the loss of order for SBA-15-SH(g) itself was more dramatic than that observed for Pd-SBA-15-SH(g) under actual Suzuki-Miyaura reaction conditions (**Figure 3-7** and **Table 3-6**).

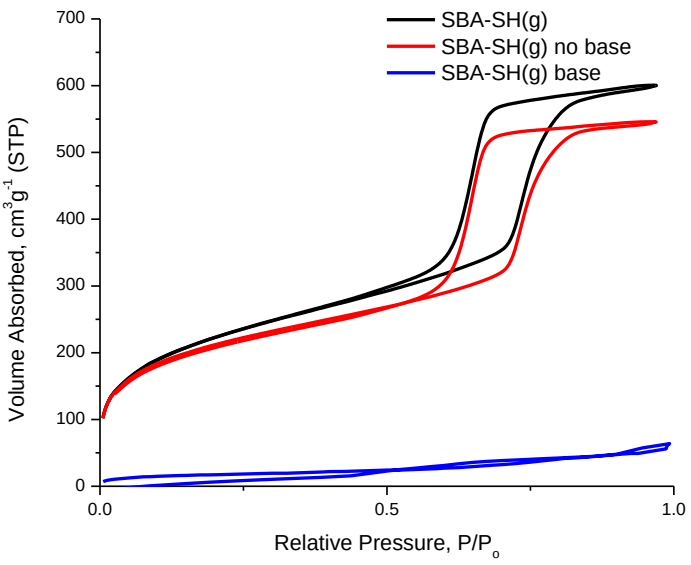

Figure 3-8. Nitrogen physisorption overlay of SBA-15-SH(g) materials used in the stability study before and after heating in 20:1 DMF:H_2O for 4 h at 80 ºC

Table 3-7. Summary of textural properties SBA-15-SH(g)[a] used in the stability study[b]

Entry	Conditions	Stir	S_{BET},[c] m^2 g^{-1}	D_{BJH},[d] nm	V_p,[d] cm^3 g^{-1}
0	Original Material	-	810	7.6	0.84
1	No Base	Yes	760	7.6	0.80
2		No	875	7.6	0.90
3	K_2CO_3[e]	Yes	60	-	0.10
4		No	550	4.4	0.46

[a] SBA-15-SH(g) had 2.4 wt% S (0.74 mmol g^{-1} S) as measured by elemental analysis; [b] Reaction conditions: 60 mg SBA-15-SH(g) in 20 mL DMF and 1 mL H_2O at 80 ºC for 4 h; [c] BET surface area; [d] Pore diameter (D_{BJH}) and pore volume (V_p) calculated using BJH adsorption branch for pores 1.0 – 300 nm in diameter; [e] 590 mg K_2CO_3

The reason for the dramatic difference between merely exposing the material to base and actually running a Suzuki-Miyaura reaction was determined by graduate student Ben Glasspoole. He demonstrated that the boric acid generated over the course of a Suzuki-Miyaura cross-coupling was able to retard the degradation of the mesostructure of the material.[47] The exact role of the boric acid remains ambiguous and it can be seen as either acting as a pH buffer or reversibly binding to accessible silanols on the surface of the mesoporous silica preventing attack by base. It was also found that base promoted leaching of Pd (**Figure 3-9**). As the order of the support decreases, thiols may become sequestered from solution; further, sulfur may be leached from the material, reducing its capacity to bind Pd.[40]

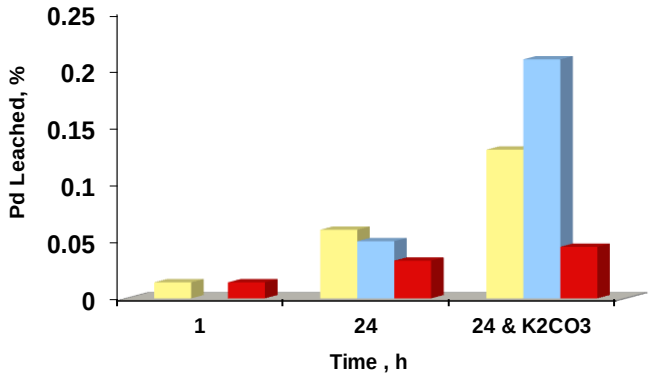

Figure 3-9. Pd leaching on treatment with 20:1 DMF:H_2O for Pd-SiO_2-SH (red), Pd-SBA-15-SH(cc) (blue) and Pd-SBA-15-SH(g) (red)

Different methods to improve the stability of the mesoporous material were explored. Pd-SBA-15-SH(g) was originally synthesized using SBA-15 which was treated using Soxhlet extraction to remove the template P123. Alternatively, calcination can be used to remove the template. This approach was employed to generate the catalyst C-Pd-SBA-15-SH(g). Calcination is known to increase the condensation of the silica network which should result in a more stable

support.[71] C-Pd-SBA-15-SH(g) (**Table 3-8** compared to **Table 3-6**) was more stable than Pd-SBA-15-SH(g) evidenced by a smaller change in pore size over the course of the recycle study. Unfortunately, during the second recycle the activity of the catalyst decreased substantially.

Table 3-8. Summary of recycling and textural properties for C-Pd-SBA-15-SH(g)[a, b]

Recycle	Yield,[c] %	Time, h	S_{BET},[d] $m^2\ g^{-1}$	D_{BJH},[e] nm	V_p,[e] $cm^3\ g^{-1}$
0	92	8	430	5.4	0.40
1	93	8	505	5.4	0.50
2	71	8	455	5.7	0.50
3	-	-	515	5.8	0.61

[a] C-SBA-15-SH(g) had 2.5 wt% S (0.79 mmol g^{-1} S) as measured by elemental analysis prior to Pd loading; [b] Reaction conditions: See Experimental for details; [c] Determined by GC-FID; [d] BET surface area; [e] Pore diameter (D_{BJH}) and pore volume (V_p) calculated using BJH adsorption branch for pores 1.0 – 300 nm in diameter

Alternatively, it was thought that if materials were prepared in such a way as to reduce the surface silanol content, then direct attack of the silica network by base would be slowed. Two approaches along these lines were explored. The first was hydrophobization[72, 73] of the SBA-15 by treatment with TMS-Cl. Silanols on the surface were end capped with TMS groups and the resulting material is referred to as TMS-Pd-SBA-15-SH(g). The second approach was to increase the sulfur content of the material. Using a modified post-grafting procedure[74] a material containing double the typical amount of sulfur (S = 2.02 mmol/g) was synthesized and is designated H-Pd-SBA-15-SH(g). Both materials (**Table 3-9** and **Table 3-10**) displayed improved stability towards the reaction conditions as compared to C-Pd-SBA-15-SH(g) (**Table 3-8**) and Pd-SBA-15-SH(g), (**Table 3-6)** but for reasons which remain unclear reduced recyclability was encountered. It is entirely likely that stability of the support is not the only parameter that is

critical to the recyclability of these heterogeneous catalysts. That said, in a more exhaustive study, fellow graduate student Ben Glasspoole examined Al stabilized SBA-15 (Al-Pd-SBA-15-SH(g))supports and found that they possessed high recyclability and low Pd leaching in addition to improved stability towards the reaction conditions.[47] Al-Pd-SBA-SH(g) could be used as a catalyst 4 times for a total of 20 h of heating with minimal loss of structural order and activity. This material represented an improvement over Pd-SBA-15-SH(g) which could also be used 4 times, albeit with significant loss of order after the first recycle (**Figure 3-7** and **Table 3-6**) and noticeable decrease in activity after the second (**Figure 3-3**).

Table 3-9. Summary of recycling and textural properties for TMS-Pd SBA-15-SH(g)[a, b]

Recycle	Yield,[c] %	Time, h	S_{BET},[d] m^2 g^{-1}	D_{BJH},[e] nm	V_p,[e] cm^3 g^{-1}
0	98	2	360	5.3	0.45
1	53	4	413	5.7	0.46
2	26	4	396	5.7	0.48
3	-	-	340	5.8	0.43

[a] TMS-SBA-15-SH(g) had 2.5 wt% S (0.78 mmol g^{-1} S) as measured by elemental analysis prior to Pd loading; [b] Reaction conditions: See Experimental for details; [c] Determined by GC-FID; [d] BET surface area; [e] Pore diameter (D_{BJH}) and pore volume (V_p) calculated using BJH adsorption branch for pores 1.0 – 300 nm in diameter

Table 3-10. Summary of recycling and textural properties for H-Pd-SBA-15-SH(g)[a, b]

Recycle	Yield,[c] %	Time, h	S_{BET},[d] m^2 g^{-1}	D_{BJH},[e] nm	V_p,[e] cm^3 g^{-1}
0	98	2	360	5.3	0.45
1	53	4	413	5.7	0.46
2	26	4	396	5.7	0.48
3	-	-	340	5.8	0.43

[a] H-SBA-15-SH(g) has 6.5 wt% S (2.0 mmol g^{-1} S) as measured by elemental analysis prior to Pd loading; [b] Reaction conditions: See Experimental for details; [c] Determined by GC-FID; [d] BET surface area; [e] Pore diameter (D_{BJH}) and pore volume (V_p) calculated using BJH adsorption branch for pores 1.0 – 300 nm in diameter

3.3.4 Heterogeneity Tests

As noted previously, there has been debate in the literature focused on the nature of the catalytically active species for supported Pd catalysts.[42, 52] While the majority of immobilized Pd catalysts acted as reservoirs for a homogeneous species, Pd-SBA-15-SH(g) and a select few other materials were outliers because traditional heterogeneity tests gave results consistent with truly heterogeneous catalysts. There were, however, results in these systems that could be considered contradictory heterogeneity test results.[40, 42, 52] In the present case recall for example, that nanoparticles are visible on the surface of Pd-SBA-15-SH(g) after use in Suzuki-Miyaura reaction. Nanoparticle formation is a hallmark of leaching of Pd from the surface; however, this analysis does not provide direct information about whether the catalytic activity stems from a supported or soluble species. On the other hand, the hot filtration showed no activity in filtered solutions, implying instead a heterogeneous catalyst. Finally, and most importantly, the three-phase test (**Scheme 3-14**) gave no reaction on the supported aryl bromide, again consistent with the catalytically active species being truly heterogeneous. Based on the available data, the

conclusion at the time was the materials were functionally heterogeneous catalysts with the preponderance of Pd remaining trapped within the pores during reaction. This conclusion, while reasonable based on the collected data, is incongruent with other mechanistic studies in the literature and as will be seen, this conclusion is inconsistent with the data collected in this study. For these reasons we thought that the supported catalysts warranted deeper analysis as to their true heterogeneity.

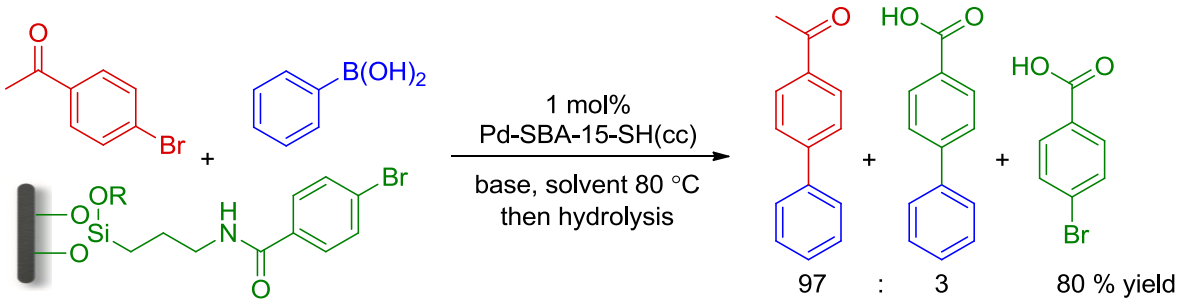

Scheme 3-14. Summary of a three phase test result from the original publication in 2005, from reference 40

As noted previously, the presence of induction periods is often indicative of loss of catalytically active Pd from the surface into solution.[55] Under the standard reaction Suzuki-Miyaura conditions used in this study, no induction period was observed; however, upon reducing the catalyst loading from 1 mol % - 0.1 mol %, a small induction period was detected (**Figure 3-10**). The combined observation of an induction period and Pd nanoparticles is indicative of a homogeneous reaction mechanism,[42, 52] but not conclusive as the nature of the active species is being probed indirectly, especially since the catalyst precursor is a Pd^{2+} species.

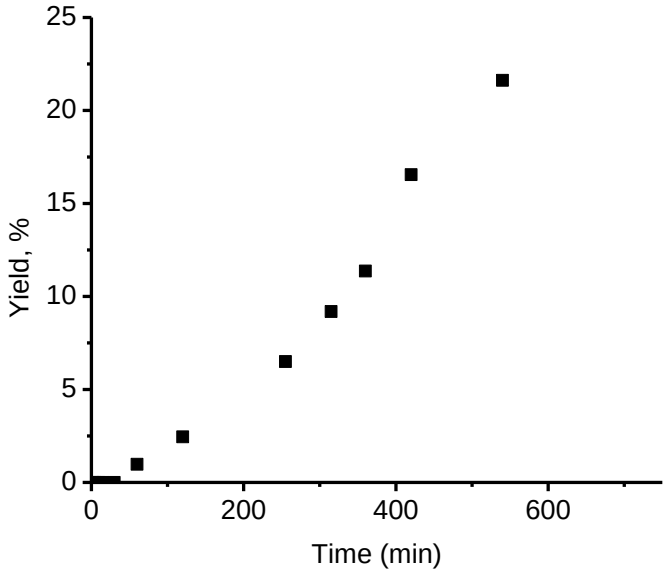

Figure 3-10. Reaction profile of an induction period; reaction was run at 0.1 M **1** and 0.15 M PhBpin at 0.1 mol% Pd-SBA-15-SH(g)

Concurrent, with our research, a report by Jones[51] outlined the use of solid phase poisons to assess Pd-SBA-15-SH type supports. Their report detailed the synthesis of a material similar to Pd-SBA-15-SH(g) discussed herein. The major difference was the S:Pd ratio which was 1:1, instead of the ratio of 2:1, used for the materials employed in our study. This difference is significant as Pd leaching is greatly increased with a 1:1 ratio; consequently, such materials would be expected to be more prone to operate via a homogeneous mechanism and indeed that was the conclusion of their report. To compare our catalysts to the Jones materials we employed the same solid phase poison test.

The activity of Pd-SBA-15-SH(g) was assessed against four solid phase poisons, PVP (poly-vinyl pyridine), Quadrapure^{TM} TU, SiO_2-NH_2 and SiO_2-SH (**Scheme 3-9**). This work was concurrent with a similar assessment by Kevin McKleny's Pd-SBA-15-SH(cc) and Stephanie Macquarie Pd-SiO_2-SH materials. High loadings of the solid phase poisons were employed to

ensure that the binding sites on the poisons were in excess to the initially added Pd, increasing the likely hood that soluble Pd would be scavenged. It was found that all the poisons decreased the activity of Pd-SBA-15-SH(g). Similar results were observed for Pd-SBA-15-SH(cc) and Pd-SiO_2-SH. The most effective of the poisons were found to be SiO_2-NH_2 and SiO_2-SH.[62] It should be noted that under the reaction conditions, SiO_2 itself does not poison Pd-SBA-15-SH(g). The effectiveness of SiO_2-SH was surprising when one considers that the same material when loaded with a 2:1 S:Pd ratio, is an active catalyst for the Suzuki reaction. In the present experiment SiO_2-SH was added to the reaction mixture based on a ratio of 35:1. It was discussed earlier that SiO_2-SH materials with a greater than 4:1 are catalytically inactive; the poisoning data is thus entirely consistent with previous results. In other words, the loss of catalytic activity observed in this case, might be due to a redistribution of Pd on the surface of the two silica-based ligands, leading to an overall greatly diminished ratio of Pd:S, well below what we have previously shown to be needed for catalytic activity. However, it should be noted that at this time, the reason for the relationship between the S:Pd ratio and catalytic activity had not been clarified.

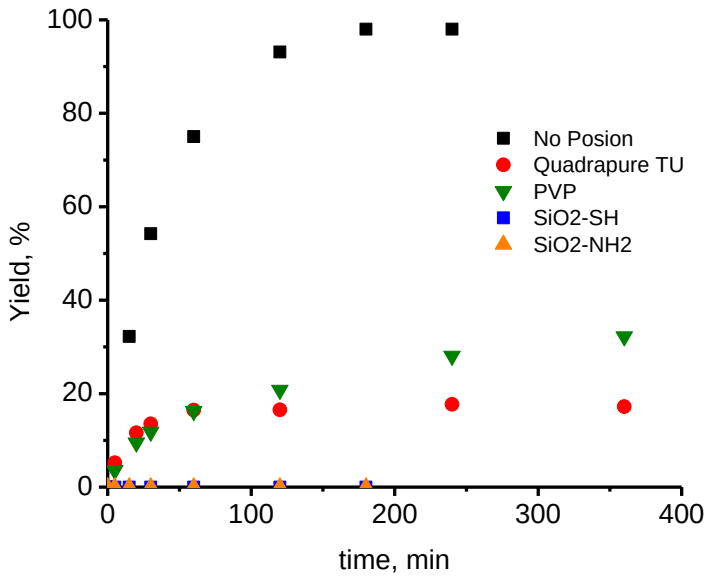

Figure 3-11. Reaction profiles from the solid phase poison test with Pd-SBA-15-SH(g)

Quadrapure™ TU and PVP were less effective poisons for Pd-SBA-15-SH(g). Reactions carried out in the presence of Quadrapure™ TU were slower than the control and arrested after 1 h, which is likely the time required for the polymer to become completely solvated. Understanding the role of PVP as a poison is a bit more complicated because the presence of the polymer increases the viscosity of the solvent, and is also known to disrupt catalytic activity just by adsorbing to the surface of the support, both of which could lead to reduced reaction rates without quenching the active Pd catalyst.[52, 61] That said the reaction did proceed to lower overall yield, 45 % after 24 hours.

Clearly, we were still left with questions as to the nature of the active catalyst after these studies. The problem is the solid phase poison test indirectly assesses the activity of a catalyst. In other words, there are always many reasons why reactions fail and making mechanistic

conclusions using failed reactions is dubious. Faced with more inconclusive data, but data that nonetheless suggest catalytic activity in solution, we turned back to the three-phase test, which is considered one of the most reliable tests as it directly assesses catalytic activity.

As mentioned in the introduction the three-phase test has the distinct advantage over the use of solid phase poisons because it directly assesses the catalytically active species.[39, 65] Recall that the test was also employed in the original publication in 2005.[40] Aryl-halide functionalized three-phase silica supports were synthesized using two methods (**Scheme 3-15**). Method A, was similar to that employed in the original publication,[40] the direct reaction of acid chloride **4** with 3-aminopropyl functionalized silica (SiO_2-NH_2) yielding material **5**. In Method B, the amide coupling step was carried out in solution by reaction of **4** with APTES (**6**) to give trialkoxysilane **7**. The three-phase material was obtained by post-grafting **7** onto amorphous SiO_2. Critically, and as before, the three-phase reactions (**Scheme 3-16**) were carried out in the presence of aryl-Br **1** and $PhB(OH)_2$. The role of both reagents was to ensure that an active catalyst was generated under the reaction conditions, assessed by monitoring formation of **3**, and to promote leaching of Pd from the support. After reaction the three-phase material was recovered by filtration and hydrolyzed in aqueous base to cleave the amide linkage. The soluble organics **8** and **9** produced during the hydrolysis reaction were recovered and the ratio of the products was assessed by ^1H NMR. An assumption in this analysis is that the two supported amides present after the cross-coupling had similar rates of hydrolysis.

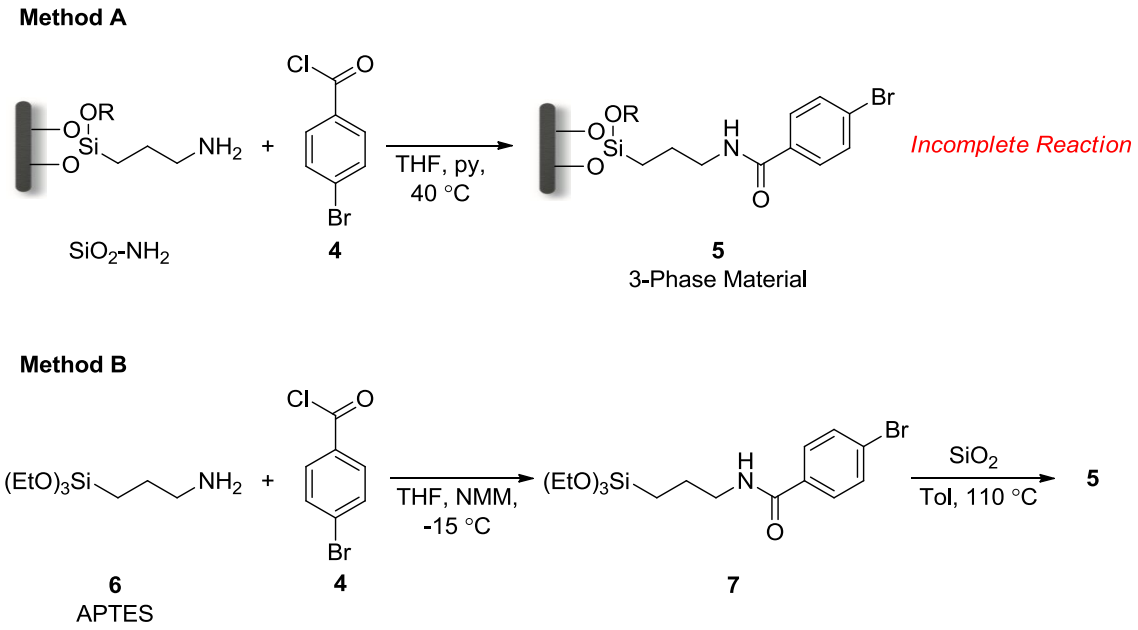

Scheme 3-15. Routes to three-phase material **5**

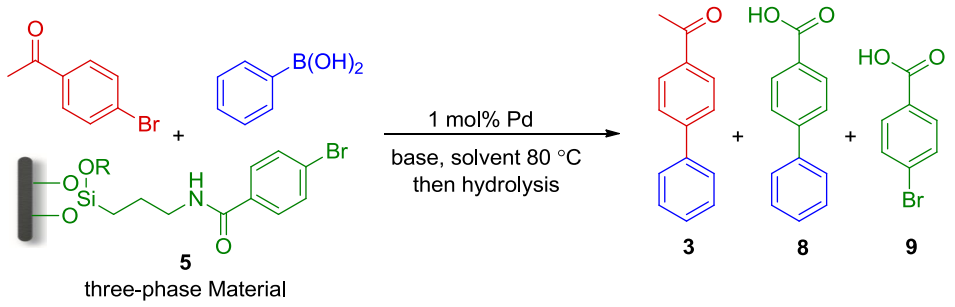

Scheme 3-16. General method for the three-phase test

It was found that the three-phase material **5** generated by Method A shut the reaction down when the coupling was carried out in DMF. Negligible product **3** was apparent after extended reaction times. Elemental analysis of **5** showed that amide formation on SiO_2-NH_2 was incomplete; approximately 30 % of the amines remained unreacted. When accounting for the amount of the three-phase material added to the reaction mixture that meant a molar ratio of

NH_2:Pd of about 35:1, more than sufficient to poison the catalyst as indicated by solid phase poisoning.

When the reaction is carried out in water for moderate reaction times (entries 1 and 3 limited cross-coupling occurred on the supported aryl-Br material **5** resulting in only a small amount of product **9**. At the same time, under these conditions, the homogeneous reaction was effective using either Pd-SBA-15-SH(g) or Pd-SBA-15-SH(cc) (**Table 3-11**) indicating that an active catalyst was generated. These results are entirely consistent with previous reports with this catalyst.[40] However, when the reaction time is increased (entries 2 and 4), and 3 equivalents of phenyl boronic acid is employed (entry 5) increased conversion on the three-phase material is observed. It should be noted that the yield of **3** in these cases was significantly lower than that observed in the absence of the three-phase material **5** because under otherwise identical conditions, >95 % yield could be obtained. It was likely that the free NH_2 groups on the surface of the material were acting to partially quench the Pd catalyst.

Table 3-11. Summary of three-phase test data for material **5** produced by Method A in **Scheme 3-16**[a]

Entry	Catalyst	Solvent	Time, h	Yield **3**,[b] %	Ratio **8**:**9**[c]
1	Pd-SBA-15-SH(g)	H_2O	5	48	2:98
2	Pd-SBA-15-SH(g)	H_2O	13	55	18:82
3	Pd-SBA-15-SH(cc)	H_2O	5	42	10:90
4	Pd-SBA-15-SH(cc)	H_2O	20	42	15:85
5[d]	Pd-SBA-15-SH(cc)	H_2O	5	69	27:73
6	Pd-SiO_2-SH	H_2O	5	94	10:90

[a] Reaction conditions: See Experimental for details; [b] Determined by GC-FID; [c] Measured by ^{1}H NMR; [d] 3 equivalents $PhB(OH)_2$.

The three-phase material **5** generated using method B had a lower free amine content as determined by elemental analysis. Use of this material under the aqueous three-phase conditions (**Table 3-12** entries 1 and 2) resulted in improved yields of **3**, as well as increased reaction on support. It is clear then that under aqueous conditions the supported Pd materials studied are likely reservoirs for homogeneous catalyst. Material **5** was also used to assess DMF:H_2O mixtures and it was found that at a ratio of 4:1 (entry 5), there was also significant conversion on support. By contrast at 20:1 DMF:H_2O, the standard solvent ratio, minimal conversion on the three-phase material was observed (entry 6). It would be tempting to conclude that the catalyst was functionally heterogeneous under these conditions but it was also entirely likely that differential solvation of the three-phase material slowed the reaction on support. To examine this possibility, Pd/C was assessed under identical three-phase conditions. Numerous studies have indicated that Pd/C operates in cross-coupling reactions via a homogeneous mechanism.[30] Employing Pd/C (entry 7) also resulted in limited conversion on the three-phase material, confirming our suspicion that material **5** was unable to detect a homogeneous Pd catalyst in 20:1 DMF:H_2O. Calibration of the three-phase test in this way, with a material well accepted to be a reservoir for a homogeneous catalyst, is rarely seen in publications purporting the discovery of a truly heterogeneous Pd cross-coupling catalyst;[53] but should be a necessary control experiment as it provides a benchmark with which to assess three-phase results.

Table 3-12. Summary of three-phase test data for material **5** produced by Method B in **Scheme 3-16**[a]

Entry	Catalyst	Solvent	Time, h	Yield **3**,[b] %	Ratio **8**:**9**[c]
1	Pd-SBA-15-SH(g)	H_2O	5	74	4:96
2	Pd-SBA-15-SH(g)	H_2O	24	90	40:60
3	Pd-SBA-15-SH(cc)	H_2O	5	63	4:96
4	Pd-SiO_2-SH	H_2O	5	95	40:60
5	Pd-SBA-15-SH(g)	4:1 DMF:H_2O	5	90	25:75
6	Pd-SBA-15-SH(g)	20:1 DMF:H_2O	5	65	4:96
7	Pd/C	20:1 DMF:H_2O	5	48	2:98

[a] Reaction conditions: See Experimental for details; [b] Determined by GC-FID; [c] Measured by ^{1}H NMR.

The preponderance of evidence from the heterogeneity tests discussed above suggests that Pd-SBA-15-SH(g), Pd-SBA-15-SH(cc) and Pd-SiO_2-SH act as reservoirs for homogenous catalytic species under Suzuki-Miyaura reaction conditions. The discussion also indicates that it is difficult to reach such a conclusion through the use of a single test, such an assessment is best made by considering data obtained from multiple methods as each test is not infallible.[55] Particular caution must also be exercised when using heterogeneity tests that do not directly probe the active species as there are always multiple reasons why reactions do not proceed. A suggestion to improve the solid phase poison test would be to add highly effective materials such as SiO_2-SH or SiO_2-NH_2 after reaction has initiated and then look for cessation of catalysis. In particular, the sensitivity of the three-phase tests to the precise conditions, particularly solvent, reaction time and amount of aryl-boronic acid partner, should serve as a caution in the use of this otherwise superb test of heterogeneity.

3.4 Conclusions

Pd-SBA-15-SH(g) is an effective and recyclable catalyst for the Suzuki-Miyaura reaction. The hallmark of this supported catalyst is the low amount of Pd leaching upon use; the amount of metal leached corresponded to <1 % of the initially added metal even after several recycles. For the reactions studied here, the concentration of Pd was always in the ppb range as measured by ICP-MS analysis. It was found that Pd-SBA-15-SH(g) was a more recyclable and active catalyst than Pd-SBA-15-SH(cc) and Pd-SiO_2-SH. A TEM study of Pd-SBA-15-SH(g) after a single use indicated that the mesostructure of the material was retained; furthermore Pd nanoparticles were also apparent. The size of the nanoparticles (3 – 6 nm) was limited by the pore dimensions (6 – 8 nm). The size distribution of the nanoparticles was used to partially rationalize the enhanced reusability of Pd-SBA-15-SH(g). By comparison, Pd-SiO_2-SH does not have ordered pores to limit particle growth and thus a variety of sizes of nanoparticles are observed on its surface. Physisorption analysis of Pd-SBA-15-SH(g) over the course of several recycles indicated that the structure of the material degrades significantly after several uses. A similar study of Pd-SBA-15-SH(cc) and analogous materials, demonstrated that collapse of the mesostructure was coincident with complete loss of catalytic activity. Loss of activity was expected in these cases because the bulk of the added Pd would be sequestered from the reagents in solution.

Control experiments indicated that the base used for the Suzuki-Miyaura reaction promoted degradation of the mesoporous support. The effect was mitigated under the reaction conditions ascribed to a stabilizing effect due to the formation of boric acid. Methods to increase condensation of the silica network enhanced the stability of the mesostructure, as well as methods that capped silanols on the external surface. While all these approaches lead to more robust

catalysts, most of these materials were less recyclable. Fellow graduate student Ben Glasspoole, was able to synthesize an Al-SBA-15 material that was stable to the reaction conditions with good recyclability and low Pd leaching.[47]

The nature of the active catalyst, homogeneous or heterogeneous, for Pd-SBA-15-SH(g) was assessed in detail in light of conflicting results from heterogeneity tests by us[51] and others.[40] As mentioned, Pd nanoparticles were observed and it is generally understood that their formation is symptomatic of a homogeneous catalytically active Pd species. Upon study, more evidence was obtained to support the contention that Pd-SBA-15-SH(g) does generate a soluble homogeneous catalyst under the reaction conditions. Evidence included the observation of an induction period upon lowering the catalyst loading. Solid phase poisons demonstrated that Pd-SBA-15-SH(g) was inactive upon exposure to materials designed to scavenge soluble Pd. Finally the three-phase test demonstrated that cross-coupling can occur on a supported aryl-halide. Pd-SBA-15-SH(cc) and Pd-SiO_2-SH materials also provided similar results. As it is difficult to ascertain catalyst heterogeneity or homogeneity by any single tests it is advisable to utilize several when interested in carrying out such an assessment. That said, the three-phase test is the most powerful of those employed herein because it directly reports on the active catalyst, it is however vitally important that suitable controls be performed to determine whether the homogeneous catalyst can detect the supported reagent.

3.5 Experimental

3.5.1 General

All reactions were performed under an Ar atmosphere unless otherwise noted. Reagents and solvents were obtained from Aldrich and used as is unless otherwise noted. Phenylboronic acid was purchased from Frontier Scientific. Palladium acetate trimer was purchased from Pressure

Chemicals. $CDCl_3$ was purchased from Cambridge Isotopes. Silica gel-100 (amorphous SiO_2) was purchased from Fluka. *p*-Bromoacetophenone was recrystallized from hot 95% ethanol prior to use. Chromatograms were collected on an Agilent Technologies 6850A Network GC System equipped with an HP-5 ((5%-phenyl)-methylpolysiloxane 30 m × 0.32 mm × 0.25 μm) column and a FID detector. Transmission electron microscopy (TEM) images were collected on a JEOL 2011 STEM at the University of New Brunswick. XRD patterns were collected on a Phillips-XRD system at the University of Laval. Elemental analysis for C,H,N and S was performed by Canadian Microanalytical Services Ltd. Nitrogen adsorption/desorption isotherms were collected at 77 K on Micrometrics ASAP 2010 instrument. SBA-15 and SBA-15-SH(g) samples were degassed at 353 K prior to analysis. Pd-SBA-15-SH(g) samples were degassed at 298 K prior to analysis. Surface area (S_{BET}) measured by the Brunauer-Emmett-Teller (BET)[75] method in region $P/P_0 = 0.07 – 0.20$. Pore size was measured from the maxima of the pore size distribution curve calculated by the Barrett-Joyner-Halenda (BJH)[76] method using the adsorption branch of the isotherm assuming a cylindrical pore structure. The pore volume was measured from the amount of gas adsorbed at a relative pressure (P / P_0) of 0.99. ^{1}H NMR spectra were collected on a Bruker Advance 300, 400 or 500 MHz NMR spectrometer as indicated, chemical shifts are reported in ppm and referenced to residual solvent.

3.5.2 Synthesis of SBA-15

The sol-gel procedure was adapted from Stucky *et al.*[71] P123 (4.0 g) was weighed into a 500 mL glass jar fitted with a stir bar, distilled H_2O (30 mL) was added and the mixture stirred for 4 h at 35 °C until homogeneous. A 2 M $HCl_{(aq)}$ solution was prepared by diluting 36.5 – 38.0 wt% HCl (20 mL) in distilled H_2O (100 mL), the 2 M $HCl_{(aq)}$ was added to the surfactant containing solution. The resulting mixture was stirred for 24 h at 35 °C. TEOS (9.0 mL) was added via

syringe over a period of 1 min to the mixture which was stirred at 35 °C for a further 24 h after which the stir bar was removed and the jar was sealed tightly for a static hydrothermal treatment at 80 °C for 48 h. The as-synthesized material (as-SBA-15) was recovered by filtration without washing and dried overnight in air and in a vacuum oven at 80 ºC for 3 days. This procedure furnished 5 g of as-synthesized SBA-15. The surfactant was removed by Soxhlet extraction or calcination. Soxhlet extraction was performed on 2.0 g batches of as-synthesized SBA-15. The material was doubly wrapped in filter paper (125 mm in diameter) placed in a 100 mL thimble and was extracted with hot 95 % ethanol for 5 days. The recovered material was dried in a vacuum oven at 80 °C overnight. Alternatively, calcination was performed on a 2.0 g batch of the material divided between two crucibles which were placed temperature controlled oven programmed with the following parameters: 1 °C/min ramp-up from 25 °C to 550 °C, hold for 480 min and a 1.5 °C/min ramp down to 25 °C.

3.5.3 Grafting MPTMS onto SBA-15: SBA-15-SH(g)

In a typical procedure, SBA-15 (900 mg) was added to a 50 mL round bottom flask, suspended in toluene (50 mL) and flushed with Ar. MPTMS (3.6 mL) was added via syringe and the suspension was stirred at 110 ºC for 18 h followed by filtration and washing with Et_2O (3 × 15 mL). The recovered powder was placed in a Soxhlet extractor fitted with a 100 mL thimble and washed with hot 95% EtOH for 1 day. The material was recovered and dried under vacuum at room temperature for 18 h. The procedure furnished 625 mg of a white powder. The final S content varied between 0.6 - 1.1 mmol S / g as determined by elemental analysis and was dependent on the batch of SBA-15 employed.

3.5.4 Grafting Large Quantities of MPTMS onto SBA-15: H-SBA-15-SH(g)

The synthesis was adapted from Fryxell *et al*.[74] SBA-15 (500 mg) was added to a 250 mL round bottom flask, suspended in toluene (90 mL), flushed with Ar and stirred at 80 ºC. H_2O (1.75 mL) was added to the solution; clumps formed and were broken up using a stirring rod. MPTMS (3.6 mL) was added via syringe and the suspension was stirred at 110 ºC for 18 h followed by filtration and washing with Et_2O (50 mL). The recovered powder was placed in a Soxhlet extractor fitted with a 100 mL thimble and washed with hot 95% EtOH for 1 day. The material was recovered and dried under vacuum at room temperature for 18 h. The procedure furnished 400 mg of a white powder. The final S content was 2.02 mmol S / g as determined by elemental analysis.

3.5.5 Treatment of SBA-15-SH(g) with trimethylsilyl chloride: TMS-SBA-15-SH(g)

SBA-15 (400 mg) was added to a 50 mL round bottom flask, suspended in toluene (25 mL) and flushed with Ar. Trimethylsilyl chloride (1.3 mL) and pyridine (0.8 mL) were added to the suspension via syringe. The mixture was stirred at room temperature for 5 h followed by heating to 110 ºC for 18 h. The powder was recovered by filtration, and then placed in a Soxhlet extractor fitted with a 100 mL thimble and washed with hot 95% EtOH for 1 day. The material was recovered and dried under vacuum at room temperature for 18 h. The procedure furnished 360 mg of a white powder.

3.5.6 Synthesis of Pd-SBA-15-SH(g)

An amount of $Pd(OAc)_2$ corresponding to half the amount of S as determined by elemental analysis was placed in a 100 mL round bottom flask and dissolved in THF (50 mL). SBA-15-SH(g) (500 mg) was added and the suspension stirred for 2 h. The solution was filtered, washed with THF (3 × 50 mL) and dried under vacuum at room temperature for 18 h. The procedure

furnished 450 mg of a red-orange powder. The amount of Pd loaded was determined by an ICP-MS analysis of the supernatant after filtration and washings (> 99.9% of initial Pd added was scavenged from solution). The final material is assumed to have a molar S : Pd ratio of 2 : 1.

3.5.7 Synthesis of PhBpin

In a typical procedure phenylboronic acid (4.00 g, 33.1 mmol) was added to a 150 mL round bottom flask and dissolved in benzene (40 mL). Pinacol (4.86 g, 39.6 mmol) was added to the above solution. The solution was stirred at 60 ºC for 2 h and the solvent was evaporated under reduced pressure. The residue was purified on the automated chromatography system Biotage Horizon^{TM} Flash Collector programmed with the following conditions: Column equilibration at 98 : 2 (Hexanes : EtOAc) for 3 column volumes (CV), sample was loaded, linear ramp from 98 : 2 to 90 : 10 (Hexanes : EtOAc) over 1 CV and hold at 90 : 10 (Hexanes : EtOAc) for 6 CV. Collection was monitored by UV at 256 nm. Fractions were concentrated under reduced pressure to give a white powder which was stored at 4 ºC. Yield: 6.10 g (90%). The NMR spectra were consistent with literature reports. ^{1}H NMR (300 MHz, $CDCl_3$): δ 1.37 (s, 12H, pincaolCH_3), 7.39 (t, 2H, $^{3}J_{H\text{-}H}$ = 8 Hz, Ar-*H*), 7.48 (t, 1H, $^{3}J_{H\text{-}H}$ = 8 Hz, Ar-*H*), 7.84 (d, 2H, $^{3}J_{H\text{-}H}$ = 8 Hz, Ar-*H*).

3.5.8 General Method for the Suzuki-Miyaura reaction

In a typical procedure an amount of Pd-SBA-15-SH(g) (5 mg, 0.0025 mmol Pd at 0.50 mmol Pd/g) corresponding to 1 mol % Pd was weighed out followed by *p*-bromoacetophenone (50 mg, 0.25 mmol), K_2CO_3 (70 mg, 0.50 mmol), PhBpin (75 mg, 0.38 mmol) and the internal standard 1,4-dimethoxybenzene (35 mg, 0.25 mmol). A 50 mL sealed tube fitted with a stir bar and septum was charged with the weighed materials and flushed with Ar. DMF (2.5 mL) and distilled H_2O (0.125 mL) freshly degassed by bubbling Ar for 15 min was added via syringe. The solution was stirred vigorously under an Ar atmosphere and the tube was heated at 80 ºC. Reaction progress

was monitored by GC-FID (Injection: Splitless, Inlet pressure: 25 psi, Temperature protocol: 40 ºC – 230 ºC at 10 ºC /min) and typically took 4 h to reach completion.

3.5.9 General Method for GC-FID Calibration

1,4-Dimethoxybenzene (27 mg, 0.20 mmol) was weighed into a 1 dram vial. One of the analytes *p*-bromoacetophenone (20 mg, 0.10 mmol), PhBpin (20 mg, 0.10 mmol), **3** (40 mg, 0.20 mmol) or bibenzyl (30 mg, 0.20 mmol) was weighed into a separate 1 dram vial. To each vial was added CH_2Cl_2 (2.00 mL) via a volumetric pipette and the vials were capped. The solutions were well mixed and in 100 µL portions the analyte (A) and 1,4-dimethoxybezene (DMB) stock were dispensed into 1 dram vials to give the volumes noted (A:DMB 100 : 500 µL, 200 : 400 µL, 300 : 300 µL, 400 : 200 µL, 500 : 100 µL). A volume (0.10 mL) from each standard solution was transferred to a 0.5 dram vial and analyzed by GC-FID (Injection: Splitless, Inlet pressure: 25 psi, Temperature protocol: 40 ºC – 230 ºC at 10 ºC /min). The obtained signal and mole ratios were plotted and fitted using linear regression analysis. The response factors and small x-intercepts are recorded in (**Table 3-13**).

Table 3-13. Summary of data from GC-FID calibration curves[a]

Analyte	Retention time, min	M	b	R^2
p-bromoacetophenone, **1**	8.24	1.017	-0.078	0.999
PhBpin, **2**	8.78	0.554	-0.029	0.998
3	14.4	0.469	0.035	0.999
Bibenzyl	8.94	0.493	0.009	0.999

[a] Fitting equation y = mx + b where y = integration DMB/integration Analyte and x = mole ratio of DMB/Analyte. The retention time of 1,4-dimethoxy benzene was 6.03 min.

3.5.10 Method for the Suzuki-Miyaura reaction under air atmosphere

An amount of Pd-SBA-15-SH(g) (5 mg, 0.0025 mmol Pd at 0.50 mmol Pd/g) corresponding to 1 mol % Pd was weighed out followed by *p*-bromoacetophenone (50 mg, 0.25 mmol), K_2CO_3 (70 mg, 0.50 mmol), PhBpin (75 mg, 0.38 mmol) and the internal standard 1,4-dimethoxybenzene (35 mg, 0.25 mmol). A 50 mL test tube fitted with a stir bar and septum was charged with the weighed materials. DMF (2.5 mL) and distilled H_2O (0.125 mL) was added via syringe. The solution was stirred vigorously and the tube was heated at 80 ºC. Reaction progress was monitored by GC-FID (Injection: Splitless, Inlet pressure: 25 psi, Temperature protocol: 40 ºC – 230 ºC at 10 ºC /min) and typically took 8 h to reach completion.

3.5.11 Method for the Suzuki-Miyaura reaction under O_2 atmosphere

An amount of Pd-SBA-15-SH(g) (5 mg, 0.0025 mmol Pd at 0.50 mmol Pd / g) corresponding to 1 mol % Pd was weighed out followed by *p*-bromoacetophenone (50 mg, 0.25 mmol), K_2CO_3 (70 mg, 0.50 mmol), PhBpin (75 mg, 0.38 mmol) and the internal standard 1,4-dimethoxybenzene (35 mg, 0.25 mmol). A 50 mL test tube fitted with a stir bar and septum was charged with the weighed materials. DMF (2.5 mL) and distilled H_2O (0.125 mL) was added via syringe. The flask was fitted with a balloon containing O_2 and the atmosphere was exchanged by evacuating the flask and back filling three times. The solution was stirred vigorously and the tube was heated at 80 ºC. Reaction progress was monitored by GC-FID (Injection: Splitless, Inlet pressure: 25 psi, Temperature protocol: 40 ºC – 230 ºC at 10 ºC /min).

3.5.12 General method for measuring Pd-SBA-15-SH(g) turnover number

In a typical procedure an amount of Pd-SBA-15-SH(g) (2.5 mg, 0.0013 mmol Pd at 0.50 mmol Pd/g) corresponding to 0.01 mol % Pd was weighed out followed by *p*-bromoacetophenone (2.50 g, 12.5 mmol), K_2CO_3 (3.50 g, 25 mmol), PhBpin (3.85 mg, 18.8 mmol) and the internal standard

1,4-dimethoxybenzene (1.70 g, 12.5 mmol). A 100 mL round bottom flask fitted with a stir bar and septum was charged with the weighed materials and flushed with Ar. DMF (25 mL) and distilled H_2O (1.25 mL) freshly degassed by bubbling Ar for 15 min was added via syringe. The solution was stirred vigorously under an Ar atmosphere and the flask was heated at 80 ºC. Reaction progress was monitored by GC-FID (Injection: Splitless, Inlet pressure: 25 psi, Temperature protocol: 40 ºC – 230 ºC at 10 ºC /min).

3.5.13 General method for measuring Pd-SBA-15-SH(g) turnover number

In a typical procedure an amount of Pd-SBA-15-SH(g) (2.5 mg, 0.0013 mmol Pd at 0.50 mmol Pd/g) corresponding to 0.01 mol % Pd was weighed out followed by *p*-bromoacetophenone (2.50 g, 12.5 mmol), K_2CO_3 (3.50 g, 25 mmol), PhBpin (3.85 mg, 18.8 mmol) and the internal standard 1,4-dimethoxybenzene (1.70 g, 12.5 mmol). A 100 mL round bottom flask fitted with a stir bar and septum was charged with the weighed materials and flushed with Ar. DMF (25 mL) and distilled H_2O (1.25 mL) freshly degassed by bubbling Ar for 15 min was added via syringe. The solution was stirred vigorously under an Ar atmosphere and the flask was heated at 80 ºC. Reaction progress was monitored by GC-FID (Injection: Splitless, Inlet pressure: 25 psi, Temperature protocol: 40 ºC – 230 ºC at 10 ºC /min).

3.5.14 General method for a Suzuki-Miyaura recycling study

In a typical procedure an amount of Pd-SBA-15-SH(g) (100 mg, 0.041 mmol Pd at 0.41 mmol Pd/g) corresponding to 1 mol % Pd was weighed out followed by *p*-bromoacetophenone (825 mg, 4.10 mmol), K_2CO_3 (1.14 g, 8.30 mmol), PhBpin (1.27 g, 6.20 mmol) and the internal standard 1,4-dimethoxybenzene (200 mg, 1.45 mmol). A 100 mL round bottom flask fitted with a stir bar and septum was charged with the weighed materials and flushed with Ar. DMF (40 mL) and distilled H_2O (2.0 mL) freshly degassed by bubbling Ar for 15 min was added via syringe.

The solution was stirred vigorously under an Ar atmosphere and the flask was heated at 80 ºC. Reaction progress was monitored by GC-FID (Injection: Splitless, Inlet pressure: 25 psi, Temperature protocol: 40 ºC – 230 ºC at 10 ºC /min). After 5 h of heating the reaction was allowed to cool to room temperature and it was filtered. The recovered solids were washed with copious amounts of EtOAc, H_2O and Et_2O and dried in vacuum at room temperature. The procedure was repeated with the recovered material, the stoichiometry was adjusted after each cycle to the recovered amount of Pd-SBA-15-SH(g) (assumed > 99 % Pd recovery as confirmed by ICP-MS).

3.5.15 Preparation of ICP-MS samples

The reaction mixture was allowed to cool from 80 ºC to room temperature. The solids were removed by Büchner filtration and they were washed with EtOAc. The filtrate was concentrated by blowing N_2 over the surface. To the residue was added EtOAc (5 mL), the suspension was sonicated for 5 min and the residual solids were filtered using a 0.10 µm PTFE membrane. A 25.00 mL volumetric flask was charged with the second filtrate. The residue washing procedure was repeated 3 times and the solution in the volumetric flask was diluted to the line. After vigorous mixing an aliquot (3.0 mL) of the volumetric stock solution was placed into a 1 dram glass vial which is sealed and submitted for ICP-MS analysis.

3.5.16 Method to assess stability of Soxhlet extracted SBA-15-SH(g) in 20 : 1 DMF : H_2O

SBA-15-SH(g) (60 mg) was weighed out and added to a 50 mL round bottom flask fitted with a stir bar and septum. DMF (20 mL) and distilled H_2O (1.0 mL) was added to the flask via syringe. The suspension was heated at 80 ºC for 1 day. The solution was filtered and the recovered material was washed with EtOAc and H_2O and dried under vacuum at room temperature

furnishing 33 mg of a white powder. The procedure was also performed without a stir bar. The recovered materials were analyzed by N_2 physisorption, see **Figure 3-8** and **Table 3-7**.

3.5.17 Method to assess stability of Soxhlet extracted SBA-15-SH(g) in 20:1 DMF:H_2O with K_2CO_3

SBA-15-SH(g) (60 mg) and K_2CO_3 (590 mg, 4.25 mmol) were weighed out and added to a 50 mL round bottom flask fitted with a stir bar and septum. DMF (20 mL) and distilled H_2O (1.0 mL) was added to the flask via syringe. The suspension was heated at 80 ºC for 4 h. The solution was filtered and the recovered material was washed with EtOAc and H_2O and dried under vacuum at room temperature furnishing 20 mg of a white powder. The procedure was also performed without a stir bar. The recovered materials were analyzed by N_2 physisorption, see **Figure 3-8** and **Table 3-7**.

3.5.18 Method to assess Pd leaching of Pd-SBA-15-SH(g) in 20:1 DMF:H_2O

Pd-SBA-15-SH(g) (6 mg, 0.0025 mmol Pd at 0.41 mmol Pd / g) was weighed and added to a 50 mL test tube fitted with a stir bar and septum. DMF (40 mL) and distilled H_2O (2.0 mL) freshly degassed by bubbling Ar for 15 min was added via syringe. The solution was stirred vigorously under an Ar atmosphere and the flask was heated at 80 ºC. After 24 h the solids were collected by Büchner filtration. The recovered material was washed with copious amounts of EtOAc and an ICP-MS sample was prepared according to the procedure outlined above.

3.5.19 Method to assess Pd leaching of Pd-SBA-15-SH(g) in 20:1 DMF:H_2O with K_2CO_3

Pd-SBA-15-SH(g) (6 mg, 0.0025 mmol Pd at 0.41 mmol Pd / g) and K_2CO_3 (590 mg, 4.25 mmol) were weighed and added to a 50 mL test tube fitted with a stir bar and septum. DMF (40 mL) and distilled H_2O (2.0 mL) freshly degassed by bubbling Ar for 15 min was added via syringe. The solution was stirred vigorously under an Ar atmosphere and the flask was heated at 80 ºC. After

24 h the solids were collected by Büchner filtration. The recovered material was washed with copious amounts of EtOAc and an ICP-MS sample was prepared according to the procedure outlined above.

3.5.20 Method to observe an induction period with Pd-SBA-15-SH(g) under Suzuki-Miyaura reaction conditions

An amount of Pd-SBA-15-SH(g) (1 mg, 0.0005 mmol Pd at 0.50 mmol Pd/g) corresponding to 0.1 mol % Pd was weighed out followed by *p*-bromoacetophenone (100 mg, 0.50 mmol), K_2CO_3 (140 mg, 1.00 mmol), PhBpin (150 mg, 0.74 mmol) and the internal standard 1,4-dimethoxybenzene (80 mg, 0.58 mmol). A 50 mL sealed tube fitted with a stir bar and septum was charged with the weighed materials and flushed with Ar. DMF (5 mL) and distilled H_2O (0.25 mL) was added via syringe. The solution was stirred vigorously and the tube was heated at 80 ºC. Reaction progress was monitored by GC-FID (Injection: Splitless, Inlet pressure: 25 psi, Temperature protocol: 40 ºC – 230 ºC at 10 ºC /min).

3.5.21 Solid phase poison test: SiO_2-SH

An amount of Pd-SBA-15-SH(g) (6 mg, 0.0025 mmol Pd at 0.41 mmol Pd / g) corresponding to 1 mol % Pd was weighed out followed by *p*-bromoacetophenone (50 mg, 0.25 mmol), K_2CO_3 (70 mg, 0.50 mmol), PhBpin (75 mg, 0.38 mmol), SiO_2-SH (75 mg, 0.10 mmol S at 1.2 mmol S / g, S : Pd = 35 : 1) and the internal standard 1,4-dimethoxybenzene (35 mg, 0.25 mmol). A 50 mL sealed tube fitted with a stir bar and septum was charged with the weighed materials and flushed with Ar. DMF (2.5 mL) and distilled H_2O (0.125 mL) freshly degassed by bubbling Ar for 15 min was added via syringe. The solution was stirred vigorously under an Ar atmosphere and the tube was heated at 80 ºC. Reaction progress was monitored by GC-FID (Injection: Splitless, Inlet pressure: 25 psi, Temperature protocol: 40 ºC – 230 ºC at 10 ºC /min).

3.5.22 Solid phase poison test: SiO_2-NH_2

An amount of Pd-SBA-15-SH(g) (6 mg, 0.0025 mmol Pd at 0.41 mmol Pd / g) corresponding to 1 mol % Pd was weighed out followed by *p*-bromoacetophenone (50 mg, 0.25 mmol), K_2CO_3 (70 mg, 0.50 mmol), PhBpin (75 mg, 0.38 mmol), SiO_2-NH_2 (85 mg, 0.10 mmol N at 1.0 mmol N / g, N : Pd = 35 : 1) and the internal standard 1,4-dimethoxybenzene (35 mg, 0.25 mmol). A 50 mL sealed tube fitted with a stir bar and septum was charged with the weighed materials and flushed with Ar. DMF (2.5 mL) and distilled H_2O (0.125 mL) freshly degassed by bubbling Ar for 15 min was added via syringe. The solution was stirred vigorously under an Ar atmosphere and the tube was heated at 80 ºC. Reaction progress was monitored by GC-FID (Injection: Splitless, Inlet pressure: 25 psi, Temperature protocol: 40 ºC – 230 ºC at 10 ºC /min).

3.5.23 Solid phase poison test: Quadrapure™ TU

An amount of Pd-SBA-15-SH(g) (5 mg, 0.0025 mmol Pd at 0.50 mmol Pd / g) corresponding to 1 mol % Pd was weighed out followed by *p*-bromoacetophenone (50 mg, 0.25 mmol), K_2CO_3 (70 mg, 0.50 mmol), PhBpin (75 mg, 0.38 mmol), Quadrapure™ TU (25 mg, 0.10 mmol N at 1.0 mmol N / g, S : Pd = 35 : 1) and the internal standard 1,4-dimethoxybenzene (35 mg, 0.25 mmol). A 50 mL sealed tube fitted with a stir bar and septum was charged with the weighed materials and flushed with Ar. DMF (2.5 mL) and distilled H_2O (0.125 mL) freshly degassed by bubbling Ar for 15 min was added via syringe. The solution was stirred vigorously under an Ar atmosphere and the tube was heated at 80 ºC. Reaction progress was monitored by GC-FID (Injection: Splitless, Inlet pressure: 25 psi, Temperature protocol: 40 ºC – 230 ºC at 10 ºC /min).

3.5.24 Solid phase poison test: Polyvinylpyridine (PVP)

An amount of Pd-SBA-15-SH(g) (5 mg, 0.0025 mmol Pd at 0.50 mmol Pd / g) corresponding to 1 mol % Pd was weighed out followed by *p*-bromoacetophenone (50 mg, 0.25 mmol), K_2CO_3 (70

mg, 0.50 mmol), PhBpin (75 mg, 0.38 mmol), polyvinylpyridine (75 mg, 0.75 mmol N at 1.0 mmol N / g, N : Pd = 300 : 1) and the internal standard 1,4-dimethoxybenzene (35 mg, 0.25 mmol). A 50 mL sealed tube fitted with a stir bar and septum was charged with the weighed materials and flushed with Ar. DMF (2.5 mL) and distilled H_2O (0.125 mL) freshly degassed by bubbling Ar for 15 min was added via syringe. The solution was stirred vigorously under an Ar atmosphere and the tube was heated at 80 ºC. Reaction progress was monitored by GC-FID (Injection: Splitless, Inlet pressure: 25 psi, Temperature protocol: 40 ºC – 230 ºC at 10 ºC /min).

3.5.25 Methods for the preparation of three-phase material: 5

Method A

The procedure was adapted from Crudden *et al*.[40] SiO_2-NH_2 (2.00g) was weighed out and added to a 100 mL round bottom flask fitted with a stir bar and septum. THF (20 mL) was added to the flask and the suspension was stirred at room temperature. 4-Bromobenzoyl chloride (1.30 g, 10.5 mmol) was weighed and added quickly to the above solution followed by the addition of pyridine (808 µL, 10.5 mmol) via syringe. The suspension was stirred at 40 ºC overnight and filtered. The recovered material was washed with CH_2Cl_2 (40 mL), 5% HCl (40 mL), 0.02 M K_2CO_3 (40 mL), H_2O (2 × 40 mL), EtOH (2 × 40 mL) and dried under vacuum at room temperature overnight giving 2.20 g of a white powder. Elemental analysis: weight %C = 10.38 (8.65 mmol/g), %H = 1.32 (13.2 mmol/g), %N = 1.51 (1.07 mmol/g), %Br = 5.60 (0.7 mmol/g).

Method B

Step 1: Preparation of 4-bromobenzamide-3-propyltriethoxysilane:

Bromo-benzoyl chloride (4.00 g, 18.2 mmol) was weighed out and quickly added to a 250 mL round bottom flask fitted with a stir bar and septum and placed under an Ar atmosphere. THF (100 mL) was added and the solution was stirred at -15 °C using an acetone ice bath. Freshly

distilled N-methyl morpholine was added dropwise followed by the addition of 3-aminopropyl triethoxysilane, a white precipitate formed. The reaction mixture was allowed to stir and warm to room temperature over 2 h. The solution was filtered and the solvent removed under reduced pressure. Care was taken to ensure that the residue never heated above 30 ºC a precaution taken to alleviate opportunity for self-condensation. The residue solidified to a beige solid under vacuum overnight. Yield: 4.30 g (55 %). ^{1}H NMR (500 MHz, $CDCl_3$): δ 0.75 (t, 2H, $^{3}J_{H\text{-}H}$ = 8 Hz, $NHCH_2CH_2CH_2Si$), 1.25 (t, 9H, $^{3}J_{H\text{-}H}$ = 7 Hz, $Si(OCH_2CH_3)_3$), 1.78 (p, 2H, $^{3}J_{H\text{-}H}$ = 8 Hz, $NHCH_2CH_2CH_2Si$), 3.50 (q, 2H, $^{3}J_{H\text{-}H}$ = 8 Hz, $NHCH_2CH_2CH_2Si$), 3.85 (q, 6H, $^{3}J_{H\text{-}H}$ = 7 Hz, $Si(OCH_2CH_3)_3$), 6.68 (br, 1H, $NHCH_2CH_2CH_2Si$), 7.60 (d, 2H, $^{3}J_{H\text{-}H}$ = 8 Hz, Ar-*H*), 7.69 (d, 2H, $^{3}J_{H\text{-}H}$ = 8 Hz, Ar-*H*).

Step 2: Preparation of 5 by grafting 4-bromobenzamide-3-propyltriethoxysilane onto amorphous SiO_2

Fluka SiO_2 (1.2 g) and freshly prepared 4-bromobenzamide 3-propyltriethoxysilane (4.20 g, 10.4 mmol) were weighed out and added to a 15 mL round bottom flask fitted with a stir bar and condenser. Toluene was added the solution was stirred. Pyridine was added via syringe. The solution was stirred at 130 °C overnight. The suspension was allowed to cool to room temperature and was filtered. The recovered solid was washed with CH_2Cl_2 (40 mL) and placed in a Soxhlet extractor equipped with 100 mL thimble and washed with hot CH_2Cl_2 overnight. The material was dried under vacuum giving 1.2 g of an off-white powder. Elemental analysis: weight %C = 12.72 (10.59 mmol/g), %H = 1.41 (14.1 mmol/g), %N = 1.53 (1.08 mmol/g), %Br = 7.91 (0.98 mmol/g).

3.5.26 General procedure for the three-phase test in H_2O

Step 1

An amount of Pd-SBA-15-SH(g) (6 mg, 0.0025 mmol Pd at 0.41 mmol Pd / g) corresponding to 1 mol % Pd was weighed out followed by *p*-bromoacetophenone (50 mg, 0.25 mmol), K_2CO_3 (70 mg, 0.50 mmol), phenylboronic acid (55 mg, 0.38 mmol) and three-phase material **5** (250 mg, 0.25 mmol Br at 1.0 mmol Br / g). A 50 mL sealed tube fitted with a stir bar and septum was charged with the weighed materials and flushed with Ar. H_2O (2.5 mL) freshly degassed by bubbling Ar for 15 min was added via syringe. The solution was stirred vigorously under an Ar atmosphere and the tube was heated at 80 ºC. After the allotted time the reaction was allowed to cool and the solution filtered and the recovered solids were washed with EtOAc. The filtrate was concentrated by blowing N_2 over the surface of the solution. The internal standard 1,4-dimethoxybenzene (35 mg, 0.25 mmol) and the yield of 3 was measured by GC-FID (Injection: Splitless, Inlet pressure: 25 psi, Temperature protocol: 40 ºC – 230 ºC at 10 ºC /min).

Step 2

The following procedure was employed to hydrolyze the amide linkages on the three-phase material. The recovered three-phase material was suspended in EtOH (10mL) and H_2O (5 mL) solution containing KOH (1.70 g, 30.0 mmol) in a 50 mL round bottom flask. The suspension was heated at 90 ºC for 3 days. The suspension was allowed to cool to room temperature, neutralized with 2 M HCl and extracted with EtOAc and CH_2Cl_2. The combined organic layers were dried with $MgSO_4$, filtered and concentrated under reduced pressure. The residue was analyzed by ^{1}H NMR the relative intensities of the following signals were used to assess the ratio of **8** : **9**. ^{1}H NMR (500 MHz, 1 : 1 $CDCl_3$: d_6-DMSO): δ 7.54 (d, 2H, $^3J_{H\text{-}H}$ = 8 Hz, Ar-*H*, 4-

bromoboronic acid **9**), 7.61 (d, 2H, $^{3}J_{H\text{-}H}$ = 8 Hz, Ar-*H*, 4-phenylboronic acid **8**), 7.85 (d, 2H, $^{3}J_{H\text{-}H}$ = 8 Hz, Ar-*H*, 4-bromoboronic acid **9**), 8.05 (d, 2H, $^{3}J_{H\text{-}H}$ = 8 Hz, Ar-*H*, 4-phenylboronic acid **8**)

3.5.27 Procedure for the three-phase test in 4:1 DMF:H_2O

An amount of Pd-SBA-15-SH(g) (6 mg, 0.0025 mmol Pd at 0.41 mmol Pd / g) corresponding to 1 mol % Pd was weighed followed by *p*-bromoacetophenone (50 mg, 0.25 mmol), K_2CO_3 (70 mg, 0.50 mmol), phenylboronic acid (55 mg, 0.38 mmol), three-phase material **5** (250 mg, 0.25 mmol Br at 1.0 mmol Br / g) and the internal standard 1,4-dimethoxybenzene (35 mg, 0.25 mmol). A 50 mL sealed tube fitted with a stir bar and septum was charged with the weighed materials and flushed with Ar. DMF (2.0 mL) and distilled H_2O (0.5 mL) freshly degassed by bubbling Ar for 15 min was added via syringe. The solution was stirred gently under an Ar atmosphere and the tube was heated at 80 ºC. Reaction progress was monitored by GC-FID (Injection: Splitless, Inlet pressure: 25 psi, Temperature protocol: 40 ºC – 230 ºC at 10 ºC /min). After reaction the suspension was allowed to cool and was filtered. The recovered solids were washed with EtOAc. The amide linkages on the three-phase material where hydrolyzed and the ratio of **8**:**9** was measured as described above.

3.5.28 General procedure for the three-phase test in 20:1 DMF:H_2O

An amount of Pd-SBA-15-SH(g) (6 mg, 0.0025 mmol Pd at 0.41 mmol Pd / g) corresponding to 1 mol % Pd was weighed out followed by *p*-bromoacetophenone (50 mg, 0.25 mmol), K_2CO_3 (70 mg, 0.50 mmol), PhBpin (75 mg, 0.38 mmol), three-phase material **5** (250 mg, 0.25 mmol Br at 1.0 mmol Br / g) and the internal standard 1,4-dimethoxybenzene (35 mg, 0.25 mmol). A 50 mL sealed tube fitted with a stir bar and septum was charged with the weighed materials and flushed with Ar. DMF (2.5 mL) and distilled H_2O (0.125 mL) freshly degassed by bubbling Ar for 15 min was added via syringe. The solution was stirred gently under an Ar atmosphere and the tube was

heated at 80 ºC. Reaction progress was monitored by GC-FID (Injection: Splitless, Inlet pressure: 25 psi, Temperature protocol: 40 ºC – 230 ºC at 10 ºC /min). After reaction the suspension was allowed to cool and was filtered. The recovered solids were washed with EtOAc. The amide linkages on the three-phase material where hydrolyzed and the ratio of **8**:**9** was measured as described above.

3.6 References

(1) Miyaura, N.; Suzuki, A. *Chem. Rev.* **1995**, *95*, 2457-83.

(2) Crudden, C. M.; Glasspoole, B. W.; Lata, C. J. *Chem. Commun.* **2009**, 6704-6716.

(3) Imao, D.; Glasspoole, B. W.; Laberge, V. S.; Crudden, C. M. *J. Am. Chem. Soc.* **2009**, *131*, 5024-5025.

(4) Sandrock, D. L.; Jean-Gerard, L.; Chen, C.; Dreher, S. D.; Molander, G. A. *J. Am. Chem. Soc.* **2010**, *132*, 17108-17110.

(5) Molander, G. A.; Shin, I.; Jean-Gerard, L. *Org. Lett.* **2010**, *12*, 4384-4387.

(6) Ohmura, T.; Awano, T.; Suginome, M. *J. Am. Chem. Soc.* **2010**, *132*, 13191-13193.

(7) Molander, G. A.; Sandrock, D. L. *Curr. Opin. Drug Discovery Dev.* **2009**, *12*, 811-823.

(8) Miyaura, N.; Yamada, K.; Suzuki, A. *Tetrahedron Lett.* **1979**, *20*, 3437-3440.

(9) Miyaura, N.; Suzuki, A. *J. Chem. Soc. Chem. Commun.* **1979**, 866-867.

(10) Suzuki, A. *Angew. Chem. Int. Ed.* **2011**, *50*, 6722-6737.

(11) Budarin, V. L.; Shuttleworth, P. S.; Clark, J. H.; Luque, R. *Curr. Org. Synth.* **2010**, *7*, 614-627.

(12) Yasuda, N. *J. Organomet. Chem.* **2002**, *653*, 279-287.

(13) Corbet, J. P.; Mignani, G. *Chem. Rev.* **2006**, *106*, 2651-2710.

(14) Larsen, R. D.; King, A. O.; Chen, C. Y.; Corley, E. G.; Foster, B. S.; Roberts, F. E.; Yang, C.; Lieberman, D. R.; Reamer, R. A. *J. Org. Chem.* **1994**, *59*, 6391-6394.

(15) Magano, J.; Dunetz, J. R. *Chem. Rev.* **2011**, *111*, 2177-2250.

(16) Ismail, M. A. H.; Barker, S.; Ella, A. E.; Abouzid, K. A. M.; Toubar, R. A.; Todd, M. H. *J. Med. Chem.* **2006**, *49*, 1526-1535.

(17) Carini, D. J.; Duncia, J. V.; Aldrich, P. E.; Chiu, A. T.; Johnson, A. L.; Pierce, M. E.; Price, W. A.; Santella, J. B.; Wells, G. J. *J. Med. Chem.* **1991**, *34*, 2525-2547.

(18) Bühlmayer, P.; Furet, P.; Criscione, L.; de Gasparo, M.; Whitebread, S.; Schmidlin, T.; Lattmann, R.; Wood, J. *Bioorg. Med. Chem. Lett.* **1994**, *4*, 29-34.

(19) Garrett, C.; Prasad, K. *Adv. Synth. Catal.* **2004**, *346*, 889-900.

(20) Slagt, V. F.; de Vries, AndreÌ • H. M.; de Vries, J. G.; Kellogg, R. M. *Org. Process Res. Dev.* **2010**, *14*, 30-47.

(21) Galaffu, N.; Man, S. P.; Wilkes, R. D.; Wilson, J. R. H. *Org. Process Res. Dev.* **2007**, *11*, 406-413.

(22) Barbaras, D.; Brozio, J.; Johannsen, I.; Allmendinger, T. *Org. Process Res. Dev.* **2009**, *13*, 1068-1079.

(23) Urawa, Y.; Miyazawa, M.; Ozeki, N.; Ogura, K. *Org. Process Res. Dev.* **2003**, *7*, 191-195.

(24) Molnár, Á. *Chem. Rev.* **2011**, *111*, 2251-2320.

(25) Yin, L.; Liebscher, J. *Chem. Rev.* **2007**, *107*, 133-173.

(26) Polshettiwar, V.; Len, C.; Fihri, A. *Coord. Chem. Rev.* **2009**, *253*, 2599-2626.

(27) Colacot, T. J. *Top. Catal.* **2008**, *48*, 91-98.

(28) Mozing, R. *Org. Synth.* **1955**, *3*, 685-685.

(29) Marck, G.; Villiger, A.; Buchecker, R. *Tetrahedron Lett.* **1994**, *35*, 3277-3280.

(30) Felpin, F.; Ayad, T.; Mitra, S. *Eur. J. Org. Chem.* **2006**, *2006*, 2679-2690.

(31) Narayanan, R.; Tabor, C.; El-Sayed, M. A. *Top. Catal.* **2008**, *48*, 60-74.

(32) Han, P.; Wang, X.; Qiu, X.; Ji, X.; Gao, L. *J. Mol. Catal. A: Chem.* **2007**, *272*, 136-141.

(33) Durap, F.; Rakap, M.; Aydemir, M.; Özkar, S. *Appl. Catal. A* **2010**, *382*, 339-344.

(34) Shylesh, S.; Wang, L.; Thiel, W. R. *Adv. Synth. Catal.* **2010**, *352*, 425-432.

(35) Yamada, Y. M. A.; Takeda, K.; Takahashi, H.; Ikegami, S. *J. Org. Chem.* **2003**, *68*, 7733-7741.

(36) Yang, H.; Han, X.; Li, G.; Wang, Y. *Green Chem.* **2009**, *11*, 1184-1193.

(37) Churruca, F.; SanMartin, R.; Ines, B.; Tellitu, I.; Dominguez, E. *Adv. Synth. Catal.* **2006**, *348*, 1836-1840.

(38) Corma, A.; Das, D.; Garcia, H.; Leyva, A. *J. Catal.* **2005**, *229*, 322-331.

(39) Baleizão, C.; Corma, A.; García, H.; Leyva, A. *J. Org. Chem.* **2004**, *69*, 439-446.

(40) Crudden, C. M.; Sateesh, M.; Lewis, R. *J. Am. Chem. Soc.* **2005**, *127*, 10045-10050.

(41) Kang, T.; Park, Y.; Yi, J. *Ind. Eng. Chem. Res.* **2004**, *43*, 1478-1484.

(42) Phan, N. T. S.; Van, D. S., Matthew; Jones, C. W. *Adv. Synth. Catal.* **2006**, *348*, 609-679.

(43) Ley, S. V.; Ramarao, C.; Gordon, R. S.; Holmes, A. B.; Morrison, A. J.; McConvey, I. F.; Shirley, I. M.; Smith, S. C.; Smith, M. D. *Chem. Commun.* **2002**, 1134-1135.

(44) Sigma Aldrich, *Pd EnCat™ Experimental Guide* [http://www.sigmaaldrich.com.proxy.queensu.ca/etc/medialib/docs/Aldrich/Bulletin/al_exp_guide_pdencat.Par.0001.File.tmp/al_exp_guide_pdencat.pdf] Retrieved: 06/07/2011.

(45) Crudden, C. M.; McEleney, K.; MacQuarrie, S. L.; Blanc, A.; Sateesh, M.; Webb, J. D. *Pure Appl. Chem.* **2007**, *79*, 247-260.

(46) Webb, J. D.; MacQuarrie, S.; McEleney, K.; Crudden, C. M. *J. Catal.* **2007**, *252*, 97-109.

(47) Glasspoole, B. W.; Webb, J. D.; Crudden, C. M. *J. Catal.* **2009**, *265*, 148-154.

(48) Nohair, B.; MacQuarrie, S.; Crudden, C. M.; Kaliaguine, S. *J. Phys. Chem. C* **2008**, *112*, 6065-6072.

(49) MacQuarrie, S.; Nohair, B.; Horton, J. H.; Kaliaguine, S.; Crudden, C. M. *J. Phys. Chem. C* **2010**, *114*, 57-64.

(50) Shimizu, K.; Koizumi, S.; Hatamachi, T.; Yoshida, H.; Komai, S.; Kodama, T.; Kitayama, Y. *J. Catal.* **2004**, *228*, 141-151.

(51) Richardson, J. M.; Jones, C. W. *J. Catal.* **2007**, *251*, 80-93.

(52) Weck, M.; Jones, C. W. *Inorg. Chem.* **2007**, *46*, 1865-1875.

(53) Dhara, K.; Sarkar, K.; Srimani, D.; Saha, S. K.; Chattopadhyay, P.; Bhaumik, A. *Dalton Trans.* **2010**, *39*, 6395-6402.

(54) Ellis, P. J.; Fairlamb, I. J. S.; Hackett, S. F. J.; Wilson, K.; Lee, A. F. L. *Angew. Chem. Int. Ed.* **2010**, *49*, 1820-1824.

(55) Widegren, J. A.; Finke, R. G. *J. Mol. Catal. A: Chem.* **2003**, *198*, 317-341.

(56) Maegawa, T.; Kitamura, Y.; Sako, S.; Udzu, T.; Sakurai, A.; Tanaka, A.; Kobayashi, Y.; Endo, K.; Bora, U.; Kurita, T.; Kozaki, A.; Monguchi, Y.; Sajiki, H. *Chem. Eur. J.* **2007**, *13*, 5937-5943.

(57) MacQuarrie, S.; Horton, J. H.; Barnes, J.; McEleney, K.; Loock, H. P.; Crudden, C. M. *Angew. Chem. Int. Ed.* **2008**, *47*, 3279-3282.

(58) Conlon, D.; Pipik, B.; Ferdinand, S.; LeBlond, C.; Sowa, J.; Izzo, B.; Collins, P.; Ho, G.; Williams, J. â.; Shi, Y.; Sun, Y. *Adv. Synth. Catal.* **2003**, *345*, 931-935.

(59) Zhao, F.; Shirai, M.; Ikushima, Y.; Arai, M. *J. Mol. Catal. A: Chem.* **2002**, *180*, 211-219.

(60) Gaikwad, A. V.; Holuigue, A.; Thathagar, M. B.; ten Elshof, J. E.; Rothenberg, G. *Chem. Eur. J.* **2007**, *13*, 6908-6913.

(61) Richardson, J. M.; Jones, C. W. *Adv. Synth. Catal.* **2006**, *348*, 1207-1216.

(62) Huang, L.; Ang, T. P.; Wang, Z.; Tan, J.; Chen, J.; Wong, P. K. *Inorg. Chem.* **2011**, *50*, 2094-2111.

(63) Rebek, J.; Gavina, F. *J. Am. Chem. Soc.* **1974**, *96*, 7112-14.

(64) Rebek, J.; Brown, D.; Zimmerman, S. *J. Am. Chem. Soc.* **1975**, *97*, 454-5.

(65) Davies, I. W.; Matty, L.; Hughes, D. L.; Reider, P. J. *J. Am. Chem. Soc.* **2001**, *123*, 10139-10140.

(66) Adamo, C.; Amatore, C.; Ciofini, I.; Jutand, A.; Lakmini, H. *J. Am. Chem. Soc.* **2006**, *128*, 6829-6836.

(67) Lakmini, H.; Ciofini, I.; Jutand, A.; Amatore, C.; Adamo, C. *J. Phys. Chem. A* **2008**, *112*, 12896-12903.

(68) Sigman, M. S.; Jensen, D. R. *Acc. Chem. Res.* **2006**, *39*, 221-229.

(69) Xie, Y.; Quinlivan, S.; Asefa, T. *J. Phys. Chem. C* **2008**, *112*, 9996-10003.

(70) McEleney, K.; Crudden, C. M.; Horton, J. H. *J. Phys. Chem. C* **2009**, *113*, 1901-1907.

(71) Zhao, D.; Huo, Q.; Feng, J.; Chmelka, B. F.; Stucky, G. D. *J. Am. Chem. Soc.* **1998**, *120*, 6024-6036.

(72) Koyano, K. A.; Tatsumi, T.; Tanaka, Y.; Nakata, S. *J. Phys. Chem. B* **1997**, *101*, 9436-9440.

(73) Kisler, J. M.; Gee, M. L.; Stevens, G. W.; O'Connor, A. J. *Chem. Mater.* **2003**, *15*, 619-624.

(74) Feng, X.; Fryxell, G. E.; Wang, L. Q.; Kim, A. Y.; Liu, J.; Kemner, K. M. *Science* **1997**, *276*, 923-926.

(75) Brunauer, S.; Emmett, P. H.; Teller, E. *J. Am. Chem. Soc.* **1938**, *60*, 309-319.

(76) Barrett, E. P.; Joyner, L. G.; Halenda, P. P. *J. Am. Chem. Soc.* **1951**, *73*, 373-380.

Chapter 4

General Introduction to Hydrogen Release and Regeneration of NH_3BH_3: A Promising Hydrogen Storage Material

4.1 Introduction

Environmental consciousness and doubts about the availability of fossil fuels in the future have raised concerns about the continued use of these materials in energy applications.[1] This reality has created an incentive to develop technologies, such as the PEM (Polymer Electrolyte Membrane) Fuel Cell that employ hydrogen as an energy carrier instead of fossil fuels. The PEM Fuel Cell is being studied for applications in stationary and mobile power generation as an alternative to the internal combustion engine for motor vehicles.[1, 2] In this type of fuel cell, the energy released from the conversion of H_2 and O_2 to H_2O is harnessed to provide power.[1] But, before this technology can be widely employed a number of challenges need to be met. As this particular topic is expansive, discussion in this manuscript will be focused on challenges associated with on-board hydrogen storage associated with light duty motor vehicles.

The DOE (US Department of Energy) has developed a set of targets that describe minimum requirements for a viable on-board hydrogen storage technology (**Table 4-1**).[3] While many technologies are being developed, there is currently no methodology that even comes close to meeting all of these standards.[2, 4] Of the different approaches, chemical hydrides are of special interest because there are several materials that exceed the volumetric and gravimetric constraints set by the DOE. One prominent example of a chemical hydride is ammonia borane (NH_3BH_3), a material which can furnish a maximum of 3 equivalents of H_2 per molecule. Because NH_3BH_3 is inherently light weight and dense, the amount of hydrogen that can be released from NH_3BH_3 is

exceptionally high as the material possesses a 0.195 kg H_2/kg (19 wt%) gravimetric and a 0.71 kg H_2/L volumetric density of hydrogen. For reference purposes **Figure 4-1** gives an idea of how NH_3BH_3 stacks up against other hydrogen storage strategies.[5] Note that it is only one of a few storage strategies that far exceed the Ultimate DOE targets, and this is a chief reason why there is significant interest in developing methods to release hydrogen from NH_3BH_3 as a hydrogen storage material.

Table 4-1. Selected DOE hydrogen storage targets[a]

Parameters	Targets		
	2010	2015	Ultimate
Gravimetric Density, kg H_2/kg (wt%)	0.045 (4.5)	0.055 (5.5)	0.075 (7.5)
Volumetric Density, kg H_2/L (vol %)	0.028 (2.8)	0.040 (4.0)	0.070 (7.0)
Operating Temperature, ºC	-30 – 50	-40 – 60	-40 – 60
Max Operating Temperature, ºC	-40 – 85	-40 – 85	-40 – 85
Fuel Cost $/gge[b]	3 – 7	2 – 6	2 – 3
Minimum Full Flow Rate (g/s)[c]	0.38	0.38	0.38
Operation Cycle Life[d]	1000	1500	1500

[a] Targets based on the entire storage system for a vehicle traveling 300 miles; [b] gge = gasoline gallon equivalent; [c] Assuming a 150 kW vehicle power plant; [d] From ¼ tank to full

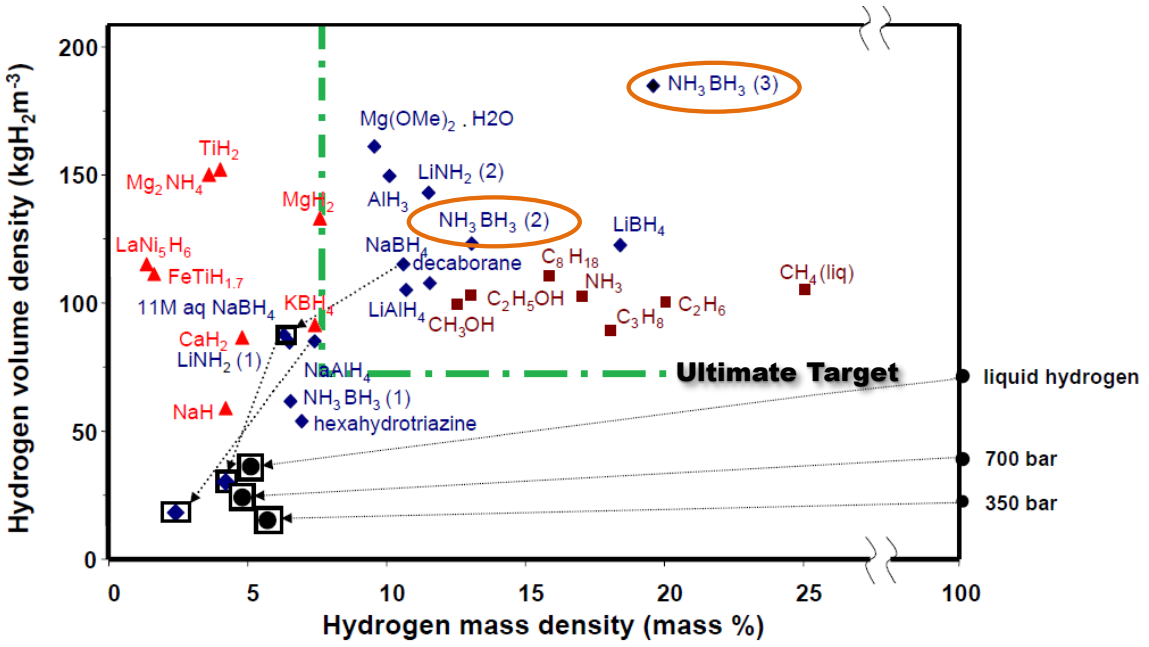

Figure 4-1. A comparison of the volumetric and gravimetric densities of some proposed hydrogen storage technologies, 2 and 3 equivalents of hydrogen release from NH_3BH_3 are marked by circles, adapted from reference 5

In addition to the properties noted in Table 4-1, an on-board hydrogen storage technology that employs ammonia borane must meet a number of other criteria.[3] The technology must be able to furnish high purity H_2 (99.97 %), free of fuel cell poisons such as NH_3 and borazine. The release must be controlled; rapid and large enough at normal operating temperatures to meet the demands of fuel cell powered motor vehicle. Last but not least, to complete the hydrogen cycle the waste material after hydrogen release must be able to be regenerated to ammonia borane efficiently (well-to-tank efficiency of 60 %). The focus of the research discussed in subsequent chapters will be on developing a strategy to address this latter point, which until recently, has been the subject of remarkably little research. However, any discussion of regeneration must

begin with a brief introduction to the methods of hydrogen release, as these strategies determine the properties of the waste material that must be reconstituted.

There has been a large amount of research focused on outlining strategies for the dehydrogenation of NH_3BH_3, and this work has been aptly reviewed by a number of groups.[4, 6-10] There are two different strategies to release hydrogen from NH_3BH_3: solvolysis and dehydrocoupling (**Scheme 4-1**). Solvolysis involves the reaction of NH_3BH_3 with water or an alcohol such as methanol. The process is normally performed in the presence of a catalyst and produces, hydrogen, ammonia and boric acid derivatives. Impressive rates have been achieved; however, these reactions possess a low gravimetric and volumetric density and are highly exothermic (*ca* -60 kcal mol^{-1} / -250 kJ mol^{-1}).[7, 11, 12] As well be discussed later on, technologies that involve a highly exothermic hydrogen release from NH_3BH_3 also produce a large energy barrier that must be overcome during regeneration. For this reason hydrogen release by solvolysis is considerably less ideal than by dehydrocoupling (*ca* -15 kcal mol^{-1} / -64 kJ mol^{-1} depending on the extent of dehydrogenation).[11, 13]

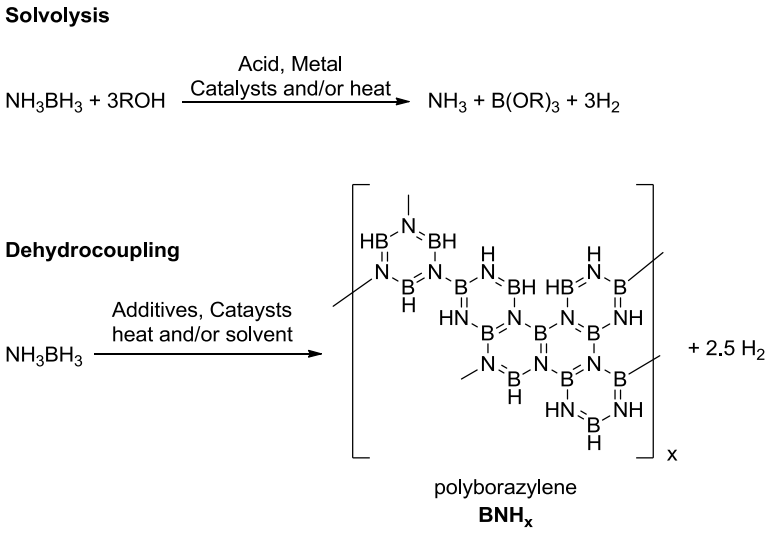

Scheme 4-1. General conceptualization of hydrogen production from NH_3BH_3 by solvolysis and dehydrocoupling

Dehydrocoupling reactions release hydrogen from NH_3BH_3 by forming new networks of B-N bonds. The structure of the boron waste product depends heavily on the approach taken. The goal in dehydrocoupling is to release ~2.5 equivalents of hydrogen gas which corresponds to a gravimetric density of ~16 wt% H_2.[14] The product of such a reaction contains B, N as well as some residual H held in N-H and B-H bonds and will be termed BNH_x. If ~ 2.5 equivalents of hydrogen are released from NH_3BH_3 the structure of BNH_x is considered to be an irregular network polymer of polyborazylene, also referred to as polyborazine. Dehydrocoupling can be accomplished by heating NH_3BH_3 in the solid state or in solution; the presence of additives and/or catalysts can improve the quantity of H_2 released as well as the kinetics on this process.

4.1.1 Solid state dehydrocoupling of NH_3BH_3

Pure NH_3BH_3 is a thermally unstable compound above 60 ºC, with the extent and rate of hydrogen release depending heavily on the heating conditions. There are three stages to the dehydrogenation, reactions 1-3 (**Scheme 4-2**).[4, 7, 15-17] Loss of the first equivalent of hydrogen forms a material termed polyaminoborane (PAB). Loss of the second gives polyiminoborane (PIB) and further dehydrogenation leads to BNH_x, then boron nitride (BN) respectively. At a heating rate of 5 ºC /min, two equivalents of hydrogen can be released as the temperature is raised to ~ 200 ºC.[15-17] Autrey[18] and co-workers studied the thermolysis of NH_3BH_3 in the solid state at 88 ºC using ^{11}B MAS NMR. They noted that during the induction period prior to hydrogen evolution from NH_3BH_3, a new mobile phase formed. The new phase is believed to result from the disruption of dihydrogen bonding network in crystalline NH_3BH_3.[18] Formation of this new solid phase is followed by partial disproportionation to give isomeric diammoniate of diborane (DADB). DADB is believed to act as a promoter for chain growth and H_2 evolution rapidly initiates after it begins to accumulate. Depicted in **Scheme 4-3** is a proposed mechanism for dehydrogenation and chain growth of PAB.

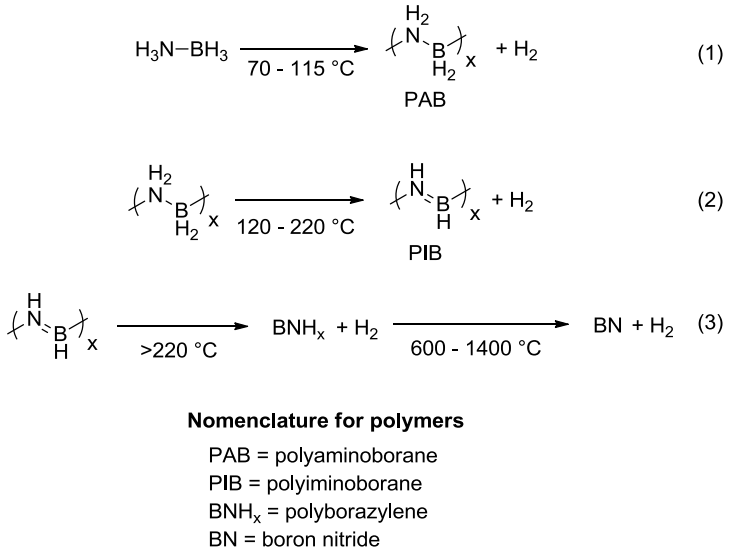

Scheme 4-2. Representative dehydrogenation reactions that occur during the thermolysis of NH_3BH_3

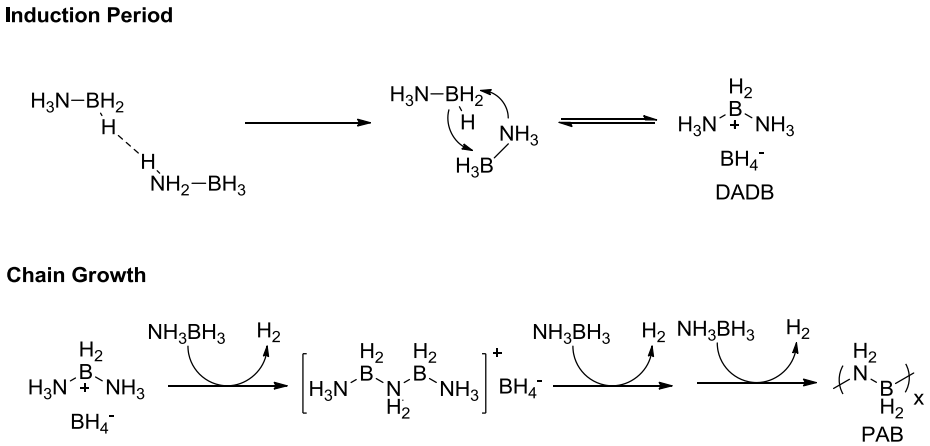

Scheme 4-3. A general decomposition pathway for thermally induced hydrogen evolution from solid NH_3BH_3

It was reported by the same group at Pacific Northwest National Labs (PNNL) that at 130 ºC up to 9 wt% of H_2 are released. Another interesting observation made during this study was that the rate of hydrogen release from solid ammonia borane could exceed the DOE target (0.38 g/s) by a factor of five.[14] The chief challenges with using solid state thermolysis in motor vehicles are management of the heat produced from dehydrogenation, reducing the temperature of dehydrogenation, developing a fuel loading strategy for solids as well as strategies to mitigate the unusual foaming/volume increase of the material that occurs during H_2 release. It was found that mesoporous materials have been able to partially address some of these challenges.[19, 20] When dispersed in the pores of SBA-15, for example, NH_3BH_3 can dehydrogenate at rates ($t_{1/2}$ < 10 min at 80 ºC)[19] that exceed DOE targets and that the reaction was less exothermic (*ca* -1 kcal mol^{-1} / -4 kJ mol^{-1}).[14] Note that this represents an improvement over solid NH_3BH_3, which dehydrogenates at 80 ºC with a substantial induction period ~ 300 min.[19, 21] The porous support does reduce the gravimetric capacity of the system to 9 wt% but it also functions to reduce foaming.[14] While it is not exactly clear why mesoporous materials have these effects on NH_3BH_3, it was postulated that confinement in the pores may produce crystal defects in NH_3BH_3 that promote dehydrogenation and/or surface silanols may provide a proton source that lower the barrier to hydrogen release.[19] In addition to porous supports, additives such as NH_4Cl and DADB have had been shown to improve NH_3BH_3 thermolysis (**Figure 4-2**).[21] Adding 5 wt% of either of these materials to solid NH_3BH_3 almost eliminates the induction period at 80 ºC with minimal material foaming.[21]

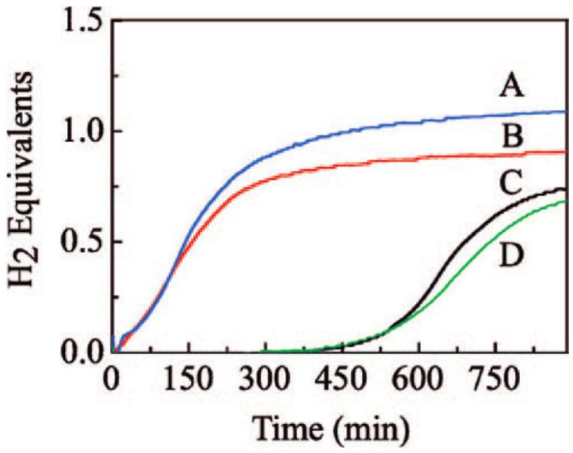

Figure 4-2. Effect of additives on hydrogen release from NH_3BH_3 at 80 ºC; A) 5 wt% NH_4Cl; B) 5 wt% DADB; C) 5 wt% $NaBH_4$; D) no additive, reproduced from reference 21 with permission

4.1.2 Dehydrocoupling of NH_3BH_3 in solution

Similar to solid state dehydrocoupling, hydrogen release from NH_3BH_3 in solution has also been extensively studied.[4, 6-10] Without catalysts or additives, the mechanism for hydrogen release in ethereal solvents is also believed to proceed through DADB (**Scheme 4-4**), but instead of oligomer formation, DADB converts first to cyclic structure CDB. Eventually CDB gives way to the trimer BCDB and hydrogen gas.[22] Note that CTB, which is isoelectric with cyclohexane and an isomer of BCDC, only appears in significant quantities in solution as borazine begins to accumulate, suggesting it is not an intermediate on the primary dehydrogenation pathway.

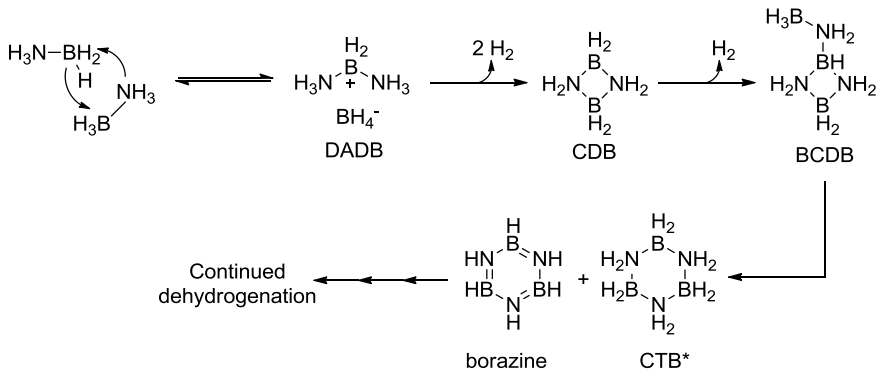

Scheme 4-4. A general decomposition pathway for thermally induced hydrogen evolution of NH_3BH_3 in solution. The asterisk denotes that it is unclear whether CTB forms from BCDB

Addition of acid[23] or transition metal catalysts[24-28] to solution has been shown to greatly enhance the rate of hydrogen release from NH_3BH_3. In 2009, Baker and Manners[6] reviewed all the catalysts reported up to that point and noted that there appears to be two distinct reaction manifolds for transition metal catalysts (**Scheme 4-5**), they either rapidly release 1 equivalent of H_2 and in some cases they exceed the DOE rate requirement or they react more slowly, but release greater than 2 equivalents of H_2.[14] The reasons for this dichotomy are still being elucidated but an ideal catalyst, which remains elusive, would be one that rapidly releases greater than 2 equivalents of H_2 from NH_3BH_3. Also efficient heterogeneous dehydrogenation catalysts are still needed, as this is a requirement for on-board storage. As of 2008, a down select process for NH_3BH_3 storage strategies indicated that homogeneous systems should only be continued to be researched in a model capacity.[14]

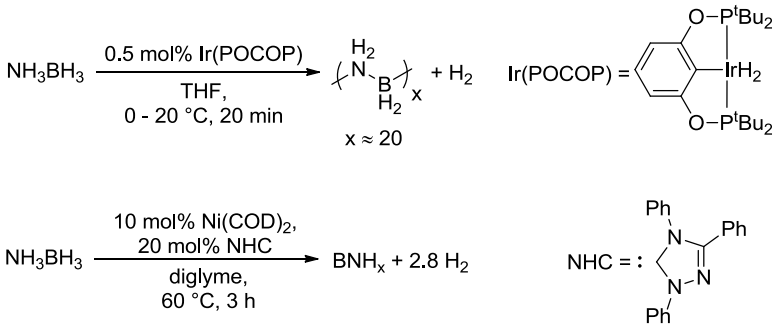

Scheme 4-5. Example catalytic dehydrocoupling reactions of NH_3BH_3 from references 24 and 26

The same report[14] also highlighted some other challenges that face solution based NH_3BH_3 dehydrogenation. An obvious issue is that the solvent dramatically reduces the gravimetric and volumetric capacity of the storage system. Also, it has become apparent that any phase change such as precipitation will be unacceptable. This is a problem for solution based approaches because the formation of precipitates is common. In fact, the formation of precipitates was key a consideration in the down select of $NaBH_4$ solvolysis as a hydrogen storage technology.[14] Nevertheless, a liquid storage technology is more ideal than employing solids alone because it fits well with existing fueling infrastructure and of late there have been some novel approaches to address the drawbacks of this type of storage.

Baker[29] recently reported dehydrocoupling of blended ammonia boranes. This system was designed to remain homogeneous over the course of the hydrogen release reaction, a parameter that necessitated the use of an ionic liquid as a co-solvent. In this system, the liquid amine borane, sec-butylamine borane serves as a solvent and mitigates the traditional loss of gravimetric capacity since it also releases hydrogen. Even though a solvent component is dehydrogenated, the overall gravimetric capacity of the system was still relatively low at 3.4 wt%

(**Scheme 4-6** and **Scheme 4-7**) and higher concentrations of NH_3BH_3 that would up the gravimetric capacity resulted in precipitation

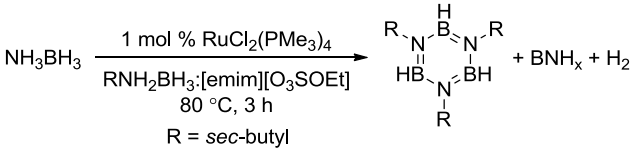

Scheme 4-6. Ru catalyzed dehydrocoupling of NH_3BH_3 with blended amine boranes; the optimum weight ratio of NH_3BH_3:RNH_2BH_3:[emim][O_3SOEt] was 6:18:15

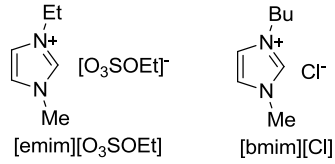

Scheme 4-7. Structure of ionic liquids [emim][O_3SOEt] and [bmim][Cl]

In 2006 Sneddon[30] reported that ionic liquids can promote hydrogen release from NH_3BH_3. It was postulated that these solvents lowered the barrier to the formation of salts, such as DADB, which have been implicated as key intermediates in dehydrocoupling reaction.[18, 22] The original ionic liquid system was reported to release up to 5.4 wt% H_2, when the weight of the solvent was taken into account. In a follow-up report, Sneddon and Baker[31] illustrated that Ru and Rh catalysts can enhance the hydrogen released from ionic liquid solutions of NH_3BH_3. A 1:1 NH_3BH_3:[bmim][Cl] (**Scheme 4-7** and **Scheme 4-8**) solution heated to 85 ºC and doped with 2.5 mol% $[Rh(COD)Cl]_2$ released an impressive ~2.5 equivalents of hydrogen which corresponds to gravimetric density of 8.1 wt% H_2, including solvent. These conditions unfortunately resulted in the formation of precipitates. The research group found that precipitation could be avoided if 1:2.5 solutions of NH_3BH_3:[emim][O_3SOEt] were used instead. While gravimetric density of the system has been lowered in this mixture, it is hoped that the solvent dependency of precipitation

demonstrates that further research into this type of dehydrocoupling is warranted especially considering they were able to achieve release of > 1 equivalent hydrogen at rates exceeding DOE targets (0.38 g/s).

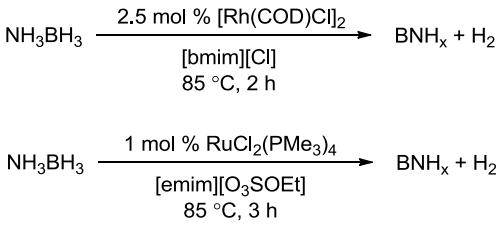

Scheme 4-8. Metal catalyzed dehydrocoupling of NH_3BH_3 in ionic liquids; optimum weight ratios of NH_3BH_3: [bmim][Cl] and NH_3BH_3:[emim][O_3SOEt] were 1:1 and 1:2.5 respectively

4.1.3 Regeneration of NH_3BH_3

Obviously, much progress has been made in developing methods to release hydrogen from NH_3BH_3 with work remaining to improve hydrogen release kinetics and the amount of hydrogen released. Nevertheless, NH_3BH_3 will not be a viable on-board hydrogen storage material in the absence of a realistic regeneration strategy to complete the hydrogen cycle.[7, 14, 32] The DOE specifications for vehicular hydrogen storage systems require that viable approaches involving chemical-hydrides must be recyclable (**Table 4-1**), otherwise the technology will not be sustainable.[33] Ideally, regeneration of NH_3BH_3 would occur on-board the vehicle presumably through a hydrogenation reaction. Unfortunately this approach has been deemed impractical for NH_3BH_3, for multiple reasons. First and most importantly, hydrogen formation from NH_3BH_3 is too exothermic to be easily reversible.[4, 7, 14] The energy released represents that minimum penalty that must be paid when regenerating the material. Recall that the dehydrocoupling route to hydrogen formation is generally exothermic, by *ca* -15 kcal mol^{-1} / -64 kJ mol^{-1},[11, 13] in the solid

state and by *ca* -60 kcal mol^{-1} / -250 kJ mol^{-1},[7, 11, 12] when solvolysis is employed. Another thermodynamic issue that an on-board regeneration scheme would have to address is the entropic penalty associated with direct hydrogenation, estimated at 8 kcal mol^{-1} / 32 kJ mol^{-1} per equivalent of hydrogen.[6] Beyond just tackling thermodynamics, a successful on-board regeneration scheme involving polyborazylene (BNH_x) would have to be effective across a structurally complex dehydrogenated material.

As can be inferred from the dehydrogenation thermodynamics of hydrogen loss from NH_3BH_3, hydrogenation of BNH_x would be highly unfavorable. The closest example of such a hydrogenation reaction is a reduction of an electronically polarized P-B bond reported by Stephan.[34] The report indicated that $^tBu_2PB(C_6F_5)_2$ could be hydrogenated at room temperature to $^tBu_2PHHB(C_6F_5)_2$ and at 1 bar hydrogen. This system, however, does not reflect the problem faced with BNH_x materials. In the Stephan system, the boron was designed to be highly electron deficient and the phosphine was electron rich. Such electronic polarization is not present in BNH_x. Furthermore, the nature of the P-B double bond is significantly different than an N-B double bond. For instance the electron cloud is less delocalized in the former bond considering the size mismatch of the atoms involved.[34] While in principle it may possible to design an analogous B-N compound that could undergo direct hydrogenation,[35-37] it is unlikely that such a substrate would reflect the electronic character of boron waste material BNH_x.

In the absence of a viable approach to an on-board regeneration strategy for NH_3BH_3, an off-board technology has been examined.[14] Off-board regeneration is less ideal for vehicular applications because it necessitates additional infrastructure to shuttle the waste material to an industrial site for reconstitution. However, this drawback may be less severe for other niche

applications of hydrogen storage materials,[2] such as those involving use as fuels for generators or fuel cells for portable electronics applications.

The general regeneration scheme for off-board regeneration of NH_3BH_3 has been outlined by multiple research groups and was summarized by Baker (**Scheme 4-9**).[7, 14] As direct hydrogenation is impractical (Step 5), the first step is digestion of BNH_x (Step 1). Effective digestion is important as it transforms BNH_x from a complex network polymer into easily handled materials such as a boron centered Lewis acid and ammonia. A generic digestion step is an important feature of this scheme because it allows the regeneration of NH_3BH_3 to be independent of the structure BNH_x, which will vary based on the extent of dehydrogenation.[38] However, regeneration schemes that do not require a digestion step, such as a direct regeneration route, would be preferable because they will have fewer steps back to NH_3BH_3.[39] It has been reported that digestion of BNH_x can be accomplished using strong acids as well as alcohols and thiols.[14, 32, 38, 40, 41] Digestion will form a boron Lewis acid(s) and may release NH_3, which can be trapped and reused for the eventually formation of NH_3BH_3.

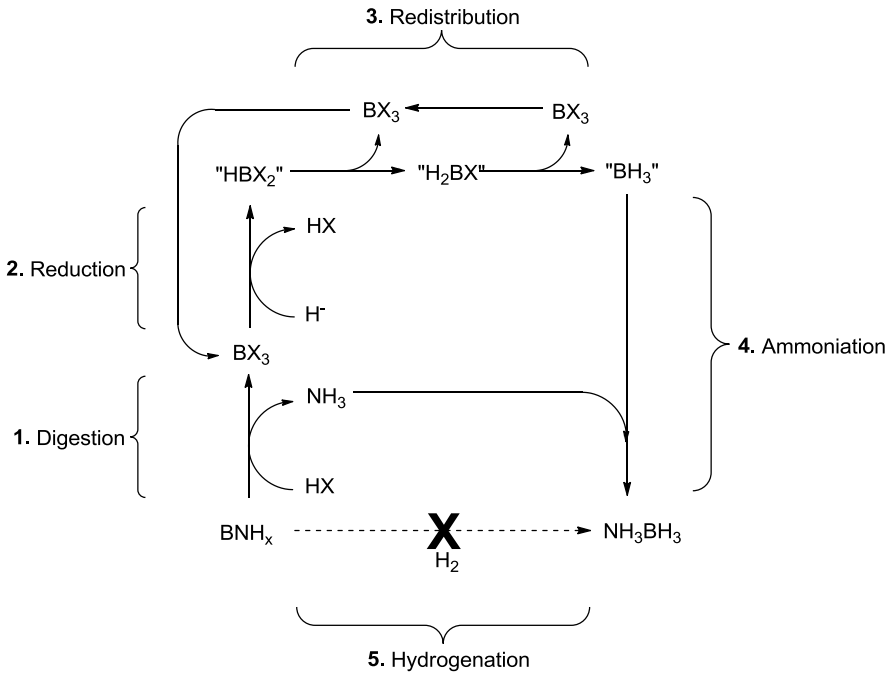

Scheme 4-9. General NH_3BH_3 regeneration scheme, from reference 14

The next step in the regeneration scheme (**Scheme 4-9**, Step 2) is the reduction of the boron Lewis acid by reaction with hydride donors (H^-) or hydrogen gas. The reduction step must form at least one B-H bond, and redistribution of these bonds will result in the formation of diborane (Step 3). Redistribution of groups on boron is common and can be facile.[38, 41-43] After reduction, NH_3BH_3 is formed by the recombination of the generated diborane with NH_3 (Step 4). In order to be effective a regeneration strategy must be energy efficient, in the near term the whole cycle should have a well-to-tank efficiency of 40 %[14] and in the long term the goal is to develop schemes with an overall efficiency of 60 % or greater.[3] An equation used by the hydrogen storage centers to evaluate the efficiency of regeneration strategies is reported below (**Eq. 3-1**).[14] The ΔH_{endo} and ΔH_{exo} are the enthalpies of reaction for the regeneration steps and 242 kJ mol^{-1} represents the lower heating value of H_2.

$$efficiency = \frac{(Equiv.\,H_2\ stored)(242\ kJ\ mol^{-1})}{(Equiv.\,H_2\ released)(57.8) + \sum(\Delta H_{endo}) - (\%\ heat\ recovery)\sum(\Delta H_{exo})}$$ **Eq. 3-1**

Effective regeneration of NH_3BH_3 requires new approaches for the production of boranes and borohydrides because the established industrial methods for the production borane[44, 45] are inefficient (**Scheme 4-10**).[7, 14] The current chemistry behind generating the B-H bond was developed initially by Schlesinger and Brown during World War II as part of a larger research project the goal which was the development of volatile uranium complexes.[46-52] The process involves the use of alkali hydrides, such as LiH and NaH, energetic materials made from reaction of Li or Na metal melts with hydrogen gas.[53] The metals themselves are generated the electrolysis process using NaCl and LiCl.[53, 54] Use of these metals or hydrides in any regeneration strategy means a significant reduction in the efficiency of the approach. As a point of reference, and as will be seen in the subsequent discussion, existing assessments of regeneration schemes that require the use Na metal at some stage have about a 45 % energy efficiency based on **Eq. 3-1**.[41] While this value exceeds the aforementioned near term goal of 40 %, it is below the minimum DOE standard of 60 % energy efficiency.[3] Current research is thus focused on developing new chemical routes for the production of boranes; regeneration schemes based on the results of some of these reports, which are also outlined below, have been calculated to have energy efficiency in excess of 70 %.

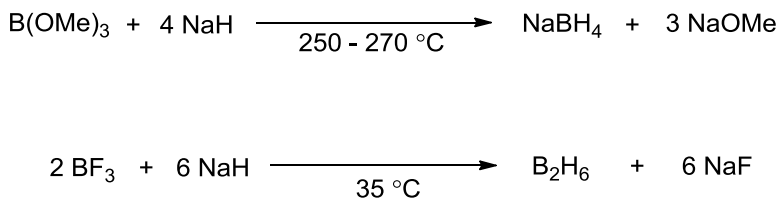

Scheme 4-10. Example reactions for the production of $NaBH_4$ and B_2H_6 from alkali metal hydrides

4.1.4 Regeneration of NH_3BH_3 using $LiAlH_4$

Ramachandran *et al.*[55] reported the first complete hydrogen cycle, which included regeneration of NH_3BH_3, in 2007 (**Scheme 4-11**). The first step of their hydrogen cycle was the methanolysis of NH_3BH_3 using a $RuCl_3$ catalyst. The system had a gravimetric density of 3.6 wt%, and it was found that $[NH_4][B(OMe)_4]$ was the main boron-containing product of reaction. A detailed comparison between the hydrolysis and alcoholysis manifolds of hydrogen production was carried out, and it was found that alcoholysis resulted in minimal release of NH_3, a known fuel cell poison. To prevent NH_3 release during the hydrolysis reaction pathways, dilute solutions, with a gravimetric density of H_2 of 1 wt% were required. NH_3BH_3 alcoholysis was superior because higher concentrations of NH_3BH_3 could be employed without NH_3 release. Instead the NH_3 was trapped as an ammonium salt. The group reported that reaction of the boron waste product $[NH_4][B(OMe)_4]$ with $LiAlH_4$ in the presence of NH_4Cl was capable of regenerating NH_3BH_3. The by-products of the regeneration were LiCl and $Al(OMe)_3$, H_2 and NH_3. Without NH_4Cl poor yields of NH_3BH_3 were observed, due to loss of NH_3.

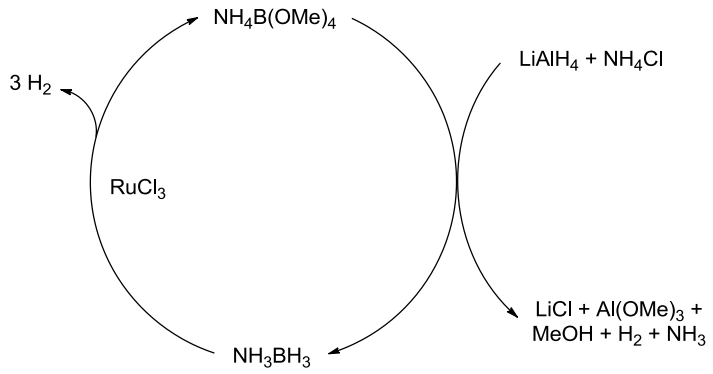

Scheme 4-11. Hydrogen cycle for methanolysis of NH_3BH_3 and regeneration based on $LiAlH_4$, adapted from reference 55

A major consideration that must be taken into account regarding the viability of this off-board regeneration strategy is the reconstitution of $LiAlH_4$ from the $Al(OMe)_3$, and LiCl by-products. $LiAlH_4$ can be made directly from the reaction of $AlCl_3$ with LiH. Note that $AlCl_3$ can be formed by reaction of $Al(OMe)_3$ with HCl.[56] Another possible route back to $LiAlH_4$ involves the reaction of Na and Al metal with hydrogen. The immediate product formed from this reaction is $NaAlH_4$ which is converted to $LiAlH_4$ by salt metathesis with LiCl.[53] Al metal can be made from $Al(OMe)_3$ by electrolysis under an atmosphere of H_2.[41] Based on the later route to the reconstitution of $LiAlH_4$, the Ramachandran regeneration scheme has energy efficiency according to **Eq 3.1** of 45 %, the most inefficient step as expected is the synthesis of Na metal from NaCl.[41]

4.1.5 Regeneration with Strong Acids and Direct Hydrogenation of BX_3 or Reaction with Inorganic Hydrides

In 2008 Mertens[38] reported a regeneration cycle (**Scheme 4-12**) for the formation of NH_3BH_3 from BNH_x. While it is clear that their process is unoptimized, several interesting results

were presented. Digestion of BNH_x was achieved using HCl and they were able to achieve 60% yield of BCl_3 after heating for 3 days at 80 ºC.[38, 40] Sneddon[40] reported to the DOE a similar digestion of BNH_x using a mixture of HBr and $AlBr_3$, in 4 h at room temperature they were able to form BBr_3. The residual boron waste from these digestion reactions was held in borazane type cyclic structures $(BX_2NH_2)_3$ the amount of which depended on the digestion conditions and the properties of BNH_x. NH_3 released during the digestion reactions was trapped as NH_4X and was recovered.

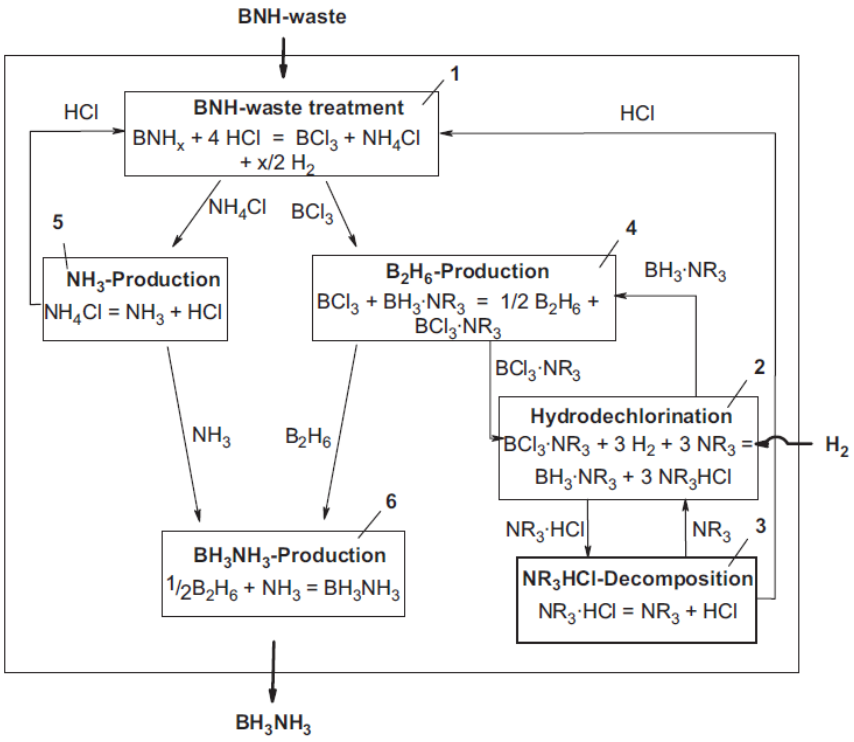

Scheme 4-12. Regeneration of NH_3BH_3 using H_2 to hydrogenate BCl_3NR_3 available from digestion BNH_x with HCl, reproduced from reference 38 with permission

It was reported in the 1960's[57, 58] that BCl_3 can be hydrogenated directly at high temperatures (> 1000 ºC) or through an Ag catalyzed reaction at 750 ºC. This reaction converts

BCl_3 to $HBCl_2$ and HCl. The reason for such harsh conditions is the thermodynamics of the reaction. Direct hydrogenation of BCl_3 is not spontaneous at ambient temperatures and pressures.[58-61] In these reports, redistribution of $HBCl_2$ to BCl_3 and BH_3 was achieved by rapidly cooling the reaction mixture to -78 ºC and distillation.[58] It is clearly more desirable for regeneration reactions to be performed under ambient or about ambient conditions; it is energy intensive to employ high temperature (750 ºC) and/or cold temperature reactions on an industrial scale (-78 ºC).

Taylor reported[42] that the addition of amine bases could reduce the temperature required for the direct hydrogenation of BCl_3. The amine base shifted the equilibrium by scavenging the HCl formed. It was noted that modulating the basicity and steric bulk of the employed amine was necessary to avoid irreversible adduct formation with BCl_3. A patent from 1960[42] demonstrated that NMe_3 could modulate the hydrogenation at temperatures of 200 ºC and high pressures, of 2000 bar. It was postulated by Mertens and coworkers[38] that milder reaction conditions could be employed if bulkier amines were used instead of NMe_3. Unfortunately such experiments were not carried out in their publication as the group did not a have suitable pressure apparatus. Instead hydrogen was substituted for the hydride donors MgH_2 and $HSiEt_3$. They found that at ambient conditions efficient redistribution of BCl_3 could be achieved using NPh_3 as the base. This reaction was carried out at 80 ºC with MgH_2 as the hydride donor and was complete in 20 min forming BH_3NPh_3 which subsequently decomposed to borane and NPh_3. Less bulky bases such as NMe_3 and NEt_3 resulted in slow reaction with MgH_2 and $HSiEt_3$. Work from the Sneddon and Thorns groups[40, 62] along these lines demonstrated that the adduct BBr_3NEt_2Ph could be converted to NH_3BH_3 on treatment with $HSiEt_3$ and NH_3. It should also be pointed out that BCl_3 can react with $HSnBu_3$ to give diborane as the major product under mild reaction conditions.[63]

Mertens[38] rightly points out that the use of inorganic hydrides for the regeneration of NH_3BH_3 can be problematic as there are only a few such hydrides that can be synthesized directly from the reaction of H_2.[38, 53] Consider as an example $HSiEt_3$, in the system described above, after reaction with BCl_3 or BBr_3 the hydride donor is converted to Cl- or $BrSiEt_3$. The standard route to reconstitute $XSiEt_3$ is reaction with NaH, which is an energy intensive material to produce.[38] Regeneration strategies that employ inorganic hydrides which can be reconstituted using H_2, or a suitable mimic, are more desirable than those that cannot.

The Sneddon iteration of the halide regeneration scheme (**Scheme 4-12**) that involved the reaction of BBr_3 with $HSnBu_3$ and NH_3 to give NH_3BH_3 and $BrSnBu_3$ was tested using **Eq. 3-1** and had 38 % overall energy efficiency.[14] It was assumed in this analysis that $BrSnBu_3$ could be reconstituted to $HSnBu_3$ by reaction with formate salt $[NHEt_3][O(O)CH]$[64] and that formic acid would be synthesized from the direct hydrogenation of CO_2, for which there is precedence.[65] While hydrogen based approach to formic acid mitigates the problem with reconstituting the Sn-H bond, formic acid is currently produced by carbonylation of methanol to give methyl formate, which is subsequently hydrolyzed to the corresponding acid.[66]

4.1.6 Regeneration using Thiols and Tin Hydrides

In 2009 the Center for Excellence in Hydrogen Storage reported a thiol based regeneration strategy (**Scheme 4-13**) for partially dehydrogenated ammonia borane.[41, 64] The waste material BNH_x was digested using 1,2-dithiobenzene yielding a mixture of $NH_4[B(PhS_2)_2]$ and $[HB(NH_3)(PhS_2)]$. On treatment with common tin hydrides, $HSnBu_3$ and H_2SnBu_2, the boron mixture was upgraded to entirely $[HB(NH_3)(PhS_2)]$ and eventually NH_3BH_3. Subsequent to the initial report, it was found that addition of NMe_3 to the reaction mixture obviated the need for H_2SnBu_2.[64]

The clear drawback of thiol based regeneration is the requirement to employ tin reagents which are highly toxic,[67] an issue that would have to be addressed if ever employed on an industrial scale. Another challenge is the high molecular weight of $HSnBu_3$ which becomes problematic on scale-up.[39] Further, at the time of publication it was not clear how the tin-thiol by-products would be reconstituted to $HSnBu_3$ without the use of energetic inorganic hydrides. Computational modeling revealed that direct hydrogenation was highly endothermic.[41] Recently, a publication from the same research group reconstituted the by-products by treatment with formic acid which was followed by thermolysis releasing CO_2 (**Scheme 4-13**).[64, 68] The overall efficiency of the thiol based regeneration scheme as calculated by **Eq. 3-1** was 78 %.

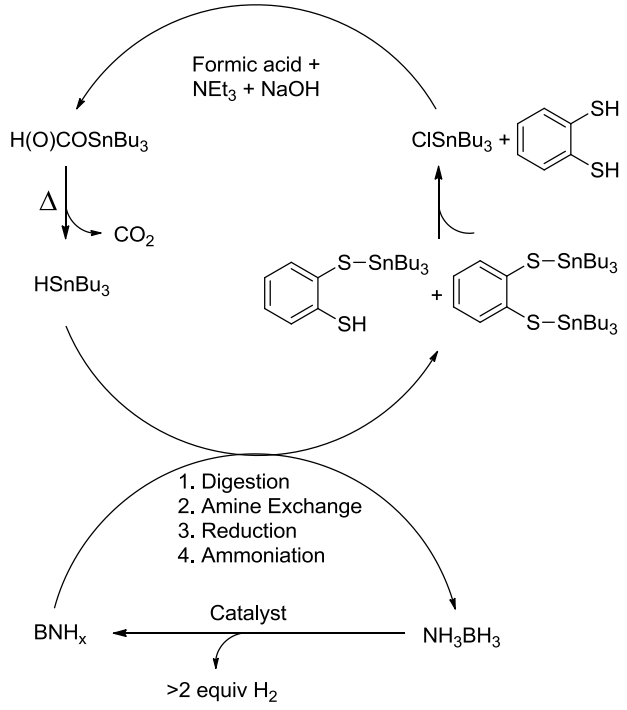

Scheme 4-13. Hydrogen cycle and regeneration of NH_3BH_3 based on $HSnBu_3$, from reference 64

4.1.7 Regeneration with Alcohols and Inorganic Hydrides

An alcohol based regeneration scheme akin to that just discussed with thiols has been proposed but has yet to be demonstrated in its entirety.[14] If successfully demonstrated, this route would have a similar theoretical efficiency to thiol based regeneration, albeit with less of a smell.[14] The BNH_x material has been treated with alcohols such as ^tBuOH and the products of the reaction preserved the residual BH bonds in the waste material giving NH_3 and $HB(O^tBu)_2$ and $B(O^tBu)_3$. Treatment of these Lewis acids with a suitable hydride donor would complete the hydrogen cycle giving NH_3BH_3. The challenges with the alcohol approach are breaking the strong B-O bonds (132 kcal mol^{-1} / 550 kJ mol^{-1}) and the low acidity of the Lewis acids,[69] theoretical calculations have suggested that strained polyols may be of some use in this regard.[14]

4.1.8 Regeneration using Transition Metal Hydrides

Dubois[43] reported an extensive study of hydride transfer from Rh-H complexes to boron Lewis acids. It was found that under these conditions reaction of $B(SPh)_3$ with Rh-H in the presence of NEt_3 resulted in exclusive formation of BH_3NEt_3 (**Scheme 4-14**), which can be converted to NH_3BH_3 on treatment with NH_3.[40] In the absence of NEt_3 several B-H containing species were formed including BH_4^-, demonstrating the significant hydricity of the Rh complexes employed. It was found that hydride could also be transferred to $B(OAr)_3$ type Lewis acids; however, efficient redistribution was not be achieved because the resulting borohydrides irreversibly disproportionated to $[B(OAr)_4]^-$ species. Similar observations were noted by Stephan when employing $B(OAr)_3$ Lewis acids for the heterolytic frustrated Lewis pair (FLP) activation of H_2.[70] While the advantage of the Dubois system over the others discussed herein is that the Rh-H complexes employed can be synthesized via direct reaction with H_2,[71] the major drawback is that the metal is prohibitively expensive.

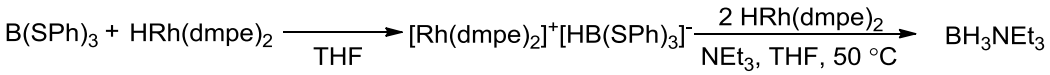

Scheme 4-14. Reaction of $B(SPh)_3$ with Rh hydrides to form BH_3NEt_3

4.1.9 Regeneration using BNH_x and Hydrazine

Recently, hydrazine (N_2H_4) was reported to react with BNH_x waste material directly to produce NH_3BH_3 (**Scheme 4-15**).[39] This regeneration scheme is particularly interesting as hydrazine is produced from NH_3 using the Olin-Raschig process. Recall that NH_3 is produced industrially from N_2 and H_2 using the Haber-Bosch process (**Scheme 4-16**).[72] Optimization of the regeneration reaction lead to the use of pressurized liquid NH_3 as solvent. The polarity of NH_3 was thought to be critical in lablizing B-N bonds, a requirement for efficient reaction of BNH_x with N_2H_4. It was found that reaction at 40 ºC for 24 h can convert BNH_x to NH_3BH_3 with 92 % yield. The excess volatiles could be removed under vacuum and the resulting NH_3BH_3 had hydrogen release properties similar to NH_3BH_3 produced using conventional methods.

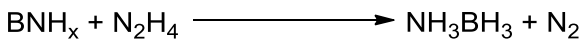

Scheme 4-15. Regeneration of NH_3BH_3 by reaction of hydrazine with BNH_x

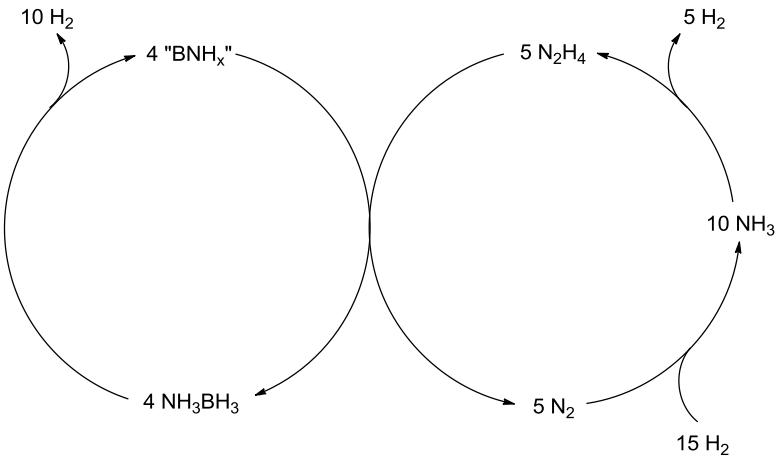

Scheme 4-16. Hydrogen cycle and regeneration of NH_3BH_3 based on N_2H_4, from reference 39

The advantage of the hydrazine based regeneration scheme (**Scheme 4-15**) over the others discussed above is that it directly converts BNH_x to NH_3BH_3 in a single processing step. Another benefit, as compared to the Bu_3SnH scheme, is the low molecular weight of N_2H_4. There are, however, some significant challenges with the use of N_2H_4 in a large scale industrial process. The current regeneration scheme uses anhydrous N_2H_4 which is dangerously reactive. The safety concerns could be partly addressed if aqueous N_2H_4 were employed instead. Also the production of N_2H_4 is energy intensive itself and the conversion of NH_3 to N_2H_4 consumes hydrogen that was fixed during the Haber-Bosch process. The authors note this in their manuscript[39] and suggest that what are needed are new methods for the production of N_2H_4. Also, they note that some of the efficiency issues could be addressed on large scale if N_2H_4 was produced at the same site where regeneration occurs.

4.1.10 Regeneration of a Hybrid Organo-Aminoborane

Part of the difficultly in regenerating NH_3BH_3 from BNH_x is a direct result of the exothermic nature the dehydrogenation reactions. Hydrocarbons by contrast are easily

hydrogenated but their dehydrogenation is strongly endothermic,[73] except for certain frameworks.[74-76] Jessop[77, 78] examined mixtures of amine boranes and organic frameworks, with the idea of using the energy released from the exothermic dehydrogenation of amine borane materials to help drive an endothermic organic dehydrogenation. While this approach does not directly address the challenge of regeneration, it lends to the possibility of using less concentrated solutions NH_3BH_3 because the solvent could potentially release H_2 as well. A challenge that he notes with his approach is matching rates of dehydrogenation of organic and inorganic components in the system.[77, 78]

Alternatively, Liu and Dixon[35, 79] have demonstrated dehydrogenation thermodynamics can be more favorable in organic molecules that possess an amine borane functional group (**Scheme 4-17**). Computational modeling indicated that dehydrogenation of their model BN heterocycles (R = H) was almost thermoneutral (ΔG = 1.9 kcal mol^{-1} / 7.9 kJ mol^{-1}). Up to this juncture dehydrogenation of their storage materials has only been modeled theoretically and their experimental efforts have been focused instead on the regeneration of the predicted waste material. So far they have been able to demonstrate that 2 equivalents of H_2 can be re-consituted by a Pd catalyzed hydrogenation (**Scheme 4-18**). Unfortunately, no hydrogenation has been observed across the BN bond. The final equivalent of H_2 is restored using KH. It is likely that milder hydrides could be used instead of this energetic material, based on the results from the NH_3BH_3 regeneration schemes discussed herein.

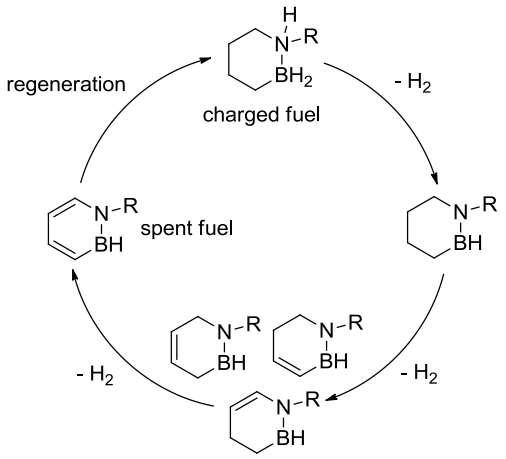

Scheme 4-17. Hydrogen cycle and regeneration of hybrid organo-amine borane hydrogen storage materials, from reference 79

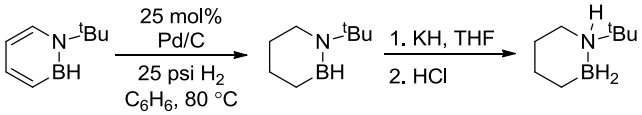

Scheme 4-18. Regeneration of a hybrid organo-amine borane hydrogen storage material

4.2 Summary

Over the last few years several amine borane regeneration schemes have begun to take shape. As outlined above each scheme has its advantages but none developed up to this juncture is wholly satisfactory and there is room for significant innovation and development of new chemistry. The discussion in the following chapters will outline progress we have made on a new regeneration scheme for BNH_x that employs organic molecules as the hydride donors to boron.

4.3 References

(1) US Department of Energy, *Multi-Year Research, Development and Demonstration Plan: Planned Program Activities for 2005-2015* [http://www1.eere.energy.gov/hydrogenandfuelcells/mypp/index.html] Retrieved: 07/03/2011.

(2) McWhorter, S.; Read, C.; Ordaz, G.; Stetson, N. *Curr. Opin. Solid State Mater. Sci.* **2011**, *15*, 29-38.

(3) US Department of Energy, *Targets for On-board Hydrogen Storage Systems for Light-Duty Vehicles* [https://www1.eere.energy.gov/hydrogenandfuelcells/storage/pdfs/targets_onboard_hydro_storage_explanation.pdf] Retrieved: 07/03/2011.

(4) Staubitz, A.; Robertson, A. P. M.; Manners, I. *Chem. Rev.* **2010**, *110*, 4079-4124.

(5) Miliken, J.; Yuzugullu, E.; Stanford, J. *The Advanced Energy Initiative: Challenges, Progress, and Opportunities* [http://repository.upenn.edu/cgi/viewcontent.cgi?article=1002&context=pennergy_presentations] Retrieved: 07/17/2011.

(6) Hamilton, C. W.; Baker, R. T.; Staubitz, A.; Manners, I. *Chem. Soc. Rev.* **2009**, *38*, 279-293.

(7) Stephens, F. H.; Pons, V.; Baker, R. T. *Dalton Trans* **2007**, 2613-2626.

(8) Han, P.; Wang, X.; Qiu, X.; Ji, X.; Gao, L. *J. Mol. Catal. A: Chem.* **2007**, *272*, 136-141.

(9) Smythe, N. C.; Gordon, J. C. *Eur. J. Inorg. Chem.* **2010**, *2010*, 509-521.

(10) Bowden, M.; Autrey, T. *Curr. Opin. Solid State Mater. Sci.* **2011**, *15*, 73-79.

(11) Dixon, D. A.; Gutowski, M. *J. Phys. Chem. A* **2005**, *109*, 5129-5135.

(12) Chase, M. W. *J. Phys. Chem. Ref. Data Monograph* **1998**, *9*, 1-1951.

(13) Miranda, C. R.; Ceder, G. *J. Chem. Phys.* **2007**, *126*, 184703.

(14) Ott, K.; Linehan, S.; Lipiecki, F.; Aradahl, C. L. *Down Select Report of Chemical Hydrogen Storage Materials, Catalysts, and Spent Fuel Regeneration Processes* [https://www1.eere.energy.gov/hydrogenandfuelcells/pdfs/chs_coe_down_select.pdf] Retrieved: 05/30/2011.

(15) Hu, M.; Geanangel, R. A.; Wendlandt, W. W. *Thermochim. Acta* **1978**, *23*, 249.

(16) Sit, V.; Geanangel, R. A.; Wendlandt, W. W. *Thermochim. Acta* **1987**, *113*, 379.

(17) Wolf, G.; Baumann, J.; Baitalow, F.; Hoffman, F. P. *Thermochim. Acta* **2000**, *343*, 19.

(18) Stowe, A. C.; Shaw, W. J.; Linehan, J. C.; Schmid, B.; Autrey, T. *Phys. Chem. Chem. Phys.* **2007**, *9*, 1831.

(19) Gutowska, A.; Li, L.; Shin, Y.; Wang, C. M.; Li, X. S.; Linehan, J. C.; Smith, R. S.; Kay, B. D.; Schmid, B.; Shaw, W. J.; Gutowski, M.; Autrey, T. *Angew. Chem. Int. Ed.* **2005**, *44*, 3578.

(20) Feaver, A.; Sepehri, S.; Shamberger, P.; Stowe, A.; Autrey, T.; Cao, G. *J. Phys. Chem. B* **2007**, *111*, 7469-7472.

(21) Heldebrant, D. J.; Karkamkar, A.; Hess, N. J.; Bowden, M.; Rassat, S.; Zheng, F.; Rappe, K.; Autrey, T. *Chem. Mater.* **2008**, *20*, 5332-5336.

(22) Shaw, W. J.; Linehan, J. C.; Szymczak, N. K.; Heldebrant, D. J.; Yonker, C.; Camaioni, D. M.; Baker, R. T.; Autrey, T. *Angew. Chem. Int. Ed.* **2008**, *47*, 7493-7496.

(23) Stephens, F. H.; Baker, R. T.; Matus, M. H.; Grant, D. J.; Dixon, D. A. *Angew. Chem. Int. Ed.* **2007**, *46*, 746.

(24) Keaton, R. J.; Blacquiere, J. M.; Baker, R. T. *J. Am. Chem. Soc.* **2007**, *129*, 1844-1845.

(25) Denney, M. C.; Pons, V.; Hebden, T. J.; Heinekey, D. M.; Goldberg, K. I. *J. Am. Chem. Soc.* **2006**, *128*, 12048-12049.

(26) Staubitz, A.; Sloan, M. E.; Robertson, A. P. M.; Friedrich, A.; Schneider, S.; Gates, P. J.; Schmedt, a.,der Gunne; Manners, I. *J. Am. Chem. Soc.* **2010**, *132*, 13332-13345.

(27) Blaquiere, N.; Diallo-Garcia, S.; Gorelsky, S. I.; Black, D. A.; Fagnou, K. *J. Am. Chem. Soc.* **2008**, *130*, 14034-14035.

(28) Staubitz, A.; Presa Soto, A.; Manners, I. *Angew. Chem. Int. Ed.* **2008**, *47*, 6212-6215.

(29) Mal, S. S.; Stephens, F. H.; Baker, R. T. *Chem. Commun.* **2011**, *47*, 2922-2924.

(30) Bluhm, M. E.; Bradley, M. G.; Butterick, R.; Kusari, U.; Sneddon, L. G. *J. Am. Chem. Soc.* **2006**, *128*, 7748-7749.

(31) Wright, W. R. H.; Berkeley, E. R.; Alden, L. R.; Baker, R. T.; Sneddon, L. G. *Chem. Commun.* **2011**, *47*, 3177-3179.

(32) Ott, K. *IV.B.1a 2010 Overview and Wrapup: DOE Chemical Hydrogen Storage Center of Excellence (CHSCoE)* [http://www.hydrogen.energy.gov/pdfs/progress10/iv_b_1a_ott.pdf] Retrieved: 05/30/2011.

(33) US Department of Energy, *DOE Targets for On-board Hydrogen Storage Systems for Light-Duty Vehicles* [http://www1.eere.energy.gov/hydrogenandfuelcells/storage/pdfs/targets_onboard_hydro_storage.pdf] Retrieved: 05/30/2011.

(34) Geier, S. J.; Gilbert, T. M.; Stephan, D. W. *J. Am. Chem. Soc.* **2008**, *130*, 12632-12633.

(35) Campbell, P. G.; Zakharov, L. N.; Grant, D. J.; Dixon, D. A.; Liu, S. *J. Am. Chem. Soc.* **2010**, *132*, 3289-3291.

(36) Matus, M. H.; Liu, S.; Dixon, D. A. *J. Phys. Chem. A* **2010**, *114*, 2644-2654.

(37) Staubitz, A.; Besora, M.; Harvey, J. N.; Manners, I. *Inorg. Chem.* **2008**, *47*, 5910-5918.

(38) Hausdorf, S.; Baitalow, F.; Wolf, G.; Mertens, F. O. R. L. *Int. J. Hydrogen Energy* **2008**, *33*, 608-614.

(39) Sutton, A. D.; Burrell, A. K.; Dixon, D. A.; Garner, E. B.; Gordon, J. C.; Nakagawa, T.; Ott, K. C.; Robinson, J. P.; Vasiliu, M. *Science* **2011**, *331*, 1426-1429.

(40) Sneddon, L. G. *Amineborane-Based Chemical Hydrogen Storage* [http://www.hydrogen.energy.gov/pdfs/review07/st_27_sneddon.pdf] Retrieved: 06/01/2011.

(41) Davis, B. L.; Dixon, D. A.; Garner, E. B.; Gordon, J. C.; Matus, M. H.; Scott, B.; Stephens, F. H. *Angew. Chem. Int. Ed.* **2009**, *48*, 6812-6816.

(42) Taylor, F. M.; Dewing, J.; Imperial Chemical Industries US 3103417, 1963.

(43) Mock, M. T.; Potter, R. G.; Camaioni, D. M.; Li, J.; Dougherty, W. G.; Kassel, W. S.; Twamley, B.; DuBois, D. L. *J. Am. Chem. Soc.* **2009**, *131*, 14454-14465.

(44) Adams, R. M.; Pearson, R. K. US Patent 2968531, 1961.

(45) Herrick, C.; Kirk, N.; Etherington, T.; Schubert, A. E. *Ind. Eng. Chem.* **1960**, *52*, 105-112.

(46) Brown, H. C.; Schlesinger, H. I.; Sheft, I.; Ritter, D. M. *J. Am. Chem. Soc.* **1953**, *75*, 192-195.

(47) Schlesinger, H. I.; Brown, H. C.; Abraham, B.; Bond, A. C.; Davidson, N.; Finholt, A. E.; Gilbreath, J. R.; Hoekstra, H.; Horvitz, L.; Hyde, E. K.; Katz, J. J.; Knight, J.; Lad, R. A.;

Mayfield, D. L.; Rapp, L.; Ritter, D. M.; Schwartz, A. M.; Sheft, I.; Tuck, L. D.; Walker, A. O. *J. Am. Chem. Soc.* **1953**, *75*, 186-190.

(48) Schlesinger, H. I.; Brown, H. C.; Abraham, B.; Davidson, N.; Finholt, A. E.; Lad, R. A.; Knight, J.; Schwartz, A. M. *J. Am. Chem. Soc.* **1953**, *75*, 191-191.

(49) Schlesinger, H. I.; Brown, H. C.; Finholt, A. E. *J. Am. Chem. Soc.* **1953**, *75*, 205-209.

(50) Schlesinger, H. I.; Brown, H. C.; Finholt, A. E.; Gilbreath, J. R.; Hoekstra, H. R.; Hyde, E. K. *J. Am. Chem. Soc.* **1953**, *75*, 215-219.

(51) Schlesinger, H. I.; Brown, H. C.; Gilbreath, J. R.; Katz, J. J. *J. Am. Chem. Soc.* **1953**, *75*, 195-199.

(52) Schlesinger, H. I.; Brown, H. C.; Hoekstra, H. R.; Rapp, L. R. *J. Am. Chem. Soc.* **1953**, *75*, 199-204.

(53) Eggeman, T. *Hydrides. Kirk-Othmer Encyclopedia of Chemical Technology;* John Wiley & Sons, Inc, **2000**, Hoboken, NJ.

(54) Downs, J. C. US Patent 1501756, 1924.

(55) Ramachandran, P. V.; Gagare, P. D. *Inorg. Chem.* **2007**, *46*, 7810-7817.

(56) Finholt, A. E.; Bond, A. C.; Schlesinger, H. I. *J. Am. Chem. Soc.* **1947**, *69*, 1199-1203.

(57) Hughes, R. L.; Smith, I. C.; Lawless, E. W. *Production of the Boranes and Related Research;* Academic Press, **1967**, New York.

(58) Murib, J. H.; Horvitz, D.; Bonecutter, C. A. *Ind. Eng. Chem. Prod. Res. Dev.* **1965**, *4*, 273-80.

(59) Jenkner, H. DE Patent 1038019, 1958.

(60) Bartsch, K.; Wolf, E. *Z. Anorg. Allg. Chem.* **1979**, *457*, 31-7.

(61) Attwood, B.; Shelton, R. A. J. *J. Less-Common Metals* **1970**, *20*, 131-4.

(62) Thorn, D. L.; Tumas, W.; Schwarz, D. E.; Burrell, A. K. PCT Int.Appl. WO2007092601A2, 2007.

(63) Gaines, D. F.; Kunz, J. C.; Kulzick, M. J. *Inorg. Chem.* **1985**, *24*, 3336-3338.

(64) Sutton, A. D.; Davis, B. L.; Bhattacharyya, K. X.; Ellis, B. D.; Gordon, J. C.; Power, P. P. *Chem. Commun.* **2010**, *46*, 148-149.

(65) Jessop, P. G.; Ikariya, T.; Noyori, R. *Chem. Rev.* **1995**, *95*, 259-72.

(66) Reutemann, W.; Kieczka, H. *Formic Acid. Ullmann's Encyclopedia of Industrial Chemistry;* Wiley-VCH, **2000**, New York, NY.

(67) Antizar-Ladislao, B. *Environ. Int.* **2008**, *34*, 292-308.

(68) Klingler, R. J.; Bloom, I.; Rathke, J. W. *Organometallics* **1985**, *4*, 1893-1894.

(69) Luo, Y. R. *Comprehensive Handbook of Chemical Bond Energies;* CRC Press, **2007**, New York, NY.

(70) Neu, R. C.; Ouyang, E. Y.; Geier, S. J.; Zhao, X.; Ramos, A.; Stephan, D. W. *Dalton Trans.* **2010**, *39*, 4285-4294.

(71) DuBois, D. L.; Blake, D. M.; Miedaner, A.; Curtis, C. J.; DuBois, M. R.; Franz, J. A.; Linehan, J. C. *Organometallics* **2006**, *25*, 4414-4419.

(72) Schmidt, E. W. *Hydrazine and its Derivatives: Preparation, Properties, Applications;* Wiley-Interscience, **2001**, New York.

(73) Hodoshima, S.; Arai, H.; Takaiwa, S.; Saito, Y. *Int. J. Hydrogen Energy* **2003**, *28*, 1255-1262.

(74) Clot, E.; Eisenstein, O.; Crabtree, R. H. *Chem. Commun.* **2007**, 2231-2233.

(75) Moores, A.; Poyatos, M.; Luo, Y.; Crabtree, R. H. *New J. Chem.* **2006**, *30*, 1675-1678.

(76) Schwarz, D. E.; Cameron, T. M.; Hay, P. J.; Scott, B. L.; Tumas, W.; Thorn, D. L. *Chem. Commun.* **2005**, 5919-5921.

(77) Wechsler, D.; Cui, Y.; Dean, D.; Davis, B.; Jessop, P. G. *J. Am. Chem. Soc.* **2008**, *130*, 17195-17203.

(78) Dean, D.; Davis, B.; Jessop, P. G. *New J. Chem.* **2011**, *35*, 417-422.

(79) Campbell, P. G.; Zakharov, L. N.; Grant, D. J.; Dixon, D. A.; Liu, S. *J. Am. Chem. Soc.* **2010**, *132*, 3289-3291.

Chapter 5

From Hantzsch Esters to Borohydrides

5.1 Introduction

5.1.1 Hantzsch Esters

Hantzsch esters are a subset of the 1,4-dihydropyridine class of organic hydrides (**Scheme 5-1**).[1] The name sake compound of this series was originally reported by Arthur Hantzsch in 1882.[2] The primary industrial application of Hantzsch esters is medicinal, as L-type calcium ion channel blockers,[3-5] but they have also been shown to have anti-bacterial,[4] anti-fungal[5] and anti-cancer[6] properties. Regulation of L-type calcium ion channels by Hantzsch esters treats hypertension and severe chest pain. There are several active pharmaceutical agents currently available on the market that contain a Hantzsch ester structural unit, including Nifepidine (Bayer), Lacidipine (Boehringer Ingelheim) and Felodipine (AstraZeneca) to name a few (**Scheme 5-2**).[3, 7] The chemical properties of Hantzsch esters and their nicotinamide counterparts are of particular interest as they are structurally related to the biological reducing agents NAD(P)H,[1] and further, it is this similarity that has inspired organic chemists to employ Hantzsch esters as reagents for the selective reduction of functional groups.[8]

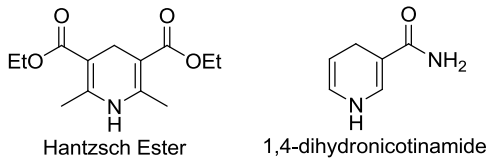

Scheme 5-1. Structure of Hantzsch Ester and 1,4-dihydronicotinamide

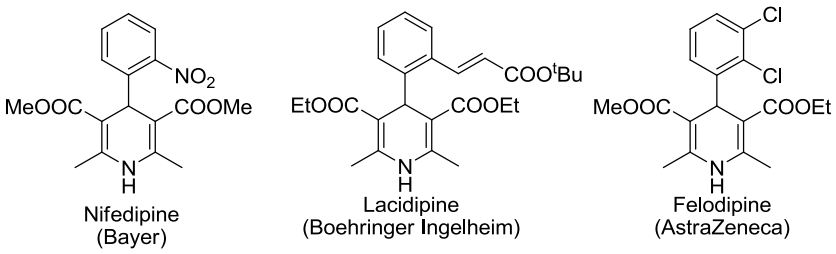

Scheme 5-2. Representative pharmaceuticals agents which are Hantzsch ester derivatives

5.1.2 Synthesis of Hantzsch Esters

Since Hantzsch ester derivatives are valued pharmaceutical targets and important synthetic intermediates on route to highly functionalized pyridines, there is a plethora of strategies to synthesize these compounds.[1, 9-12] Herein our discussion will be briefly focused on the generation of symmetrically substituted Hantzsch esters derivatives.

Hantzsch esters are typically synthesized using a multi-component reaction (**Scheme 5-3**), the details of which have not changed much since the original report.[2, 9] All the components employed can be adjusted to provide the desired substitution pattern in high yield.[11] Substitution of alkyl and aryl groups at the 4-position is typically achieved by employing the appropriate aldehyde. The carbonyl substituent comes from the appropriate 1,3-dicarbonyl reagent. N-alkylation is typically achieved after the multi-component reaction by S_N2 substitution of the deprotonated Hantzsch ester using the appropriate alkyl electrophile.[13] N-arylation, is more challenging requiring an alternative synthetic strategy, an example of which was reported by Singh[14] via reaction of a protected formaldehyde with an enamine (**Scheme 5-4**).

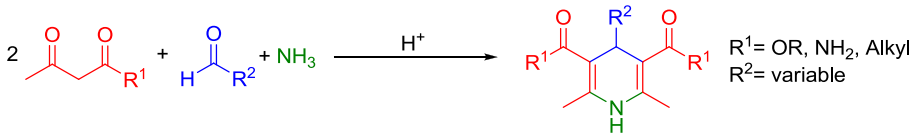

Scheme 5-3. Hantzsch ester multicomponent synthesis

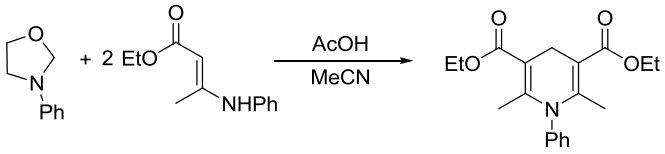

Scheme 5-4. N-Ph Hantzsch ester synthesis

Highly functionalized pyridines are obtained by oxidation of Hantzsch esters and there are several high yielding procedures that employ heat, microwaves, light, air as well as single and two electron oxidants.[15, 16] The main consideration when choosing to employ a Hantzsch ester oxidation procedure is the substitution pattern desired for the resulting pyridine.[15] Substitution on the N can be lost due to nucleophilic displacement from the resulting pyridinium salt, which is electrophilic at that position. Loss of substitution at the 4-position can occur if the oxidation is carried out using single electron oxidants, as intermediates along the reaction pathway can fragment to form carbocations.[17-19]

5.1.3 Hantzsch Esters as Reducing Agents

There are numerous examples of the application of Hantzsch esters as an organic hydride in the literature and the field has been aptly reviewed by a number of groups.[8, 20, 21] The reducing capacity of Hantzsch esters has been shown to be comparable to BH_3NEt_3[22] and is marked by unusually low C4-H heterolytic bond dissociation energies of ~70 kcal mol^{-1} / ~290 kJ mol^{-1}.[23] Hantzsch esters have been applied to the reduction of organic architectures for over 30 years and

the list of substrates for these reactions include heterocycles,[24, 25] nitryl-[26] and nitro-alkenes,[27, 28] imines,[29] iminium ions,[30, 31] 1,2-dicarbonyl-[32] and α,β-unsaturated carbonyl compounds.[33, 34] An interesting report Zu et al. applied Hantzsch ester in a reductive cyclization reaction (**Scheme 5-5**), their synthetic approach was amenable to the formation of 3 to 7 membered rings.[35]

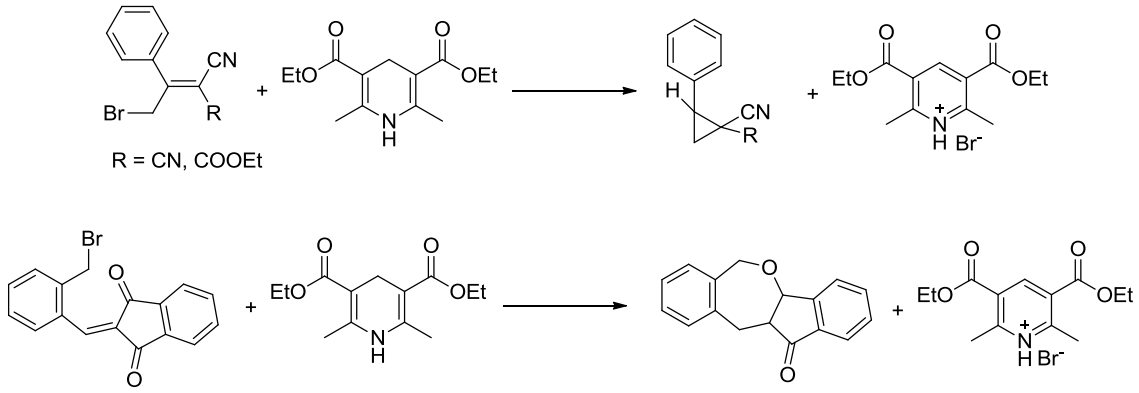

Scheme 5-5. Cyclizations promoted by Hantzsch esters

In 1981, designer chiral Hantzsch esters were employed successfully in enantioselective reductions (**Scheme 5-6**).[32] Since the Hantzsch ester is employed as a stoichiometric or even super stoichiometric reagent, this was not a particularly efficient method for enantioselective reductions. However, recent developments from the groups of List[36] and Macmillan[37] and others[25, 38] using regular Hantzsch esters as a reducing agent along with chiral organo-,[36, 37] hydrogen bonding[38] and Brønsted acid catalysts.[24, 25, 39] An example of a metal free reaction of this type is the enantioselective reduction of enals reported by the Macmillan group[37] (**Scheme 5-7a**) which utilizes an imidazolidinone salt as an organo-iminium ion catalyst. High catalyst loadings plagued the Macmillan approach; lower loadings were achieved without loss of selectivity through use of either hybrid organo-Brønsted acid systems[40] or Brønsted acid catalysts

on their own, this is demonstrated by considering the reduction of 2-substituted quinolines (**Scheme 5-7b**).[24, 25]

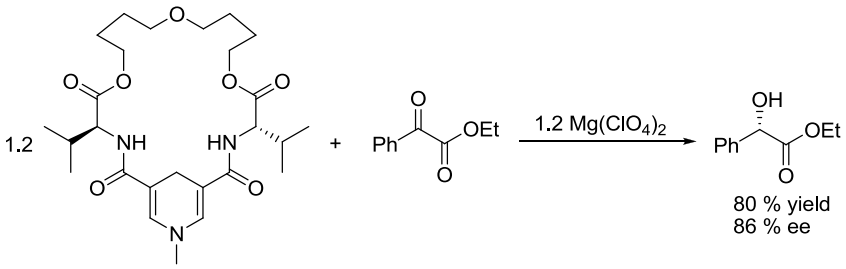

Scheme 5-6. An asymmetric reduction of an α-ketoester by a chiral Hantzsch ester

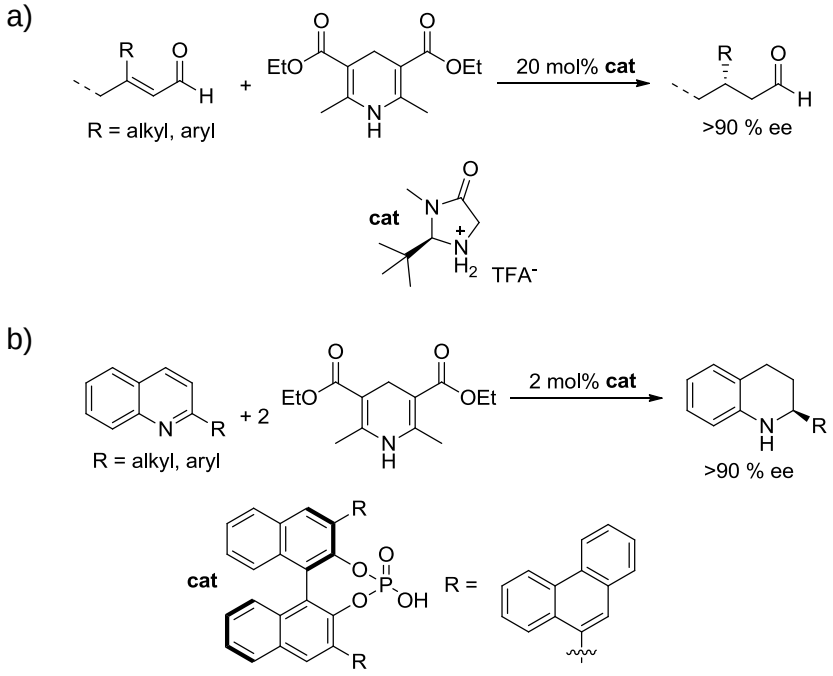

Scheme 5-7. Select Examples of catalytic reductions involving Hantzsch esters, a) reduction of enals and b) reduction of N-heterocycles

However, even in these latter cases, a full equivalent of the Hantzsch esters or their dihydronicotinamide relatives is required, and on large scale the cost of these reagents and the

large amount of pyridine waste generated is prohibitive. Two strategies designed to address these issues are recovery and recycling of the spent reagent,[41, 42] and cascade catalysis,[43-46] which allows for *in-situ* regeneration of the dihydropyridine, reducing the equivalents required. The recovery and recycling approach was demonstrated by immobilizing nicotinamide derivatives on silica[41] and a polymer support.[42] After reaction, the spent organic hydride was recovered by filtration, reduced, and then reused.

Up to now, *in-situ* regeneration of 1,4-dihydropyridines has only been reported for nicotinamides.[44-46] The catalytic approach is inspired by the $NAD(P)^+$/NAD(P)H redox couple present in biochemical pathways. In biological systems spent $NAH(P)^+$ is not discarded but regenerated through enzymatic reduction. In organic systems, the regeneration of the nicotinamide is carried out by a metal catalyst; where the reducing agent is hydrogen,[46] formate or electrons.[43] Fish[45] reported one such system (**Scheme 5-8**) that used a Rh catalyst (3 mol%) to regenerate dihydronicotinamide which had been used in enzymatic reduction of a ketone to an alcohol. While the preliminary reports in this field are interesting, more work is needed to expand the number of 1, 4-dihydropyridine processes amenable to this type of cascade catalysis.

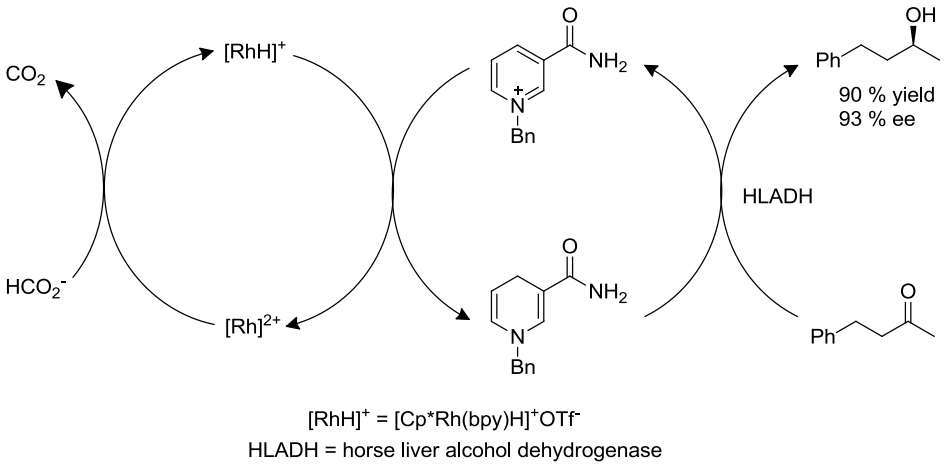

Scheme 5-8. Cascade catalysis with dihydronicotinamides

5.1.4 Mechanism of Hydride Transfer

There has been much study of the hydride transfer mechanism for Hantzsch esters and the associated nicotinamide analogues because of their structural relationship to the biological reducing agent NAD(P)H.[1, 12, 21] Several hydride transfer mechanisms have been proposed and are summarized in (**Scheme 5-9**).[23] The concerted hydride transfer mechanism (Path A) is typically proposed when Hantzsch ester is employed in the reduction of organic substrates,[21, 47, 48] This mechanism is characterized by a pronounced primary KIE at the C4-H/D ring position, indicating that a hydride is transferred in the rate determining step.[48, 49]

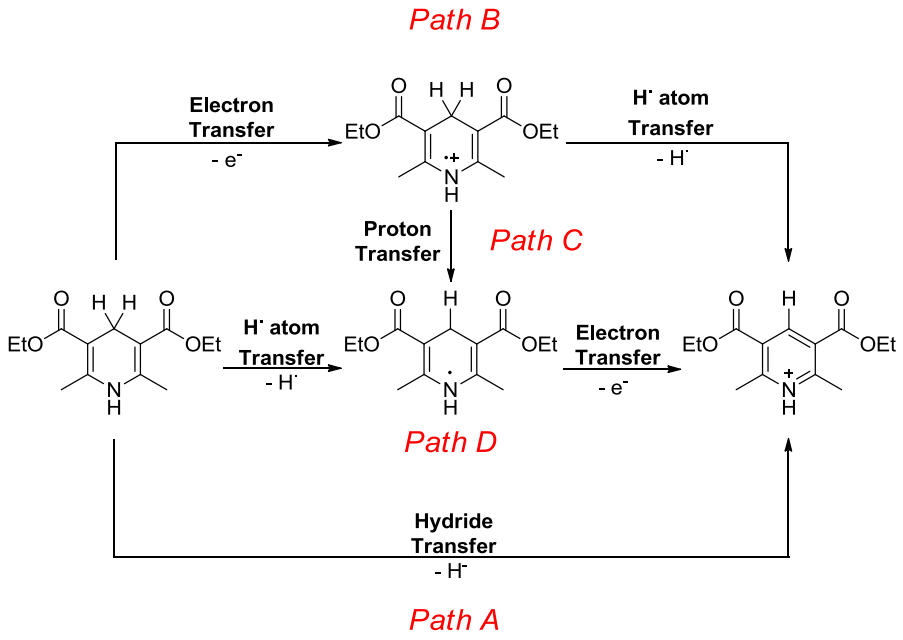

Scheme 5-9. Summary of proposed Hantzsch ester hydride transfer mechanisms

There are several potential stepwise hydride transfer mechanisms (Paths B – D), the most commonly invoked of which involves an initial electron transfer followed by an H atom transfer

(Path B) or sequential proton electron transfers (Path C).[23] The initial electron transfer step in both mechanisms is typically considered to be rate determining, resulting in a small KIE (~1.0). The observation of this type of KIE is used as supporting evidence that the hydride transfer proceeds via one of these two multistep pathways.[48, 49] The reduction of trityl, xanthylium ions and single electron metal oxidants by Hantzsch esters (**Scheme 5-10**) most likely proceeds via atom transfer (Path B) or through a highly as-synchronous transition state.[49]

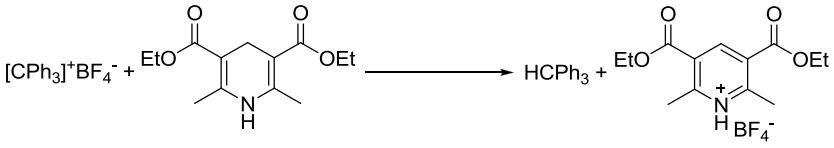

Scheme 5-10. Reduction of trityl cation by Hantzsch ester

Path C has been found to be consistent with experiment when the hydride acceptor can behave as a Brønsted base (**Scheme 5-11**).[23] An encounter complex is formed prior to the initial electron transfer in stepwise mechanisms. This is necessary as the actual electron transfer proceeds faster than atomic motion, which is not however to suggest that there is no energy barrier to an electron transfer, the barrier arises from the energy required to pre-organize the reagents and the solvent cage as described by Marcus theory.[50] The initial electron transfer can be spontaneous or non-spontaneous and the spontaneity can be estimated by comparing the relative oxidation ($E^o(DHP^{+\bullet}/DHP)$) and reduction potentials ($E^o(A^+/A^\bullet)$) (**Eq. 5-1**) of Hantzsch ester (DHP) and the hydride acceptor (A). [49] The Hantzsch ester reaction with trityl is an example of a reaction that proceeds with non-spontaneous initial electron transfer.

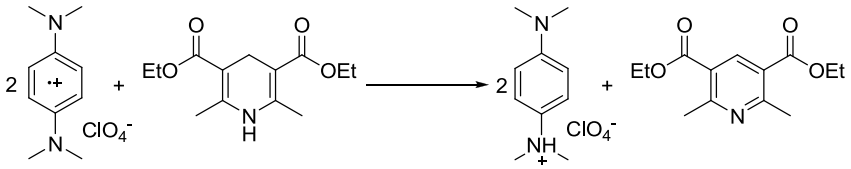

Scheme 5-11. Reaction of tetramethyl-phenyldiamine radical cation with Hantzsch ester

$$\Delta G(ET) = -F[\Delta E(\mathrm{A}^{+}/A^{\cdot}) - \Delta E(\mathrm{DHP}^{+\cdot}/\mathrm{DHP})] \qquad \textbf{Eq. 5-1}$$

5.1.5 Tris(pentafluorophenyl)boron

The Lewis acid $B(C_6F_5)_3$ was originally reported in 1963 by Massey as the product from action of $[Li][C_6F_5]$ on BCl_3 in pentane (**Scheme 5-12**).[51, 52] $B(C_6F_5)_3$is a strong Lewis acid, its strength on the Childs acidity scale lies between BF_3 and BCl_3.[53] It is a popular initiator for Ziegler-Natta polymerization reactions,[54, 55] because of its stability and ability to cleanly abstract hydride, halides and methyl groups from transition metal complexes.[56, 57]

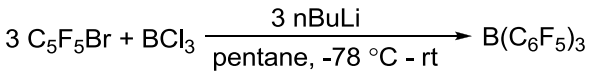

Scheme 5-12. Synthesis of $B(C_6F_5)_3$

Piers, Gevorgian and others have highlighted the utility of $B(C_6F_5)_3$ as a catalyst for the hydrosilylation of alkenes,[58] imines,[59] alcohols,[60] thiols, enol ethers,[61] carbonyl compounds[61-63] and the reduction of CO_2 to methane.[64] Detailed mechanistic studies of the hydrosilylation reaction, exemplified by the reduction of benzyl carbonyl substrates,[62, 63] revealed that the role of $B(C_6F_5)_3$ was to abstract a hydride from the silane and not to act as a Lewis acid activator for the carbonyl group (**Scheme 5-13**).

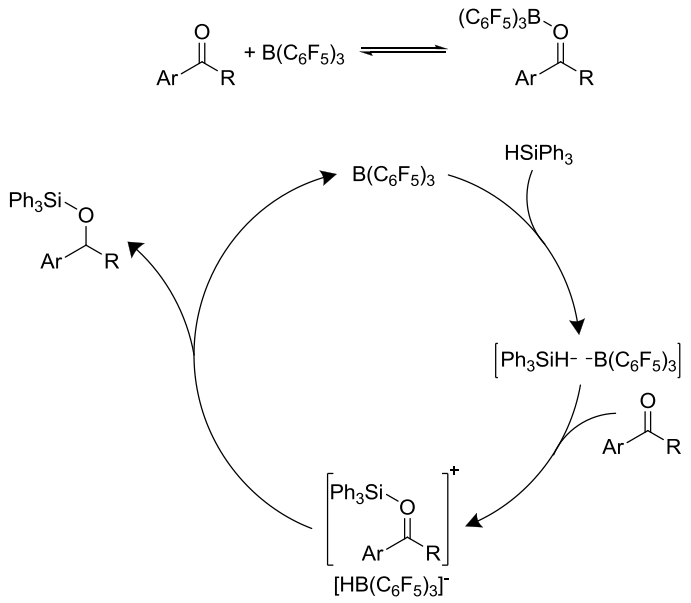

Scheme 5-13. Proposed mechanism for the $B(C_6F_5)_3$ catalyzed silylation of ketones

Besides the observation of $[HB(C_6F_5)_3]^-$ under some catalytic conditions,[59, 61] evidence in support of the abstraction pathway came from observing that the turnover frequency was inversely dependent on the basicity of the carbonyl oxygen.[62, 63] Aldehyde and ketones reacted more slowly than esters, which is inverse to the strength of their respective Lewis acid-base adducts with $B(C_6F_5)_3$.[62, 65] Thus, binding of the Lewis acid catalyst to the carbonyl group served to inhibit reaction rather than activate the substrate. The rate determining step for the catalytic cycle was established to be hydride transfer from the silane to $B(C_6F_5)_3$.[63] Further, activation of the Si-H bond, regardless of the silylation reaction studied, only occurred in the presence of a Lewis base.[61-63] The silylium cation activated the carbonyl group to hydride attack, which results in product formation and regeneration of the catalyst. In addition, when the silylium cation is bound to an alcohol or thiol it serves to increases the acidity of the proton promoting the liberation of H_2 upon reaction $[HB(C_6F_5)_3]^-$.

More recently, $B(C_6F_5)_3$ has received attention owed to the extensive research into its activity as the Lewis acid component of a Frustrated Lewis Pair (FLP).[66] FLPs are Lewis acid-base mixtures that would otherwise form stable adducts save for unfavorable steric interactions, the systems are thus described as being electronically frustrated.[67-70] An early example of steric frustration was reported in the 1940's, when H. C. Brown noted that sterics could inhibit adduct formation between boranes and pyridines.[71] Subsequently, it was found that trityl cation abstracts hydride from bulky amines,[72] demonstrating that steric frustration can impart unusual reactivity in these systems. The field remained unexplored until recently and exploded upon the observation of reversible heterolytic H_2 activation by Stephan in 2006.[67] Prior to the report by Stephan, H_2 activation under mild reaction conditions was only common with transition metal complexes. Subsequently, $B(C_6F_5)_3$ was found to be a particularly important FLP reagent due to its combination of high Lewis acidity and steric bulk.[67-70] H_2 activation where $B(C_6F_5)_3$ is the Lewis acid has been reported for a number of Lewis bases including hindered phosphines,[66] carbenes,[73-75] amines[76, 77] and pyridines[67-70] (**Scheme 5-14**).

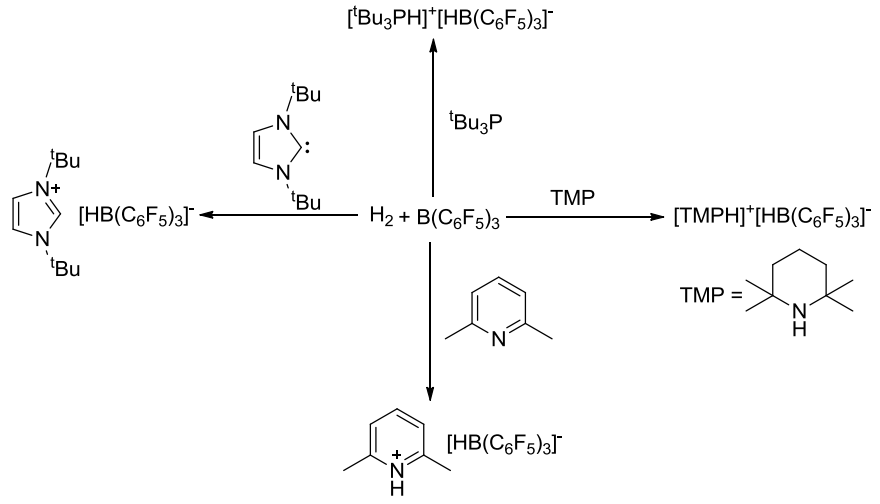

Scheme 5-14. Examples of FLP promoted heterolytic H_2 activations involving $B(C_6F_5)_3$

Initial reports of FLPs hinted that the usual reactivity stemmed from prevention of Lewis acid-base adduct formation by steric encumbrance.[66] Subsequent reports, typified by the 2,6-lutidine $B(C_6F_5)_3$ system,[78, 79] have suggested that Lewis acid-base adduct formation could occur but must be reversible in order to effect H_2 activation (**Scheme 5-15**). Such a necessity has been used to great effect in the development of FLP catalysts for metal-free hydrogenation reactions. $B(C_6F_5)_3$ catalyzed hydrogenations have been employed to reduce many functional groups including imines,[80-83] N-heterocycles[83, 84] and silyl-enol ethers.[83, 85] Beyond H_2 activation, FLPs involving $B(C_6F_5)_3$ have also been used to activate N-H,[75] and B-H bonds,[86] mediate the ring opening of THF[75] and promote addition across C-C double bonds.[87, 88]

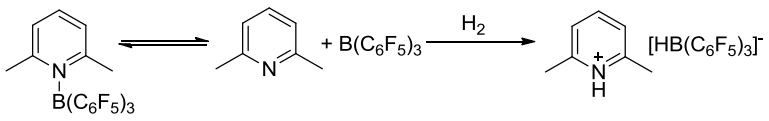

Scheme 5-15. Heterolytic H_2 activation with the 2,6-lutidine $B(C_6F_5)_3$ FLP

Akin to the reactivity of trityl with bulky amines, $B(C_6F_5)_3$ has been shown to abstract hydride from the C alpha to N in systems where stable Lewis acid-base adduct formation is prohibited due to sterics encumbrance (**Scheme 5-16**).[89] These reactions are typically less efficient at generating $[HB(C_6F_5)_3]^-$ than their FLP counterparts requiring either 2 equivalents of $B(C_6F_5)_3$ or amine to proceed to completion.[89] It is important to note that hydride abstractions from Hünig's base, triethylamine[76, 90] and dimethylaniline[57, 91] are reversible under ambient conditions, as this reversibility will come to play in the subsequent discussion.

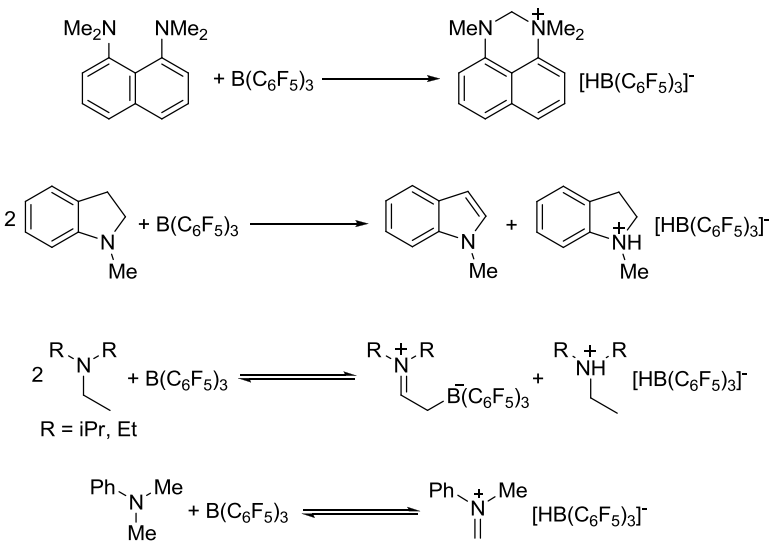

Scheme 5-16. Examples of hydride transfers to $B(C_6F_5)_3$ involving bulky amines

5.2 Research Objectives

As was introduced in Chapter 4 the current industrial approach to the synthesis of borane and borohydrides involves the reaction of NaH with a boron Lewis acid, BF_3OEt_2 and $B(OMe)_3$ respectively.[92] While this method is acceptable to meet the existing demand for borane and borohydride reagents, it would be insufficient to meet societal demands for B-H containing compounds if boron based hydrogen storage materials were to see wide spread application in electronics, stationary power generation and/or in the transportation sector, providing the impetus for research into alternative strategies to generate B-H bonds. These new approaches have generally substituted NaH for other inorganic hydrides of the form, $LiAlH_4$,[93] $HSnBu_3$,[94, 95] N_2H_4,[96] and transition metal hydrides such as $[HRh(dmpe)_2]$ (dmpe = 1,2-dimethylphosphinoethane).[97] Each method has its merits and disadvantages but the use of these

inorganic strategies in a large scale process would be prohibitive. Clearly, more research into regeneration of B-H bonds is necessary.

Inspired by the biological reducing agents NAD(P)H, we wondered about the capacity for organic hydrides such as 1,4-dihydropyridines to affect the formation of B-H bonds (**Scheme 5-17**). The general regeneration scheme to form boranes from 1,4-dihydropyridines would be as follows: a boron Lewis acid BX_3, available from the digestion of spent NH_3BH_3 hydrogen storage material (BNH_x), would be reacted with a 1,4-dihydropyridine transferring a hydride equivalent to boron initiating a redistribution cascade to give a borane adduct or diborane. The borane formed would be recombined with NH_3, also produced during the digestion of BNH_x, to yield ammonia borane (NH_3BH_3). The pyridinium, Py-HX, formed from the hydride transfer reaction would then be recovered and reduced back to the 1,4-dihydropyridine using a hydrogenation reaction which would also liberate HX. Recall that it is generally preferable to digest BNH_x because this type of processing transforms this network polymer into more easily handled materials.

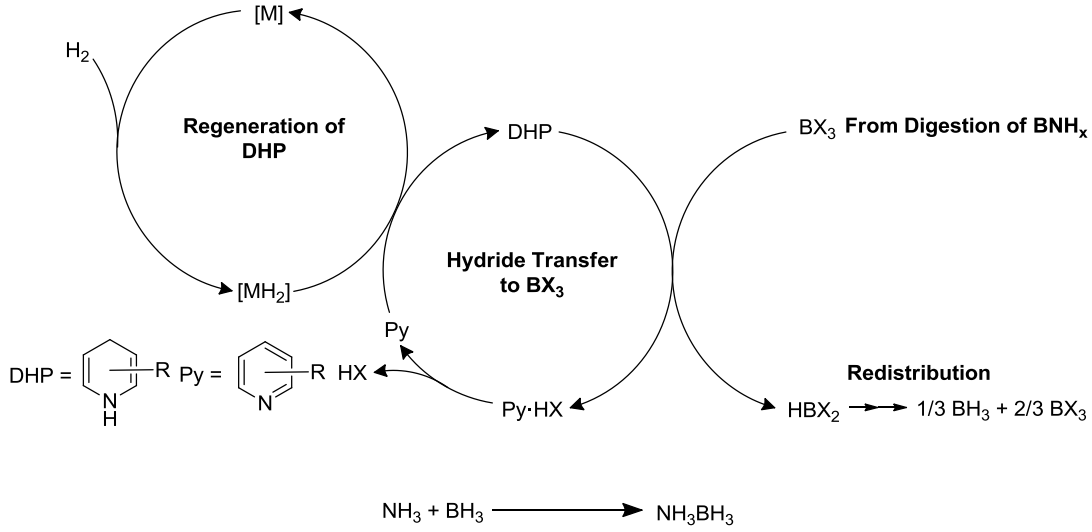

Scheme 5-17. Proposed regeneration scheme for NH_3BH_3 involving 1,4-dihydropyridines

The scheme is ambitious considering there is no precedence for the formation of BH_3 from organic hydrides and in addition to this, the details of how to modulate the redistribution process that produces borane would have to be ironed out. Further, there are only a few catalytic reductions capable of converting pyridines to 1,4-dihydropyridines[98-101] and their substrate scope is limited (**Scheme 5-18**), thus it may be necessary to optimize a new reaction along these lines. If all aspects of the regeneration cycle were eventually shown to be successful on the lab scale, the efficiency of the scheme would need to be assessed to determine how our approach compares with the inorganic alternatives.[102]

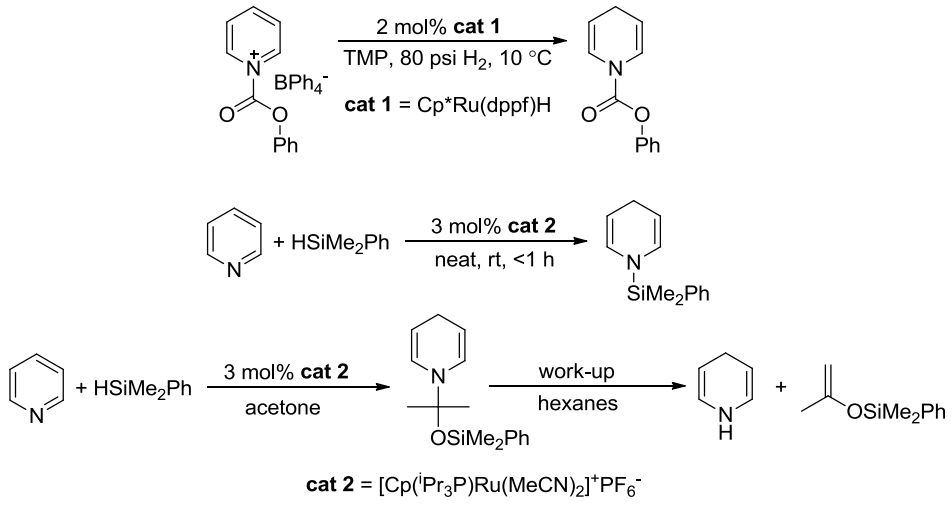

Scheme 5-18. Examples of catalytic methods to 1,4-dihydropyridines

The first phase of the research project was to study the reactivity of 1,4-dihydropyrdines with a boron Lewis acid for which, to the best of our knowledge at the time, there was no literature precedence, although the reverse reaction the reduction of pyridines with $NaBH_4$ was known.[103] The goal was to observe a clean hydride transfer from a 1,4-dihydropyridine to a boron Lewis acid. Hantzsch esters were chosen as the model 1,4-dihydropyridine because of their

relative stability, ease of synthesis and the large amount of literature describing their properties. $B(C_6F_5)_3$ was chosen as the model boron Lewis acid, because of the multiple NMR handles available and the literature surrounding the study of the hydride $[HB(C_6F_5)_3]^-$. Another advantage of $B(C_6F_5)_3$ was it reflected the Lewis acidity of BX_3 species available from digestion BNH_x, but the resulting hydride is generally stable to redistribution.[104] Subsequent to our work, Nikonov[99] reported hydride transfer from a silylated 1,4-dihydropyridine to $B(C_6F_5)_3$ (**Scheme 5-19**), the reaction produced a pyridinium borohydride salt that disproportionated to silane and a pyridine-$B(C_6F_5)_3$ Lewis acid-base adduct.

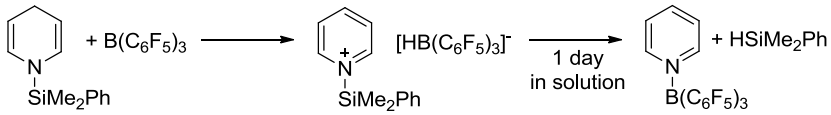

Scheme 5-19. Reaction of a silylated 1,4-dihydropyridine with $B(C_6F_5)_3$ reported by Nikonov in 2011 as described in reference 99

5.3 Results and Discussion

5.3.1 Reaction N-alkylated Hantzsch Esters with $B(C_6F_5)_3$

At the outset of the project the Lewis acid-base adduct chemistry between Hantzsch esters and $B(C_6F_5)_3$ was not well understood. In principle there were three potential coordination sites, the two carbonyl oxygens of the esters and the nitrogen. Detailed studies by other groups established that $B(C_6F_5)_3$ binding to esters was reversible, so this did not appear to be a significant concern at the outset.[57, 62, 63, 65, 105] The effect of possible binding to the nitrogen was not known and it was for this reason that the *N*-alkylated Hantzsch ester **1a** (*N*-Me) was prepared, with the understanding that the added steric hindrance would disfavor any potential adduct formation. Work by us, which will be discussed below, and Stephan[83] ultimately demonstrated that $B(C_6F_5)_3$

does not bind to doubly vinylic amines through the N lone pair. It was found, that **1a** undergoes a clean hydride transfer reaction with $B(C_6F_5)_3$ at room temperature providing the salt **2a** in high NMR yield (98 %) (**Scheme 5-20** and **Table 5-1** entry 2). The N-phenyl Hantzsch ester **1b**, prepared by fellow graduate student Véronique Laberge, was also found to react in a similar fashion to give **2b**, albeit with slightly lower yield (90 %). Formation of the borohydride anion was confirmed by its characteristic doublet at -25 ppm in the ^{11}B NMR spectrum which became a singlet on decoupling. Reaction of d_2-**1a** with $B(C_6F_5)_3$ yielded d_2-**2a**, the singlet at -25 ppm in the ^{11}B NMR confirmed that source of hydride was the C4-H position of **1a** (**Figure 5-1**). The hydride transfer reaction initiated rapidly at temperatures below -40 ˚C, with no further conversion being observed after 30 min at -20 ˚C.

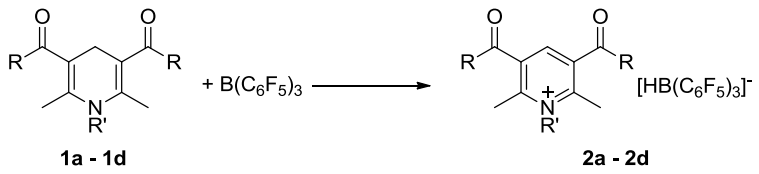

Scheme 5-20. Hydride transfer reaction of Hantzsch esters with $B(C_6F_5)_3$

Table 5-1. Yield of pyridinium borohydride salts **2a-d**

Entry	Substrate	R, R'	**1** : $B(C_6F_5)_3$	Yield **2** (%)[a]
1	**1a**	OEt, Me	1 : 1	95
2	**1a**	OEt, Me	1 : 1	98[b]
3	**1b**	OEt, Ph	1 : 1	90[b]
4	**1c**	OEt, H	1 : 1	60
5	**1d**	O^{t}Bu, H	1 : 1	90[c]

[a] Reactions carried out in 0.03 M **1** in CD_2Cl_2 at -20 ˚C, ^{1}H NMR yields based on limiting reagent with bibenzyl as an internal standard; [b] Reaction carried out at 25 ˚C; [c] Reaction carried out at -30 ˚C

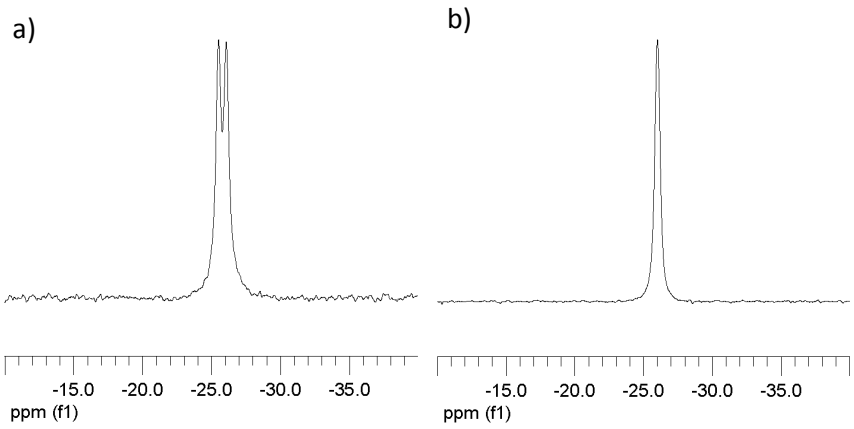

Figure 5-1. ^{11}B NMR of a) **2a** and b) ***d_2*-2a** in CD_2Cl_2 at 25 ºC

Salts **2a** and **2b** were formed at room temperature in less than 5 minutes, although decomposition was observed in solution upon standing for extended times (hours to days). The decomposition pathways will be discussed in more detail in section 5.3.2. It was also found that in solution the pyridinium borohydride salts were slightly light sensitive and as a result all

reactions were carried out in the dark. An X-ray crystal structure of the salt **2a** confirmed the expected connectivity (**Figure 5-2**). The metric parameters of the resolved structure were similar to those recently reported by Geier and Stephan for the pyridinium borohydride salt $[C_5H_3Me_2NH][HB(C_6F_5)_3]$.[78] The closest approach of the BH and NR fragments of **2a** in the solid state was 3.59 Å demonstrating that the two ions are well separated.

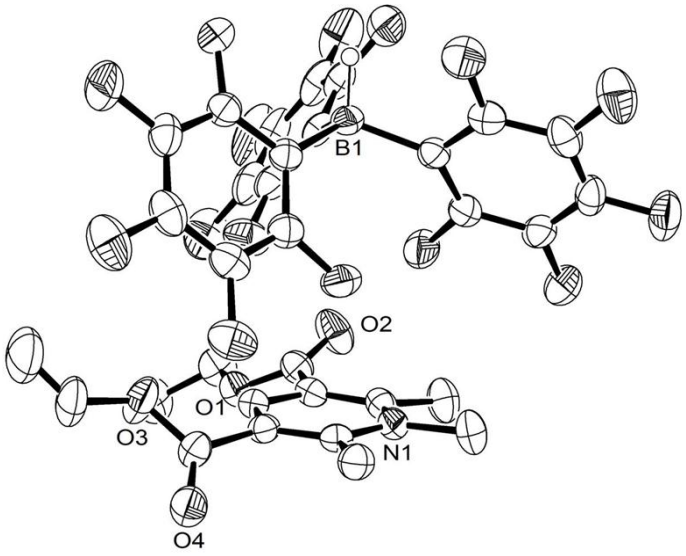

Figure 5-2. ORTEP structure of salt **2a** the thermal ellipsoids were drawn at 50 % probability. All hydrogen atoms were omitted for clarity except for B-H

5.3.2 Reaction of Hantzsch Ester with $B(C_6F_5)_3$

In a similar fashion to **1a** and **1b**, the reaction of Hantzsch ester itself, **1c**, with $B(C_6F_5)_3$ resulted in formation of the borohydride salt **2c** in 60% yield at –20 ˚C. A ^{1}H NMR NOESY experiment performed on salt **2c** (**Figure C-1** in **Appendix C**) revealed a correlation between the pyridinium proton (δ 12.5 ppm) and the $[HB(C_6F_5)_3]^-$ hydride (δ 3.5 ppm), consistent with ion pairing. Similar interactions have been observed in related compounds.[66, 76, 78, 90] At -20 ˚C, the

balance of the initially added 1, 4-dihydropyridine **1c** was sequestered as the Lewis acid-base adduct **3c** (**Scheme 5-21**). Although the carbonyl oxygen atoms were expected to be less basic than the amine nitrogen, steric congestion about nitrogen and its vinylogous placement can be used to rationalize the formation of the adduct at the carbonyl oxygen. Evidence in support of the connectivity of adduct **3c** came upon cooling a solution below -40 ˚C, which resulted in resolved peaks representing distinct ethyl ester moieties that suggest an un-symmetrical compound (**Figure C-2** in **Appendix C**). Binding to the nitrogen would be expected to result in a symmetrical adduct.

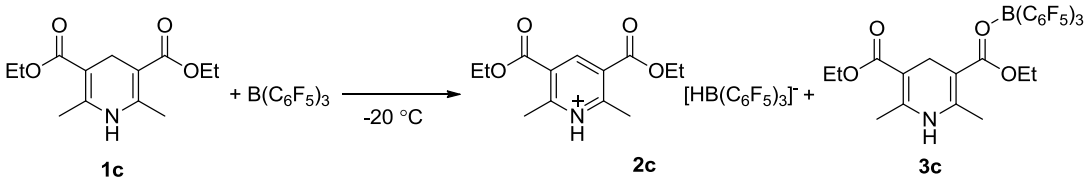

Scheme 5-21. Product distribution for the reaction of **1c** with $B(C_6F_5)_3$ at -20 ˚C in CD_2Cl_2

Warming the reaction mixture containing **2c** and **3c** from -20 ˚C to room temperature, resulted in partial conversion of **2c** to the 1,2-dihydropyridine-$B(C_6F_5)_3$ adduct **4c** (**Scheme 5-22**). A significant amount, 55 % of the material in solution was the 1,2–dihydropyridine adduct after 30 min at room temperature, and the proportion increased to 70 % over 24 h in CD_2Cl_2. The rapidity with which **4c** forms stands in contrast to the corresponding 1,2-dihydropyridine adducts **4a** and **4b**, derived from **1a** and **1b** (**Scheme 5-23** and **Figure C-3** in **Appendix C**). Significant decomposition of **2a** and **2b** takes hours in solution at room temperature whereas **2c** decomposes in minutes. It is important to note that the formation of the 1,2-dihydropyridines adduct **4a-c** is negligible for all substrates at -20 ˚C even after standing for several hours. Since adducts **4a-c** likely result from attack of $[HB(C_6F_5)_3]^-$ at the 2 position of the pyridinium ring, increased steric

bulk about the N in salts **2a** and **2b**, likely slows attack, making these species more kinetically stable. The 1,2-dihydropyridine adducts **4a-c** are readily identifiable by their ^{1}H NMR spectra, for example **4c** is characterized by a pentet at δ 4.60 ppm (p, 1H, $^{3}J_{H\text{-}H}$ = 7 Hz) in CD_2Cl_2 representing the methine proton and a doublet at δ 1.10 ppm (d, 3H, $^{3}J_{H\text{-}H}$ = 7 Hz) from the adjacent methyl group.[103, 106, 107]

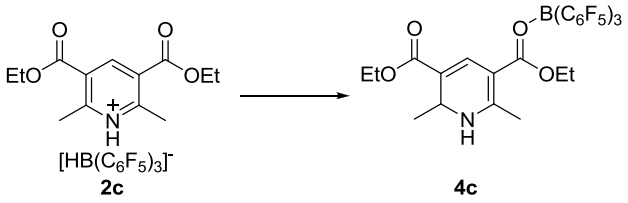

Scheme 5-22. Conversion of **2c** to 1,2-dihydropyridine **4c**

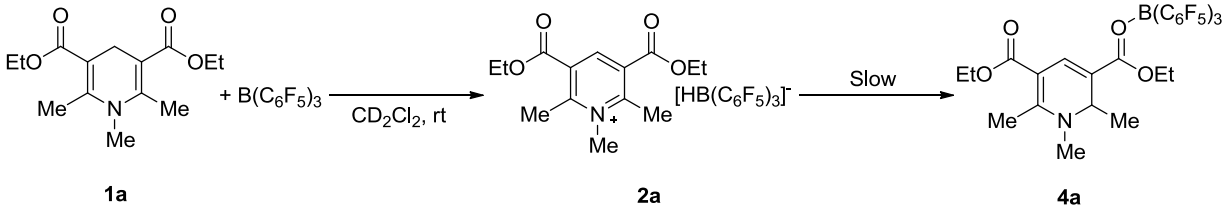

Scheme 5-23. Formation of 1,2-dihydropyridine **4a** from salt **2a**

Product **4c** can be isolated in 45% yield when the reaction of **1c** and $B(C_6F_5)_3$ is carried out in a mixture of CH_2Cl_2 and hexanes at room temperature for 1 h and cooled to induce crystallization. The ^{19}F and ^{11}B NMR spectra were consistent with $B(C_6F_5)_3$ remaining complexed to the carbonyl oxygen, an observation confirmed by X-ray crystallography (**Figure 5-3**). The structure of **4c**, depicts $B(C_6F_5)_3$ binding to the ester *trans* to the centre of hydride addition. The geometry about the B centre of **4c** was pseudo-tetrahedral with an O-B distance of 1.547(4) Å, which is similar in length to analogous ester adducts.[65, 105] Even though X-ray data indicates that

$B(C_6F_5)_3$ is bound to the ester *trans* to the centre of hydride addition, NMR data suggests that exchange between the two carbonyls is rapid at room temperature. It was found that formation of **4c** from **2c** was also somewhat reversible. The characteristic signal for $[HB(C_6F_5)_3]^-$ appeared slowly, among other decomposition products, when monitoring the ^1H and ^{11}B NMR of solutions initially enriched in **4c** at room temperature. The initial solutions of **4c** contained no resonance attributable to $[HB(C_6F_5)_3]^-$.

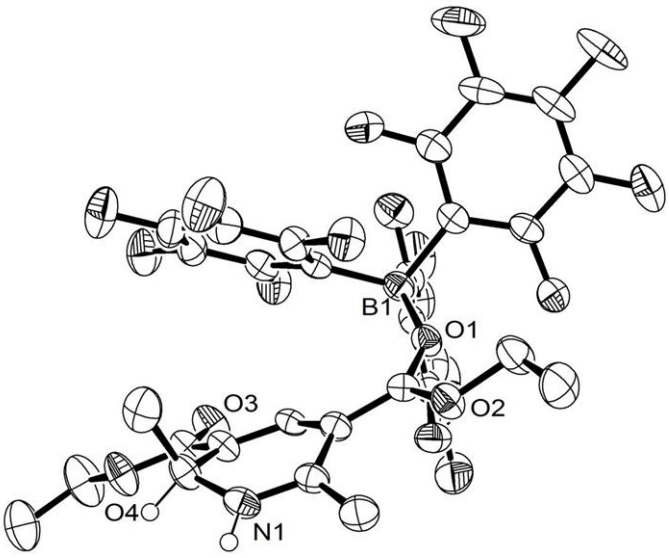

Figure 5-3. ORTEP structure of 1,2-dihydropyridine **4c** the thermal ellipsoids were drawn at 50 % probability. All hydrogen atoms were omitted for clarity except for C2-H and N-H

A solvent screen was performed in an effort to maximize **2c** formation at the expense of **3c** and **4c**, with the goal of establishing a procedure to isolate the salt. It was found that solvents such as THF, Et_2O and nitromethane yielded only trace amounts of the salt **2c**. The ineffectiveness of these solvents is likely the result of sequestration of $B(C_6F_5)_3$ by coordination. Hydride transfer products were favoured in non-coordinating solvents (**Figure 5-4**). Solvents

which were less-polar than CD_2Cl_2 including $CDCl_3$, C_6D_6 and $CF_3C_6H_5$ favoured the formation of **4c**, possibly due to their reduced capacity to stabilize charge; while 1,2-dichloroethane (CH_2ClCH_2Cl), which is slightly more polar than CD_2Cl_2, favoured the formation of **2c**.[108] The data also suggested that aromatic solvents disfavour formation of adduct **3c**, the balance of material in solution was either **2c** or **4c**. None of the solvents screened resulted in exclusive formation or precipitation of **2c**, it thus seemed unlikely that changing solvent alone would provide for conditions to allow for isolation of the salt. As mentioned earlier lowering the reaction temperature could eliminate the formation of **4c**, however large quantities of **3c** still existed in solution. Further, **2c** is highly soluble at temperatures below -50 ºC in CH_2Cl_2 and CH_2ClCH_2Cl, ruling out crystallization as a route to isolation. Decomposition of the borohydride salt was facile upon removal of the solvent under vacuum, which may be due to the presence of advantageous water. For all the above reasons, attempts to isolate **2c** were abandoned.

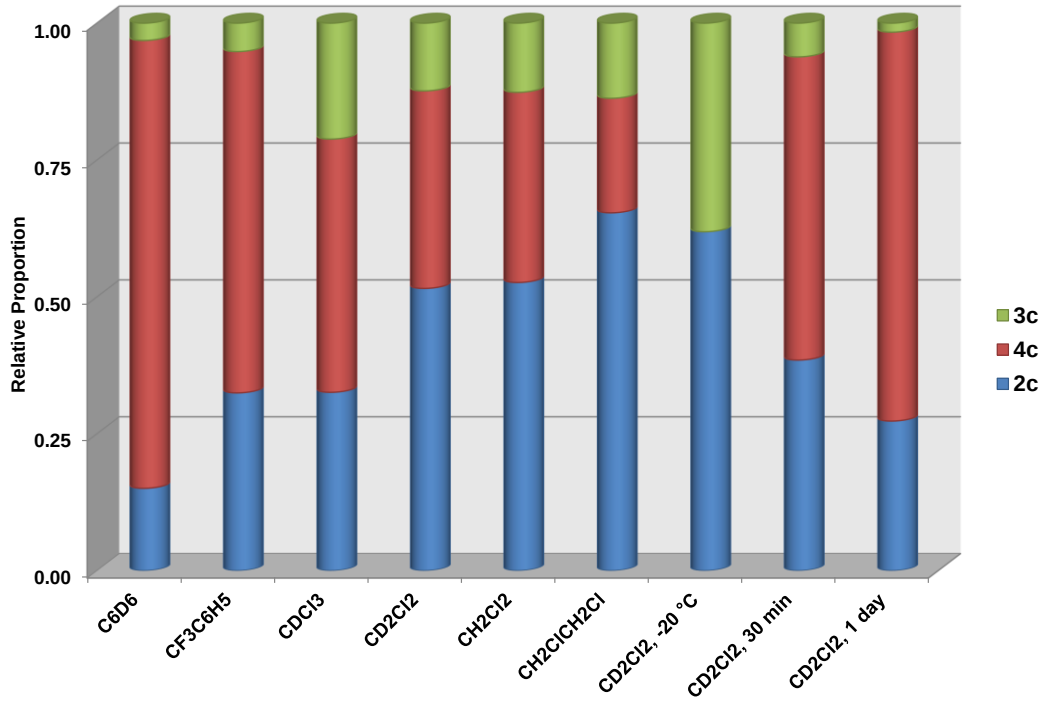

Figure 5-4. Product distribution as measured by ^{1}H NMR[109] for the reaction of **1c** with $B(C_6F_5)_3$ in various solvents

Concurrent with the solvent screen, an effort was made to disfavor the formation of the 1,2-dihydropyridine and Lewis acid-base adducts (**4** and **3**) by modifying the steric bulk about the carbonyl oxygen of unprotected Hantzsch ester derivatives. Fellow graduate student Véronique Laberge examined the reaction of the *t*-butyl-ester derivative **1d** with $B(C_6F_5)_3$. The increased bulk about the esters proved successful, as a 1:1 molar ratio of **1d** and $B(C_6F_5)_3$ afforded the pyridinium borohydride salt **2d** in good yield (90 %) (**Scheme 5-20** and **Table 5-1** entry 5). Unfortunately, isolation of borohydride salt **2d** was hampered its instability above -20 ˚C; thus, the reaction was carried out at -30 ˚C and **2d** was only characterized in solution.

5.3.3 Lewis Acid-base Adducts of Hantzsch Ester Derivatives with $B(C_6F_5)_3$

In contrast to **1c** and **1d**, the dimethylketone analog **1e** reacted with $B(C_6F_5)_3$ affording exclusively the Lewis acid-base adduct **3e** with no evidence of the hydride transfer product (**Scheme 5-24**). The preferential formation of the adduct **3e** was consistent with the decreased steric congestion and increased Lewis basicity of the carbonyl oxygen which is now a vinylogous amide.[62] As with adducts **3c** and **4c**, exchange between the two carbonyl groups was facile at room temperature, as determined by NMR, and desymmetrization of the Me resonances was observed in CD_2Cl_2 upon cooling to 0 ˚C (**Figure C-4** in **Appendix C**). Further evidence of carbonyl binding came from crystallographic data for **3e** (**Figure 5-5**). Similar to **4c**, the $B(C_6F_5)_3$ fragment of **3e** had a pseudo-tetrahedral geometry about B and an O-B distance of 1.538(5) Å, consistent with similar structural motifs in the literature.[65]

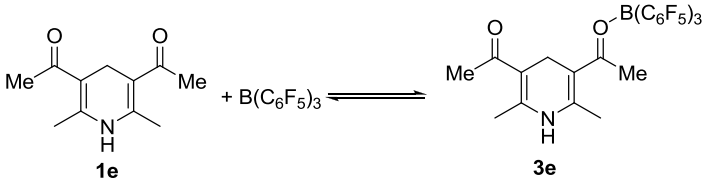

Scheme 5-24. Reaction of Hantzsch esters **1e** with $B(C_6F_5)_3$

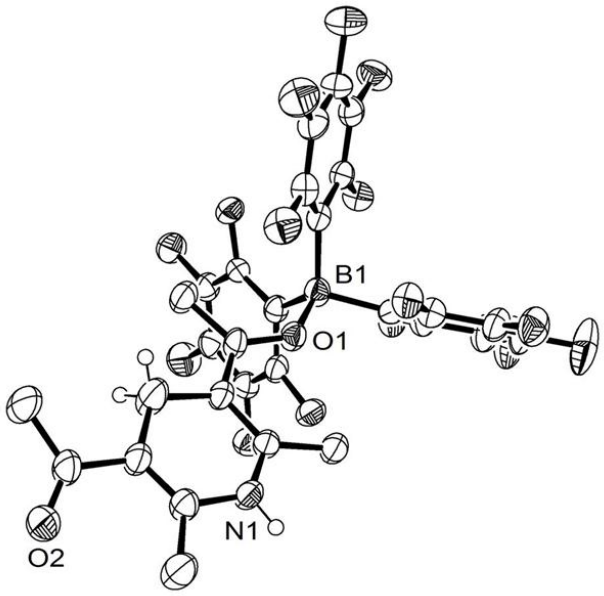

Figure 5-5. ORTEP structure of adduct **3e** the thermal ellipsoids were drawn at 50 % probability. All hydrogen atoms were omitted for clarity except for C4-H and N-H

The shifts in product distributions observed for the un-substituted Hantzsch ester derivatives **1c**, **1d** and **1e** illustrate that electronic and steric influences about the carbonyl groups impact the effectiveness of the hydride transfer and the stability of the borohydride salt. Reaction of **1c** with $B(C_6F_5)_3$ results in formation of **2c**, **3c** and **4c** and their relative proportion depends on the conditions. The bulk of **1d** favors formation of **2d** and the increased basicity and low steric bulk of **1e** promotes exclusive Lewis acid-base adduct formation. Recall that the reaction of **1a** and **1b** with $B(C_6F_5)_3$ was highly selective producing the borohydrides **2a** and **2b** almost exclusively.

The Hantzsch ester **1f** reacted with $B(C_6F_5)_3$ to yield a carbonyl bound Lewis acid-base adduct **3f** (**Scheme 5-25**) as evidenced by NMR and the connectivity was confirmed by X-ray crystallographic analysis (**Figure 5-6**). Again the boron atom is in a pseudo-tetrahedral

environment with a O-B bond length of 1.581(7) Å, which is consistent with the structures reported herein and elsewhere.[65, 105] Observation of the adduct **3f** was interesting considering it is a constitutional isomer of salt **2b**, illustrating clearly that substitution about the Hantzsch ester ring can shift the reaction outcome with $B(C_6F_5)_3$.

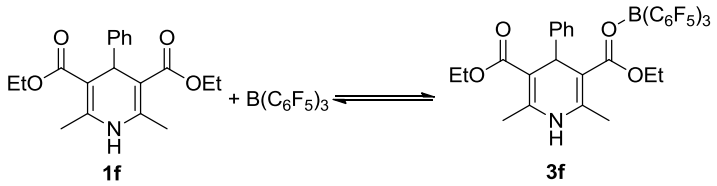

Scheme 5-25. Reaction of Hantzsch esters **1f** with $B(C_6F_5)_3$

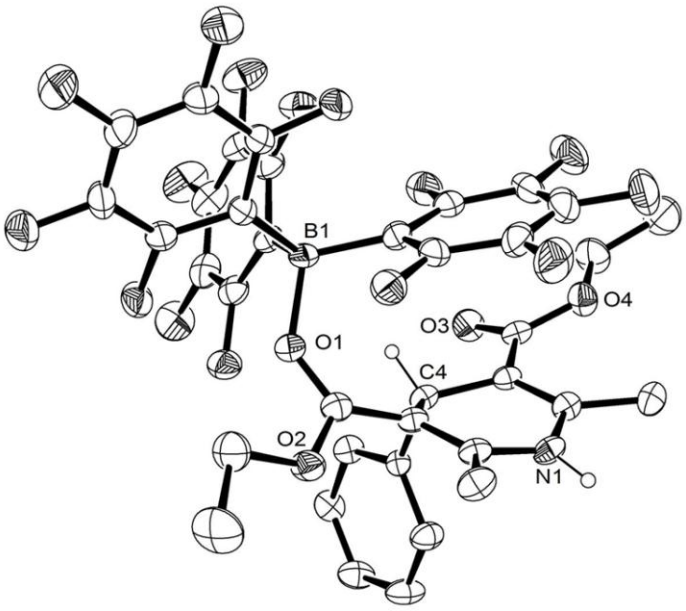

Figure 5-6. ORTEP structure of adduct **3f** the thermal ellipsoids were drawn at 50 % probability. All hydrogen atoms were omitted for clarity except for C4-H and N-H

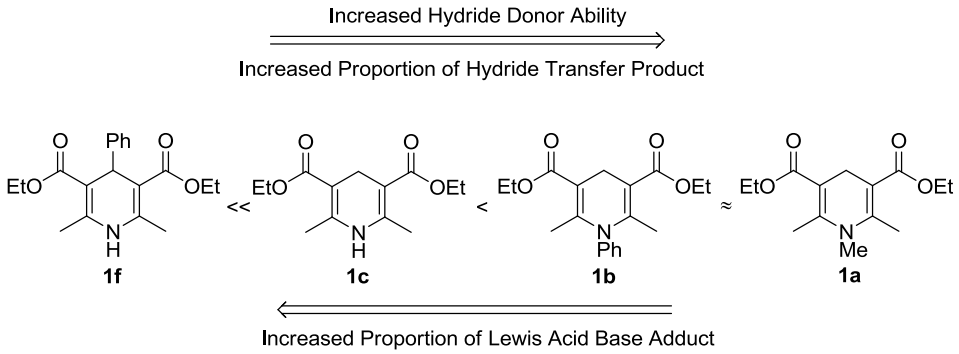

Scheme 5-26. Trend in reactivity of Hantzsch esters with $B(C_6F_5)_3$

It is known that substitution at the C4-ring position of a Hantzsch ester results in a reduction in hydride donating ability of the substrate, an effect that is ascribed to the additional energy required to move that substituent into the plane of the ring during reaction.[110, 111] Conversely, N-substituents promote the hydride transfer reaction because the C4-H is more electron rich.[112] These electronic perturbations can be used to rationalize why of all the Hantzsch esters examined only **1a** and **1b** react selectively to form **2a** and **2b** (**Scheme 5-26**). By this interpretation, substrate **1c** would be considered to be less hydridic than **1a** and **1b** but more hydridic than **1f**. This placement of **1c** is consistent with the observation of the formation of significant quantities of **2c** and **3c** under most reaction conditions. The preceding comparison assumes that the Lewis basicity of the esters is similar for **1a-c** and **1f** and as a result, illustrates that perturbations in the hydricity of the ring can explain some of the observed trends in reactivity. As described above the Hantzsch esters **1d** and **1e** illustrate that the Lewis basicity of the esters can influence the outcome of the hydride transfer reaction as well.

The homo exchange rate (k_{ex}) between Hantzsch ester **1f** and adduct **3f** (**Scheme 5-27**) was measured by VT NMR in CD_2Cl_2 by employing Mexico peak simulation software. An

Eyring Plot (**Figure 5-7**) of the extracted rate constants (**Table C-1** in **Appendix C**) determined at temperatures between 25 °C and -60 ºC showed overall nonlinear behavior, which is commonly observed if there is a change in the rate determining step of the exchange mechanism. The curve did display good linearity below 5 ºC, with activation parameters of $\Delta H^{\ddagger}$ = 11 ± 1 kcal mol^{-1} / 46 ± 4 kJ mol^{-1} and $\Delta S^{\ddagger}$ = -1 ± 2 cal mol^{-1} K^{-1} / -4 ± 2 J mol^{-1} K^{-1}(**Figure C-5** in **Appendix C**). Above 5 ºC there was a second region of linearity ($\Delta H^{\ddagger}$ = 2 ± 1 kcal mol^{-1} / 8 ± 4 kJ mol^{-1} and $\Delta S^{\ddagger}$ = -33 ± 3 cal mol^{-1} K^{-1} / -138 J mol^{-1} K^{-1}) although the regression fit (**Figure C-6** in **Appendix C**) was not as good because the peaking fitting strategy was hampered by the lower sensitivity of the exchange process to temperature. The coalescence temperature of the adduct was -35 ºC and the exchange rate at this temperature was 300 s^{-1}. The temperature of coalescence was higher and the rate of homo exchange was slightly lower than that observed for $B(C_6F_5)_3$ ethylbenzoate exchange (-70 ºC, k_{ex} = 811 s^{-1})[65] measured under similar experimental conditions by Piers.

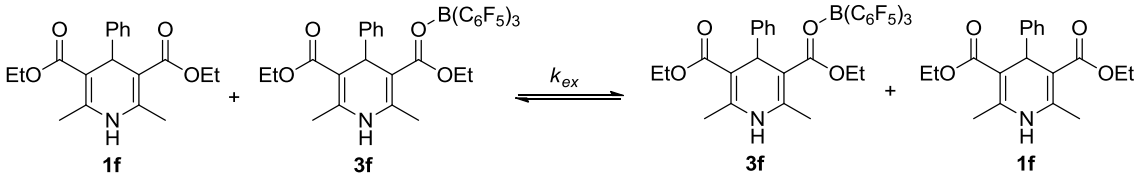

Scheme 5-27. Homo-exchange reaction between Hantzsch ester **1f** and adduct **3f**

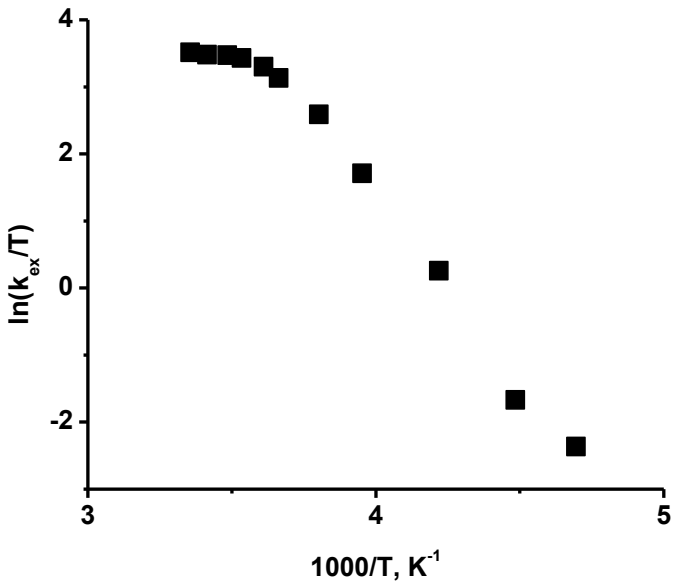

Figure 5-7. Eyring plot of **1f** and **3f** homo-exchange rate constants

5.3.4 Pyridinium Borohydrides via an FLP approach

An alternative strategy for the preparation of pyridinium borohydride salts employs frustrated Lewis pair (FLP) heterolytic H_2 activation.[78, 79] As was discussed previously, 2,6-lutidine, a sterically hindered pyridine, and $B(C_6F_5)_3$ are a sufficiently active FLP to cleave H_2 (**Scheme 5-15**). If pyridine **5c** could be employed instead of lutidine the resulting pyridinium-borohydride salt obtained would be identical to those obtained from hydride abstraction from Hantzsch ester **1c**.

The key to the success of the lutidine system in the original publication was the reversibility of adduct formation between the pyridine and $B(C_6F_5)_3$.[78, 79] The equilibrium allowed for a steady state quantity of free lutidine and $B(C_6F_5)_3$.[78, 79] In the absence of hydrogen, we found that $B(C_6F_5)_3$ became bound to the ester group of **5c** rather than the N (**Scheme 5-28**), as was

observed with 1,6-lutidine. The structure of **6c** was confirmed by X-ray crystallographic analysis (**Figure 5-8**). The O-B bond distance of **6c** was found to be 1.589(2) Å which was slightly longer than that observed for **4c**, reflecting slightly weaker binding with $B(C_6F_5)_3$, expected because of reduced electron donation from the aromatic ring.

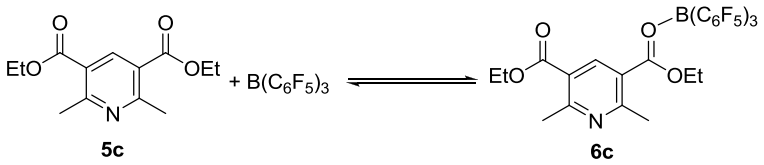

Scheme 5-28. Formation of adduct **6c** from reaction of **5c** with $B(C_6F_5)_3$

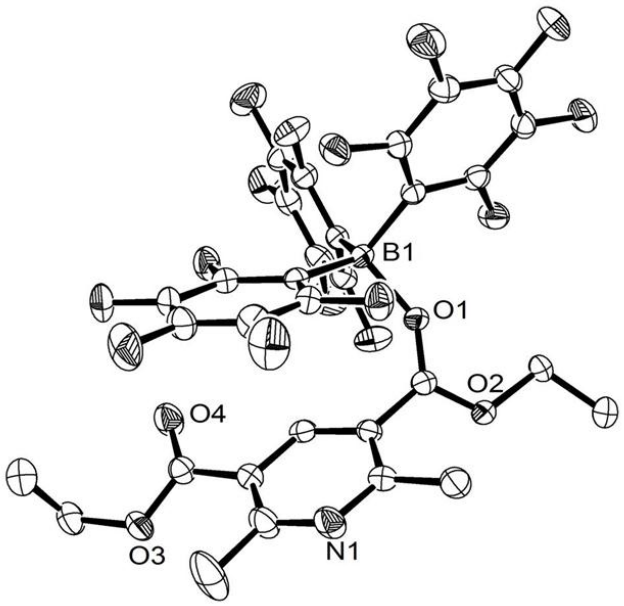

Figure 5-8. ORTEP structure of adduct **3f** the thermal ellipsoids were drawn at 50 % probability. All hydrogen atoms were omitted for clarity

The FLP heterolytic H_2 activation work was performed in collaboration with the Stephan group; unfortunately, conditions to form **2c** selectively were not found (**Scheme 5-29**). At room temperature, after 2 days the reaction afforded a mixture of starting material **6c**, oxygen-bound 1,2-dihydropyridine adduct **4c**, and the desired salt **2c** in a 40:51:9 ratio. Not surprising considering that **2c** readily disproportionates to **4c** in the presence of $B(C_6F_5)_3$. At -15 ˚C only trace amounts of **2c** and **4c** formed on standing for weeks. On the other hand the **6c**:**4c**:**2c** ratio was 3:86:11 when two equivalents of $B(C_6F_5)_3$ were employed, reflecting increased formation of 1,2-dihydropyridine. The increased heterolytic H_2 activation coincided with increased availability of free $B(C_6F_5)_3$. All the data suggests that the barrier to H_2 activation is higher for **6c** than for the lutidine system, which readily reacted at room temperature. [78, 79] A more detailed interpretation of the data is not possible considering the binding constant and exchange rates for **6c** under relevant reaction conditions were not determined. It would have been interesting to look at the FLP reactivity of the pyridine of the t-butyl ester **1d**, as the bulk about the carbonyl groups would disfavor adduct formation but we were discouraged from doing so because of the instability of **2d**.

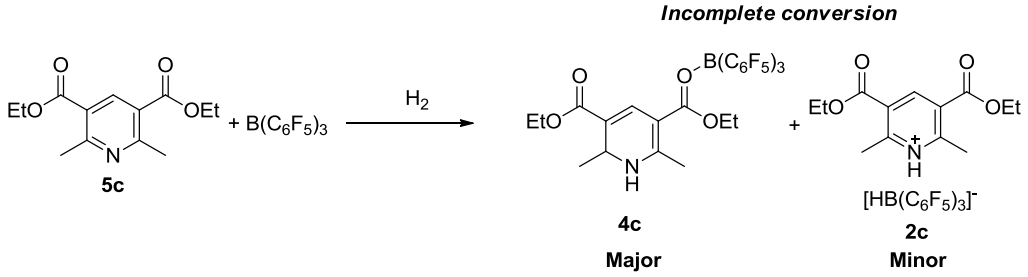

Scheme 5-29. Product distribution of H_2 activation by **5c** and $B(C_6F_5)_3$

5.3.5 Mechanism of Hydride Transfer: Stepwise of Concerted

All hydride transfers involving Hantzsch ester are subject to the same question, does the reaction proceed via a concerted polar transition state or does the reaction proceed through stepwise SET transfer mechanism (**Scheme 5-30**)?

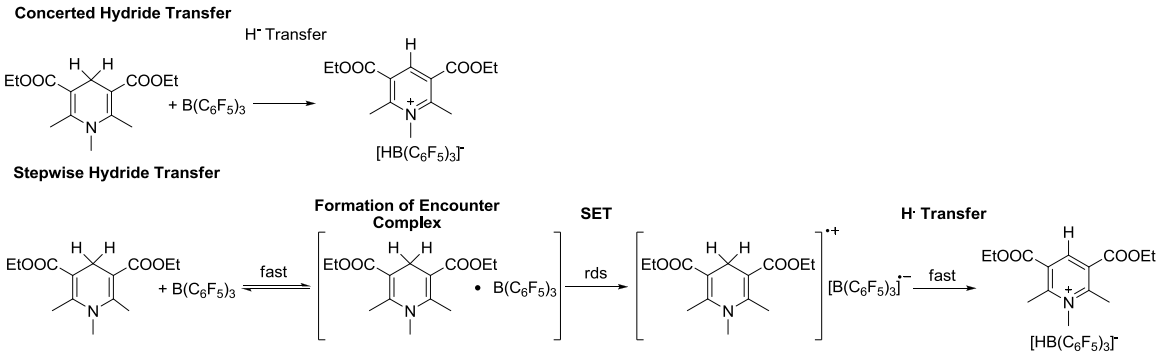

Scheme 5-30. Hydride transfer mechanisms for the reaction of **1a** with $B(C_6F_5)_3$

$$\Delta G(ET) = -F[\Delta E(A^{+}/A\cdot) - \Delta E(1^{+\cdot}/1)] \qquad \textbf{Eq. 5-2}$$

Based solely on one electron oxidation potentials for Hantzsch esters ($E^{o}(1^{+\bullet}/1)$ **1a** = 0.51 V, **1c** = 0.50 V verses $Fc^{+/0}$)[23] and the estimated reduction potential of $B(C_6F_5)_3$ ($E^{o}(B(C_6F_5)_3/B(C_6F_5)_3^{-\bullet})$ -1.17 V verses $Fc^{+/0}$)[113], electron transfer would be predicted to be non-spontaneous (**Eq. 5-2** where A = $B(C_6F_5)_3$) Non-spontaneous electron transfer, however, is not sufficient to rule out a SET reaction mechanism. An example is the hydride transfer reaction between Hantzsch ester **1c** and trityl cation ($E^{o}(CPh_3^{+}/CPh_3^{\bullet})$ = -0.26 V verses $Fc^{+/0}$),[49] which is isoelectric with $B(C_6F_5)_3$. In this particular case, it was also postulated that the electron transfer and the hydride transfer processes maybe closely linked, so much so that the barrier for the electron transfer might be overlapped with that of the hydrogen transfer, this would be an example of a highly asynchronous transition state.[49, 114-116]

The KIE of a hydride transfer reaction is a good way to discriminate between the concerted and stepwise mechanisms. An observation of a primary KIE is indicative of concerted hydride transfer while the absence of any KIE or the presence of a small KIE favors a stepwise SET pathway because the initial electron transfer is considered to be rate limiting.[48, 49] The KIE for the hydride transfer reaction between **1a** and $B(C_6F_5)_3$ was measured using two different methods (**Scheme 5-31**), by comparing the relative pseudo-first order rate constants for hydride versus deuteride transfer and by measuring the product distribution from NMR competition experiments (**Table 5-2**). The values obtained were 0.94 ± 0.09 and 1.05 ± 0.01 respectively. For comparison we also measured the KIE for the hydride transfer between **1c** and trityl 1.12 ± 0.14 under similar conditions and found it to be in good agreement with the transfer reaction with $B(C_6F_5)_3$. Rate determining carbonyl adduct formation/ decomposition was ruled out as the rate of carbonyl exchange as measured for the model adduct **3f**, see above discussion, was found to be much faster than the rate of reaction as measured by stop flow methods. While we cannot definitively rule out the possibility of a concerted hydride transfer mechanism, these data are consistent with a SET manifold or a highly asynchronous transition state. We propose then that the mechanism of hydride transfer between **1c** and $B(C_6F_5)_3$, under these conditions, is similar to that reported for trityl. That is, it proceeds with rapid and reversible formation of an encounter complex followed by a rate determining electron transfer and fast hydrogen atom transfer (**Scheme 5-30**).[49] It is also entirely possible that the hydride transfer is concerted but the transition state is asynchronous.[49] Currently this possibilty is being examined computationally in the Crudden group.

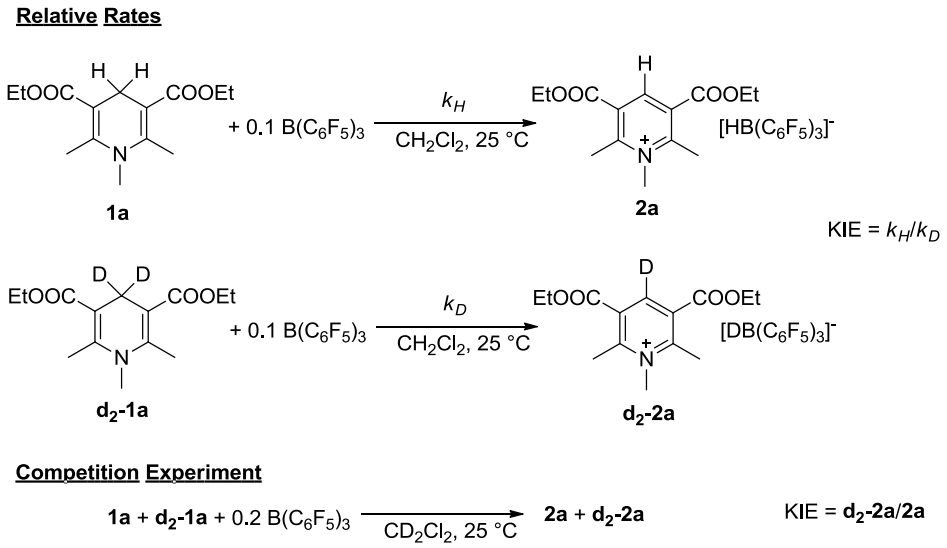

Scheme 5-31. Methods employed to measure the KIE of reaction

Table 5-2. Summary of KIE data for the reaction of **1a** and ***d*$_2$-1a** with $B(C_6F_5)_3$

Substrate	k_{obs}, s^{-1} [a]	KIE	
1a	0.030 ± 0.002	0.94 ± 0.09 [b]	1.05 ± 0.04 [c]
***d*$_2$-1a**	0.032 ± 0.003		

[a] Initial [**1a**], [***d*$_2$-1a**] and [$B(C_6F_5)_3$] concentrations were 0.18mM, 0.18 mM and 0.018 mM in CH_2Cl_2 at 25 ˚C; [b] Calculated from the ratio of the pseudo-first order rate constants, collected from monitoring the the decay of $B(C_6F_5)_3$ adsorption at 305 nm; [c] Calculated from NMR integrations where the initial [**1a**], [***d*$_2$-1a**] and [$B(C_6F_5)_3$] concentrations were 0.04 M, 0.04 M and 0.004 M respectively in CD_2Cl_2

We are not the only group to propose a SET mechanism for a hydride transfer reaction involving $B(C_6F_5)_3$. The Piers group reported the observation of an ESR signal for the radical anion $[B(C_6F_5)_3]^{\cdot-}$ in the equilibrium between *N*,*N*-dimethylaniline and $B(C_6F_5)_3$ (**Scheme 5-32**).[57] While care must be exercised when interpreting an ESR result, it is nonetheless possible that

multistep hydride transfer mechanisms are more common with $B(C_6F_5)_3$ than is currently appreciated and mechanistic studies into $B(C_6F_5)_3$ mediated reductions should reflect this possibility. In fact, it has already been established that $B(C_6F_5)_3$ is an electron acceptor in the presence of strong inorganic single electron reductants.[117-119] For example, $B(C_6F_5)_3$ has been observed to oxidize select Zr and Mo complexes and the radical anion $[B(C_6F_5)_3^{\bullet-}]$ was observed by ESR when $B(C_6F_5)_3$ was treated with the reductant Cp^*_2Co.

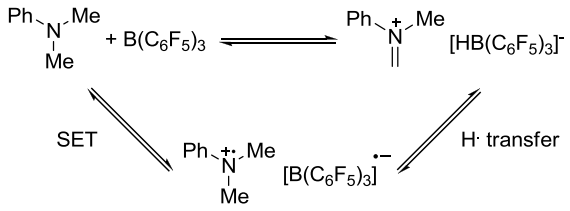

Scheme 5-32. The Piers mechanism for hydride transfer from *N*,*N*-dimethylaniline to $B(C_6F_5)_3$ from reference 57

5.3.6 Estimating the Hydride Affinity of $B(C_6F_5)_3$

In view of the importance of $[HB(C_6F_5)_3]^-$ to FLP[70] and silylation[57] reduction reactions it would be useful to have an experimental measurement of the hydride affinity (ΔH_{aff}) of $B(C_6F_5)_3$ because the value could be used to improve mechanistic models and aid reaction development.

Hydride affinity is defined as the negative of the heat of reaction ($\Delta H_{rxn}(H^-)$) for the addition of H^- to an acceptor, and is considered to be equal to the corresponding heterolytic bond dissociation energy. **Scheme 5-33** illustrates the definition for $B(C_6F_5)_3$.[97, 120] To the best of our knowledge the only values reported for the hydride affinity of $B(C_6F_5)_3$ (ΔH_{aff} = 100 kcal mol^{-1} / 420 kJ mol^{-1})[121] and other highly acidic boranes, other than BH_3 (ΔH_{aff} = 73 kcal mol^{-1} / 305 kJ mol^{-1}),[97, 120, 122] have been gas phase theoretical calculations. The ΔH_{aff} of $B(C_6F_5)_3$ can be estimated experimentally (**Eq. 5-3**) using calorimetry by subtracting the enthalpy of reaction

(ΔH_{rxn}(**1a**/$B(C_6F_5)_3$) from the value for the heterolytic bond dissociation energy of a Hantzsch ester (ΔH_{het}(**1a**) = 69.9 kcal mol^{-1} / 292 kJ mol^{-1}).[23, 47, 123]

$$B(C_6F_5)_3 + H^- \underset{\Delta H_{het}([HB(C_6F_5)_3]^-)}{\overset{-\Delta H_{aff}(B(C_6F_5)_3)}{\rightleftharpoons}} [HB(C_6F_5)_3]^- \quad \Delta H_{rxn}(H^-)$$

Scheme 5-33. Defining hydride affinity

$$\Delta H_{aff}(B(C_6F_5)_3) = \Delta H_{het}(\mathbf{1a}) - \Delta H_{rxn} \qquad \textbf{Eq. 5-3}$$

Using reaction calorimetry, the ΔH_{rxn}(**1a**/$B(C_6F_5)_3$) for hydride transfer from **1a** to $B(C_6F_5)_3$ was measured to be -10.6 ± 1 kcal mol^{-1} / -44.3 ± 4 kJ mol^{-1}. This value was used to estimate the hydride affinity of $B(C_6F_5)_3$ (ΔH_{aff} = 80.5 ± 1 kcal mol^{-1} / 338 ± 4.2 kJ mol^{-1}). A portion of the measured ΔH_{rxn}(**1a**/$B(C_6F_5)_3$) may be the result of charge pairing in the product **2a**, but we think that due to the large size of both the cation and anion, the effect is minimal. In support of this contention, it was found that two successive additions of $B(C_6F_5)_3$ to a solution containing excess **1a** were similarly exothermic. With charge pairing in mind the hydride affinity of $B(C_6F_5)_3$ reported above can be considered to be an overestimation.

Our value for the hydride affinity of $B(C_6F_5)_3$ is substantially smaller than that estimated from gas phase calculations, but seems reasonable considering observed patterns of reactivity. $B(C_6F_5)_3$ readily abstracts hydride from Hantzsch esters, but does not react with $HCPh_3$ (ΔH_{het} = 99.1 kcal mol^{-1} / 414 kJ mol^{-1})[124] even when heated (**Scheme 5-34**). The reverse reaction of **2a** with trityl to yield $HCPh_3$ however, is rapid (**Scheme 5-35**). 9,10-dihydroacridine (ΔH_{het} = 81.1 kcal mol^{-1} / 339 kJ mol^{-1})[23, 47] also does not react with $B(C_6F_5)_3$ at room temperature but a slow dehydrogenation reaction can be observed upon heating (**Scheme 5-34**). The reverse reaction, a $B(C_6F_5)_3$ catalyzed hydrogenation of acridine was recently reported by Geier and Stephan.[84]

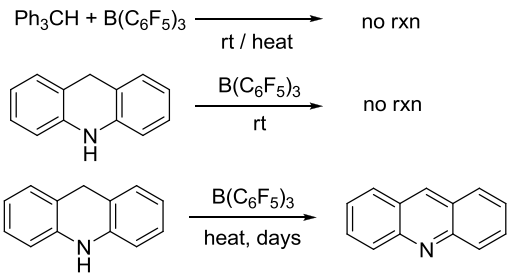

Scheme 5-34. Reactivity of $B(C_6F_5)_3$ toward $HCPh_3$ and 9,10-dihydroacridine

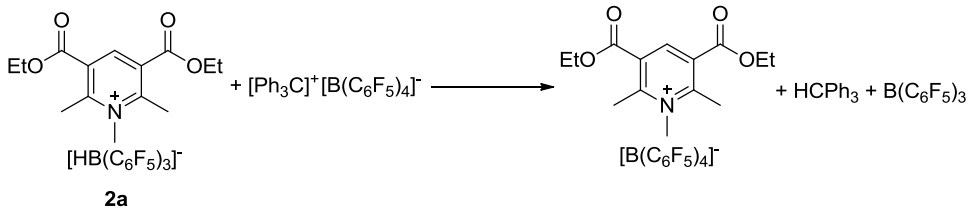

Scheme 5-35. Reaction of trityl with **2a**

Hydride Transfer Equilibrium

Esters **1b** and **1f** illustrate (**Table 5-1** entry 3 and **Scheme 5-25**) an effect that was common throughout this study, that small structural differences between Hantzsch ester derivatives result in large shifts in reactivity with $B(C_6F_5)_3$. The reason for the shift between hydride transfer and Lewis acid-base adduct formation is likely a consequence of the small thermodynamic driving force for hydride abstraction, as evidenced by the relatively small heat of reaction (ΔH_{rxn}(**1a**/$B(C_6F_5)_3$) = -10.6 kcal mol^{-1} / -44.3 kJ mol^{-1}), measurement of which was just discussed.

The reaction of unsubstituted Hantzsch ester **1c** with $B(C_6F_5)_3$, in contrast to the other derivatives discussed herein, represents a balance between these two extremes because significant amounts of hydride transfer product **2c** and Lewis acid-base adduct **3c** are formed.[104] In an effort

to better understand the interplay between hydride transfer and adduct formation, we examined the speciation between **2c** and **3c** as a function of $B(C_6F_5)_3$ concentration. It was observed that hydride transfer was favored under conditions where $B(C_6F_5)_3$ was present as a limiting reagent (**Figure 5-9**). This effect can be visualized by ^{19}F NMR, (**Figure 5-10**). At a 1:1 ratio of **1c**:$B(C_6F_5)_3$ the peaks for the adduct **3c** are readily observed and they diminished in intensity relative **2c** as the molar ratio was increased to 2:1.

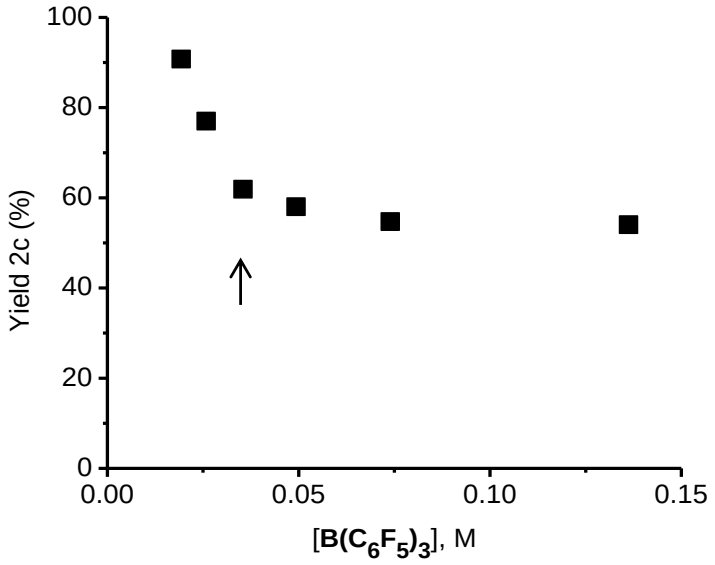

Figure 5-9. Yield of **2c** as a function of $[B(C_6F_5)_3]$ at -20 ºC as determined by ^1H NMR. Initial [**1c**] concentration was 0.03 M in CD_2Cl_2. The arrows indicate the point where the initial molar ratio of **1c**:$B(C_6F_5)_3$ was 1:1

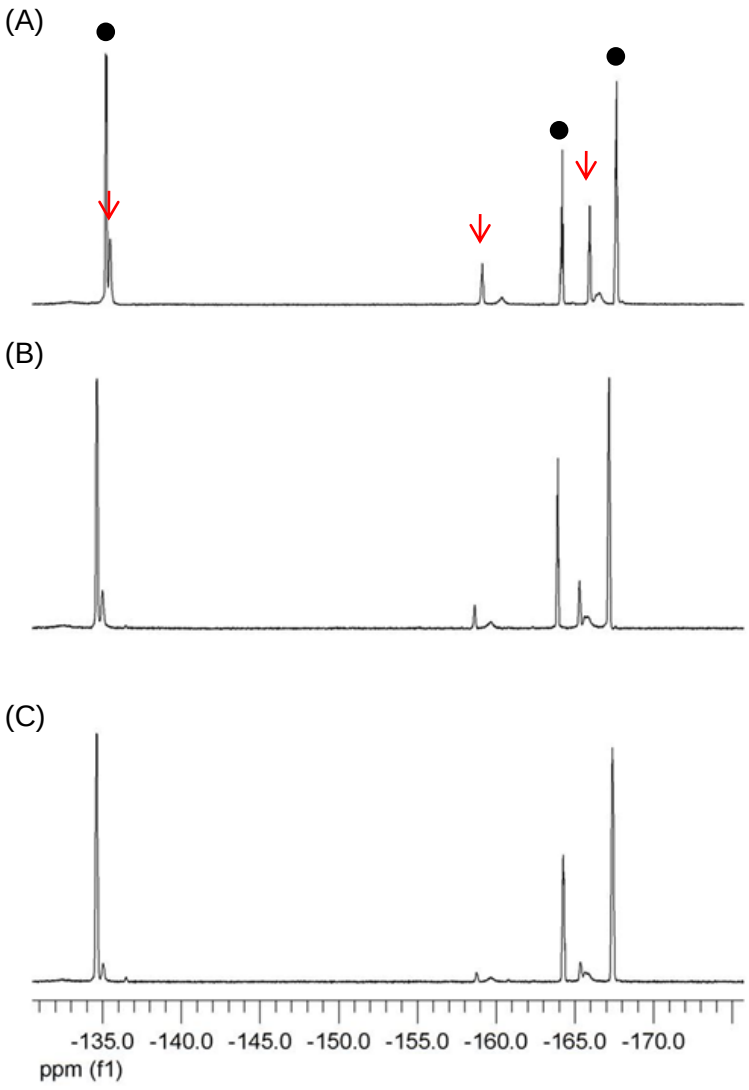

Figure 5-10. ^{19}F NMR indicates the speciation between **2c** (circle) and **3c** (arrow) at -20 ºC at different initial molar ratios of **1c**:$B(C_6F_5)_3$ A) 1:1; B) 1.5:1; C) 2:1. Initial [**1c**] concentration was held constant at 0.03 M in CD_2Cl_2

The fact that hydride transfer is favored over adduct formation as the amount of $B(C_6F_5)_3$ added is decreased (**Figure 5-9**) demonstrates that **1c** is a better hydride donor to this Lewis acid than a Lewis base. In other words the energy gained from aromaticity and forming a B-H bond as

a result of hydride transfer is greater than that from the formation of a B-O bond in the adduct. If the opposite were true and **1c** was a better Lewis base than hydride donor, decreasing the amount of $B(C_6F_5)_3$ added would have favored adduct formation instead i.e. the curve in **Figure 5-9** would have tended to 0 % yield of **2c**.

The temperature dependence of the concentration of **2c** in the reaction of **1c** with $B(C_6F_5)_3$ at a 1:4 molar ratio was examined by performing the reaction at -20 ºC, raising the solution temperature to -10 ºC and subsequently lowering the temperature in 5 degree increments to -30 ºC (**Figure 5-11** and **Figure 5-12**). It was found that adduct **3c** was favored at the expense of **2c** when the temperature was lowered, the same dependence was also observed for a 1:2 ratio. At a 2:1 ratio, a condition where $B(C_6F_5)_3$ was the limiting reagent, the concentration of **2c** did not change on the time scale of the experiment. Under these conditions no reversibility was observed. It is worth noting that we were able to mimic the temperature dependence of **2c** and **3c** by adding $B(C_6F_5)_3$ to a reaction with an initial molar ratio of 2:1.

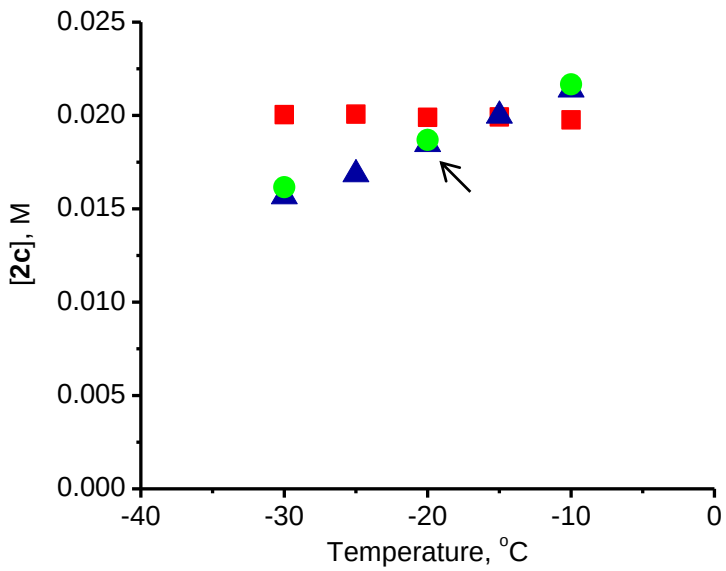

Figure 5-11. Temperature dependence of [**2c**] at different initial molar ratios of **1c**:$B(C_6F_5)_3$, 2:1 (square), 1:2 (circle) and 1:4 (triangle). The arrow indicates the starting [**2c**] and temperature for the 1:4 experiments. Initial [**1c**] concentration was held constant at 0.03 M in CD_2Cl_2

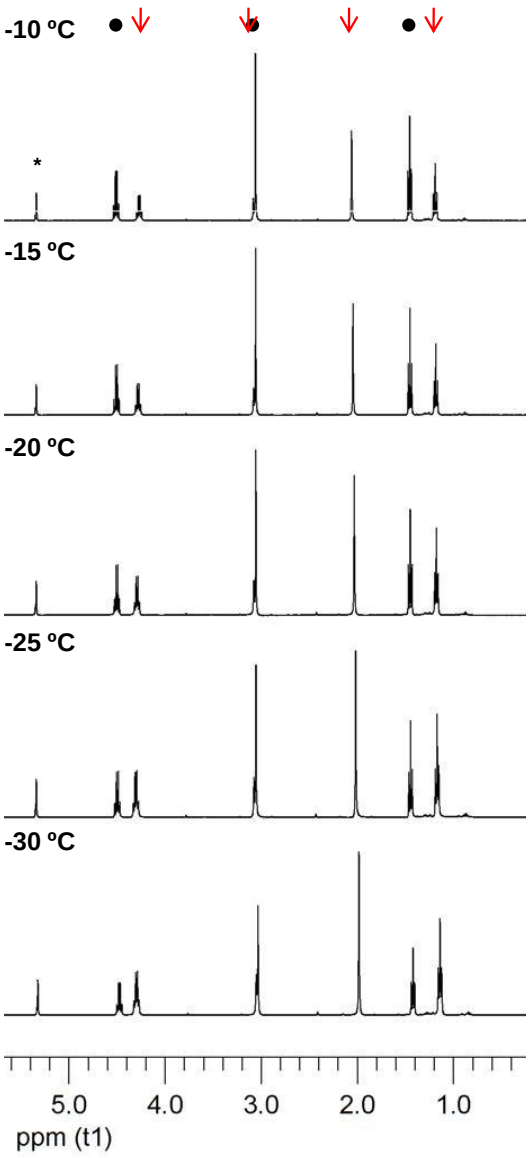

Figure 5-12. Interconversion of **2c** (circle) and **3c** (arrow) at an initial molar ratio of **1c**:$B(C_6F_5)_3$ of 1:4. The temperature was lowered from -10 ºC in 5 ºC increments. Initial [**1c**] concentration was 0.03 M in CD_2Cl_2. The asterisk represents the solvent peak

The observation of temperature dependence under conditions with excess Lewis acid (**Figure 5-11**) suggests that $B(C_6F_5)_3$ mediates an equilibrium between **2c** and **3c** (**Scheme 5-36**). This is an interesting circumstance in which a hydride abstraction is in equilibrium with a borohydride reduction, especially considering the equilibrium takes place at temperatures below -10 ºC. There are several of reports of similar reactions between $B(C_6F_5)_3$ and certain bulky amines at higher temperatures,[57, 76, 89-91] but these studies contained little information regarding the thermodynamics and dynamics of those systems.

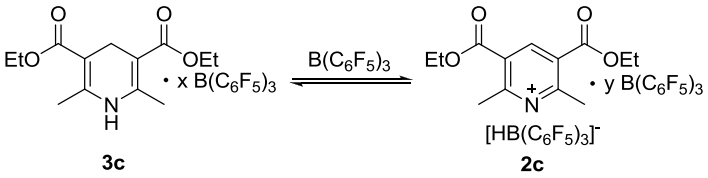

3c **2c**

Scheme 5-36. General expression for the equilibrium between **3c** and **2c**

A more detailed analysis of the equilibrium requires an understanding of the Lewis acid-base behavior of **2c** and **3c** under conditions where $B(C_6F_5)_3$ is held in large excess, i.e. at an initial 1:4 molar ratio of **1c**:$B(C_6F_5)_3$. Such an analysis is complicated by the fact that **2c** and **3c** have, in principle, multiple sites capable of binding to $B(C_6F_5)_3$. What was needed is a $B(C_6F_5)_3$ binding study of **2c** and **3c**. Unfortunately, we were unable to devise conditions to isolate the two components of the equilibrium; therefore, we thought it would be appropriate to interpolate their structure by examining instead the Lewis acid-base behavior of model compounds (**1f** and **8c**) as a function of $B(C_6F_5)_3$ concentration. Model Hantzsch ester **1f** was chosen because it was structurally related to **1c** and, as discussed in the previous section, forms adducts with $B(C_6F_5)_3$ rather than undergoing a hydride transfer reaction. Model substrate **8c** resembles the borohydride

2c and was synthesized from the corresponding Hantzsch pyridinium chloride salt **7c** by salt metathesis with $LiB(C_6F_5)_4$.

In order to qualitatively estimate the extent of adduct formation between $B(C_6F_5)_3$ and a Lewis base, one can look at the Δ_{m-p} (δ_{meta}- δ_{para}) value calculated using ^{19}F NMR chemical shifts.[61, 125, 126] Unbound $B(C_6F_5)_3$ has a Δ_{m-p} = 17, which is compared to tetravalent $[HB(C_6F_5)_3]^-$ and $[B(C_6F_5)_4]^-$, which have Δ_{m-p} values of 3.0 and 4.0, respectively. Thus small Δ_{m-p} values are indicative of strong binding of $B(C_6F_5)_3$ to a Lewis base and larger values represent weaker binding.[61, 125, 126] Significantly different Δ_{m-p} values were observed for **1f** (8.5) and **8c** (15.2), which mirror the expectation that **1f** should be a better Lewis donor than **8c**. That being said, regardless of how potentially marginal, $B(C_6F_5)_3$ does interact with ester groups of **8c** and as a result this observation is relevant to the adduct-borohydride equilibrium condition (**Scheme 5-36**).

The Δ_{m-p} analysis provided some information regarding the Lewis basicity of the model substrates **1f** and **5c** but it did not give much indication about how many equivalents of $B(C_6F_5)_3$ bind to these species. To get a better idea of the quantitative nature of $B(C_6F_5)_3$ binding to the model substrates (**Scheme 5-37**) and hence the structure of **2c** and **3c** under the equilibrium condition (**Scheme 5-36**) we analyzed changes in the ^1H NMR spectra as a function of Lewis acid concentration (**Figure 5-13**). The multiple Lewis basic sites of **1f** and **5c** required that the data be analyzed by a generalized binding equation[127-130] rather than a more standard approach of estimating the mole fraction of free substrate,[65] details of the modeling are discussed in the experimental section.

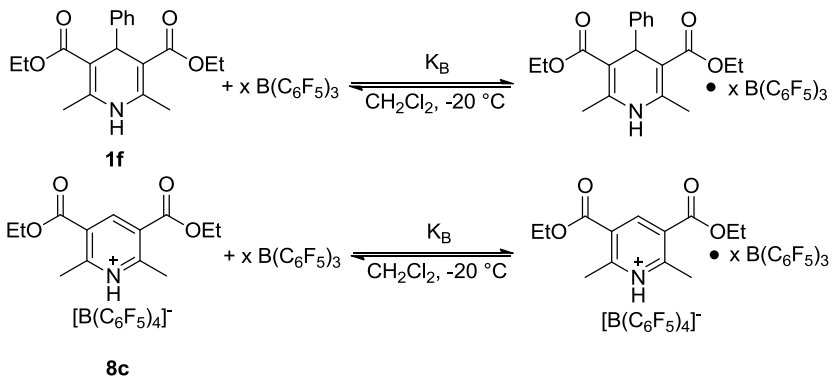

Scheme 5-37. General conditions for the bind study of model substrates **1f** and **8c**

A plot of ^{1}H NMR $\Delta\delta_{C4\text{-}H}$ vs. [$B(C_6F_5)_3$] for **1f** at -20 ºC (**Figure 5-13a**) exhibited a small but significant x-intercept (5.3 ± 0.8) × 10^{-3} M and sharp rise, both are suggestive of a multiple binding event of Lewis acid to **1f**.[127-130] We believe that a maximum of 2 equivalents of $B(C_6F_5)_3$ bind to this substrate even though there are in principle 3 Lewis base sites, two esters and a N. Observations in support of our contention are, the resonance for the 2,6–Me groups of **1f** does not change as the concentration of $B(C_6F_5)_3$ is increased and there is no evidence of $B(C_6F_5)_3$ binding to the N in 9,10-dihydroacridine ($\Delta_{m\text{-}p}$ = 17.0), which is structurally related to Hantzsch esters. As it is reasonable to assume that 2 equivalents of $B(C_6F_5)_3$ bind to **1f**, the curve displayed in **Figure 5-13a** gives information regarding the binding constant (K_b) for the second binding event (K_b = 5.2 ± 1.7) × 10^{2} M^{-1}. A similar observation was made for adduct **3c**, although it could not be quantified (**Figure C-2** and **Figure C-9** in **Appendix C**). When the molar ratio of **1c**:$B(C_6F_5)_3$ was set at 1:1, desymmetrization of **3c** could be observed upon cooling below -30 ºC. However at a 1:4 ratio, recall these are the conditions in which **3c** and the borohydride salt **2c** interconvert no desymmetrization of **3c** was observed even upon cooling to -80 ºC.

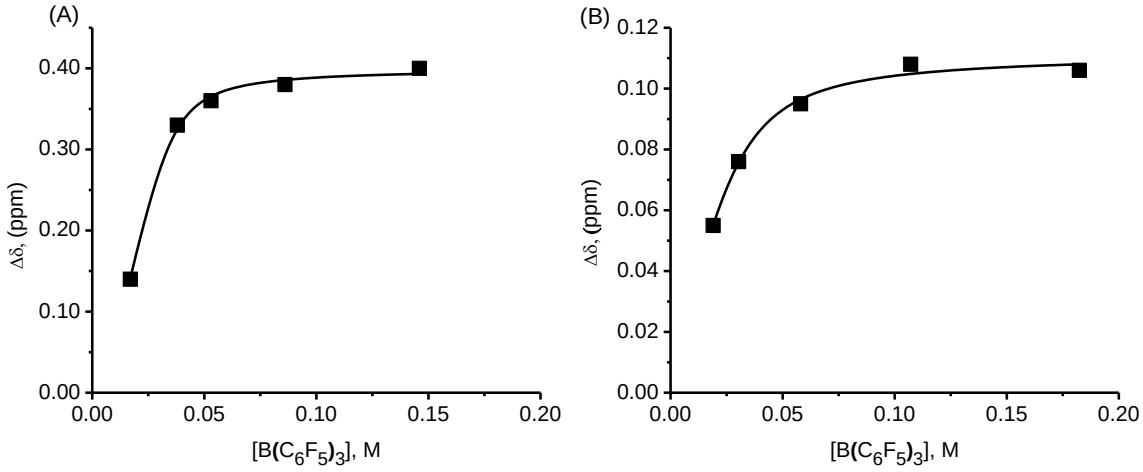

Figure 5-13. Plot of $\Delta\delta_{C4\text{-}H}$ verses $[B(C_6F_5)_3]$ for (a) **1f**, 0.03 M and (b) **8c**, 0.03 M calculated from the C4-H signal in the ^1H NMR in CD_2Cl_2 at -20 ºC

A binding curve was also obtained in a similar manner for the pyridinium borohydride structural analogue **8c** (**Figure 5-13b**).[127-130] This curve was more consistent with the formation of a 1:1 Lewis acid-base adduct, evidenced by less curvature and the absence of a significant x-intercept $(-0.8 \pm 2.2) \times 10^{-3}$ M. The calculated K_b of $(1.9 \pm 0.7) \times 10^2$ M^{-1} was slightly smaller than that observed for the second binding event to **1f**, which is expected considering the ring is electron deficient. Recall that the relatively large $\Delta_{m\text{-}p}$ value (15.2) was also consistent with weaker binding. The modeled K_b value for $B(C_6F_5)_3$ to **8c** was in agreement with a K_b value calculated ($K_b = 2.2 \pm 0.9) \times 10^2$ M^{-1} from more generic mole fraction of free substrate equation which is described in the experimental section and is similar to a value reported by Piers for the binding of $B(C_6F_5)_3$ to ethylbenzoate, $K_b = 1.1 \times 10^2$ M^{-1}.[65]

The binding study of the model substrates (**Scheme 5-37**) provided evidence that 2 equivalents of $B(C_6F_5)_3$ bind to **1f** and 1 equivalent binds to **8c**. When these results are applied to

the equilibrium between **2c** and **3c** (**Scheme 5-38**) an equilibrium expression can be derived (**Eq. 5-4**). Notice that $B(C_6F_5)_3$ appears on both sides of the equilibrium, for this reason it falls out of the simplified equilibrium expression. It should be emphasized that **Eq. 5-4** only applies under the conditions where $B(C_6F_5)_3$ is held in excess of Hantzsch ester, i.e. a molar ratio of **1c**:$B(C_6F_5)_3$ >1:2. The equilibrium equation is in line with the observation that when held in excess, the Lewis acid does not influence the distribution between **2c** and **3c** (**Figure 5-9**). The horizontal asymptote in this graph can be interpreted as the regime where **Eq. 5-4** is valid because $B(C_6F_5)_3$ has saturated all the available binding sites in solution and can no longer influence speciation.

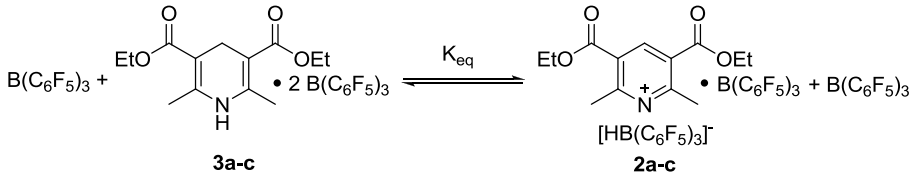

Scheme 5-38. $B(C_6F_5)_3$ mediated equilibrium between **3a-c** and **2a-c**

$$K_{eq} = \frac{[py]^+[HB(C_6F_5)_3]^-[\cancel{B(C_6F_5)_3}]}{[Adduct][\cancel{B(C_6F_5)_3}]} \qquad \textbf{Eq. 5-4}$$

Throughout the discussion we mention that $B(C_6F_5)_3$ is a mediator for the equilibrium between **2c** and **3c**. This statement is based on the temperature dependence of the concentration of **2c** and **3c** presented in **Figure 5-11** because interconversion of these species is only observed when $B(C_6F_5)_3$ is in excess of the initially added **1c**. Due to the structure of and the strength of binding in the Lewis acid-base adducts involved in the equilibrium (**Scheme 5-38**) there is necessarily some free $B(C_6F_5)_3$ present in solution. To confirm the function of $B(C_6F_5)_3$ as a mediator for the equilibrium a reaction was performed at a **1c**:$B(C_6F_5)_3$ molar ratio of 2:1. As mentioned earlier, at this initial condition, there is no temperature dependence on the

concentration of **2c**; but, the temperature dependency seen in **Figure 5-11** was initiated on addition of 2 equivalents of $B(C_6F_5)_3$ to the solution.

The equilibrium (**Scheme 5-38**) described for **1c** in the presence of excess $B(C_6F_5)_3$ was also observed for **1a** and **1b**. The thermodynamic parameters for all three reactions were measured experimentally using van't Hoff plots (**Table 5-3**). The van't Hoff plot for **1b** was recorded by Véronique Laberge. Notice that the ΔH_{rxn} for the equilibria with Hantzsch esters **1a-c** is endothermic. These values are in contrast to the exothermic reaction (ΔH_{rxn}(**1a**/$B(C_6F_5)_3$) = -10.6 kcal mol^{-1} / 44.3 kJ mol^{-1}) measured when $B(C_6F_5)_3$ was added in sub-stoichiometric quantities. It would be expected that the hydricity of the Hantzsch esters is decreased by coordination to $B(C_6F_5)_3$, resulting in a more endothermic reaction. The entropy values for the equilibria appear to be related to the size of the substituent on N, possibly reflecting increased dissociation of the ion pair. The balance of enthalpy and entropy contributions for the equilibria resulted in endergonic reactions under the conditions studied with equilibrium constants on the order of $6.5 \times 10^{-2} - 2.9 \times 10^{-3}$ M at -20 °C. While the N-substituted Hantzsch esters **1a** and **1b** are more efficient at transferring hydride to $B(C_6F_5)_3$ than **1c** under stoichiometric conditions (**Table 5-3**), there is no clear trend in the magnitude of K_{eq} and structure of the substrate.

Table 5-3. Physical parameters for the equilibria between **2a-c** and **3a-c**[a]

Substrate	R	ΔH_{rxn}, kcal mol^{-1} (kJ mol^{-1})	ΔS_{rxn}, cal mol^{-1} K^{-1} (J mol^{-1} K^{-1})	ΔG_{rxn}, kcal mol^{-1} (kJ mol^{-1})[b]	K_{eq}, M[b]
1a	Me	9.3 ± 0.1 (38.9 ± 0.4)	31.4 ± 0.3 (131 ± 1)	1.5 ± 0.1 (6.2 ± 0.4)	(6.5 ± 0.5) ×10^{-2}
1b	Ph	14.1 ± 0.1 (58.9 ± 0.4)	43.3 ± 0.1 (181 ± 0.4)	3.2 ± 0.1 (13.4 ± 0.4)	(2.9 ± 0.2) ×10^{-3}
1c	H	7.5 ± 0.3 (31.4 ± 1.2)	20.8 ± 0.9 (86.9 ± 3.8)	2.3 ± 0.6 (9.6 ± 4.5)	(1.2 ± 0.1) ×10^{-2}

[a] van't Hoff plots were obtained from reactions with initial concentrations 0.02 – 0.03 M **1a** – **c** in CD_2Cl_2 at temperatures -10 to -30 ˚C with 4 equivalents of $B(C_6F_5)_3$. The equilibrium distributions of **2a** – **c** and **3a** – **c** were determined by ^{1}H NMR. [b] Calculated at -20 ˚C

5.4 Conclusions

In conclusion, it was demonstrated that *N*-alkylated and arylated Hantzsch ester are effective hydride donors to $B(C_6F_5)_3$. The hydride transfer reactions described herein were observed at temperatures as low as -50 °C. It was found that the selectivity of the reaction was highly sensitive to the structure of the organic hydride. The most stable pyridinium borohydride products, **2a** and **2b**, resulted from hydride transfer from **1a** and **1b** to $B(C_6F_5)_3$. In solution the salts **2a** and **2b** did disproportionate slowly, over hours to days, to the corresponding 1,2-dihydropyridine adducts at room temperature. The same disproportionation reaction was more rapid for the less hindered salt **2c**.

In collaboration with our work on 1,4-dihydropyridines, the Stephan group explored heterolytic H_2 activation using **5c** and $B(C_6F_5)_3$ as an FLP. They observed the formation of trace amounts of borohydride salt **2c** and found that H_2 activation was slow in comparison to the

hydride transfer reaction. The decreased reactivity of the FLP was attributed to the lower basicity of the pyridine nitrogen as compared to successful FLPs such as 2,6-lutidine $B(C_6F_5)_3$ and the presence of a second complexation site for boron at the carbonyl oxygen.

The KIE of the hydride transfer reaction of **1a** with $B(C_6F_5)_3$ was measured and was found to be consistent with literature reports of studies on related systems and supported a SET reaction pathway or a highly asynchronous transition state. Calorimetry was used to estimate the hydride affinity of $B(C_6F_5)_3$, which was found to be 80 kcal mol^{-1} / 334 kJ mol^{-1} significantly lower than that calculated computationally but consistent with the observed patterns of reactivity explored herein and described in the literature. This value must be considered to be a maximum as there could be ion pairing between the cation and ion of **2a**. Controls suggested that the enthalpy contribution from ion pairing is likely minimal and an X-ray structure of **2a** showed that the cation and anion were well separated in the solid state.

Exploration of the product distribution of the reaction of **1c** with $B(C_6F_5)_3$ by varying the stoichiometry led to the observation of a dynamic equilibrium when the Lewis acid was present in excess of the organic hydride. This process was interesting because $B(C_6F_5)_3$ appeared to be necessary for interconversion of **3c** and **2c** but at high concentrations it did not influence the speciation.

The overall goal of this project was to assess the inherent capacity of 1,4-dihydropyridines to act as hydride donors in the synthesis of borohydrides. In this regard the project was a success as a rapid hydride transfer reaction to the model Lewis acid $B(C_6F_5)_3$ was developed and was amenable to study. Continuing on the path of establishing an organic hydride based regeneration scheme for ammonia borane (NH_3BH_3), the next step is to establish that organic hydrides can be used to generate boron compounds with more than one B-H bond. The

results of this Hantzsch ester study demonstrate that organic hydrides of interest in the next step should possess few if any accessible Lewis base sites, in this way reaction pathways leading to unproductive adducts can be avoided. These results also demonstrate the importance of screening out organic scaffolds that may undergo unwanted disproportionation reactions with boranes or borohydrides, such as what was observed for the conversion of the salt **2c** to the 1,2-dihydropyridine **4c**. It was with these considerations in mind that we began exploring the reactivity of organic hydrides with boron Lewis acids relevant to the regeneration of hydrogen storage materials, the subject of Chapter 6.

5.5 Experimental

5.5.1 General

Manipulations were performed either in an mBraun glovebox or on a double manifold Ar/vacuum line using standard Schlenk technique unless otherwise noted. All solvents were of Certified A.C.S. grade, purchased from Aldrich Chemical Co. unless otherwise note and distilled prior to use from an appropriate drying agent (pentane: P_2O_5; hexanes: Na; THF: Na ketyl; Et_2O, CH_2Cl_2, toluene, trifluorotoluene, CD_2Cl_2 and 1,2-dichloroethane: CaH_2; $CDCl_3$: Na_2SO_4) degassed by three freeze- pump-thaw cycles and stored in a glovebox over 4 Å molecular sieves and basic Al_2O_3. CD_2Cl_2 was purchased from Cambridge Isotopes, ethyl acetoacetate from Acros Organics, ceric ammonium nitrate from Anachemia Chemicals, $[CPh_3][B(C_6F_5)_4]$ from Strem and ammonium acetate from BDH Chemicals. $B(C_6F_5)_3$ was purchased from Strem and sublimed under static vacuum at 80 ˚C prior to use. ^{1}H, ^{13}C, ^{11}B and ^{19}F NMR spectra were collected on Bruker Advance 400, 500 and 600 MHz NMR spectrometers as indicated and referenced to residual solvent (^{1}H, ^{13}C) or externally (^{11}B: BF_3OEt_2, ^{19}F: $CFCl_3$).

5.5.2 Synthesis of ($C_5H_2Me_2(CO_2Et)_2NMe$): 1a

NaH (90 mg, 3.79 mmol) was weighed in a glovebox, suspended in dry THF (5 mL) and transferred via cannula to **1c** (400 mg, 1.58 mmol) suspended in THF (5 mL) in a 25 mL round bottom flask at 0 ˚C. The solution developed a bright orange color over 10 min and was warmed to room temperature. Methyl *p*-toluene sulfonate (0.60 mL, 5.91 mmol) was added drop wise over 30 min. The suspension was stirred for a further 2 hours after which the solvent was removed under vacuum. The residue was cooled in an ice bath, the excess NaH was quenched by slow addition of a dilute aqueous solution of *p*-toluene sulfonic acid (0.05 M, 25 mL) and the crude product was recovered by extraction with CH_2Cl_2. The organic layer was washed with brine and dried with $MgSO_4$, followed by the addition of 1,4-diazabicyclo[2.2.2]octane (500 mg, 4.44 mmol) to quench excess methyl *p*-toluene sulfonate. The solvent was removed under vacuum and the residue was purified by chromatography (3:1 Hexanes:EtOAc). The recovered white solid was dried over P_2O_5 under vacuum. The collected spectra were consistent with literature reports.[131] Yield: 210 mg (50 %). ^{1}H NMR (400 MHz, CD_2Cl_2, 298 K) δ: 1.31 (t, 6H, $^3J_{H\text{-}H}$ = 6 Hz, OCH_2CH_3), 2.39 (s, 6H, CH_3), 3.14 (s, 2H, CH_2), 3.18 (s, 3H, N-CH_3), 4.17 (q, 4H, $^3J_{H\text{-}H}$ = 6 Hz, OCH_2CH_3); ^{13}C NMR (100 MHz, $CDCl_3$, 298 K) δ: 14.4, 15.9, 23.9, 33.8, 59.7, 101.5, 150.6, 167.8.

5.5.3 Synthesis of Hantzsch ester ($C_5H_2Me_2(CO_2Et)_2NH$): 1c

The procedure was adapted from Wang *et al*.[132] Paraformaldehyde (300 mg, 10 mmol) and ammonium acetate (3.10 g, 40 mmol) were weighed into a 50 mL round bottom and suspended in distilled water (10 mL). Ethyl acetoacetate (3.80 mL, 30 mmol) was then added to the mixture, the flask was fitted with a condenser and heated at 80 ˚C for 4 hours. The reaction mixture was then cooled to 0 ˚C, filtered and washed with Et_2O and EtOAc. The crude product was further

purified by passing the material through a silica plug (EtOAc), recrystallized from a H_2O:MeOH mixture and dried over P_2O_5 under vacuum. The collected spectra were consistent with literature reports.[133] Yield: 2.0 g (80 %). ^{1}H NMR (300 MHz, $CDCl_3$, 298 K) δ: 1.27 (t, 6H, $^3J_{H-H}$= 7.1 Hz, OCH_2CH_3); 2.18 (s, 6H, Me); 3.26 (s, 2H, CH_2); 4.16 (q, 4H, $^3J_{H-H}$= 7.1 Hz, OCH_2CH_3); 5.09 (bs, 1H, NH).

5.5.4 Synthesis of ($C_5HMe_2Ph(CO_2Et)_2NH$): 1f

The procedure was adapted from Wang *et al*.[132] Benzaldehyde (4.25 g, 40 mmol) and ammonium acetate (6.20 g, 80 mmol) were weighed into a 100 mL round bottom and suspended in distilled water (20 mL). Ethyl acetoacetate (7.80 mL, 60 mmol) was added to the above mixture, the flask was fitted with a condenser and heated at 80 ˚C for 4 hours. The reaction mixture was then cooled to room temperature and extracted with CH_2Cl_2, the organic layer was dried with brine and $MgSO_4$. The solvent was removed under reduced pressure and the residue was heated under vacuum to remove excess ethylacetoacetate, followed by trituration with Et_2O. The crude product was further purified by passing the material through a silica plug (1:1 Hexanes:EtOAc), triturated again with Et_2O and dried over P_2O_5. The collected spectra were consistent with literature reports.[134] Yield: 2.0 g (20 %). ^{1}H NMR (300 MHz, C_6D_6, 298 K) δ: 1.04 (t, 6H, $^3J_{H-H}$= 7 Hz, OCH_2CH_3); 2.12 (s, 6H, Me); 4.16 (m, 4H, OCH_2CH_3); 4.83 (s, 1H, CH); 5.60 (s, 1H, NH), 7.15 (t, 1H, $^3J_{H-H}$ = 7 Hz, para-C_6H_5), 7.34 (t, 2H, $^3J_{H-H}$ = 7 Hz, meta-C_6H_5), 7.72 (d, 1H, $^3J_{H-H}$ = 7 Hz, ortho-C_6H_5).

5.5.5 Synthesis of [$C_5HMe_2(CO_2Et)_2NMe$][$HB(C_6F_5)_3$]: 2a

$B(C_6F_5)_3$ (100 mg, 0.19 mmol) was weighed in a glovebox, dissolved in CH_2Cl_2 (1.5 mL) and was added drop wise, in the dark, to a solution of **1a** (50 mg, 0.19 mmol) in CH_2Cl_2 (1.5 mL) in a 4 dram glass vial at room temperature. A bright yellow solution formed on addition and after 5 min

Et_2O (15 mL) was added. The solvent was removed under vacuum to yield a white powder. X-ray quality crystals were grown from Et_2O at -25 ˚C. Anal. Calcd. for $C_{32}H_{21}BF_{15}NO_4 \cdot 0.5CH_2Cl_2$: C, 47.50%; H, 2.70%; N, 1.70%. Found: C, 47.51%; H, 2.50%; N, 1.71%. ^{1}H NMR (500 MHz, CD_2Cl_2, 298 K) δ: 1.45 (t, 6H, $^3J_{H\text{-}H}$ = 7 Hz, OCH_2CH_3), 3.16 (ov s, 6H, CH_3), 3.42 (br ov q, 1H, $^1J_{B\text{-}H}$ = 88 Hz, B-*H*), 4.25 (s, 3H, N-CH_3), 4.52 (q, 4H, $^3J_{H\text{-}H}$ = 7 Hz, OCH_2CH_3), 9.14 (s, 1H, para-H); ^{13}C NMR (125 MHz, CD_2Cl_2 273 K) δ: 14.1, 20.3, 42.5, 64.6, 125.4 (br m, *C*-B), 130.4, 136.8 (dm, $^1J_{C\text{-}F}$ = 257 Hz, *C*-F), 138.1 (dm, $^1J_{C\text{-}F}$ = 244 Hz, *C*-F), 146.7, 148.28 (dm, $^1J_{C\text{-}F}$ = 244 Hz, *C*-F), 160.7, 162.6; ^{19}F NMR (376 MHz, CD_2Cl_2, 298 K) δ: -134.6 (br m, 6F, ortho-C_6F_5), -164.6 (br m, 3F, para-C_6F_5), -167.6 (br m, 6F, meta-C_6F_5); ^{11}B NMR (160 MHz, CD_2Cl_2, 298 K) δ: -25.8 (d, $^1J_{B\text{-}H}$ = 88 Hz).

5.5.6 Synthesis of $[C_5HMe_2(CO_2Et)_2NH][HB(C_6F_5)_3]$: 2c and $(C_5H_2Me_2(CO_2Et)(CO_2EtB(C_6F_5)_3)NH)$: 3c

$B(C_6F_5)_3$ (10 mg, 0.02 mmol) was weighed in a glovebox, dissolved in CD_2Cl_2 (0.25 mL) and was added in the dark to a suspension of **1c** (5 mg, 0.02 mmol) frozen in CD_2Cl_2 (0.25 mL) in an NMR tube. On warming, a bright yellow solution formed. The solution was characterized by VT multi-nuclear NMR. **2c** ^{1}H (400 MHz, CD_2Cl_2, 253 K) δ: 1.46 (t, 6H, $^3J_{H\text{-}H}$ = 7 Hz, OCH_2CH_3), 3.06 (s, 6H, CH_3), 3.53 (br ov q, 1H, $^1J_{B\text{-}H}$ = 80 Hz, B-*H*), 4.50 (q, 4H, $^3J_{H\text{-}H}$ = 7 Hz, OCH_2CH_3), 9.42 (s, 1H, para-*H*), 13.05 (br s, 1H, N-*H*); ^{13}C NMR (125 MHz, CD_2Cl_2 253 K, HSQC and HMBC) δ: 14.3 (s, OCH_2CH_3), 21.2 (s, CH_3), 64.3 (s, OCH_2CH_3), 124.0 (br m, *C*-B), 128.0 (s, py*C*), 136.8 (dm, $^1J_{C\text{-}F}$ = 244 Hz, *C*-F), 138.4 (dm, $^1J_{C\text{-}F}$ = 235 Hz, *C*-F), 148.2 (dm, $^1J_{C\text{-}F}$ = 231 Hz, *C*-F), 149.5 (s, py*C*H), 159.3 (s, py*C*), 161.7 (s, *C*OOEt); ^{19}F NMR (376 MHz, CD_2Cl_2, 253 K) δ: -135.3 (d, 6F, $^3J_{F\text{-}F}$ = 22 Hz, ortho-C_6F_5), -164.1 (t, 3F, $^3J_{F\text{-}F}$ = 20 Hz, para-C_6F_5), -167.7 (t, 6F, $^3J_{F\text{-}F}$ = 20 Hz, meta-C_6F_5); ^{11}B (168 MHz, CD_2Cl_2, 263K) δ: -24.4 (d, $^1J_{B\text{-}H}$ = 80 Hz, *B*-H). **3c**

^{1}H (400 MHz, CD_2Cl_2, 253 K) δ: 1.23 (br m, 6H, OCH_2CH_3), 2.11 (s, 6H, CH_3), 3.22 (s, 2H, CH_2), 4.20 (q, 4H, $^{3}J_{H\text{-}H}$ = 7 Hz, OCH_2CH_3), 5.94 (br s, 1H, N-*H*); Partial ^{13}C (125 MHz, CD_2Cl_2, 263 K, HSQC and HMBC) δ: 13.1 (s, OCH_2CH_3), 18.9 (s, CH_3), 23.3 (s, CH_2), 66.1 (s, OCH_2CH_3), 97.1 (s, *C*=C), 149.8 (s, *C*=C), 174.9 (s, *C*OOEt); ^{19}F NMR (376 MHz, CD_2Cl_2, 253 K) δ: -135.6 (br m, 6F, ortho-C_6F_5), -159.1 (br m, 3F, para-C_6F_5), -165.9 (br m, 6F, meta-C_6F_5); ^{11}B (168 MHz, CD_2Cl_2, 263K) δ: 2.4 (br s, *B*-O).

5.5.7 Synthesis of ($C_5H_2Me_2(COMe)(COMeB(C_6F_5)_3)NH$): 3e

$B(C_6F_5)_3$ (25 mg, 0.05 mmol) was weighed in a glovebox, dissolved in CD_2Cl_2 (0.25 mL) and was added in the dark, to a suspension of $C_5H_2Me_2(COMe)_2NH$ **1e** (9 mg, 0.05 mmol) in CD_2Cl_2 (0.25 mL) in an NMR tube. The solution was characterized by VT multi-nuclear NMR. X-ray quality crystals were grown from 1,2-DCE layered with pentane at -25 ˚C. Anal. Calcd for $C_{32}H_{21}BF_{15}NO_4 \cdot 0.5CH_2Cl_2$: C, 49.39 %; H, 2.14 %; N, 1.99 %. Found: C, 49.22 %; H, 2.03 %; N, 1.96 %. ^{1}H (600 MHz, CD_2Cl_2, 273 K) δ: 2.10 (s, 3H, CH_3), 2.21 (s, 3H, CH_3), 2.28 (s, 3H, CH_3), 2.45 (s, 3H, CH_3), 3.34 (s, 2H, CH_2), 7.10 (s, 1H, N*H*); ^{13}C NMR (125 MHz, CD_2Cl_2 273 K) δ: 19.1, 23.9, 25.3, 27.0, 30.4, 105.9, 116.6, 119.6 (br m, C-B), 137.3 (dm, $^{1}J_{C\text{-}F}$ = 246 Hz, *C*-F), 139.3, 140.2 (dm, $^{1}J_{C\text{-}F}$ = 253 Hz, *C*-F), 148.0 (dm, $^{1}J_{C\text{-}F}$ = 240 Hz, *C*-F), 164.7, 197.9, 198.5; ^{19}F NMR (376 MHz, CD_2Cl_2, 250 K) δ: -134.0 (br m, 6F, ortho-C_6F_5), -155 (br m, 3F, para-C_6F_5), -163.3 (br m, 6F, meta-C_6F_5); ^{11}B (168 MHz, CD_2Cl_2, 273K) δ: -2.0 (br s, *B*-O).

5.5.8 Synthesis of ($C_5HMe_2Ph(CO_2Me)(CO_2EtB(C_6F_5)_3)NH$): 3f

$B(C_6F_5)_3$ (15 mg, 0.03 mmol) was weighed in a glovebox, dissolved in DCE (0.25 mL) and added to a solution of $C_5HMe_2Ph(CO_2Et)_2NH$ **1f** (10 mg, 0.03 mmol) in DCE (0.25 mL) and was layered with pentane. The solution was allowed to stand at -20 ºC and the resulting crystals recovered, washed with pentane and dried in vacuum. Yield 20 mg (80 %). Anal. Calcd. for

$C_{37}H_{23}BF_{15}NO_4$: C, 52.80 %; H, 2.87 %; N, 1.66 %. Found: C, 52.80 %; H, 3.02 %; N, 1.66 %. ^{1}H (500 MHz, CD_2Cl_2, 298 K) δ: 1.21 (t, 6H, $^3J_{H-H}$ = 7 Hz, OCH_2CH_3), 2.29 (s, 6H, CH_3), 4.24 (q, 4H, $^3J_{H-H}$ = 7 Hz, OCH_2CH_3), 4.73 (s, 1H, C-*H*), 6.27 (br s, 1H, N-H), 7.13 (d, 2H, $^3J_{H-H}$ = 7 Hz, ortho-C_6H_5), 7.24 (ov m, 3H, meta-para-C_6H_5); ^{13}C (100 MHz, CD_2Cl_2, 298 K) δ: 14.1, 19.3, 39.8, 64.6, 103.1, 117.2 (br-s, B-*C*), 127.3, 127.5, 128.6, 137.5 (dm, $^1J_{C-F}$ = 244 Hz, *C*-F), 141.1 (dm, $^1J_{C-F}$ = 238 Hz, *C*-F), 145.4, 145.9, 148.3 (dm, $^1J_{C-F}$ = 233 Hz, *C*-F), 172.2; ^{19}F (376 MHz, CD_2Cl_2, 298 K) δ: -133.0 (br m, ortho-C_6F_5), -155.9 (br m, para-C_6F_5), -164.5 (br m, meta-C_6F_5); ^{11}B (160 MHz, CD_2Cl_2, 298 K) δ: 7.2 (br s, *B*-O).

5.5.9 Synthesis of ($C_5H_2Me_2(CO_2Et)(CO_2EtB(C_6F_5)_3)NH$): 4c

$B(C_6F_5)_3$ (100 mg, 0.19 mmol) was weighed in a glovebox, dissolved in CH_2Cl_2 (1.5 mL) and was added drop wise, in the dark, to a solution of **1c** (50 mg, 0.19 mmol) in CH_2Cl_2 (1.5 mL) in a 4 dram glass vial at room temperature. A bright yellow solution formed on addition, after 5 min hexanes (10 mL) was added and the solution was allowed to stand at -25 ˚C. The resulting precipitate was filtered and recrystallized from CH_2Cl_2 layered from pentane, filtered and dried under vacuum. Yield: 60 mg (40 %). **3c** slowly decomposes in solution to **2c** and as a result it was not possible to obtain an analytically pure sample. X-ray quality crystals were grown from CH_2Cl_2 layered with pentane at -25 ˚C. ^{1}H NMR (400 MHz, $CDCl_3$, 298 K) δ: 1.10 (ov d, 3H, $^3J_{H-H}$ = 7 Hz, $CHCH_3$), 1.13 (ov br m, 3H, OCH_2CH_3), 1.44 (br, 3H, OCH_2CH_3), 2.39 (s, 3H, CH_3), 4.13 (br m, 2H, OCH_2CH_3), 4.22 (br m, 2H, OCH_2CH_3), 4.56 (p, 1 H, $^3J_{H-H}$ = 7 Hz, $CHCH_3$), 6.06 (br s), 7.41 (br s); Partial ^{13}C (125 MHz, CD_2Cl_2, 298 K, HSQC) δ: 13.5, 13.7, 21.7, 23.7, 48.6, 62.1, 65.4, 138.6; ^{19}F NMR (376 MHz CD_2Cl_2, 298 K) δ: -134.2 (br m, 6F, ortho-C_6F_5), -157.3 (br m, 3F, para-C_6F_5), -164.3 (br m, 6F, meta-C_6F_5); ^{11}B NMR (160 MHz, C_6D_6, 298 K) δ: 2.9 (br s, *B*-O).

5.5.10 Synthesis of ($C_5H(CO_2Et)_2NH$): 5c

Synthesis was adapted from Pfister *et al.*[16] Ceric ammonium nitrate (2.25 g, 4.10 mmol) was weighed into a 4 dram vial, dissolved in H_2O (5 mL) and added dropwise to diethyl 1,4-dihydro-2,6-dimethylpyridine-3,5-dicarboxylate (**1a**, 500 mg, 2.0 mmol) suspended in acetone (15 mL) at 0 ˚C in a 50 mL round bottom flask. After addition, the solution was stirred for 30 min and the acetone was evaporated under vacuum. The aqueous solution was extracted with CH_2Cl_2 and the organic layer was dried with brine and $MgSO_4$. A silica plug (8:1 Hexanes : Ethyl Acetate) was used to further purify the residue obtained after extraction, the recovered white solid was dried over P_2O_5 under vacuum. The collected spectra were consistent with literature reports.[135] Yield: 430 mg (87 %). ^{1}H NMR (300 MHz, $CDCl_3$, 298 K) δ: 1.43 (t, 6H, $^3J_{H\text{-}H}$ = 7 Hz, OCH_2CH_3), 2.87 (s, 6H, CH_3), 4.43 (q, 4H, $^3J_{H\text{-}H}$ = 7 Hz, OCH_2CH_3), 8.69 (s, 1H, p; *para-H*); ^{13}C NMR (100 MHz, $CDCl_3$, 298 K) δ: 15.0, 24.9, 61.4, 123.1, 140.9, 162.2, 166.0. HRMS (TOF EI^+) exact mass calculated for $[M]^+$ required *m/z* 251.1158 ($C_{13}H_{17}NO_4$), found *m/z* 251.1153.

5.5.11 Synthesis of ($C_5HMe_2(CO_2Et)(CO_2EtB(C_6F_5)_3)N$): 6c

$B(C_6F_5)_3$ (100 mg, 0.19 mmol) was weighed in a glovebox, dissolved in CH_2Cl_2 (1.5 mL) at room temperature and was added to a 4 dram glass vial which contained diethyl 2,6-dimethylpyridine-3,5-dicarboxylate **5c** (50 mg, 0.19 mmol) dissolved in CH_2Cl_2 (1.5 mL). The solution was allowed to stand room temperature for 1 h and the solvent was removed under vacuum. X-Ray quality crystals were grown from CH_2Cl_2: pentane at -25 ˚C. Anal. Calcd. for $C_{31}H_{17}BF_{15}NO_4$: C, 48.78 %; H, 2.24 %; N, 1.84 %. Found: C, 48.59 %; H, 2.17 %; N, 1.85 %. ^{1}H NMR (500 MHz, $CDCl_3$, 298 K) δ: 1.42 (t, 6H, $^3J_{H\text{-}H}$ = 7 Hz, OCH_2CH_3),), 2.18 (s, 6H, CH_3), 4.45 (q, 4H, $^3J_{H\text{-}H}$ = 7 Hz, OCH_2CH_3), 8.61 (s, 1H, *para-H*); ^{13}C NMR (125 MHz, $CDCl_3$ 298 K) δ: 14.5, 25.0, 63.2, 114.4 (br m, *C*-B), 123.1, 137.8 (dm, $^1J_{C\text{-}F}$ = 252 Hz, *C*-F), 141.1, 144.3 (dm, $^1J_{C\text{-}F}$ = 266 Hz, *C*-

F), 148.5 (dm, $^{1}J_{C\text{-}F}$ = 247 Hz, *C*-F), 162.5, 167.5; ^{19}F NMR (376 MHz, $CDCl_3$, 298 K) δ: -129.4 (br d, 6F, $^{3}J_{F\text{-}F}$ = 16 Hz, *ortho*-C_6F_5), -145.7 (br m, 3F, *para*-C_6F_5), (t d, 6F, $^{3}J_{F\text{-}F}$ = 16 Hz & $^{5}J_{F\text{-}F}$ = 6 Hz, *meta*-C_6F_5); ^{11}B NMR (160 MHz, $CDCl_3$, 298 K) δ: 44.2 (br s, *B*-O).

5.5.12 Synthesis of $(C_5HMe_2(CO_2Et)_2NH)Cl$: 7c

To a solution of 3,5-bis(ethoxycarbonyl)-2,6-dimethylpyridine **5c** (280 mg, 1.10 mmol) in Et_2O (3 mL) was added 1 N HCl in Et_2O (3 mL). The precipitate was isolated by filtration and washed with Et_2O and dried over P_2O_5 under vacuum. Yield: 180 mg (55 %). Anal. Calcd. for $C_{13}H_{18}NO_4Cl$: C, 54.26 %; H, 6.31 %; N, 4.87 %. Found: C, 54.52 %; H, 6.26 %; N, 4.87 %. ^{1}H (300 MHz, d_6-DMSO, 298 K) δ: 1.33 (t, 6H, $^{3}J_{H\text{-}H}$ = 7 Hz, OCH_2CH_3), 2.80 (s, 6H, CH_3), 4.35 (q, 4H, $^{3}J_{H\text{-}H}$ = 7 Hz, OCH_2CH_3), 8.62 (s, 1H, C-*H*), 8.83 (br s, 1H, N-*H*); ^{13}C (120 MHz, d_6-DMSO, 298 K) δ: 14.8, 23.6, 62.5, 124.7, 142.6, 161.3, 165.2.

5.5.13 Synthesis of $(C_5HMe_2(CO_2Et)_2NH)(B(C_6F_5)_4)$: 8c

To a solution of $(C_5HMe_2(CO_2Et)_2NH)Cl$ **7c** (33 mg, 0.11 mmol) in MeCN (2 mL) was added $LiB(C_6F_5)_4$ (100 mg, 0.11 mmol). The solution was stirred overnight at room temperature and the solvent was removed under vacuum. The residue was washed with CH_2Cl_2 (1 mL) and the solution was filtered to remove solids which were dried over P_2O_5 under vacuum. Yield: 84 mg, (70 %). ^{1}H (400 MHz, CD_2Cl_2, 298 K) δ: 1.47 (t, 6H, $^{3}J_{H\text{-}H}$ = 7 Hz, OCH_2CH_3), 3.15 (s, 6H, CH_3), 4.54 (q, 4H, $^{3}J_{H\text{-}H}$ = 7 Hz, OCH_2CH_3), 9.40 (1H, s, C-*H*), 12.57 (br s, 1H, N-*H*); ^{13}C (100 MHz, CD_2Cl_2, 298 K) δ: 14.1, 21.6, 64.1, 128.1, 136.6 (dm, $^{1}J_{C\text{-}F}$ = 238 Hz, *C*-F), 138.5 (dm, $^{1}J_{C\text{-}F}$ = 242, *C*-F), 148.4 (dm, $^{1}J_{C\text{-}F}$ = 238 Hz, *C*-F), 149.0, 159.1, 161.8; ^{19}F (376 MHz, CD_2Cl_2, 298 K) δ: -133.6 (br m, ortho-C_6F_5), -163.9 (t, $^{3}J_{F\text{-}F}$ = 21 Hz, para-C_6F_5), -167.7 (br m, $^{3}J_{F\text{-}F}$ = 21 Hz, meta-C_6F_5); ^{11}B (160 MHz, CD_2Cl_2, 298 K) δ: -17.0 (br s, B-C4). HRMS (ESI^+) exact mass

calculated for $[M]^+$ required *m/z* 252.1236 ($C_{13}H_{18}NO_4$) found *m/z* 252.1238. HRMS (ESI^-) exact mass calculated for $[M]^-$ 678.9778 ($C_{24}BF_{20}$) found *m/z* 678.9794.

5.5.14 Determination of Kinetic Isotope Effects

Kinetic Measurement

Kinetic measurements were obtained on an Applied Photophysics 5X-17MV stopped flow reaction analyzer with a 10 mm light path and thermostated at 25.0 ± 0.1 ºC. Data was collected by monitoring the decay in the $B(C_6F_5)_3$ fluorescence excitation band at 305 nm.[136] CH_2Cl_2 stock solutions which were 0.037 mM in $B(C_6F_5)_3$, 0.37 mM in **1a** and 0.37 mM ***d*$_2$-1a** were prepared in volumetric flasks by serial dilution in a glovebox. Two gas tight syringe were loaded, one with 2.0 mL of the $B(C_6F_5)_3$ stock solution and the other was loaded with 2.0 mL of either **1a** or ***d*$_2$-1a**. These solutions were injected into the stopped flow instrument; the reactions were monitored over 5 half-lives and fitted to pseudo-first order decays. The k_{obs} values reported were averaged from three runs. The initial concentration of the reagents at the beginning of each run would have been 0.018 mM $B(C_6F_5)_3$ and 0.18 mM **1a** or ***d*$_2$-1a**. The KIE value was obtained from ratio of the k_{obs} values for **1a** and ***d*$_2$-1a**.

Table 5-4. Measured pseudo-first order rate constants

Run	k_{obs}, s^{-1}		KIE
	1a	***d*$_2$-1a**	
1	0.030	0.032	0.92
2	0.031	0.034	0.92
3	0.028	0.029	0.95
Average	0.030	0.032	0.93
STDEV	0.002	0.003	0.09

NMR Competition Experiments

$B(C_6F_5)_3$ (4.5 mg, 0.010 mmol) or $[CPh_3][B(C_6F_5)_4]$ (8.0 mg, 0.010 mmol) was weighed in a glovebox and dissolved in CD_2Cl_2 (0.50 mL) to generate a 0.018 M solution of which 0.10 mL was added to a well-mixed solution of **1a** (5 mg, 0.018 mmol) and ***d*$_2$-1a** (5 mg, 0.018 mmol) in CD_2Cl_2 (0.40 mL). The relative ratio of **2a** and ***d*$_2$-2a** or $HCPh_3$ and $DCPh_3$ was determined by ^1H NMR and was found to be 1:1. A *protio* control was performed to optimize the acquisition parameters, the T_1 relaxation time was determined to be 14.4 sec and the delay was 5 x T_1.

Table 5-5. ^{1}H NMR data from $B(C_6F_5)_3$ KIE competition experiments

Run	**1a**, mmol	***d*$_2$-1a**, mmol	Integration		KIE
			C4py-H (assumed)	CH_3CH_2O/4	
standard	0.040	-	1	1.10	-
1	0.020	0.020	1	2.16	1.03
2	0.020	0.019	1	2.11	1.08
				AVERAGE	1.05
				STDEV	0.04

Table 5-6. ^{1}H NMR data from trityl KIE competition experiments

Run	**1a**, mmol	***d*$_2$-1a**, mmol	Integration		KIE
			C4py-H (assumed)	CH_3CH_2O/4	
standard	0.037	-	1	1.05	-
1	0.021	0.021	1	1.87	1.26
2	0.020	0.021	1	1.92	1.23

Run	**1a**, mmol	***d*$_2$-1a**, mmol	Integration		KIE
			CPh_3-H	Ph-*H*/15	
standard	0.037	-	1.05	1.01	-
1	0.021	0.021	0.97	1.941	1.05
2	0.020	0.021	0.94	2.07	0.96
				AVERAGE	1.12
				STDEV	0.14

5.5.15 Estimation of $B(C_6F_5)_3$ hydride affinity

Calorimetric measurements were obtained on an Omnical SuperCRC Reaction Calorimeter. **1a** (15 mg, 0.06 mmol) was weighed into a 4 dram vial fitted with a stir bar, dissolved in CH_2Cl_2 (1.5 mL) and fitted with a Teflon lined septum cap. A gas tight syringe was loaded with 0.6 mL or 0.4 mL from a CH_2Cl_2 (5 mL) stock solution of $B(C_6F_5)_3$ (50 mg, 0.10 mmol). Both the vial and the syringe were allowed to equilibrate at room temperature in the calorimeter for ~ 30 min prior to injection. Post injection heat flow data points were collected every 3 s and heats of reaction were obtained from the integration of heat flow curves and were corrected for the heats dilution of $B(C_6F_5)_3$ (-7.6 kcal mol^{-1} / -31.8 kJ mol^{-1}) and **1a** (-1.2 kcal mol^{-1} / 5.0 kJ mol^{-1}) as calculated from blanks. The heat of reaction was calculated from average of four measurements and this value was used to estimate hydride affinity.

Table 5-7. Heat flow and $B(C_6F_5)_3$ hydride affinity measurements[a]

Heat Flow, J	ΔH_{rxn},[d] kcal mol^{-1} (kJ mol^{-1})	ΔH_{aff} $B(C_6F_5)_3$,[e] kcal mol^{-1} (kJ mol^{-1})
0.69[b]	-10.8 (45.1)	80.7 (337.3)
0.67[b]	-11.8 (-49.3)	81.7 (341.5)
0.89[c]	-9.5 (-39.7)	79.4 (331.9)
0.98[c]	-10.4 (-43.5)	80.3 (335.7)
Average	-10.6 (-44.3)	80.5 (336.5)
STDEV	1.0 (4.2)	1.0 (4.2)

[a] A stock $[B(C_6F_5)_3]$ = 0.020 M was added via syringe to a 1.5 mL solution of [**1a**] = 0.040 M in the following volumes; [b] 0.40 mL; [c] 0.60 mL; [d] corrected for heats associated with solvation of **1a** and $B(C_6F_5)_3$ under comparable conditions; [e] assumed **1a** ΔH_{het}(**1a**) = 69.9 kcal mol^{-1} / 292.2 kJ mol^{-1} [23]

5.5.16 Reaction of 2a or *d*$_2$-2a with $[CPh_3][B(C_6F_5)_4]$

$B(C_6F_5)_3$ (10 mg, 0.02 mmol) was weighed in a glovebox, dissolved in CD_2Cl_2 (0.2 mL) and added to a solution of **1a** (5 mg, 0.02 mmol) or ***d*$_2$-1a** (5 mg, 0.02 mmol) in CD_2Cl_2 (0.2 mL). The solution was monitored by multinuclear NMR to ensure formation of **2a** or ***d*$_2$-2a**. $[CPh_3][B(C_6F_5)_4]$ (18 mg, 0.02 mmol) was weighed, dissolved in CD_2Cl_2 (0.2 mL) in a glovebox

and added to a solution containing **2a** or ***d*$_2$-2a**. Formation of $HCPh_3$ or $DCPh_3$ was monitored multinuclear NMR (**Figure C-7** in **Appendix C**).

5.5.17 Determination of Binding Constants and Dependence on $B(C_6F_5)_3$

Various CD_2Cl_2 solutions which were 0.02 – 0.2 M in $B(C_6F_5)_3$ and 0.03 M in either **1c, 1f** or **8c** were prepared in a glovebox. The solutions were characterized by multinuclear NMR at room temperature and cooled to -20 ºC. They were allowed to equilibrate at this temperature for at least 10 min prior to acquisition. The binding constants can be calculated by fitting a plot of $\Delta\delta_{C4\text{-}H}$ verses $[B(C_6F_5)_3]$ with a NLSSQ (non-linear least squares) model (**Eq. 5-5**) which applies to both strong and weak binding events and has been described elsewhere in detail.[127-130] In the equation $\Delta\delta$ represented the $(\delta_{obs}- \delta_{sub})$ for the C4-H resonance, δ_b was the chemical shift of the Lewis acid-base adduct, A was the x-intercept and [Sub] was the [**1f**] or [**8c**]. For comparative purposes the K_B between **8c** and $B(C_6F_5)_3$ was also calculated from the mole fraction N_F (**Eq. 5-6**) of free carbonyl from the same ratios of [**2i**]:$[B(C_6F_5)_3]$ entered into the modelling equation.[65]

Table 5-8. Chemical Shifts for the binding study of **1f**[a]

$[B(C_6F_5)_3]$, M	δC4-*H*, ppm	Δ δC4-*H*, ppm
0.000	4.91	0.000
0.017	4.77	0.140
0.038	4.58	0.330
0.053	4.55	0.360
0.086	4.53	0.380
0.146	4.51	0.400

[a] [**1f**] = 0.030 M

Table 5-9. Chemical Shifts for the binding study of **8c**

[$B(C_6F_5)_3$], M	δC4-*H*, ppm	Δ δC4-*H*, ppm
0.000	9.398	0.000
0.019	9.453	0.055
0.030	9.474	0.076
0.058	9.493	0.095
0.107	9.506	0.108
0.182	9.504	0.106

[a] [**8c**] = 0.030 M

$$\Delta\delta = \delta_b\ (1 + K_B\ [B(C_6\ F_5)_3 - A] + K_B[Sub]\ - X)/(2K_B\ )/[Sub]$$

$$X = (1 + 2K_B[Sub] + 2K_B[B(C_6F_5)_3 - A] + K_B^2[Sub]^2 - 2K_B^2[Sub][B(C_6F_5)_3 - A] + K_B^2[B(C_6F_5)_3 - A]^2)^{0.5}$$

Eq. 5-5

$$N_F = (\delta_{obs} - \delta_b)/(\delta_{sub} - \delta_b)$$

Eq. 5-6

Table 5-10. Fitted NLLSQ equation (**Eq. 5-5**) parameters for the **1f** and **8c** binding study

Parameter	**1f**	Error	**5c**	Error
[Sub], M	0.030	-	0.030	-
K_B, M^{-1}	525	169	190	77
δ_b, ppm	0.400	0.008	0.112	0.003
A, M	0.0054	0.0008	-0.00084	0.002

Table 5-11. K_B and N_F calculated (**Eq. 5-6**) for **5c** at various $B(C_6F_5)_3$ concentrations[a]

$[B(C_6F_5)_3]$, M	δ_{obs}- δ_b[b], ppm	N_F	K_B, M^{-1}
0.000	-0.112	1	-
0.019	-0.057	0.055	230
0.030	-0.036	0.076	214
0.058	-0.017	0.095	176
0.107	-0.0036	0.108	384
0.182	-0.0056	0.106	123
		Average	226
		STDEV	98

[a] [**5c**] = 0.030 M; [b] δ_b = XX ppm

5.5.18 van't Hoff plots

In a typical experiment $B(C_6F_5)_3$ (40 mg, 0.07 mmol) was weighed in a glovebox, dissolved in CD_2Cl_2 (0.25 mL) and was layered onto a frozen suspension of either **1a** or **1c** (5 - 6 mg, 0.02 mmol) in CD_2Cl_2 (0.25 mL) for a final reaction volume of 0.50 mL. The reaction mixture was allowed to warm to -20 ºC in the NMR instrument and was monitored over 30 min to ensure completion. The tube was warmed to -10 ºC and allowed to equilibrate for 10 min and monitored by NMR and in this fashion the reaction mixture was cooled to -30 ºC in 5 ºC increments. Thermodynamic parameters for the equilibria were calculated from van't Hoff plots assuming (**Eq. 5-4**) described the equilibrium condition.

Table 5-12. Parameters for the **3c** – **2c** equilibrium extracted from van't Hoff plots at 253 K[a]

Run	slope	intercept	ΔH, kcal mol^{-1} (kJ mol^{-1})	ΔS, cal mol^{-1} K^{-1} (J mol^{-1} K^{-1})	ΔG, kcal mol^{-1} (kJ mol^{-1})	Keq, M
1	3316	8.7	6.6 (27.6)	17.0 (71.1)	2.3 (9.6)	0.0126
2	3536	9.5	7.0 (29.3)	18.4 (76.9)	2.4 (10.0)	0.0108
Average	3426	9.1	6.8 (28.4)	17.7 (74.0)	2.3 (9.6)	0.0117
STDEV	155	0.6	0.3 (1.2)	1.0 (4.2)	0.1 (0.4)	0.0013

[a] R^2 = 0.997 or greater for the linear regressions

Table 5-13. Parameters for the **3a** – **2a** equilibrium extracted from van't Hoff plots at 253 K[a]

Run	slope	intercept	ΔH, kcal mol^{-1} (kJ mol^{-1})	ΔS, cal mol^{-1} K^{-1} (J mol^{-1} K^{-1})	ΔG, kcal mol^{-1} (kJ mol^{-1})	Keq, M
1	4731	16	9.4 (39.3)	31.2 (130.4)	1.5 (6.3)	0.0694
2	4822	16.2	9.6 (40.1)	31.6 (132.1)	1.6 (6.7)	0.0610
Average	4776	16.1	9.5 (39.7)	31.4 (131.3)	1.5 (6.3)	0.0652
STDEV	64	0.1	0.1 (0.4)	0.3 (1.2)	0.05 (0.2)	0.0060

[a] R^2 = 0.997 or greater for the linear regressions

5.5.19 X-Ray Data Collection and Reduction

X-Ray quality crystals were grown at -20 °C from Et_2O for **2a** and DCE layered with pentane for **3e, 3f** and **6c**. Crystals were mounted on a glass fiber with grease and cooled to -93 °C in a stream of nitrogen gas controlled with Cryostream Controller 700. Data collection was performed on a Bruker SMART APEX II X-ray diffractometer. Data was processed using the Bruker AXS Crystal Structure Analysis Package.

5.5.20 Structure Solution and Refinement

Neutral atom scattering factors were taken from Cromer and Waber.[137] The heavy atom positions were determined using direct methods and all other non-hydrogen atoms were refined anisotropically. The refinements were carried out by using full-matrix least squares techniques on F, minimizing the function $\omega(F_o-F_c)^2$. In the final cycles of each refinement, all non-hydrogen atoms were assigned anisotropic temperature factors in the absence of disorder or insufficient data. In the latter cases atoms were treated isotropically. The B-H hydrogen atom was located from the difference Fourier maps, and all of the other H atoms were placed in geometrically calculated positions, with C-H = 0.95 (aromatic), 0.99 (CH_2) and 0.98 Å (CH_3), and refined as riding atoms. The H-atom contributions were calculated, but not refined. The locations of the largest peaks in the final difference Fourier map calculation as well as the magnitude of the residual electron densities in each case were of no chemical significance.

5.6 References

(1) Stout, D. M.; Meyers, A. I. *Chem. Rev.* **1982**, *82*, 223-243.

(2) Hantzsch, A. *Justus Liebigs Ann. Chem.* **1882**, *215*, 1-82.

(3) Triggle, D. J. *Cell. Mol. Neurobiol.* **2003**, *23*, 293-303.

(4) Sirisha, K.; Bikshapathi, D.; Achaiah, G.; Reddy, V. M. *Eur. J. Med. Chem.* **2011**, *46*, 1564-1571.

(5) Mithlesh; Pawan, K. P.; Kant, R.; Shukla, S.; Ojha, K. *Cent. Eur. J. Chem.* **2010**, *8*, 163-173.

(6) Zarrin, A.; Mehdipour, A. R.; Miri, R. *Chem. Biol. Drug Des.* **2010**, *76*, 369-381.

(7) Triggle, D. J. *Curr. Pharm. Des.* **2006**, *12*, 443-457.

(8) Ouellet, S. G.; Walji, A. M.; Macmillan, D. W. C. *Acc. Chem. Res.* **2007**, *40*, 1327-1339.

(9) Quirion, J. -.; Leclerc, E.; Jubault, P. *Science of Synthesis* **2006**, *33*, 601-628.

(10) Christen, D. P. *Art of Drug Synth.* **2007**, 159-167.

(11) Kuthan, J.; Kurfurst, A. *Ind. Eng. Chem. Prod. Res. Dev.* **1982**, *21*, 191-261.

(12) Eisner, U.; Kuthan, J. *Chem. Rev.* **1972**, *72*, 1-42.

(13) Sausin, A. É.; Lusis, V. K.; Dubur, G. Y.; Beilis, Y. I. *Chem. Heterocycl. Compd.* **1978**, *14*, 1226-1231.

(14) Singh, H.; Singh, K. *Tetrahedron* **1989**, *45*, 3967-3974.

(15) Saini, A.; Kumar, S.; Sandhu, J. S. *J. Sci. Ind. Res.* **2008**, *67*, 95-111.

(16) Pfister, J. R. *Synthesis* **1990**, 689-690.

(17) Lee, K. H.; Ko, K. Y. *Bull. Korean Chem. Soc.* **2002**, *23*, 1505-1506.

(18) Varma, R.,S.; Kumar, D. *J. Chem. Soc. Perkin Trans. 1* **1999**, 1755-1758.

(19) Engelmenn, F. *Justus Liebigs Ann. Chem.* **1885**, *231*, 37-71.

(20) Rueping, M.; Sugiono, E.; Schoepke, F. R. *Synlett* **2010**, 852-865.

(21) Connon, S. J. *Org. Biomol. Chem.* **2007**, *5*, 3407-3417.

(22) Richter, D.; Mayr, H. *Angew. Chem. Int. Ed.* **2009**, *48*, 1958-1961.

(23) Zhu, X.; Li, H.; Li, Q.; Ai, T.; Lu, J.; Yang, Y.; Cheng, J. *Chem. Eur. J.* **2003**, *9*, 871-880.

(24) Rueping, M.; Antonchick, A. *Angew. Chem. Int. Ed.* **2007**, *46*, 4562-4565.

(25) Rueping, M.; Antonchick, A. P.; Theissmann, T. *Angew. Chem. Int. Ed.* **2006**, *45*, 3683-3686.

(26) Zhu, X.; Zou, H.; Yuan, P.; Liu, Y.; Cao, L.; Cheng, J. *J. Chem. Soc. Perkin Trans. 2* **2000**, 1857-1861.

(27) Zhang, Z.; Schreiner, P. R. *Synthesis* **2007**, 2559-2564.

(28) Nakamura, K.; Fujii, M.; Oka, S.; Ohno, A. *Chem. Lett.* **1985**, 523-526.

(29) Singh, S.; Sharma, V. K.; Gill, S.; Sahota, R. I. K. *J. Chem. Soc. Perkin Trans. 1* **1985**, 437-440.

(30) Pandit, U. K.; Gase, R. A.; Cabre, F. R. M.; de Nie-Sarink, M. J. *J. Chem. Soc. Chem. Commun.* **1975**, 211-212.

(31) de Nie-Sarink, M. J.; Pandit, U. K. *Tetrahedron Lett.* **1979**, *20*, 2449-2452.

(32) Jouin, P.; Troostwijk, C. B.; Kellogg, R. M. *J. Am. Chem. Soc.* **1981**, *103*, 2091-2093.

(33) Inoue, Y.; Inoue, Y.; Imaizumi, S.; Ito, H.; Shinya, T.; Hashimoto, H.; Miyano, S. *Bull. Chem. Soc. Jpn.* **1988**, *61*, 3020-3022.

(34) Norcross, B. E.; Klinedinst, P. E.; Westheimer, F. H. *J. Am. Chem. Soc.* **1962**, *84*, 797-802.

(35) Zhu, X.; Wang, H.; Wang, J.; Liu, Y. *J. Org. Chem.* **2001**, *66*, 344-347.

(36) Yang, J. W.; Hechavarria, F. M. T.; Vignola, N.; List, B. *Angew. Chem. Int. Ed.* **2005**, *44*, 108-110.

(37) Ouellet, S. G.; Tuttle, J. B.; MacMillan, D. W. C. *J. Am. Chem. Soc.* **2005**, *127*, 32-33.

(38) Menche, D.; Hassfeld, J.; Li, J.; Menche, G.; Ritter, A.; Rudolph, S. *Org. Lett.* **2006**, *8*, 741-744.

(39) Rueping, M.; Sugiono, E.; Azap, C.; Theissmann, T.; Bolte, M. *Org. Lett.* **2005**, *7*, 3781-3783.

(40) Mayer, S.; List, B. *Angew. Chem. Int. Ed.* **2006**, *45*, 4193-4195.

(41) Zhang, B.; Zhu, X.; Lu, J.; He, J.; Wang, P. G.; Cheng, J. *J. Org. Chem.* **2003**, *68*, 3295-3298.

(42) Vitry, C.; Vasse, J.; Dupas, G.; Levacher, V.; Quéguiner, G.; Bourguignon, J. *Tetrahedron* **2001**, *57*, 3087-3098.

(43) Chenault, H.; Whitesides, G. *Appl. Biochem. Biotechnol.* **1987**, *14*, 147-197.

(44) Abril, O.; Whitesides, G. M. *J. Am. Chem. Soc.* **1982**, *104*, 1552-1554.

(45) Lo, H. C.; Fish, R. H. *Angew. Chem. Int. Ed.* **2002**, *41*, 478-481.

(46) Wagenknecht, P. S.; Penney, J. M.; Hembre, R. T. *Organometallics* **2003**, *22*, 1180-1182.

(47) Zhu, X.; Zhang, M.; Yu, A.; Wang, C.; Cheng, J. *J. Am. Chem. Soc.* **2008**, *130*, 2501-2516.

(48) Powell, M. F.; Bruice, T. C. *J. Am. Chem. Soc.* **1983**, *105*, 7139-7149.

(49) Cheng, J.; Lu, Y. *J. Phys. Org. Chem.* **1997**, *10*, 577-584.

(50) Marcus, R. A. *Rev. Mod. Phys.* **1993**, *65*, 599.

(51) Massey, A. G.; Park, A. J.; Stone, F. G. A. *Proc. Chem. Soc.* **1963**, 212-213.

(52) Massey, A. G.; Park, A. J. *J. Organomet. Chem.* **1964**, *2*, 245-250.

(53) Döring, S.; Erker, G.; Fröhlich, R.; Meyer, O.; Bergander, K. *Organometallics* **1998**, *17*, 2183-2187.

(54) Marks, T. J. *Acc. Chem. Res.* **1992**, *25*, 57-65.

(55) Yang, X.; Stern, C. L.; Marks, T. J. *J. Am. Chem. Soc.* **1994**, *116*, 10015-10031.

(56) Erker, G. *Dalton Trans.* **2005**, 1883-1890.

(57) Piers, W. E. *Adv. Organomet. Chem.* **2005**, *52*, 1-76.

(58) Rubin, M.; Schwier, T.; Gevorgyan, V. *J. Org. Chem.* **2002**, *67*, 1936-1940.

(59) Blackwell, J. M.; Sonmor, E. R.; Scoccitti, T.; Piers, W. E. *Org. Lett.* **2000**, *2*, 3921-3923.

(60) Blackwell, J. M.; Foster, K. L.; Beck, V. H.; Piers, W. E. *J. Org. Chem.* **1999**, *64*, 4887-4892.

(61) Blackwell, J. M.; Morrison, D. J.; Piers, W. E. *Tetrahedron* **2002**, *58*, 8247-8254.

(62) Parks, D. J.; Piers, W. E. *J. Am. Chem. Soc.* **1996**, *118*, 9440-9441.

(63) Parks, D. J.; Blackwell, J. M.; Piers, W. E. *J. Org. Chem.* **2000**, *65*, 3090-3098.

(64) Berkefeld, A.; Piers, W. E.; Parvez, M. *J. Am. Chem. Soc.* **2010**, *132*, 10660-10661.

(65) Parks, D. J.; Piers, W. E.; Parvez, M.; Atencio, R.; Zaworotko, M. J. *Organometallics* **1998**, *17*, 1369-1377.

(66) Welch, G. C.; Stephan, D. W. *J. Am. Chem. Soc.* **2007**, *129*, 1880-1881.

(67) Welch, G. C.; Juan, R. R. S.; Masuda, J. D.; Stephan, D. W. *Science* **2006**, *314*, 1124-1126.

(68) Stephan, D. W. *Dalton Trans.* **2009**, 3129-3136.

(69) Stephan, D. W. *Org. Biomol. Chem.* **2008**, *6*, 1535-1539.

(70) Stephan, D.; Erker, G. *Angew. Chem. Int. Ed.* **2010**, *49*, 46-76.

(71) Brown, H. C.; Schlesinger, H. I.; Cardon, S. Z. *J. Am. Chem. Soc.* **1942**, *64*, 325-329.

(72) Damico, R.; Broaddus, C. D. *J. Org. Chem.* **1966**, *31*, 1607-1612.

(73) Chase, P. A.; Gille, A. L.; Gilbert, T. M.; Stephan, D. W. *Dalton Trans.* **2009**, 7179-7188.

(74) Holschumacher, D.; Bannenberg, T.; Hrib, C.; Jones, P.; Tamm, M. *Angew. Chem. Int. Ed.* **2008**, *47*, 7428-7432.

(75) Chase, P. A.; Stephan, D. W. *Angew. Chem. Int. Ed.* **2008**, *47*, 7433-7437.

(76) Sumerin, V.; Schulz, F.; Nieger, M.; Leskelä, M.; Repo, T.; Rieger, B. *Angew. Chem. Int. Ed.* **2008**, *47*, 6001-6003.

(77) Jiang, C.; Blacque, O.; Fox, T.; Berke, H. *Organometallics* **2011**, *30*, 2117-2124.

(78) Geier, S. J.; Stephan, D. W. *J. Am. Chem. Soc.* **2009**, *131*, 3476-3477.

(79) Geier, S. J.; Gille, A. L.; Gilbert, T. M.; Stephan, D. W. *Inorg. Chem.* **2009**, *48*, 10466-10474.

(80) Chase, P.; Welch, G.; Jurca, T.; Stephan, D. *Angew. Chem. Int. Ed.* **2007**, *46*, 8050-8053.

(81) Chase, P. A.; Jurca, T.; Stephan, D. W. *Chem. Commun.* **2008**, 1701-1703.

(82) Chen, D.; Klankermayer, J. *Chem. Commun.* **2008**, 2130-2131.

(83) Stephan, D. W.; Greenberg, S.; Graham, T. W.; Chase, P.; Hastie, J. J.; Geier, S. J.; Farrell, J. M.; Brown, C. C.; Heiden, Z. M.; Welch, G. C.; Ullrich, M. *Inorg. Chem.* **2011**, null-null.

(84) Geier, S. J.; Chase, P. A.; Stephan, D. W. *Chem. Commun.* **2010**, *46*, 4884-4886.

(85) Wang, H.; Frohlich, R.; Kehr, G.; Erker, G. *Chem. Commun.* **2008**, 5966-5968.

(86) Dureen, M. A.; Lough, A.; Gilbert, T. M.; Stephan, D. W. *Chem. Commun.* **2008**, 4303-4305.

(87) Ullrich, M.; Seto, K. S.; Lough, A. J.; Stephan, D. W. *Chem. Commun.* **2009**, 2335-2337.

(88) McCahill, J. .; Welch, G.; Stephan, D. *Angew. Chem. Int. Ed.* **2007**, *46*, 4968-4971.

(89) Focante, F.; Mercandelli, P.; Sironi, A.; Resconi, L. *Coord. Chem. Rev.* **2006**, *250*, 170-188.

(90) Di Saverio, A.; Focante, F.; Camurati, I.; Resconi, L.; Beringhelli, T.; D'Alfonso, G.; Donghi, D.; Maggioni, D.; Mercandelli, P.; Sironi, A. *Inorg. Chem.* **2005**, *44*, 5030-5041.

(91) Millot, N.; Santini, C. C.; Fenet, B.; Basset, J. M. *Eur. J. Inorg. Chem.* **2002**, *2002*, 3328-3335.

(92) Mohring, R. M.; Wu, Y. *AIP Conf. Proc.* **2003**, *671*, 90-100.

(93) Ramachandran, P. V.; Gagare, P. D. *Inorg. Chem.* **2007**, *46*, 7810-7817.

(94) Davis, B. L.; Dixon, D. A.; Garner, E. B.; Gordon, J. C.; Matus, M. H.; Scott, B.; Stephens, F. H. *Angew. Chem. Int. Ed.* **2009**, *48*, 6812-6816.

(95) Sutton, A. D.; Davis, B. L.; Bhattacharyya, K. X.; Ellis, B. D.; Gordon, J. C.; Power, P. P. *Chem. Commun.* **2010**, *46*, 148-149.

(96) Sutton, A. D.; Burrell, A. K.; Dixon, D. A.; Garner, E. B.; Gordon, J. C.; Nakagawa, T.; Ott, K. C.; Robinson, J. P.; Vasiliu, M. *Science* **2011**, *331*, 1426-1429.

(97) Mock, M. T.; Potter, R. G.; Camaioni, D. M.; Li, J.; Dougherty, W. G.; Kassel, W. S.; Twamley, B.; DuBois, D. L. *J. Am. Chem. Soc.* **2009**, *131*, 14454-14465.

(98) Shaw, A. P.; Ryland, B. L.; Franklin, M. J.; Norton, J. R.; Chen, J. Y. -.; Hall, M. L. *J. Org. Chem.* **2008**, *73*, 9668-9674.

(99) Osakada, K. *Angew. Chem. Int. Ed.* **2011**, *50*, 3845-3846.

(100) Cook, N. C.; Lyons, J. E. *J. Am. Chem. Soc.* **1966**, *88*, 3396-403.

(101) Cook, N. C.; Lyons, J. E. *J. Am. Chem. Soc.* **1965**, *87*, 3283-4.

(102) Ott, K.; Linehan, S.; Lipiecki, F.; Aradahl, C. L. *Down Select Report of Chemical Hydrogen Storage Materials, Catalysts, and Spent Fuel Regeneration Processes* [https://www1.eere.energy.gov/hydrogenandfuelcells/pdfs/chs_coe_down_select.pdf] Retrieved: 05/30/2011.

(103) Van Bergen, T. J.; Mulder, T.; Kellogg, R. M. *J. Am. Chem. Soc.* **1976**, *98*, 1960-1962.

(104) Webb, J.; Laberge, V.; Geier, S.; Stephan, D.; Crudden, C. *Chem. Eur. J.* **2010**, *16*, 4895-4902.

(105) Mitu, S.; Baird, M. C. *Organometallics* **2006**, *25*, 4888-4896.

(106) Biellmann, J. F.; Callot, H. J.; Pilgrim, W. R. *Tetrahedron* **1972**, *28*, 5911-5921.

(107) Kano, K.; Matsuo, T. *Tetrahedron Lett.* **1975**, *16*, 1389-1392.

(108) Marcus, Y. *Chem. Soc. Rev.* **1993**, *22*, 409-416.

(109) Hoye, T. R.; Eklov, B. M.; Ryba, T. D.; Voloshin, M.; Yao, L. J. *Org. Lett.* **2004**, *6*, 953-956.

(110) Zhao, B.; Zhu, X.; Lu, Y.; Xia, C.; Cheng, J. *Tetrahedron Lett.* **2000**, *41*, 257-260.

(111) Cheng, J.; Lu, Y.; Zhu, X.; Sun, Y.; Bi, F.; He, J. *J. Org. Chem.* **2000**, *65*, 3853-3857.

(112) López-Alarcón, C.; Núñez-Vergara, L. J.; Squella, J. A. *Electrochim. Acta* **2003**, *48*, 2505-2516.

(113) Cummings, S. A.; Iimura, M.; Harlan, C. J.; Kwaan, R. J.; Trieu, I. V.; Norton, J. R.; Bridgewater, B. M.; Jäkle, F.; Sundararaman, A.; Tilset, M. *Organometallics* **2006**, *25*, 1565-1568.

(114) Xu, H.; Dai, D.; Liu, Y.; Li, J.; Luo, S.; Wu, Y. *Tetrahedron Lett.* **2005**, *46*, 5739-5742.

(115) Fang, X.; Xu, H.; Jiang, H.; Liu, Y.; Fu, Y.; Wu, Y. *Tetrahedron Lett.* **2009**, *50*, 312-315.

(116) Walling, C. *J. Am. Chem. Soc.* **1980**, *102*, 6854-6855.

(117) Harlan, C. J.; Hascall, T.; Fujita, E.; Norton, J. R. *J. Am. Chem. Soc.* **1999**, *121*, 7274-7275.

(118) Beddows, C. J.; Burrows, A. D.; Connelly, N. G.; Green, M.; Lynam, J. M.; Paget, T. J. *Organometallics* **2001**, *20*, 231-233.

(119) Kwaan, R. J.; Harlan, C. J.; Norton, J. R. *Organometallics* **2001**, *20*, 3818-3820.

(120) Grant, D. J.; Dixon, D. A.; Camaioni, D.; Potter, R. G.; Christe, K. O. *Inorg. Chem.* **2009**, *48*, 8811-8821.

(121) Timoshkin, A. Y.; Frenking, G. *Organometallics* **2008**, *27*, 371-380.

(122) Vianello, R.; Maksić, Z. B. *Inorg. Chem.* **2005**, *44*, 1095-1102.

(123) Zhu, X.; Yang, Y.; Zhang, M.; Cheng, J. *J. Am. Chem. Soc.* **2004**, *126*, 6833-6833.

(124) Zhang, X.; Bruno, J. W.; Enyinnaya, E. *J. Org. Chem.* **1998**, *63*, 4671-4678.

(125) Horton, A. D.; de With, J. *Organometallics* **1997**, *16*, 5424-5436.

(126) Blackwell, J. M.; Piers, W. E.; Parvez, M. *Org. Lett.* **2000**, *2*, 695-698.

(127) Neverov, A. A.; Lu, Z.; Maxwell, C. I.; Mohamed, M. F.; White, C. J.; Tsang, J. S. W.; Brown, R. S. *J. Am. Chem. Soc.* **2006**, *128*, 16398-16405.

(128) Lu, Z.; Liu, C. T.; Neverov, A. A.; Brown, R. S. *J. Am. Chem. Soc.* **2007**, *129*, 11642-11652.

(129) Bunn, S. E.; Liu, C. T.; Lu, Z.; Neverov, A. A.; Brown, R. S. *J. Am. Chem. Soc.* **2007**, *129*, 16238-16248.

(130) Edwards, D. R.; Liu, C. T.; Garrett, G. E.; Neverov, A. A.; Brown, R. S. *J. Am. Chem. Soc.* **2009**, *131*, 13738-13748.

(131) Brignell, P. J.; Eisner, U.; Farrell, P. G. *J. Chem. Soc. B* **1966**, 1083-1089.

(132) Xia, J.; Wang, G. *Synthesis* **2005**, *2005*, 2379-2383.

(133) Cheung, L. L. W.; Styler, S. A.; Dicks, A. P. *J. Chem. Educ.* **2010**, *87*, 628-630.

(134) Sridhar, R.; Perumal, P. T. *Tetrahedron* **2005**, *61*, 2465-2470.

(135) Nakamichi, N.; Kawashita, Y.; Hayashi, M. *Synthesis* **2004**, 1015-1020.

(136) Chojnowski, J.; Rubinsztajn, S.; Cella, J. A.; Fortuniak, W.; Cypryk, M.; Kurjata, J.; Kaźmierski, K. *Organometallics* **2005**, *24*, 6077-6084.

(137) Cromer, D. T.; Waber, J. T. In *International Tables for X-ray. Crystallography;* International Tables for X-ray Crystallography; Kynoch Press: Burningham, UK, 1974; Vol. 4, pp Table 2.2 A.

Chapter 6

Hydride Transfer from 2,3-Dihydroimidazoles to Boron Lewis Acids

6.1 Introduction

Our previously discussed work on Hantzsch esters illustrated that hydride transfer to boron from organic molecules can occur in high yield, but in some circumstances the pendant functionality results in unwanted reactivity. As a result, our focus shifted to probing the capacity of less functionalized organic molecules to transfer hydride to boron. Depicted in **Scheme 6-1** are general structural motifs for organic molecules that are as strong as, if not stronger hydride donors than Hantzsch esters or dihydronicotinamides.[1] The strongest hydride donors of this series are 2,3-dihydroimidazoles and tricyclic orthoformamides, and it was for this reason they were selected to be screened for reaction with boron Lewis acids. Key to their reactivity is the hyperconjugation between the N lone pair(s) and the $\sigma^*_{C\text{-}H}$ orbital of an adjacent C-H bond, which has been shown to be particularly effective at activating that bond toward hydride transfer.[1-4] This electronic effect operates in alkyl amines, an example of which was discussed in the previous chapter, recall that hydride transfer from bulky amines was observed to take place to trityl and $B(C_6F_5)_3$.[5]

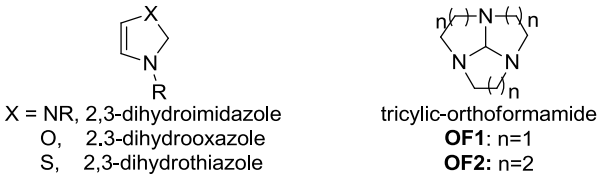

Scheme 6-1. General structures of N-heterocyclic organic hydride donors

6.1.1 2,3-Dihydroimidazoles

The first research into 2,3-dihydroimidazoles as hydride donors appeared in the 1960's.[6, 7] Nonetheless, the literature on this class of donor is less extensive than that of their Hantzsch ester counterparts. Hydride transfer from 2,3-dihydroimidazoles is favored because of the gain of aromaticity. This is also true for 2,3-dihydrooxazoles and 2,3-dihydrothiazoles (**Scheme 6-1**) which are related architectures, but experimentally they are weaker donors because hyperconjugation of the (X = O, S) lone pair to the $\sigma^*_{C\text{-}H}$ orbital is inferior to donation from an N lone pair.[1] 2,3-Dihydroimidazoles are stronger donors than Hantzsch esters as measured by their C-H heterolytic bond dissociation energy (ΔH_{het}). For *N,N*-dimethyl-dihydrobenzimidazoles ΔH_{het} varies from 49.5 – 62 kcal mol^{-1} / 205 – 259 kJ mol^{-1} (ΔH_{het} = 49.5 kcal mol^{-1} / 210 kJ mol^{-1} for R_1 and R_2 = H) depending on the substitution pattern (**Scheme 6-2**), compared to Hantzsch ester which has a ΔH_{het} of 63 kcal mol^{-1} / 263 kJ mol^{-1}.[1] It was found that substitution at position R_1 with electron withdrawing groups decreased the donating ability, with the maximum effect observed with R_1 = CF_3 (ΔH_{het} = 63 kcal mol^{-1} / 263 kJ mol^{-1}) while electron donating groups minimally increased the donating ability. Substitution at R_2 had the effect of reducing the donating ability of the molecule regardless of the electronics of the aromatic ring employed (ΔH_{het} = 50.6 – 56.7 kcal mol^{-1} / 211 – 237 kJ mol^{-1} for R = *p*-C_6H_5-NMe_2 to *p*-C_6H_5-NO_2).

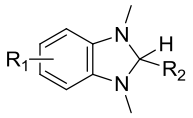

Scheme 6-2. General structure of N,N-dimethyl-dihydrobenzimidazole

2,3-Dihydroimizdazoles are generally synthesized by one of three routes. If the corresponding imidazolium salt is available it can be reduced to a 2,3-dihydroimidazole with a

strong reducing agent such as $NaBH_4$,[1, 8] $NaBH(OMe)_3$[9] or formate.[10] The reduction route is typically employed when R_2 = H (**Scheme 6-2**). When R_2 is an aryl group, the typical approach is condensation of the diamine with the corresponding aldehyde.[1] Alkyl substitution at R_2 is achieved by nucleophilic substitution of the corresponding imidazolium salt with a Grignard reagent.[11] It should be noted that 2,3-dihydroimidazoles are known to undergo ring opening reactions in water and that these processes are accelerated by acid and base.[7, 11]

The main application of 2,3-dihydroimidazoles in the literature has been to study the mechanisms of hydride transfer.[1, 12-14] They are particularly amenable to such studies due to their ease of synthesis and functionalization. As with Hantzsch esters, concerted hydride transfer is expected when 2,3-dihydroimidazoles reduce organic electrophiles.[13] Stepwise hydride transfer is also known because these hydrides are good single electron reducing agents.[1] In organic synthesis 2,3-dihydroimidazoles have been applied as reducing agents for dehalogenation of α-halocarbonyl compounds,[15] the conversion of α-nitrosulfones to nitroalkanes,[16] and the reduction of electron deficient alkenes to alkanes (**Scheme 6-3**).[17]

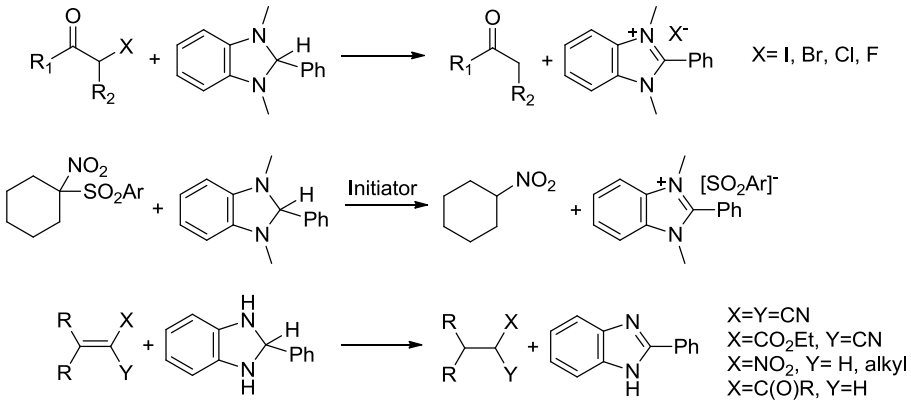

Scheme 6-3. Selected synthetic applications of 2,3-dihydroimidazoles

A particularly interesting application of 2,3-dihydrobenzamidazoles was as chemical hydrogen storage materials. The concept was proposed and explored by Wuest,[2, 3, 18, 19] who reported the synthesis of dihydroimidazoles which had intramolecular acidic functional groups in close proximity to the hydridic C-H bond. Unfortunately, upon heating no evidence of dehydrogenation could be observed, instead disproportionation reactions occurred leading to the conclusion that there was a high intrinsic barrier to hydrogen release. Thorn[8] showed subsequently (**Scheme 6-4**) that hydrogen release from these organic molecules can proceed at room temperature on addition of a Pd catalyst. Hydrogen release can also occur in an intermolecular fashion on treatment of *N*,*N*-dimethyl dihydrobenzimidazole with acid. These systems represent one of the few examples of an exothermic (ΔH_{rxn} = -10 kcal mol^{-1} / -42 kJ mol^{-1}) hydrogen release from organic molecules. The chief drawback to the wide spread application of this approach to hydrogen storage is the low gravimetric density (1 wt% H_2) of the organic scaffold, although it may be possible to improve this value through substrate design.[8]

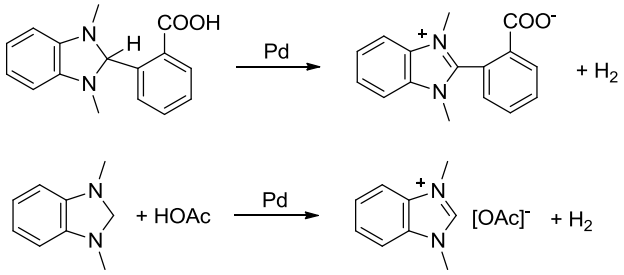

Scheme 6-4. Examples of intra- and inter- molecular H_2 evolution from 2,3-dihydroimidazoles

6.1.2 Tricyclic Orthoformamides

Tricylic orthoformamides are macrocyclic amines with bridgehead nitrogens and the structure of orthoformaides **OF1** (n=1) and **OF2** (n=2) are depicted in **Scheme 6-1**. The hydride

donating ability of these compounds has not been measured experimentally although low level gas phase calculations predict the ΔH_{het} for the central methine C-H of **OF2** is 40 kcal mol^{-1} / 167 kJ mol^{-1}. This value can be compared the ΔH_{het} of *N*,*N*-dimethyl-dihydroimidazole which was calculated to be 47 kcal mol^{-1} / 196 kJ mol^{-1} at the same level of theory.[3] It is then inferred that orthoformamides can be similarly hydridic, if not slightly more hydridic than dihydroimidazoles.

The same set of gas phase calculations predicted that hydrogen evolution from the orthoformamide **OF2** (**Scheme 6-1**) on treatment with weak acid would be more exothermic than the reaction of acid with dihydroimidazoles, which was discussed above. The trend established in these calculations was consistent with and borne out by experiment. Orthoformamide **OF2**, and others based on the same core structure, in contrast to the dihydroimidazole systems (**Scheme 6-4**), are converted to the corresponding guanidinium salts on treatment with acid and heat without the need of a catalyst (**Scheme 6-5**). This reaction represents a rare example of non-catalyzed hydrogen evolution from an organic compound. Wuest[20, 21] studied these systems in detail and concluded that the transition state for hydrogen formation is likely linear.

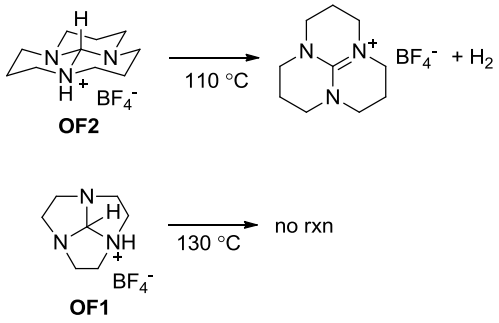

Scheme 6-5. Thermolysis of protonated orthoformamides **OF1** and **OF2**

The relative orientation of the N lone pairs and the central C-H methine of tricyclic-orthoformamides helps to determine their relative hydride donating ability. Notice in **Scheme 6-5**

that while protonated orthoformamide **OF2** dehydrogenated on heating, the related orthoformamide **OF1** does not release hydrogen gas. Early on, there was much research performed to ascertain the conformation of ring junctures of tricyclic orthoformamides.[22-24] Compounds **OF1** and **OF2**, as well as derivatives thereof, were characterized spectroscopically in solution and in the solid state. Both **OF1** and **OF2** are symmetrical and there is little evidence of conformational equilibria, i.e. ring inversion, on cooling to -100 ºC. These structural studies concluded that the relationship between N lone pairs and the methine C-H is syn-periplanar for orthoformamide **OF1** and antiperiplanar for **OF2** (**Scheme 6-6**). There is also ^{1}H NMR evidence[22-24] of hyperconjugation between the N lone pairs and the $\sigma^{*}_{C\text{-}H}$ orbital of the central methine of **OF2**. The ^{1}H NMR resonance (δ = 2.25 ppm in $CDCl_3$) for the methine proton is shifted significantly up field due to electron donation from the lone pairs. When compared with the same resonance in **OF1**, (δ = 5.03 ppm in $CDCl_3$), it is clear that the chemical shift of the methine is much more similar to what would be expected based on inductive arguments in the absence of any similar hyperconjugation effects.

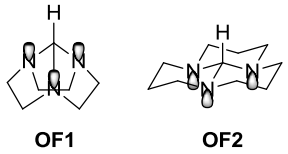

OF1 **OF2**

Scheme 6-6. A depiction of the relative orientation of the N-lone pair to the methine C-H for orthoformamides **OF1** and **OF2**

The relative orientations of the N lone pair and the methine C-H have important consequence for the hydride donating ability of the ortho-formamide. The anti-periplanar arrangement in **OF2** makes it more apt than **OF1** to donate hydride and this can be observed experimentally (**Scheme 6-5** and **Scheme 6-7**). As mentioned earlier, protonated derivatives of

OF2 dehydrogenate upon heating, while **OF1** is unreactive. Also illustrative is the reduction of $Hg(OAc)_2$ to Hg metal with **OF2**, while **OF1** forms a Lewis acid-base adduct. It is however, possible for **OF1** to act as a hydride donor as it reacts with $[CPh_3]^+$ cleanly to form $HCPh_3$ and the corresponding guanidinium salt. The same reaction of **OF2** also forms $[CPh_3]^+$ although hydride is abstracted from various positions about the rings.[4]

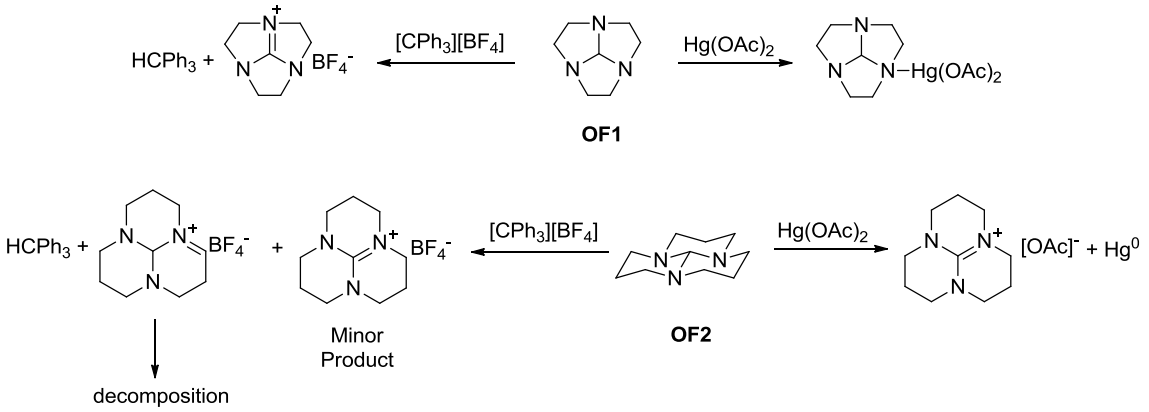

Scheme 6-7. Reactions of orthoformamides **OF1** and **OF2** with trityl cation and $Hg(OAc)_2$

The current strategy to synthesize tricyclic orthoformamides is by reaction of a guanidine base with a dihalo-alkane (**Scheme 6-8**). The guanidinium salt is isolated and reduced with either $NaBH_4$ or $LiAlH_4$.[25, 26] This approach is preferable to the original synthetic strategy which involved a low yielding synthesis of the corresponding macrocyclic triamine that was converted to the orthoformamide through reaction with an orthoformate. It is ironic that currently the main application of tricyclic orthoformamides in the literature is as precursors to macrocyclic amines, valued ligands for monometallic and bimetallic catalysts (**Scheme 6-9**).[26-28]

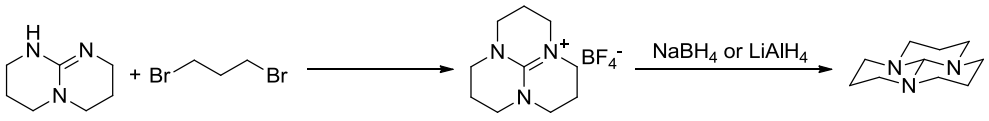

Scheme 6-8. Synthesis of tricyclic orthoformamide **OF2**

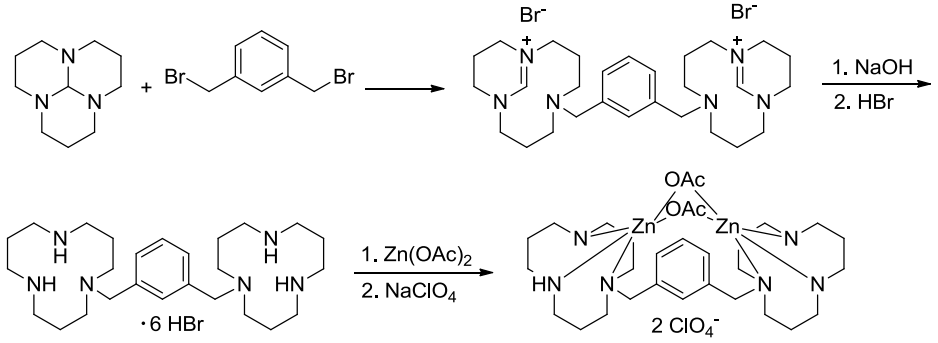

Scheme 6-9. Synthesis of a bimetallic catalyst for ester hydrolysis

The potential of 2,3-dihydroimidazoles and tricyclic-orthoformamides to behave as hydride donors has been demonstrated in the literature. These compounds have been reported to be able to reduce organic compounds and form hydrogen gas on treatment with acid. The focus of the following discussion is to illustrate their applicability as hydride donors to boron Lewis acids.

6.2 Research Objectives

The goal of this research project is to demonstrate that organic hydrides can react with boron Lewis acids to form boranes of the type $BH_{4-y}X_y$ (y = 1or 2). Previous work by us, on Hantzsch esters,[29] and others with amines,[5, 30-33] has only been able to demonstrate that a single hydride equivalent can be transferred from an organic scaffold to boron. Recall briefly that the key step in our ammonia borane (NH_3BH_3) regeneration strategy proposed in Chapter 4 involves the reaction of an organic hydride with a boron Lewis acid to produce diborane or a borane Lewis acid-base adduct. To the best of our knowledge there has been no report in the literature, up to the

time of the preparation of this chapter, which indicates that one or more equivalents of an organic molecule can react with a boron Lewis acid in this fashion. This work may serve as a launching pad for the eventual design of an organic hydride that could be employed in our NH_3BH_3 regeneration strategy.

Our study of the reactivity of Hantzsch's esters towards $B(C_6F_5)_3$ demonstrated that excellent selectivity for the hydride transfer product could be obtained by judicious choice of functional groups.[29] N-substituted esters reacted with $B(C_6F_5)_3$ to produce borohydride salts in high yields. However, significant quantities of Lewis acid-base adducts or 1,2-dihydropyridines could be obtained depending on the reaction conditions or substrate employed. It was our view that these undesirable reaction manifolds could be avoided by examining less functionalized and more reactive organic hydrides. It was for this reason that structures with either 2,3-dihydroimidazole **1a-c** or orthoformamide, **1d**, architectures were synthesized (**Scheme 6-10**). This work was concurrent with efforts by fellow graduate student Véronique Laberge to synthesize less functionalized 1,4-dihydropyridines.

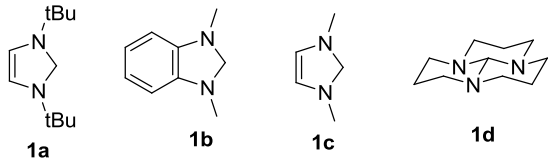

Scheme 6-10. Structures of organic hydrides used in this study

$B(C_6F_5)_3$ will continue to serve as our benchmark Lewis acid. Clean reaction with $B(C_6F_5)_3$ will be a prerequisite for further screening of these model organic hydrides. However, while this Lewis acid is relatively well behaved, it is only amenable to accepting a single hydride equivalent. With the goal of forming diborane or adducts thereof, we targeted Lewis acids of the

type $B(OAr)_3$ and $B(SAr)_3$ as hydride acceptors for two reasons: (1) these Lewis acids are accessible from the waste material, BNH_x of NH_3BH_3 dehydrogenation and (2) they have been shown to disproportionate to BH_3NEt_3 and other boranes/ borohydrides on treatment with inorganic species.[34]

6.3 Results and Discussion

6.3.1 Reaction of Organic Hydrides with $B(C_6F_5)_3$

A series of organic hydrides (**1a-d**) were synthesized and reacted with $B(C_6F_5)_3$. As with the reaction of Hantzsch esters with $B(C_6F_5)_3$, the hydride transfer was rapid at room temperature (**Scheme 6-11**). It was found that the 2,3-dihydroimidazoles **1a** and **1b** reacted cleanly to yield the corresponding borohydride salts **2a** and **2b**. The reaction of **1c** and **1d** with $B(C_6F_5)_3$ resulted in some measure of hydride transfer but other boron containing products were observed and as a result these compounds were not pursued further as hydride donors to boron. In fact, the ^{1}H NMR of the reaction of **1d** with $B(C_6F_5)_3$ suggested that multiple organic species were formed; a similar observation was made by Wuest when **1d** was reacted with trityl.[4]

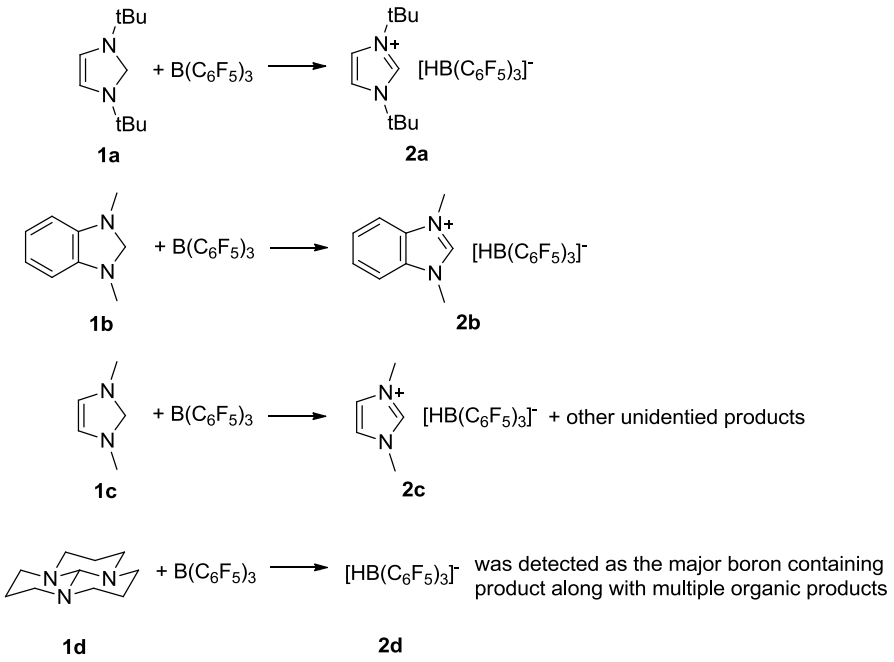

Scheme 6-11. Reactivity of **1a-d** with $B(C_6F_5)_3$

The borohydride salt **2a** was previously synthesized by groups employing the aforementioned Frustrated Lewis Pair (FLP) methodology (**Scheme 6-12**).[35-37] Salt **2a** is the product of reaction of N-heterocyclic carbene **3a** with $B(C_6F_5)_3$ in the presence of H_2. It is unlikely that a similar FLP approach would succeed in generating **2b** or **2c** for two reasons. It was found in the same report that $B(C_6F_5)_3$ formed stable Lewis acid-base adducts with less-encumbered carbenes[35-37] and the free carbene analogues of **3a** that would be required are not sufficiently bulky to be stable at room temperature.[38, 39]

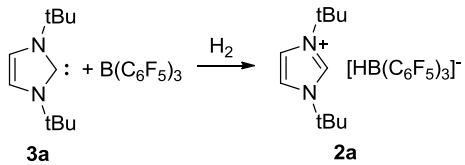

Scheme 6-12. Alternate route to **2a** utilizing an FLP strategy

6.3.2 Reaction of 1a and 1b with $B(SPh)_3$

$B(SPh)_3$ was chosen as a test hydride acceptor based on the results of Dubois[34] who reported that on exposure to Rh-hydrides and NEt_3, the Lewis acid could be converted to BH_3NEt_3. We adopted screening procedures similar to those reported by Dubois. The first set of reactions were carried out at room temperature in the absence of NEt_3 to get an idea of the intrinsic capacity of **1a** and **1b** to act as hydride donors to $B(SPh)_3$ (**Scheme 6-13** and **Figure D-1** in **Appendix D**). The purpose of using 3 equivalents of organic hydride to Lewis acid was to ensure that there would be sufficient donor present to completely convert $B(SPh)_3$ to diborane or an amine borane adduct, if such a reaction manifolds were operational. These reactions were monitored by ^1H NMR and ^{11}B NMR. It was found that the dihydroimidazoles **1a** and **1b** transferred hydride to $B(SPh)_3$ forming $[HB(SPh)_3]^-$ and that the Lewis acid was consumed in 1 h at room temperature (**Figure 6-1b**).

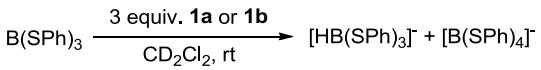

Scheme 6-13. Reaction of $B(SPh)_3$ with hydrides **1a** and **1b**

The other major boron containing species observed was $[B(SPh)_4]^-$ which was formed to a greater degree when **1a** was the hydride source.[34] Resonances consistent with the corresponding imidazolium cations **1a** and **1b** were also apparent by ^1H NMR. The formation of $[B(SPh)_4]^-$ was reversible in CD_2Cl_2 as, upon standing the resonance would diminish in intensity relative to $[HB(SPh)_3]^-$ (**Figure 6-1b** and **c**). After 2 days at room temperature the major boron containing species in solution was $[HB(SPh)_3]^-$. There was something unique about this reaction when carried out in chlorinated solvents since the formation of $[B(SPh)_4]^-$ in THF and DME appeared to

be irreversible (**Figure D-2** in **Appendix D**), because the relative intensity of the resonance for $[B(SPh)_4]^-$ as compared to $[HB(SPh)_3]^-$ did not change over time in these solvents.

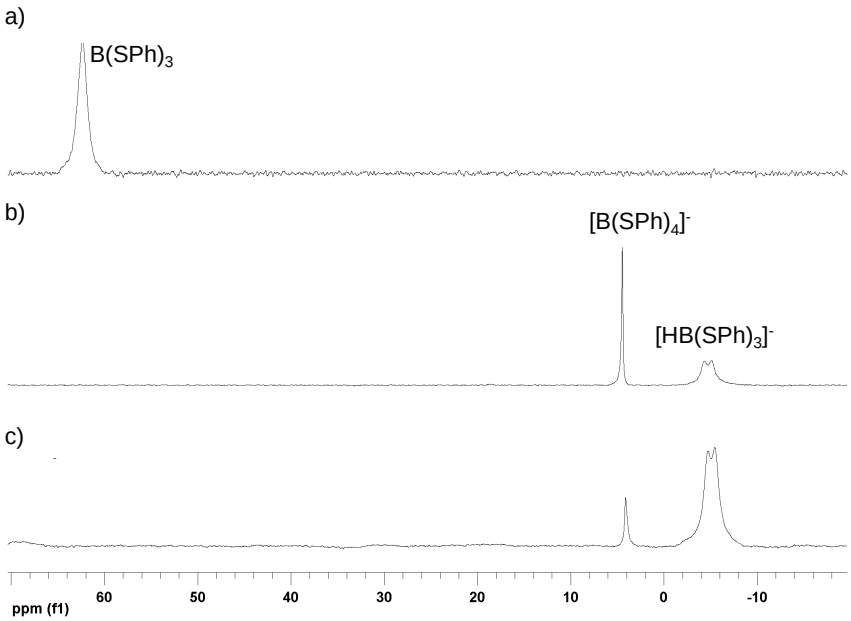

Figure 6-1. ^{11}B NMR overlay for the redistribution reaction of $B(SPh)_3$ with hydride donor **1a**; a) before addition of **1a**; b) after 1 h at room temperature; c) after 2 days at room temperature.

A survey of reaction conditions led to the isolation of the borohydride salt **4a** (**Scheme 6-14**). The same conditions also afforded small amounts of the salt **5a** for which X-ray quality crystals were grown (**Figure 6-2**). The metric parameters for the imidazolium cation such as the N1-C1-N2 bond angle (107.87(17)º) as well as the N1-C1 (1.331(2) Å) and N2-C1 (1.375(2) Å) bond lengths were similar to those reported elsewhere.[35, 36] The geometry about $[B(SPh)_4]^-$ was essentially tetrahedral with bond angles ranging from 105 – 118º. The B-S bond lengths were 1.914(2) Å, 1.919(2) Å, 1.924(2) Å and 1.950(2) Å and compared well to those reported for $[HB(SPh)_3]^-$.[40]

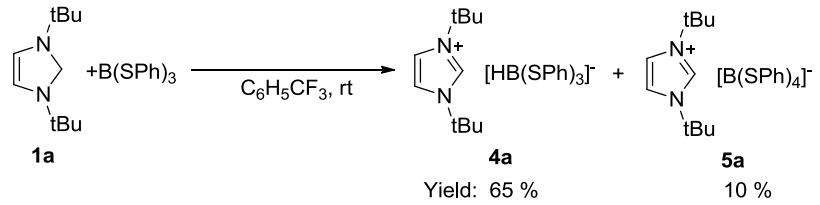

Scheme 6-14. Synthesis of salts **4a** and **5a**

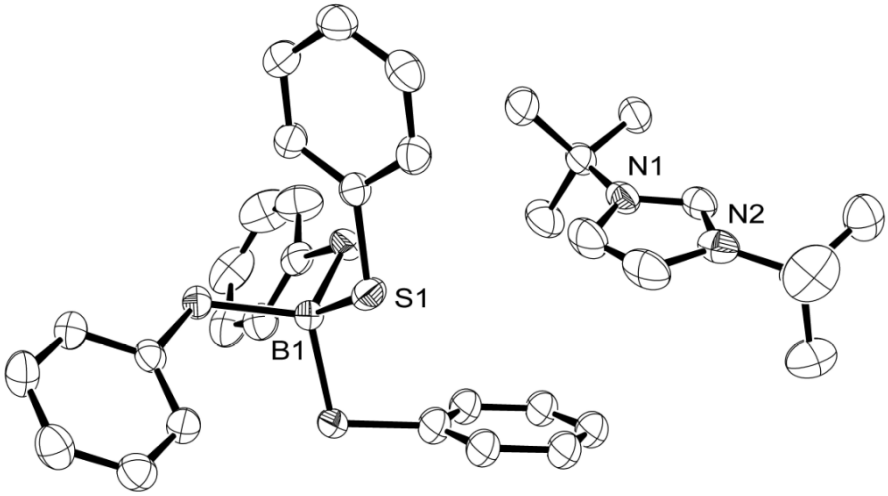

Figure 6-2. ORTEP drawing of salt **5a**, thermal ellipsoids were drawn at 50 % probability and hydrogen atoms were eliminated for clarity

The salt **4a** served as a convenient source of $[HB(SPh)_3]^-$ and was used to probe reaction conditions to generate higher boranes (**Figure 6-3**). When **4a** was heated to 50 ºC in CD_2Cl_2 small quantities of $[H_2B(SPh)_2]^-$ were observed on short reaction times but ultimately $[HB(SPh)_3]^-$ redistributed into a complex mixture of unidentified B-H containing species. On addition of excess NEt_3 the reaction manifold changed and **4a** redistributed to species consistent with $H_2B(NEt_3)(SPh)$, $[B(SPh)_4]^-$ and $HB(NEt_3)(SPh)_2$.[34] Importantly, addition of excess organic

hydride **1a** (4 equivalents) to the redistribution of **4a** produced $H_2B(NEt_3)(SPh)$, as the only observable boron containing species.

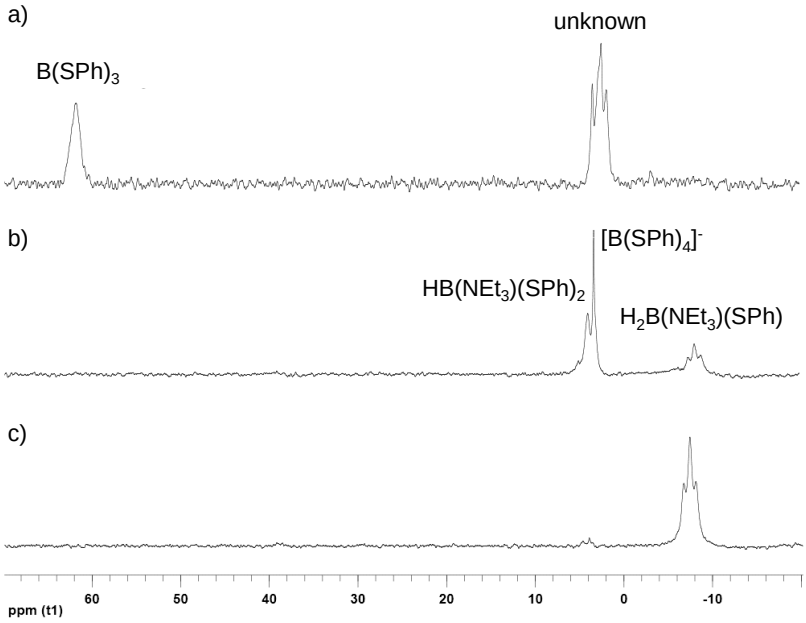

Figure 6-3. ^{11}B NMR overlay for the redistribution reactions of **4a** under different conditions in CD_2Cl_2; a) 18 h at 50 ºC no additives; b) 18 h at 50 ºC excess NEt_3; c) 18 h at 50 ºC excess NEt_3 and **1a** (4 equivalents)

Encouraged by the redistribution results using **4a**, focus shifted to developing a route to $H_2B(NEt_3)(SPh)$ with **1a** and **1b** as hydride donors to $B(SPh)_3$. THF was chosen as the solvent because anecdotal evidence suggested that **1a** decomposes slowly in CD_2Cl_2. The redistribution reaction was performed initially at room temperature in the absence of NEt_3. After consumption of $B(SPh)_3$, NEt_3 was added and the solution was heated at 50 ºC (**Figure D-2** in **Appendix D**). Unfortunately, no change in the product distribution between $[HB(SPh)_3]^-$ and $[B(SPh)_4]^-$ was observed after 3 days of heating. This result was surprising because these redistribution

conditions were analogous to those employed in the Dubois Rh-hydride system that resulted in almost exclusive formation of BH_3NEt_3[34] and hints that redistribution in the presence of organic hydrides proceeds through an alternative reaction pathway which will be discussed later on.

Subsequently, redistribution was examined in a 1:1 mixture of THF:CH_2Cl_2 with excess NEt_3 (**Scheme 6-15**). After heating overnight at 50 ºC the only species evident by ^{11}B NMR was $H_2B(NEt_3)(SPh)$ (**Figure 6-4**). $H_2B(NEt_3)(SPh)$ was also formed when $B(SPh)_3$ redistribution was carried out in the presence of **1b**, but the reaction was not selective. It may be that **1b** is an inferior hydride donor to $B(SPh)_3$ as compared to **1a**.

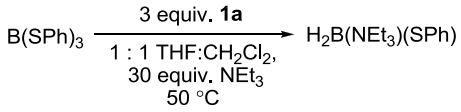

Scheme 6-15. Redistribution of $B(SPh)_3$ with hydride donor **1a** in 1:1 THF:CH_2Cl_2

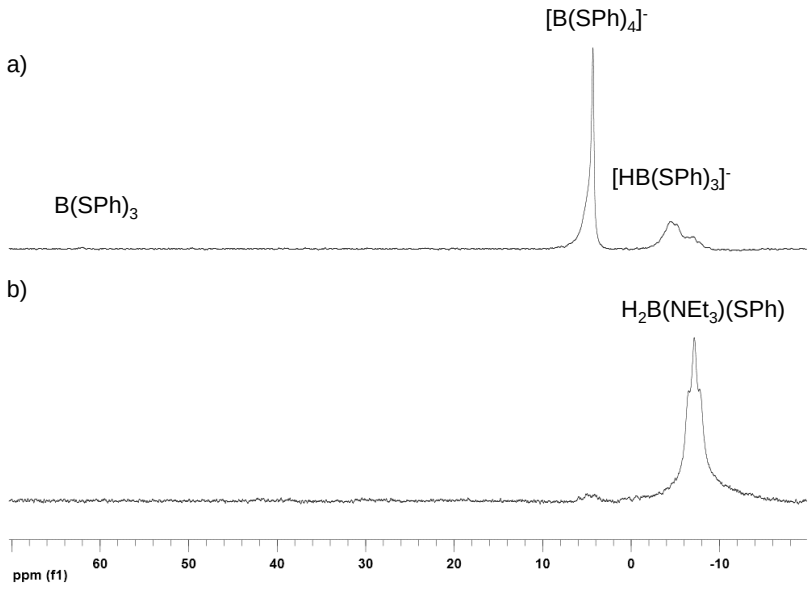

Figure 6-4. ^{11}B NMR overlay for redistribution reaction of $B(SPh)_3$ with hydride donor **1a** in 1:1 THF:CH_2Cl_2 with excess NEt_3; a) after 1 h at room temperature; b) after 18 h at 50 ºC

Based on the results of redistribution with **1a**, CH_2Cl_2 is critical for selective formation of $H_2B(NEt_3)(SPh)$. The role of CH_2Cl_2 in the reaction is not known definitively at this time, although it is reasonable to suspect that it acts as a thiolate scavenger. Other research groups[41-43] have demonstrated that thiolates can react with CH_2Cl_2 under mild conditions. In our hands the disulfide $CH_2(SPh)_2$ has been detected in GC-MS chromatograms of redistribution reactions. It is noted that NEt_3 also reacts with CH_2Cl_2 under these conditions to form quaternary ammonium salts, and this may be the material that occasionally precipitates on prolonged heating. An alternative explanation for the effect of CH_2Cl_2 could be that an increase in ionic strength of the solvent due to the formation of these ammonium salts helps with redistribution. To probe this possibility the non-coordinating salts $[NEt_4][SbF_6]$ and $[Na][BPh_4]$ were added to a redistribution reaction in THF without CH_2Cl_2. While trace amounts of $H_2B(NEt_3)(SPh)$ could be observed at room temperature, these salts did not promote additional formation of $H_2B(NEt_3)(SPh)$ after heating overnight.

When the redistribution reaction of $B(SPh)_3$ with **1a** was carried out at 80 ºC instead of 50 °C, ^{11}B NMR spectra with poor signal to noise ratios were collected (**Figure 6-5a**). The same observation was obtained from heating a solution of $H_2B(NEt_3)(SPh)$ with excess **1a** under the same conditions. While these results are inconclusive, they hinted at the possibility that diborane might have been formed under these redistribution conditions, rather than BH_3NEt_3 which was observed in the Rh-hydride system of Dubois.[34] To test this possibility, 1-octene was added to the reaction mixture to act as a trap for diborane (**Scheme 6-16**). After heating at 80 ºC overnight the only resonance in the ^{11}B NMR was at 86 ppm consistent with the formation of trioctylborane ($B(nOc)_3$) (**Figure 6-5c**).[44] Interestingly the resonance at 86 ppm was a minor peak when the

redistribution was carried out at 50 ºC (**Figure 6-5d**) suggesting some diborane may be formed along with $H_2B(NEt_3)(SPh)$ under these conditions but has thus far gone undetected.

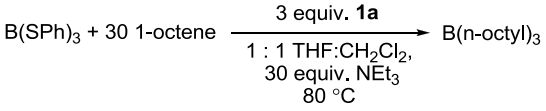

Scheme 6-16. General conditions for the 1-octene trapping experiment

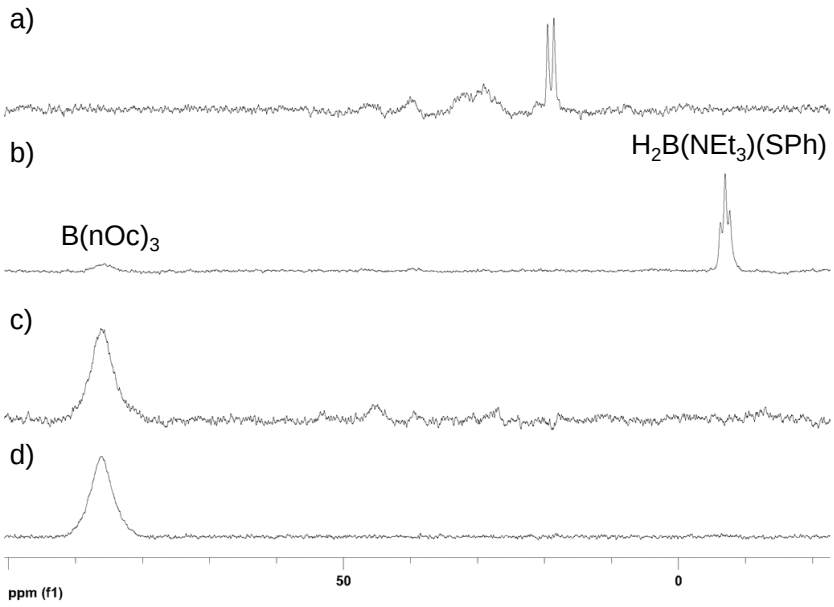

Figure 6-5. ^{11}B NMR overlay for the redistribution of $B(SPh)_3$ with hydride donor **1a** with excess NEt_3; a) after overnight at 80 ºC; b) after overnight at 50 ºC; c) after overnight at 80 ºC with excess octene; d) spectra of trioctylborane formed from a hydroboration reaction in 1:1 THF:CH_2Cl_2

Monitoring the reaction periodically at 80 ºC, showed that after 20 min the major boron species was $H_2B(NEt_3)(SPh)$, along with lesser quantities of $[HB(SPh)_3]^-$ and $B(nOc)_3$. After 4 h

the major detectible boron species was trioctylborane (**Figure 6-6** and **Figure D-3** in **Appendix D**). Neither, BH_3NEt_3 or $[BH_3SPh]^-$ accumulated at any time during the redistribution reaction and no significant resonances associated with dialkyl or monoalkyl boranes were observed.[45, 46] These observations indicate that under the our redistribution conditions, $H_2B(NEt_3)(SPh)$ likely disproportionates to form diborane. The diborane is then removed from the system through reaction with 1-octene, giving $B(nOc)_3$.

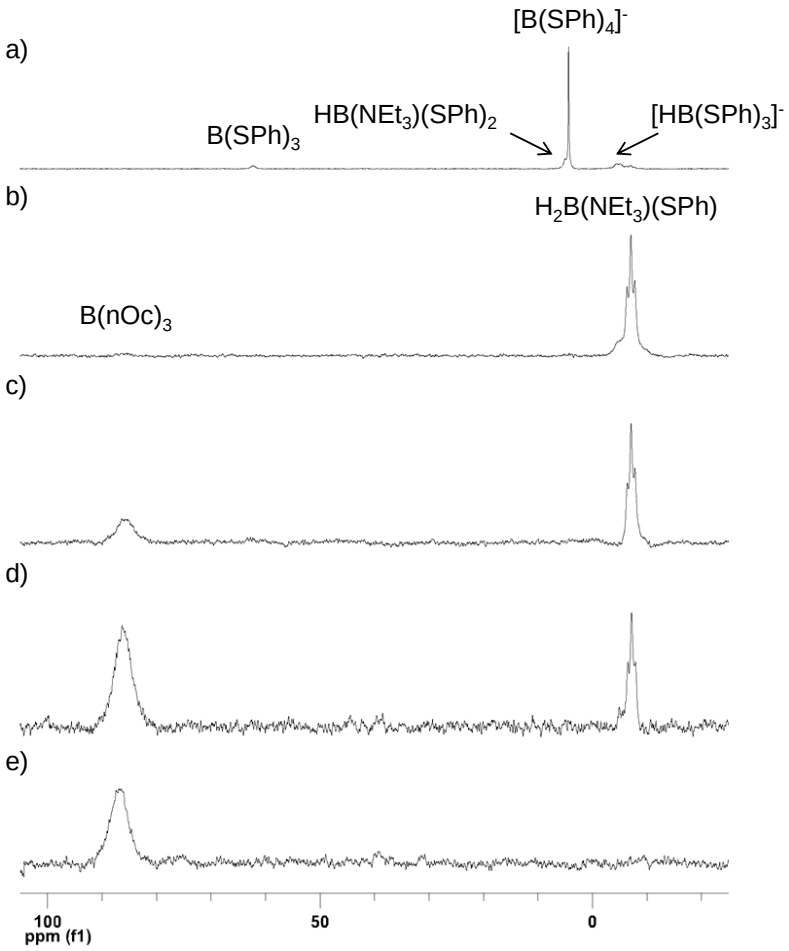

Figure 6-6. ^{11}B NMR overlay for redistribution of $B(SPh)_3$ with hydride donor **1a** with excess NEt_3 and 1-octene; a) after 1 h at room temperature; after b) 20 min; c) 1 h; d) 2 h; e) 4h at 80 °C

The $B(nOc)_3$ generated under the redistribution conditions was subjected to a standard peroxide oxidation protocol with H_2O_2 and NaOH to produce 1-octanol (**Table 6-1**). The typical yield of 1-octanol was about 50 %, which is based on the amount of $B(SPh)_3$ added to the reaction mixture and the amount formed was insensitive to heating the reaction for longer periods of time or scale (entry 1-3). For reference, a hydroboration reaction with BH_3NEt_3 (entry 7) was performed under similar conditions to the redistribution reaction and the yield of 1-octanol was 45 %. It is likely that 1-octene is not completely effective at trapping diborane under the redistribution conditions. The yield of 1-octanol then serves instead as a lower indicator of the amount of diborane formed. Note that 1-octanol was not formed when a control reaction was carried out in the absence of $B(SPh)_3$ (entry 8) and heating $B(SPh)_3$ in the absence of **1a** did not result in the formation of detectible quantities of trialkylboranes (**Figure D-5** in **Appendix D**).

Table 6-1. Yields of 1-octanol from diborane trapping experiments

Entry	Lewis acid	NEt_3, mmol	Time, h	Yield 1-octanol, (%)[b]
1	$B(SPh)_3$	1.0	5	55
2[c]	$B(SPh)_3$	1.0	5	48
3	$B(SPh)_3$	1.0	18	50
4	$B(SPh)_3$	None	18	30
5	BH_3NEt_3	1.0	18	11
6	BH_3NEt_3	None	18	44
7[c]	BH_3NEt_3	None	18	45
8	None	1.0	18	-

[a] Reaction conditions: Boron Lewis acid (0.03 mmol), **1a** (0.11 mmol), NEt_3, 1-octene (1.0 mmol) were combined in 1:1 THF:CH_2Cl_2 (1 mL) and the solution was heated at 80 ºC. After heating the solution was cooled to 0 ºC and 1 mL of 1:1 solution of 2 M NaOH: 36 wt% H_2O_2 was added to the reaction mixture; [b] Yield was measured by GC-FID and 1,4-dimethyoxybenzene added as an internal standard; [c] Double scale.

The ^{11}B NMR reaction profile (**Figure 6-6**) suggests that 1-octene is reacting with diborane formed under the redistribution conditions; the reaction pathway is unclear but efforts to

detect the gas directly are on-going. It can be said definitively that neither BH_3NEt_3 or $[BH_3SPh]^-$ accumulate in solution under our redistribution conditions and these are boranes that were detected by Dubois as products from the redistribution of $B(SPh)_3$ in the presence of Rh-hydrides. This is more evidence suggesting that our redistribution process is different than that observed in the Dubois system.[34] We were able to establish that BH_3NEt_3 is fairly stable to our redistribution conditions at 80 ºC as heating overnight in the presence of excess NEt_3 and 1-octene resulted in only trace hydroboration (**Table 6-1** entry 5 and **Figure D-4** in **Appendix D**). Based on this observation it is likely that $H_2B(NEt_3)(SPh)$ does not redistribute to BH_3NEt_3 prior to the formation of diborane in our system. Alternatively, $[BH_3SPh]^-$ could be forming under the reaction conditions but decomposes to diborane, rather than accumulate in solution, due to the presence of CH_2Cl_2 which scavenges the thiolate formed when the adduct dissociates.

An alternative explanation for $B(nOc)_3$ formation in the presence of 1-octene is that $H_2B(NEt_3)(SPh)$ decomposes under the redistribution conditions to give H_2BSPh which undergoes a hydroboration reaction rather than diborane and the resulting dialkylborane, $B(nOc)_2(SPh)$, disproportionates to $B(nOc)_3$. To get an idea about whether this process can occur, we performed control reactions where $H_2B(NEt_3)(SPh)$ was formed and heated at 50 ºC and/or 80 ºC in the presence of excess 1-octene. In these experiments $H_2B(NEt_3)(SPh)$ was generated *in-situ*, along with trace quantities of $HB(NEt_3)_2(SPh)$, $[B(SPh)_4]^-$, by heating 2.2 equivalents of **1a** with $B(SPh)_3$ and NEt_3 in 1:1 THF:CH_2Cl_2 at 50 ºC (**Figure 6-7** and **Figure 6-8**). Once $H_2B(NEt_3)(SPh)$ was formed all the added **1a** was consumed. At this point 1-octene was added to the solution. Heating $H_2B(NEt_3)(SPh)$ overnight at 50 ºC produced three new boranes including $B(nOc)_3$ (**Figure 6-7b**). The other two are thought to be $B(nOc)_2(SPh)$ and $B(nOc)(SPh)_2$, as their chemical shifts are consistent with similar species reported in the literature.[45, 46] A ^{11}B NMR time

course at 80 ºC (**Figure 6-8**), showed that $B(nOc)_2(SPh)$ and $B(nOc)(SPh)_2$ form alongside $B(nOc)_3$ and resembled what was observed in the 1960's when H_2BSPh was tested as a hydroborating agent.[47] That said, the product distributions at 50 ºC and 80 ºC in these controls are different than what is observed under the standard redistribution conditions (**Figure 6-6**, **Figure 6-7** and **Figure 6-8**), where the only alkyl borane detected was $B(nOc)_3$. This data suggests that the redistribution of $H_2B(NEt_3)(SPh)$ proceeds through a different reaction pathway when **1a** is present and that **1a** is required for the efficient formation of $B(nOc)_3$. It may be that **1a** reacts with either $H_2B(NEt_3)(SPh)$ or H_2BSPh under the redistribution conditions forming $[BH_3SPh]^-$ that decomposes to diborane.

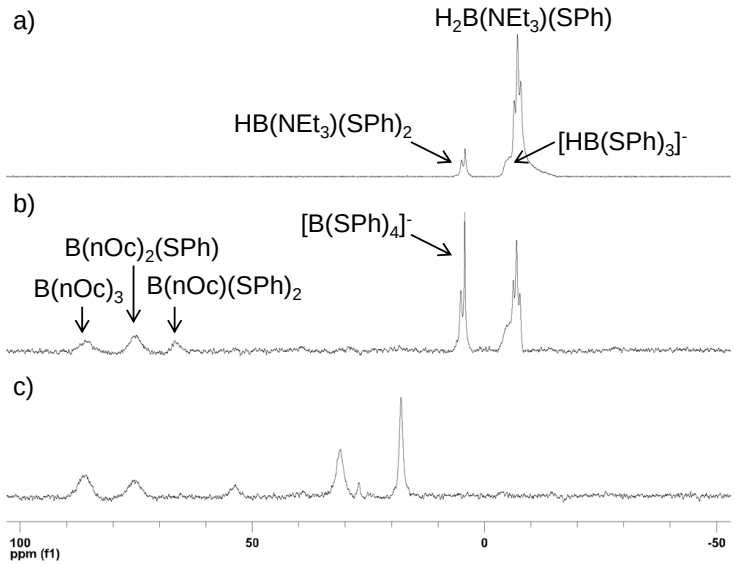

Figure 6-7. ^{11}B NMR for the redistribution of $B(SPh)_3$ with 2.2 equivalents of hydride **1a** in 1:1 THF:CH_2Cl_2 with excess NEt_3; a) after overnight at 50 ºC; b) after heating solution in a) with excess 1-octene overnight at 50 ºC; c) after heating solution b) overnight at 80 ºC

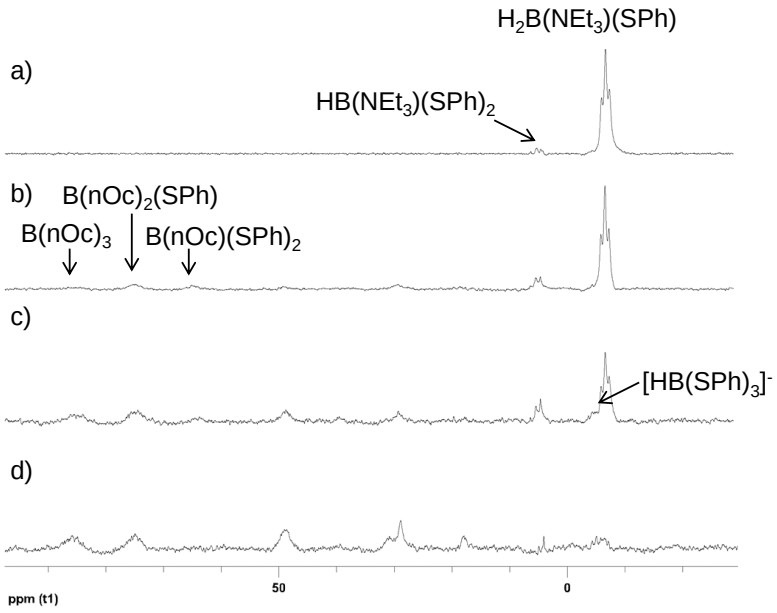

Figure 6-8. ^{11}B NMR for the redistribution of $B(SPh)_3$ with 2.2 equivalents of hydride **1a** in 1:1 THF:CH_2Cl_2 with excess NEt_3; a) after overnight at 50 ºC b) after heating solution in a) with excess 1-octene for 20 min; c) 1 h; d) 2 h at 80 ºC

While 1-octene trapping has produced good indirect evidence for the formation of diborane under the redistribution conditions, direct observation would clearly be ideal. Currently we are looking into approaches of sampling the head space of the vessel by MS and/or by trapping the gas in either THF or NEt_3, a method similar to that used when forming diborane in lab for synthetic applications.[48, 49]

We have also attempted to modify the redistribution system in the hopes of directly observing BH_3-adducts. First we exchanged NE_3 for the bulkier Hünigs base (**Figure D-6** in **Appendix D**). The rationale for the change was that increased bulk about $H_2B(NR_3)(SPh)$ intermediated would promote further disproportionation to a borane. Unfortunately Hünigs base disrupted formation of $H_2B(NR_3)(SPh)$ and the approach was abandoned.

We also explored the possibilty of modulating disproportionation by modifying the structure and electronics of the boron Lewis acid with varying success. The bulky Lewis acid *ortho*-$B(SC_6H_5CH_3)_3$ was synthesized using a procedure similar to that used to make $B(SPh)_3$. Substantially longer reaction times were required for the synthesis an observation that was attributed to the steric bulk of the thiol (**Scheme 6-17**).

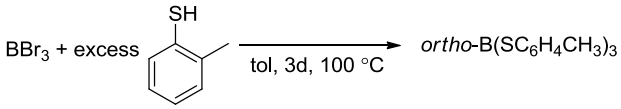

Scheme 6-17. Synthesis of *ortho*-$B(SC_6H_4CH_3)_3$

It was thought that the steric bulk of *ortho*-$B(SC_6H_4CH_3)_3$ would promote disproportionation of the $H_2B(NR_3)(SAr)$ intermediate. On exposure to **1a** (**Scheme 6-18**), redistribution occurred to form the borohydride *ortho*-$[HB(SC_6H_4CH_3)_3]^-$ although the hydride transfer reaction was slower than that in the $B(SPh)_3$ system (**Figure D-7** in **Appendix D**). After 2 days at room temperature the free Lewis acid was still evident in ^{11}B NMR spectra. On heating the reaction mixture to 50 ºC, additional disproportionation occurred giving *ortho*-$H_2B(NEt_3)(SC_6H_4CH_3)$ which eventually decomposed when the temperature was raised to 80 ºC. Unfortunately, no resonances consistent with BH_3-adducts were observed.

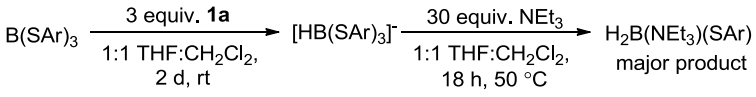

Scheme 6-18. Redistribution experiment with *ortho*-$B(SC_6H_4CH_3)_3$ and hydride donor **1a**.

Ar = *ortho*-$SC_6H_4CH_3$

Alternatively, the Lewis acid $B(SC_6F_5)_3$ was synthesized from BF_3OEt_2 and $LiS(C_6F_5)_3$ using a procedure outlined by Naumann.[50] The purpose of screening the redistribution reaction with $B(SC_6F_5)_3$ was to examine the effect of increasing the electron withdrawing character of the thiol on the $H_2B(NR_3)(SAr)$ intermediate. Unfortunately, formation of $H_2B(NR_3)(SAr)$ was disrupted (**Scheme 6-19**) and no BH_3-adducts were observed by ^{11}B NMR (**Figure D-8** and **Figure D-9** in **Appendix D**).

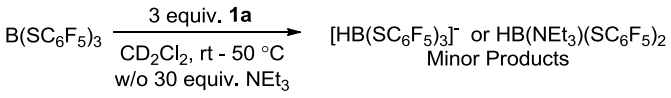

Scheme 6-19. Redistribution experiment with $B(SC_6F_5)_3$ and hydride donor **1a**

6.3.3 Exploring the factors that govern formation of $[B(SPh)_4]^-$ at room temperature

As mentioned earlier, a significant quantity of $[B(SPh)_4]^-$ forms alongside $[HB(SPh)_3]^-$ on short reaction times during the redistribution reaction of $B(SPh)_3$ with the hydride donor **1a** (**Figure 6-1**). A similar observation was also made by Dubois,[34] in their Rh-hydride system. They found that when sub-stoichiometric quantities of Rh-hydrides were reacted with $B(SPh)_3$, a significant amount of $[B(SPh)_4]^-$ was formed alongside $[HB(SPh)_3]^-$. Besides $B(SPh)_3$, no other boron species were detected under these conditions. Currently, there is no satisfactory explanation for why $[B(SPh)_4]^-$ can form alongside $[HB(SPh)_3]^-$. It would be convenient to rationalize the formation of $[B(SPh)_4]^-$ as the result of a disproportionation reaction between $B(SPh)_3$ and $[HB(SPh)_3]^-$ but no such reaction occurred when $B(SPh)_3$ was added to the borohydride salt **4a** after 3 h at room temperature (**Figure D-10** in **Appendix D**). $[B(SPh)_4]^-$ only formed when **1a** was added to the reaction mixture. The formation of $[B(SPh)_4]^-$ under our redistribution conditions seems to be related to the organic hydride employed. As compared to **1a**, *N*,*N*-

dimethyl-dihydroimidazole **1b** disfavours formation of $[B(SPh_4)]^-$. It may be that the extent of formation of $[B(SPh)_4]^-$ is related to strength of organic hydride because anecdotal evidence hints that **1a** is more hydridic than **1b**.

6.3.4 Reaction of 1e with $B(SPh)_3$

The 1,4-dihydropyridine **1e** was generously prepared for this study by Nikonov[51] and was screened under the redistribution conditions with $B(SPh)_3$. It was observed that **1e** was only capable of transferring one equivalent of hydride to $B(SPh)_3$ forming $HB(py)(SPh)_2$ (**Scheme 6-20**). No further redistribution was observed even upon heating in presence of NEt_3. As was mentioned previously **1e**, was shown by Nikonov[51] to undergo a hydride transfer reaction with $B(C_6F_5)_3$ (**Scheme 6-21**). The resulting borohydride salt, however, decomposed upon standing. It was our contention that the pyridine stabilized silylium cation formed from the hydride transfer reaction with $B(SPh)_3$ might act as a thiol scavenger, instead of a hydride scavenger, obviating for the need for CH_2Cl_2 in the redistribution reactions. The selective formation of a species consistent with $HB(py)(SPh)_2$ demonstrated the veracity of this approach. Unfortunately, further redistribution of $HB(py)(SPh)_2$ to $[BH_2X_2]^-$ and $[BH_3X]^-$ adducts was not observed. The problem may be that pyridine behaves as an inhibitor to redistribution because it is insufficiently basic/ bulky to promote ligand dissociation. Alternatively, **1e** may be insufficiently hydridic to donate to promote further redistribution. Future design of 1,4-dihydropyridine targets for the redistribution reaction should take these potential issues into account.

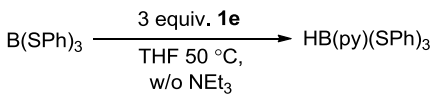

Scheme 6-20. Redistribution of $B(SPh)_3$ with hydride donor **1e**

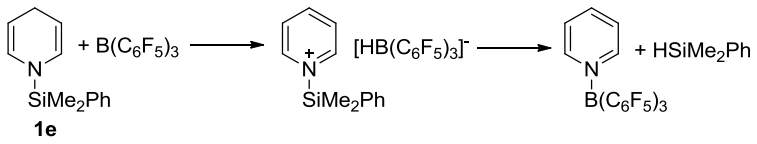

Scheme 6-21. Reaction of **1e** with $B(C_6F_5)_3$

6.3.5 Reaction of 1a and 1b with other boron Lewis acids

Early on in the redistribution screening process BBr_3 and BF_3OEt_2 were examined as potential boron Lewis acids. It was found that BF_3OEt_2 was insufficiently reactive to consume the organic hydrides **1a** and **1b**. While BBr_3 did undergo reaction with **1a** and **1b**, many organic and boron containing products were formed. The use of these Lewis acids was ultimately abandoned because BBr_3 is also a potent reagent for the removal of alkyl groups from ethers and amines, which may account for some of the products formed under these redistribution conditions.

The phenol-derived Lewis acid $B(OC_6F_5)_3$ was also screened under the redistribution reaction conditions with **1a** and **1b**. No hydride containing species were observed during the redistribution reactions when 3 equivalents, of hydride donors **1a** or **1b** were employed (**Scheme 6-22**). The major boron species had a chemical shift consistent with $[B(OC_6F_5)_4]^-$ (**Figure D-11** and **Figure D-12** in **Appendix D**). However, the borohydride $[HB(OC_6F_5)_3]^-$ was detected as a trace product, when **1b** was employed in deficiency (**Figure 6-9**). The anion $[B(OC_6F_5)_4]^-$ likely results from disproportionation reactions of $BH_x(OC_6F_5)_{3-x}$ species, that can be formed under the redistribution reaction conditions as discussed by Dubois and Stephan.[34, 52]

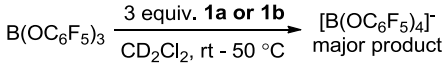

Scheme 6-22. Redistribution of $B(OC_6F_5)_3$ with hydride donors **1a** and **1b**

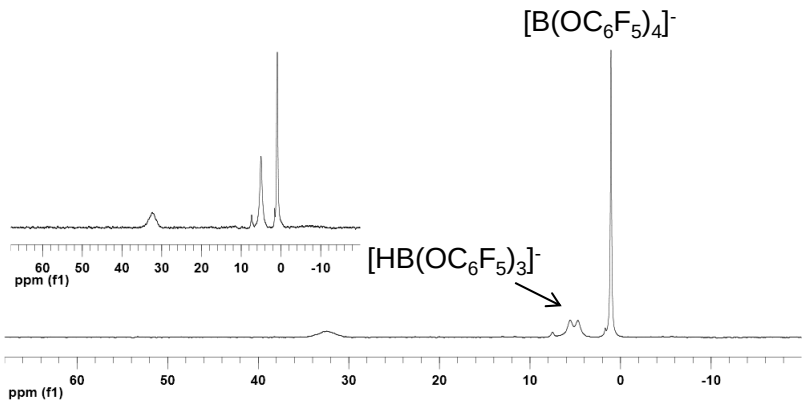

Figure 6-9. ^{11}B NMR for the redistribution of $B(OC_6F_5)_3$ at 50 C with 0.75 equiv. of hydride **1b** and 30 equiv. 1-octene. The corresponding ^{11}B $\{^1H\}$ NMR spectrum is displayed as an inlay

6.3.6 Hydride Transfer between Boron Lewis Acids

In our system there are two general routes that will lead to the formation of higher boranes. One path involves successive hydride transfers from an organic scaffold to a boron Lewis acid. The other route involves hydride exchange between boron atoms. It is likely that both paths are kinetically relevant to the redistribution processes discussed here. Hydride transfer between boron atoms is a well reported phenomenon;[53-55] however, considering its central importance to this research project we thought that it was important to study the process using model systems.

Hydride Exchange between $B(C_6F_5)_3$ and $[HB(C_6F_5)_3]^-$

$B(C_6F_5)_3$ was chosen as the model Lewis acid and **1b** was selected as the hydride donor for the study of the identity hydride transfer reaction (**Scheme 6-11** and **Scheme 6-23**). The hydride transfer reaction between **1b** and $B(C_6F_5)_3$ was performed by varying the equivalents of

$B(C_6F_5)_3$. Speciation was monitored with VT multinuclear NMR methods. It was found that regardless of the excess quantity of $B(C_6F_5)_3$ employed, consumption of **1b** was complete. This observation is in contrast to the previous discussion on the reaction of Hantzsch esters with the same Lewis acid. It was observed that the peak for the $[HB(C_6F_5)_3]^-$ anion broadened in the ^{11}B NMR with increasing equivalents of $B(C_6F_5)_3$ (**Figure D-13** in **Appendix D**). This observation suggested an identity hydride exchange process which was ultimately confirmed by monitoring the same solutions by ^{19}F NMR. A 2D ^{19}F EXSY experiment (**Figure 6-10**) performed at -20 ºC showed cross peaks for resonances attributed to $B(C_6F_5)_3$ and $[HB(C_6F_5)_3]^-$. The mechanism of exchange likely involves a bridging hydride but it is unknown if this species is a true intermediate or a transition state; if it is an intermediate its concentration is too low or lifetime is too short to be observed directly by these NMR methods.

$$[HB(C_6F_5)_3]^- + B(C_6F_5)_3 \rightleftharpoons B(C_6F_5)_3 + [HB(C_6F_5)_3]^-$$

Scheme 6-23. Identity hydride exchange between $B(C_6F_5)_3$ and $[HB(C_6F_5)_3]^-$

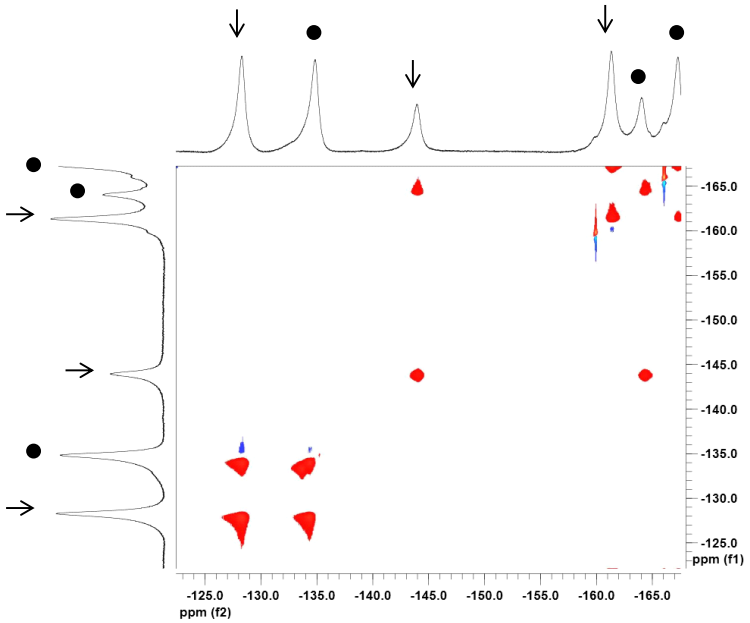

Figure 6-10. 2D ^{19}F EXSY NMR spectrum collected at -20 ºC depicting the identity hydride exchange between $B(C_6F_5)_3$ (circles) and $[HB(C_6F_5)_3]^-$ (arrows)

Hydride transfer from HBpin to $B(C_6F_5)_3$

Stephan[56] reported that the FLP of P^tBu_3 and $B(C_6F_5)_3$ can activate the B-H bond of 1,3,2-benzodioxaborole (HBcat, **Scheme 6-24**). The product was the borenium cation borohydride salt $[^tBu_3PBcat][HB(C_6F_5)_3]$. Prior to their work, mechanistic investigations into the transition metal catalyzed hydroboration reaction revealed that phosphine bases can disproportionate HBcat to BH_3PR_3 adducts in coordinating solvents.[57] In addition, work from our lab indicated that THF can act as a Lewis base to promote the cleavage of B-H bonds of HBpin.[58] By comparison there has been comparatively little work on whether amine bases promote B-H bond activation. The experiments discussed subsequently were performed in conjunction with fellow researcher Chris Lata.

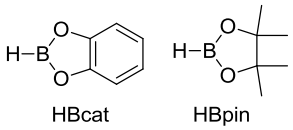

Scheme 6-24. Structure of HBcat and HBpin

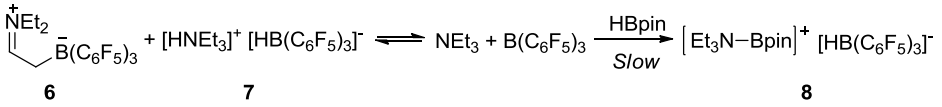

Scheme 6-25. Reaction of HBpin with NEt_3 and $B(C_6F_5)_3$ in CH_2Cl_2 to give borenium cation **8**

The first base examined was NEt_3. On mixing with 4,4,5,5-tetramethyl-1,3,2-dioxaborolane (HBpin, **Scheme 6-24**) no adduct or redistribution was observed. However, addition of $B(C_6F_5)_3$ resulted in C-H activation to form **6** and **7** (**Scheme 6-25**),[30, 31] Interestingly, B-H bond activation did in fact occur but was slow. The activation proceeded over the course of a week to give a borenium cation consistent with the structure of **8**.[59] Evidence for reaction was obtained by monitoring speciation by ^{11}B NMR (**Figure D-14** in **Appendix D**). A new resonance consistent with borenium cation **8**[59] grows in as the resonance for $[HB(C_6F_5)_3]^-$ increases in intensity and HBpin is consumed. Similar correlations were observed in ^1H NMR spectra (**Figure D-15** in **Appendix D**). The formation of salt **8** from this mixture confirms that the reaction of $B(C_6F_5)_3$ with NEt_3 to give **6** and **7** is reversible, an observation that has also been made by other research groups.[30, 31]

The experiment with NEt_3 demonstrated that $B(C_6F_5)_3$ reacts more rapidly with alpha-C-H bonds than the B-H bond of HBpin. For this reason the focus shifted from NEt_3 to amines such as tetramethylpiperidine (TMP) and diazabicyclo[2.2.2]octane (Dabco) because they do not possess C-H bonds that can be activated by $B(C_6F_5)_3$. Dabco reacted with HBpin and $B(C_6F_5)_3$ in

less than 30 min at room temperature to give the borenium cation salt **9** (**Scheme 6-26**). Unfortunately, TMP proved to be too bulky to promote efficient B-H activation. Chris Lata also studied the reaction of *N*,*N*-dimethylaniline with HBpin and $B(C_6F_5)_3$ and showed that some H-B activation did occur.[58]

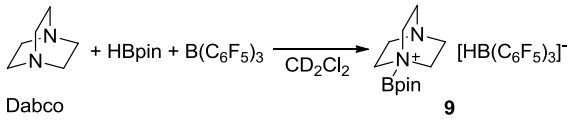

Scheme 6-26. Reaction of Dabco with HBpin and $B(C_6F_5)_3$ to give borenium cation **9**

The order of reagent addition is important to realize clean B-H activation, best results are obtained when HBpin is added to solutions already containing Dabco and $B(C_6F_5)_3$. It should be noted that Dabco reversibly binds to $B(C_6F_5)_3$ to form an insoluble species, presumably a Lewis acid-base adduct. If the Lewis acid-base behaviour is similar to that observed between Dabco and BF_3, both mono- and bis- adducts are possible.[60, 61] The fact that Dabco promotes borenium cation formation demonstrates that FLP promoted B-H activation, like heterolytic H_2 activation, can occur in the presence of Lewis bases that reversibly bind to $B(C_6F_5)_3$.

Fellow graduate student, Chris Lata,[58] observed that $B(C_6F_5)_3$ promoted B-H bond activation played a critical role in a Lewis acid accelerated metal catalyzed hydroboration reaction. In his system, it was found that trace quantities of THF in the reaction mixture acted as the Lewis base for the B-H bond activation. This reaction provided a continuous supply of catalytic quantities of borenium cation and the overall process is thought to be critical for rapid oxidative addition of the hydroborating reagent HBpin to the Rh catalyst under his conditions. The work suggests that B-H bond activation can occur in presence of weak Lewis bases. The problem with THF as a Lewis base is its propensity to ring open in the presence of strong Lewis

acids, however since it is only used in catalytic quantities, sufficient amounts are not present for polymerization to be significant.[62]

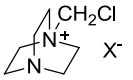

X = Cl, SelectCl; BF_4, SelectBF_4

Scheme 6-27. Weak nucleophiles screened to activate B-H bonds

To further explore B-H activation with weak Lewis bases, nucleophiles inspired by the fluorinating agent Selectfluor were synthesized (**Scheme 6-27**).[63] Two equivalents of $B(C_6F_5)_3$ to the Lewis base were used in these experiments to ensure that scavenging of Cl^- and BF_4^- anions would not interfere with the B-H activation reaction.[58] Fairly clean reaction was observed between SelectCl and HBpin in the presence of $B(C_6F_5)_3$, although it is likely the Cl^- counter ion is acting as the nucleophile to form Cl-Bpin (**Figure D-16** in **Appendix D**).[64, 65] Small amounts of H-B activation were also observed with SelectBF_4 (**Figure D-17** in **Appendix D**). While the borenium cation was not observed directly $[HB(C_6F_5)_3]^-$ did accumulate in solution over time. It is possible that the borenium cation is unstable and decomposes under the reaction conditions. It is likely that the weakly basic N of SelectBF_4 is responsible for heterolytic cleavage observed. Evidence in support of this contention are, a control without any Lewis base present resulted in decomposition of HBpin without $[HB(C_6F_5)_3]^-$ formation and Chris Lata previously established that BF_4^- does not promote activation of HBpin in the presence of $B(C_6F_5)_3$.[58]

N-bound borenium cations are interesting because they are electrophilic. In principle, these borenium cations may be displaced by nucleophiles or serve as Lewis acid activators and promote nucleophilic attack on substrates. Current research in the laboratory is focused on

applications of these new routes to borenium cations. Specifically, N-Lewis base promoted B-H activation is being used to develop new metal free reactions including an electrophilic borylation.

To the best of our knowledge there are no examples of metal free catalytic borylation reactions,[66] although the stoichiometric version was recently reported using ClBcat (**Scheme 6-28**).[59] NEt_3 and $AlCl_3$ promoted the B-Cl activation in this system and the resulting borenium cation was quenched by electron rich N-heterocycles such as indoles. Interestingly, the group reported that HBpin and HBcat did not produce product under the same conditions. The reactivity of $AlCl_3$ with HBpin and HBcat was not disclosed. However, substituting $AlCl_3$ for $B(C_6F_5)_3$ or another Lewis acid may be able to promote borylation of these reagents (**Scheme 6-29**) and/or the borylation of other aromatic reagents. The challenge in particular with indoles is to make the reaction catalytic and find conditions that selectively promote dehydrogenation rather than reduction of the substrate.

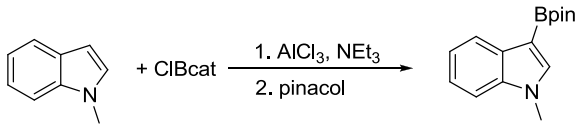

Scheme 6-28. Stoichiometric borylation of indoles via a borenium cation intermediate

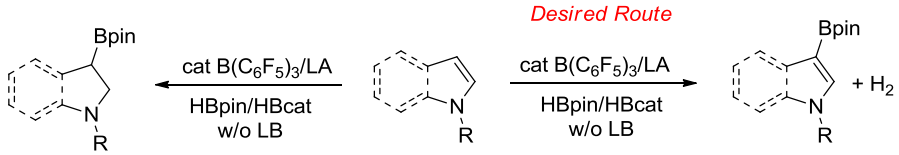

Scheme 6-29. Proposed Lewis acid catalyzed borylation of electron rich heterocycles such as indoles

6.4 Conclusions

This work represents the second phase in the development of a regeneration scheme for ammonia borane (NH_3BH_3) that employs organic molecules as hydride donors to boron Lewis acids. Previously it was established that Hantzsch esters were effective hydride donors to $B(C_6F_5)_3$. But, in order to make our regeneration scheme relevant it is necessary to demonstrate hydride transfer to boron Lewis acids that are more closely related to compounds produced from the digestion of the waste hydrogen storage material, BNH_x. Unfortunately Hantzsch esters were insufficiently reactive to transfer hydride to these Lewis acids; as a result, more hydridic model organic scaffolds were synthesized. The 2,3-dihydroimidazoles **1a** and **1b** as well as the 1,4-dihydropyridine **1e** were found to be effective hydride donors to $B(SPh)_3$. Of the model hydrides **1a** was found to be the most effective transferring two equivalents of hydride to $B(SPh)_3$ in the presence of NEt_3 and CH_2Cl_2 to form $H_2B(NEt_3)(SPh)$. The likely role of CH_2Cl_2 under these reaction conditions is as a thiol scavenger. When the redistribution experiment was carried out at 80 ºC, in the presence of a 1-octene trap, indirect evidence for the formation of diborane was obtained. Unfortunately, BH_3NEt_3 was not observed under any redistribution condition. Efforts to observe diborane directly under the redistribution conditions are ongoing.

Formation of $[H_2BX_2]^-$ species from an organic hydride was unprecedented and represents a significant advance along the road to a full regeneration scheme. This work, however, points to challenges that need to be addressed. First, the model hydrides **1a** and **1b** used in this study were synthesized from borohydrides that are made from NaH, which is highly inefficient. This problem may be rectified if a new synthetic approach to 2,3-dihydroimidazoles were developed. Ideally, the new approach would involve the hydrogenation of an imidazolium cation or employment of a mild reducing agent such as formic acid.[10] Even though the current

synthesis of **1a** and **1b** is inefficient, their use in this study was justified considering the dearth of examples of hydride transfers from organic molecules to boron Lewis acids. Another challenge that needs to be addressed is the requirement of CH_2Cl_2 as a thiol scavenger. Thiol-scavengers are also present in NH_3BH_3 regeneration schemes that deal with sulfur based boron Lewis acids.[34, 67, 68] Consider that when redistribution is carried out with $HSn(Bu)_3$ and Rh-H complexes that the thiolates formed end up bound to Sn and Rh. It is entirely possible that removing thiolates from these redistribution processes in this way is more important to the outcome of the reaction than is currently appreciated. In the present system with 2,3-dihydroimidazoles what would be needed is a route to easily liberate the thiol from $CH_2(SPh)_2$, which is formed from the reaction of CH_2Cl_2 and $[SPh]^-$ under the redistribution conditions. The current strategy would be to subject the sulfide to birch reduction conditions[69] and is clearly not satisfactory. A better solution would be to forgo the use of chlorinated solvents all together. The impetus of studying the redistribution of $B(SPh)_3$ using the 1,4-dihydropyridine **1e** was to begin to address both the synthetic and scavenging challenges.

Substrate **1e** is synthesized from a selective hydrosilylation of pyridine and [51] the silylium cation formed from the hydride transfer behaved like a thiol scavenger, to form $HB(py)(SPh)_2$. Unfortunately, no further redistribution was observed. The benefit of using 1,4-dihydropyridines as the hydride donor is methods already exist to generate them from pyridines without the need for strong reducing agents.[51, 70-73]

The focus now should be to use the lessons learned from **1a**, **1b** and **1e** and synthesize 1,4-dihydropyridines that can produce diborane or BH_3-adducts such as BH_3NEt_3 on exposure to boron Lewis acids. The same 1,4-dihydropyridines must also be able to be reconstituted from pyridines by hydrogenation or by reaction with mild reducing agents. Also 1,4-dihydropyridines

of the form in **Scheme 6-30** are of particular interest as they may be competent to regenerate BNH_x waste material back to NH_3BH_3 without the need of a distinct digestion step. This hypothetical regeneration scheme is conceptually similar to that reported for hydrazine.[74] Now that some of the fundamental chemistry behind organic hydride regeneration has been established we should put priority on performing a global analysis of the efficiency of our NH_3BH_3 regeneration scheme(s).[75] The analysis will allow us compare our approach(es) to existing strategies and better refine our research goals.

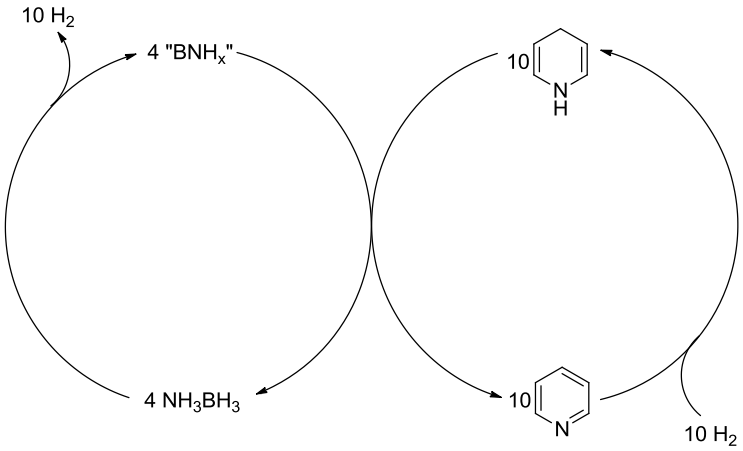

Scheme 6-30. A hypothetical regeneration scheme for BNH_x on treatment with 1,4-dihydropyridine without need of a distinct digestion step

Finally, while exploring the hydride transfer between borohydrides and boron Lewis acids a facile route to borenium cations was developed using the readily available hydroborating agent HBpin. This route is currently serving as inspiration for new catalytic transformations.

6.5 Experimental

6.5.1 General

Manipulations were performed either in an mBraun glovebox or on a double manifold Ar/vacuum line using standard Schlenk technique unless otherwise noted. All solvents were of Certified A.C.S. grade, purchased from Aldrich Chemical Co. unless otherwise noted. The solvents were distilled prior to use from an appropriate drying agent (pentane: P_2O_5; hexanes: Na; THF, toluene and Et_2O: Na ketyl; CH_2Cl_2, trifluorotoluene, CD_2Cl_2 and 1,2-dichloroethane: CaH_2; $CDCl_3$: Na_2SO_4), degassed by three freeze- pump-thaw cycles and stored in a glovebox over 4 Å molecular sieves and basic Al_2O_3. CD_2Cl_2 was purchased from Cambridge Isotopes. $B(C_6F_5)_3$ was purchased from Strem and sublimed under static vacuum at 80 ˚C prior to use. NEt_3 was a distilled from CaH_2 and stored over Al_2O_3 prior to use. t-Butylamine was stored over $MgSO_4$ and decolorizing charcoal and was filtered through Celite prior to use. ^{1}H, ^{13}C, ^{11}B and ^{19}F NMR spectra were collected on Bruker Advance 400, 500 and 600 MHz NMR spectrometers as indicated and referenced to residual solvent (^{1}H, ^{13}C) or externally (^{11}B: BF_3OEt_2, ^{19}F: $CFCl_3$). Chromatograms were collected on an Agilent Technologies 6850A Network GC System equipped with a HP-Chiral ((20% permethylated)-β-cyclodextrin 30 m × 0.32 mm × 0.25 μm) column and an FID detector.

6.5.2 Synthesis of *N,N*-ditertbutyl-imidazolium tetrafluoroborate

The synthesis was adapted from a procedure reported by Hermann *et al.*[76] Paraformaldehyde (2.00 g, 66 mmol) was weighed into a 250 mL round bottom flask fitted with a septum and a stir bar and was suspended in toluene (20 mL). t-Butylamine (4.80 g, 65.6 mmol) was added to the suspension which was subsequently heated to 60 ºC for 20 min at which point the solution was clear and water droplets were visible. The solution was cooled to 0 ºC with an ice bath and t-

butylamine (4.80 g, 65.6 mmol) was added followed by HBF_4 (54 wt% in Et_2O, 8.9 mL, 66 mmol). After 15 min the solution was warmed to room temperature and glyoxal (40 wt% in H_2O, 9.5 mL, 79.2 mmol) was added. The reaction mixture was heated at 40 ºC for 18 h; after 2 h a viscous precipitate was visible. The precipitate was collected by filtration, washed with Et_2O and was recrystallized from 95 % EtOH (150 mL). The collected spectra were consistent with literature reports.[76] Yield: 10.5 g (60 %). ^{1}H (500 MHz, d_6-DMSO) δ: 1.16 (s, 18H, C(C*H*$_3$)$_3$), 8.06 (s, 2H, C=C*H*), 9.00 (s, 1H, N$_2$-C*H*); ^{13}C (125 MHz, d_6-DMSO) δ: 29.0, 59.6, 120.4, 132.2.

6.5.3 Synthesis of *N,N*-ditertbutyl-dihydroimidazole: 1a

NaH (99 wt%, 1.28 g, 53.3 mmol) was weighed in a glovebox into a 250 mL round bottom flask fitted with a septum and a stir bar and was suspended in THF (30 mL). The suspension was cooled in an ice bath and $B(OMe)_3$ (6.11 mL, 53.3 mmol) was added dropwise via syringe. *Caution, the action of B(OMe)$_3$ on NaH is exothermic.* The suspension was allowed to warm slowly to room temperature, then heated to 60 ºC for 30 min and cooled back to room temperature. *N,N*-ditertbutyl-imidazolium tetrafluoroborate (4.0 g, 15.2 mmol) was weighed into a 250 mL round bottom flask fitted with a septum and a stir bar and was suspended in THF (30 mL). The borohydride solution was transferred via cannula into the imidazolium suspension and the mixture was allowed to stir overnight at room temperature. The solvent was removed by distillation at atmospheric pressure. The residue was extracted with pentane and water. The organic layer was dried with brine and $MgSO_4$, filtered and the pentane was removed by distillation at atmospheric pressure. The oil was transferred to a glovebox, filtered through basic Al_2O_3 and stored at -25 ºC. The oil partially crystallized and the supernatant was discarded. The resulting solid contained trace quantities of THF. Yield: 2.7 g (50 %). ^{1}H (500 MHz, C_6D_6, 298 K) δ: 1.15 (s, 18 H, C(C*H*$_3$)$_3$), 4.36 (s, 2H, N$_2$-C*H*$_2$), 5.58 (s, 2H, C=C-*H*); ^{13}C (125 MHz, C_6D_6,

298 K) δ: 27.0, 52.7, 66.5, 116.2. HRMS (TOF EI^+) exact mass calculated for $[M]^+$ required *m/z* 182.1776 ($C_{11}H_{22}N_2$), found *m/z* 182.1783.

6.5.4 Synthesis of *N,N*-dimethyl-benzimidazolium iodide

The synthesis was adapted from a procedure reported by Higashino *et al*.[77] To a 50 mL sealed test tube containing a stir bar was added *N*-methylbenzimidazole (3.40 g, 26.7 mmol), methyl iodide (2.30 mL, 37.5 mmol) and MeOH (20 mL). The reaction tube was heated at 90 ºC for 3 h, and after cooling the solvent was removed under vacuum. To the residue was added EtOAc, the solid that formed was recovered by filtration and was washed with additional EtOAc. The solid was dried under vacuum. Yield: 7.0 g (95 %). The collected spectra were consistent with literature reports.[77] ^{1}H NMR (300 MHz, d_6-DMSO) δ: 4.07 (s, 6H, N-C*H*$_3$), 7.72 (d, 2H, $^3J_{H\text{-}H}$ = 8 Hz, Ar-*H*), 8.03 (d, 2H, $^3J_{H\text{-}H}$ = 8 Hz, Ar-*H*), 9.73 (s, 1H, N_2-C*H*); ^{13}C (100 MHz, d_6-DMSO) δ: 33.7, 113.9, 126.9, 132.1, 143.6.

6.5.5 Synthesis of *N,N*-dimethyl-dihydrobenzimidazole: 1b

N,N-Dimethyl-benzimidazolium iodide (7.0 g, 25.5 mmol) was weighed into a 500 mL round bottom flask fitted with a septum and a stir bar and was dissolved in MeOH (150 mL). The solution was cooled to -40 ºC with an acetonitrile dry ice bath. To the solution was added $NaBH_4$ (1.9 g, 51 mmol) in portions over 1 h after which the reaction mixture was allowed to warm to room temperature slowly. After bubbling ceased the reaction was quenched by the addition of water and was concentrated under vacuum. The residue was extracted with CH_2Cl_2 (250 mL) and the organic layer was dried by washing with brine and $MgSO_4$ and was concentrated under vacuum. The crude product was further purified by fractional distillation under vacuum. The product fraction boiling from 45 – 55 ºC was collected and transferred into the glovebox. The product was percolated through a basic Al_2O_3 column and was stored at -25 ºC. The collected

spectra were consistent with literature reports.[1] Yield: 4.8 g (60 %). ^{1}H NMR (500 MHz, CD_2Cl_2) δ: 2.77 (s, 6H, N-CH_3), 4.36 (s, 2H, N_2-CH_2), 6.46 (dd, 2H, $^{3}J_{H\text{-}H}$ = 8 Hz, $^{4}J_{H\text{-}H}$ = 4 Hz, Ar-*H*), 6.70 (dd, 2H, $^{3}J_{H\text{-}H}$ = 8 Hz, $^{4}J_{H\text{-}H}$ = 4 Hz, Ar-*H*); ^{13}C NMR (125 MHz, CD_2Cl_2) δ: 34.3, 80.3, 106.0, 119.0, 143.5.

6.5.6 Synthesis of *N*-*N*-dimethyl-imidazolium tosylate

The synthesis was adapted from a procedure reported by Lieder *et al*.[9] To a 200 mL round bottom flask fitted with a septum and a stir bar, was added THF (70 mL) and *N*-methylimidazole (5.30 mL, 65.0 mmol). Methyl tosylate (10.0 mL, 66.5 mmol) was added to the solution dropwise using a syringe. After 10 min of stirring the homogeneous solution became turbid. The reaction mixture was stirred overnight and the solvent was evaporated under vacuum. To the residue was added Et_2O (10 mL) during which a solid precipitate formed that was recovered by filtration. The hydroscopic solid was dried over P_2O_5 and stored in a desiccator. The collected spectra were consistent with literature reports.[9] Yield: 17.5 g (95 %). ^{1}H (300 MHz, d_6-DMSO) δ: 2.28 (s, 3H, Ar-CH_3), 3.83 (s, 6H, N-CH_3), 7.11 (d, 2H, $^{3}J_{H\text{-}H}$ = 8 Hz, Ar-*H*), 7.13 (d, 2H, $^{3}J_{H\text{-}H}$ = 8 Hz, Ar-*H*), 7.67 (s, 1H, C=C-*H*), 7.68 (s, 1H, C=C-*H*), 9.06 (s, 1H, N_2-C-*H*); 13C (100 MHz, d_6-DMSO) δ: 20.8, 35.6, 123.4, 126.3, 128.1, 137.7, 145.8.

6.5.7 Synthesis of *N*,*N*-dimethyl-dihydroimidazole: 1c

The synthesis was adapted from a procedure reported by Lieder *et al*.[9] NaH (99 wt%, 2.35 g, 97.5 mmol) was weighed in a glovebox into a 250 mL round bottom flask fitted with a septum and a stir bar and was suspended in THF (50 mL). The suspension was cooled in an ice bath and $B(OMe)_3$ (10.7 mL 112 mmol) was added dropwise via syringe. *Caution, the action of $B(OMe)_3$ on NaH is exothermic.* The suspension was allowed to warm slowly to room temperature, then heated to 70 ºC for 15 min and cooled back to room temperature. *N*,*N*-dimethyl-imidazolium

tosylate (7.0 g, 26 mmol) was weighed into a 250 mL round bottom flask fitted with a septum and a stir bar and was suspended in THF (25 mL). The borohydride solution was transferred via cannula into the imidazolium solution. The reaction mixture was stirred overnight at room temperature and then heated to 70 ºC for 4 h. The solution was cooled to 0 ºC and was concentrated to 25 % of the original volume, under vacuum. The volatiles of the residue were vacuum transferred to a 50 mL round bottom flask. The product (105 – 110 ºC) was collected by fractional distillation at atmospheric temperature. A THF fraction from 65 – 80 ºC and a yellow fraction from 80 - 105 ºC were discarded. The product was stored at -25 ºC in the glovebox. The collected spectra were consistent with literature reports.[9] Yield: 300 mg (10 %) contaminated with trace amounts of THF. ^{1}H NMR (500 MHz, C_6D_6) δ: 2.17 (s, 6H, N-C*H*$_3$), 3.59 (s, 2H, N_2-C*H*$_2$), 5.26 (s, 2H, C=C*H*); ^{13}C NMR (125 MHz, C_6D_6) δ: 40.4, 81.8, 122.9.

6.5.8 Synthesis of hexahydrotriazaphenalene tetrafluoroborate

The synthesis was adapted from a procedure reported by Weisman *et al.*[25] 1,5,7-triazabicyclo[4.4.0]dec-5-ene (4.0 g, 28.7 mmol) was weighed into a 250 mL round bottom flask fitted with a septum and a stir bar and was dissolved in THF (30 mL). The solution was cooled to 0 ºC with an ice bath. NaH (99 wt%, 775 mg, 32.3 mmol) weighed in a glovebox into a 50 mL round bottom flask and suspended in THF (25 mL). The NaH suspension was transferred via cannula into the above solution and the mixture was allowed to stir for 15 min after which 1,3-dibromopropane (2.9 mL, 28.2 mmol) was added dropwise via syringe. The reaction mixture was allowed to stir overnight after which EtOH (2 mL) was added slowly to quench the excess NaH. The hygroscopic precipitate was recovered by filtration and was dissolved in saturated $NaBF_4$ (50 mL) and extracted with CH_2Cl_2. The organic layer was dried with $MgSO_4$ and solvent was removed under vacuum. Yield: 4.4 g (40 %) of crude material which was approximately 90 %

pure, the main contaminant was residual 1,5,7-triazabicyclo[4.4.0]dec-5-ene and this material was used without further purification. ^{1}H NMR (500 MHz, $CDCl_3$) δ: 2.09 (p, 6H, $^{3}J_{H\text{-}H}$ = 8 Hz, $CH_2CH_2CH_2$), 3.38 (t, 12H, $^{3}J_{H\text{-}H}$ = 8 Hz, $CH_2CH_2CH_2$); ^{11}B NMR (160 MHz, $CDCl_3$) δ: -1.25 (s, BF_4).

6.5.9 Synthesis of perhydrotriazaphenalene: 1d

The synthesis was adapted from a procedure reported by Weisman *et al*.[25] Hexahydrotriazaphenalene tetrafluoroborate (4.40 g, 11.2 mmol) was weighed into a 250 mL round bottom flask and suspended in THF (50 mL). The suspension was cooled to 0 ºC with an ice bath. $LiAlH_4$ (1.0 M in THF, 33.5 mL 33.5 mmol) was added dropwise via syringe. The reaction mixture was stirred at 0 ºC for 3 h then was allowed to warm slowly to room temperature and was stirred for 2 h. The reaction was quenched by the slow addition of hexanes, Et_2O, EtOH and H_2O, *caution, of potential exotherm.* The precipitates were filtered and the product was extracted with CH_2Cl_2. The organic layer was dried with $MgSO_4$ and the solvent was removed under reduced pressure. The residue was purified by sublimation under static vacuum at 45 ºC. The collected spectra were consistent with literature reports.[25] Yield: 500 mg (25 %). ^{1}H NMR (300 MHz, CD_2Cl_2) δ: 1.44 (dt, 3H, $^{3}J_{H\text{-}H}$ = 8 Hz, $^{3}J_{H\text{-}H}$ = 2 Hz), 1.93 (m, 3H), 2.13 (t, 6H, $^{3}J_{H\text{-}H}$ = 8 Hz), 2.26 (s, 1H), 2.80 (d, 2H, $^{3}J_{H\text{-}H}$ = 8 Hz).

6.5.10 Reaction of 1a with $B(C_6F_5)_3$, in situ formation of 2a

$B(C_6F_5)_3$ (20 mg, 0.04 mmol) was weighed in a glovebox, dissolved in CD_2Cl_2 (0.25 mL) and was added to a solution of *N*,*N*-ditertbutyl-dihydroimidazole **1a** (7 mg, 0.04 mmol) in CD_2Cl_2 (0.25 mL) in a 1 dram vial. The reaction mixture was transferred to an NMR tube and was characterized by multi-nuclear NMR. The collected spectra were consistent with literature reports[37] and the formation of **2a**, (recall that **1a** was contaminated with trace quantities of THF).

^{1}H (500 MHz, CD_2Cl_2) δ: 1.68 (s, 18H, C(CH_3)$_3$), 3.53 (br q, 1H, $^{1}J_{B\text{-}H}$ = 86 Hz, B-*H*), 7.48 (s, 2H, C=C-*H*), 8.18 (s, 1H, N_2-C*H*); ^{13}C (100 MHz, CD_2Cl_2) δ: 29.8, 120.9, 124.9 (br, *C*-B), 129.4, 136.9 (dm, $^{1}J_{C\text{-}F}$ = 247 Hz, *C*-F), 138.4 (dm, $^{1}J_{C\text{-}F}$ = 247 Hz, *C*-F), 148.4 (dm, $^{1}J_{C\text{-}F}$ = 237 Hz, *C*-F). 19F (376 MHz, CD_2Cl_2) δ: -134.1 (br s, ortho-C_6F_5), -164.9 (br s, para-C_6F_5), -167.8 (br s, ortho-C_6F_5); ^{11}B (160 MHz, CD_2Cl_2) δ: -26.7 (br d, $^{1}J_{B\text{-}H}$ = 85 Hz, *B*-H).

6.5.11 Reaction of 1b with $B(C_6F_5)_3$, synthesis of 2b

$B(C_6F_5)_3$ (100 mg, 0.18 mmol) was dissolved in CH_2Cl_2 (2 mL) and was added slowly to a solution of *N*,*N*-dimethyl dihydrobenzimidazole **1b** (26 mg, 0.18 mmol) dissolved in CH_2Cl_2 in a 4 dram vial. The reaction mixture was allowed to stand for 30 min at room temperature. Hexane was added to the reaction mixture and the precipitate was isolated by filtration and dried in vacuum. Yield: 70 mg (55 %). ^{1}H (500 MHz, CD_2Cl_2) δ: 3.53 (br q, 1H, $^{1}J_{B\text{-}H}$ = 86 Hz, B-*H*), 4.13 (s, 6H, N-CH_3), 7.80 (a s, 4H, Ar-*H*), 8.76 (s, 1H, N_2-C*H*); ^{13}C (125 MHz, CD_2Cl_2) δ: 34.0, 113.2, 124.2 (br, *C*-B), 125.2, 132.2, 136.9 (dm, $^{1}J_{C\text{-}F}$ = 227 Hz, *C*-F), 138.2 (dm, $^{1}J_{C\text{-}F}$ = 242 Hz, *C*-F), 140.1, 148.5 (dm, $^{1}J_{C\text{-}F}$ = 234 Hz, *C*-F); ^{19}F (376 MHz, CD_2Cl_2) δ: -134.7 (br s, ortho-C_6F_5), -164.5 (br s, para-C_6F_5), -167.7 (br s, ortho-C_6F_5); ^{11}B (160 MHz, CD_2Cl_2) δ: -25.3 (d, $^{1}J_{B\text{-}H}$ = 85 Hz, *B*-H).

6.5.12 Reaction of 1b with 1 to 4 equivalents of $B(C_6F_5)_3$

$B(C_6F_5)_3$ (0.07 – 0.028 mmol) was dissolved in CD_2Cl_2 (0.2 mL) and was added slowly to a solution of *N*,*N*-dimethyl dihydrobenzimidazole **1b** (10 mg, 0.07 mmol) dissolved in CD_2Cl_2 (0.2 mL). The reaction mixtures were transferred to a J-Young NMR tube and analyzed by VT-multinuclear NMR methods, see **Figure D-13** in **Appendix D** for spectral overlays.

6.5.13 Reaction of 1c with $B(C_6F_5)_3$

$B(C_6F_5)_3$ (25 mg, 0.05 mmol) was weighed in a glovebox, dissolved in CD_2Cl_2 (0.25 mL) and was added to a solution of *N*,*N*-dimethyl-dihydroimidazole **1c** (5 mg, 0.05 mmol) in CD_2Cl_2 (0.25 mL) in a 1 dram vial. The reaction mixture was transferred to a J-Young NMR tube and was characterized by ^{11}B NMR. Hydride transfer was observed and is reported as a percentage of the total area. ^{11}B (160 MHz, CD_2Cl_2) δ: -25.2 (d, $^{1}J_{B\text{-}H}$ = 85 Hz, *B*-H, 76 %), -13.2 (br s, unknown, 20 %), -2.9 (br s, unknown, 4 %).

6.5.14 Reaction of 1d with $B(C_6F_5)_3$

$B(C_6F_5)_3$ (15 mg, 0.03 mmol) was weighed in a glovebox, dissolved in CD_2Cl_2 (0.25 mL) and was added to a solution of *N*,*N*-dimethyl-dihydroimidazole **1c** (5 mg, 0.03 mmol) in CD_2Cl_2 (0.25 mL) in a 1 dram vial. The reaction mixture was transferred to a J-Young NMR tube and was characterized by ^{11}B NMR. Hydride transfer was observed and is reported as a percentage of the total area. ^{11}B (160 MHz, CD_2Cl_2) δ: -25.2 (d, $^{1}J_{B\text{-}H}$ = 85 Hz, *B*-H, 77 %), -13.3 (br s, unknown, 12 %), -12.2 (br s, unknown, 11 %).

6.5.15 Synthesis of $B(SC_6H_5)_3$

Neat BBr_3 (2.65 g, 10.5 mmol) was weighed in a glovebox and transferred into a 50 mL Schlenk flask fitted with a septum and a stir bar and was dissolved in dry toluene (15 mL). The Schlenk flask was removed from the glovebox, cooled to 0 ºC with an ice bath and flushed with argon. Benzenethiol (3.00 mL, 31.7 mmol), *caution of mercaptan odor*, was added to the BBr_3 solution dropwise via syringe. The solution was allowed to stir at 0 ºC for 10 min after which the septum was replaced by a glass stopper. The solution was slowly warmed to 100 ºC and stirred for 18 h. The solvent was removed under vacuum and the residue was transferred to a glovebox. The residue was then dissolved in a minimum volume of toluene and CH_2Cl_2 and crystallized at room

temperature by layering an equivalent volume of pentane. The crystals were collected by filtration, washed with pentane and dried under vacuum. *Caution, the material has a mercaptan odor when exposed to air.* The collected spectra were consistent with literature reports.[34] Yield: 1.90 g (50 %). ^{1}H (500 MHz, CD_2Cl_2) δ: 7.38 (ov, m, 3H, $SC_6\mathit{H}_5$), 7.51 (m, 2H, $SC_6\mathit{H}_5$); ^{13}C (125 MHz, CD_2Cl_2) δ: 128.9, 129.5, 129.7, 135.2; ^{11}B (160 MHz, CD_2Cl_2) δ: 62.0 (br s, $S_3\mathit{B}$).

6.5.16 General Procedure for redistribution of $B(SPh)_3$ with 1a or 1b at room temperature in CH_2Cl_2

$B(SPh)_3$ (12 mg, 0.04 mmol) was weighed in a glovebox, dissolved in CD_2Cl_2 (0.25 mL) and was added to a solution of *N,N*-ditertbutyl-dihydroimidazole **1a** (20 mg, 0.12 mmol) or *N,N*-dimethyl-dihydroimidazole **1b** (16 mg, 0.012 mmol) in CD_2Cl_2 (0.25 mL) in a 1 dram vial. The reaction mixture was transferred to a J-Young NMR tube and was monitored periodically by ^{11}B NMR; see **Figure 6-1** and see **Figure D-1** in **Appendix D** for spectral overlays of reaction with **1a** and **1b** respectively. The observed boron species are also reported alongside their percentage of total area. Redistribution with **1a** after 1 h at room temperature resulted in the following spectra ^{11}B (160 MHz, CD_2Cl_2) δ: -4.7 (br d, $^{1}J_{B\text{-}H}$ = 118, $[HB(SPh)_3]^-$, 59 %), 4.1 (s, $[B(SPh)_4]^-$, 41 %); after 2 days at room temperature (160 MHz, CD_2Cl_2) δ -4.7 (br d, $^{1}J_{B\text{-}H}$ = 118, $[HB(SPh)_3]^-$, 86 %), 4.1 (s, $[B(SPh)_4]^-$, 9 %), 69.3 (br s, unknown, 5 %). Redistribution with **1b** after 1 h at room temperature ^{11}B (160 MHz, CD_2Cl_2) δ: -4.8 (br d, $^{1}J_{B\text{-}H}$ = 118, $[HB(SPh)_3]^-$, 98 %), 4.0 (s, $[B(SPh)_4]^-$, 2 %).

6.5.17 Synthesis of 4a and 5a

$B(SPh)_3$ (50 mg, 0.15 mmol) was weighed in a glovebox, dissolved in trifluorotoluene (1.5 mL) and was added drop wise, in the dark, to a solution of **1a** (50 mg, 0.27 mmol) in trifluorotoluene (1.5 mL) in a 1 dram vial at room temperature. The reaction mixture was allowed to stand

overnight at room temperature, then NEt_3 (0.4 mL) was layered on top of the solution. The solution stood again overnight during which time crystals formed. The product **4a** was recovered by filtration and washed with trifluorotoluene. Yield: 50 mg (65 %). Anal. Calcd. for **4a** $C_{29}H_{37}BN_2S_3$: C, 66.90 %; H, 7.16 %; N, 5.38 %; S, 18.48 %. Found C, 66.62 %; H, 6.91 %; N, 5.42 %; S, 18.16 %. ^{1}H (500 MHz, CD_2Cl_2, 298 K) δ: 1.59 (s, 18 H, C(C*H*$_3$)$_3$), 4.49 (br q, 1H, $^1J_{B\text{-}H}$ = 118 Hz, B-*H*), 6.92 (t, 3H, $^3J_{H\text{-}H}$ = 8 Hz, para-SC$_6$*H*$_5$), 7.10, (t, 6H, $^3J_{H\text{-}H}$ = 8 Hz, para-SC$_6$*H*$_5$), 7.38 (s, 2H, C=C-*H*), 7.50 (d, 3H, $^3J_{H\text{-}H}$ = 8 Hz, para-SC$_6$*H*$_5$), 8.33 (s, 1H, N$_2$-C*H*); ^{13}C (125 MHz, CD_2Cl_2, 298 K) δ: 30.1, 61.2, 121.2, 122.7, 128.1, 129.4, 130.1, 144.0; ^{11}B (160 MHz, CD_2Cl_2, 298 K) δ: -5.0 (br d, $^1J_{B\text{-}H}$ = 118 Hz, S$_3$*B*-H). The product **5a** crystallized from the filtrate, which was stored at -25 ˚C. X-ray quality crystals of **5a** were grown from a trifluorotoluene / NEt_3 solvent mixture at -25 ˚C. Yield: 10 mg (5 %). ^{1}H (500 MHz, CD_2Cl_2, 298 K) δ: 1.60 (s, 18 H, C(C*H*$_3$)$_3$), 7.00 (t, 3H, $^3J_{H\text{-}H}$ = 8 Hz, para-SC$_6$*H*$_5$), 7.12, (t, 6H, $^3J_{H\text{-}H}$ = 8 Hz, para-SC$_6$*H*$_5$), 7.32 (s, 2H, C=C-*H*), 7.68 (d, 3H, $^3J_{H\text{-}H}$ = 8 Hz, para-SC$_6$*H*$_5$), 8.30 (s, 1H, N$_2$-C*H*); ^{13}C (125 MHz, CD_2Cl_2, 298 K) δ: 30.1, 61.2, 121.0, 124.1, 127.7, 129.6, 133.2, 141.0; ^{11}B (160 MHz, CD_2Cl_2, 298 K) δ: -4.1 (s, S$_4$*B*).

6.5.18 Procedures for redistribution with salt 4a

Method A

4a (9 mg, 0.02 mmol) was weighed in a glovebox, dissolved in CD_2Cl_2 (0.4 mL) and added to a J-Young tube. The solution was heated at 50 ºC for 18 h and monitored periodically by ^{11}B NMR; see **Figure 6-3** for spectral overlay. The observed boron species are also reported alongside their percentage of total area. After 50 ºC for 30 min resulted in the following spectra ^{11}B NMR (160 MHz, CD_2Cl_2) δ: -15.6 (br t, $^1J_{B\text{-}H}$ = 106 Hz, $[H_2B(SPh)_2]^-$, 3 %), 4.5 (br d, $^1J_{B\text{-}H}$ = 118, $[HB(SPh)_3]^-$, 89 %), 61.0 (br s, $B(SPh)_3$, 8 %); after 10 h ^{11}B NMR (160 MHz, CD_2Cl_2) δ: 2.3 (d,

$^{1}J_{B\text{-}H}$ = 114 Hz, unknown, 35 %), 2.9 (d, $^{1}J_{B\text{-}H}$ = 114 Hz, unknown, 35 %), 61.8 (br s, $B(SPh)_3$, 31 %).

Method B

Similar to Method A with the following exception, NEt_3 (100 mg, 1.00 mmol) was added to the reaction mixture. After 50 ºC for 18 h resulted in the following spectra ^{11}B NMR (160 MHz, CD_2Cl_2) δ: -7.5 (br t, $^{1}J_{B\text{-}H}$ = 110, $H_2B(NEt_3)(SPh)$, 31 %), 3.8 (s, $[B(SPh)_4]^-$, 15 %), 5.4 (ov d, $HB(NEt)_3(SPh)_2$, 54 %).

Method C

Similar to Method A with the following exception, **1a** (12 mg, 0.08 mmol) was added to the reaction mixture. After 50 ºC for 18 h resulted in the following spectra ^{11}B NMR (160 MHz, CD_2Cl_2) δ: -7.1 (br t, $^{1}J_{B\text{-}H}$ = 110, $H_2B(NEt_3)(SPh)$, 97 %), 4.6 (ov, $HB(NEt)_3(SPh)_2$ and $[B(SPh)_4]^-$, 3 %).

Method D

4a (9 mg, 0.02 mmol) was weighed in a glovebox, dissolved in CD_2Cl_2 (0.2 mL) and added to a solution of $B(SPh)_3$ (12 mg, 0.04 mmol) in CD_2Cl_2 (0.2 mL) in a 1 dram vial. The solution was transferred to a J-Young tube and monitored periodically by ^{11}B NMR; see **Figure D-10** in **Appendix D** for a spectral overlay.

6.5.19 General Procedure for Redistribution of $B(SPh)_3$ with 1a at 50 ºC and 80 ºC in 1:1 THF:CH_2Cl_2

Method A

In a typical procedure $B(SPh)_3$ (11 mg, 0.03 mmol) was weighed in a glovebox, dissolved in CH_2Cl_2 (0.25 mL) and was added to a solution of *N*,*N*-ditertbutyl-dihydroimidazole **1a** (20 mg, 0.10 mmol) and NEt_3 (100 mg, 1.0 mmol) in THF (0.25 mL) in a 1 dram vial. The reaction

mixture was transferred to a J-Young NMR tube and allowed to stand at room temperature for 1 h prior to heating at either 50 ºC or 80 ºC for the indicated periods of time. The solution was monitored periodically by ^{11}B NMR; see **Figure 6-4** for spectral overlay. The observed boron species are also reported alongside their percentage of total area. Redistribution with **1a** at room temperature for 1 h resulted in the following spectra ^{11}B (160 MHz, 1:1 THF:CH_2Cl_2) δ: -7.0 (br t, $^1J_{B\text{-}H}$ = 110 Hz, $H_2B(NEt_3)(SPh)$, 9 %), -4.7 (br d, $^1J_{B\text{-}H}$ = 116 Hz, $[HB(SPh)_3]^-$, 22 %), 4.3 (ov s, $[B(SPh)_4]^-$, 54 %), 4.9 (ov d, $HB(NEt_3)(SPh)_2$, 15 %); at 50 ºC for 18 h ^{11}B (160 MHz, 1:1 THF:CH_2Cl_2) δ: -7.0 (br t, $^1J_{B\text{-}H}$ = 110 Hz, $H_2B(NEt_3)(SPh)$, 97 %), -4.7 (ov, $HB(NEt_3)(SPh)_2$ and $[B(SPh)_4]^-$, 3 %); at 80 ºC for 18 h δ: 18.6 (br d, $^1J_{B\text{-}H}$ = 150 Hz, unknown).

Method B

Similar to Method A with the following exceptions, 1-octene (112 mg, 1.0 mmol) was added to the solution of **1a** and NEt_3 prior to the addition of $B(SPh)_3$. The reaction mixture was heated in a J-Young NMR tube or was heated in a 1 dram vial equipped with a stir bar and a Teflon septum cap. Reactions carried out in a J-Young NMR tube were monitored periodically by ^{11}B NMR; see **Figure 6-5**, **Figure 6-6** and **Figure D-3** in **Appendix D** for spectral overlays. The observed boron species are also reported alongside their percentage of total area. Redistribution with **1a** at room temperature for 40 min resulted in the following spectra ^{11}B (160 MHz, 1:1 THF:CH_2Cl_2) δ -7.0 (br t, $^1J_{B\text{-}H}$ = 110 Hz, $H_2B(NEt_3)(SPh)$, 16 %), -4.7 (br d, $^1J_{B\text{-}H}$ = 116 Hz, $[HB(SPh)_3]^-$, 16 %), 4.3 (ov s, $[B(SPh)_4]^-$, 49 %), 4.9 (ov d, $HB(NEt_3)(SPh)_2$, 11 %), 62.0 (br s, $B(SPh)_3$, 8 %); at 80 ºC for 20 min ^{11}B (160 MHz, 1:1 THF:CH_2Cl_2) δ: -7.0 (br t, $^1J_{B\text{-}H}$ = 110 Hz, $H_2B(NEt_3)(SPh)$, 85 %), -5.0 (br d, $^1J_{B\text{-}H}$ = 116 Hz, $[HB(SPh)_3]^-$, 12 %), 4.3 (ov s, $[B(SPh)_4]^-$, 49 %), 86.5 (br s, $B(n\text{-octyl})_3$, 3 %); for 5 h ^{11}B (160 MHz, 1:1 THF:CH_2Cl_2) δ: -6.3 (br t, $^1J_{B\text{-}H}$ = 110 Hz, $H_2B(NEt_3)(SPh)$, 5

%), -4.5 (br d, $^{1}J_{B\text{-}H}$ = 116 Hz, $[HB(SPh)_3]^-$, 6 %), 40.0 (br d, $^{1}J_{B\text{-}H}$ = 116 Hz, unknown, 2 %), 86.5 (br s, $B(SPh)_3$, 87 %).

Oxidation Protocol

A freshly degassed solution of 1:1 2 M NaOH : 35 wt % H_2O_2 was prepared, 1.5 mL of which was added to the reaction mixtures that were heated at 80 ºC. The solutions were cooled in an ice bath, stirred for 6 h and extracted with CH_2Cl_2 (3 × 5 mL). The aqueous layer was acidified (pH ≈ 2) with 2 M HCl and further extracted with CH_2Cl_2 (3 × 5 mL). The combined organic layers were dried with $MgSO_4$ and 1,4-dimethoxybenzene (10 mg, 0.07 mmol) was added as an internal standard. The solution was then transferred to a 0.5 dram vial without further dilution and analyzed by GC-FID (Injection: Splitless, Inlet pressure: 25 psi, Temperature protocol: 40 ºC – 230 ºC at 20 ºC /min, then hold for 10 min) to measure 1-octanol content.

6.5.20 Calibration of GC-FID with 1-octanol

1-octanol (130 mg, 1.00 mmol) was weighed into a 5 mL volumetric flask diluted to the mark with CH_2Cl_2. In addition 1,4-dimethoxybenzene (DMB, 138 mg, 1.00 mmol) was weighed into a 5 mL volumetric flask and diluted to the 5 mL mark with CH_2Cl_2. In 100 µL portions the 1-octanol (A) and DMB stock solutions were dispensed into 1 dram vials to give the volumes noted (A:DMB 100 : 500 µL, 200 : 400 µL, 300 : 300 µL, 400 : 200 µL, 500 : 100 µL). A volume (0.10 mL) from each 1-octanol and DMB solution was transferred to a 0.5 dram vial and analyzed by GC-FID (Injection: Splitless, Inlet pressure: 25 psi, Temperature protocol: 40 ºC – 230 ºC at 20 ºC /min, then hold for 10 min) (**Table 6-2**).

Table 6-2. Summary of data from GC-FID calibration of 1-octanol

Analyte	Retention time, min	M	B	R^2
1-octanol	4.30	1.090	0.030	0.999

[a] Fitting equation y = mx + b where y = integration 1-octanol/integration DMB and x = mole ratio of 1-octanol/DMB. The retention time of DMB was 5.06 min

6.5.21 General Procedure for Redistribution of $B(SPh)_3$ with 2 equivalents 1a at 50 ºC and 80 ºC in 1:1 THF:CH_2Cl_2

In a typical procedure $B(SPh)_3$ (18 mg, 0.05 mmol) was weighed in a glovebox, dissolved in CH_2Cl_2 (0.25 mL) and was added to a solution of *N*,*N*-ditertbutyl-dihydroimidazole **1a** (22 mg, 0.12 mmol) and NEt_3 (100 mg, 1.0 mmol) in THF (0.25 mL) in a 1 dram vial. The reaction mixture was transferred to a J-Young NMR tube and allowed to stand at room temperature for 1 h prior to heating at either 50 ºC for 18 h. The reaction mixture was analyzed by ^{11}B NMR to ensure formation of $H_2B(NEt_3)(SPh)$ after which 1-octene (110 mg, 1.0 mmol) was added. The solution was then heated at 50 ºC or 80 ºC and monitored periodically by ^{11}B NMR; see **Figure 6-7** and **Figure 6-8** for spectral overlays.

6.5.22 Control reactions involving BH_3NEt_3

Method A

BH_3NEt_3 (7.5 mg, 0.066 mmol) was weighed in a glovebox, dissolved in CH_2Cl_2 (0.2 mL) and was added to a solution of NEt_3 (100 mg, 1.00 mmol) and 1-octene (112 mg, 1.00 mmol) in THF (0.2 mL) in a 1 dram vial. The reaction mixture was transferred to a J-Young NMR tube which was heated to 80 ºC and was monitored periodically by ^{11}B NMR; see **Figure D-4** in **Appendix D** for a spectral overlay.

Method B

Similar to Method A with the following exception, NEt_3 was omitted from the reaction mixture.

Method C

Similar to Method A with the following exception, 1-octene was omitted from the reaction mixture.

Method D

BH_3NEt_3 (25 mg, 0.22 mmol) was weighed in a glovebox, dissolved in CH_2Cl_2 (0.5 mL) and was added to a solution of 1-octene (224 mg, 2.00 mmol) in THF (0.5 mL) in a 1 dram vial fitted with a stir bar and a Teflon septum cap. After reaction the solution was subjected to the oxidation conditions described for the redistribution reaction of $B(SPh)_3$ with **1a**.

6.5.23 Control of 1a with 1-octene

N,*N*-ditertbutyl-dihydroimidazole **1a** (18 mg, 0.10 mmol) was weighed in a glovebox, dissolved in CH_2Cl_2 (0.25 mL) and was added to a solution of 1-octene (112 mg, 1.0 mmol) in THF (0.25 mL) in a 1 dram vial sealed with a Teflon cap and heated at 80 ºC for 18 h. After reaction the solution was subjected to the oxidation conditions described for the redistribution reaction of $B(SPh)_3$ with **1a**. 1-octanol was not observed by GC-FID (Injection: Splitless, Inlet pressure: 25 psi, Temperature protocol: 40 ºC – 230 ºC at 20 ºC /min, then hold for 10 min).

6.5.24 Control of $B(SPh)_3$ with NEt_3 and 1-octene

$B(SPh)_3$ (11 mg, 0.03 mmol) was weighed in a glovebox, dissolved in CH_2Cl_2 (0.25 mL) and was added to a solution of 1-octene (112 mg, 1.0 mmol) and NEt_3 (100 mg, 1.0 mmol) in THF (0.25 mL) in a 1 dram vial. The reaction mixture was transferred to a J-Young NMR tube and allowed to stand at room temperature for 1 h prior to heating at 80 ºC for 18 h. The solution was monitored by ^{11}B NMR; see **Figure D-5** in **Appendix D** for a spectral overlay.

6.5.25 Synthesis of *ortho*-$B(SC_6H_4CH_3)_3$

Neat BBr_3 (1.00 g, 4.0 mmol) was weighed in a glovebox and transferred into a 50 mL Schlenk flask fitted with a septum and a stir bar and dissolved in dry toluene (10 mL). The Schlenk flask was removed from the glovebox, cooled to 0 ºC with an ice bath and flushed with argon. *ortho*-Methylbenzenethiol (1.40 mL, 12.0 mmol), *caution mercaptan odour*, was added to the BBr_3 solution dropwise via syringe. The solution was allowed to stir at 0 ºC for 10 min after which the septum was replaced by a glass stopper. The solution was slowly warmed to 50 ºC and stirred at temperature for 2 days. After 2 days additional 2-methylbenzenethiol (0.23 mL, 2.0 mmol) was added and the solution was heated at 100 ºC for 3 days. The reaction was monitored by ^{11}B NMR periodically. The solvent was removed under vacuum and excess 2-methylbenzenethiol was removed by distillation. The residue was transferred to a glovebox and solidified on addition of pentane. The solid was collected and dried under vacuum. *Caution, the material has a mercaptan odour.* Yield: 450 mg (30 %). ^1H (500 MHz, CD_2Cl_2, 298 K) δ: 2.50 (s, 9H, $SC_6H_4CH_3$), 7.22 (t, 1H, $^3J_{H\text{-}H}$ = 7 Hz, $SC_6H_4CH_3$), 7.12, (ov m, 2H, $SC_6H_4CH_3$), 7.49 (d, 3H, $^3J_{H\text{-}H}$ = 7 Hz, $SC_6H_4CH_3$); ^{13}C (125 MHz, CD_2Cl_2, 298 K) δ: 21.5, 126.9, 129.3, 130.2, 131.0, 136.3, 142.2; ^{11}B (160 MHz, CD_2Cl_2, 298 K) δ: 61.3 (s, S_3B).

6.5.26 Redistribution of *ortho*-$B(SC_6H_4CH_3)_3$ with 1a at room temperature and 50 ºC in CD_2Cl_2

ortho-$B(SC_6H_4CH_3)_3$ (14 mg, 0.04 mmol) was weighed in a glovebox, dissolved in CD_2Cl_2 (0.25 mL) and was added to a solution of *N*,*N*-ditertbutyl-dihydroimidazole **1a** (20 mg, 0.12 mmol) and NEt_3 (100 mg, 1.0 mmol) in CD_2Cl_2 (0.25 mL) in a 1 dram vial. The reaction mixture was transferred to a J-Young NMR tube and allowed to stand at room temperature for 2 days prior to

heating at 50 ºC. The solution was monitored periodically by ^{11}B NMR; see **Figure D-7** in **Appendix D** for a spectral overlay.

6.5.27 Synthesis of $B(SC_6F_5)_3$

The synthesis was adapted from Naumann *et al*.[50] Pentafluorobenzenethiol (1.3 mL, 10 mmol) was added to a 50 mL Schlenk tube fitted with a septum and a stir bar. The thiol was dissolved in freshly distilled Et_2O (10 mL) and pentane (2 mL). The solution was cooled to -60 ºC with an isopropanol:H_2O dry ice bath and *n*-BuLi (2.5 M in hexanes, 4 mL, 10 mmol) was added slowly down the side of the flask. The solution was allowed to stir at temperature for 2 h. BF_3-OEt_2 (48 wt% solution in Et_2O, 0.80 mL, 3 mmol) was diluted in Et_2O (2 mL) and added to the thiolate solution slowly down the side of the flask. The septum was exchanged quickly for a glass stopper. The solution was allowed to warm to room temperature slowly over 6 h and the solvent was removed under vacuum. The glass stopper was exchanged for a coldfinger in a glovebox. The residue was heated to 120 ºC under vacuum to distill off excess pentafluorobenzenethiol which collected on the coldfinger. Subsequently, CH_2Cl_2 (20 mL) was added to the residue which was filtered in a glovebox and the solvent was removed under vacuum and the resulting powder was sublimed at 130 ºC under static vacuum. *Caution, the material has a mercaptan odour*. Yield: 650 mg (35 %). ^{13}C (125 MHz, CD_2Cl_2, 273 K) δ: 102.7, 138.5 (dm, $^1J_{C\text{-}F}$ = 255 Hz, *C*-F), 143.2 (dm, $^1J_{C\text{-}F}$ = 256 Hz, *C*-F), 147.4 (dm, $^1J_{C\text{-}F}$ = 248 Hz, *C*-F); ^{19}F (376 MHz, CD_2Cl_2, 298 K) δ: -131.1 (d, $^3J_{F\text{-}F}$ = 21 Hz, ortho-C_6F_5), -150.0 (t, $^3J_{F\text{-}F}$ = 21 Hz, meta-C_6F_5), -160.2 (t, $^3J_{F\text{-}F}$ = 21 Hz, para-C_6F_5); ^{11}B (160 MHz, CD_2Cl_2, 298 K) δ: 60.0 (br s, S_3B).

6.5.28 Redistribution of $B(SC_6F_5)_3$ with 1a at room temperature and 50 ºC in CD_2Cl_2

$B(SC_6F_5)_3$ (20 mg, 0.03 mmol) was weighed in a glovebox, dissolved in CD_2Cl_2 (0.25 mL) and was added to a solution of *N*,*N*-ditertbutyl-dihydroimidazole **1a** (18 mg, 0.10 mmol) and NEt_3

(100 mg, 1.0 mmol) in CD_2Cl_2 (0.25 mL) in a 1 dram vial. The reaction mixture was transferred to a J-Young NMR tube and allowed to stand at room temperature for 1 h prior to heating at 50 ºC for 18 h. The solution was monitored periodically by ^{11}B NMR; see **Figure D-8** in **Appendix D** for a spectral overlay.

6.5.29 Synthesis of $B(OC_6F_5)_3$

The synthesis was adapted from Naumann *et al*.[50] Neat BBr_3 (450 mg, 1.80 mmol) was weighed in a glovebox and transferred to a 50 mL Schlenk flask fitted with a septum and a stir bar and dissolved in dry CH_2Cl_2 (5 mL). Pentafluorophenol (1.00g, 5.43 mmol) was weighed into a 5 mL round bottom flask and dissolved in dry CH_2Cl_2 (2 mL). Both solutions were removed from the glovebox and purged with Ar. The Schlenk flask was cooled to -50 ºC with a DME dry ice bath. The pentafluorophenol solution was added to the BBr_3 solution slowly via syringe, and the round bottom flask was washed with CH_2Cl_2 (3 x 2 mL) to complete the transfer of the phenol. The reaction mixture was stirred at temperature for 4 h, and then slowly warmed to room temperature. The septum was replaced with a glass stopper and the solvent was removed under vacuum. In a glovebox the glass stopper was replaced with a cold finger and the residue was sublimed under static vacuum at 85 ºC. The collected spectra were consistent with literature reports.[50] Yield: 450 mg (45 %). ^{19}F (376 MHz, CD_2Cl_2, 298 K) δ: -157.4 (d, $^3J_{F\text{-}F}$ = 21 Hz, ortho-C_6F_5), -161.8 (t, $^3J_{F\text{-}F}$ = 21 Hz, meta-C_6F_5), -163.5 (t, $^3J_{F\text{-}F}$ = 21 Hz, para-C_6F_5); ^{11}B (160 MHz, CD_2Cl_2, 298 K) δ: 13.2 (br s, O_3B).

6.5.30 Redistribution of $B(OC_6F_5)_3$ with 1a at 50 ºC in CD_2Cl_2

$B(OC_6F_5)_3$ (10 mg, 0.018 mmol) was weighed in a glovebox, dissolved in CD_2Cl_2 (0.25 mL) and was added to a solution of *N*,*N*-ditertbutyl-dihydroimidazole **1a** (12 mg, 0.07 mmol) in CD_2Cl_2 (0.25 mL) in a 1 dram vial. The reaction mixture was transferred to a J-Young NMR tube and was

heated at 50 ºC. The solution was monitored periodically by ^{11}B NMR; see **Figure D-11** in **Appendix D** for a spectral overlay.

6.5.31 Redistribution of $B(OC_6F_5)_3$ with 1b at 50 ºC in CD_2Cl_2

Method A

$B(OC_6F_5)_3$ (15 mg, 0.025 mmol) was weighed in a glovebox, dissolved in CD_2Cl_2 (0.25 mL) and was added to a solution of *N*,*N*-dimethyl-dihydrobenzimidazole **1b** (12 mg, 0.08 mmol) in CD_2Cl_2 (0.25 mL) in a 1 dram vial. The reaction mixture was transferred to a J-Young NMR tube and was heated at 50 ºC. The solution was monitored periodically by ^{11}B NMR; see **Figure D-12** in **Appendix D** for a spectral overlay.

Method B

$B(OC_6F_5)_3$ (30 mg, 0.05 mmol) was weighed in a glovebox, dissolved in CD_2Cl_2 (0.25 mL) and was added to a solution of *N*,*N*-dimethyl-dihydroimidazole **1b** (6 mg, 0.04 mmol) and 1-octene (112 mg, 1.00 mmol) in CD_2Cl_2 (0.25 mL) in a 1 dram vial. The reaction mixture was transferred to a J-Young NMR tube and was heated at 50 ºC. The solution was monitored periodically by ^{11}B NMR; see **Figure 6-9** for a spectral overlay.

6.5.32 Redistribution of $B(SPh)_3$ with 1e

Method A

$B(SPh)_3$ (11 mg, 0.03 mmol) was weighed in a glovebox, dissolved in THF (0.25 mL) and was added to a solution of *N*-(dimethyl(phenyl)silyl)dihydropyridine **1e** (22 mg, 0.10 mmol) and NEt_3 (100 mg, 1.0 mmol) in THF (0.25 mL) in a 1 dram vial. The reaction mixture was transferred to a J-Young NMR tube and allowed to stand at room temperature for 1 h prior to heating at 50 ºC for the indicated period of time. The solution was monitored by ^{11}B NMR. The observed boron species are reported alongside their percentage of total area. After 18 h at 50 ºC ^{11}B (160 MHz,

THF) δ: 3.0 (br d, $^{1}J_{B\text{-}H}$ = 130 Hz, $HB(py)(SPh)_2$, 85 %), 4.3 (s, $[B(SPh)_4]^-$, 5 %), 9 (br s, unknown, 10 %).

Method B

$B(SPh)_3$ (11 mg, 0.03 mmol) was weighed in a glovebox, dissolved in C_6D_6 (0.25 mL) and was added to a solution of *N*-(dimethyl(phenyl)silyl)dihydropyridine **1e** (7 mg, 0.03 mmol) in C_6D_6 (0.25 mL) in a 1 dram vial. The reaction mixture was transferred to a J-Young NMR tube and allowed to stand at room temperature for 1 h prior to heating at 50 ºC for 5 days. The solution was monitored by ^{11}B NMR. The observed boron species are reported alongside their percentage of total area. After 5 days at 50 ºC ^{11}B (160 MHz, C_6D_6) δ: 3.1 (br d, $^{1}J_{B\text{-}H}$ = 130 Hz, $HB(py)(SPh)_2$, 93 %), 8.6 (br s, unknown, 3 %), 62.0 (br s, $B(SPh)_3$, 4 %).

6.5.33 Reaction of triethylamine with 4,4,5,5-tetramethyl-1,3,2-dioxaborolane (HBpin) and $B(C_6F_5)_3$

NEt_3 (5 mg, 0.05 mmol) was weighed in a glovebox, dissolved in CD_2Cl_2 (0.2 mL) and was added to HBpin (6 mg, 0.05 mmol) in CD_2Cl_2 (0.2 mL) in a 1 dram vial. After 15 min $B(C_6F_5)_3$ (25 mg, 0.05 mmol) was weighed, dissolved in CD_2Cl_2 (0.2 mL) and added to the above solution. The reaction was monitored periodically by ^{11}B NMR; see **Figure D-14** and **Figure D-15** in **Appendix D** for spectral overlays.

6.5.34 Reaction of 1,4-diazabicyclo[2.2.2]octane (Dabco) with HBpin and $B(C_6F_5)_3$

$B(C_6F_5)_3$ (30 mg, 0.06 mmol) was weighed in a glovebox, dissolved in CD_2Cl_2 (0.2 mL) and was added to Dabco (6 mg, 0.06 mmol) frozen in CD_2Cl_2 (0.2 mL) in an NMR tube. On addition of $B(C_6F_5)_3$, the solution became turbid and was frozen in a coldwell. HBpin (8 mg, 0.06 mmol) was weighed, dissolved in CD_2Cl_2 (0.2 mL) and layered on the frozen solution. The reaction mixture was warmed to room temperature and became homogeneous after 10 min with periodic shaking.

The solution was characterized by VT multi-nuclear NMR. ^{1}H (500 MHz, CD_2Cl_2, 298 K) δ: 1.40 (s, 12H, B*pin*), 3.21 (t, 6H, $^{3}J_{H\text{-}H}$ = 8 Hz, CH_2-CH_2), 3.29 (t, 6H, $^{3}J_{H\text{-}H}$ = 8 Hz, CH_2-CH_2), 3.55 (bro v q. $^{1}J_{B\text{-}H}$ = 88 Hz, B-*H*); ^{13}C (125 MHz, CD_2Cl_2, 273 K) δ: 24.4, 44.4, 46.4, 48.8, 90.6, 125.2 (br m, *C*-B), 136.8 (dm, $^{1}J_{C\text{-}F}$ = 245 Hz, *C*-F), 138.2 (dm, $^{1}J_{C\text{-}F}$ = 244 Hz, *C*-F), 148.5 (dm, $^{1}J_{C\text{-}F}$ = 239 Hz, *C*-F); ^{19}F (376 MHz, CD_2Cl_2, 298 K) δ: -134.5 (d, $^{3}J_{F\text{-}F}$ = 23 Hz, ortho-C_6F_5), -164.8 (t, $^{3}J_{F\text{-}F}$ = 23 Hz, para-C_6F_5), -167.9 (t, $^{3}J_{F\text{-}F}$ = 23 Hz, meta-C_6F_5); ^{11}B 160 MHz, CD_2Cl_2, 298 K) δ: -25 (br d, $^{1}J_{B\text{-}H}$ = 88 Hz, *B*-H) 25.6 (br s, N-*B*pin).

6.5.35 Synthesis of 1-(chloromethyl)-4-aza-1-azoniabicyclo[2.2.2]octane chloride: SelectCl

Dabco (200 mg, 1.80 mmol) was weighed into a 4 dram vial in a glovebox and was dissolved in CH_2Cl_2 (5 mL). The solution was allowed to stand at room temperature for 3 days. The solvent was removed and to the residue was added 95 % EtOH (2 mL). Et_2O was added until the solution became slightly turbid and the new precipitates were removed by filtration. The solvent was removed under reduced pressure and the resulting powder was dried under vacuum over P_2O_5. The collected spectra were consistent with literature reports.[63] Yield: 70 mg (40 %). ^{1}H (300 MHz, d_6-DMSO) δ: 3.10 (t, 6H, $^{3}J_{H\text{-}H}$ = 7 Hz, CH_2-CH_2), 3.49 (t, 6H, $^{3}J_{H\text{-}H}$ = 7 Hz, CH_2-CH_2), 5.55 (s, 2H, NCH_2Cl); ^{13}C (100 MHz, d_6-DMSO) δ: 44.4, 50.5, 67.4.

6.5.36 Synthesis of 1-(chloromethyl)-4-aza-1-azoniabicyclo[2.2.2]octane tetrafluoroborate: SelectBF$_4$

The synthesis was adapted from Banks *et al*.[63] Dabco (500 mg, 4.45 mmol) was weighed into a 4 dram vial fitted with a stir bar and Teflon cap in a glovebox and was dissolved in CH_2Cl_2 (10 mL). The solution was stirred at 40 ºC for 4 h and the solvent was removed under reduced pressure. The residue solidified under vacuum and was washed with CH_2Cl_2. The recovered material was placed in a 25 mL round bottom flask and was dissolved in acetonitrile (5 mL). A

stoichiometric amount of $NaBF_4$ (488 mg, 2.28 mmol) was added to the above solution which was stirred under an argon atmosphere overnight. The solution was filtered and the solvent was removed under vacuum. The residue was crystallized from 1:1 95 % EtOH:EtOAc. The crystals were collected by filtration and dried under vacuum over P_2O_5. The collected spectra were consistent with literature reports.[63] Yield: 100 mg (10 %). ^{1}H (300 MHz, d_6-DMSO) δ: 3.10 (t, 6H, $^3J_{H\text{-}H}$ = 7 Hz, CH_2-CH_2), 3.38 (t, 6H, $^3J_{H\text{-}H}$ = 7 Hz, CH_2-CH_2), 5.27 (s, 2H, NCH_2Cl); ^{13}C (100 MHz, d_6-DMSO) δ: 44.4, 50.8, 67.6.

6.5.37 Reaction of SelectCl and SelectBF_4 with HBpin and $B(C_6F_5)_3$

$B(C_6F_5)_3$ (40 mg, 0.08 mmol) was weighed in a glovebox, dissolved in CD_2Cl_2 (00.2 mL) and was added to SelectCl (8 mg, 0.04 mmol) or SelectBF_4 (12 mg, 0.04) dissolved in CD_2Cl_2 (0.2 mL) in a J-Young NMR tube. HBpin (25 mg, 0.20 mmol) was weighed, dissolved in CD_2Cl_2 (0.2 mL) and was added to the NMR tube. The reaction mixture was monitored periodically by ^{11}B NMR; see **Figure D-16** and **Figure D-17** in **Appendix D** for spectral overlays.

6.5.38 X-Ray Data Collection and Reduction

X-ray quality crystals of **5a** were grown from a trifluorotoluene / NEt_3 solvent mixture at -25 ˚C. Crystals were mounted on a glass fiber with grease and cooled to -93 °C in a stream of nitrogen gas controlled with Cryostream Controller 700. Data collection was performed on a Bruker SMART APEX II X-ray diffractometer. Data was processed using the Bruker AXS Crystal Structure Analysis Package.

6.5.39 Structure Solution and Refinement

Neutral atom scattering factors were taken from Cromer and Waber.[78] The heavy atom positions were determined using direct methods and all other non-hydrogen atoms were refined

anisotropically. The refinements were carried out by using full-matrix least squares techniques on F, minimizing the function $\omega(F_o-F_c)^2$. In the final cycles of each refinement, all non-hydrogen atoms were assigned anisotropic temperature factors in the absence of disorder or insufficient data. In the latter cases atoms were treated isotropically. H atoms were placed in geometrically calculated positions, with C-H = 0.95 (aromatic), 0.99 (CH_2) and 0.98 Å (CH_3), and refined as riding atoms. The H-atom contributions were calculated, but not refined. The locations of the largest peaks in the final difference Fourier map calculation as well as the magnitude of the residual electron densities in each case were of no chemical significance.

6.6 References

(1) Zhu, X.; Zhang, M.; Yu, A.; Wang, C.; Cheng, J. *J. Am. Chem. Soc.* **2008**, *130*, 2501-2516.

(2) Bachand, B.; Ramos, S. M.; Wuest, J. D. *J. Org. Chem.* **1987**, *52*, 5443-5446.

(3) Ramos, S. M.; Tarazi, M.; Wuest, J. D. *J. Org. Chem.* **1987**, *52*, 5437-5442.

(4) Erhardt, J. M.; Grover, E. R.; Wuest, J. D. *J. Am. Chem. Soc.* **1980**, *102*, 6365-6369.

(5) Focante, F.; Mercandelli, P.; Sironi, A.; Resconi, L. *Coord. Chem. Rev.* **2006**, *250*, 170-188.

(6) El'tsov, I. A. V.; Muravich-Aleksandr, K. L. *Zh. Org. Khim.* **1965**, *1*, 1307-14.

(7) Eltsov, A. V. *Zh. Org. Khim.* **1967**, *3*, 199-204.

(8) Schwarz, D. E.; Cameron, T. M.; Hay, P. J.; Scott, B. L.; Tumas, W.; Thorn, D. L. *Chem. Commun.* **2005**, 5919-5921.

(9) Schank, K.; Bouillon, G.; Fünfrocken, M.; Lick, C.; Lieder, R. *Helv. Chim. Acta* **2002**, *85*, 1295-1326.

(10) Korotkikh, M. I.; Rayenko, G. F.; Shvaika, O. P. *Dopov. Nats. Akad. Nauk Ukr.* **2001**, 130-133.

(11) Shi, Z.; Gu, H. *Synth. Commun.* **1996**, *26*, 4175-4178.

(12) Lee, I. H.; Jeoung, E. H.; Kreevoy, M. M. *J. Am. Chem. Soc.* **1997**, *119*, 2722-2728.

(13) Han Lee, I.; Jeoung, E. H.; Kreevoy, M. M. *J. Am. Chem. Soc.* **2001**, *123*, 7492-7496.

(14) Lee, I. H.; Ji, Y. R.; Jeoung, E. H. *J. Phys. Chem. C* **2006**, *110*, 3875-3881.

(15) Chikashita, H.; Ide, H.; Itoh, K. *J. Org. Chem.* **1986**, *51*, 5400-5405.

(16) Chen, J.; Tanner, D. D. *J. Org. Chem.* **1988**, *53*, 3897-3900.

(17) Chikashita, H.; Nishida, S.; Miyazaki, M.; Morita, Y.; Itoh, K. *Bull. Chem. Soc. Jpn.* **1987**, *60*, 737-46.

(18) Brunet, P.; Wuest, J. D. *J. Org. Chem.* **1996**, *61*, 2020-6.

(19) Montgrain, F.; Ramos, S. M.; Wuest, J. D. *J. Org. Chem.* **1988**, *53*, 1489-1492.

(20) Erhardt, J. M.; Wuest, J. D. *J. Am. Chem. Soc.* **1980**, *102*, 6363-6364.

(21) Brunet, P.; Wuest, J. D. *J. Org. Chem.* **1996**, *61*, 2020-2026.

(22) Weisman, G. R.; Johnson, V.; Fiala, R. E. *Tetrahedron Lett.* **1980**, *21*, 3635-8.

(23) Beddoes, R. L.; Edwards, W. D.; Joule, J. A.; Mills, O. S.; Street, J. D. *Tetrahedron* **1987**, *43*, 1903-20.

(24) Atkins, T. J. *J. Am. Chem. Soc.* **1980**, *102*, 6364-6365.

(25) Alder, R. W.; Mowlam, R. W.; Vachon, D. J.; Weisman, G. R. *J. Chem. Soc. Chem. Commun.* **1992**, 507-508.

(26) Long, N. J.; Parker, D. G.; Speyer, P. R.; White, A. J. P.; Williams, D. J. *J. Chem. Soc. Dalton Trans.* **2002**, 2142-2150.

(27) Ren.Yan-Wei; Guo, H.; Wang, C.; Liu, J.; Jiao, H.; Zhang, F. *Transition Met. Chem.* **2006**, *31*, 611-615.

(28) Neverov, A. A.; Liu, C. T.; Bunn, S. E.; Edwards, D.; White, C. J.; Melnychuk, S. A.; Brown, R. S. *J. Am. Chem. Soc.* **2008**, *130*, 6639-6649.

(29) Webb, J.; Laberge, V.; Geier, S.; Stephan, D.; Crudden, C. *Chem. Eur. J.* **2010**, *16*, 4895-4902.

(30) Di Saverio, A.; Focante, F.; Camurati, I.; Resconi, L.; Beringhelli, T.; D'Alfonso, G.; Donghi, D.; Maggioni, D.; Mercandelli, P.; Sironi, A. *Inorg. Chem.* **2005**, *44*, 5030-5041.

(31) Sumerin, V.; Schulz, F.; Nieger, M.; Leskelä, M.; Repo, T.; Rieger, B. *Angew. Chem. Int. Ed.* **2008**, *47*, 6001-6003.

(32) Piers, W. E. *Adv. Organomet. Chem.* **2005**, *52*, 1-76.

(33) Millot, N.; Santini, C. C.; Fenet, B.; Basset, J. M. *Eur. J. Inorg. Chem.* **2002**, *2002*, 3328-3335.

(34) Mock, M. T.; Potter, R. G.; Camaioni, D. M.; Li, J.; Dougherty, W. G.; Kassel, W. S.; Twamley, B.; DuBois, D. L. *J. Am. Chem. Soc.* **2009**, *131*, 14454-14465.

(35) Holschumacher, D.; Bannenberg, T.; Hrib, C.; Jones, P.; Tamm, M. *Angew. Chem. Int. Ed.* **2008**, *47*, 7428-7432.

(36) Chase, P. A.; Stephan, D. W. *Angew. Chem. Int. Ed.* **2008**, *47*, 7433-7437.

(37) Chase, P. A.; Gille, A. L.; Gilbert, T. M.; Stephan, D. W. *Dalton Trans.* **2009**, 7179-7188.

(38) Liu, Y.; Lindner, P. E.; Lemal, D. M. *J. Am. Chem. Soc.* **1999**, *121*, 10626-10627.

(39) Schaub, T.; Backes, M.; Radius, U. *Organometallics* **2006**, *25*, 4196-4206.

(40) DuBois, D. L.; Blake, D. M.; Miedaner, A.; Curtis, C. J.; DuBois, M. R.; Franz, J. A.; Linehan, J. C. *Organometallics* **2006**, *25*, 4414-4419.

(41) Sulzer-Mossé, S.; Alexakis, A.; Mareda, J.; Bollot, G.; Bernardinelli, G.; Filinchuk, Y. *Chem. Eur. J.* **2009**, *15*, 3204-3220.

(42) Screttas, C. G.; Micha-Screttas, M. *J. Org. Chem.* **1979**, *44*, 713-719.

(43) Ono, N.; Miyake, H.; Saito, T.; Kaji, A. *Synthesis* **1980**, 952-953.

(44) Zaidlewicz, M.; Kanth, J. V. B.; Brown, H. C. *J. Org. Chem.* **2000**, *65*, 6697-6702.

(45) Cragg, R. H.; Husband, J. P. N.; Weston, A. F. *J. Inorg. Nucl. Chem.* **1973**, *35*, 3685-3689.

(46) Vahrenkamp, H. *J. Organomet. Chem.* **1971**, *28*, 167-179.

(47) Pasto, D. J.; Cumbo, C. C.; Balasubramaniyan, P. *J. Am. Chem. Soc.* **1966**, *88*, 2187-2194.

(48) Kanth, J. V. B.; Brown, H. C. *Inorg. Chem.* **2000**, *39*, 1795-1802.

(49) Narayana, C.; Periasamy, M. *J. Organomet. Chem.* **1987**, *323*, 145-147.

(50) Naumann, D.; Butler, H.; Gnann, R. *Z. anorg. allg. Chem.* **1992**, *618*, 74-76.

(51) Gutsulyak, D. V.; van der Est, A.; Nikonov, G. I. *Angew. Chem. Int. Ed.* **2011**, *50*, 1384-1387.

(52) Neu, R. C.; Ouyang, E. Y.; Geier, S. J.; Zhao, X.; Ramos, A.; Stephan, D. W. *Dalton Trans.* **2010**, *39*, 4285-4294.

(53) Hausdorf, S.; Baitalow, F.; Wolf, G.; Mertens, F. O. R. L. *Int. J. Hydrogen Energy* **2008**, *33*, 608-614.

(54) Mikhailov, B. M. *Russ. Chem. Rev.* **1968**, *37*, 935-953.

(55) Hughes, R. L.; Smith, I. C.; Lawless, E. W. *Production of the Boranes and Related Research;* Academic Press, **1967**, New York.

(56) Dureen, M. A.; Lough, A.; Gilbert, T. M.; Stephan, D. W. *Chem. Commun.* **2008**, 4303-4305.

(57) Westcott, S. A.; Blom, H. P.; Marder, T. B.; Baker, R. T.; Calabrese, J. C. *Inorg. Chem.* **1993**, *32*, 2175-2182.

(58) Lata, C. J.; Crudden, C. M. *J. Am. Chem. Soc.* **2010**, *132*, 131-137.

(59) Del Grosso, A.; Singleton, P. J.; Muryn, C. A.; Ingleson, M. J. *Angew. Chem. Int. Ed.* **2011**, *50*, 2102-2106.

(60) Nöth, H. *Prog. Boron Chem.* **1970**, *3*, 211-311.

(61) Van Paasschen, J. M.; Geanangel, R. A. *Can. J. Chem.* **1975**, *53*, 723-726.

(62) Pruckmayr, G.; Dreyfuss, P.; Dreyfuss, M. P. *Polyethers, Tetrahydrofuran and Oxetane Polymers;* John Wiley & Sons, Inc, **1996**, New York.

(63) Banks, R. E.; Besheesh, M. K.; Mohialdin-Khaffaf, S.; Sharif, I. *J. Fluorine Chem.* **1996**, *78*, 43-50.

(64) Bettinger, H.; Filthaus, M.; Bornemann, H.; Oppel, I. *Angew. Chem. Int. Ed.* **2008**, *47*, 4744-4747.

(65) Blackwell, J. M.; Morrison, D. J.; Piers, W. E. *Tetrahedron* **2002**, *58*, 8247-8254.

(66) Mkhalid, I. A. I.; Barnard, J. H.; Marder, T. B.; Murphy, J. M.; Hartwig, J. F. *Chem. Rev.* **2010**, *110*, 890-931.

(67) Davis, B. L.; Dixon, D. A.; Garner, E. B.; Gordon, J. C.; Matus, M. H.; Scott, B.; Stephens, F. H. *Angew. Chem. Int. Ed.* **2009**, *48*, 6812-6816.

(68) Sutton, A. D.; Davis, B. L.; Bhattacharyya, K. X.; Ellis, B. D.; Gordon, J. C.; Power, P. P. *Chem. Commun.* **2010**, *46*, 148-149.

(69) Yu, Z.; Verkade, J. G. *Phosphorus, Sulfur Silicon Relat. Elem.* **1998**, *133*, 79-82.

(70) Shaw, A. P.; Ryland, B. L.; Franklin, M. J.; Norton, J. R.; Chen, J. Y. C.; Hall, M. L. *J. Org. Chem.* **2008**, *73*, 9668-9674.

(71) Osakada, K. *Angew. Chem. Int. Ed.* **2011**, *50*, 3845-3846.

(72) Cook, N. C.; Lyons, J. E. *J. Am. Chem. Soc.* **1966**, *88*, 3396-403.

(73) Cook, N. C.; Lyons, J. E. *J. Am. Chem. Soc.* **1965**, *87*, 3283-4.

(74) Sutton, A. D.; Burrell, A. K.; Dixon, D. A.; Garner, E. B.; Gordon, J. C.; Nakagawa, T.; Ott, K. C.; Robinson, J. P.; Vasiliu, M. *Science* **2011**, *331*, 1426-1429.

(75) Ott, K.; Linehan, S.; Lipiecki, F.; Aradahl, C. L. *Down Select Report of Chemical Hydrogen Storage Materials, Catalysts, and Spent Fuel Regeneration Processes* [https://www1.eere.energy.gov/hydrogenandfuelcells/pdfs/chs_coe_down_select.pdf] Retrieved: 05/30/2011.

(76) Herrmann, W. A.; Böhm, V. P. W.; Gstöttmayr, C. W. K.; Grosche, M.; Reisinger, C.; Weskamp, T. *J. Organomet. Chem.* **2001**, *617-618*, 616-628.

(77) Miyashita, A.; Matsuda, H.; Higashino, T. *Chem. Pharm. Bull.* **1990**, *38*, 1147-1152.

(78) Cromer, D. T.; Waber, J. T. In *International Tables for X-ray. Crystallography;* International Tables for X-ray Crystallography; Kynoch Press: Burningham, UK, 1974; Vol. 4, pp Table 2.2 A.

Chapter 7

Conclusions and Future Work

This thesis was divided into two parts. Part A of this thesis described applications of mesoporous silicas and Part B described the initial stages of the development of an organic hydride based regeneration scheme for the promising hydrogen storage material ammonia borane (NH_3BH_3). The first research chapter in Part A of this thesis was Chapter 2 where we outlined a procedure to selectively graft functionality on to the mesopores of SBA-15 and MCM-41. The selective grafting strategy employed was pore protection passivation. This approach uses the structure directing agent contained within the pores of as-synthesized materials to protect silanols on that domain from being passivated while those on the external surface are capped with TMS groups. Once the external surface is capped, the mesopores can be functionalized using conventional post-synthesis grafting methods. Based on our analysis of literature selective grafting protocols it was found that loading additional P123 into the pores of as-SBA-15 was necessary to protect the mesostructure from unwanted silylation during passivation. The second part of the chapter described our efforts towards the development of a test for selective grafting that could easily evaluate a bulk amount of material. Of the different schemes that were evaluated the most informative results were obtained from a FloDot adsorption test. It was found that FloDots, large fluorescent silica nanospheres, adsorbed more strongly onto hydrophilic surfaces than hydrophobic ones. This property was used to demonstrate that passivation layers formed on the external surface of SBA-15 and MCM-41.

Future work on this project should focus on developing a test to look at the localization of functionality on selective grafted materials. In that vein, a selective grafting test based on

analyzing pyrene quenching on differently functionalized materials as a function of adsorption of large gold nanoparticles was proposed. Once selective grafting is definitively established the research project should shift focus and start to critically assess the role of mesopores in catalysis namely, whether or not they can influence the enantioselectivity and regioselectivity of reactions. These effects have been postulated by other research groups but not rigorously tested. Another emerging application of selective grafted materials may be to see whether these mesoporous silicas can serve as improved nanoreactors for polymerization reactions, this is an application being explored by fellow graduate student Tomohiro Seki.

Chapter 3 described the study of the immobilized Suzuki-Miyaura catalyst Pd-SBA-15-SH(g). The material was low leaching (<1 ppm Pd) and recyclable, up to 4 times and it was found to be more active and recyclable than comparable catalysts Pd-SBA-15-SH(cc) and Pd-SiO_2-SH. Previous work in our group demonstrated the versatility of these materials as catalysts for cross-coupling reactions. Changes in the textural properties of Pd-SBA-15-SH(g) upon reuse suggested that loss of structural order was one reason why activity of this material decreased upon prolonged recycling. The culprit was the base necessary for reaction. While attempts to stabilize the support including calcination and silanol capping were successful, none of these new catalysts were as recyclable as Pd-SBA-15-SH(g). That said, fellow graduate student Ben Glasspoole developed an Al-Pd-SBA-15-SH(g) that had improved recyclability and stability. The second part of the study of Pd-SBA-15-SH(g) was focused on probing the active species. The results of three-phase tests and solid phase poisoning tests suggested that Pd-SBA-15-SH(g) is a reservoir for a soluble molecular Pd catalyst.

Research on these mesoporous Pd catalysts has reached a mature state; the work reported herein represents only a sample of the studies carried out in the Crudden group. Collectively, we

understand much about the mode of action of these materials, their scope, as well as their advantages and disadvantages as compared to other catalysts available commercially and in the literature. Beyond this, there are 100's of manuscripts devoted to immobilized Pd catalysts and while more research can be done on these low leaching materials, we should keep in mind the origin of this project was a result from a happy accident the occurred during the study of a novel Pd remediation approach developed in our laboratory. The future direction, as was the past, is also in remediation research as there is still much need for approaches that will be generally useful at removing Pd from contaminated organic substances.

Part B of this thesis was focused on describing the initial steps towards the development of an organic hydride based regeneration scheme for the chemical hydrogen storage material NH_3BH_3. The first step in this research program was to establish that organic molecules can be efficient hydride donors to boron Lewis acids. This was the goal of Chapter 5 where studies of the hydride transfer between Hantzsch esters and the model Lewis acid $B(C_6F_5)_3$ were discussed. It was found that N-substituted derivatives were efficient hydride donors to boron giving pyridinium borohydride salt products rapidly (<5 min at room temperature) and in high yield (>90 %). This reaction allowed for an experimental determination of the hydride affinity of $B(C_6F_5)_3$ which was consistent with observed patterns of reactivity discussed here and elsewhere. The KIE of reaction was consistent with either a SET reaction pathway or a highly asynchronous transition state. This mechanistic ambiguity is currently being studied computationally in model systems. Unsubstituted Hantzsch ester was a less efficient hydride donor with the balance of the material being held as a Lewis acid-base adduct and studying this reaction lead to the observation of an equilibrium between the borohydride salt and the adduct, a process which was promoted by $B(C_6F_5)_3$. This transformation was interesting because it represented a hydride transfer in one

direction and a borohydride reduction in the other and was operative at temperatures below -10 ºC.

The research in Chapter 5 led directly into Chapter 6 which described the study of hydride transfer from other organic molecules to boron Lewis acids that were more relevant from a regeneration point of view. In particular it was found that *N*,*N*-ditertbutyl-dihydroimidazole was a particularly effective hydride donor to $B(SPh)_3$ in the presence of excess NEt_3 and CH_2Cl_2. When the reaction was carried out at 50 ºC, $B(SPh)_3$ redistributed to $H_2B(NEt_3)(SPh)$, which was the major boron containing product. Indirect evidence for the formation of diborane was obtained from 1-octene trapping experiments when the redistribution reaction was carried out at 80 ºC. Diborane is a useful precursor to NH_3BH_3. The role of CH_2Cl_2 in the reaction is likely to act as a thiol-scavenger, without which the second equivalent of hydride is not transferred to boron. A variety of experiments designed to observe another useful precursor BH_3NEt_3 were met with varying success and the observation of this borane remains elusive. Studies designed to look at the nature the exchange of hydride between boron Lewis acids lead to the development of a facile route to borenium cations from readily available boranes. This chemistry is currently being exploited as part of a research program interested in developing new catalytic strategies for the reduction of organic substrates.

The future of the regeneration project is bright indeed. The challenge that must be addressed is isolating diborane from the redistribution reaction. After the formation of diborane is confirmed the next step should be to study redistribution with Lewis acids formed directly from the digestion of polyborazylene (BNH_x). The results of these experiments will ultimately dictate the next phase of the regeneration project. If it turns out that dihydroimidazoles can generate high yields of NH_3BH_3 precursors from relevant waste streams, new chemistry to synthesize these

organic hydrides from imidazoles is required, as well as strategies to obviate the use of CH_2Cl_2. It may be interesting to look at the possibility of using formate as the ultimate hydride source for the reconstitution of dihydroimidazoles. Another road to take is to further develop the 1,4-dihydropyridine hydride transfer chemistry to boron. As shown, hydrosilylated dihydropyridines can scavenge thiols from boron Lewis acids without the need of chlorinated solvents. There is also some literature precedence that suggests that pyridines can be selectively hydrogenated to unsubstituted 1,4-dihydropyridines and as previously mentioned there is the possibility that these hydrides may have the capacity to regenerate NH_3BH_3 directly from BNH_x without the need of a distinct digestion step. As there are so many potential roads to take with this regeneration project, effort should be put into some computational analysis of these different schemes and assess them for general energy efficiency, especially against literature approaches, as well as overall thermodynamic and kinetic viability.

Appendix A: Supplementary Data for Chapter 2

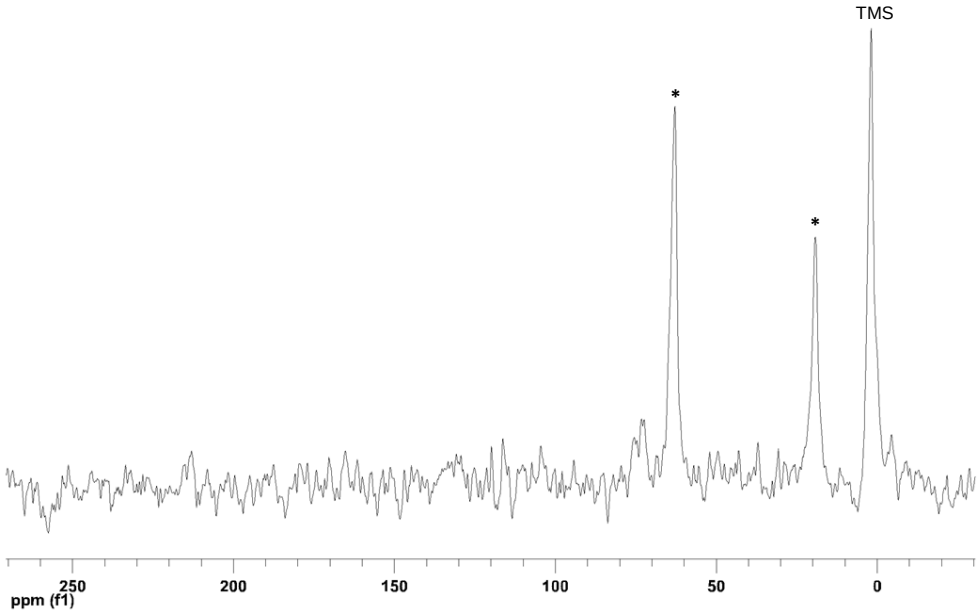

Figure A-1. ^{13}C CP-MAS-NMR for TMSOEt-SBA-15, the asterisk denote ethanol incorporated during Soxhlet extraction

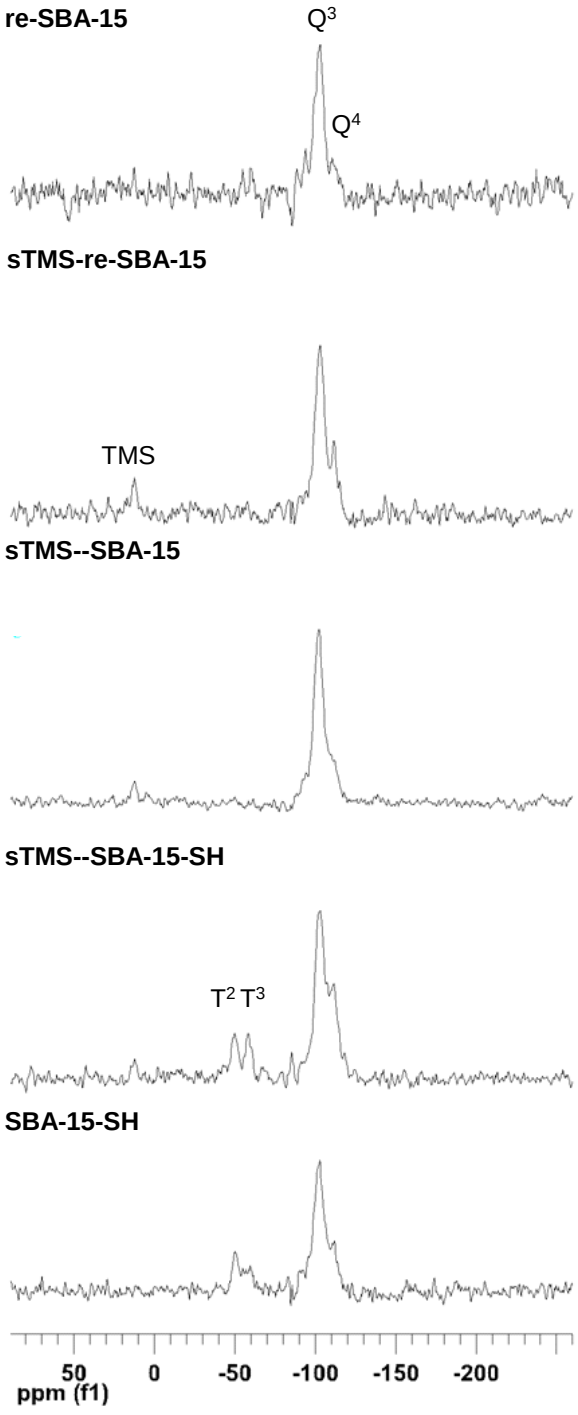

Figure A-2. ^{29}Si CP-MAS NMR overlay for selective grafted SBA-15 materials

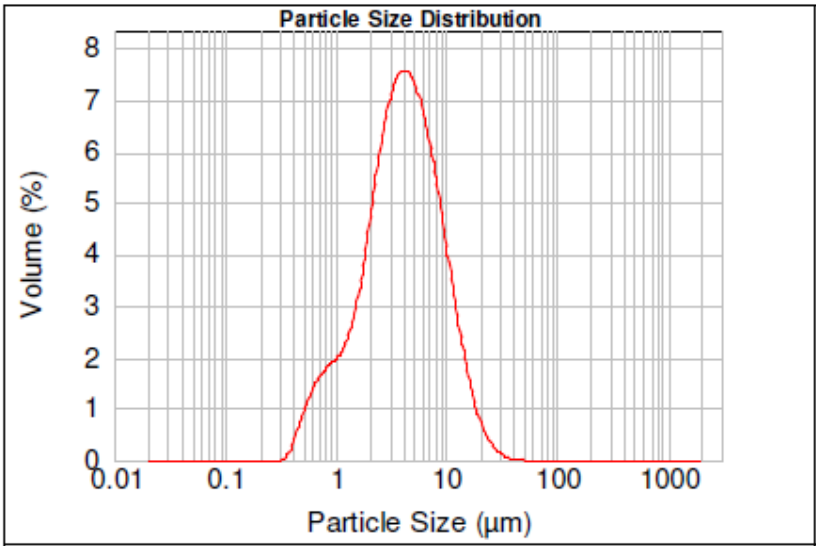

Figure A-3. Laser diffraction particle size distribution for SBA-15-NH_2 after treatment with poly-isocyanate

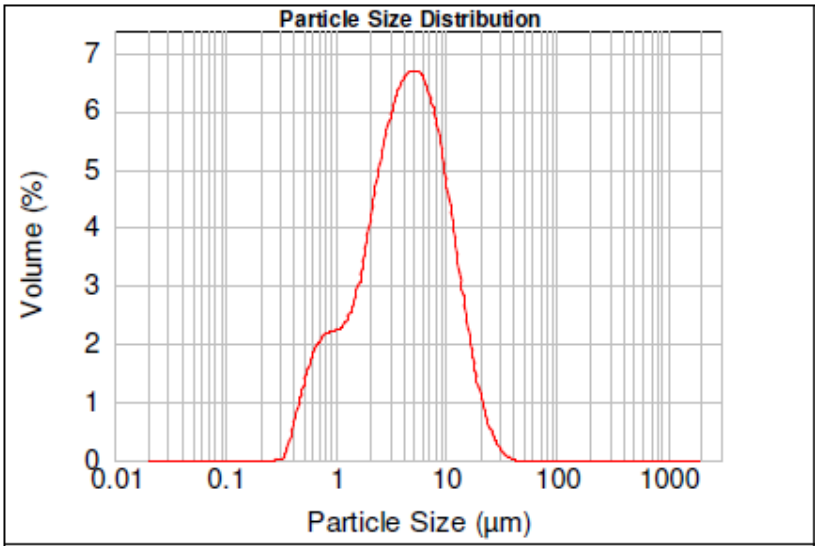

Figure A-4. Laser diffraction particle size distribution for sTMS-SBA-15-NH_2 after treatment with poly-isocyanate

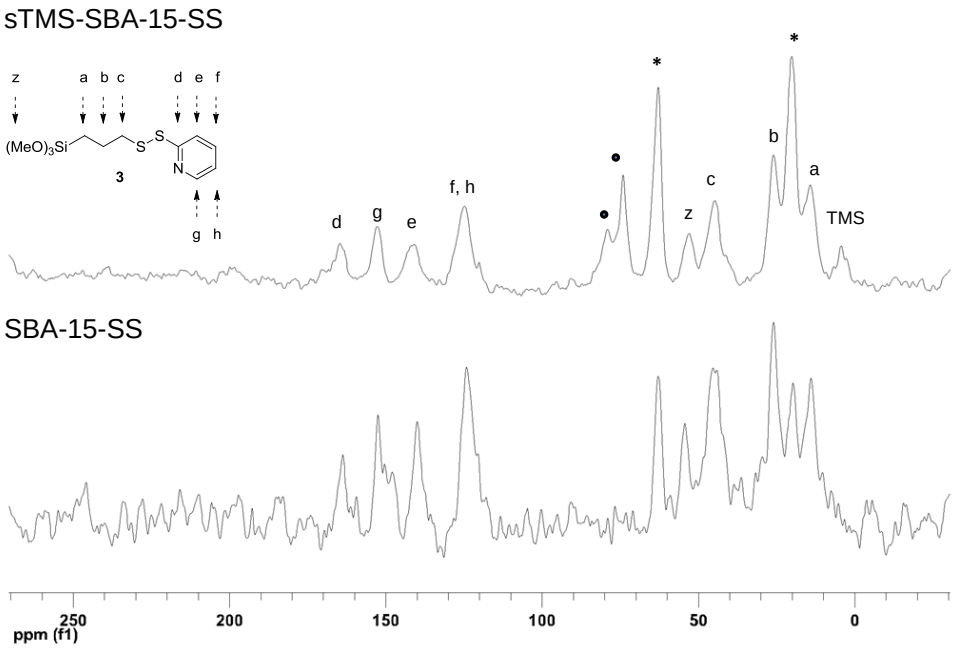

Figure A-5. ^{13}C CP-MAS NMR overlay of TMS-SBA-15-SS and SBA-15-SS synthesized by post-grafting heterodisulfide **3**, residual P123 (circles) and ethanol (asterisk) are labeled

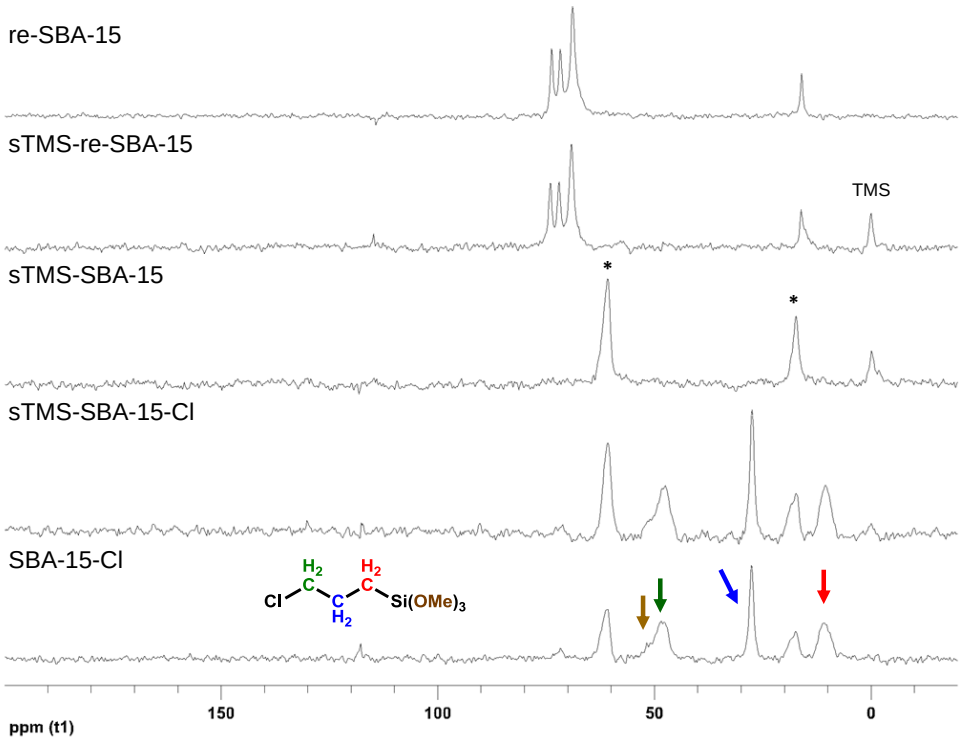

Figure A-6. ^{13}C CP-MAS NMR overlay for selective grafted SBA-15 post-grafted with ClPTMS, the asterisk denote ethanol incorporated during Soxhlet extraction

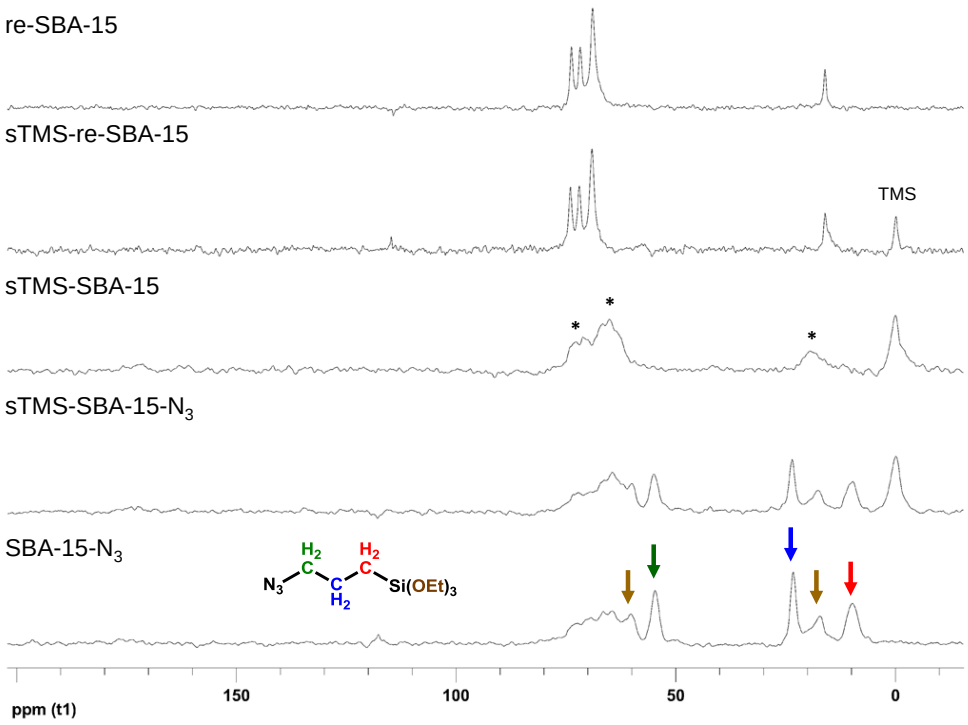

Figure A-7. ^{13}C CP-MAS NMR overlay for selective grafted SBA-15 post-grafted with N_3PTES, the asterisk denote residual P123 from the acetone Soxhlet extraction

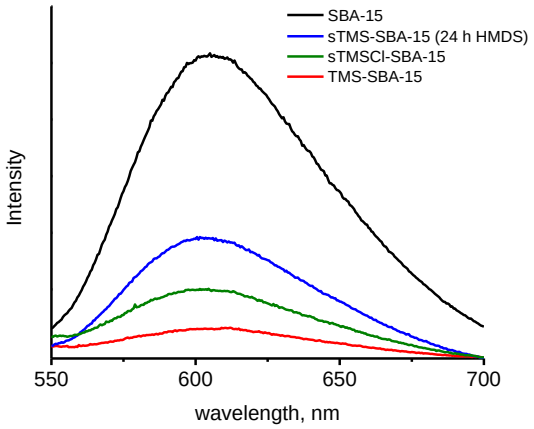

Figure A-8. Fluorescence overlay (λ_{ex} = 450 nm) the adsorption of FloDots on to sTMS-SBA-15 (24 h in HMDS), re-SBA-15 was dried at 80 ºC under high vacuum

Appendix B: Supplementary Data for Chapter 3

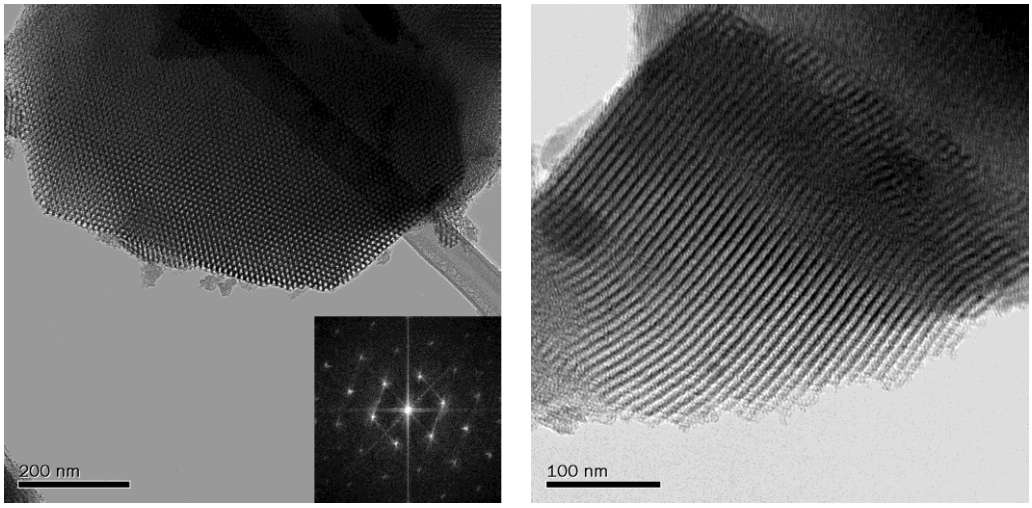

Figure B-1. TEM images of Pd-SBA-SH(g), inlay shows Fourier Transform of image

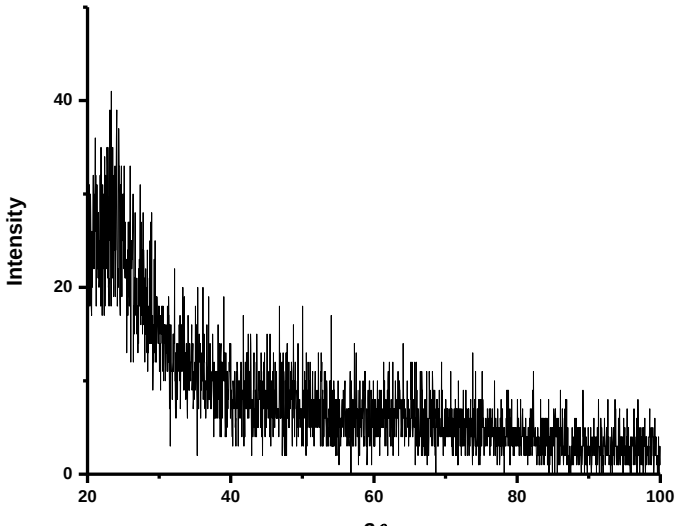

Figure B-2. Wide angle XRD pattern for Pd-SBA-SH(g)

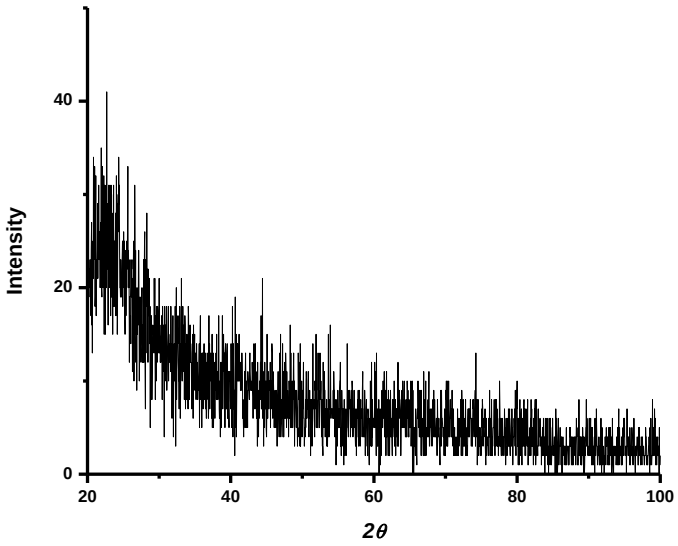

Figure B-3. Wide angle XRD pattern for Pd-SBA-SH(g) after 1 use

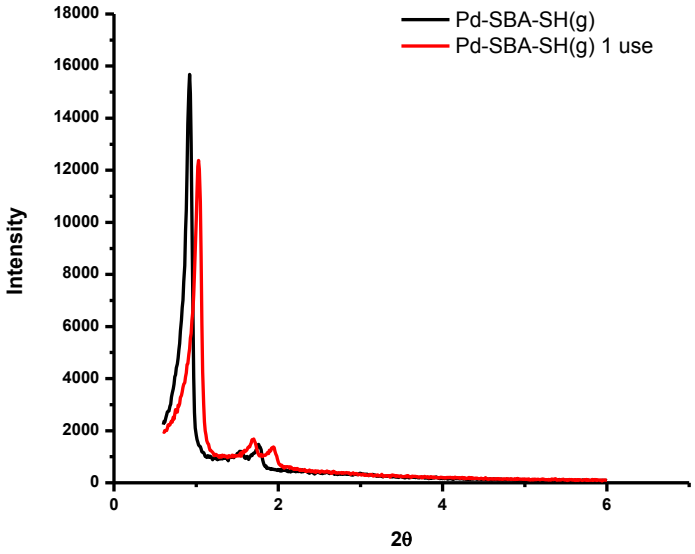

Figure B-4. pXRD pattern for Pd-SBA-15-SH(g) before and after use

Table B-1. Summary of XRD unit cell data for Pd-SBA-SH(g)

Material	hkl, d(Å)			
	100	**110**	**200**	a_o [a]
SBA-15	93.9	56.2	49.0	108
SBA-SH(g)	92.9	55.9	49.6	107
SBA-SH(g)-Pd	96.0	57.7	50.1	111
SBA-SH(g)-Pd 1st Use	85.7	51.9	45.5	99

[a] a_o = cell parameter = $2 \times d_{100}/\sqrt{3}$

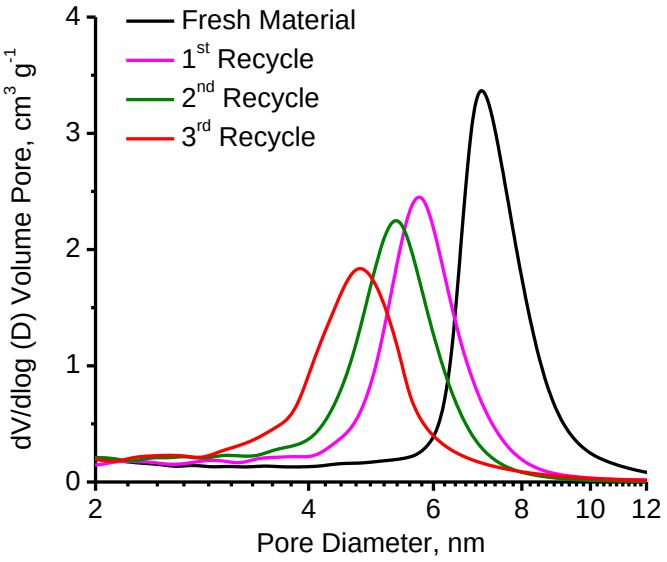

Figure B-5. BJH adsorption overlay of pore size distributions for Pd-SBA-SH(g) upon recycle

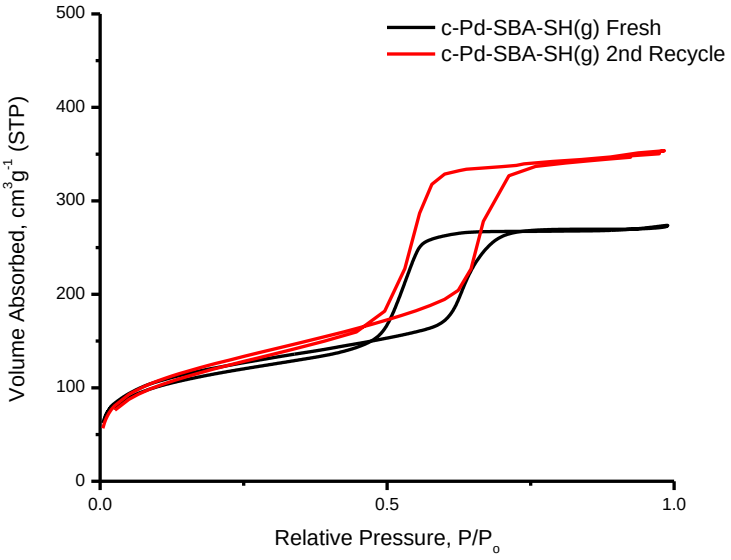

Figure B-6. Physisorption Overlay for c-Pd-SBA-SH(g)

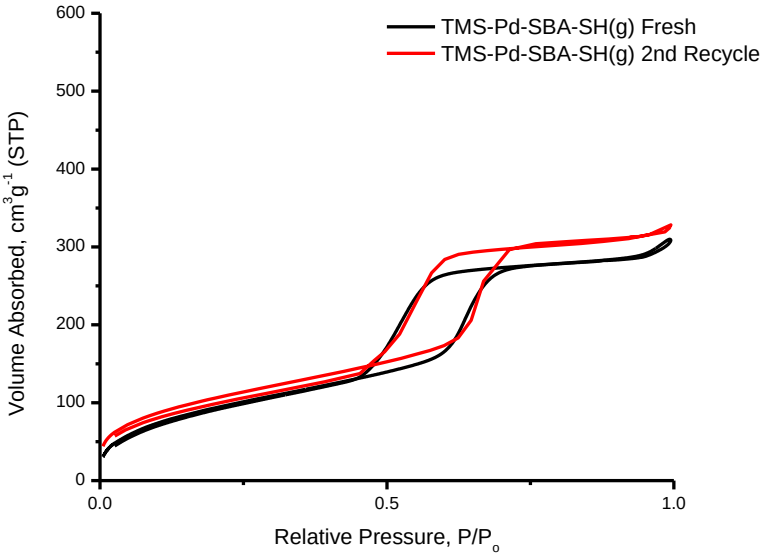

Figure B-7. Physisorption Overlay for TMS-Pd-SBA-SH(g)

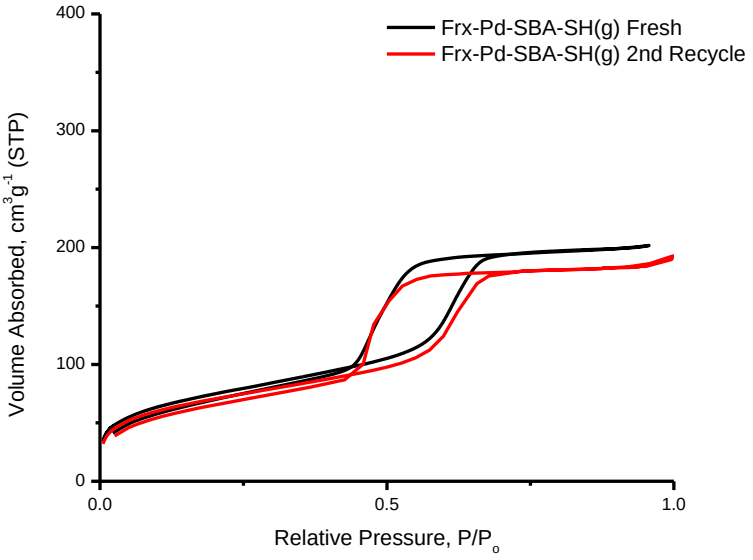

Figure B-8. Physisorption Overlay for high sulfur H-Pd-SBA-SH(g

Appendix C: Supplementary Data for Chapter 5

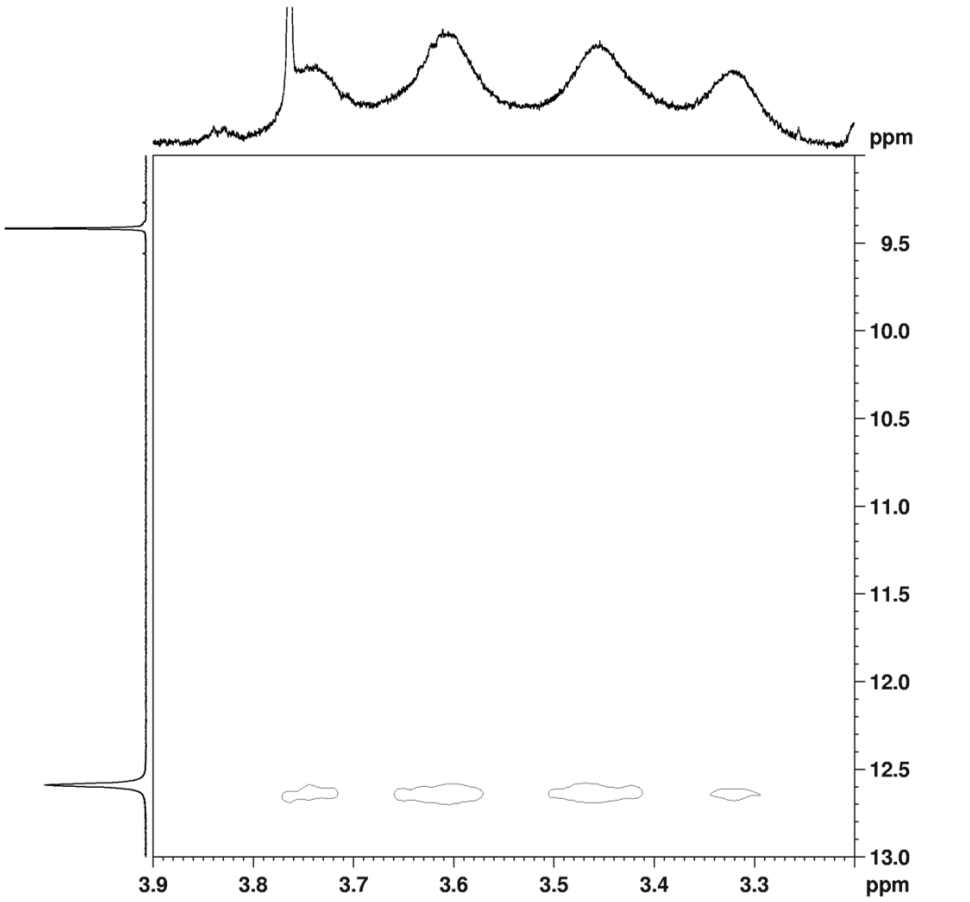

Figure C-1. ^{1}H NMR NOESY 600 MHz of **2c** in CD_2Cl_2 at -10 ºC

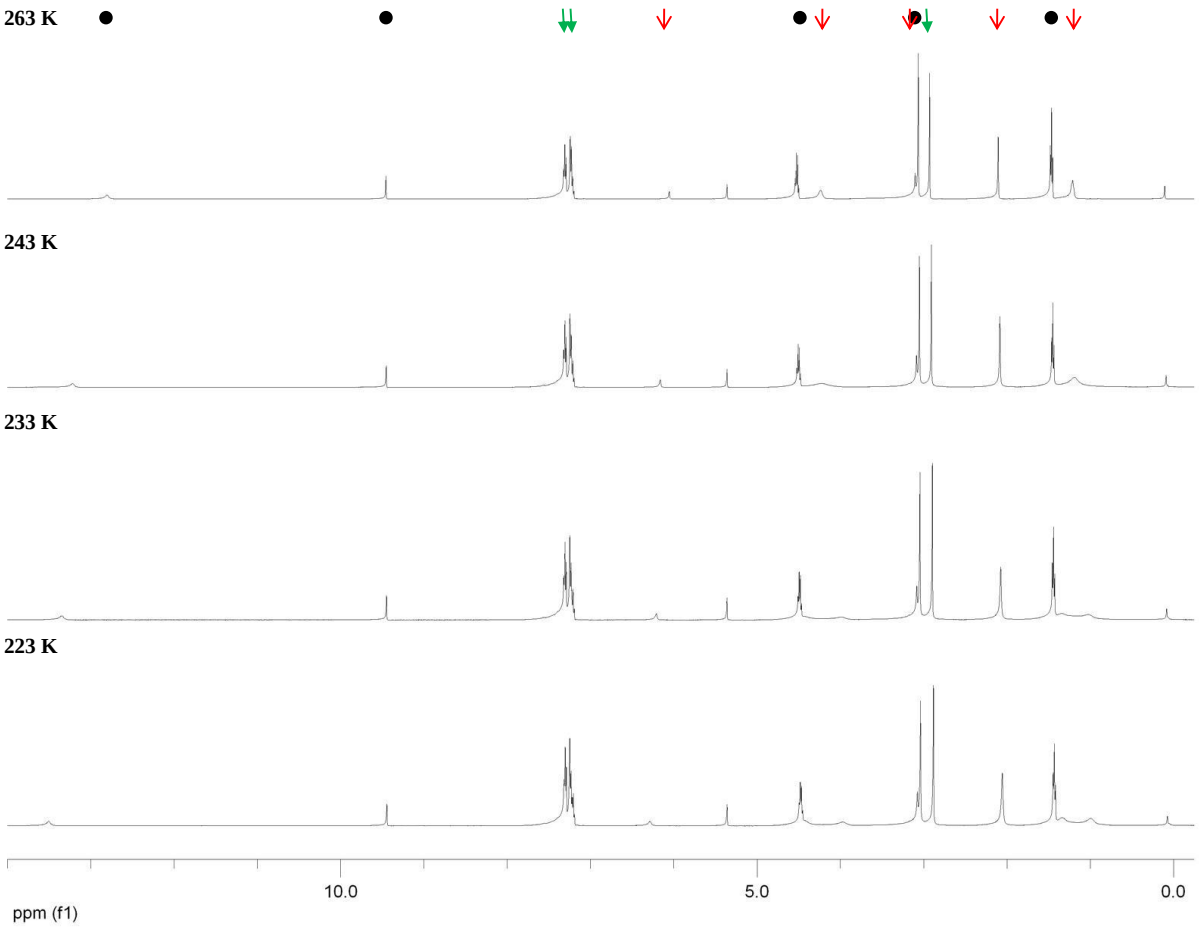

Figure C-2. ^{1}H NMR overlay for **2c** (circle), **3c** (red arrow) and bibenzyl internal standard (green arrow) in CD_2Cl_2 as the temperature is lowered from -10 ºC to -50 ºC

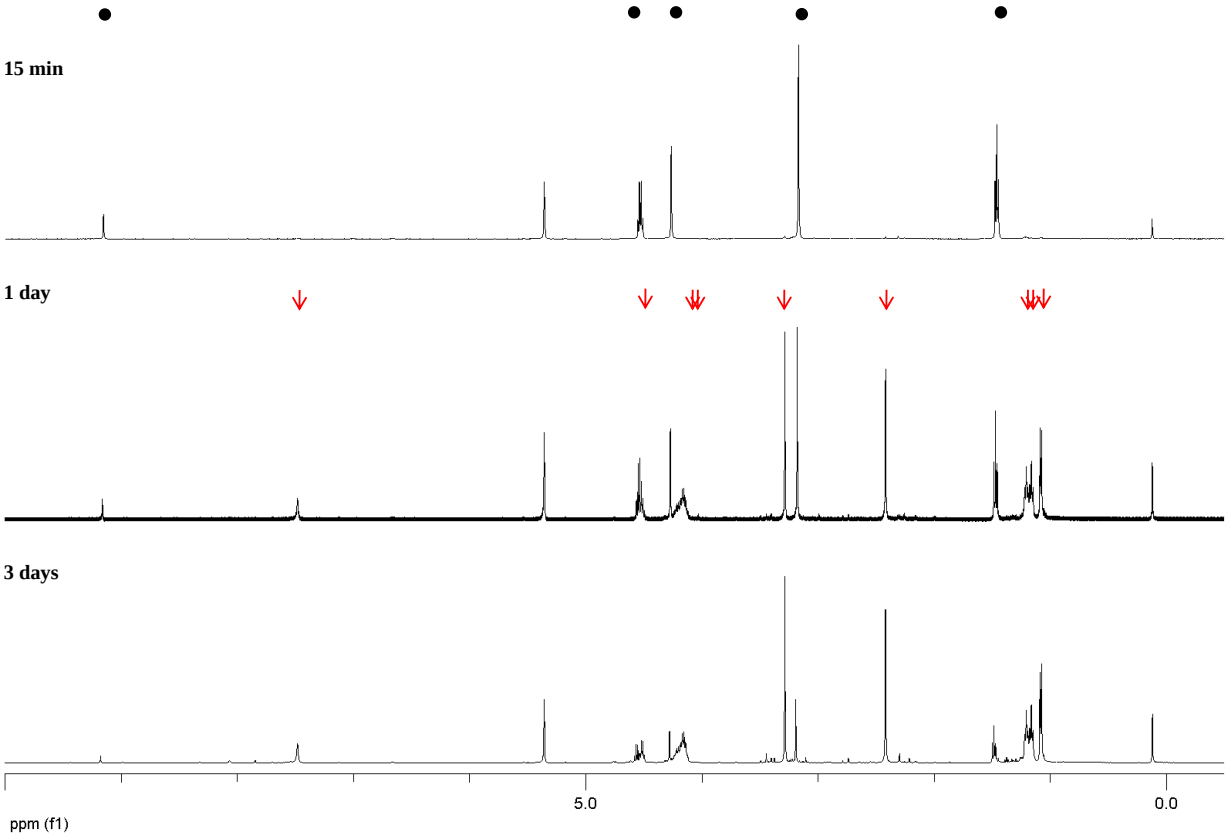

Figure C-3. ^{1}H NMR overlay for the conversion of **2a** (circle) to **4a** (red arrow) in CD_2Cl_2 at room temperature

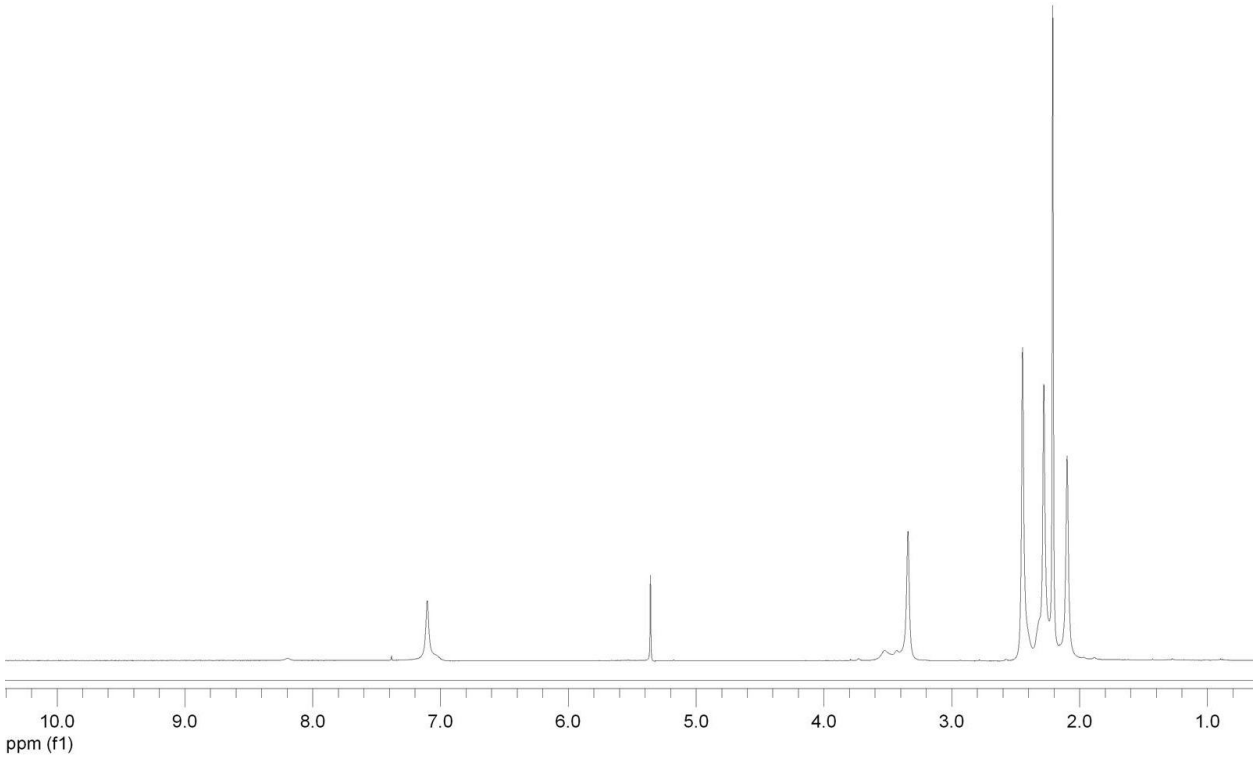

Figure C-4. ^{1}H NMR of adduct **3e** in CD_2Cl_2 collected at 0 ºC

Table C-1. Rate constants for the Homo-exchange between **1f** and **3f** [a]

T, K	k_{ex}, s^{-1}
298	10000
293	9500
287	9250
283	8750
277	7500
273	6250
263	3500
253	1400
238[b]	300
223	40
213	20

[a] Reaction was carried out at 0.03 M **1f** and 0.015 M $B(C_6F_5)_3$ in CD_2Cl_2 and was monitored by ^1H NMR. [b] Coalescence temperature

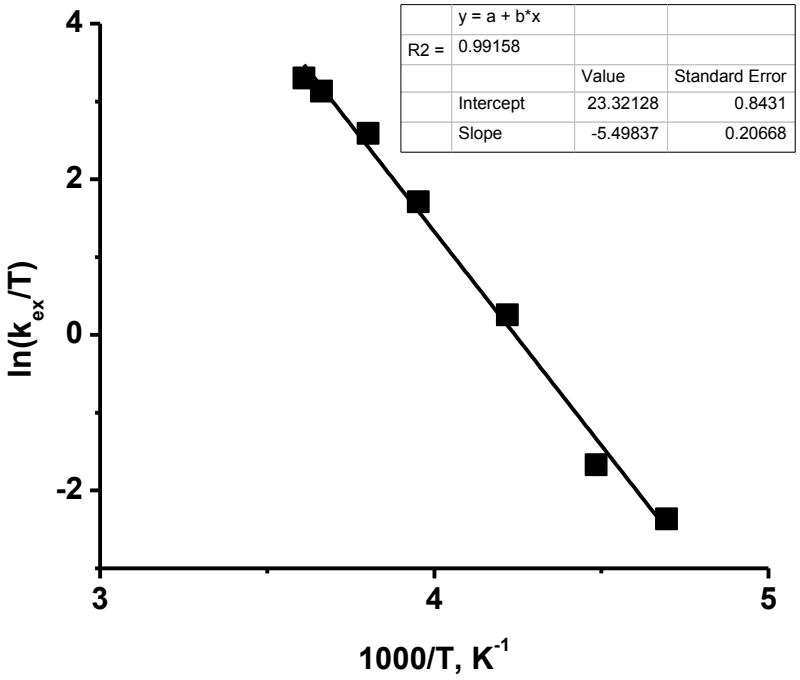

Figure C-5. Linearization of the Eyring plot of **1f** and **3f** homo-exchange rate constants between 5 ºC and -60 ºC

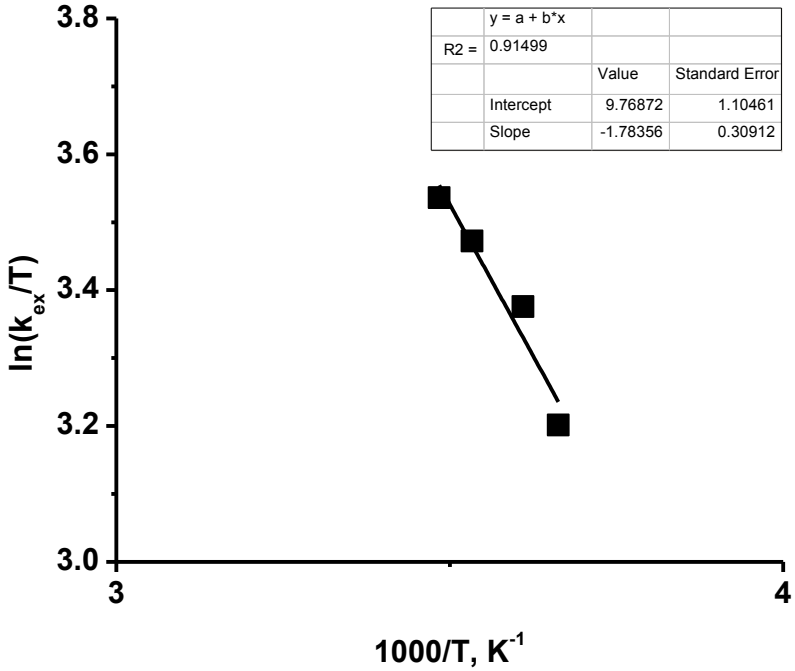

Figure C-6. Linearization of the Eyring plot of **1f** and **3f** homo-exchange rate constants between 25 ºC and 5 ºC

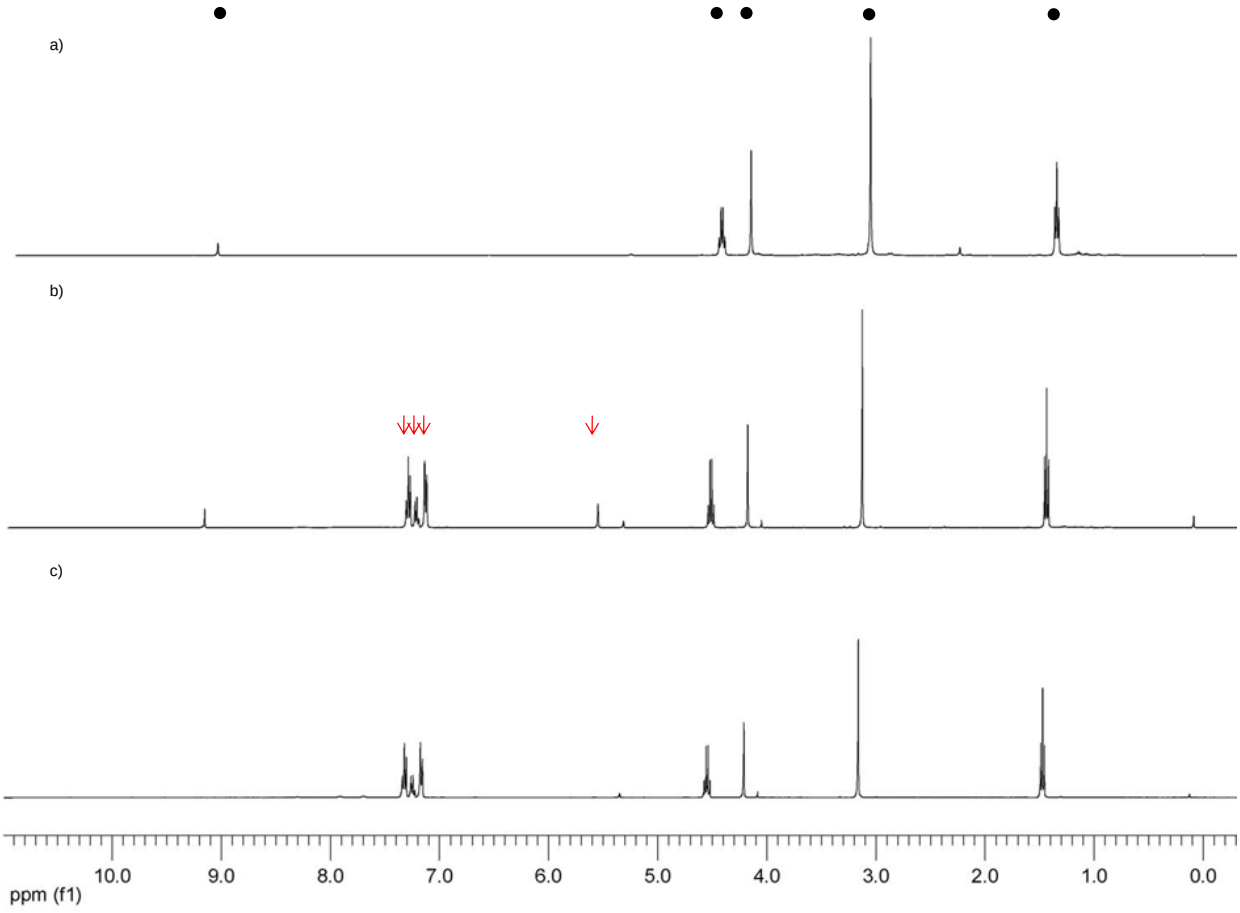

Figure C-7. ^{1}H NMR overlay for reaction of **2a** (black circle) or ***d*$_2$-2a** with $[CPh_3][B(C_6F_5)_4]$ in CD_2Cl_2 at 25 ºC to produce $HCPh_3$ or $DCPh_3$ (red arrow); a) ^{1}H NMR of **2a**; b) ^{1}H NMR post addition of $[CPh_3][B(C_6F_5)_4]$ to **2a**; c) post addition of $[CPh_3][B(C_6F_5)_4]$ to ***d*$_2$-2a**

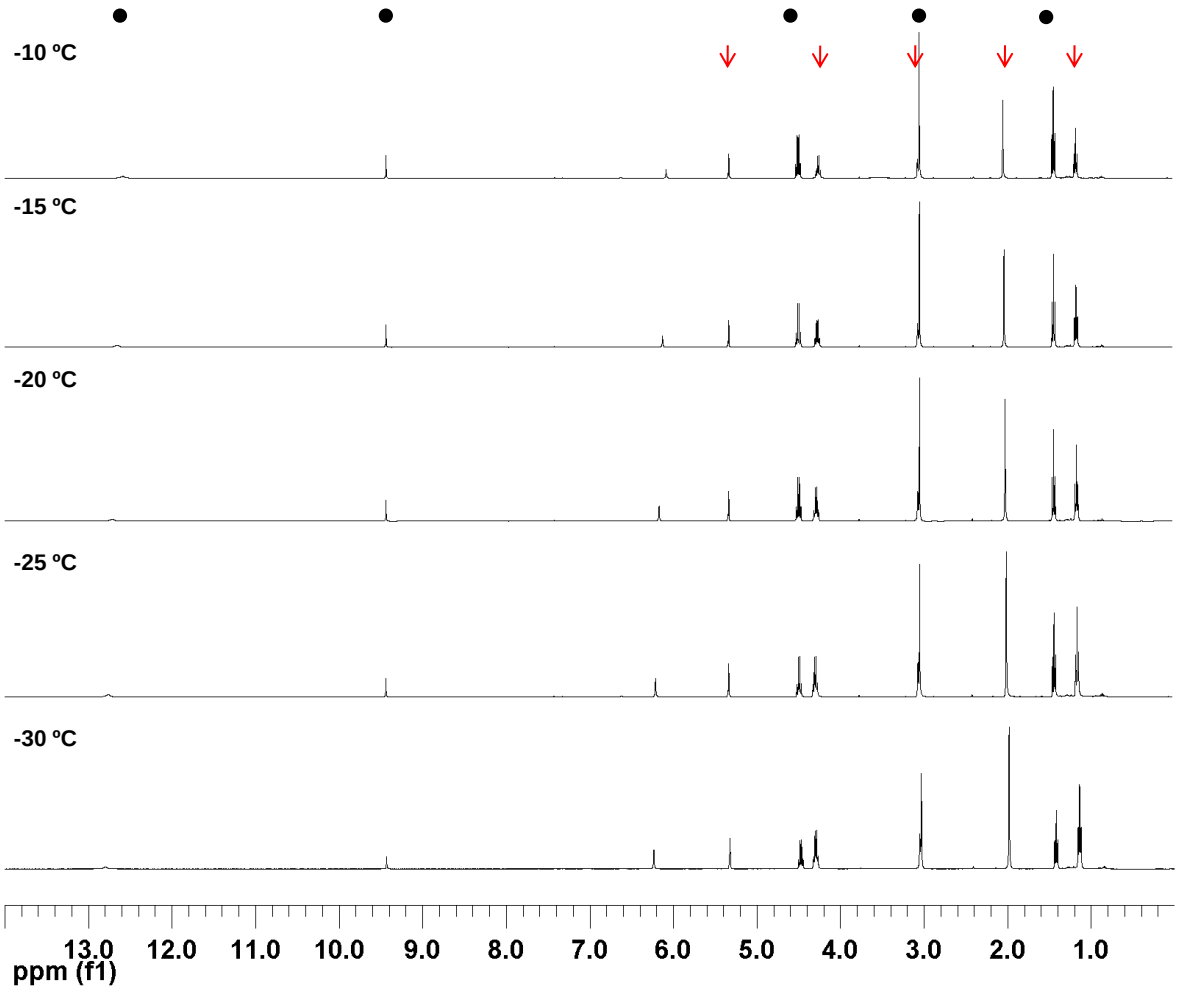

Figure C-8. Equilibrium between **2c** (black circles) and **3c** (red arrows) at an initial molar ratio of **1c**:$B(C_6F_5)_3$ of 1:4 as the temperature was lowered

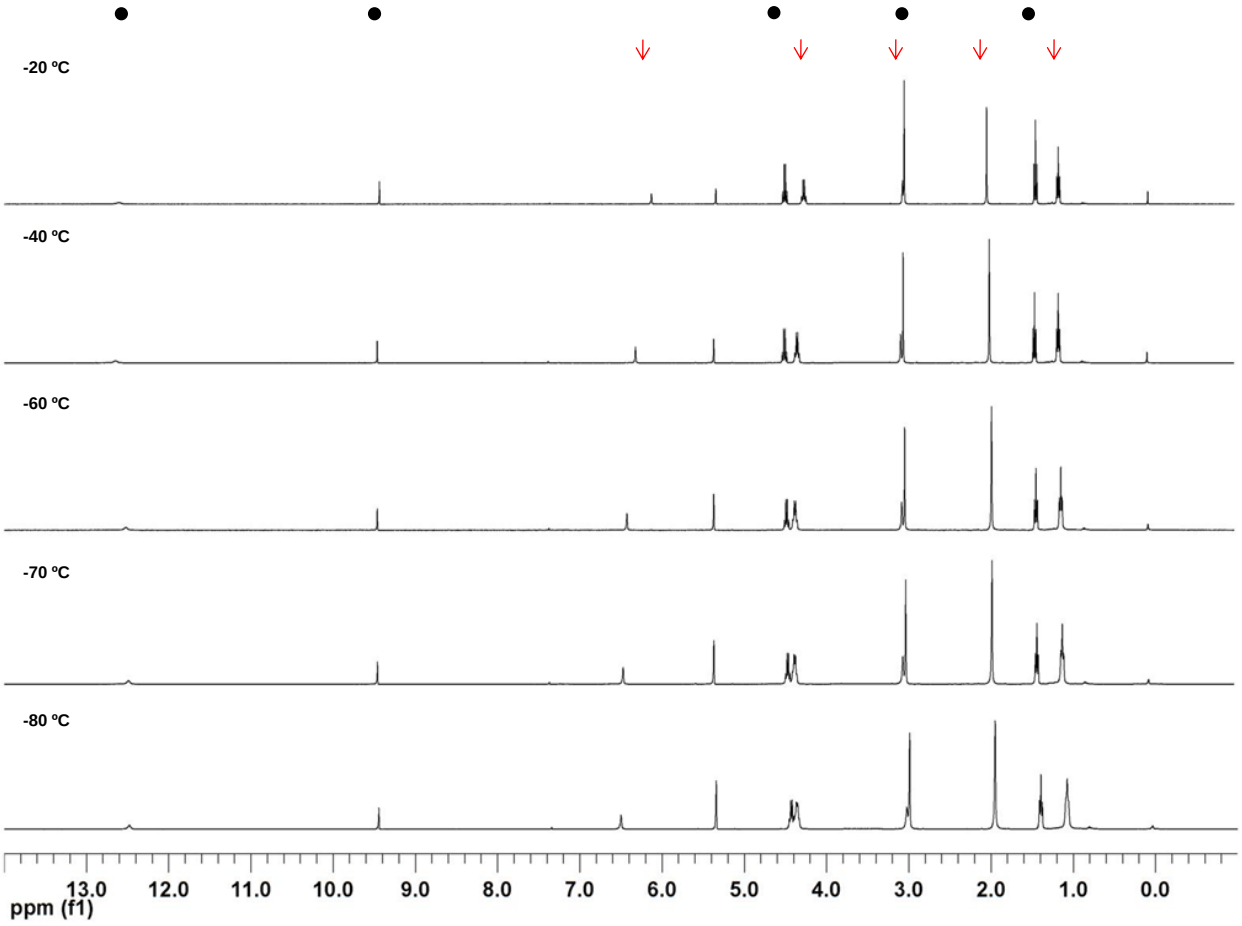

Figure C-9. VT ^{1}H NMR overlay of **2c** (black circle) and adduct **3c** (red arrows). Initial stoichiometry **1c**:$B(C_6F_5)_3$ of 1:4 and concentration of [**1c**] = 0.03 M in CD_2Cl_2

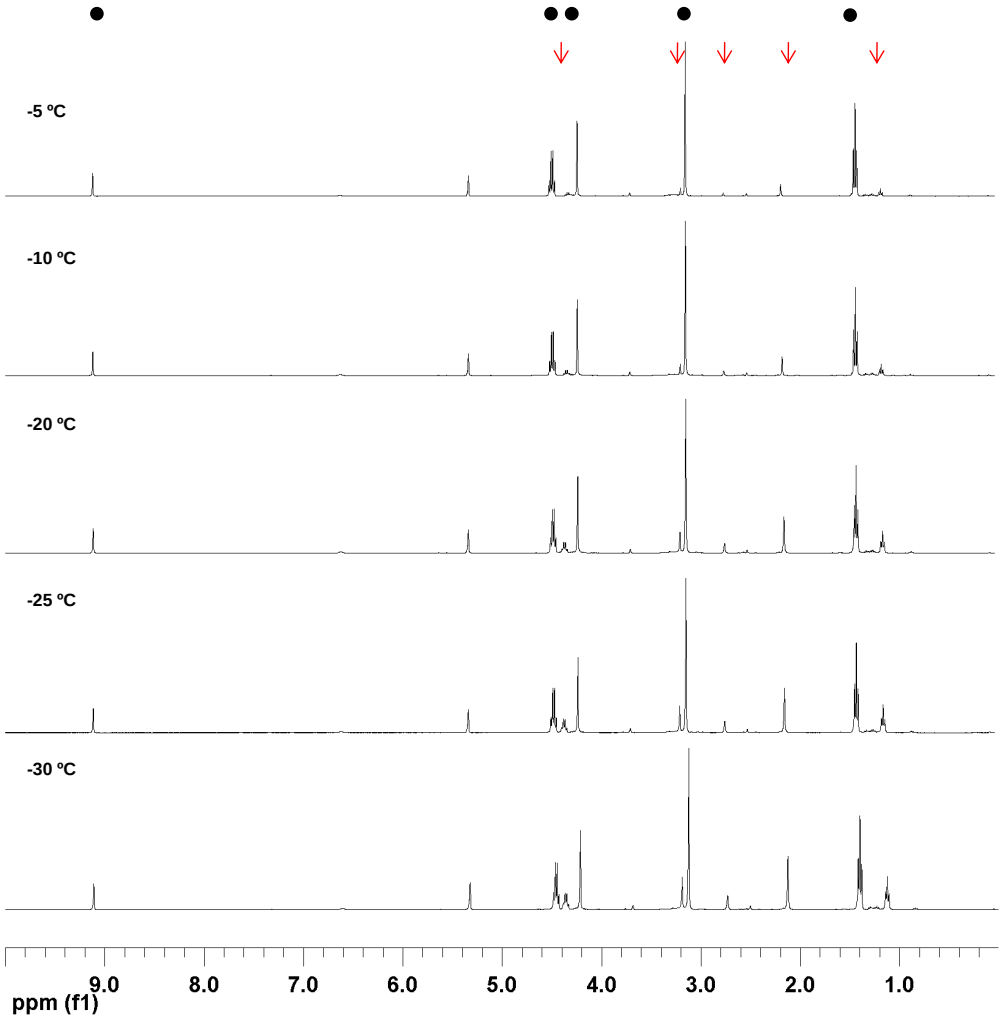

Figure C-10. Equilibrium between **2a** (black circle) and **3a** (red arrow) at an initial molar ratio of **1a**:$B(C_6F_5)_3$ of 1:4 as the temperature was lowered

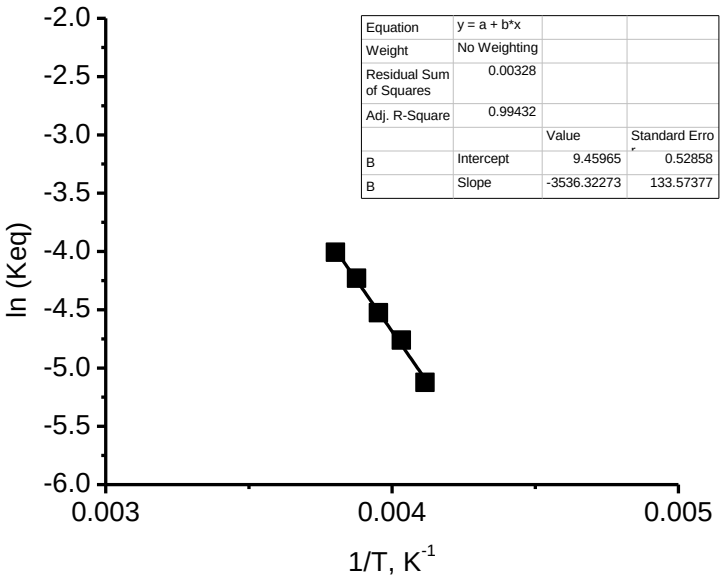

Figure C-11. Sample van`t Hoff plot for **3c**–**2c** equilibrium. The molar ratio of **1c**:$B(C_6F_5)_3$ was 1:4 and the initial [**1c**] was 0.030 M

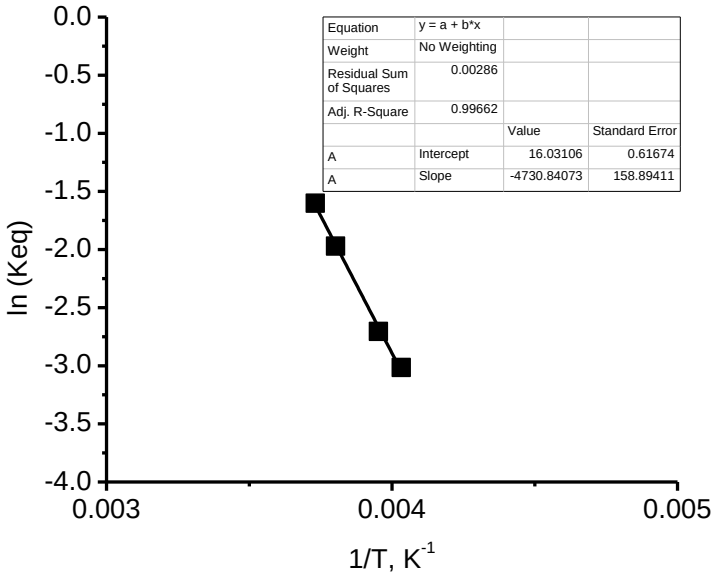

Figure C-12. Sample van`t Hoff plot for **3a**–**2a** equilibrium. The molar ratio of **1a**:$B(C_6F_5)_3$ was 1:4 and the initial [**1a**] was 0.030 M

Appendix D: Supplementary Data for Chapter 6

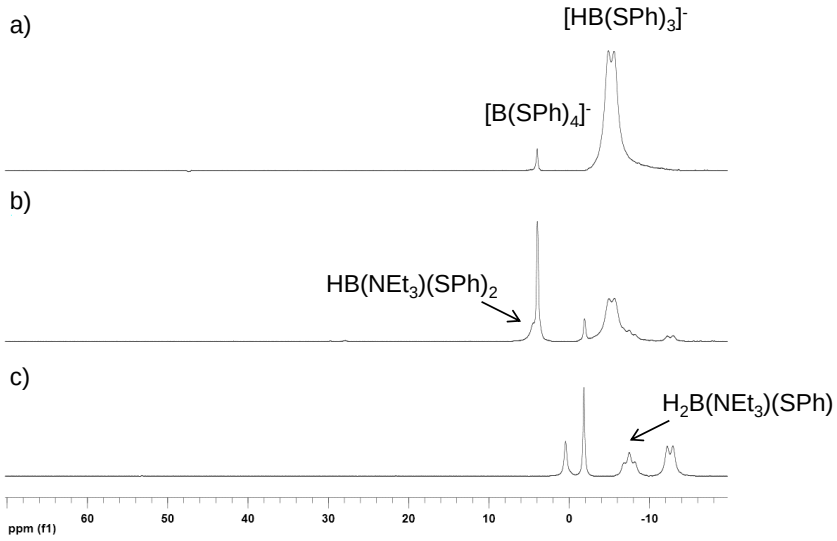

Figure D-1. ^{11}B NMR overlay for redistribution of $B(SPh)_3$ with the hydride donor **1b** in CD_2Cl_2; a) after 3 h at room temperature; b) 1h after addition of excess NEt_3; c) after overnight at 50 ºC

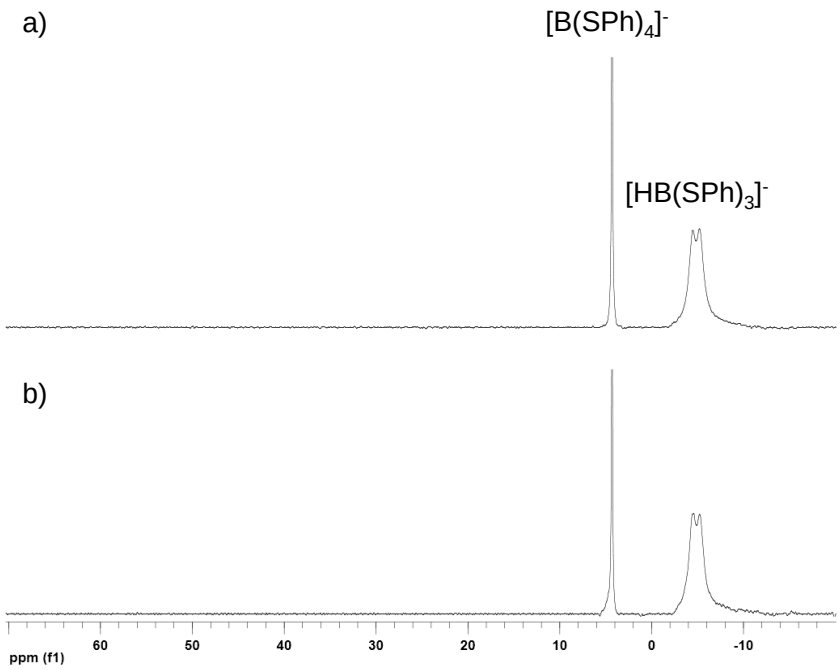

Figure D-2. ^{11}B NMR overlay for redistribution of $B(SPh)_3$ with hydride donor **1a** in THF; a) after 1 h at room temperature; b) after addition of excess NEt_3 and 3 days at 50 ºC

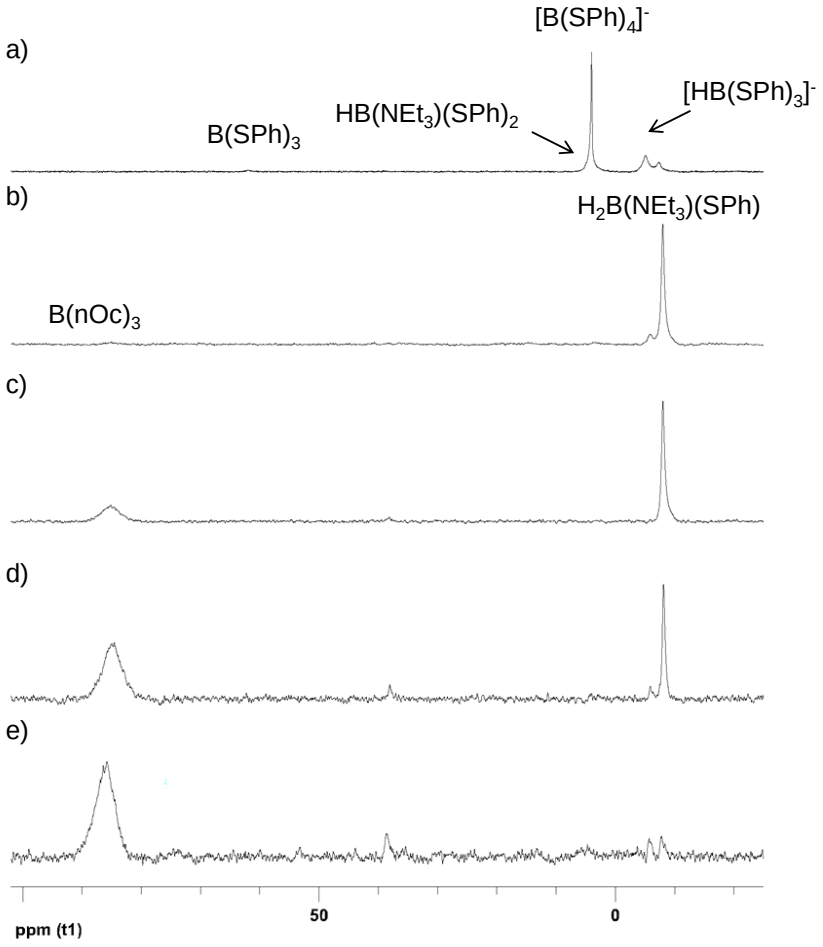

Figure D-3. $^{11}B\{H\}$ NMR overlay for redistribution of $B(SPh)_3$ with hydride donor **1a** with excess NEt_3 and 1-octene; a) after 1 h at room temperature; after b) 20 min; c) 1 h; d) 2 h and e) 4h at 80 ºC

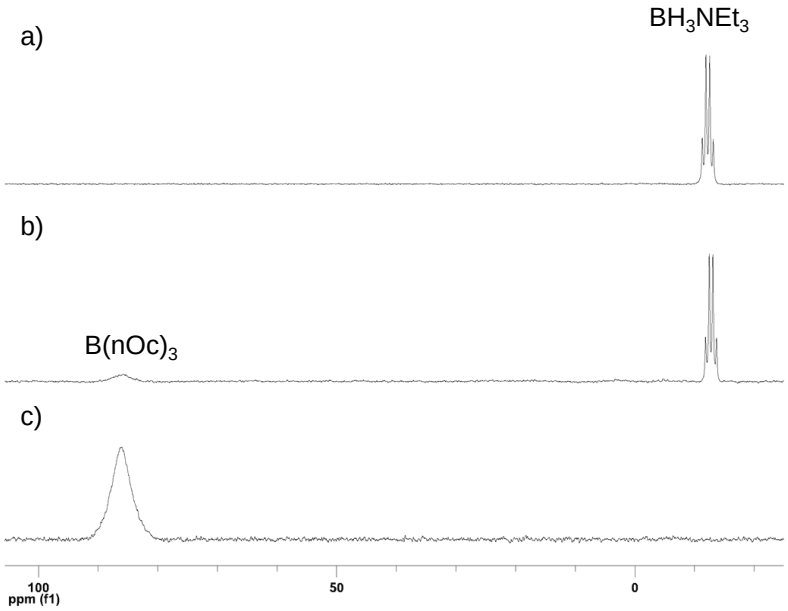

Figure D-4. ^{11}B NMR overlay of BH_3NEt_3 control experiments in 1:1 THF:CH_2Cl_2 with excess NEt_3 and 1-octene; a) after 1 h at room temperature; b) after 18 h at 80 ºC; c) same conditions as b) at 80 ºC without excess NEt_3

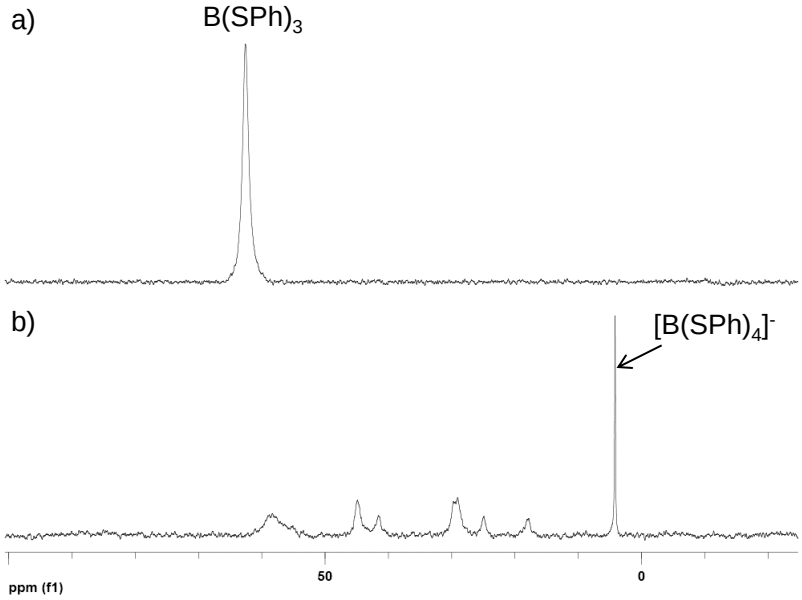

Figure D-5. ^{11}B NMR overlay for the control of $B(SPh)_3$ in 1:1 THF:CH_2Cl_2 with excess NEt_3 and 1-octene; a) after 1 h at room temperature; b) after 18 h at 80 ºC

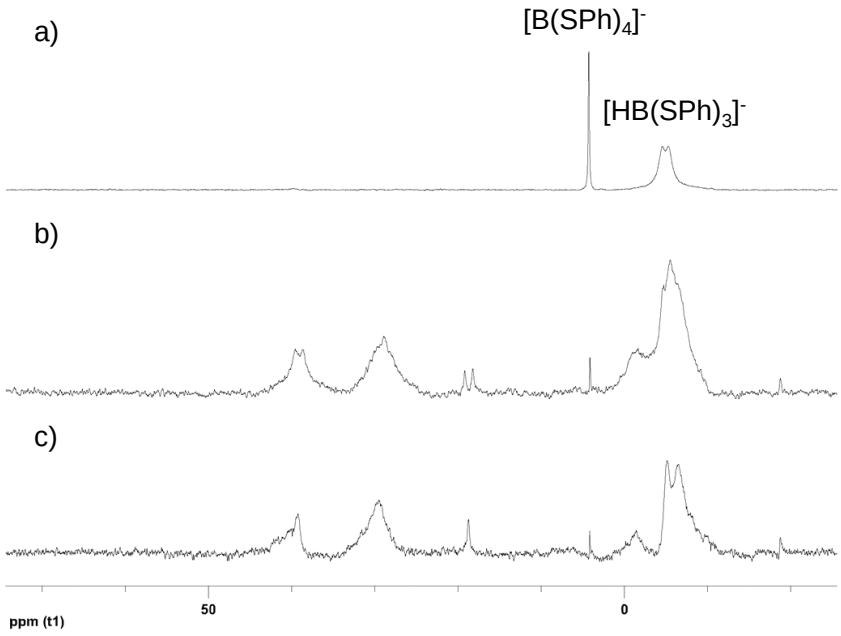

Figure D-6. ^{11}B NMR overlay for the redistribution of $B(SPh)_3$ in 1:1 THF:CH_2Cl_2 with hydride **1a** and excess Hünig's base; a) after 1h at room temperature; b) after 18 h at 50 ºC; c) corresponding ^{11}B {^1H} NMR spectrum

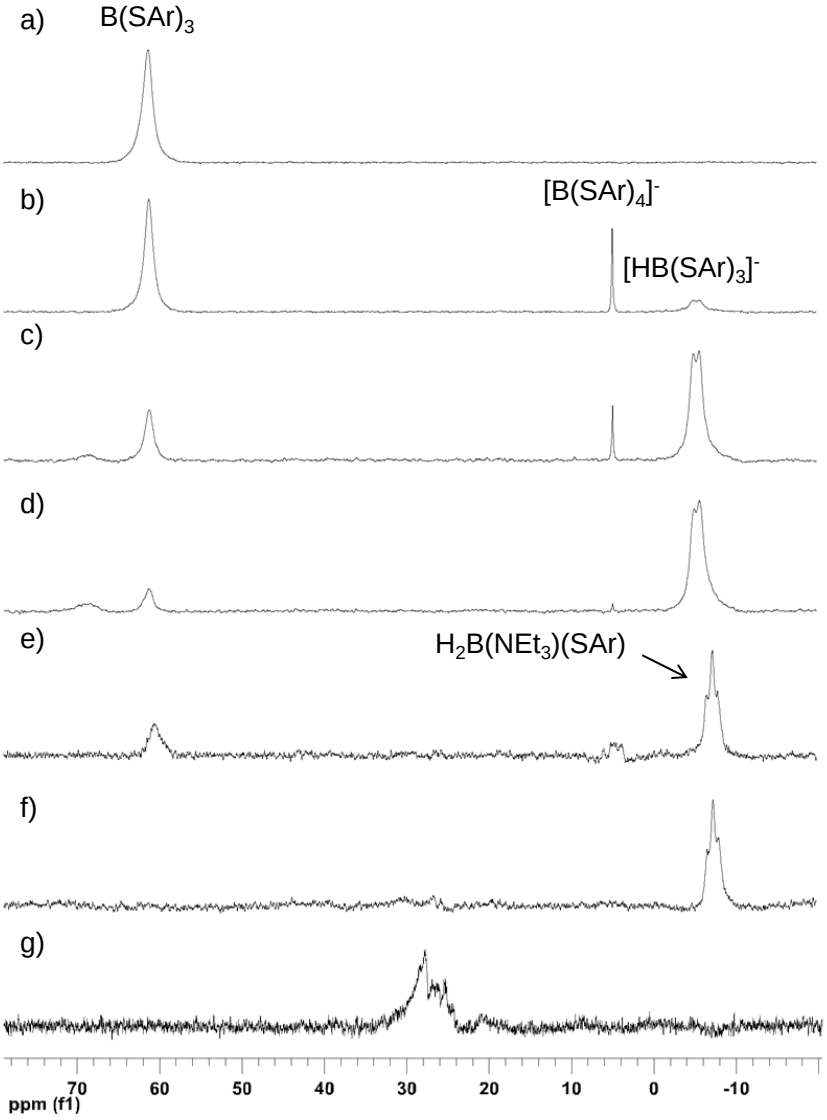

Figure D-7. ^{11}B NMR overlay for redistribution of *ortho*-B($SC_6H_4CH_3$) with hydride **1a** in CD_2Cl_2; a) starting material; b) after addition of 3 equiv. of **1a** and 1 h at room temperature; c) 1 d; d) 2 d; e) after addition of NEt_3 and 18 h at 50 ºC; f) after addition of 3 equiv. of **1a** and 1 h at 80 ºC; g) after 18 h at 80 ºC. Ar = *ortho*-$SC_6H_4CH_3$

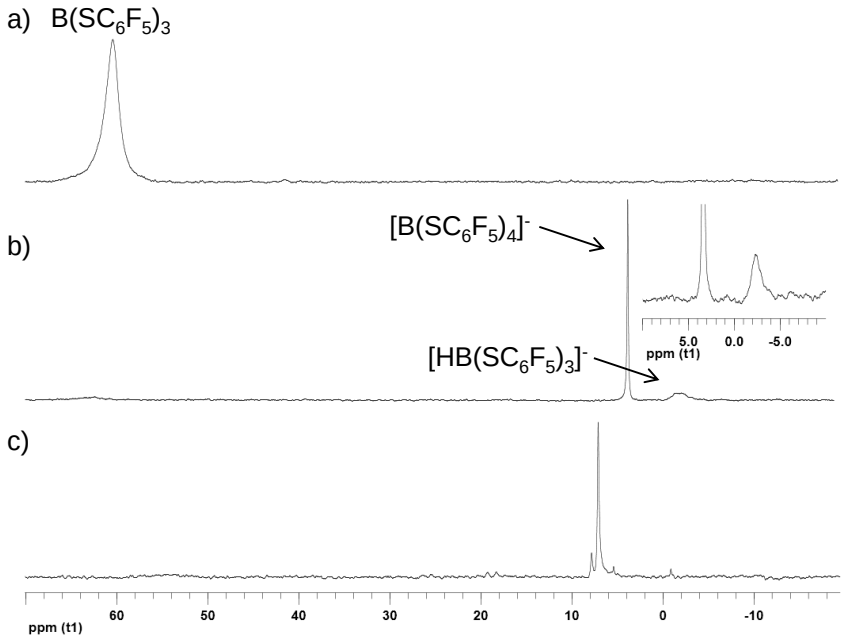

Figure D-8. ^{11}B NMR overlay for the redistribution of $B(SC_6F_5)_3$ in CD_2Cl_2; a) starting material; b) after addition of **1a** and 15 min at room temperature; c) after 3 d at room temperature. Inlay represents the $^{11}B\{^1H\}$ NMR spectrum of b)

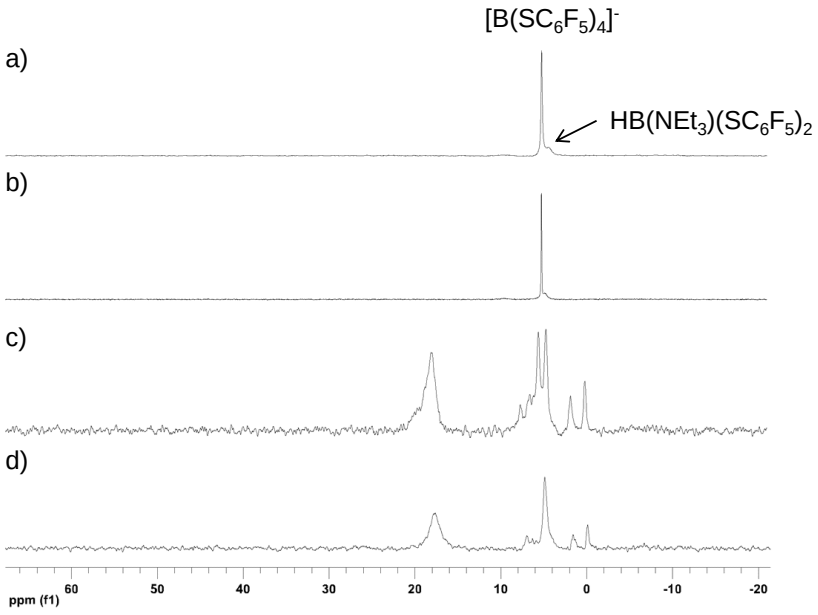

Figure D-9. ^{11}B NMR overlay for redistribution of $B(SC_6F_5)_3$ with hydride **1a** and excess NEt_3; a) after 5 min at room temperature; c) after 18 h at 50 ºC; b) and d) are the corresponding $^{11}B\{^1H\}$ NMR spectra

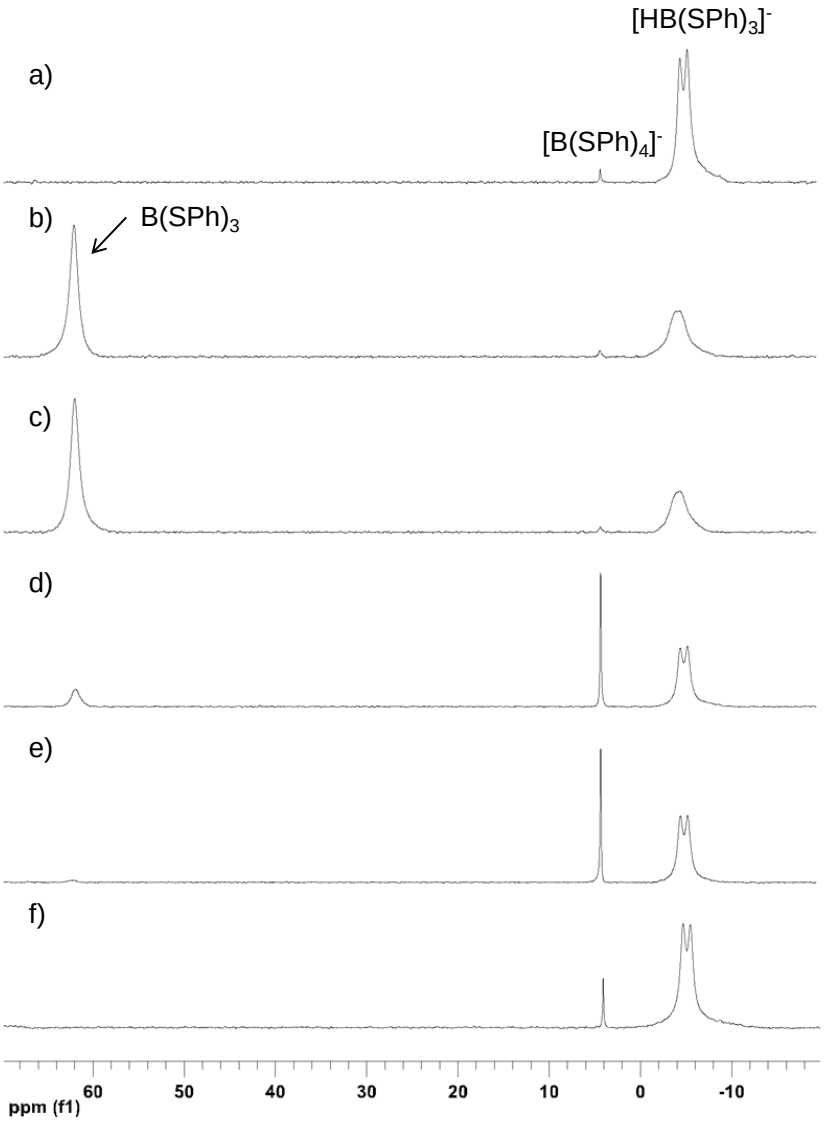

Figure D-10. ^{11}B NMR overlay for redistribution of $B(SPh)_3$ with $[HB(SPh)_3]^-$, looking for conditions that favour formation of $[B(SPh)_4]^-$; a) spectrum of $[HB(SPh)_3]^-$ starting material; b) after addition of $B(SPh)_3$ and 15 min at room temperature; c) after 3 h at room temperature; d) after addition of **1a** and 15 min at room temperature; e) after 1 h at room temperature; f) after 18 h at room temperature

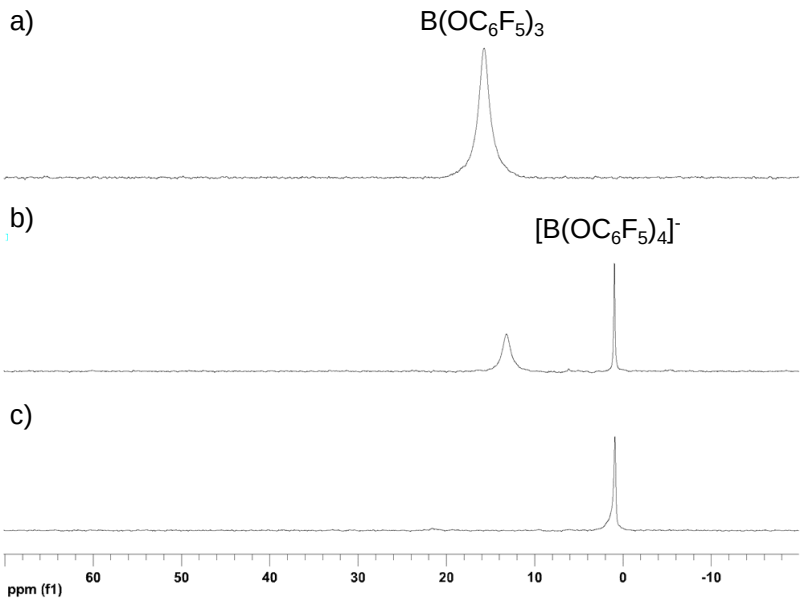

Figure D-11. ^{11}B NMR overlay for the redistribution of $B(OC_6F_5)_3$ in CD_2Cl_2 with 3 equiv. of hydride donor **1a**; a) starting material; b) after 30 min at room temperature; c) after 18 h at 50 ºC

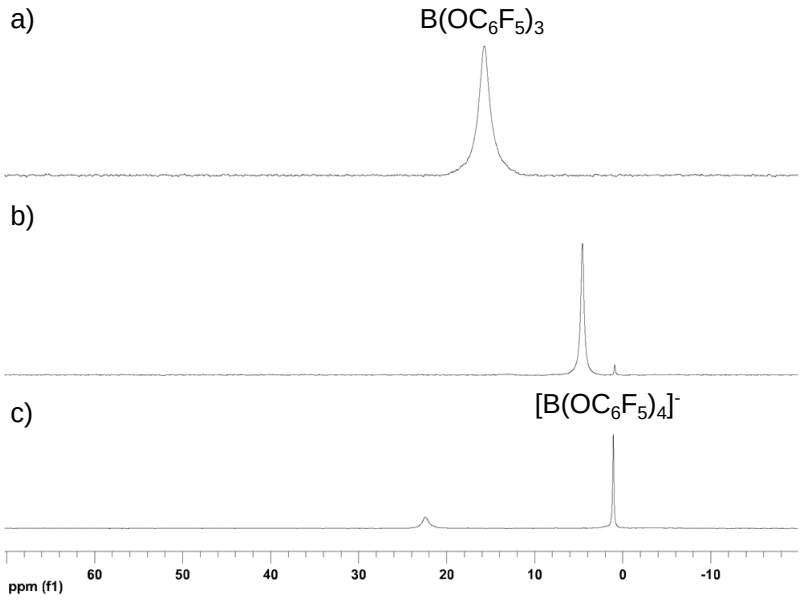

Figure D-12. ^{11}B NMR overlay for the redistribution of $B(OC_6F_5)_3$ in CD_2Cl_2 with 3 equiv. of hydride donor **1b**; a) starting material; b) after 30 min at room temperature; c) after 18 h at 50 ºC

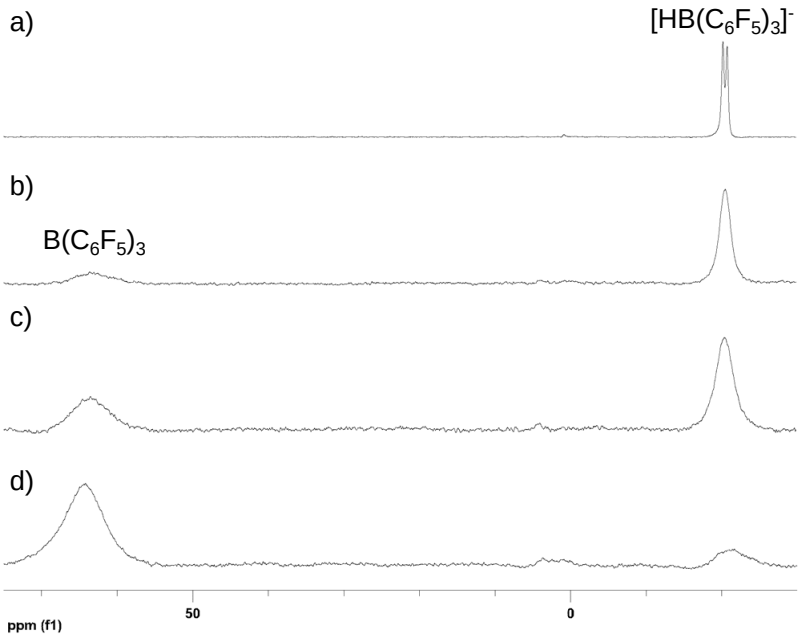

Figure D-13. ^{11}B NMR overlay depicting broadening of the resonance for $[HB(C_6F_5)_3]^-$ with increasing quantities of free $B(C_6F_5)_3$; a) starting material; b) mole ratio $B(C_6F_5)_3$: $[HB(C_6F_5)_3]^-$ of 1:2; c) 1:1; d) 3:1

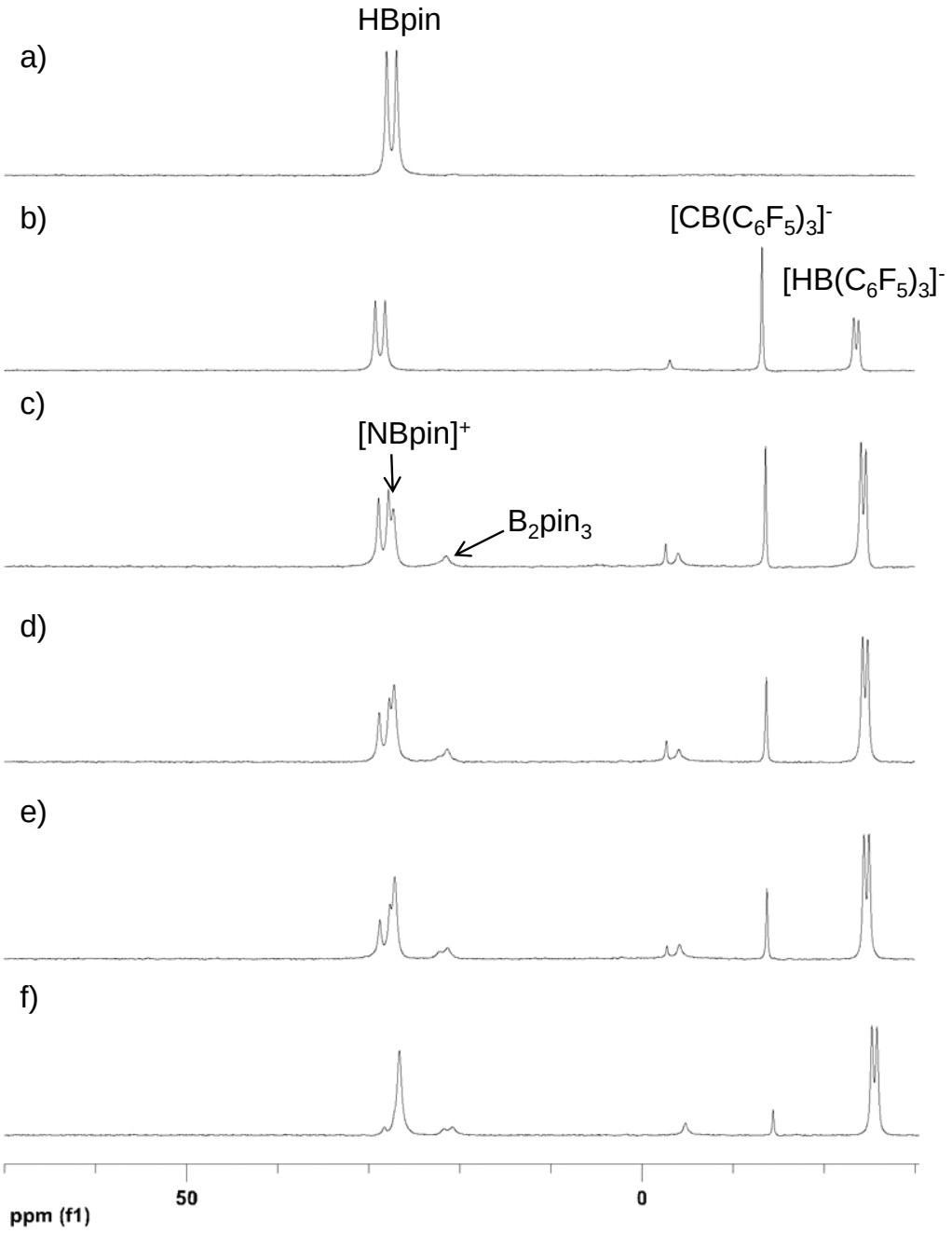

Figure D-14. ^{11}B NMR overlay depicting borenium cation formation from the reaction of HBpin with NEt_3 and $B(C_6F_5)_3$ in CD_2Cl_2; a) HBpin with NEt_3; b) after addition of $B(C_6F_5)_3$ and 30 min; c) 1 d; d) 2 d; e) 3 d; f) 7 d at room temperature

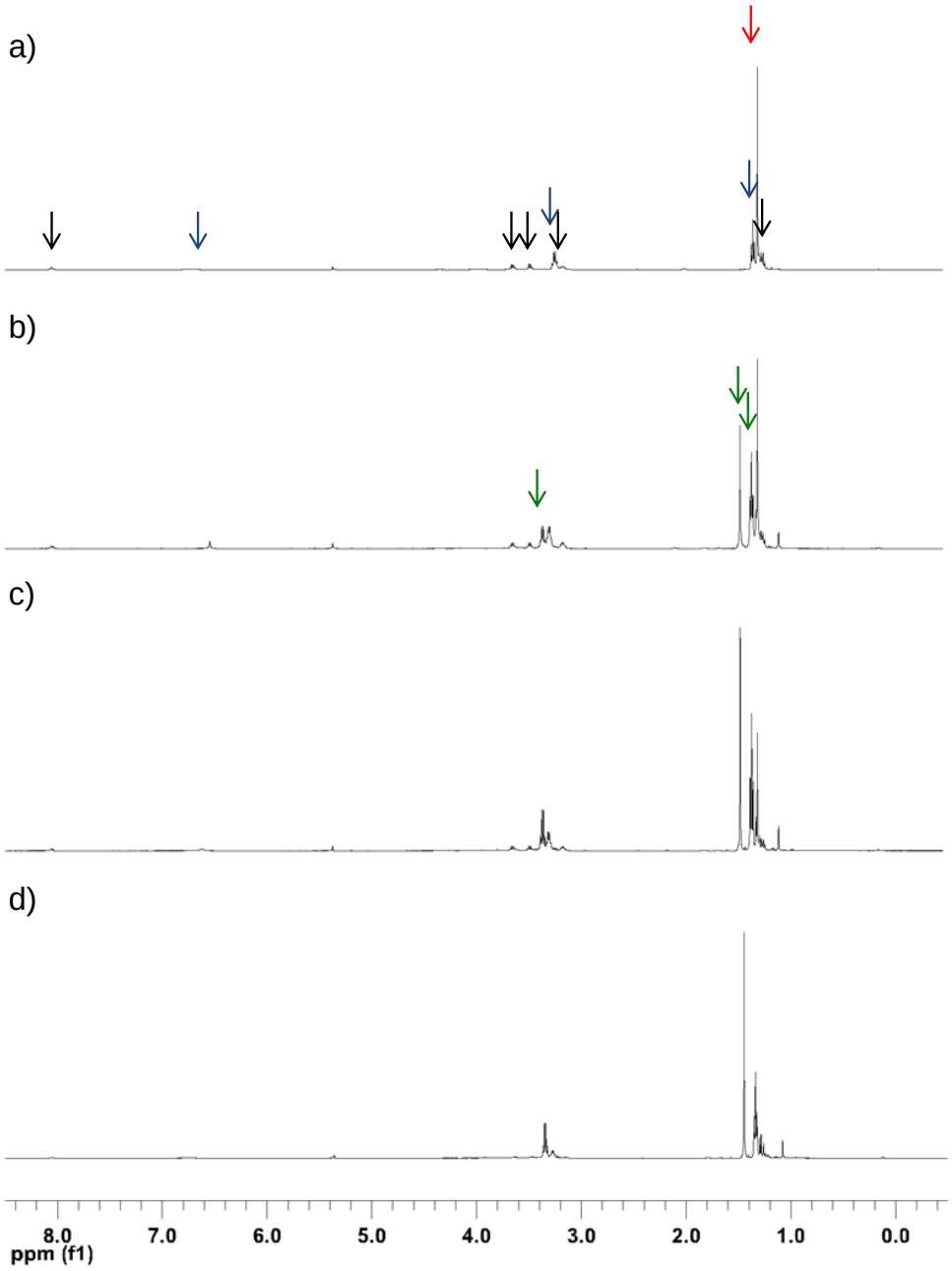

Figure D-15. ^{1}H NMR overlay depicting borenium cation formation from the reaction of HBpin (red arrow) with NEt_3 and $B(C_6F_5)_3$ in CD_2Cl_2; a) after 30 min, b) 1 d, c) 3 d and d) 7 d at room temperature $[Et_3NH][HB(C_6F_5)_3]$ (black arrow); $Et_2N{=}CHCH_2B(C_6F_5)_3$ (blue arrows) and $[Et_3NBpin][HB(C_6F_5)_3]$ (green arrow)

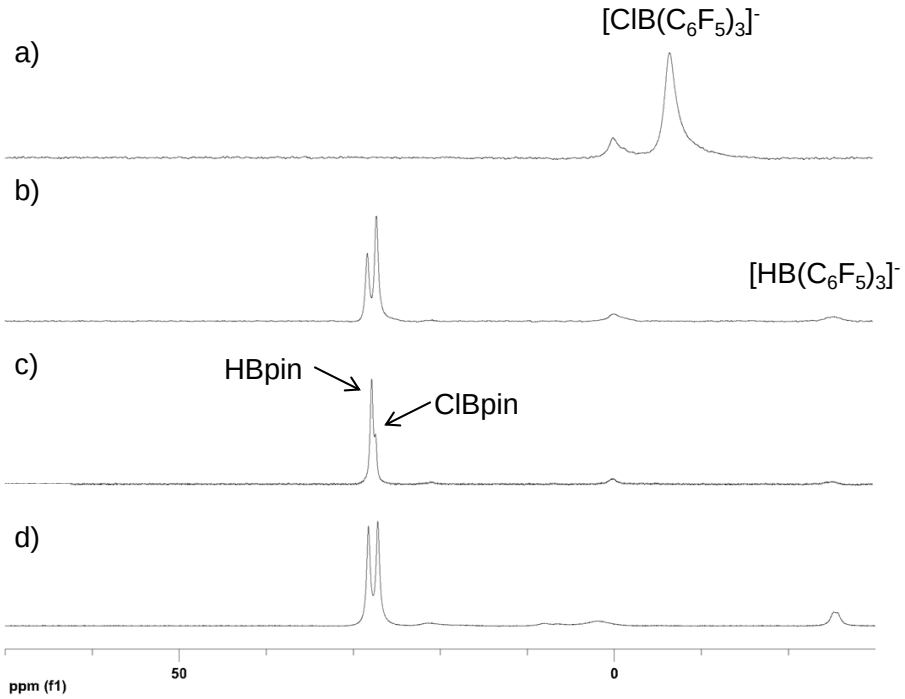

Figure D-16. ^{11}B NMR overlay for the reaction of HBpin with SelectCl and 2 equiv. of $B(C_6F_5)_3$; a) SelectCl with 2 equiv. of $B(C_6F_5)_3$; b) after addition of 1 equiv. of HBpin and 30 min at room temperature; c) the corresponding ^{11}B {^{1}H} NMR spectrum; d) after addition of 10 equiv. HBpin and 30 min at room temperature.

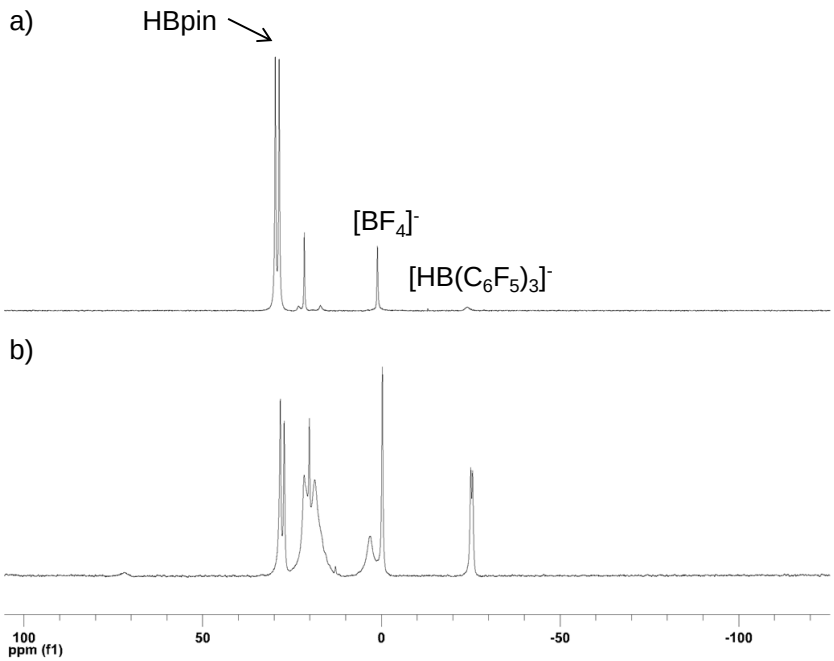

Figure D-17. ^{11}B NMR overlay for the reaction of 10 equiv. HBpin with SelectBF_4 and 2 equiv. of $B(C_6F_5)_3$; a) after 30 min at room temperature; b) after 18 h at room temperature

Appendix E: Relevant Crystallographic Data

Chapter 5

Table E-1. Cystal data and structural refinements

Crystal	**2a**	**4c**
Formula	$C_{32}H_{21}BF_{15}NO_4$	$C_{31}H_{19}BF_{15}NO_4$
Formula weight	780.35	765.28
Crystal system	Triclinic	Monoclinic
Space group	P-1	$P2_{1/n}$
a(Å)	9.7091(9)	13.7038(3)
b(Å)	12.2814(12)	27.7497(5)
c(Å)	14.0010(14)	18.4929(3)
α(°)	78.055	90.00
β(°)	82.764(1)	97.925(1)
γ(°)	86.857(1)	90.00
Volume ($Å^3$)	1619.6(3)	6965.2(2)
Z	2	8
Density (calc), g cm^{-3}	1.598	1.460
μ, mm^{-1}	0.162	0.149
Data: total (independent reflections)	6337	13625
Data $F_o^2>3\sigma(F_o^2)$	5062	7111
R^a	0.0374	0.0576
$R_w{}^b$	0.1013	0.1652
Goodness of Fit	1.036	0.933

$^aR = \Sigma(F_o-F_c)/\Sigma F_o$ $^bR_w = (\Sigma[w(F_o^2-F_c^2)^2] /\Sigma[w(F_o)^2])^{½}$

3e	**6c**	**4c**
$C_{29}H_{15}BF_{15}NO_2$	$C_{31}H_{17}BF_{15}NO_4$	$C_{37}H_{23}BF_{15}NO_4$
705.23	763.27	841.37
Monoclinic	Monoclinic	Triclinic
$P2_1/n$	$P2_1/c$	$P\bar{1}$
15.7452(13)	11.4131(2)	14.1716(6)
24.0777(18)	18.7242(3)	15.5119(6)
20.9825(18)	15.061(2)	20.4571(7)
90.00	90.00	102.540(2)
109.924(2)	108.4620(10)	95.498(3)
90.00	90.00	90.875(2)
7478.5(11)	3052.72(8)	4366.6(3)
8	4	4
1.253	1.661	1.474
0.129	0.170	0.225
14587	5983	32666
6244	4479	16989
0.0616	0.0357	0.0792
0.1747	0.0856	0.1887
0.819	1.006	0.942

Table E-2. Atomic coordinates and equivalent isotropic displacement parameters ($Å^2$) for $[C_5HMe_2(CO_2Et)_2NMe][HB(C_6F_5)_3]$ 2a

Atom	X	Y	Z	U(eq)
N1	0.80960(14)	0.00744(11)	0.22349(10)	0.0358
O1	0.87730(13)	0.33539(10)	0.32776(9)	0.0426
O2	0.75011(17)	0.21328(13)	0.44029(10)	0.0634
O3	0.79169(17)	0.33753(11)	-0.00507(10)	0.0622
O4	0.93725(14)	0.21131(10)	-0.06075(9)	0.0487
C1	0.81256(17)	0.06035(14)	0.30023(12)	0.0371
C2	0.81778(16)	0.17583(14)	0.27964(12)	0.0352
C3	0.82788(16)	0.23286(14)	0.18293(12)	0.0338
C4	0.83393(16)	0.17628(13)	0.10679(12)	0.0323
C5	0.82214(16)	0.06156(13)	0.12730(12)	0.0329
C6	0.81091(19)	0.24113(15)	0.35950(13)	0.041
C7	0.8737(2)	0.40845(17)	0.39807(15)	0.0533
C8	0.9624(3)	0.50472(19)	0.34908(18)	0.0703
C9	0.86054(18)	0.24111(14)	0.00348(12)	0.038
C10	0.7819(14)	0.4023(11)	-0.1035(11)	0.0591
C11	0.6538(16)	0.4799(16)	-0.0990(14)	0.0916
C12	0.8167(2)	-0.00871(17)	0.40119(14)	0.0533
C13	0.7935(2)	-0.11514(15)	0.24371(15)	0.0506
C14	0.81849(18)	-0.00575(14)	0.05035(13)	0.0403
B1	0.25212(19)	0.13866(16)	0.22499(14)	0.0342
H1	0.1356(19)	0.1477(14)	0.2311(13)	0.039
C15	0.30815(16)	0.18371(13)	0.10895(12)	0.0334
C16	0.42995(18)	0.14952(15)	0.05955(13)	0.0389
C17	0.47478(19)	0.18987(16)	-0.03804(14)	0.0448
C18	0.3952(2)	0.26863(16)	-0.09262(13)	0.0468
C19	0.2729(2)	0.30653(15)	-0.04864(14)	0.0447
C20	0.23281(17)	0.26389(14)	0.05009(13)	0.0379
C21	0.30040(18)	0.21727(14)	0.29555(12)	0.0378
C22	0.4171(2)	0.28077(15)	0.27798(14)	0.0458
C23	0.4494(2)	0.34958(16)	0.33808(17)	0.0571
C24	0.3633(3)	0.35534(17)	0.42260(17)	0.0628
C25	0.2472(3)	0.29168(17)	0.44516(14)	0.0574
C26	0.2186(2)	0.22575(15)	0.38182(13)	0.0449

C27	0.29056(16)	0.00698(14)	0.26621(12)	0.0341
C28	0.40046(17)	-0.03589(14)	0.31807(13)	0.0392
C29	0.42101(18)	-0.14727(15)	0.35781(13)	0.0424
C30	0.3293(2)	-0.22312(14)	0.34666(13)	0.0436
C31	0.2188(2)	-0.18590(15)	0.29601(13)	0.0436
C32	0.20317(17)	-0.07416(15)	0.25688(12)	0.0376
F16	0.51552(10)	0.07314(9)	0.10875(8)	0.0513
F17	0.59679(12)	0.15352(11)	-0.08031(9)	0.0634
F18	0.43659(14)	0.30818(11)	-0.18842(8)	0.0677
F19	0.19470(13)	0.38505(10)	-0.10065(9)	0.0672
F20	0.11285(10)	0.30753(8)	0.08887(8)	0.0482
F22	0.50891(11)	0.27882(11)	0.19707(9)	0.0611
F23	0.56437(15)	0.41059(11)	0.31368(12)	0.0827
F24	0.3925(2)	0.42030(11)	0.48289(11)	0.0927
F25	0.16252(18)	0.29397(12)	0.52892(9)	0.0837
F26	0.10172(12)	0.16585(10)	0.40987(8)	0.0566
F28	0.49749(11)	0.03319(9)	0.33123(9)	0.0574
F29	0.52980(12)	-0.18162(10)	0.40853(9)	0.063
F30	0.34806(14)	-0.33178(9)	0.38461(8)	0.0617
F31	0.12532(14)	-0.25891(10)	0.28589(10)	0.0681
F32	0.09249(11)	-0.04461(9)	0.20545(8)	0.0535

Table E-3. Atomic coordinates and equivalent isotropic displacement parameters ($Å^2$) for $[C_5H_2Me_2(CO_2Et)(CO_2EtB(C_6F_5)_3)NH]$ **4c**

Atom	X	Y	Z	U(eq)
B1	0.3547(2)	0.80505(13)	0.7968(2)	0.0322
N1	0.69992(17)	0.90004(9)	0.74956(15)	0.0379
O1	0.45839(13)	0.80404(7)	0.84218(11)	0.0335
O2	0.61601(14)	0.79169(7)	0.87699(12)	0.0384
O3	0.37856(15)	0.96459(8)	0.70125(14)	0.0502
O4	0.49920(15)	0.99001(8)	0.63999(14)	0.0498
C1	0.6782(2)	0.86789(11)	0.79749(18)	0.0331
C2	0.5774(2)	0.85717(10)	0.79907(17)	0.0308
C3	0.5079(2)	0.89142(10)	0.76366(17)	0.0298
C4	0.5315(2)	0.92336(11)	0.71501(18)	0.0342
C5	0.6315(2)	0.91990(11)	0.68969(18)	0.0364
C6	0.5466(2)	0.81779(10)	0.83902(17)	0.0302

C7	0.5887(2)	0.74759(13)	0.9119(2)	0.049
C8	0.6817(2)	0.72726(14)	0.9521(2)	0.0557
C9	0.4618(2)	0.96054(11)	0.68622(19)	0.0384
C10	0.4385(3)	1.03022(14)	0.6109(3)	0.0684
C11	0.5018(3)	1.06348(15)	0.5757(2)	0.0741
C12	0.7638(2)	0.84854(13)	0.8469(2)	0.0447
C13	0.6311(2)	0.88854(14)	0.6222(2)	0.0535
C14	0.3115(2)	0.75108(11)	0.81147(18)	0.0329
C15	0.3173(2)	0.73313(11)	0.88168(19)	0.0354
C16	0.2836(2)	0.68816(12)	0.8988(2)	0.0464
C17	0.2417(3)	0.65888(12)	0.8441(3)	0.0522
C18	0.2321(3)	0.67494(13)	0.7737(2)	0.0529
C19	0.2651(2)	0.72022(12)	0.7587(2)	0.0428
C20	0.3659(2)	0.81383(10)	0.71103(17)	0.0322
C21	0.4328(2)	0.78592(11)	0.67823(18)	0.0365
C22	0.4490(2)	0.79113(13)	0.6070(2)	0.0454
C23	0.3969(3)	0.82566(14)	0.56360(19)	0.0469
C24	0.3296(2)	0.85304(12)	0.5922(2)	0.0422
C25	0.3155(2)	0.84671(11)	0.66456(19)	0.0361
C26	0.2872(2)	0.84471(10)	0.83322(17)	0.0323
C27	0.3197(2)	0.87989(11)	0.88393(18)	0.0387
C28	0.2583(3)	0.91157(12)	0.9137(2)	0.0493
C29	0.1589(3)	0.90911(14)	0.8928(2)	0.0554
C30	0.1220(2)	0.87478(14)	0.8441(2)	0.048
C31	0.1856(2)	0.84376(12)	0.81552(19)	0.0389
F15	0.35709(13)	0.76022(7)	0.93906(10)	0.0444
F16	0.29329(16)	0.67261(8)	0.96856(13)	0.0649
F17	0.20993(18)	0.61438(7)	0.85928(16)	0.0833
F18	0.18826(18)	0.64685(8)	0.71932(15)	0.0812
F19	0.24943(15)	0.73346(7)	0.68784(12)	0.0589
F21	0.48583(13)	0.75151(7)	0.71755(10)	0.0481
F22	0.51504(15)	0.76379(8)	0.57916(12)	0.0674
F23	0.41246(16)	0.83193(9)	0.49459(11)	0.0682
F24	0.27911(15)	0.88713(8)	0.55154(12)	0.0638
F25	0.24850(13)	0.87606(7)	0.68851(11)	0.0492
F27	0.41715(14)	0.88554(7)	0.90726(10)	0.0494
F28	0.29688(19)	0.94454(7)	0.96265(12)	0.0706
F29	0.09851(19)	0.93995(9)	0.92067(12)	0.0802
F30	0.02381(14)	0.87147(9)	0.82336(13)	0.0688

F31	0.14411(12)	0.81146(7)	0.76582(11)	0.0513

Table E-4. Atomic coordinates and equivalent isotropic displacement parameters ($Å^2$) for $[C_5H_2Me_2(COMe)(COMeB(C_6F_5)_3)NH]$ **3e**

Atom	X	Y	Z	U(eq)
B1	0.3202(3)	0.73788(17)	0.3543(2)	0.0321
N1	0.3904(2)	0.68140(14)	0.11586(16)	0.0409
O1	0.31703(14)	0.72025(10)	0.28303(12)	0.0349
O2	0.31753(17)	0.79515(11)	-0.04934(13)	0.0471
C1	0.3648(2)	0.68958(16)	0.17052(19)	0.0364
C2	0.3054(2)	0.73266(15)	0.16895(18)	0.0322
C3	0.2652(2)	0.76732(16)	0.10552(17)	0.0372
C4	0.3050(2)	0.75510(15)	0.05067(17)	0.0327
C5	0.3643(2)	0.71363(16)	0.05668(18)	0.0367
C6	0.4073(3)	0.65019(16)	0.2281(2)	0.0459
C7	0.2839(2)	0.74813(15)	0.22623(18)	0.0324
C8	0.2238(2)	0.79670(15)	0.22227(19)	0.0389
C9	0.2741(2)	0.78982(16)	-0.01067(19)	0.0383
C10	0.1850(2)	0.81937(18)	-0.0264(2)	0.0478
C11	0.4081(3)	0.69503(19)	0.0071(2)	0.0527
C12	0.2212(2)	0.73574(15)	0.36347(19)	0.0351
C13	0.2127(3)	0.75141(16)	0.4246(2)	0.0423
C14	0.1336(3)	0.74898(17)	0.4383(2)	0.0491
C15	0.0579(3)	0.72824(17)	0.3915(2)	0.05
C16	0.0617(2)	0.70945(17)	0.3309(2)	0.0465
C17	0.1421(2)	0.71349(16)	0.3182(2)	0.0392
C18	0.3789(2)	0.68834(15)	0.40484(17)	0.0316
C19	0.4450(2)	0.69561(15)	0.46750(18)	0.0343
C20	0.4875(2)	0.65263(16)	0.50998(18)	0.0366
C21	0.4641(2)	0.59957(17)	0.4914(2)	0.0458
C22	0.3982(3)	0.58956(16)	0.4302(2)	0.043
C23	0.3578(2)	0.63331(15)	0.38920(19)	0.0345
C24	0.3711(2)	0.79865(16)	0.36799(18)	0.0384
C25	0.3366(3)	0.84928(18)	0.3762(2)	0.0475
C26	0.3824(3)	0.89950(18)	0.3855(2)	0.0567
C27	0.4690(4)	0.8994(2)	0.3854(2)	0.0594

C28	0.5081(3)	0.8505(2)	0.3757(2)	0.0567
C29	0.4593(3)	0.80194(17)	0.36717(19)	0.0421
F13	0.28644(15)	0.77201(10)	0.47417(11)	0.0552
F14	0.13077(17)	0.76743(11)	0.49915(13)	0.0706
F15	-0.02074(16)	0.72654(11)	0.40385(15)	0.074
F16	-0.01177(14)	0.68697(10)	0.28497(13)	0.0637
F17	0.13986(13)	0.69416(9)	0.25685(11)	0.0477
F19	0.47374(13)	0.74706(9)	0.49082(11)	0.0463
F20	0.55253(14)	0.66397(9)	0.56987(11)	0.0539
F21	0.50393(17)	0.55726(10)	0.53267(13)	0.0734
F22	0.37272(16)	0.53654(9)	0.41129(12)	0.0631
F23	0.29055(12)	0.61966(8)	0.33049(10)	0.0412
F25	0.24870(15)	0.85364(9)	0.37473(12)	0.0576
F26	0.34378(19)	0.94675(10)	0.39434(13)	0.0732
F27	0.5162(2)	0.94705(11)	0.39494(14)	0.0888
F28	0.59345(18)	0.85004(12)	0.37409(15)	0.0854
F29	0.50190(13)	0.75489(10)	0.35828(11)	0.0514

Table E-5. Atomic coordinates and equivalent isotropic displacement parameters ($Å^2$) for $[C_5HMe_2Ph(CO_2Me)(CO_2EtB(C_6F_5)_3)NH]$ **3f**

Atom	X	Y	Z	U(eq)
B1	0.6166(5)	0.1298(4)	0.3523(3)	0.0489
N1	0.8642(3)	0.3527(3)	0.2894(2)	0.0415
O1	0.6680(3)	0.2085(3)	0.40706(17)	0.0535
O3	0.5416(3)	0.3449(3)	0.20955(19)	0.0581
O4	0.6455(3)	0.3369(3)	0.13421(17)	0.057
C1	0.8475(4)	0.3204(4)	0.3450(3)	0.0433
C2	0.7558(4)	0.3082(4)	0.3564(2)	0.043
C3	0.6746(4)	0.3423(4)	0.3163(2)	0.0404
C4	0.7029(4)	0.3460(3)	0.2478(2)	0.0358
C5	0.7942(4)	0.3566(3)	0.2379(2)	0.0348
C6	0.9371(4)	0.2973(4)	0.3818(3)	0.0566
C7	0.8345(4)	0.3722(4)	0.1760(3)	0.0495
C8	0.7361(5)	0.2628(4)	0.4086(3)	0.0539
O2	0.8119(10)	0.2670(13)	0.4556(6)	0.0466
C9	0.813(2)	0.2147(15)	0.5041(10)	0.0729
C10	0.7631(16)	0.2624(13)	0.5645(9)	0.0705

C11	0.6224(4)	0.3424(4)	0.1967(3)	0.0421
C12	0.5690(5)	0.3355(6)	0.0814(3)	0.0812
C13	0.603(2)	0.326(3)	0.0170(10)	0.116
C14	0.6445(4)	0.4335(4)	0.3537(2)	0.0383
C15	0.7009(4)	0.5095(4)	0.3585(3)	0.0472
C16	0.6742(4)	0.5911(4)	0.3913(3)	0.0535
C17	0.5901(5)	0.5981(4)	0.4205(3)	0.0514
C18	0.5335(4)	0.5244(4)	0.4167(3)	0.0482
C19	0.5597(4)	0.4424(4)	0.3826(2)	0.043
C20	0.5037(5)	0.1456(4)	0.3482(3)	0.0505
C21	0.4560(5)	0.2107(5)	0.3879(3)	0.0585
C22	0.3583(6)	0.2166(5)	0.3826(4)	0.0673
C23	0.3040(6)	0.1542(6)	0.3369(4)	0.0772
C24	0.3458(6)	0.0861(5)	0.2984(4)	0.0681
C25	0.4416(5)	0.0827(4)	0.3042(3)	0.0589
C26	0.6681(5)	0.1227(4)	0.2833(3)	0.0468
C27	0.6258(5)	0.1301(4)	0.2209(3)	0.0528
C28	0.6755(6)	0.1218(4)	0.1647(3)	0.0598
C29	0.7703(6)	0.1071(4)	0.1696(3)	0.0657
C30	0.8161(6)	0.1000(4)	0.2301(3)	0.0621
C31	0.7641(5)	0.1080(4)	0.2851(3)	0.0524
C32	0.6324(4)	0.0424(4)	0.3856(3)	0.0487
C33	0.6135(4)	0.0451(4)	0.4520(3)	0.0507
C34	0.6204(5)	-0.0249(5)	0.4821(3)	0.0592
C35	0.6441(5)	-0.1042(4)	0.4470(3)	0.0629
C36	0.6625(5)	-0.1126(4)	0.3814(3)	0.0637
C37	0.6552(5)	-0.0399(4)	0.3522(3)	0.0563
F21	0.5046(3)	0.2737(2)	0.43600(16)	0.0698
F22	0.3179(3)	0.2848(3)	0.4219(2)	0.092
F23	0.2096(3)	0.1621(4)	0.3305(2)	0.1093
F24	0.2923(3)	0.0241(3)	0.2539(2)	0.0996
F25	0.4812(3)	0.0131(2)	0.26562(16)	0.0658
F27	0.5345(3)	0.1484(2)	0.21142(15)	0.0632
F28	0.6313(3)	0.1283(3)	0.10567(16)	0.0815
F29	0.8202(3)	0.0984(3)	0.11591(18)	0.0884
F30	0.9102(3)	0.0853(3)	0.23705(19)	0.0811
F31	0.8136(2)	0.1003(2)	0.34402(16)	0.0626
F32	0.5844(3)	0.1211(2)	0.48972(15)	0.0647
F33	0.6029(3)	-0.0157(2)	0.54746(16)	0.0708

F35	0.6490(3)	-0.1755(3)	0.47494(19)	0.0859
F36	0.6842(3)	-0.1918(3)	0.34478(19)	0.0894
F37	0.6748(3)	-0.0551(2)	0.28756(16)	0.0697

Table E-6. Atomic coordinates and equivalent isotropic displacement parameters ($Å^2$) for $[C_5HMe_2(CO_2Et)(CO_2EtB(C_6F_5)_3)N]$ **6c**

Atom	X	Y	Z	U(eq)
N1	0.54175(14)	0.21399(8)	0.60957(12)	0.0371
B1	0.97152(19)	0.21971(10)	0.89849(14)	0.0234
O1	0.89802(11)	0.12691(6)	0.66531(8)	0.0278
O2	0.95408(11)	0.18052(6)	0.80162(8)	0.0243
O3	0.56787(12)	0.44011(7)	0.61580(10)	0.0377
O4	0.74952(13)	0.42983(7)	0.72881(11)	0.0416
C1	0.64732(17)	0.17725(9)	0.64141(13)	0.0281
C2	0.75958(16)	0.21239(9)	0.68474(12)	0.0234
C3	0.75969(16)	0.28601(9)	0.69249(12)	0.0237
C4	0.65093(16)	0.32403(9)	0.65699(13)	0.0269
C5	0.54195(18)	0.28577(10)	0.61607(15)	0.0367
C6	0.63498(18)	0.09737(10)	0.63077(14)	0.0347
C7	0.87654(16)	0.17281(9)	0.72251(12)	0.0229
C8	1.01192(17)	0.08308(9)	0.69807(13)	0.0292
C9	1.0047(2)	0.02843(11)	0.62481(15)	0.0452
C10	0.4154(2)	0.31899(13)	0.5777(2)	0.0707
C11	0.66236(17)	0.40322(10)	0.67172(13)	0.0292
C12	0.5680(2)	0.51679(10)	0.63435(15)	0.0416
C13	0.5223(2)	0.53016(12)	0.71500(17)	0.0519
C14	0.84114(16)	0.25478(9)	0.90014(12)	0.023
C15	0.73743(17)	0.21275(9)	0.88732(13)	0.0275
C16	0.62425(18)	0.23835(11)	0.88667(15)	0.0366
C17	0.60995(18)	0.31023(11)	0.89777(15)	0.0383
C18	0.70870(19)	0.35471(10)	0.91115(14)	0.0332
C19	0.82116(17)	0.32681(9)	0.91205(12)	0.0266
C20	1.02264(16)	0.15410(9)	0.97306(12)	0.024
C21	0.98150(17)	0.13735(9)	1.04776(13)	0.0278
C22	1.02748(18)	0.08235(10)	1.10929(13)	0.0309
C23	1.12102(18)	0.04047(9)	1.09902(13)	0.0311
C24	1.16724(16)	0.05472(9)	1.02713(13)	0.0288

C25	1.11930(16)	0.11087(9)	0.96750(12)	0.0258
C26	1.08199(16)	0.27762(9)	0.91038(12)	0.0237
C27	1.12646(16)	0.30406(10)	0.84176(13)	0.0283
C28	1.21713(17)	0.35598(10)	0.85759(14)	0.0333
C29	1.26802(17)	0.38388(9)	0.94571(15)	0.0341
C30	1.22833(18)	0.35890(10)	1.01696(14)	0.0338
C31	1.13805(17)	0.30737(9)	0.99833(13)	0.029
F15	0.74543(10)	0.14176(5)	0.87380(8)	0.0371
F16	0.52739(11)	0.19417(7)	0.87435(11)	0.0596
F17	0.49963(11)	0.33642(7)	0.89504(11)	0.0603
F18	0.69647(12)	0.42505(6)	0.92221(9)	0.0468
F19	0.91195(10)	0.37494(5)	0.92366(8)	0.0361
F21	0.89167(10)	0.17655(6)	1.06492(8)	0.0396
F22	0.98332(11)	0.06979(6)	1.18050(8)	0.0466
F23	1.16662(11)	-0.01301(6)	1.15912(8)	0.0455
F24	1.25950(10)	0.01478(6)	1.01612(8)	0.0429
F25	1.17345(9)	0.12373(6)	0.90107(7)	0.0335
F27	1.07968(10)	0.28126(6)	0.75202(7)	0.0401
F28	1.25391(11)	0.38018(7)	0.78650(9)	0.0496
F29	1.35310(10)	0.43547(6)	0.96123(9)	0.0483
F30	1.27545(11)	0.38624(7)	1.10336(9)	0.0507
F31	1.09848(11)	0.28736(6)	1.07038(8)	0.0408

Table E-7. Cystal data and structural refinements

Crystal	**5a**
Formula	$C_{35}H_{41}BN_2S_4$
Formula weight	628.75
Crystal system	Triclinic
Space group	P-1
a(Å)	10.6039(8)
b(Å)	11.1039(9)
c(Å)	14.9573(11)
α(°)	92.347(1)
β(°)	105.624(1)
γ(°)	96.677(1)
Volume (Å^3)	1679.7(2)
Z	2
Density (calc), g cm^{-3}	1.243
μ, mm^{-1}	0.310
Data: total (independent reflections)	6558
Data $F_o^2>3\sigma(F_o^2)$	5897
R^a	0.0370
R_w^b	0.0970
Goodness of Fit	0.992

$^aR = \Sigma(F_o-F_c)/\Sigma F_o$ $^bR_w = (\Sigma[w(F_o^2-F_c^2)^2] /\Sigma[w(F_o)^2])^{½}$

Table E-8. Atomic coordinates and equivalent isotropic displacement parameters ($Å^2$) for $[C_2H_2(NtBu)_2CH][B(SC_6H_5)_4]$ **5a**

Atom	X	Y	Z	U(eq)
B1	0.16238(19)	0.19748(17)	0.28817(13)	0.0301
S1	0.29982(4)	0.30089(4)	0.37813(3)	0.0367
S2	0.03472(5)	0.30055(4)	0.23281(3)	0.0369
S3	0.06684(4)	0.06514(4)	0.33192(3)	0.0324
S4	0.25273(5)	0.13115(4)	0.20356(3)	0.0356
N1	0.27633(16)	0.70947(13)	0.22454(10)	0.0373
N2	0.48515(16)	0.78158(14)	0.25825(10)	0.0397
C1	0.36288(19)	0.80301(16)	0.21743(12)	0.0357
C2	0.3460(2)	0.62397(19)	0.27223(15)	0.0522
C3	0.4741(3)	0.66825(19)	0.29293(15)	0.0548
C4	0.12872(19)	0.69480(16)	0.18638(13)	0.0387
C5	0.0693(2)	0.66012(19)	0.26568(15)	0.0532
C6	0.0868(2)	0.81373(17)	0.15082(14)	0.0438
C7	0.0902(3)	0.59433(19)	0.10733(15)	0.0554
C8	0.6122(2)	0.8584(2)	0.25947(14)	0.0451
C9	0.5865(2)	0.9889(2)	0.24284(17)	0.055
C10	0.7095(2)	0.8544(3)	0.35426(18)	0.0696
C11	0.6616(3)	0.8039(3)	0.1819(2)	0.0712
C12	0.23545(16)	0.37225(15)	0.46181(11)	0.0305
C13	0.11601(18)	0.33206(16)	0.47981(12)	0.0364
C14	0.07912(19)	0.38986(18)	0.55089(13)	0.0417
C15	0.1601(2)	0.48676(17)	0.60608(13)	0.0416
C16	0.27799(19)	0.52806(17)	0.58796(13)	0.0415
C17	0.31464(18)	0.47263(16)	0.51577(13)	0.0379
C18	-0.09935(18)	0.21307(18)	0.14971(12)	0.0387
C19	-0.0943(2)	0.10048(19)	0.10684(13)	0.0452
C20	-0.2050(2)	0.0397(2)	0.04186(14)	0.0564
C21	-0.3211(2)	0.0898(3)	0.01816(15)	0.0674
C22	-0.3266(3)	0.2015(3)	0.05911(19)	0.0775
C23	-0.2176(2)	0.2625(3)	0.12428(16)	0.0605
C24	0.17810(16)	-0.02213(14)	0.40322(11)	0.0301
C25	0.30600(17)	-0.03052(16)	0.39790(12)	0.0352
C26	0.38221(18)	-0.10776(17)	0.45267(13)	0.0394
C27	0.33465(19)	-0.17567(18)	0.51428(14)	0.0436

C28	0.20826(19)	-0.16679(18)	0.52112(14)	0.0439
C29	0.13014(18)	-0.09157(16)	0.46563(13)	0.0362
C30	0.3227(3)	0.2603(2)	0.1577(2)	0.0444
C31	0.2514(3)	0.3128(2)	0.0801(2)	0.0444
C32	0.3099(3)	0.4145(2)	0.04752(18)	0.0444
C33	0.4398(3)	0.46367(18)	0.09248(19)	0.0444
C34	0.5111(3)	0.41116(19)	0.17003(19)	0.0444
C35	0.4525(3)	0.3095(2)	0.20261(19)	0.0444

Appendix F: Rights and Permissions

Home | Create Account | Help

Title: On the Controllable Soft-Templating Approach to Mesoporous Silicates

Author: Ying Wan et al.

Publication: Chemical Reviews

Publisher: American Chemical Society

Date: Jul 1, 2007

User ID

Password

Enable Auto Login

LOGIN

Forgot Password/User ID?

If you're a copyright.com user, you can login to Rightslink using your copyright.com credentials.

Already **a Rightslink user** or want to learn more?

No charge permission and attribution

Permission for this particular request is granted for print and electronic formats at no charge. Figures and tables may be modified. Appropriate credit should be given. Please print this page for your records and provide a copy to your publisher. Requests for up to 4 figures require only this record. Five or more figures will generate a printout of additional terms and conditions. Appropriate credit should read: "Reprinted with permission from {COMPLETE REFERENCE CITATION}. Copyright {YEAR} American Chemical Society." Insert appropriate information in place of the capitalized words.

This permission does not apply to images that are credited to publications other than ACS journals. For images credited to non-ACS journal publications, you will need to obtain permission from the journal referenced in the Table/Figure/Micrograph legend or credit line before making any use of the image(s) or table(s).

BACK | CLOSE WINDOW

JOHN WILEY AND SONS LICENSE TERMS AND CONDITIONS

Jul 27, 2011

This is a License Agreement between Jonathan D Webb ("You") and John Wiley and Sons ("John Wiley and Sons") provided by Copyright Clearance Center ("CCC"). The license consists of your order details, the terms and conditions provided by John Wiley and Sons, and the payment terms and conditions.

All payments must be made in full to CCC. For payment instructions, please see information listed at the bottom of this form.

License Number	2717101230248
License date	Jul 27, 2011
Licensed content publisher	John Wiley and Sons
Licensed content publication	Angewandte Chemie International Edition
Licensed content title	Silica-Based Mesoporous Organic–Inorganic Hybrid Materials
Licensed content author	Frank Hoffmann,Maximilian Cornelius,Jürgen Morell,Michael Fröba
Licensed content date	May 12, 2006
Start page	3216
End page	3251
Type of use	Dissertation/Thesis
Requestor type	University/Academic
Format	Print and electronic
Portion	Figure/table
Number of figures/tables	4
Number of extracts	
Original Wiley figure/table number(s)	Figure 2, Figure 3, Figure 4, Figure 5
Will you be translating?	No
Order reference number	
Total	0.00 USD
Terms and Conditions	

TERMS AND CONDITIONS

This copyrighted material is owned by or exclusively licensed to John Wiley & Sons, Inc. or one of its group companies (each a "Wiley Company") or a society for whom a Wiley Company has exclusive publishing rights in relation to a particular journal (collectively WILEY"). By clicking "accept" in connection with completing this licensing transaction, you agree that the following terms and conditions apply to this transaction (along with the billing and payment terms and conditions established by the Copyright Clearance Center Inc., ("CCC's Billing and Payment terms

and conditions"), at the time that you opened your Rightslink account (these are available at any time at http://myaccount.copyright.com)

Terms and Conditions

1. The materials you have requested permission to reproduce (the "Materials") are protected by copyright.

2. You are hereby granted a personal, non-exclusive, non-sublicensable, non-transferable, worldwide, limited license to reproduce the Materials for the purpose specified in the licensing process. This license is for a one-time use only with a maximum distribution equal to the number that you identified in the licensing process. Any form of republication granted by this licence must be completed within two years of the date of the grant of this licence (although copies prepared before may be distributed thereafter). The Materials shall not be used in any other manner or for any other purpose. Permission is granted subject to an appropriate acknowledgement given to the author, title of the material/book/journal and the publisher. You shall also duplicate the copyright notice that appears in the Wiley publication in your use of the Material. Permission is also granted on the understanding that nowhere in the text is a previously published source acknowledged for all or part of this Material. Any third party material is expressly excluded from this permission.

3. With respect to the Materials, all rights are reserved. Except as expressly granted by the terms of the license, no part of the Materials may be copied, modified, adapted (except for minor reformatting required by the new Publication), translated, reproduced, transferred or distributed, in any form or by any means, and no derivative works may be made based on the Materials without the prior permission of the respective copyright owner. You may not alter, remove or suppress in any manner any copyright, trademark or other notices displayed by the Materials. You may not license, rent, sell, loan, lease, pledge, offer as security, transfer or assign the Materials, or any of the rights granted to you hereunder to any other person.

4. The Materials and all of the intellectual property rights therein shall at all times remain the exclusive property of John Wiley & Sons Inc or one of its related companies (WILEY) or their respective licensors, and your interest therein is only that of having possession of and the right to reproduce the Materials pursuant to Section 2 herein during the continuance of this Agreement. You agree that you own no right, title or interest in or to the Materials or any of the intellectual property rights therein. You shall have no rights hereunder other than the license as provided for above in Section 2. No right, license or interest to any trademark, trade name, service mark or other branding ("Marks") of WILEY or its licensors is granted hereunder, and you agree that you shall not assert any such right, license or interest with respect thereto.

5. NEITHER WILEY NOR ITS LICENSORS MAKES ANY WARRANTY OR REPRESENTATION OF ANY KIND TO YOU OR ANY THIRD PARTY, EXPRESS, IMPLIED OR STATUTORY, WITH RESPECT TO THE MATERIALS OR THE ACCURACY OF ANY INFORMATION CONTAINED IN THE MATERIALS, INCLUDING, WITHOUT LIMITATION, ANY IMPLIED WARRANTY OF MERCHANTABILITY, ACCURACY, SATISFACTORY QUALITY, FITNESS FOR A PARTICULAR PURPOSE, USABILITY, INTEGRATION OR NON-INFRINGEMENT AND ALL SUCH WARRANTIES ARE HEREBY EXCLUDED BY WILEY AND ITS LICENSORS AND WAIVED BY YOU.

6. WILEY shall have the right to terminate this Agreement immediately upon breach of this Agreement by you.

7. You shall indemnify, defend and hold harmless WILEY, its Licensors and their respective directors, officers, agents and employees, from and against any actual or threatened claims, demands, causes of action or proceedings arising from any breach of this Agreement by you.

8. IN NO EVENT SHALL WILEY OR ITS LICENSORS BE LIABLE TO YOU OR ANY OTHER PARTY OR ANY OTHER PERSON OR ENTITY FOR ANY SPECIAL, CONSEQUENTIAL, INCIDENTAL, INDIRECT, EXEMPLARY OR PUNITIVE DAMAGES, HOWEVER CAUSED, ARISING OUT OF OR IN CONNECTION WITH THE DOWNLOADING, PROVISIONING, VIEWING OR USE OF THE MATERIALS REGARDLESS

OF THE FORM OF ACTION, WHETHER FOR BREACH OF CONTRACT, BREACH OF WARRANTY, TORT, NEGLIGENCE, INFRINGEMENT OR OTHERWISE (INCLUDING, WITHOUT LIMITATION, DAMAGES BASED ON LOSS OF PROFITS, DATA, FILES, USE, BUSINESS OPPORTUNITY OR CLAIMS OF THIRD PARTIES), AND WHETHER OR NOT THE PARTY HAS BEEN ADVISED OF THE POSSIBILITY OF SUCH DAMAGES. THIS LIMITATION SHALL APPLY NOTWITHSTANDING ANY FAILURE OF ESSENTIAL PURPOSE OF ANY LIMITED REMEDY PROVIDED HEREIN.

9. Should any provision of this Agreement be held by a court of competent jurisdiction to be illegal, invalid, or unenforceable, that provision shall be deemed amended to achieve as nearly as possible the same economic effect as the original provision, and the legality, validity and enforceability of the remaining provisions of this Agreement shall not be affected or impaired thereby.

10. The failure of either party to enforce any term or condition of this Agreement shall not constitute a waiver of either party's right to enforce each and every term and condition of this Agreement. No breach under this agreement shall be deemed waived or excused by either party unless such waiver or consent is in writing signed by the party granting such waiver or consent. The waiver by or consent of a party to a breach of any provision of this Agreement shall not operate or be construed as a waiver of or consent to any other or subsequent breach by such other party.

11. This Agreement may not be assigned (including by operation of law or otherwise) by you without WILEY's prior written consent.

12. Any fee required for this permission shall be non-refundable after thirty (30) days from receipt.

13. These terms and conditions together with CCC's Billing and Payment terms and conditions (which are incorporated herein) form the entire agreement between you and WILEY concerning this licensing transaction and (in the absence of fraud) supersedes all prior agreements and representations of the parties, oral or written. This Agreement may not be amended except in writing signed by both parties. This Agreement shall be binding upon and inure to the benefit of the parties' successors, legal representatives, and authorized assigns.

14. In the event of any conflict between your obligations established by these terms and conditions and those established by CCC's Billing and Payment terms and conditions, these terms and conditions shall prevail.

15. WILEY expressly reserves all rights not specifically granted in the combination of (i) the license details provided by you and accepted in the course of this licensing transaction, (ii) these terms and conditions and (iii) CCC's Billing and Payment terms and conditions.

16. This Agreement will be void if the Type of Use, Format, Circulation, or Requestor Type was misrepresented during the licensing process.

17. This Agreement shall be governed by and construed in accordance with the laws of the State of New York, USA, without regards to such state's conflict of law rules. Any legal action, suit or proceeding arising out of or relating to these Terms and Conditions or the breach thereof shall be instituted in a court of competent jurisdiction in New York County in the State of New York in the United States of America and each party hereby consents and submits to the personal jurisdiction of such court, waives any objection to venue in such court and consents to service of process by registered or certified mail, return receipt requested, at the last known address of such party.

Wiley Open Access Terms and Conditions

All research articles published in Wiley Open Access journals are fully open access: immediately freely available to read, download and share. Articles are published under the terms of the Creative Commons Attribution Non Commercial License. which permits use, distribution and

reproduction in any medium, provided the original work is properly cited and is not used for commercial purposes. The license is subject to the Wiley Open Access terms and conditions: Wiley Open Access articles are protected by copyright and are posted to repositories and websites in accordance with the terms of the Creative Commons Attribution Non Commercial License. At the time of deposit, Wiley Open Access articles include all changes made during peer review, copyediting, and publishing. Repositories and websites that host the article are responsible for incorporating any publisher-supplied amendments or retractions issued subsequently. Wiley Open Access articles are also available without charge on Wiley's publishing platform, **Wiley Online Library** or any successor sites.

Use by non-commercial users

For non-commercial and non-promotional purposes individual users may access, download, copy, display and redistribute to colleagues Wiley Open Access articles, as well as adapt, translate, text- and data-mine the content subject to the following conditions:

- The authors' moral rights are not compromised. These rights include the right of "paternity" (also known as "attribution" - the right for the author to be identified as such) and "integrity" (the right for the author not to have the work altered in such a way that the author's reputation or integrity may be impugned).
- Where content in the article is identified as belonging to a third party, it is the obligation of the user to ensure that any reuse complies with the copyright policies of the owner of that content.
- If article content is copied, downloaded or otherwise reused for non-commercial research and education purposes, a link to the appropriate bibliographic citation (authors, journal, article title, volume, issue, page numbers, DOI and the link to the definitive published version on Wiley Online Library) should be maintained. Copyright notices and disclaimers must not be deleted.
- Any translations, for which a prior translation agreement with Wiley has not been agreed, must prominently display the statement: "This is an unofficial translation of an article that appeared in a Wiley publication. The publisher has not endorsed this translation."

Use by commercial "for-profit" organisations

Use of Wiley Open Access articles for commercial, promotional, or marketing purposes requires further explicit permission from Wiley and will be subject to a fee. Commercial purposes include:

- Copying or downloading of articles, or linking to such articles for further redistribution, sale or licensing;
- Copying, downloading or posting by a site or service that incorporates advertising with such content;
- The inclusion or incorporation of article content in other works or services (other than normal quotations with an appropriate citation) that is then available for sale or licensing, for a fee (for example, a compilation produced for marketing purposes, inclusion in a sales pack)
- Use of article content (other than normal quotations with appropriate citation) by for-profit organisations for promotional purposes

- Linking to article content in e-mails redistributed for promotional, marketing or educational purposes;
- Use for the purposes of monetary reward by means of sale, resale, licence, loan, transfer or other form of commercial exploitation such as marketing products
- Print reprints of Wiley Open Access articles can be purchased from: corporatesales@wiley.com

Other Terms and Conditions:

BY CLICKING ON THE "I AGREE..." BOX, YOU ACKNOWLEDGE THAT YOU HAVE READ AND FULLY UNDERSTAND EACH OF THE SECTIONS OF AND PROVISIONS SET FORTH IN THIS AGREEMENT AND THAT YOU ARE IN AGREEMENT WITH AND ARE WILLING TO ACCEPT ALL OF YOUR OBLIGATIONS AS SET FORTH IN THIS AGREEMENT.

v1.7

Gratis licenses (referencing $0 in the Total field) are free. Please retain this printable license for your reference. No payment is required.

If you would like to pay for this license now, please remit this license along with your payment made payable to "COPYRIGHT CLEARANCE CENTER" otherwise you will be invoiced within 48 hours of the license date. Payment should be in the form of a check or money order referencing your account number and this invoice number RLNK11027775.
Once you receive your invoice for this order, you may pay your invoice by credit card. Please follow instructions provided at that time.

Make Payment To:
Copyright Clearance Center
Dept 001
P.O. Box 843006
Boston, MA 02284-3006

For suggestions or comments regarding this order, contact Rightslink Customer Support: customercare@copyright.com or +1-877-622-5543 (toll free in the US) or +1-978-646-2777.

No charge permission and attribution

Permission for this particular request is granted for print and electronic formats at no charge. Figures and tables may be modified. Appropriate credit should be given. Please print this page for your records and provide a copy to your publisher. Requests for up to 4 figures require only this record. Five or more figures will generate a printout of additional terms and conditions. Appropriate credit should read: "Reprinted with permission from {COMPLETE REFERENCE CITATION}. Copyright {YEAR} American Chemical Society." Insert appropriate information in place of the capitalized words.

This permission does not apply to images that are credited to publications other than ACS journals. For images credited to non-ACS journal publications, you will need to obtain permission from the journal referenced in the Table/Figure/Micrograph legend or credit line before making any use of the image(s) or table(s).

BACK CLOSE WINDOW

RightsLink®

Home | Account Info | Help

Title: Selective Functionalization of the Outer and Inner Surfaces in Mesoporous Silica Nanoparticles

Author: Johann Kecht et al.

Publication: Chemistry of Materials

Publisher: American Chemical Society

Date: Dec 1, 2008

Logged in as:
Jonathan Webb
Account #:
3000432578

LOGOUT

No charge permission and attribution

Permission for this particular request is granted for print and electronic formats at no charge. Figures and tables may be modified. Appropriate credit should be given. Please print this page for your records and provide a copy to your publisher. Requests for up to 4 figures require only this record. Five or more figures will generate a printout of additional terms and conditions. Appropriate credit should read: "Reprinted with permission from {COMPLETE REFERENCE CITATION}. Copyright {YEAR} American Chemical Society." Insert appropriate information in place of the capitalized words.

This permission does not apply to images that are credited to publications other than ACS journals. For images credited to non-ACS journal publications, you will need to obtain permission from the journal referenced in the Table/Figure/Micrograph legend or credit line before making any use of the image(s) or table(s).

BACK CLOSE WINDOW

JOHN WILEY AND SONS LICENSE TERMS AND CONDITIONS

Jul 27, 2011

This is a License Agreement between Jonathan D Webb ("You") and John Wiley and Sons ("John Wiley and Sons") provided by Copyright Clearance Center ("CCC"). The license consists of your order details, the terms and conditions provided by John Wiley and Sons, and the payment terms and conditions.

All payments must be made in full to CCC. For payment instructions, please see information listed at the bottom of this form.

License Number	2717110664683
License date	Jul 27, 2011
Licensed content publisher	John Wiley and Sons
Licensed content publication	Angewandte Chemie International Edition
Licensed content title	Controlling and Imaging the Functional-Group Distribution on Mesoporous Silica
Licensed content author	Nando Gartmann,Dominik Brühwiler
Licensed content date	Aug 10, 2009
Start page	6354
End page	6356
Type of use	Dissertation/Thesis
Requestor type	University/Academic
Format	Print and electronic
Portion	Figure/table
Number of figures/tables	1
Number of extracts	
Original Wiley figure/table number(s)	Figure 2
Will you be translating?	No
Order reference number	
Total	0.00 USD
Terms and Conditions	

TERMS AND CONDITIONS

This copyrighted material is owned by or exclusively licensed to John Wiley & Sons, Inc. or one of its group companies (each a "Wiley Company") or a society for whom a Wiley Company has exclusive publishing rights in relation to a particular journal (collectively WILEY"). By clicking "accept" in connection with completing this licensing transaction, you agree that the following terms and conditions apply to this transaction (along with the billing and payment terms and

conditions established by the Copyright Clearance Center Inc., ("CCC's Billing and Payment terms and conditions"), at the time that you opened your Rightslink account (these are available at any time at http://myaccount.copyright.com)

Terms and Conditions

1. The materials you have requested permission to reproduce (the "Materials") are protected by copyright.

2. You are hereby granted a personal, non-exclusive, non-sublicensable, non-transferable, worldwide, limited license to reproduce the Materials for the purpose specified in the licensing process. This license is for a one-time use only with a maximum distribution equal to the number that you identified in the licensing process. Any form of republication granted by this licence must be completed within two years of the date of the grant of this licence (although copies prepared before may be distributed thereafter). The Materials shall not be used in any other manner or for any other purpose. Permission is granted subject to an appropriate acknowledgement given to the author, title of the material/book/journal and the publisher. You shall also duplicate the copyright notice that appears in the Wiley publication in your use of the Material. Permission is also granted on the understanding that nowhere in the text is a previously published source acknowledged for all or part of this Material. Any third party material is expressly excluded from this permission.

3. With respect to the Materials, all rights are reserved. Except as expressly granted by the terms of the license, no part of the Materials may be copied, modified, adapted (except for minor reformatting required by the new Publication), translated, reproduced, transferred or distributed, in any form or by any means, and no derivative works may be made based on the Materials without the prior permission of the respective copyright owner. You may not alter, remove or suppress in any manner any copyright, trademark or other notices displayed by the Materials. You may not license, rent, sell, loan, lease, pledge, offer as security, transfer or assign the Materials, or any of the rights granted to you hereunder to any other person.

4. The Materials and all of the intellectual property rights therein shall at all times remain the exclusive property of John Wiley & Sons Inc or one of its related companies (WILEY) or their respective licensors, and your interest therein is only that of having possession of and the right to reproduce the Materials pursuant to Section 2 herein during the continuance of this Agreement. You agree that you own no right, title or interest in or to the Materials or any of the intellectual property rights therein. You shall have no rights hereunder other than the license as provided for above in Section 2. No right, license or interest to any trademark, trade name, service mark or other branding ("Marks") of WILEY or its licensors is granted hereunder, and you agree that you shall not assert any such right, license or interest with respect thereto.

5. NEITHER WILEY NOR ITS LICENSORS MAKES ANY WARRANTY OR REPRESENTATION OF ANY KIND TO YOU OR ANY THIRD PARTY, EXPRESS, IMPLIED OR STATUTORY, WITH RESPECT TO THE MATERIALS OR THE ACCURACY OF ANY INFORMATION CONTAINED IN THE MATERIALS, INCLUDING, WITHOUT LIMITATION, ANY IMPLIED WARRANTY OF MERCHANTABILITY, ACCURACY, SATISFACTORY QUALITY, FITNESS FOR A PARTICULAR PURPOSE, USABILITY, INTEGRATION OR NON-INFRINGEMENT AND ALL SUCH WARRANTIES ARE HEREBY EXCLUDED BY WILEY AND ITS LICENSORS AND WAIVED BY YOU.

6. WILEY shall have the right to terminate this Agreement immediately upon breach of this Agreement by you.

7. You shall indemnify, defend and hold harmless WILEY, its Licensors and their respective directors, officers, agents and employees, from and against any actual or threatened claims, demands, causes of action or proceedings arising from any breach of this Agreement by you.

8. IN NO EVENT SHALL WILEY OR ITS LICENSORS BE LIABLE TO YOU OR ANY OTHER PARTY OR ANY OTHER PERSON OR ENTITY FOR ANY SPECIAL, CONSEQUENTIAL, INCIDENTAL, INDIRECT, EXEMPLARY OR PUNITIVE DAMAGES, HOWEVER CAUSED, ARISING OUT OF OR IN CONNECTION

WITH THE DOWNLOADING, PROVISIONING, VIEWING OR USE OF THE MATERIALS REGARDLESS OF THE FORM OF ACTION, WHETHER FOR BREACH OF CONTRACT, BREACH OF WARRANTY, TORT, NEGLIGENCE, INFRINGEMENT OR OTHERWISE (INCLUDING, WITHOUT LIMITATION, DAMAGES BASED ON LOSS OF PROFITS, DATA, FILES, USE, BUSINESS OPPORTUNITY OR CLAIMS OF THIRD PARTIES), AND WHETHER OR NOT THE PARTY HAS BEEN ADVISED OF THE POSSIBILITY OF SUCH DAMAGES. THIS LIMITATION SHALL APPLY NOTWITHSTANDING ANY FAILURE OF ESSENTIAL PURPOSE OF ANY LIMITED REMEDY PROVIDED HEREIN.

9. Should any provision of this Agreement be held by a court of competent jurisdiction to be illegal, invalid, or unenforceable, that provision shall be deemed amended to achieve as nearly as possible the same economic effect as the original provision, and the legality, validity and enforceability of the remaining provisions of this Agreement shall not be affected or impaired thereby.

10. The failure of either party to enforce any term or condition of this Agreement shall not constitute a waiver of either party's right to enforce each and every term and condition of this Agreement. No breach under this agreement shall be deemed waived or excused by either party unless such waiver or consent is in writing signed by the party granting such waiver or consent. The waiver by or consent of a party to a breach of any provision of this Agreement shall not operate or be construed as a waiver of or consent to any other or subsequent breach by such other party.

11. This Agreement may not be assigned (including by operation of law or otherwise) by you without WILEY's prior written consent.

12. Any fee required for this permission shall be non-refundable after thirty (30) days from receipt.

13. These terms and conditions together with CCC's Billing and Payment terms and conditions (which are incorporated herein) form the entire agreement between you and WILEY concerning this licensing transaction and (in the absence of fraud) supersedes all prior agreements and representations of the parties, oral or written. This Agreement may not be amended except in writing signed by both parties. This Agreement shall be binding upon and inure to the benefit of the parties' successors, legal representatives, and authorized assigns.

14. In the event of any conflict between your obligations established by these terms and conditions and those established by CCC's Billing and Payment terms and conditions, these terms and conditions shall prevail.

15. WILEY expressly reserves all rights not specifically granted in the combination of (i) the license details provided by you and accepted in the course of this licensing transaction, (ii) these terms and conditions and (iii) CCC's Billing and Payment terms and conditions.

16. This Agreement will be void if the Type of Use, Format, Circulation, or Requestor Type was misrepresented during the licensing process.

17. This Agreement shall be governed by and construed in accordance with the laws of the State of New York, USA, without regards to such state's conflict of law rules. Any legal action, suit or proceeding arising out of or relating to these Terms and Conditions or the breach thereof shall be instituted in a court of competent jurisdiction in New York County in the State of New York in the United States of America and each party hereby consents and submits to the personal jurisdiction of such court, waives any objection to venue in such court and consents to service of process by registered or certified mail, return receipt requested, at the last known address of such party.

Wiley Open Access Terms and Conditions

All research articles published in Wiley Open Access journals are fully open access: immediately freely available to read, download and share. Articles are published under the terms of the

- Linking to article content in e-mails redistributed for promotional, marketing or educational purposes;
- Use for the purposes of monetary reward by means of sale, resale, licence, loan, transfer or other form of commercial exploitation such as marketing products
- Print reprints of Wiley Open Access articles can be purchased from: corporatesales@wiley.com

Other Terms and Conditions:

BY CLICKING ON THE "I AGREE..." BOX, YOU ACKNOWLEDGE THAT YOU HAVE READ AND FULLY UNDERSTAND EACH OF THE SECTIONS OF AND PROVISIONS SET FORTH IN THIS AGREEMENT AND THAT YOU ARE IN AGREEMENT WITH AND ARE WILLING TO ACCEPT ALL OF YOUR OBLIGATIONS AS SET FORTH IN THIS AGREEMENT.

v1.7

Gratis licenses (referencing $0 in the Total field) are free. Please retain this printable license for your reference. No payment is required.

If you would like to pay for this license now, please remit this license along with your payment made payable to "COPYRIGHT CLEARANCE CENTER" otherwise you will be invoiced within 48 hours of the license date. Payment should be in the form of a check or money order referencing your account number and this invoice number RLNK11027789.
Once you receive your invoice for this order, you may pay your invoice by credit card. Please follow instructions provided at that time.

Make Payment To:
Copyright Clearance Center
Dept 001
P.O. Box 843006
Boston, MA 02284-3006

For suggestions or comments regarding this order, contact Rightslink Customer Support: customercare@copyright.com or +1-877-622-5543 (toll free in the US) or +1-978-646-2777.

Reply Reply to all Forward | Close | Help

From: CONTRACTS-COPYRIGHT (shared) [Contracts-Copyright@rsc.org] Sent: Thu 7/28/2011 2:54 AM

To: Jonathan Webb

Cc:

Subject: RE: Permission Request Form: Jonathan Webb

Attachments:

View As Web Page

Dear Dr Webb

The Royal Society of Chemistry hereby grants permission for the use of the material specified below in the work described and in all subsequent editions of the work for distribution throughout the world, in all media including electronic and microfilm. You may use the material in conjunction with computer-based electronic and information retrieval systems, grant permissions for photocopying, reproductions and reprints, translate the material and to publish the translation, and authorize document delivery and abstracting and indexing services. The Royal Society of Chemistry is a signatory to the STM Guidelines on Permissions (available on request).

Please note that if the material specified below or any part of it appears with credit or acknowledgement to a third party then you must also secure permission from that third party before reproducing that material.

Please ensure that the published article carries a credit to The Royal Society of Chemistry in the following format:

[Original citation] – Reproduced by permission of The Royal Society of Chemistry

and that any electronic version of the work includes a hyperlink to the article on the Royal Society of Chemistry website. The recommended form for the hyperlink is http://dx.doi.org /10.1039/*DOI suffix*, for example in the link http://dx.doi.org/10.1039/b110420a the DOI suffix is 'b110420a'. To find the relevant DOI suffix for the RSC paper in question, go to the Journals section of the website and locate your paper in the list of papers for the volume and issue of your specific journal. You will find the DOI suffix quoted there.

Regards

Gill Cockhead

Contracts & Copyright Executive

Gill Cockhead (Mrs), Contracts & Copyright Executive

Royal Society of Chemistry, Thomas Graham House

Science Park, Milton Road, Cambridge CB4 0WF, UK

Tel +44 (0) 1223 432134, Fax +44 (0) 1223 423623

http://www.rsc.org

-----Original Message-----
From: jonathan.webb@chem.queensu.ca [mailto:jonathan.webb@chem.queensu.ca]
Sent: 27 July 2011 17:15
To: CONTRACTS-COPYRIGHT (shared)
Subject: Permission Request Form: Jonathan Webb

Name : Jonathan Webb

Address :

PO Box 1495 Station Main

Kingston ON

K7L 5C7

Tel : 613-484-9734

Fax :

Email : jonathan.webb@chem.queensu.ca

I am preparing the following work for publication:

Article/Chapter Title : ADDRESSING CHALLENGES IN CATALYSIS AND ENERGY: SELECTIVE GRAFTING FUNCTIONALITY ONTO MESOPOROUS SILICAS AND ORGANIC HYDRIDES FOR THE REGENERATION OF AMMONIA BORANE, A HYDROGEN STORAGE MATERIAL

Journal/Book Title : Thesis

Editor/Author(s) : Jonathan Webb

Publisher : Queen's University

I would very much appreciate your permission to use the following material:

Journal/Book Title : Chemical Communication

Editor/Author(s) : Lunn J.D.; Shantz, D.F.

Volume Number : 46

Year of Publication : 2010

Description of Material : Figure 1

Page(s) : 2926

Any Additional Comments :

This is for a PhD Thesis and is non-profit

JOHN WILEY AND SONS LICENSE TERMS AND CONDITIONS

Jul 27, 2011

This is a License Agreement between Jonathan D Webb ("You") and John Wiley and Sons ("John Wiley and Sons") provided by Copyright Clearance Center ("CCC"). The license consists of your order details, the terms and conditions provided by John Wiley and Sons, and the payment terms and conditions.

All payments must be made in full to CCC. For payment instructions, please see information listed at the bottom of this form.

License Number	2717111173158
License date	Jul 27, 2011
Licensed content publisher	John Wiley and Sons
Licensed content publication	Angewandte Chemie International Edition
Licensed content title	Bifunctionalized Mesoporous Materials with Site-Separated Brønsted Acids and Bases: Catalyst for a Two-Step Reaction Sequence
Licensed content author	Yulin Huang,Shu Xu,Victor S.-Y. Lin
Licensed content date	Jan 17, 2011
Start page	661
End page	664
Type of use	Dissertation/Thesis
Requestor type	University/Academic
Format	Print and electronic
Portion	Figure/table
Number of figures/tables	1
Number of extracts	
Original Wiley figure/table number(s)	Figure 1
Will you be translating?	No
Order reference number	
Total	0.00 USD
Terms and Conditions	

TERMS AND CONDITIONS

This copyrighted material is owned by or exclusively licensed to John Wiley & Sons, Inc. or one of its group companies (each a "Wiley Company") or a society for whom a Wiley Company has exclusive publishing rights in relation to a particular journal (collectively WILEY"). By clicking "accept" in connection with completing this licensing transaction, you agree that the following

conditions established by the Copyright Clearance Center Inc., ("CCC's Billing and Payment terms and conditions"), at the time that you opened your Rightslink account (these are available at any time at http://myaccount.copyright.com)

Terms and Conditions

1. The materials you have requested permission to reproduce (the "Materials") are protected by copyright.

2. You are hereby granted a personal, non-exclusive, non-sublicensable, non-transferable, worldwide, limited license to reproduce the Materials for the purpose specified in the licensing process. This license is for a one-time use only with a maximum distribution equal to the number that you identified in the licensing process. Any form of republication granted by this licence must be completed within two years of the date of the grant of this licence (although copies prepared before may be distributed thereafter). The Materials shall not be used in any other manner or for any other purpose. Permission is granted subject to an appropriate acknowledgement given to the author, title of the material/book/journal and the publisher. You shall also duplicate the copyright notice that appears in the Wiley publication in your use of the Material. Permission is also granted on the understanding that nowhere in the text is a previously published source acknowledged for all or part of this Material. Any third party material is expressly excluded from this permission.

3. With respect to the Materials, all rights are reserved. Except as expressly granted by the terms of the license, no part of the Materials may be copied, modified, adapted (except for minor reformatting required by the new Publication), translated, reproduced, transferred or distributed, in any form or by any means, and no derivative works may be made based on the Materials without the prior permission of the respective copyright owner. You may not alter, remove or suppress in any manner any copyright, trademark or other notices displayed by the Materials. You may not license, rent, sell, loan, lease, pledge, offer as security, transfer or assign the Materials, or any of the rights granted to you hereunder to any other person.

4. The Materials and all of the intellectual property rights therein shall at all times remain the exclusive property of John Wiley & Sons Inc or one of its related companies (WILEY) or their respective licensors, and your interest therein is only that of having possession of and the right to reproduce the Materials pursuant to Section 2 herein during the continuance of this Agreement. You agree that you own no right, title or interest in or to the Materials or any of the intellectual property rights therein. You shall have no rights hereunder other than the license as provided for above in Section 2. No right, license or interest to any trademark, trade name, service mark or other branding ("Marks") of WILEY or its licensors is granted hereunder, and you agree that you shall not assert any such right, license or interest with respect thereto.

5. NEITHER WILEY NOR ITS LICENSORS MAKES ANY WARRANTY OR REPRESENTATION OF ANY KIND TO YOU OR ANY THIRD PARTY, EXPRESS, IMPLIED OR STATUTORY, WITH RESPECT TO THE MATERIALS OR THE ACCURACY OF ANY INFORMATION CONTAINED IN THE MATERIALS, INCLUDING, WITHOUT LIMITATION, ANY IMPLIED WARRANTY OF MERCHANTABILITY, ACCURACY, SATISFACTORY QUALITY, FITNESS FOR A PARTICULAR PURPOSE, USABILITY, INTEGRATION OR NON-INFRINGEMENT AND ALL SUCH WARRANTIES ARE HEREBY EXCLUDED BY WILEY AND ITS LICENSORS AND WAIVED BY YOU.

6. WILEY shall have the right to terminate this Agreement immediately upon breach of this Agreement by you.

7. You shall indemnify, defend and hold harmless WILEY, its Licensors and their respective directors, officers, agents and employees, from and against any actual or threatened claims, demands, causes of action or proceedings arising from any breach of this Agreement by you.

8. IN NO EVENT SHALL WILEY OR ITS LICENSORS BE LIABLE TO YOU OR ANY OTHER PARTY OR ANY OTHER PERSON OR ENTITY FOR ANY SPECIAL, CONSEQUENTIAL, INCIDENTAL, INDIRECT, EXEMPLARY OR PUNITIVE DAMAGES, HOWEVER CAUSED, ARISING OUT OF OR IN CONNECTION

WITH THE DOWNLOADING, PROVISIONING, VIEWING OR USE OF THE MATERIALS REGARDLESS OF THE FORM OF ACTION, WHETHER FOR BREACH OF CONTRACT, BREACH OF WARRANTY, TORT, NEGLIGENCE, INFRINGEMENT OR OTHERWISE (INCLUDING, WITHOUT LIMITATION, DAMAGES BASED ON LOSS OF PROFITS, DATA, FILES, USE, BUSINESS OPPORTUNITY OR CLAIMS OF THIRD PARTIES), AND WHETHER OR NOT THE PARTY HAS BEEN ADVISED OF THE POSSIBILITY OF SUCH DAMAGES. THIS LIMITATION SHALL APPLY NOTWITHSTANDING ANY FAILURE OF ESSENTIAL PURPOSE OF ANY LIMITED REMEDY PROVIDED HEREIN.

9. Should any provision of this Agreement be held by a court of competent jurisdiction to be illegal, invalid, or unenforceable, that provision shall be deemed amended to achieve as nearly as possible the same economic effect as the original provision, and the legality, validity and enforceability of the remaining provisions of this Agreement shall not be affected or impaired thereby.

10. The failure of either party to enforce any term or condition of this Agreement shall not constitute a waiver of either party's right to enforce each and every term and condition of this Agreement. No breach under this agreement shall be deemed waived or excused by either party unless such waiver or consent is in writing signed by the party granting such waiver or consent. The waiver by or consent of a party to a breach of any provision of this Agreement shall not operate or be construed as a waiver of or consent to any other or subsequent breach by such other party.

11. This Agreement may not be assigned (including by operation of law or otherwise) by you without WILEY's prior written consent.

12. Any fee required for this permission shall be non-refundable after thirty (30) days from receipt.

13. These terms and conditions together with CCC's Billing and Payment terms and conditions (which are incorporated herein) form the entire agreement between you and WILEY concerning this licensing transaction and (in the absence of fraud) supersedes all prior agreements and representations of the parties, oral or written. This Agreement may not be amended except in writing signed by both parties. This Agreement shall be binding upon and inure to the benefit of the parties' successors, legal representatives, and authorized assigns.

14. In the event of any conflict between your obligations established by these terms and conditions and those established by CCC's Billing and Payment terms and conditions, these terms and conditions shall prevail.

15. WILEY expressly reserves all rights not specifically granted in the combination of (i) the license details provided by you and accepted in the course of this licensing transaction, (ii) these terms and conditions and (iii) CCC's Billing and Payment terms and conditions.

16. This Agreement will be void if the Type of Use, Format, Circulation, or Requestor Type was misrepresented during the licensing process.

17. This Agreement shall be governed by and construed in accordance with the laws of the State of New York, USA, without regards to such state's conflict of law rules. Any legal action, suit or proceeding arising out of or relating to these Terms and Conditions or the breach thereof shall be instituted in a court of competent jurisdiction in New York County in the State of New York in the United States of America and each party hereby consents and submits to the personal jurisdiction of such court, waives any objection to venue in such court and consents to service of process by registered or certified mail, return receipt requested, at the last known address of such party.

Wiley Open Access Terms and Conditions

All research articles published in Wiley Open Access journals are fully open access: immediately freely available to read, download and share. Articles are published under the terms of the

- Linking to article content in e-mails redistributed for promotional, marketing or educational purposes;
- Use for the purposes of monetary reward by means of sale, resale, licence, loan, transfer or other form of commercial exploitation such as marketing products
- Print reprints of Wiley Open Access articles can be purchased from: corporatesales@wiley.com

Other Terms and Conditions:

BY CLICKING ON THE "I AGREE..." BOX, YOU ACKNOWLEDGE THAT YOU HAVE READ AND FULLY UNDERSTAND EACH OF THE SECTIONS OF AND PROVISIONS SET FORTH IN THIS AGREEMENT AND THAT YOU ARE IN AGREEMENT WITH AND ARE WILLING TO ACCEPT ALL OF YOUR OBLIGATIONS AS SET FORTH IN THIS AGREEMENT.

v1.7

Gratis licenses (referencing $0 in the Total field) are free. Please retain this printable license for your reference. No payment is required.

If you would like to pay for this license now, please remit this license along with your payment made payable to "COPYRIGHT CLEARANCE CENTER" otherwise you will be invoiced within 48 hours of the license date. Payment should be in the form of a check or money order referencing your account number and this invoice number RLNK11027789.
Once you receive your invoice for this order, you may pay your invoice by credit card. Please follow instructions provided at that time.

Make Payment To:
Copyright Clearance Center
Dept 001
P.O. Box 843006
Boston, MA 02284-3006

For suggestions or comments regarding this order, contact Rightslink Customer Support: customercare@copyright.com or +1-877-622-5543 (toll free in the US) or +1-978-646-2777.

JOHN WILEY AND SONS LICENSE
TERMS AND CONDITIONS

Jul 27, 2011

This is a License Agreement between Jonathan D Webb ("You") and John Wiley and Sons ("John Wiley and Sons") provided by Copyright Clearance Center ("CCC"). The license consists of your order details, the terms and conditions provided by John Wiley and Sons, and the payment terms and conditions.

All payments must be made in full to CCC. For payment instructions, please see information listed at the bottom of this form.

License Number	2717120629858
License date	Jul 27, 2011
Licensed content publisher	John Wiley and Sons
Licensed content publication	Angewandte Chemie International Edition
Licensed content title	Site-Directed Surface Derivatization of MCM-41: Use of High-Resolution Transmission Electron Microscopy and Molecular Recognition for Determining the Position of Functionality within Mesoporous Materials
Licensed content author	Douglas S. Shephard,Wuzong Zhou,Thomas Maschmeyer,Justin M. Matters,Caroline L. Roper,Simon Parsons,Brian F. G. Johnson,Melinda J. Duer
Licensed content date	Oct 16, 1998
Start page	2719
End page	2723
Type of use	Dissertation/Thesis
Requestor type	University/Academic
Format	Print and electronic
Portion	Figure/table
Number of figures/tables	1
Number of extracts	
Original Wiley figure/table number(s)	Figure 5
Will you be translating?	No
Order reference number	
Total	0.00 USD
Terms and Conditions	

TERMS AND CONDITIONS

conditions established by the Copyright Clearance Center Inc., ("CCC's Billing and Payment terms and conditions"), at the time that you opened your Rightslink account (these are available at any time at http://myaccount.copyright.com)

Terms and Conditions

1. The materials you have requested permission to reproduce (the "Materials") are protected by copyright.

2. You are hereby granted a personal, non-exclusive, non-sublicensable, non-transferable, worldwide, limited license to reproduce the Materials for the purpose specified in the licensing process. This license is for a one-time use only with a maximum distribution equal to the number that you identified in the licensing process. Any form of republication granted by this licence must be completed within two years of the date of the grant of this licence (although copies prepared before may be distributed thereafter). The Materials shall not be used in any other manner or for any other purpose. Permission is granted subject to an appropriate acknowledgement given to the author, title of the material/book/journal and the publisher. You shall also duplicate the copyright notice that appears in the Wiley publication in your use of the Material. Permission is also granted on the understanding that nowhere in the text is a previously published source acknowledged for all or part of this Material. Any third party material is expressly excluded from this permission.

3. With respect to the Materials, all rights are reserved. Except as expressly granted by the terms of the license, no part of the Materials may be copied, modified, adapted (except for minor reformatting required by the new Publication), translated, reproduced, transferred or distributed, in any form or by any means, and no derivative works may be made based on the Materials without the prior permission of the respective copyright owner. You may not alter, remove or suppress in any manner any copyright, trademark or other notices displayed by the Materials. You may not license, rent, sell, loan, lease, pledge, offer as security, transfer or assign the Materials, or any of the rights granted to you hereunder to any other person.

4. The Materials and all of the intellectual property rights therein shall at all times remain the exclusive property of John Wiley & Sons Inc or one of its related companies (WILEY) or their respective licensors, and your interest therein is only that of having possession of and the right to reproduce the Materials pursuant to Section 2 herein during the continuance of this Agreement. You agree that you own no right, title or interest in or to the Materials or any of the intellectual property rights therein. You shall have no rights hereunder other than the license as provided for above in Section 2. No right, license or interest to any trademark, trade name, service mark or other branding ("Marks") of WILEY or its licensors is granted hereunder, and you agree that you shall not assert any such right, license or interest with respect thereto.

5. NEITHER WILEY NOR ITS LICENSORS MAKES ANY WARRANTY OR REPRESENTATION OF ANY KIND TO YOU OR ANY THIRD PARTY, EXPRESS, IMPLIED OR STATUTORY, WITH RESPECT TO THE MATERIALS OR THE ACCURACY OF ANY INFORMATION CONTAINED IN THE MATERIALS, INCLUDING, WITHOUT LIMITATION, ANY IMPLIED WARRANTY OF MERCHANTABILITY, ACCURACY, SATISFACTORY QUALITY, FITNESS FOR A PARTICULAR PURPOSE, USABILITY, INTEGRATION OR NON-INFRINGEMENT AND ALL SUCH WARRANTIES ARE HEREBY EXCLUDED BY WILEY AND ITS LICENSORS AND WAIVED BY YOU.

6. WILEY shall have the right to terminate this Agreement immediately upon breach of this Agreement by you.

7. You shall indemnify, defend and hold harmless WILEY, its Licensors and their respective directors, officers, agents and employees, from and against any actual or threatened claims, demands, causes of action or proceedings arising from any breach of this Agreement by you.

8. IN NO EVENT SHALL WILEY OR ITS LICENSORS BE LIABLE TO YOU OR ANY OTHER PARTY OR ANY OTHER PERSON OR ENTITY FOR ANY SPECIAL, CONSEQUENTIAL, INCIDENTAL, INDIRECT, EXEMPLARY OR PUNITIVE DAMAGES, HOWEVER CAUSED, ARISING OUT OF OR IN CONNECTION

WITH THE DOWNLOADING, PROVISIONING, VIEWING OR USE OF THE MATERIALS REGARDLESS OF THE FORM OF ACTION, WHETHER FOR BREACH OF CONTRACT, BREACH OF WARRANTY, TORT, NEGLIGENCE, INFRINGEMENT OR OTHERWISE (INCLUDING, WITHOUT LIMITATION, DAMAGES BASED ON LOSS OF PROFITS, DATA, FILES, USE, BUSINESS OPPORTUNITY OR CLAIMS OF THIRD PARTIES), AND WHETHER OR NOT THE PARTY HAS BEEN ADVISED OF THE POSSIBILITY OF SUCH DAMAGES. THIS LIMITATION SHALL APPLY NOTWITHSTANDING ANY FAILURE OF ESSENTIAL PURPOSE OF ANY LIMITED REMEDY PROVIDED HEREIN.

9. Should any provision of this Agreement be held by a court of competent jurisdiction to be illegal, invalid, or unenforceable, that provision shall be deemed amended to achieve as nearly as possible the same economic effect as the original provision, and the legality, validity and enforceability of the remaining provisions of this Agreement shall not be affected or impaired thereby.

10. The failure of either party to enforce any term or condition of this Agreement shall not constitute a waiver of either party's right to enforce each and every term and condition of this Agreement. No breach under this agreement shall be deemed waived or excused by either party unless such waiver or consent is in writing signed by the party granting such waiver or consent. The waiver by or consent of a party to a breach of any provision of this Agreement shall not operate or be construed as a waiver of or consent to any other or subsequent breach by such other party.

11. This Agreement may not be assigned (including by operation of law or otherwise) by you without WILEY's prior written consent.

12. Any fee required for this permission shall be non-refundable after thirty (30) days from receipt.

13. These terms and conditions together with CCC's Billing and Payment terms and conditions (which are incorporated herein) form the entire agreement between you and WILEY concerning this licensing transaction and (in the absence of fraud) supersedes all prior agreements and representations of the parties, oral or written. This Agreement may not be amended except in writing signed by both parties. This Agreement shall be binding upon and inure to the benefit of the parties' successors, legal representatives, and authorized assigns.

14. In the event of any conflict between your obligations established by these terms and conditions and those established by CCC's Billing and Payment terms and conditions, these terms and conditions shall prevail.

15. WILEY expressly reserves all rights not specifically granted in the combination of (i) the license details provided by you and accepted in the course of this licensing transaction, (ii) these terms and conditions and (iii) CCC's Billing and Payment terms and conditions.

16. This Agreement will be void if the Type of Use, Format, Circulation, or Requestor Type was misrepresented during the licensing process.

17. This Agreement shall be governed by and construed in accordance with the laws of the State of New York, USA, without regards to such state's conflict of law rules. Any legal action, suit or proceeding arising out of or relating to these Terms and Conditions or the breach thereof shall be instituted in a court of competent jurisdiction in New York County in the State of New York in the United States of America and each party hereby consents and submits to the personal jurisdiction of such court, waives any objection to venue in such court and consents to service of process by registered or certified mail, return receipt requested, at the last known address of such party.

Wiley Open Access Terms and Conditions

All research articles published in Wiley Open Access journals are fully open access: immediately freely available to read, download and share. Articles are published under the terms of the

- Linking to article content in e-mails redistributed for promotional, marketing or educational purposes;
- Use for the purposes of monetary reward by means of sale, resale, licence, loan, transfer or other form of commercial exploitation such as marketing products
- Print reprints of Wiley Open Access articles can be purchased from: corporatesales@wiley.com

Other Terms and Conditions:

BY CLICKING ON THE "I AGREE..." BOX, YOU ACKNOWLEDGE THAT YOU HAVE READ AND FULLY UNDERSTAND EACH OF THE SECTIONS OF AND PROVISIONS SET FORTH IN THIS AGREEMENT AND THAT YOU ARE IN AGREEMENT WITH AND ARE WILLING TO ACCEPT ALL OF YOUR OBLIGATIONS AS SET FORTH IN THIS AGREEMENT.

v1.7

Gratis licenses (referencing $0 in the Total field) are free. Please retain this printable license for your reference. No payment is required.

If you would like to pay for this license now, please remit this license along with your payment made payable to "COPYRIGHT CLEARANCE CENTER" otherwise you will be invoiced within 48 hours of the license date. Payment should be in the form of a check or money order referencing your account number and this invoice number RLNK11027789.
Once you receive your invoice for this order, you may pay your invoice by credit card. Please follow instructions provided at that time.

Make Payment To:
Copyright Clearance Center
Dept 001
P.O. Box 843006
Boston, MA 02284-3006

For suggestions or comments regarding this order, contact Rightslink Customer Support: customercare@copyright.com or +1-877-622-5543 (toll free in the US) or +1-978-646-2777.

Copyright Clearance Center RightsLink®

Home | Account Info | Help

ACS Publications High quality. High impact.

Title: Synthesis of Gold Nanoparticles via Electroless Deposition in SBA-15

Author: Tewodros Asefa et al.

Publication: Chemistry of Materials

Publisher: American Chemical Society

Date: May 1, 2005

Logged in as:
Jonathan Webb
Account #:
3000432578

LOGOUT

No charge permission and attribution

Permission for this particular request is granted for print and electronic formats at no charge. Figures and tables may be modified. Appropriate credit should be given. Please print this page for your records and provide a copy to your publisher. Requests for up to 4 figures require only this record. Five or more figures will generate a printout of additional terms and conditions. Appropriate credit should read: "Reprinted with permission from {COMPLETE REFERENCE CITATION}. Copyright {YEAR} American Chemical Society." Insert appropriate information in place of the capitalized words.

This permission does not apply to images that are credited to publications other than ACS journals. For images credited to non-ACS journal publications, you will need to obtain permission from the journal referenced in the Table/Figure/Micrograph legend or credit line before making any use of the image(s) or table(s).

BACK CLOSE WINDOW

RightsLink®

Home | Account Info | Help

Title: Selective Surface Functionalization and Metal Deposition in the Micropores of Mesoporous Silica SBA-15

Author: Chia-Min Yang et al.

Publication: Chemistry of Materials

Publisher: American Chemical Society

Date: Jun 1, 2007

Logged in as:
Jonathan Webb
Account #:
3000432578

LOGOUT

No charge permission and attribution

Permission for this particular request is granted for print and electronic formats at no charge. Figures and tables may be modified. Appropriate credit should be given. Please print this page for your records and provide a copy to your publisher. Requests for up to 4 figures require only this record. Five or more figures will generate a printout of additional terms and conditions. Appropriate credit should read: "Reprinted with permission from {COMPLETE REFERENCE CITATION}. Copyright {YEAR} American Chemical Society." Insert appropriate information in place of the capitalized words.

This permission does not apply to images that are credited to publications other than ACS journals. For images credited to non-ACS journal publications, you will need to obtain permission from the journal referenced in the Table/Figure/Micrograph legend or credit line before making any use of the image(s) or table(s).

BACK | CLOSE WINDOW

JOHN WILEY AND SONS LICENSE TERMS AND CONDITIONS

Jul 27, 2011

This is a License Agreement between Jonathan D Webb ("You") and John Wiley and Sons ("John Wiley and Sons") provided by Copyright Clearance Center ("CCC"). The license consists of your order details, the terms and conditions provided by John Wiley and Sons, and the payment terms and conditions.

All payments must be made in full to CCC. For payment instructions, please see information listed at the bottom of this form.

License Number	2717121400155
License date	Jul 27, 2011
Licensed content publisher	John Wiley and Sons
Licensed content publication	Angewandte Chemie International Edition
Licensed content title	Introducing Distinctly Different Chemical Functionalities onto the Internal and External Surfaces of Mesoporous Materials
Licensed content author	Kristopher A. Kilian,Till Böcking,Katharina Gaus,J. Justin Gooding
Licensed content date	Mar 25, 2008
Start page	2697
End page	2699
Type of use	Dissertation/Thesis
Requestor type	University/Academic
Format	Print and electronic
Portion	Figure/table
Number of figures/tables	1
Number of extracts	
Original Wiley figure/table number(s)	Figure 1
Will you be translating?	No
Order reference number	
Total	0.00 USD
Terms and Conditions	

TERMS AND CONDITIONS

This copyrighted material is owned by or exclusively licensed to John Wiley & Sons, Inc. or one of its group companies (each a "Wiley Company") or a society for whom a Wiley Company has exclusive publishing rights in relation to a particular journal (collectively WILEY"). By clicking "accept" in connection with completing this licensing transaction, you agree that the following terms and conditions apply to this transaction (along with the billing and payment terms and

conditions established by the Copyright Clearance Center Inc., ("CCC's Billing and Payment terms and conditions"), at the time that you opened your Rightslink account (these are available at any time at http://myaccount.copyright.com)

Terms and Conditions

1. The materials you have requested permission to reproduce (the "Materials") are protected by copyright.

2. You are hereby granted a personal, non-exclusive, non-sublicensable, non-transferable, worldwide, limited license to reproduce the Materials for the purpose specified in the licensing process. This license is for a one-time use only with a maximum distribution equal to the number that you identified in the licensing process. Any form of republication granted by this licence must be completed within two years of the date of the grant of this licence (although copies prepared before may be distributed thereafter). The Materials shall not be used in any other manner or for any other purpose. Permission is granted subject to an appropriate acknowledgement given to the author, title of the material/book/journal and the publisher. You shall also duplicate the copyright notice that appears in the Wiley publication in your use of the Material. Permission is also granted on the understanding that nowhere in the text is a previously published source acknowledged for all or part of this Material. Any third party material is expressly excluded from this permission.

3. With respect to the Materials, all rights are reserved. Except as expressly granted by the terms of the license, no part of the Materials may be copied, modified, adapted (except for minor reformatting required by the new Publication), translated, reproduced, transferred or distributed, in any form or by any means, and no derivative works may be made based on the Materials without the prior permission of the respective copyright owner. You may not alter, remove or suppress in any manner any copyright, trademark or other notices displayed by the Materials. You may not license, rent, sell, loan, lease, pledge, offer as security, transfer or assign the Materials, or any of the rights granted to you hereunder to any other person.

4. The Materials and all of the intellectual property rights therein shall at all times remain the exclusive property of John Wiley & Sons Inc or one of its related companies (WILEY) or their respective licensors, and your interest therein is only that of having possession of and the right to reproduce the Materials pursuant to Section 2 herein during the continuance of this Agreement. You agree that you own no right, title or interest in or to the Materials or any of the intellectual property rights therein. You shall have no rights hereunder other than the license as provided for above in Section 2. No right, license or interest to any trademark, trade name, service mark or other branding ("Marks") of WILEY or its licensors is granted hereunder, and you agree that you shall not assert any such right, license or interest with respect thereto.

5. NEITHER WILEY NOR ITS LICENSORS MAKES ANY WARRANTY OR REPRESENTATION OF ANY KIND TO YOU OR ANY THIRD PARTY, EXPRESS, IMPLIED OR STATUTORY, WITH RESPECT TO THE MATERIALS OR THE ACCURACY OF ANY INFORMATION CONTAINED IN THE MATERIALS, INCLUDING, WITHOUT LIMITATION, ANY IMPLIED WARRANTY OF MERCHANTABILITY, ACCURACY, SATISFACTORY QUALITY, FITNESS FOR A PARTICULAR PURPOSE, USABILITY, INTEGRATION OR NON-INFRINGEMENT AND ALL SUCH WARRANTIES ARE HEREBY EXCLUDED BY WILEY AND ITS LICENSORS AND WAIVED BY YOU.

6. WILEY shall have the right to terminate this Agreement immediately upon breach of this Agreement by you.

7. You shall indemnify, defend and hold harmless WILEY, its Licensors and their respective directors, officers, agents and employees, from and against any actual or threatened claims, demands, causes of action or proceedings arising from any breach of this Agreement by you.

8. IN NO EVENT SHALL WILEY OR ITS LICENSORS BE LIABLE TO YOU OR ANY OTHER PARTY OR ANY OTHER PERSON OR ENTITY FOR ANY SPECIAL, CONSEQUENTIAL, INCIDENTAL, INDIRECT, EXEMPLARY OR PUNITIVE DAMAGES, HOWEVER CAUSED, ARISING OUT OF OR IN CONNECTION

WITH THE DOWNLOADING, PROVISIONING, VIEWING OR USE OF THE MATERIALS REGARDLESS OF THE FORM OF ACTION, WHETHER FOR BREACH OF CONTRACT, BREACH OF WARRANTY, TORT, NEGLIGENCE, INFRINGEMENT OR OTHERWISE (INCLUDING, WITHOUT LIMITATION, DAMAGES BASED ON LOSS OF PROFITS, DATA, FILES, USE, BUSINESS OPPORTUNITY OR CLAIMS OF THIRD PARTIES), AND WHETHER OR NOT THE PARTY HAS BEEN ADVISED OF THE POSSIBILITY OF SUCH DAMAGES. THIS LIMITATION SHALL APPLY NOTWITHSTANDING ANY FAILURE OF ESSENTIAL PURPOSE OF ANY LIMITED REMEDY PROVIDED HEREIN.

9. Should any provision of this Agreement be held by a court of competent jurisdiction to be illegal, invalid, or unenforceable, that provision shall be deemed amended to achieve as nearly as possible the same economic effect as the original provision, and the legality, validity and enforceability of the remaining provisions of this Agreement shall not be affected or impaired thereby.

10. The failure of either party to enforce any term or condition of this Agreement shall not constitute a waiver of either party's right to enforce each and every term and condition of this Agreement. No breach under this agreement shall be deemed waived or excused by either party unless such waiver or consent is in writing signed by the party granting such waiver or consent. The waiver by or consent of a party to a breach of any provision of this Agreement shall not operate or be construed as a waiver of or consent to any other or subsequent breach by such other party.

11. This Agreement may not be assigned (including by operation of law or otherwise) by you without WILEY's prior written consent.

12. Any fee required for this permission shall be non-refundable after thirty (30) days from receipt.

13. These terms and conditions together with CCC's Billing and Payment terms and conditions (which are incorporated herein) form the entire agreement between you and WILEY concerning this licensing transaction and (in the absence of fraud) supersedes all prior agreements and representations of the parties, oral or written. This Agreement may not be amended except in writing signed by both parties. This Agreement shall be binding upon and inure to the benefit of the parties' successors, legal representatives, and authorized assigns.

14. In the event of any conflict between your obligations established by these terms and conditions and those established by CCC's Billing and Payment terms and conditions, these terms and conditions shall prevail.

15. WILEY expressly reserves all rights not specifically granted in the combination of (i) the license details provided by you and accepted in the course of this licensing transaction, (ii) these terms and conditions and (iii) CCC's Billing and Payment terms and conditions.

16. This Agreement will be void if the Type of Use, Format, Circulation, or Requestor Type was misrepresented during the licensing process.

17. This Agreement shall be governed by and construed in accordance with the laws of the State of New York, USA, without regards to such state's conflict of law rules. Any legal action, suit or proceeding arising out of or relating to these Terms and Conditions or the breach thereof shall be instituted in a court of competent jurisdiction in New York County in the State of New York in the United States of America and each party hereby consents and submits to the personal jurisdiction of such court, waives any objection to venue in such court and consents to service of process by registered or certified mail, return receipt requested, at the last known address of such party.

Wiley Open Access Terms and Conditions

All research articles published in Wiley Open Access journals are fully open access: immediately freely available to read, download and share. Articles are published under the terms of the

- Linking to article content in e-mails redistributed for promotional, marketing or educational purposes;
- Use for the purposes of monetary reward by means of sale, resale, licence, loan, transfer or other form of commercial exploitation such as marketing products
- Print reprints of Wiley Open Access articles can be purchased from: corporatesales@wiley.com

Other Terms and Conditions:

BY CLICKING ON THE "I AGREE..." BOX, YOU ACKNOWLEDGE THAT YOU HAVE READ AND FULLY UNDERSTAND EACH OF THE SECTIONS OF AND PROVISIONS SET FORTH IN THIS AGREEMENT AND THAT YOU ARE IN AGREEMENT WITH AND ARE WILLING TO ACCEPT ALL OF YOUR OBLIGATIONS AS SET FORTH IN THIS AGREEMENT.

v1.7

Gratis licenses (referencing $0 in the Total field) are free. Please retain this printable license for your reference. No payment is required.

If you would like to pay for this license now, please remit this license along with your payment made payable to "COPYRIGHT CLEARANCE CENTER" otherwise you will be invoiced within 48 hours of the license date. Payment should be in the form of a check or money order referencing your account number and this invoice number RLNK11027789.
Once you receive your invoice for this order, you may pay your invoice by credit card. Please follow instructions provided at that time.

Make Payment To:
Copyright Clearance Center
Dept 001
P.O. Box 843006
Boston, MA 02284-3006

For suggestions or comments regarding this order, contact Rightslink Customer Support: customercare@copyright.com or +1-877-622-5543 (toll free in the US) or +1-978-646-2777.

SPRINGER LICENSE
TERMS AND CONDITIONS

Jul 27, 2011

This is a License Agreement between Jonathan D Webb ("You") and Springer ("Springer") provided by Copyright Clearance Center ("CCC"). The license consists of your order details, the terms and conditions provided by Springer, and the payment terms and conditions.

All payments must be made in full to CCC. For payment instructions, please see information listed at the bottom of this form.

License Number	2717130297991
License date	Jul 27, 2011
Licensed content publisher	Springer
Licensed content publication	Analytical and Bioanalytical Chemistry
Licensed content title	FloDots: luminescent nanoparticles
Licensed content author	Gang Yao
Licensed content date	Jun 1, 2006
Volume number	385
Issue number	3
Type of Use	Thesis/Dissertation
Portion	Figures
Author of this Springer article	No
Order reference number	
Title of your thesis / dissertation	ADDRESSING CHALLENGES IN CATALYSIS AND ENERGY: SELECTIVE GRAFTING FUNCTIONALITY ONTO MESOPOROUS SILICAS AND ORGANIC HYDRIDES FOR THE REGENERATION OF AMMONIA BORANE, A HYDROGEN STORAGE MATERIAL
Expected completion date	Sep 2011
Estimated size(pages)	450
Total	0.00 USD
Terms and Conditions	

Introduction
The publisher for this copyrighted material is Springer Science + Business Media. By clicking "accept" in connection with completing this licensing transaction, you agree that the following terms and conditions apply to this transaction (along with the Billing and Payment terms and conditions established by Copyright Clearance Center, Inc. ("CCC"), at the time that you opened your Rightslink account and that are available at any time at http://myaccount.copyright.com).

Limited License
With reference to your request to reprint in your thesis material on which Springer Science and Business Media control the copyright, permission is granted, free of charge, for the use indicated in your enquiry. Licenses are for one-time use only with a maximum distribution equal to the number that you identified in the licensing process.

This License includes use in an electronic form, provided it is password protected or on the university's intranet, destined to microfilming by UMI and University repository. For any other electronic use, please contact Springer at (permissions.dordrecht@springer.com or permissions.heidelberg@springer.com)

The material can only be used for the purpose of defending your thesis, and with a maximum of 100 extra copies in paper.

Although Springer holds copyright to the material and is entitled to negotiate on rights, this license is only valid, provided permission is also obtained from the (co) author (address is given with the article/chapter) and provided it concerns original material which does not carry references to other sources (if material in question appears with credit to another source, authorization from that source is required as well). Permission free of charge on this occasion does not prejudice any rights we might have to charge for reproduction of our copyrighted material in the future.

Altering/Modifying Material: Not Permitted
However figures and illustrations may be altered minimally to serve your work. Any other abbreviations, additions, deletions and/or any other alterations shall be made only with prior written authorization of the author(s) and/or Springer Science + Business Media. (Please contact Springer at permissions.dordrecht@springer.com or permissions.heidelberg@springer.com)

Reservation of Rights
Springer Science + Business Media reserves all rights not specifically granted in the combination of (i) the license details provided by you and accepted in the course of this licensing transaction, (ii) these terms and conditions and (iii) CCC's Billing and Payment terms and conditions.

Copyright Notice:
Please include the following copyright citation referencing the publication in which the material was originally published. Where wording is within brackets, please include verbatim.
"With kind permission from Springer Science+Business Media: <book/journal title, chapter/article title, volume, year of publication, page, name(s) of author(s), figure number(s), and any original (first) copyright notice displayed with material>."

Warranties: Springer Science + Business Media makes no representations or warranties with respect to the licensed material.

Indemnity
You hereby indemnify and agree to hold harmless Springer Science + Business Media and CCC, and their respective officers, directors, employees and agents, from and against any and all claims arising out of your use of the licensed material other than as specifically authorized pursuant to this license.

No Transfer of License
This license is personal to you and may not be sublicensed, assigned, or transferred by you to any other person without Springer Science + Business Media's written permission.

No Amendment Except in Writing
This license may not be amended except in a writing signed by both parties (or, in the case of Springer Science + Business Media, by CCC on Springer Science + Business Media's behalf).

Objection to Contrary Terms
Springer Science + Business Media hereby objects to any terms contained in any purchase order, acknowledgment, check endorsement or other writing prepared by you, which terms are inconsistent with these terms and conditions or CCC's Billing and Payment terms and conditions. These terms and conditions, together with CCC's Billing and Payment terms and conditions (which are incorporated herein), comprise the entire agreement between you and Springer Science + Business Media (and CCC) concerning this licensing transaction. In the event of any conflict between your obligations established by these terms and conditions and those established by CCC's Billing and Payment terms and conditions, these terms and conditions shall control.

Jurisdiction
All disputes that may arise in connection with this present License, or the breach thereof, shall be settled exclusively by the country's law in which the work was originally published.

Other terms and conditions:

v1.2

Gratis licenses (referencing $0 in the Total field) are free. Please retain this printable license for your reference. No payment is required.

If you would like to pay for this license now, please remit this license along with your payment made payable to "COPYRIGHT CLEARANCE CENTER" otherwise you will be invoiced within 48 hours of the license date. Payment should be in the form of a check or money order referencing your account number and this invoice number RLNK11027833.
Once you receive your invoice for this order, you may pay your invoice by credit card. Please follow instructions provided at that time.

Make Payment To:
Copyright Clearance Center
Dept 001

P.O. Box 843006
Boston, MA 02284-3006

For suggestions or comments regarding this order, contact Rightslink Customer Support: customercare@copyright.com or +1-877-622-5543 (toll free in the US) or +1-978-646-2777.

JOHN WILEY AND SONS LICENSE TERMS AND CONDITIONS

Jul 27, 2011

This is a License Agreement between Jonathan D Webb ("You") and John Wiley and Sons ("John Wiley and Sons") provided by Copyright Clearance Center ("CCC"). The license consists of your order details, the terms and conditions provided by John Wiley and Sons, and the payment terms and conditions.

All payments must be made in full to CCC. For payment instructions, please see information listed at the bottom of this form.

License Number	2717130924307
License date	Jul 27, 2011
Licensed content publisher	John Wiley and Sons
Licensed content publication	Advanced Synthesis & Catalysis
Licensed content title	Suzuki–Miyaura Cross-Coupling With Quasi-Heterogeneous Palladium
Licensed content author	David A. Conlon,Brenda Pipik,Simone Ferdinand,Carl R. LeBlond,John R. Sowa,Bill Izzo,Paul Collins,Guo-Jie Ho,J. Michael Williams,Yao-Jun Shi,Yongkui Sun
Licensed content date	Aug 1, 2003
Start page	931
End page	935
Type of use	Dissertation/Thesis
Requestor type	University/Academic
Format	Print and electronic
Portion	Figure/table
Number of figures/tables	1
Number of extracts	
Original Wiley figure/table number(s)	Figure 1
Will you be translating?	No
Order reference number	
Total	0.00 USD
Terms and Conditions	

TERMS AND CONDITIONS

This copyrighted material is owned by or exclusively licensed to John Wiley & Sons, Inc. or one of its group companies (each a "Wiley Company") or a society for whom a Wiley Company has

exclusive publishing rights in relation to a particular journal (collectively WILEY"). By clicking "accept" in connection with completing this licensing transaction, you agree that the following terms and conditions apply to this transaction (along with the billing and payment terms and conditions established by the Copyright Clearance Center Inc., ("CCC's Billing and Payment terms and conditions"), at the time that you opened your Rightslink account (these are available at any time at http://myaccount.copyright.com)

Terms and Conditions

1. The materials you have requested permission to reproduce (the "Materials") are protected by copyright.

2. You are hereby granted a personal, non-exclusive, non-sublicensable, non-transferable, worldwide, limited license to reproduce the Materials for the purpose specified in the licensing process. This license is for a one-time use only with a maximum distribution equal to the number that you identified in the licensing process. Any form of republication granted by this licence must be completed within two years of the date of the grant of this licence (although copies prepared before may be distributed thereafter). The Materials shall not be used in any other manner or for any other purpose. Permission is granted subject to an appropriate acknowledgement given to the author, title of the material/book/journal and the publisher. You shall also duplicate the copyright notice that appears in the Wiley publication in your use of the Material. Permission is also granted on the understanding that nowhere in the text is a previously published source acknowledged for all or part of this Material. Any third party material is expressly excluded from this permission.

3. With respect to the Materials, all rights are reserved. Except as expressly granted by the terms of the license, no part of the Materials may be copied, modified, adapted (except for minor reformatting required by the new Publication), translated, reproduced, transferred or distributed, in any form or by any means, and no derivative works may be made based on the Materials without the prior permission of the respective copyright owner. You may not alter, remove or suppress in any manner any copyright, trademark or other notices displayed by the Materials. You may not license, rent, sell, loan, lease, pledge, offer as security, transfer or assign the Materials, or any of the rights granted to you hereunder to any other person.

4. The Materials and all of the intellectual property rights therein shall at all times remain the exclusive property of John Wiley & Sons Inc or one of its related companies (WILEY) or their respective licensors, and your interest therein is only that of having possession of and the right to reproduce the Materials pursuant to Section 2 herein during the continuance of this Agreement. You agree that you own no right, title or interest in or to the Materials or any of the intellectual property rights therein. You shall have no rights hereunder other than the license as provided for above in Section 2. No right, license or interest to any trademark, trade name, service mark or other branding ("Marks") of WILEY or its licensors is granted hereunder, and you agree that you shall not assert any such right, license or interest with respect thereto.

5. NEITHER WILEY NOR ITS LICENSORS MAKES ANY WARRANTY OR REPRESENTATION OF ANY KIND TO YOU OR ANY THIRD PARTY, EXPRESS, IMPLIED OR STATUTORY, WITH RESPECT TO THE MATERIALS OR THE ACCURACY OF ANY INFORMATION CONTAINED IN THE MATERIALS, INCLUDING, WITHOUT LIMITATION, ANY IMPLIED WARRANTY OF MERCHANTABILITY, ACCURACY, SATISFACTORY QUALITY, FITNESS FOR A PARTICULAR PURPOSE, USABILITY, INTEGRATION OR NON-INFRINGEMENT AND ALL SUCH WARRANTIES ARE HEREBY EXCLUDED BY WILEY AND ITS LICENSORS AND WAIVED BY YOU.

6. WILEY shall have the right to terminate this Agreement immediately upon breach of this Agreement by you.

7. You shall indemnify, defend and hold harmless WILEY, its Licensors and their respective directors, officers, agents and employees, from and against any actual or threatened claims, demands, causes of action or proceedings arising from any breach of this Agreement by you.

8. IN NO EVENT SHALL WILEY OR ITS LICENSORS BE LIABLE TO YOU OR ANY OTHER PARTY OR ANY OTHER PERSON OR ENTITY FOR ANY SPECIAL, CONSEQUENTIAL, INCIDENTAL, INDIRECT, EXEMPLARY OR PUNITIVE DAMAGES, HOWEVER CAUSED, ARISING OUT OF OR IN CONNECTION WITH THE DOWNLOADING, PROVISIONING, VIEWING OR USE OF THE MATERIALS REGARDLESS OF THE FORM OF ACTION, WHETHER FOR BREACH OF CONTRACT, BREACH OF WARRANTY, TORT, NEGLIGENCE, INFRINGEMENT OR OTHERWISE (INCLUDING, WITHOUT LIMITATION, DAMAGES BASED ON LOSS OF PROFITS, DATA, FILES, USE, BUSINESS OPPORTUNITY OR CLAIMS OF THIRD PARTIES), AND WHETHER OR NOT THE PARTY HAS BEEN ADVISED OF THE POSSIBILITY OF SUCH DAMAGES. THIS LIMITATION SHALL APPLY NOTWITHSTANDING ANY FAILURE OF ESSENTIAL PURPOSE OF ANY LIMITED REMEDY PROVIDED HEREIN.

9. Should any provision of this Agreement be held by a court of competent jurisdiction to be illegal, invalid, or unenforceable, that provision shall be deemed amended to achieve as nearly as possible the same economic effect as the original provision, and the legality, validity and enforceability of the remaining provisions of this Agreement shall not be affected or impaired thereby.

10. The failure of either party to enforce any term or condition of this Agreement shall not constitute a waiver of either party's right to enforce each and every term and condition of this Agreement. No breach under this agreement shall be deemed waived or excused by either party unless such waiver or consent is in writing signed by the party granting such waiver or consent. The waiver by or consent of a party to a breach of any provision of this Agreement shall not operate or be construed as a waiver of or consent to any other or subsequent breach by such other party.

11. This Agreement may not be assigned (including by operation of law or otherwise) by you without WILEY's prior written consent.

12. Any fee required for this permission shall be non-refundable after thirty (30) days from receipt.

13. These terms and conditions together with CCC's Billing and Payment terms and conditions (which are incorporated herein) form the entire agreement between you and WILEY concerning this licensing transaction and (in the absence of fraud) supersedes all prior agreements and representations of the parties, oral or written. This Agreement may not be amended except in writing signed by both parties. This Agreement shall be binding upon and inure to the benefit of the parties' successors, legal representatives, and authorized assigns.

14. In the event of any conflict between your obligations established by these terms and conditions and those established by CCC's Billing and Payment terms and conditions, these terms and conditions shall prevail.

15. WILEY expressly reserves all rights not specifically granted in the combination of (i) the license details provided by you and accepted in the course of this licensing transaction, (ii) these terms and conditions and (iii) CCC's Billing and Payment terms and conditions.

16. This Agreement will be void if the Type of Use, Format, Circulation, or Requestor Type was misrepresented during the licensing process.

17. This Agreement shall be governed by and construed in accordance with the laws of the State of New York, USA, without regards to such state's conflict of law rules. Any legal action, suit or proceeding arising out of or relating to these Terms and Conditions or the breach thereof shall be instituted in a court of competent jurisdiction in New York County in the State of New York in the United States of America and each party hereby consents and submits to the personal jurisdiction of such court, waives any objection to venue in such court and consents to service of process by registered or certified mail, return receipt requested, at the last known address of such party.

Wiley Open Access Terms and Conditions

a fee (for example, a compilation produced for marketing purposes, inclusion in a sales pack)
- Use of article content (other than normal quotations with appropriate citation) by for-profit organisations for promotional purposes
- Linking to article content in e-mails redistributed for promotional, marketing or educational purposes;
- Use for the purposes of monetary reward by means of sale, resale, licence, loan, transfer or other form of commercial exploitation such as marketing products
- Print reprints of Wiley Open Access articles can be purchased from: corporatesales@wiley.com

Other Terms and Conditions:

BY CLICKING ON THE "I AGREE..." BOX, YOU ACKNOWLEDGE THAT YOU HAVE READ AND FULLY UNDERSTAND EACH OF THE SECTIONS OF AND PROVISIONS SET FORTH IN THIS AGREEMENT AND THAT YOU ARE IN AGREEMENT WITH AND ARE WILLING TO ACCEPT ALL OF YOUR OBLIGATIONS AS SET FORTH IN THIS AGREEMENT.

v1.7

Gratis licenses (referencing $0 in the Total field) are free. Please retain this printable license for your reference. No payment is required.

If you would like to pay for this license now, please remit this license along with your payment made payable to "COPYRIGHT CLEARANCE CENTER" otherwise you will be invoiced within 48 hours of the license date. Payment should be in the form of a check or money order referencing your account number and this invoice number RLNK11027841.
Once you receive your invoice for this order, you may pay your invoice by credit card. Please follow instructions provided at that time.

Make Payment To:
Copyright Clearance Center
Dept 001
P.O. Box 843006
Boston, MA 02284-3006

For suggestions or comments regarding this order, contact Rightslink Customer Support: customercare@copyright.com or +1-877-622-5543 (toll free in the US) or +1-978-646-2777.

Copyright Clearance Center RightsLink®

Home | Account Info | Help

ACS Publications High quality. High impact.

Title: The Effects of Chemical Additives on the Induction Phase in Solid-State Thermal Decomposition of Ammonia Borane

Author: David J. Heldebrant et al.

Publication: Chemistry of Materials

Publisher: American Chemical Society

Date: Aug 1, 2008

Logged in as:
Jonathan Webb
Account #:
3000432578

LOGOUT

No charge permission and attribution

Permission for this particular request is granted for print and electronic formats at no charge. Figures and tables may be modified. Appropriate credit should be given. Please print this page for your records and provide a copy to your publisher. Requests for up to 4 figures require only this record. Five or more figures will generate a printout of additional terms and conditions. Appropriate credit should read: "Reprinted with permission from {COMPLETE REFERENCE CITATION}. Copyright {YEAR} American Chemical Society." Insert appropriate information in place of the capitalized words.

This permission does not apply to images that are credited to publications other than ACS journals. For images credited to non-ACS journal publications, you will need to obtain permission from the journal referenced in the Table/Figure/Micrograph legend or credit line before making any use of the image(s) or table(s).

BACK CLOSE WINDOW

ELSEVIER LICENSE
TERMS AND CONDITIONS

Jul 27, 2011

This is a License Agreement between Jonathan D Webb ("You") and Elsevier ("Elsevier") provided by Copyright Clearance Center ("CCC"). The license consists of your order details, the terms and conditions provided by Elsevier, and the payment terms and conditions.

All payments must be made in full to CCC. For payment instructions, please see information listed at the bottom of this form.

Supplier	Elsevier Limited The Boulevard,Langford Lane Kidlington,Oxford,OX5 1GB,UK
Registered Company Number	1982084
Customer name	Jonathan D Webb
Customer address	PO Box 1495 Station Main Kingston, ON K7L 5C7
License number	2717140548457
License date	Jul 27, 2011
Licensed content publisher	Elsevier
Licensed content publication	International Journal of Hydrogen Energy
Licensed content title	A procedure for the regeneration of ammonia borane from BNH-waste products
Licensed content author	Steffen Hausdorf, Felix Baitalow, Gert Wolf, Florian O.R.L. Mertens
Licensed content date	January 2008
Licensed content volume number	33
Licensed content issue number	2
Number of pages	7
Start Page	608
End Page	614
Type of Use	reuse in a thesis/dissertation
Intended publisher of new work	other
Portion	figures/tables/illustrations
Number of figures/tables /illustrations	1
Format	both print and electronic

Are you the author of this Elsevier article?	No
Will you be translating?	No
Order reference number	
Title of your thesis/dissertation	ADDRESSING CHALLENGES IN CATALYSIS AND ENERGY: SELECTIVE GRAFTING FUNCTIONALITY ONTO MESOPOROUS SILICAS AND ORGANIC HYDRIDES FOR THE REGENERATION OF AMMONIA BORANE, A HYDROGEN STORAGE MATERIAL
Expected completion date	Sep 2011
Estimated size (number of pages)	450
Elsevier VAT number	GB 494 6272 12
Permissions price	0.00 USD
VAT/Local Sales Tax	0.0 USD / 0.0 GBP
Total	0.00 USD
Terms and Conditions	

INTRODUCTION

1. The publisher for this copyrighted material is Elsevier. By clicking "accept" in connection with completing this licensing transaction, you agree that the following terms and conditions apply to this transaction (along with the Billing and Payment terms and conditions established by Copyright Clearance Center, Inc. ("CCC"), at the time that you opened your Rightslink account and that are available at any time at http://myaccount.copyright.com).

GENERAL TERMS

2. Elsevier hereby grants you permission to reproduce the aforementioned material subject to the terms and conditions indicated.

3. Acknowledgement: If any part of the material to be used (for example, figures) has appeared in our publication with credit or acknowledgement to another source, permission must also be sought from that source. If such permission is not obtained then that material may not be included in your publication/copies. Suitable acknowledgement to the source must be made, either as a footnote or in a reference list at the end of your publication, as follows:

"Reprinted from Publication title, Vol /edition number, Author(s), Title of article / title of chapter, Pages No., Copyright (Year), with permission from Elsevier [OR APPLICABLE SOCIETY COPYRIGHT OWNER]." Also Lancet special credit - "Reprinted from The Lancet, Vol. number, Author(s), Title of article, Pages No., Copyright (Year), with permission from Elsevier."

4. Reproduction of this material is confined to the purpose and/or media for which

permission is hereby given.

5. Altering/Modifying Material: Not Permitted. However figures and illustrations may be altered/adapted minimally to serve your work. Any other abbreviations, additions, deletions and/or any other alterations shall be made only with prior written authorization of Elsevier Ltd. (Please contact Elsevier at permissions@elsevier.com)

6. If the permission fee for the requested use of our material is waived in this instance, please be advised that your future requests for Elsevier materials may attract a fee.

7. Reservation of Rights: Publisher reserves all rights not specifically granted in the combination of (i) the license details provided by you and accepted in the course of this licensing transaction, (ii) these terms and conditions and (iii) CCC's Billing and Payment terms and conditions.

8. License Contingent Upon Payment: While you may exercise the rights licensed immediately upon issuance of the license at the end of the licensing process for the transaction, provided that you have disclosed complete and accurate details of your proposed use, no license is finally effective unless and until full payment is received from you (either by publisher or by CCC) as provided in CCC's Billing and Payment terms and conditions. If full payment is not received on a timely basis, then any license preliminarily granted shall be deemed automatically revoked and shall be void as if never granted. Further, in the event that you breach any of these terms and conditions or any of CCC's Billing and Payment terms and conditions, the license is automatically revoked and shall be void as if never granted. Use of materials as described in a revoked license, as well as any use of the materials beyond the scope of an unrevoked license, may constitute copyright infringement and publisher reserves the right to take any and all action to protect its copyright in the materials.

9. Warranties: Publisher makes no representations or warranties with respect to the licensed material.

10. Indemnity: You hereby indemnify and agree to hold harmless publisher and CCC, and their respective officers, directors, employees and agents, from and against any and all claims arising out of your use of the licensed material other than as specifically authorized pursuant to this license.

11. No Transfer of License: This license is personal to you and may not be sublicensed, assigned, or transferred by you to any other person without publisher's written permission.

12. No Amendment Except in Writing: This license may not be amended except in a writing signed by both parties (or, in the case of publisher, by CCC on publisher's behalf).

13. Objection to Contrary Terms: Publisher hereby objects to any terms contained in any purchase order, acknowledgment, check endorsement or other writing prepared by you, which terms are inconsistent with these terms and conditions or CCC's Billing and Payment

terms and conditions. These terms and conditions, together with CCC's Billing and Payment terms and conditions (which are incorporated herein), comprise the entire agreement between you and publisher (and CCC) concerning this licensing transaction. In the event of any conflict between your obligations established by these terms and conditions and those established by CCC's Billing and Payment terms and conditions, these terms and conditions shall control.

14. Revocation: Elsevier or Copyright Clearance Center may deny the permissions described in this License at their sole discretion, for any reason or no reason, with a full refund payable to you. Notice of such denial will be made using the contact information provided by you. Failure to receive such notice will not alter or invalidate the denial. In no event will Elsevier or Copyright Clearance Center be responsible or liable for any costs, expenses or damage incurred by you as a result of a denial of your permission request, other than a refund of the amount(s) paid by you to Elsevier and/or Copyright Clearance Center for denied permissions.

LIMITED LICENSE

The following terms and conditions apply only to specific license types:

15. **Translation**: This permission is granted for non-exclusive world **English** rights only unless your license was granted for translation rights. If you licensed translation rights you may only translate this content into the languages you requested. A professional translator must perform all translations and reproduce the content word for word preserving the integrity of the article. If this license is to re-use 1 or 2 figures then permission is granted for non-exclusive world rights in all languages.

16. **Website**: The following terms and conditions apply to electronic reserve and author websites:
Electronic reserve: If licensed material is to be posted to website, the web site is to be password-protected and made available only to bona fide students registered on a relevant course if:
This license was made in connection with a course,
This permission is granted for 1 year only. You may obtain a license for future website posting,
All content posted to the web site must maintain the copyright information line on the bottom of each image,
A hyper-text must be included to the Homepage of the journal from which you are licensing at http://www.sciencedirect.com/science/journal/xxxxx or the Elsevier homepage for books at http://www.elsevier.com , and
Central Storage: This license does not include permission for a scanned version of the material to be stored in a central repository such as that provided by Heron/XanEdu.

17. **Author website** for journals with the following additional clauses:

All content posted to the web site must maintain the copyright information line on the

bottom of each image, and
he permission granted is limited to the personal version of your paper. You are not allowed to download and post the published electronic version of your article (whether PDF or HTML, proof or final version), nor may you scan the printed edition to create an electronic version,
A hyper-text must be included to the Homepage of the journal from which you are licensing at http://www.sciencedirect.com/science/journal/xxxxx , As part of our normal production process, you will receive an e-mail notice when your article appears on Elsevier's online service ScienceDirect (www.sciencedirect.com). That e-mail will include the article's Digital Object Identifier (DOI). This number provides the electronic link to the published article and should be included in the posting of your personal version. We ask that you wait until you receive this e-mail and have the DOI to do any posting.
Central Storage: This license does not include permission for a scanned version of the material to be stored in a central repository such as that provided by Heron/XanEdu.

18. **Author website** for books with the following additional clauses:
Authors are permitted to place a brief summary of their work online only.
A hyper-text must be included to the Elsevier homepage at http://www.elsevier.com

All content posted to the web site must maintain the copyright information line on the bottom of each image
You are not allowed to download and post the published electronic version of your chapter, nor may you scan the printed edition to create an electronic version.
Central Storage: This license does not include permission for a scanned version of the material to be stored in a central repository such as that provided by Heron/XanEdu.

19. **Website** (regular and for author): A hyper-text must be included to the Homepage of the journal from which you are licensing at http://www.sciencedirect.com/science/journal/xxxxx. or for books to the Elsevier homepage at http://www.elsevier.com

20. **Thesis/Dissertation**: If your license is for use in a thesis/dissertation your thesis may be submitted to your institution in either print or electronic form. Should your thesis be published commercially, please reapply for permission. These requirements include permission for the Library and Archives of Canada to supply single copies, on demand, of the complete thesis and include permission for UMI to supply single copies, on demand, of the complete thesis. Should your thesis be published commercially, please reapply for permission.

21. **Other Conditions**:

v1.6

Gratis licenses (referencing $0 in the Total field) are free. Please retain this printable license for your reference. No payment is required.

If you would like to pay for this license now, please remit this license along with your payment made payable to "COPYRIGHT CLEARANCE CENTER" otherwise you will be invoiced within 48 hours of the license date. Payment should be in the form of a check or money order referencing your account number and this invoice number RLNK11027847.
Once you receive your invoice for this order, you may pay your invoice by credit card. Please follow instructions provided at that time.

Make Payment To:
Copyright Clearance Center
Dept 001
P.O. Box 843006
Boston, MA 02284-3006

For suggestions or comments regarding this order, contact Rightslink Customer Support: customercare@copyright.com or +1-877-622-5543 (toll free in the US) or +1-978-646-2777.